

Mechanisms and Machine Science

Constantinos Frangos

Mathematical
Modelling,
Nonlinear Control
and Performance
Evaluation of a
Ground Based
Mobile Air Defence
System

 Springer

Volume 76

Mechanisms and Machine Science

Series Editor

Marco Ceccarelli

*Department of Industrial Engineering, University of Rome Tor Vergata,
Roma, Italy*

Editorial Board

Alfonso Hernandez

*Mechanical Engineering, University of the Basque Country, Bilbao,
Vizcaya, Spain*

Tian Huang

*Department of Mechatronical Engineering, Tianjin University, Tianjin,
China*

Yukio Takeda

Mechanical Engineering, Tokyo Institute of Technology, Tokyo, Japan

Burkhard Corves

*Institute of Mechanism Theory, Machine Dynamics and Robotics, RWTH
Aachen University, Aachen, Nordrhein-Westfalen, Germany*

Sunil Agrawal

*Department of Mechanical Engineering, Columbia University, New York,
NY, USA*

This book series establishes a well-defined forum for monographs, edited Books, and proceedings on mechanical engineering with

particular emphasis on MMS (Mechanism and Machine Science). The final goal is the publication of research that shows the development of mechanical engineering and particularly MMS in all technical aspects, even in very recent assessments. Published works share an approach by which technical details and formulation are discussed, and discuss modern formalisms with the aim to circulate research and technical achievements for use in professional, research, academic, and teaching activities.

This technical approach is an essential characteristic of the series. By discussing technical details and formulations in terms of modern formalisms, the possibility is created not only to show technical developments but also to explain achievements for technical teaching and research activity today and for the future.

The book series is intended to collect technical views on developments of the broad field of MMS in a unique frame that can be seen in its totality as an Encyclopaedia of MMS but with the additional purpose of archiving and teaching MMS achievements. Therefore, the book series will be of use not only for researchers and teachers in Mechanical Engineering but also for professionals and students for their formation and future work.

The series is promoted under the auspices of International Federation for the Promotion of Mechanism and Machine Science (IFToMM).

Prospective authors and editors can contact Mr. Pierpaolo Riva (publishing editor, Springer) at: pierpaolo.riva@springer.com

Indexed by SCOPUS and Google Scholar.

More information about this series at <http://www.springer.com/series/8779>

Constantinos Frangos

Mathematical Modelling, Nonlinear Control and Performance Evaluation of a Ground Based Mobile Air Defence System

1st ed. 2021



Dr. Constantinos Frangos, PhD
Electrical Engineer working in Decision and Control, Pretoria, South
Africa

ISSN 2211-0984 e-ISSN 2211-0992
Mechanisms and Machine Science
ISBN 978-3-030-55497-2 e-ISBN 978-3-030-55498-9
<https://doi.org/10.1007/978-3-030-55498-9>

© Springer Nature Switzerland AG 2021

This work is subject to copyright. All rights are reserved by the Publisher, whether the whole or part of the material is concerned, specifically the rights of translation, reprinting, reuse of illustrations, recitation, broadcasting, reproduction on microfilms or in any other physical way, and transmission or information storage and retrieval, electronic adaptation, computer software, or by similar or dissimilar methodology now known or hereafter developed.

The use of general descriptive names, registered names, trademarks, service marks, etc. in this publication does not imply, even in the absence of a specific statement, that such names are exempt from the relevant protective laws and regulations and therefore free for general use.

The publisher, the authors and the editors are safe to assume that the advice and information in this book are believed to be true and accurate at the date of publication. Neither the publisher nor the authors or the editors give a warranty, expressed or implied, with respect to the material contained herein or for any errors or omissions that may have been made. The publisher remains neutral with regard to jurisdictional claims in published maps and institutional affiliations.

This Springer imprint is published by the registered company Springer
Nature Switzerland AG

The registered company address is: Gewerbestrasse 11, 6330 Cham,
Switzerland

This work is gratefully dedicated to the memory of our unforgettable and beloved mother Angeliki Frangos (Αγγελική

Φράγκου του Γεωργίου και της Ευαγγελίας Πελέκη), 1926–2016.

Our mother raised us with loving care and attention, and with wise words of advice and consolation. Every thought of our mother fills us with happiness and pride. Our mother was very talented and worked professionally as a master dress-maker. She performed her craft with great skill and style, creating elegant garments and earning the respect and admiration of colleagues and friends. Our mother inspired us to become dedicated professionals driven by innovation, ethics and a deep respect for other professionals.

Constantinos Frangos

Evangelia Frangos

Preface

This research monograph deals with the dynamic modelling, nonlinear control and performance evaluation of a ground based mobile air defence system (ADS).

The present work complements existing references on ground based ADSs ([69, 108, 142]). The afore-mentioned publications deal mainly with static or non-mobile ADSs, that is, ADSs that are deployed at a fixed location. This research monograph deals with a mobile ADS that consists of an armoured ground vehicle with an integrated rotating turret and anti-aircraft (AA) gun.

A mobile ADS has several advantages over a fixed ADS as follows.

1. A mobile ADS can move relatively quickly between various locations and defend against attacking aerial targets (AATs) as needed.
2. A mobile ADS can engage mainly AATs and also fixed or moving ground targets. The mobile ADS can engage targets from a stationary position or while it is maneuvering on the horizontal plane and can thus support fast moving motorized ground forces.
3. A mobile ADS can be designed to transport personnel and cargo internally, and provide protection against a range of battlefield threats.
4. A mobile ADS can lead to tactical advantages in military deployments and engagements.

The mobile ADS is modelled as a constrained rigid multibody system. The ground vehicle of the mobile ADS has 4 wheels. It is assumed that all 4 wheels roll perfectly thus resulting in nonholonomic velocity constraints. Furthermore, the mobile ADS is controlled by 4 applied torques that are implemented by suitable actuators (for example, electric motors). First, there is a torque that steers the front wheels via a steering system (similar to an Ackermann steering system) leading to holonomic velocity constraints. Second, there is a torque

driving the rear wheels via a differential gearbox and sids shafts resulting in a holonomic velocity constraint. Third, there is a torque that rotates the turret in azimuth via a gearbox based mechanism. Fourth, there is a torque that rotates the AA gun in elevation via a gearbox based mechanism. The afore-mentioned gearbox based mechanisms lead to holonomic velocity constraints. It turns out that the specified configuration of the mobile ADS results in a set of holonomic and nonholonomic velocity constraints that are not independent.

Thus, kinematic and dynamic models of the mobile ADS need to be developed. In addition, nonlinear feedback control laws need to be derived for the applied torques such that given variables associated with the motion of the vehicle body, the turret and the AA gun asymptotically track reference command trajectories. Furthermore, the performance of the mobile ADS needs to be evaluated in engaging a specified AAT.

Part 1 of the book deals with the dynamic modelling and nonlinear control of the mobile ADS while Part 2 deals with the performance evaluation of the mobile ADS against a given AAT. In order to address these topics several interesting mathematical modelling and nonlinear control methodologies are presented and applied as follows.

1. Kinematic modelling of constrained rigid multibody systems subject to velocity constraints that may not be independent.
2. Extension of the Lagrange equations for the dynamic modelling of constrained rigid multibody systems subject to velocity constraints that may not be independent.
3. By applying the above-mentioned methodologies, the kinematic and dynamic models of the mobile ADS are derived by using all the velocity constraints in their original form (that is, the redundant velocity constraints are not deleted).
4. Nonlinear control of constrained rigid multibody systems using inverse dynamics transformations. Analysis of the zero dynamics of the controlled dynamic model of the multibody system. A nonlinear feedback control law is derived for the mobile ADS that provides maneuvering control of the vehicle body and rotational control of the turret and AA gun. This enables the mobile ADS to track and

the target and AA gun. This enables the mobile ADS to track and engage AATs with the AA gun while independently maneuvering the vehicle body on the horizontal plane.

5. Derivation and numerical solution of the point mass flight dynamics model of the AA projectile consisting of a set of nonlinear ordinary differential equations (ODEs).
6. Formulation and numerical solution of a conceptual fire control problem using constrained optimization. The fire control problem involves the computation of the aiming angles of the AA gun and the time of flight of the AA projectile to the intercept point with the center of mass (CM) of the AAT. Reformulation of the fire control problem using feasible control (co-developed with Prof. Yaakov Yavin (1935–2006)).
7. Application of a methodology for computing the impact point of the AA projectile on the three-dimensional body of the AAT.
8. Stochastic modelling of the dispersion of the AA projectiles fired by the AA gun by considering random initial conditions for the point mass flight dynamics model of the AA projectile. Computation of the probability that the AA projectile will impact the body of the AAT.
9. Application of advanced scientific computing systems, mainly Maple, MATLAB/MATLAB Symbolic Toolbox, Octave/Octave Symbolic Package (and also of other systems such as Mathematica, Maxima), all running under the Linux operating system, in order to perform the complicated symbolic and numerical computations required to obtain the above-mentioned results.¹ In particular, machines running Ubuntu Linux and Linux Mint with the MATE desktop manager are employed.

Although a particular type of ground based mobile ADS is considered in this work, the methodologies presented in Part 1 of the book can be applied to model the given mobile ADS in greater detail, to model a mobile ADS with a different configuration, or to model an ADS that operates in a different domain. Similarly, the methodologies

presented in Part 2 of the book can be applied to evaluate the performance of the mobile ADS against a variety of AATs. In addition, different types of AA projectiles and alternative weapon systems can be considered. Some examples of the above are as follows.

1. The case where the mobile ADS is moving on a three-dimensional terrain. In this instance, the rigid bodies comprising the mobile ADS will rotate in yaw, pitch and roll.
2. More detailed modelling of the mobile ADS, for example, the case where each wheel consists of a tyre mounted on a hub thus leading to the possibility of slipping of the wheel, a suspension system for each wheel, a detailed implementation of the steering system for the front wheels, etc. More detailed modelling will generally result in more complicated kinematic and dynamic models of the mobile ADS.
3. A land based mobile ADS with alternative vehicle configurations, for example, a vehicle with six or eight wheels, or a vehicle with tracks.
4. A mobile ADS engaging ground targets and aerial targets using the following.
 - (a) Missiles.
 - (b) Ray based guns employing high power lasers.
5. Weapon systems having a generic turret and gun configuration and operating in different domains as follows.
 - (a) Sea based weapon systems, for example, a turret with a relevant gun or weapon mounted on a ship.
 - (b) Air based weapon systems, for example, a turret with a relevant gun or weapon mounted on a helicopter or aircraft.
 - (c) Future space based weapon systems, for example, a turret

with a relevant weapon mounted on a space craft, space station or satellite.

6. Application of some of the methodologies presented in this work to the case of aerial vehicles engaging moving ground targets, for example, air-to-ground gunnery ([118]).

Part 1 of the book consists of Chaps. 2–5 and Appendices A, B, while Part 2 includes Chaps. 6–9, as follows.

Chapter 1 : Introduction

A summary is presented of Part 1 and Part 2.

Chapter 2 : Overview of the Mobile Air Defence System

A mathematical description of each rigid body is given, together with the associated holonomic and nonholonomic velocity constraints. The mobile ADS comprises $N = 11$ rigid bodies and is controlled by

$m_c = 4$ applied torques (variable names like N , m_c , n , m , etc. are introduced here in order to conveniently denote various quantities). There are a total of $n = 15$ generalized co-ordinates and thus 15 generalized velocities. In addition, there are a total of $m = 13$ velocity constraints of which only $r_G = 11$ are independent. Thus,

$n_s = n - r_G = 4$ of the 15 generalized velocities can be selected to be independent generalized velocities. In this case, the number of independent generalized velocities is equal to the number of applied torques, $n_s = m_c = 4$.

Chapter 3 : Kinematic Model of the Mobile Air Defence System

Using all 13 holonomic and nonholonomic velocity constraints and the methods presented in Appendix A, the kinematic model of the mobile ADS is derived. The kinematic model describes the 15 generalized velocities in terms of the selected 4 independent generalized velocities. Note that the inertial velocity of the muzzle of the AA gun depends on the motions of the AA gun, the turret and the vehicle body of the mobile ADS.

Chapter 4 : Dynamic Model and Nonlinear Control of the Mobile Air Defence System

By using the methods presented in Appendix B the basic dynamic model of the mobile air defence system is derived. The basic dynamic model describes the 15 generalized accelerations in terms of 15 generalized applied forces and 13 Lagrange multipliers. Four of the generalized applied forces are nonzero and correspond to the 4 applied torques. The kinematic model of the mobile ADS is applied in order to derive the reduced dynamic model of the mobile ADS. The reduced dynamic model describes the 4 independent generalized accelerations in terms of the 4 applied torques and does not contain the Lagrange multipliers.

Thus, the reduced dynamic model is employed in order to derive a nonlinear feedback control law for the mobile ADS by using inverse dynamics transformations. The nonlinear feedback control law is for the 4 applied torques and enables control of 4 variables related to the motion of the vehicle body, the turret and the AA gun. The zero dynamics of the controlled dynamic model of the mobile ADS is analyzed.

A methodology is presented for the computation of the constrained motion of the controlled dynamic model of the mobile ADS satisfying all the holonomic and nonholonomic velocity constraints. In addition, methodologies are presented for computing the vector of generalized constraint forces and the vector of Lagrange multipliers. Since the velocity constraints are not independent the vector of Lagrange multipliers is not unique. Based on the results presented in Appendix B the Moore-Penrose generalized inverse is applied in order to compute the vector of Lagrange multipliers having minimum Euclidean norm.

Chapter 5 : Operational Modes of the Mobile Air Defence System

The operational modes of the mobile ADS consist of various combinations of the tracking modes of the vehicle body and of the AA gun. The afore-mentioned tracking modes are based on the nonlinear feedback control law developed in Chap. 4. In addition, some results based on the firing rate of the AA gun are presented.

Chapter 6 : Point Mass Flight Dynamics Model of the Anti-Aircraft Projectile

The point mass flight dynamics model of the AA projectile consists of a set of nonlinear ODEs and includes a speed-dependent drag coefficient. The trajectory of the AA projectile is computed by assuming a completely stationary vehicle body, for a fixed aiming azimuth angle, and for various aiming elevation angles of the AA gun. The case of zero wind velocity and the case of non-zero wind velocity are considered. Note that the inertial velocity of the AA projectile on exit from the muzzle of the AA gun is the vector sum of the generic firing velocity of the AA projectile and the inertial velocity of the muzzle of the AA gun.

Chapter 7 : The Fire Control Problem

The formulation and numerical solution of a conceptual fire control problem FCA is presented. This involves the specification of a finite number of intercept times of the AA projectile with the CM of the AAT. For each given intercept time, the required aiming azimuth and elevation angles of the AA gun are computed as well as the time of flight of the AA projectile to the CM of the AAT. The fire control problem is also formulated using feasible control.

The numerical solution of fire control problem FCA is obtained for the case where the vehicle body of the mobile ADS is completely stationary and for the case where the vehicle body of the mobile ADS is moving forward at constant speed and in a straight line. The obtained numerical results for fire control problem FCA are applied in Chaps. 8 and 9.

Chapter 8 : Computation of the Impact Point of the AA Projectile on the Body of the Attacking Aerial Target

The geometry of the three-dimensional body of the AAT is specified and the relative kinematics between the AA projectile and the AAT are derived. A methodology is presented for computing the impact point of the AA projectile on the body of the AAT.

Chapter 9 : Computation of the Probability that the AA Projectile Will Impact the Body of the Attacking Aerial Target

A stochastic model is proposed for the random direction of the generic firing velocity vector of the AA projectile relative to the longitudinal axis of the AA gun. The random direction is constructed by using a random azimuth error angle and a random elevation error angle.

Thus, the point mass flight dynamics model of the AA projectile is subject to random initial conditions that are a function of the above-mentioned random error angles. A computational method is applied in order to compute the probability that the AA projectile will impact the body of the AAT. In addition, the computation of the probability that a burst of AA projectiles will destroy the AAT, and the accumulative probability that a burst of AA projectiles will destroy the AAT, is presented. A verification method is applied in order to verify the computational method used to obtain the probability that the AA projectile will impact the body of the AAT.

Appendix A: Kinematics of Constrained Rigid Multibody Systems Subject to Velocity Constraints that May Not be Independent

Basic assumptions, results and methods are presented on the kinematics of constrained rigid multibody systems subject to velocity constraints that may not be independent. For example, the specified configuration of the mobile ADS leads to a set of holonomic and nonholonomic velocity constraints that are not independent. The presented methods can be applied in order to derive the kinematic model of the multibody system using all the velocity constraints. The resulting kinematic model describes the generalized velocities in terms of the selected independent generalized velocities.

Appendix B: Lagrange Equations for Constrained Rigid Multibody Systems Subject to Velocity Constraints that May Not be Independent

Basic assumptions, results and methods are presented on the dynamics of constrained rigid multibody systems. By using the d'Alembert-Lagrange principle, the Lagrange equations are extended for the case where the velocity constraints may not be independent. The results indicate that in the case of independent velocity constraints the Lagrange multipliers are unique while in the case of dependent velocity constraints the Lagrange multipliers are not unique. The Moore-Penrose generalized inverse is applied in order to compute the vector of Lagrange multipliers having minimum Euclidean norm.

In the literature, the Lagrange equations are usually derived by assuming that the velocity constraints are independent. Thus, in order to apply the Lagrange equations to the mobile ADS the set of not

independent velocity constraints has to be converted to a set of independent velocity constraints (for example, by deleting the redundant velocity constraints). In general, this approach may imply a corresponding modification of the given physical configuration of the multibody system (Chap. 1). Some auxiliary results are presented dealing with the computation of a general solution of consistent simultaneous linear equations.

It is recommended that Appendices A, B, are consulted in parallel with Chaps. 1–9, and particularly with Chaps. 1–5. This will familiarize the reader with the assumptions and notations used in the derivation of the kinematic and dynamic models of the mobile ADS and of the nonlinear feedback control law. Thus, the contents of the book can be studied in the following sequence.

1. Chapter 1. (Appendices A, B)
2. Chapter 2.
3. Chapter 3.
4. Chapter 4.
5. Chapter 5.
6. Chapters 6–9.

This work will be of interest to the following audiences.

1. Postgraduate students and advanced undergraduate students studying at general universities and at national defence universities for degrees in the following fields.
 - (a) Electrical, Mechanical, Aerospace and Industrial Engineering.
 - (b) Applied Mathematics, Physics, Statistics/Stochastics and Scientific Computing.

- Academic staff working at the above-mentioned university
2. departments.
 3. Engineering and science professionals working for the following organizations.
 - (a) Defence-related companies dealing with the development and manufacture of wheeled vehicles, motorized systems and mobile air defence systems.
 - (b) Defence-related research institutes.
 - (c) Research institutes working in the dynamic modelling and nonlinear control of transportation systems.
 - (d) Industrial companies dealing with the development and manufacture of ground vehicles and interested in comparing alternative approaches to the dynamic modelling of wheeled vehicles. For example, assuming perfect rolling of the wheels compared to the case where tyre models are used and where slipping of the wheels does take place.

In particular, the research monograph is intended for those that are interested in one or more of the topics and methodologies enumerated on p. viii–ix. Enumeration is used in this work in order to present in a compact form various assumptions, results and methods, as appropriate.

Constantinos Frangos
Pretoria, South Africa
March 2020

Acknowledgements

I would like to sincerely thank the teachers, colleagues and family that supported my professional career over the past few decades.

In this regard, I would like to gratefully acknowledge the research collaboration with Prof. Yaakov Yavin (1935–2006) as follows.

1. Co-founded with Prof. Yavin the Laboratory for Decision and Control, Department of Electrical, Electronic and Computer Engineering, University of Pretoria.
2. Co-developed with Prof. Yavin feasible control that circumvents certain difficulties of optimal control and facilitates the design of control strategies for linear and nonlinear dynamic systems such that a wide range of practical performance specifications and constraints are satisfied. Feasible control has been applied to solve a number of otherwise intractable control problems (Sect. 7.2).
3. Collaborated with Prof. Yavin in research on the mathematical modelling and control of land, sea and air transportation systems, for example, various types of wheeled ground vehicles, super tanker ships, aerial vehicles and projectiles (Chaps. 1–9, Sects. 7.2, 9.1.1).
4. Collaborated with Prof. Yavin in research on the optimal and suboptimal feedback control of nonlinear stochastic systems subject to complicated performance requirements, control constraints and state constraints. This involves the numerical solution of the Hamilton-Jacobi-Bellman (HJB) partial differential equation (PDE) subject to boundary conditions, for the optimal objective function and the optimal feedback control function (Sect. 9.1.1). The HJB PDE is discretized by using a unique numerical approximation method developed by Prof. Harold J. Kushner, Division of Applied Mathematics, Brown University, USA.

I appreciate the comments and suggestions that were provided by colleagues for improving the contents of the book. I would also like to

thank the many dedicated professionals all over the world who have contributed for more than 25 years to the development of the Linux operating system and of numerous open source software systems.

My professional work has benefitted from Linux and from open source and private source scientific computing systems that run easily and efficiently on Linux. The results presented in this research monograph are obtained by employing large scale scientific computing on machines running Ubuntu Linux and Linux Mint with the MATE desktop manager.

Lastly, I would like to express my thanks to all the Springer staff for their kind assistance during the writing of this book. In particular, I would like to thank Ms. Charlotte Cross and Mr. Anthony Doyle, Springer, Great Britain, Mr. Arulmurugan Venkatasalam and team, Springer production department, India, and Mr. Faruk Ali Syed, SPS, India.

Constantinos Frangos

Acronyms

AA Anti-Aircraft

AAT Attacking Aerial Target

ADS Air Defence System

CM Center of Mass

CPA Closest Point of Approach

FC Fire Control

FCA Fire Control Problem FCA

GM1 AA Gun Tracking Mode GM1

GM1A AA Gun Tracking Mode GM1A

GM1B AA Gun Tracking Mode GM1B

GM2 AA Gun Tracking Mode GM2

HJB Hamilton-Jacobi-Bellman

ICR Instantaneous Center of Rotation

IID Independent Identically Distributed

ILBS Integration Limits Bounding Sphere

ISA International Standard Atmosphere

LOI Line-Of-Intercept

LOS Line-Of-Sight

LQG Linear Quadratic Gaussian

NM1 Numerical Method NM1

NM2 Numerical Method NM2

ODE Ordinary Differential Equation

OM1 Mobile ADS Operational Mode OM1

OM1A Mobile ADS Operational Mode OM1A

OM1B Mobile ADS Operational Mode OM1B

OM2 Mobile ADS Operational Mode OM2

OM3 Mobile ADS Operational Mode OM3

PDE Partial Differential Equation
PDF Probability Density Function
PMF Probability Mass Function
SLEs Simultaneous Linear Equations
TBS Target Bounding Sphere
TPBVP Two-Point-Boundary-Value-Problem
VM1 Vehicle Body Tracking Mode VM1
VM1A Vehicle Body Tracking Mode VM1A
VM2 Vehicle Body Tracking Mode VM2
VMB Verification Method VMB

Contents

1 Introduction

1.1 Part 1: Kinematics, Dynamics and Nonlinear Control of the Mobile Air Defence System Subject to Holonomic and Nonholonomic Velocity Constraints

1.2 Part 2: Performance Evaluation of the Mobile Air Defence System Against an Attacking Aerial Target

2 Overview of the Mobile Air Defence System

2.1 Multibody System Representation of the Mobile Air Defence System

2.2 Vehicle Body (Body 5)

2.2.1 Electric Motors EM_{γ_0} , EM_{α_s} and EM_{δ_v}

2.3 Wheels 1, 2, 3 and 4 (Body 1 to Body 4)

2.3.1 Velocity Constraints

2.4 Turret (Body 6)

2.4.1 Electric Motor EM_{δ_v}

2.5 Anti-Aircraft Gun (Body 7)

2.6 Drive System and Differential Gearbox (Body 8)

2.6.1 Velocity Constraint

2.7 Steering System (Body 9)

2.7.1 Geometric Constraints

2.7.2 Velocity Constraints

2.8 Rotor of the Turret Electric Motor EM_{γ_0} (Body 10)

2.8.1 Velocity Constraint

2.9 Rotor of the AA Gun Electric Motor EM_{δ_v} (Body 11)

2.9.1 Velocity Constraint

2.10 Definition of Generalized Co-Ordinates n and Generalized Velocities p

2.11 Inertial Azimuth and Elevation Angles of a Vector

2.12 Line-of-Sight Vector from the Mobile ADS to the AAT

2.13 Aiming Vector of the AA Gun

2.14 Inertial Position and Velocity of the AA Gun Muzzle

3 Kinematic Model of the Mobile Air Defence System

3.1 Velocity Constraints of the Mobile ADS

3.2 Kinematic Model of the Mobile ADS

3.3 Decoupled Kinematic Models of the Vehicle System and of the Turret and AA Gun System

4 Dynamic Model and Nonlinear Control of the Mobile Air Defence System

4.1 Basic Dynamic Model of the Mobile ADS

4.2 Reduced Dynamic Model of the Mobile ADS

4.3 Nonlinear Feedback Control of the Reduced Dynamic Model of the Mobile ADS

4.3.1 Analysis of the Zero Dynamics

4.4 Constrained Motion of the Controlled Dynamic Model of the Mobile ADS

4.5 Generalized Constraint Forces

4.6 Lagrange Multipliers

5 Operational Modes of the Mobile Air Defence System

5.1 Asymptotic Tracking Results

5.2 Vehicle Body Tracking Mode VM1: Vehicle Body is Maneuvering

5.3 Vehicle Body Tracking Mode VM1A: Vehicle Body is Moving in a Straight Line

5.4 Vehicle Body Tracking Mode VM2: Vehicle Body is Stationary

5.5 AA Gun Tracking Mode GM1: AA Gun is Rotating Relative to the Vehicle Body

5.6 AA Gun Tracking Mode GM1A: AA Gun Aiming Vector is Tracking the LOS Vector

5.7 AA Gun Tracking Mode GM1B: AA Gun Aiming Vector is Tracking the Fire Control Vector

5.8 AA Gun Tracking Mode GM2: AA Gun is not Rotating Relative to the Vehicle Body

5.9 Main Operational Modes of the Mobile ADS

5.10 Operational Mode OM1: Mobile ADS is Maneuvering

5.11 Operational Mode OM1A: Vehicle Body is Moving in a Straight Line (VM1A) and the AA Gun is Rotating Relative to the Vehicle Body (GM1)

5.12 Operational Mode OM1B: Vehicle Body is Moving in a Straight Line (VM1A) and the AA Gun is not Rotating Relative to the Vehicle Body (GM2)

5.13 Operational Mode OM2: Vehicle Body is Stationary (VM2) and the AA Gun is Rotating Relative to the Vehicle Body (GM1)

5.14 Operational Mode OM3: Vehicle Body is Stationary (VM2) and the AA Gun is not Rotating Relative to the Vehicle Body (GM2)

5.15 Firing Rate of the AA Gun and Firing Times of the AA Projectiles

6 Point Mass Flight Dynamics Model of the Anti-Aircraft Projectile

6.1 Inertial Position and Velocity of the AA Projectile

6.2 Point Mass Flight Dynamics Model of the AA Projectile

6.3 Parameter Values for the Anti-Aircraft Projectile

6.4 Parameter Values for the Mobile ADS

6.5 Computation of the AA Projectile Trajectory with No Wind

6.6 Computation of the AA Projectile Trajectory with a Cross Wind

7 The Fire Control Problem

7.1 Fire Control Problem FCA

7.2 Fire Control Problem Formulation Using Feasible Control

7.3 Air Defence System Deployment and Attacking Aerial Target Engagement Scenario

7.4 Computational Results for Fire Control Problem FCA: Vehicle Body of Mobile ADS is Completely Stationary

7.5 Computational Results for Fire Control Problem FCA: Vehicle Body of Mobile ADS is Moving in a Straight Line at Constant Speed

8 Computation of the Impact Point of the AA Projectile on the Body of the Attacking Aerial Target

8.1 Geometry of the Attacking Aerial Target

8.2 Inertial Trajectory of the Attacking Aerial Target

8.3 Computation of the Impact Point of the AA Projectile on the Body of the Attacking Aerial Target

8.4 Vulnerability Model of the Attacking Aerial Target

8.5 Computational Results

9 Computation of the Probability that the AA Projectile Will Impact the Body of the Attacking Aerial Target

9.1 Stochastic Model of the Dispersion of the AA Projectiles Fired by the AA Gun

9.1.1 Remarks on Applications of Stochastic Optimal Control

9.2 Computation of the Probability that the AA Projectile Will Impact the Body of the Attacking Aerial Target, $P_{hitT,k}$

9.3 Computational Method NM1 for the Computation of $P_{hitT,k}$

9.4 Computational Method NM2 for the Computation of $P_{hitT,k}$

9.5 Probability of Destroying the AAT for the Case Where a Burst of AA Projectiles is Fired

9.6 Accumulative Probability of Destroying the AAT for the Case Where a Burst of AA Projectiles is Fired

9.7 Computational Results

9.8 Verification Method VMB for the Computation of the Probability $P_{hitT,k}$

9.8.1 Computational Results

Appendix A: Kinematics of Constrained Rigid Multibody Systems Subject to Velocity Constraints that May Not be Independent

Appendix B: Lagrange Equations for Constrained Rigid Multibody Systems Subject to Velocity Constraints that May Not be Independent

References

Index

Footnotes

- 1 However, no programs or software will be provided with this book.

1. Introduction

Constantinos Frangos¹ 

(1) Electrical Engineer working in Decision and Control, Pretoria,
South Africa

This Chapter presents a summary of Part 1 and Part 2 of the research monograph as follows.

1. Part 1: Kinematics, dynamics and nonlinear control of the mobile air defence system subject to holonomic and nonholonomic velocity constraints (Chaps. 2, 3, 4, 5 and Appendices A, B).
 2. Part 2: Performance evaluation of the mobile ADS against an attacking aerial target (Chaps. 6, 7, 8 and 9).
-

1.1 Part 1: Kinematics, Dynamics and Nonlinear Control of the Mobile Air Defence System Subject to Holonomic and Nonholonomic Velocity Constraints

The mathematical modelling of the mobile ADS is considered by using the Lagrange equations ([10, 81, 94, 107, 117, 125, 147, 167, 172, 179, 215]). Related applications dealing with the dynamic modelling and nonlinear control of front-wheel-drive and rear-wheel-drive vehicles are presented in [60–63].

In this work, the term holonomic velocity constraint is used to refer to a velocity constraint that can be integrated analytically with respect to time, to yield a geometric constraint. It follows that if a geometric constraint is differentiated with respect to time then a holonomic velocity constraint is obtained. In addition, this work uses the term nonholonomic velocity constraint to refer to a velocity constraint that cannot be integrated analytically with respect to time. Thus, it is not possible to convert a nonholonomic velocity constraint to a geometric constraint ([23, 101, 129, 147]).

Many references use a more compact terminology as follows. Firstly, the term holonomic constraint is used to refer to a geometric constraint and to a holonomic velocity constraint. Secondly, any constraint that cannot be converted to a holonomic constraint is referred to as a nonholonomic constraint ([81, 147]).

The mobile ADS consists of $N = 11$ rigid bodies and is controlled by $m_c = 4$ applied torques. The vector of generalized co-ordinates \mathbf{q} consists of a total of $n = 15$ elements, $\mathbf{q} \in \mathbb{R}^n$, and the vector of generalized velocities $\mathbf{p} = d\mathbf{q}/dt$ consists of $n = 15$ elements, $\mathbf{p} \in \mathbb{R}^n$ (bold letters are used to denote vector and matrix quantities). In order to simplify the presentation it is assumed that the applied torques are implemented by electric motors. The following holds with regard to the applied torques.

Firstly, there is a steering system torque associated with the steering system rotation angle relative to the vehicle body, δ_v . If the steering system is rotated through an angle δ_v then the left and right front wheels are steered through angles δ_3 and δ_3 , respectively (Fig. 1.1).

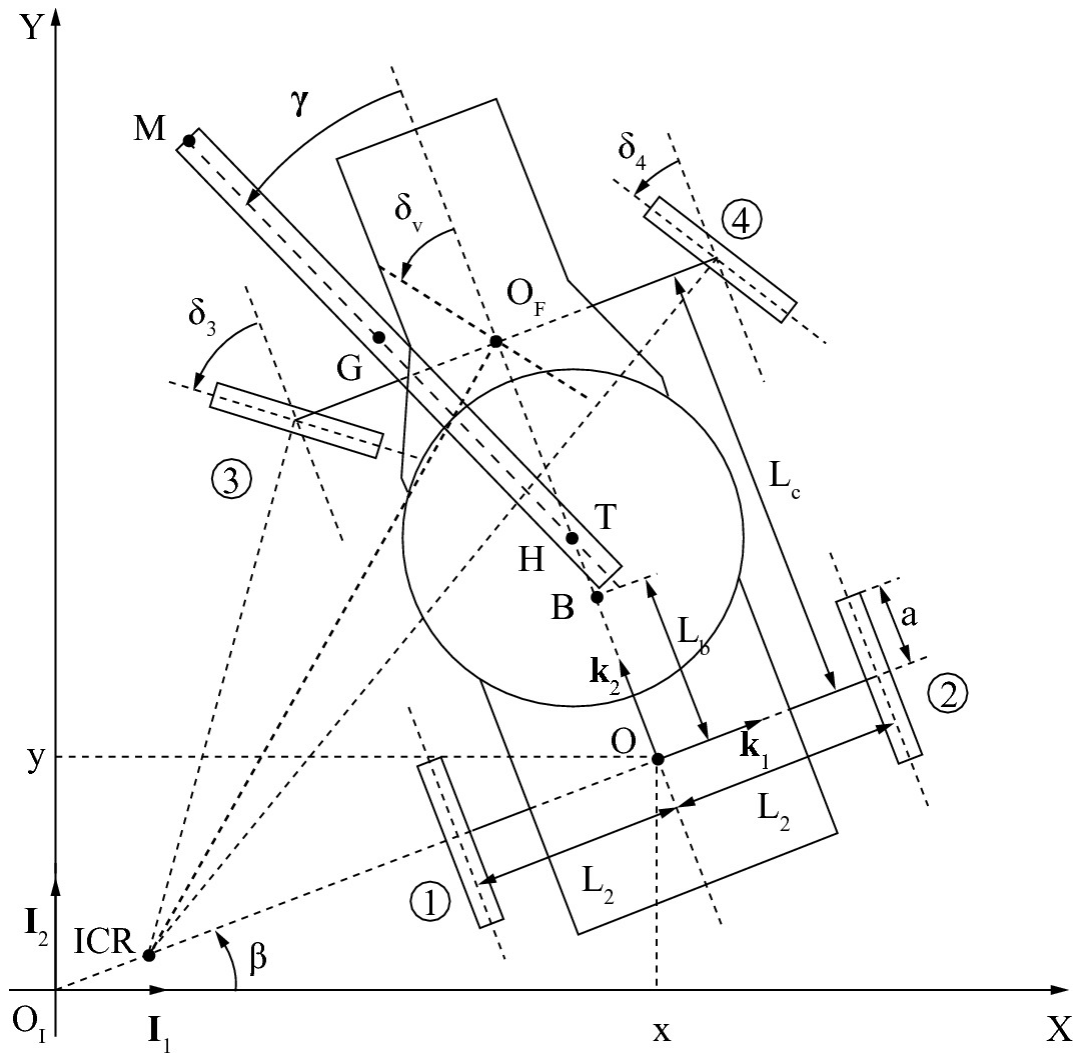


Fig. 1.1 Schematic of the mobile air defence system

Secondly, there is a drive system torque associated with the rotation angle of the drive system relative to the vehicle body, α_s . The drive system drives (or rotates) the rear wheels 1 and 2 via a differential gearbox and side shafts.

Thirdly, there is a torque associated with the rotation angle of the turret electric motor rotor in azimuth relative to the vehicle body, γ_0 .

The turret electric motor rotor drives a gearbox based mechanism that rotates the turret in azimuth relative to the vehicle body by an angle γ .

Fourthly, there is a torque associated with the rotation angle of the AA gun electric motor rotor in elevation relative to the turret, ζ_0 . The

AA gun electric motor rotor drives a gearbox based mechanism that rotates the AA gun in elevation relative to the turret by an angle ζ .

The operation of the front wheel steering system, the rear-wheel-drive system, the turret motor drive system and the AA gun motor drive system lead to holonomic velocity constraints. The assumption that all four wheels roll perfectly leads to nonholonomic velocity constraints ([23, 73, 129, 147]). Thus, the systems comprising the mobile ADS result in a total of $m = 13$ holonomic and nonholonomic velocity

constraints of which only $r_G = 11$ are independent. Thus,

$n_s = n - r_G = 4$ of the 15 generalized velocities can be selected to be

independent generalized velocities. In this case, the vector of independent generalized velocities is selected as follows $\mathbf{p}_s = [\dot{\delta}_v, \alpha_s,$

$\gamma, \dot{\zeta}]^T \in \mathbb{R}^4$. Hence, for the mobile ADS, the number of applied torques

is equal to the number of independent generalized velocities,

$$n_s = m_c = 4.$$

Let $(\delta_{v,ref}(t), \dot{\alpha}_{s,ref}(t), \gamma_{ref}(t), \zeta_{ref}(t))$, $t \geq 0$, denote reference trajectories for the steering system rotation angle $\delta_v(t)$, the drive system rotational velocity $\dot{\alpha}_s(t)$, the turret azimuth rotation angle $\gamma(t)$, and the AA gun elevation rotation angle $\zeta(t)$, respectively.

Let the vectors $\boldsymbol{\eta}_i(t)$ and $\boldsymbol{\eta}_{i,ref}(t)$, $t \geq 0$, $\boldsymbol{\eta}_{i,ref}(t)$, be defined as follows

$$\boldsymbol{\eta}_1(t) = \left[\delta_v(t), \frac{d\delta_v(t)}{dt}, \frac{d^2\delta_v(t)}{dt^2}, \frac{d\alpha_s(t)}{dt}, \frac{d^2\alpha_s(t)}{dt^2} \right]^\top,$$

$$\boldsymbol{\eta}_2(t) = \left[\gamma(t), \frac{d\gamma(t)}{dt}, \frac{d^2\gamma(t)}{dt^2}, \zeta(t), \frac{d\zeta(t)}{dt}, \frac{d^2\zeta(t)}{dt^2} \right]^\top,$$

$$\boldsymbol{\eta}_{1,ref}(t) = \left[\delta_{v,ref}(t), \frac{d\delta_{v,ref}(t)}{dt}, \frac{d^2\delta_{v,ref}(t)}{dt^2}, \frac{d\alpha_{s,ref}(t)}{dt}, \frac{d^2\alpha_{s,ref}(t)}{dt^2} \right]^\top,$$

$$\boldsymbol{\eta}_{2,ref}(t) = \left[\gamma_{ref}(t), \frac{d\gamma_{ref}(t)}{dt}, \frac{d^2\gamma_{ref}(t)}{dt^2}, \zeta_{ref}(t), \frac{d\zeta_{ref}(t)}{dt}, \frac{d^2\zeta_{ref}(t)}{dt^2} \right]^\top.$$

A nonlinear feedback control law is required for the four applied torques such that $\boldsymbol{\eta}_i(t)$, $t \geq 0$, $\boldsymbol{\eta}_{i,ref}(t)$, asymptotically tracks the reference trajectory $\boldsymbol{\eta}_{i,ref}(t)$, $t \geq 0$, $\boldsymbol{\eta}_{i,ref}(t)$, as follows

$$\begin{aligned} \lim_{t \rightarrow \infty} (\boldsymbol{\eta}_1(t) - \boldsymbol{\eta}_{1,ref}(t)) &= \mathbf{0}_{5 \times 1}, \\ \lim_{t \rightarrow \infty} (\boldsymbol{\eta}_2(t) - \boldsymbol{\eta}_{2,ref}(t)) &= \mathbf{0}_{6 \times 1}. \end{aligned} \tag{1.1}$$

The initial values $\boldsymbol{\eta}_1(0)$ and $\boldsymbol{\eta}_{1,ref}(0)$ may possibly not coincide with the initial reference values $\boldsymbol{\eta}_{1,ref}(0)$ and $\boldsymbol{\eta}_{1,ref}(0)$. In this case, the

nonlinear feedback control law should rotate the steering system, the drive system, the turret and the AA gun such that asymptotic tracking of the reference trajectories is achieved, (1.1). It is assumed throughout that the mobile ADS is moving forward at all times.

Most texts on classical mechanics formally derive the Lagrange equations for constrained rigid multibody systems, by assuming that the velocity constraints are independent ([10, 36, 81, 147, 172]). Thus, in order to directly apply the Lagrange equations to a system like the mobile ADS, not independent velocity constraints have to be converted to a set of independent velocity constraints. This approach is followed in [60, 61], for the case of a ground vehicle.

Each velocity constraint is associated with a different Lagrange multiplier. Furthermore, in some applications Lagrange multipliers correspond directly to constraint forces or to constraint torques and thus have units of force (N) or torque (Nm), respectively ([36, 85, 179]). However, as mentioned in [61], the particular interpretation of the Lagrange multipliers depends partly on the form and structure of the velocity constraints.

There are many multibody systems with a given physical configuration consisting of rigid bodies connected by various types of joints or links leading to velocity constraints that are not independent. References [158, 159, 176, 177], discuss the fact that dependent velocity constraints are common in practical applications. In such cases, removal of the redundant velocity constraints may imply a corresponding modification of the given physical configuration of the multibody system.

Thus, if the specified configuration of a multibody system leads to a set of velocity constraints that are not independent then the following should be considered.

1. If the redundant velocity constraints are directly deleted then this results in the removal of the associated Lagrange multipliers (Chaps. 3 and 4).
2. If a reduction procedure is applied (for example, transformation of the velocity constraints matrix to reduced row echelon form, Chap. 3) then the form and structure of the resulting independent velocity constraints may be different to the form and structure of the original not independent velocity constraints.
3. Deletion or reduction of the redundant velocity constraints may imply a corresponding modification of the given physical configuration of the multibody system.
4. Deletion or reduction of the redundant velocity constraints may limit the possibility of a direct correspondence between the Lagrange multipliers of the resulting system and the constraint forces and torques present in the original system subject to all the velocity constraints.

Based on the above it appears advantageous to consider all the velocity constraints together, preserving the original form and structure of the constraints (Chap. 3).

By using the d'Alembert-Lagrange principle, the Lagrange equations for constrained rigid multibody systems are extended for the case where the velocity constraints may not be independent (Appendices A, B and [62]). It is assumed that the rank of the velocity constraints matrix is constant for all motions of the system. It is shown that the following holds.

1. If the velocity constraints are independent then the vector of Lagrange multipliers is unique.
2. If the velocity constraints are not independent then the vector of Lagrange multipliers is not unique.
3. The vector of generalized constraint forces is equal to a unique vector of expressions.

In addition, a method is proposed to practically compute the vector of Lagrange multipliers using the Moore-Penrose generalized inverse (Appendix B, and [80, 125, 126]). The proposed method results in the vector of Lagrange multipliers that has minimum Euclidean norm and is applicable to cases of independent and not independent velocity constraints.

References [158, 159, 176, 177], consider the simulation of large-scale rigid multibody systems subject to dependent velocity constraints by using the Newton-Euler equations ([50, 155]). The afore-mentioned references follow an approach that is similar to the one used here and employ all the velocity constraints and the Moore-Penrose generalized inverse in order to compute the vector of Lagrange multipliers. The Moore-Penrose generalized inverse is also widely used in the control of constrained rigid multibody systems with redundant actuators and/or redundant sensors ([125, 215]).

Reference [145] considers the case of nonlinear nonholonomic velocity constraints that may not be independent by applying a general approach based on the Gauss principle and differential algebraic

equations (DAEs). The framework of DAEs does not seem to be directly applicable to the derivation of nonlinear feedback control laws for constrained rigid multibody systems ([154]). In addition, Ref. [145] considers computational examples involving mainly uncontrolled multibody systems subject to linear nonholonomic velocity constraints that are independent.

In summary, the following analyses and derivations regarding the kinematics, dynamics and nonlinear control of the mobile ADS are presented ([60–62]).

1. Basic description of the rigid bodies comprising the mobile ADS and the resulting holonomic and nonholonomic velocity constraints. In this case, the velocity constraints are not independent.
2. Derivation of the kinematic model of the mobile ADS by using all the velocity constraints. The kinematic model describes the vector of generalized velocities \mathbf{q} in terms of the vector of independent generalized velocities \mathbf{p}_s ([23, 73, 81, 147, 155, 174]).
3. Derivation of the basic dynamic model of the mobile ADS describing the vector of generalized accelerations $d\mathbf{p}/dt$ in terms of the vector of generalized applied forces \mathbf{Q}_A , $\mathbf{Q}_A \in \mathbb{R}^n$, and the vector of Lagrange multipliers $\boldsymbol{\lambda}$, $\boldsymbol{\lambda} \in \mathbb{R}^m$. The 4 nonzero elements of the vector of generalized applied forces \mathbf{Q}_A have units of torque (Nm) and correspond to the 4 applied torques.
4. Derivation of the reduced dynamic model of the mobile ADS describing the vector of independent generalized accelerations $d\mathbf{p}_s/dt$ in terms of the 4 applied torques. The reduced dynamic model does not include the vector of Lagrange multipliers $\boldsymbol{\lambda}$ ([23, 73, 81, 147, 155, 174]). Thus, the reduced dynamic model of the mobile ADS is used in

5. order to derive a nonlinear feedback control law by employing inverse dynamics transformations. In particular, the nonlinear feedback control law is derived for the applied torques such that the mobile ADS achieves the specified asymptotic tracking performance, (1.1) ([35, 99, 124, 153]). The closed loop nonlinear control system consists of the combination of the kinematic and reduced dynamic models of the mobile ADS and of the nonlinear feedback control law, and is referred to as the controlled dynamic model of the mobile ADS.
6. Analysis of the zero dynamics of the controlled dynamic model of the mobile ADS.
7. Methodology for the computation of the constrained motion of the controlled dynamic model of the mobile ADS satisfying all the holonomic and nonholonomic velocity constraints.
8. Methodology for the computation of the vector of generalized constraint forces Q_C , $Q_C \in \mathbb{R}^n$, by using the constrained motion of the controlled dynamic model of the mobile ADS.
9. Methodology for the computation of the vector of Lagrange multipliers λ by using the vector of generalized constraint forces Q_C and by computing the Moore-Penrose generalized inverse of the transpose of the velocity constraints matrix.

The Newton-Euler equations for constrained rigid multibody systems subject to velocity constraints that are independent are presented in [10, 81, 125, 215] (for computer implementations, extensions and applications see [3, 50, 117, 141, 150, 151, 154, 160, 162, 174, 181]).

In [63, 64], by using the d'Alembert principle ([81]), the Newton-Euler equations for constrained rigid multibody systems are extended for the case where the velocity constraints may not be independent ([158, 159, 176, 177]). By applying the Newton-Euler equations developed in [63, 64], the basic dynamic model of the mobile ADS is

derived, and is verified to be identical to the basic dynamic model obtained by using the Lagrange equations (Chap. 4).

The approach followed in this work is similar to the approach followed in [129] (see also [26, 45, 106, 107, 146]). Reference [129] considers the mathematical modelling of various types of vehicles and assumes in some cases perfect rolling of the wheels. The assumption of perfect rolling of the wheels leads to nonholonomic velocity constraints being imposed on the motion of the vehicle ([23]). In this case, the framework of Lagrangian mechanics generates the required generalized constraint forces in order to enforce the velocity constraints.

Alternative methods have been used in the modelling and control of various ground vehicles, see for example [25, 86, 87, 129, 185], and the references given there. Reference [25] presents the modelling and control of a four-wheel mobile robot with skid-steering. In this case, the wheels skid in order to maneuver the vehicle. In [86, 87], the modelling and control of a heavy truck is presented, and the wheels are allowed to slip during vehicle maneuvers. Thus, in [25, 86, 87], perfect rolling of the wheels is not assumed, and specific models are used in order to compute the forces at the point of contact of each wheel with the horizontal plane. Since perfect rolling of the wheels is not assumed, the corresponding nonholonomic velocity constraints are not applicable. Reference [185] presents a number of additional vehicle drive system configurations including tracked vehicles.

The control design procedure used in this work employs inverse dynamics transformations ([25, 35, 41, 99, 153, 154, 162, 167, 182]). The control design procedure has been used to develop nonlinear feedback control laws for ground vehicles ([60–64]), a rolling disk ([47, 58]), and an autonomous bicycle¹ ([213]). One advantage of this approach is that a nonlinear feedback control law is obtained for a complicated nonlinear dynamic model of the mobile ADS with vector of generalized co-ordinates in \mathbb{R}^{15} .

Alternative methods for the control of nonlinear systems are presented in [88, 99, 109, 130, 167]. Some of these methods are based on differential geometric techniques, and seem difficult to apply to nonlinear systems of high order. For additional references on nonlinear

control methods and applications see [28, 29, 31, 49, 53, 54, 103, 134, 170].

1.2 Part 2: Performance Evaluation of the Mobile Air Defence System Against an Attacking Aerial Target

The performance evaluation of the mobile ADS against a given AAT is considered (Chaps. 6, 7, 8 and 9).

Chapter 6 deals with the point mass flight dynamics model of the AA projectile ([8, 9, 24, 79, 115, 116, 122]) as follows.

1. The AA projectile is considered to be a point mass and the flight dynamics model describes the inertial motion of the point mass using a set of nonlinear differential equations ([79, 115]). The rotational motion of the actual AA projectile is not considered.
2. The differential equations of the point mass model together with the specified initial condition define an initial value problem. The final time of the initial value problem is determined by the impact of the AA projectile on the ground represented by the inertial (X, Y) plane ([44, 119]).
3. The AA gun fires a single projectile at a sequence of increasing aiming elevation angles and at a fixed aiming azimuth angle. It is assumed throughout that the mobile ADS remains completely stationary from the firing time until the time the projectile impacts the inertial (X, Y) plane. The case of zero wind velocity and the case of a given cross wind velocity are considered.
4. In all cases, the trajectory of the AA projectile is computed by solving numerically the initial value problem using a fourth order Runge-Kutta algorithm with a fixed time-step ([44]).

Chapter 7 presents the formulation and numerical solution of a conceptual fire control problem FCA as follows.

1. Fire control problem FCA involves the specification of a finite number of intercept times of the AA projectile with the CM of the

AAT, $t \geq 0$, $k = 1, 2, \dots, n_f$. The associated firing times $t \geq 0$, $k = 1, 2, \dots, n_f$, are obtained as shown below.

2. For each given intercept time $t \geq 0$ the following quantities are computed.
 - a. The inertial azimuth and elevation angles of the fire control (FC) vector, $\mathbf{a}_{FC}(t_{fire,k})$, $\mathbf{a}_{FC}(t_{fire,k})$. At time $t \geq 0$, the aiming azimuth and elevation angles of the AA gun are equal to $\mathbf{a}_{FC}(t_{fire,k})$ and $\mathbf{a}_{FC}(t_{fire,k})$, respectively.
 - b. The time of flight of the AA projectile to the CM of the AAT, $\Delta_{tofC,k}$.
 - c. It follows that the firing time of the AA projectile is $t_{fire,k} = t_{hitC,k} - \Delta_{tofC,k}$.
3. The fire control problem is also formulated using feasible control ([55, 56, 59, 210–212]).
4. A schematic of the deployment of the mobile ADS and the trajectory of the AAT is shown in Fig. 1.2. The defended location is at the origin O_I of the inertial co-ordinate system (X, Y, Z) . The computational results obtained for fire control problem FCA are applied directly in the performance evaluation of the mobile ADS against the AAT in Chaps. 8 and 9.

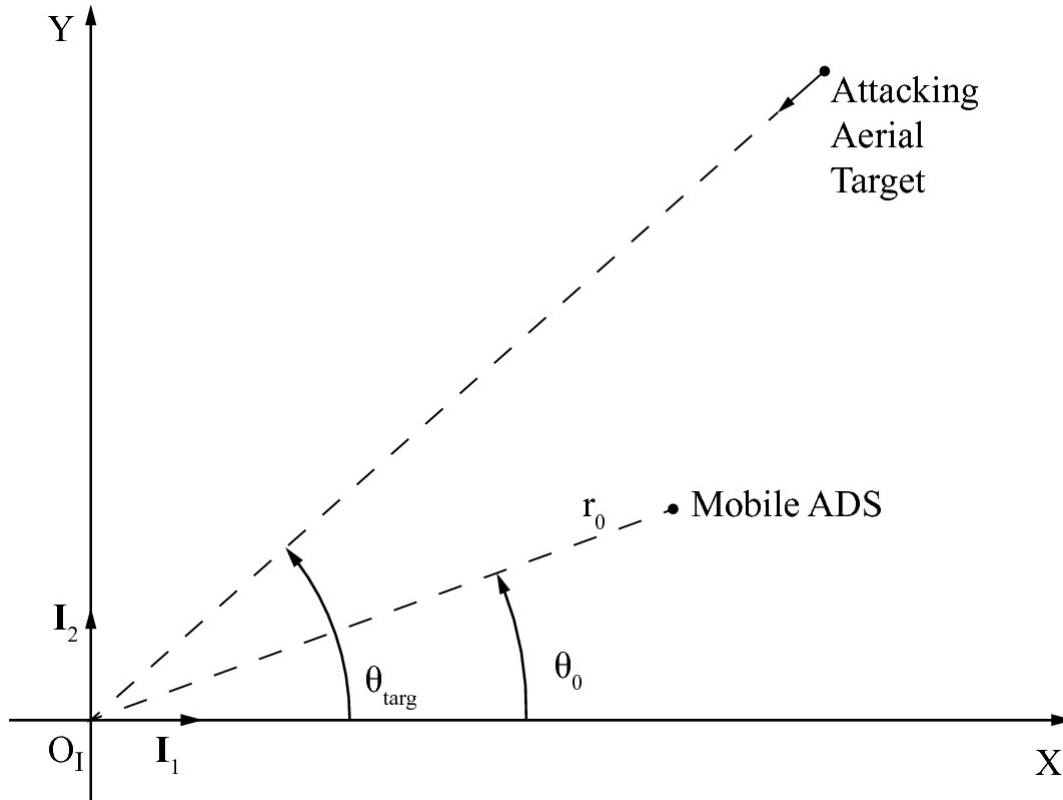


Fig. 1.2 Schematic of the deployment of the mobile ADS and the attacking aerial target; the defended location is at the origin O_1

Chapter 8 deals with the following.

1. The geometry of the three-dimensional body of the AAT is given in Fig. 1.3. A body reference frame B_{targ} is defined with origin fixed at the center of mass of the AAT.
2. A methodology is presented for computing the impact point of the AA projectile on the body of the AAT relative to the origin of the body reference frame B_{targ} and expressed in B_{targ} .

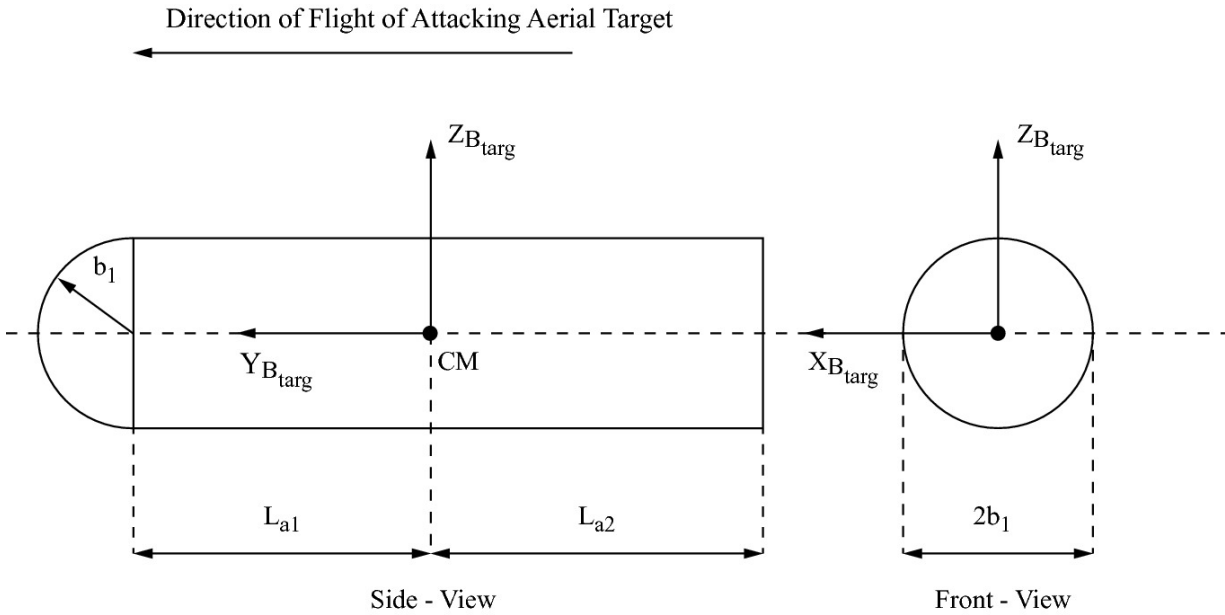


Fig. 1.3 Schematic of the attacking aerial target

Chapter 9 deals with the following.


1. The stochastic model describing the dispersion of the AA projectiles fired by the AA gun.
2. Computation of the probability that the AA projectile fired at time $t \geq 0$ will impact any point on the body of the AAT, $P_{hitT,k}$.
3. The vulnerability model of the AAT assumes that if one or more AA projectiles impact the body of the AAT then the AAT is destroyed. Thus, if one AA projectile is fired then the probability that the AAT will be destroyed is $P_{hitT,k}$.
4. Computation of the probability that a burst of N_p AA projectiles will destroy the AAT, and the accumulative probability that a burst of N_p AA projectiles will destroy the AAT.
5. A verification method is applied in order to verify the computational method used to obtain the probability $P_{hitT,k}$.

Subsequent Chapters refer to Figs. [1.1](#), [1.2](#) and [1.3](#). These Figures are repeated there for convenience and for ease of reference.

Footnotes

¹ “Life is like riding a bicycle. To keep your balance you must keep moving”— Albert Einstein, world famous physicist and winner of the 1921 Nobel Prize in Physics for his discovery of the law of the photoelectric effect, [48].

2. Overview of the Mobile Air Defence System

Constantinos Frangos¹ 

(1) Electrical Engineer working in Decision and Control, Pretoria, South Africa

This Chapter presents an overview of the mobile air defence system as follows.

1. The mobile ADS is a constrained rigid multibody system consisting of several connected rigid bodies (Fig. 2.1).
 2. A detailed description of each rigid body is given together with the associated holonomic and nonholonomic velocity constraints.
 3. A number of variables related mainly to the AA gun are defined.
-

2.1 Multibody System Representation of the Mobile Air Defence System

The mobile air defence system considered in this work is modelled as a constrained rigid multibody system (Fig. 2.1). It is assumed that the mobile ADS is controlled by $m_c = 4$ applied torques.

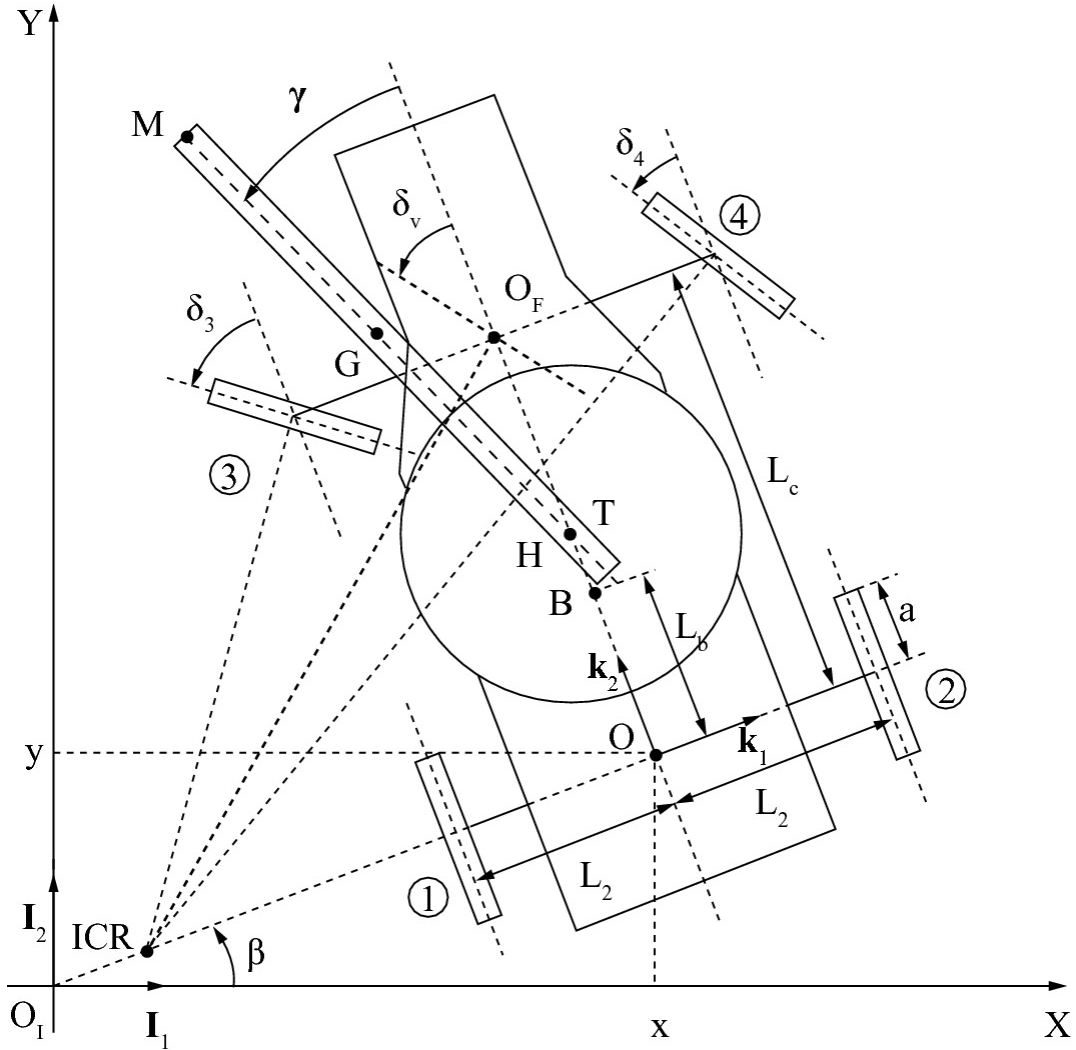


Fig. 2.1 Schematic of the mobile air defence system

First, there is a steering system torque T_{δ_v} that steers the front wheels via a steering system. Second, there is a drive system torque T_{α_s} that drives the rear wheels via a differential gearbox and sideshafts. Third, there is a torque T_{γ_0} that rotates the turret in azimuth via a gearbox based mechanism. Fourth, there is a torque T_{δ_v} that rotates the AA gun in elevation via a gearbox based mechanism.

In order to simplify the presentation it is assumed that the applied torques are implemented by 4 electric motors denoted by EM_{δ_v} , EM_{α_s}

, EM_{γ_0} and EM_{δ_v} , respectively. The electromagnetic transients of the electric motors are not taken into account. In particular, it is assumed that there is an ideal closed-loop controller for each of the 4 electric motors ensuring that each motor produces the specified reference torque value instantaneously, that is, T_{δ_v} , T_{α_s} , T_{γ_0} and T_{δ_v} , respectively.

The mobile ADS consists of a total of $N = 11$ rigid bodies,

$$N = 11. \quad (2.1)$$

The designation of each rigid body is indicated in subsequent Sections. All co-ordinate systems used in this work are right-handed Cartesian co-ordinate systems. It is assumed that there is an inertial reference frame I and an associated co-ordinate system (X, Y, Z) with unit vectors $(\mathbf{I}_1, \mathbf{I}_2, \mathbf{I}_3)$ and with origin fixed at point O_I , Fig. 2.1 (Appendix A).

Furthermore, for each rigid body i , there is a body reference frame B_i and an associated co-ordinate system $(X_{B_i}, Y_{B_i}, Z_{B_i})$ with unit vectors $(\mathbf{I}_{B_i}, \mathbf{J}_{B_i}, \mathbf{K}_{B_i})$ and with origin fixed at the center of mass of rigid body i , $(X_{B_i}, Y_{B_i}, Z_{B_i})$ ((A.3), Appendix A). Thus, body reference frame B_i translates and rotates together with rigid body i .

In order to simplify the dynamic model of the mobile ADS the following assumptions are made.

1. The centers of mass of the four wheels, the turret, the drive system, the steering system and the turret electric motor rotor are fixed relative to the origin of the body reference frame of the vehicle body.
2. The center of mass of the AA gun electric motor rotor is fixed relative to the origin of the body reference frame of the turret.

The following quantities and notations are relevant in the kinematic and dynamic modelling of the mobile ADS (Appendices A and B).

1. The unit vectors of body reference frame B_i expressed in the inertial reference frame I are denoted by $(\mathbf{I}_{B_i}^{(I)}, \mathbf{J}_{B_i}^{(I)}, \mathbf{K}_{B_i}^{(I)})$. The rotation matrix from the body reference frame B_i to the inertial reference frame I , \mathbf{R}_{B_i2I} , is defined in terms of the aforementioned unit vectors as follows

$$\mathbf{R}_{B_i2I} = [\mathbf{I}_{B_i}^{(I)} : \mathbf{J}_{B_i}^{(I)} : \mathbf{K}_{B_i}^{(I)}]. \quad (2.2)$$

2. The rotation axis sequence is $\mathcal{Z} \rightarrow \mathcal{X} \rightarrow \mathcal{Y}$. The associated Euler angles are denoted by α_s in azimuth, Θ_i in elevation, and Φ_i in roll and are provided for the case of the vehicle body, the turret and the AA gun, that is, for rigid bodies 5, 6, 7, respectively. It follows that

$$\mathbf{R}_Y(\Phi_i)\mathbf{R}_X(\Theta_i)\mathbf{R}_Z(\Psi_i) = \mathbf{R}_{I2B_i} = \mathbf{R}_{B_i2I}^\top, \quad i = 5, 6, 7. \quad (2.3)$$

3. All four wheels have equal radius denoted by a .
4. The angular velocity $\omega_{B_i r I}^{(B_i)}$ of the body reference frame B_i with respect to the inertial reference frame I and expressed in the body reference frame B_i is given by

$$\omega_{B_i r I}^{(B_i)} = [\omega_{B_i r I x}^{(B_i)}, \omega_{B_i r I y}^{(B_i)}, \omega_{B_i r I z}^{(B_i)}]^\top. \quad (2.4)$$

5. The inertial position $\mathbf{r}_i^{(I)}$ and the inertial velocity $\mathbf{v}_i^{(I)} = d_I \mathbf{r}_i^{(I)} / dt$ of the center of mass of rigid body i are given by

$$\mathbf{r}_i^{(I)} = [r_{ix}^{(I)}, r_{iy}^{(I)}, r_{iz}^{(I)}]^\top, \quad \mathbf{v}_i^{(I)} = [v_{ix}^{(I)}, v_{iy}^{(I)}, v_{iz}^{(I)}]^\top. \quad (2.5)$$

For each rigid body i , Θ_i denotes the mass $m_i > 0$ and $\mathcal{I}^{(B_i)}$

6. For each rigid body i , \mathcal{V}_i denotes the mass, $m_i > 0$, and $\mathcal{J}_i^{(C)}$

denotes the inertia matrix about the center of mass and expressed in the body reference frame B_i , $\mathcal{J}_i^{(B_i)} = (\mathcal{J}_i^{(B_i)})^\top$, $\det(\mathcal{J}_i^{(B_i)}) > 0$

(Appendix B).

7. The gravitational force acting at the center of mass of rigid body i and expressed in the inertial reference frame I is given by

$$\mathbf{F}_{grav,i}^{(I)} = -m_i g \mathbf{I}_3, \quad (2.6)$$

where g is the gravitational acceleration, $g = 9.81 \text{ m/s}^2$.

8. In the case of the mobile ADS, the resultant applied forces are all zero, $\mathbf{F}_{A,i}^{(I)} = \mathbf{0}_{3 \times 1}$, $(X_{B_i}, Y_{B_i}, Z_{B_i})$.

9. The resultant applied torque $\mathbf{T}_{A,i}^{(B_i)}$ acting about the center of mass of rigid body i and expressed in the body reference frame B_i is given by $\mathbf{T}_{A,i}^{(B_i)} = [T_{A,ix}^{(B_i)}, T_{A,iy}^{(B_i)}, T_{A,iz}^{(B_i)}]^\top$, and $\mathbf{T}_{A,i}^{(I)} = \mathbf{R}_{B_i I} \mathbf{T}_{A,i}^{(B_i)}$. The resultant applied torque $\mathbf{T}_{A,i}^{(B_i)}$ is expressed in terms of the applied torques T_{δ_v} , T_{α_s} , T_{γ_0} , T_{δ_v} , as appropriate.

10. The geometric and velocity constraints applicable to rigid body i . The time derivative of the geometric constraints together with the velocity constraints result in a set of holonomic and nonholonomic velocity constraints for the mobile ADS that are not independent.

11. The kinetic energy, \mathcal{E}_i , and potential energy, \mathcal{V}_i , of rigid body i are given by

$$\mathcal{E}_i = \frac{1}{2} m_i \dot{\mathbf{x}}_i^T \dot{\mathbf{x}}_i + \frac{1}{2} \dot{\boldsymbol{\theta}}_i^T \mathcal{J}_i^{(C)} \dot{\boldsymbol{\theta}}_i$$

$$\mathcal{E}_i = \frac{1}{2}m_i(\mathbf{v}_i^{(I)})^\top \mathbf{v}_i^{(I)} + \frac{1}{2}(\boldsymbol{\omega}_{B_i I}^{(B_i)})^\top \mathcal{J}_i^{(B_i)} \boldsymbol{\omega}_{B_i I}^{(B_i)}, \quad (2.7)$$

$$\mathcal{V}_i = m_i g r_{iz}^{(I)}. \quad (2.8)$$

12.

The notation \dot{n} and n denotes the first and second derivatives of x with respect to time t .

Hereafter, the details of each rigid body comprising the mobile ADS are presented.

2.2 Vehicle Body (Body 5)

The vehicle body is designated as *Body 5*. The body reference frame B_5 has an associated co-ordinate system $(X_{B_5}, Y_{B_5}, Z_{B_5})$ with unit vectors $(\mathbf{I}_{B_5}^{(I)}, \mathbf{J}_{B_5}^{(I)}, \mathbf{K}_{B_5}^{(I)})$ defined below, and with origin fixed at the center of mass of the vehicle body, that is, point B in Fig. 2.1. The relevant rotation matrix is given by

$$\mathbf{R}_{B_5 2I} = [\mathbf{I}_{B_5}^{(I)} \ : \ \mathbf{J}_{B_5}^{(I)} \ : \ \mathbf{K}_{B_5}^{(I)}]. \quad (2.9)$$

It is assumed that the vehicle body translates parallel to the inertial (X, Y) plane and rotates about the Z_{B_5} axis that is always parallel to the inertial Z axis. It follows that the (X_{B_5}, Y_{B_5}) plane is always parallel to the inertial (X, Y) plane. Various systems of the mobile ADS rotate with respect to the vehicle body. In some cases this involves rotation about an axis that is parallel to the Z_{B_5} axis.

Define \mathbf{k}_1 to be a unit vector along the line that passes through the centers of wheels 1 and 2 (Fig. 2.1) given by

$$(2.10)$$

$$\mathbf{k}_1 = \cos(\beta)\mathbf{I}_1 + \sin(\beta)\mathbf{I}_2.$$

Let \mathbf{k}_2 be a unit vector orthogonal to \mathbf{k}_1 given by

$$\mathbf{k}_2 = -\sin(\beta)\mathbf{I}_1 + \cos(\beta)\mathbf{I}_2. \quad (2.11)$$

The unit vectors of the body reference frame B_5 are given by

$$\mathbf{I}_{B_5}^{(I)} = \mathbf{k}_1, \quad \mathbf{J}_{B_5}^{(I)} = \mathbf{k}_2, \quad \mathbf{K}_{B_5}^{(I)} = \mathbf{I}_3. \quad (2.12)$$

The Euler angles of the vehicle body are obtained from (2.3), and are given by

$$\Psi_5 = \beta, \quad \Theta_5 = 0, \quad \Phi_5 = 0. \quad (2.13)$$

The angular velocity of the body reference frame B_5 with respect to the inertial reference frame I is given by

$$\omega_{B_5 r I}^{(B_5)} = \dot{\beta}\mathbf{K}_{B_5} = \dot{\beta}\mathbf{K}_{B_5}^{(I)} = \dot{\beta}\mathbf{I}_3. \quad (2.14)$$

Let $\mathbf{r}_i^{(I)}$ denote the inertial position of point O in the vehicle body

(Fig. 2.1), and $\mathbf{r}_{OA}^{(I)}$ the inertial position of the vertical projection of

point O onto the inertial (X, Y) plane, given by

$$\mathbf{r}_O^{(I)} = x\mathbf{I}_1 + y\mathbf{I}_2 + a\mathbf{I}_3, \quad (2.15)$$

$$\mathbf{r}_{OA}^{(I)} = x\mathbf{I}_1 + y\mathbf{I}_2. \quad (2.16)$$

Let $\mathbf{r}_i^{(I)}$ denote the inertial position of the center of mass of the vehicle

body (point B in Fig. 2.1) given by

$$\mathbf{r}_5^{(I)} = x\mathbf{I}_1 + y\mathbf{I}_2 + h_b\mathbf{I}_3 + L_b\mathbf{k}_2, \quad (2.17)$$

where p_s denotes the vertical distance of point B above the inertial (X, Y) plane, $h_b > a$, $L_b > 0$. By using (2.15), (2.16), (2.17), the inertial velocities $\mathbf{r}_j^{(I)}$, $j = O, OA, 5$, are obtained as follows

$$\mathbf{v}_j^{(I)} = \frac{d_I \mathbf{r}_j^{(I)}}{dt}, \quad j = O, OA, 5, \quad (2.18)$$

$$\Rightarrow \mathbf{v}_O^{(I)} = \begin{bmatrix} \dot{x} \\ \dot{y} \\ 0 \end{bmatrix}, \quad \mathbf{v}_{OA}^{(I)} = \begin{bmatrix} \dot{x} \\ \dot{y} \\ 0 \end{bmatrix}, \quad \mathbf{v}_5^{(I)} = \begin{bmatrix} \dot{x} - L_b \cos(\beta) \dot{\beta} \\ \dot{y} - L_b \sin(\beta) \dot{\beta} \\ 0 \end{bmatrix}. \quad (2.19)$$

The variables x , y and n are part of the generalized co-ordinates of the mobile ADS. The mass of the vehicle body m_5 is given by

$$m_5 = m_b. \quad (2.20)$$

It is assumed that the inertia matrix of the vehicle body, $\mathcal{J}_5^{(B5)}$, is given by ([10, 81])

$$\mathcal{J}_5^{(B5)} = \begin{bmatrix} J_{b1} & 0 & 0 \\ 0 & J_{b2} & -J_{b23} \\ 0 & -J_{b23} & J_{b3} \end{bmatrix}, \quad (2.21)$$

where J_{b1} , J_{b1} , J_{b23} , $m = 13$.

2.2.1 Electric Motors EM_{γ_0} , EM_{α_s} and EM_{δ_v}

The following assumptions are employed with regard to the electric motors EM_{γ_0} , EM_{α_s} and EM_{δ_v} .

1. The stators of the electric motors EM_{γ_0} , EM_{α_s} and EM_{δ_v} are rigidly mounted on the vehicle body, and thus form part of the

vehicle body.

2. The rotor of the drive system electric motor EM_{α_s} forms part of the drive system that extends outside of the electric motor. Thus, the resultant applied torque acting about the center of mass of the drive system (*Body 8*) is given by

$$\mathbf{T}_{A,8}^{(I)} = T_{\alpha_s} \mathbf{k}_2. \quad (2.22)$$

3. The rotor of the steering system electric motor EM_{δ_v} forms part of the steering system that extends outside of the electric motor. Thus, the resultant applied torque acting about the center of mass of the steering system (*Body 9*) is given by

$$\mathbf{T}_{A,9}^{(I)} = T_{\delta_v} \mathbf{I}_3. \quad (2.23)$$

4. The rotor of the turret electric motor EM_{γ_0} drives a gearbox based mechanism whose output rotates the turret relative to the vehicle body in azimuth. Thus, the resultant applied torque acting about the center of mass of the rotor of electric motor EM_{γ_0} (*Body 10*) is given by

$$\mathbf{T}_{A,10}^{(I)} = T_{\gamma_0} \mathbf{I}_3. \quad (2.24)$$

5. Newton's third law states that "for every action there is an equal and opposite reaction" ([10, 81]). It is assumed here that electric motors EM_{α_s} , EM_{δ_v} and EM_{γ_0} satisfy Newton's third law

(extended for the case of torques).

6. Thus, it follows from the above that there is a reaction torque $-T_{\alpha_s} \mathbf{k}_2$ acting on the stator of electric motor EM_{α_s} , a reaction torque $-T_{\delta_v} \mathbf{I}_3$ acting on the stator of electric motor EM_{δ_v} , and a reaction torque $-T_{\gamma_0} \mathbf{I}_3$ acting on the stator of electric motor EM_{γ_0}

(pp. 573–575, [42]).

7.

Furthermore, since the stators of the electric motors EM_{α_s} , EM_{δ_v} and EM_{γ_0} , form part of the vehicle body, it follows that the above-mentioned reaction torques sum to a resultant applied torque acting about the center of mass of the vehicle body (*Body 5*) given by ((2.12))

$$\mathbf{T}_{A,5}^{(I)} = -T_{\alpha_s} \mathbf{k}_2 - T_{\delta_v} \mathbf{I}_3 - T_{\gamma_0} \mathbf{I}_3, \quad \mathbf{T}_{A,5}^{(B_5)} = \mathbf{R}_{I_2 B_5} \mathbf{T}_{A,5}^{(I)}. \quad (2.25)$$

(For other applications involving electric motor reaction torques refer to Example 9.2, pp. 494–496, and Exercises 4, 6, 20, pp. 542–544, [10].)

2.3 Wheels 1, 2, 3 and 4 (Body 1 to Body 4)

The vehicle wheels 1, 2, 3 and 4 are designated as *Body 1*, *Body 2*, *Body 3* and *Body 4*, respectively (Fig. 2.1). The body reference frame of wheel i is B_i and has an associated co-ordinate system $(X_{B_i}, Y_{B_i}, Z_{B_i})$ with unit vectors $(\mathbf{I}_{B_i}^{(I)}, \mathbf{J}_{B_i}^{(I)}, \mathbf{K}_{B_i}^{(I)})$ defined below, and with origin fixed at the center of mass of wheel i , that is, at the center of wheel i , $i = 1, 2, 3, 4$.

The relevant rotation matrix of wheel i is given by

$$\mathbf{R}_{B_i 2I} = [\mathbf{I}_{B_i}^{(I)} \vdots \mathbf{J}_{B_i}^{(I)} \vdots \mathbf{K}_{B_i}^{(I)}], \quad i = 1, 2, 3, 4. \quad (2.26)$$

With regard to wheels 1 and 2, define the vectors

$$\begin{aligned} \mathbf{i}_i &= \cos(\alpha_i)(-\mathbf{I}_3) + \sin(\alpha_i)\mathbf{k}_2, \\ \mathbf{j}_i &= -\sin(\alpha_i)(-\mathbf{I}_3) + \cos(\alpha_i)\mathbf{k}_2, \quad i = 1, 2, \end{aligned} \quad (2.27)$$

where δ_v is the rotation angle of wheel i relative to the vehicle body and about an axis through the center of wheel i and parallel to \mathbf{k}_1 , $\boldsymbol{\eta}_{i,ref}(t)$, respectively (Fig. 2.1). Hence, $\boldsymbol{\gamma}$ and \mathbf{j}_i are always in the plane of wheel i , $\boldsymbol{\eta}_{i,ref}(t)$. The unit vectors of the body reference frame B_i of wheel i , $\boldsymbol{\eta}_{i,ref}(t)$, are given by

$$\mathbf{I}_{B_i}^{(I)} = \mathbf{i}_i, \quad \mathbf{J}_{B_i}^{(I)} = \mathbf{j}_i, \quad \mathbf{K}_{B_i}^{(I)} = \mathbf{k}_1, \quad i = 1, 2. \quad (2.28)$$

The angular velocity of the body reference frame B_i , $\boldsymbol{\eta}_{i,ref}(t)$, with respect to the inertial reference frame I is given by

$$\boldsymbol{\omega}_{B_i/I}^{(B_i)} = -\dot{\beta} \cos(\alpha_i) \mathbf{I}_{B_i} + \dot{\beta} \sin(\alpha_i) \mathbf{J}_{B_i} + \dot{\alpha}_i \mathbf{K}_{B_i}, \quad (2.29)$$

$$i = 1, 2,$$

$$\boldsymbol{\omega}_{B_i/I}^{(I)} = \dot{\alpha}_i \cos(\beta) \mathbf{I}_1 + \dot{\alpha}_i \sin(\beta) \mathbf{I}_2 + \dot{\beta} \mathbf{I}_3, \quad i = 1, 2. \quad (2.30)$$

With regard to wheels 3 and 4, define the vectors

$$\mathbf{i}_i = \cos(\alpha_i) (-\mathbf{I}_3) + \sin(\alpha_i) \mathbf{v}_i, \quad (2.31)$$

$$\mathbf{j}_i = -\sin(\alpha_i) (-\mathbf{I}_3) + \cos(\alpha_i) \mathbf{v}_i, \quad i = 3, 4,$$

$$\boldsymbol{\xi}_i = \cos(\beta + \delta_i) \mathbf{I}_1 + \sin(\beta + \delta_i) \mathbf{I}_2, \quad i = 3, 4, \quad (2.32)$$

where

$$\mathbf{v}_i = -\sin(\beta + \delta_i) \mathbf{I}_1 + \cos(\beta + \delta_i) \mathbf{I}_2, \quad i = 3, 4, \quad (2.33)$$

and where δ_v is the rotation angle of wheel i relative to the vehicle body and about an axis through the center of wheel i and parallel to m , and δ_i is the steering angle of wheel i relative to the vehicle body and about an axis through the center of wheel i and perpendicular to the

(X_{B_5}, Y_{B_5}) plane, $\boldsymbol{\eta}_{i,ref}(t)$, respectively (Fig. 2.1). Hence, $\boldsymbol{\gamma}$ and \boldsymbol{j}_i are always in the plane of wheel i , $\boldsymbol{\eta}_{i,ref}(t)$. The unit vectors of the body reference frame B_i of wheel i , $\boldsymbol{\eta}_{i,ref}(t)$, are given by

$$\boldsymbol{I}_{B_i}^{(I)} = \boldsymbol{i}_i, \quad \boldsymbol{J}_{B_i}^{(I)} = \boldsymbol{j}_i, \quad \boldsymbol{K}_{B_i}^{(I)} = \boldsymbol{\xi}_i, \quad i = 3, 4. \quad (2.34)$$

The angular velocity of the body reference frame B_i , $\boldsymbol{\eta}_{i,ref}(t)$, with respect to the inertial reference frame I is given by

$$\boldsymbol{\omega}_{B_i r I}^{(B_i)} = -(\dot{\beta} + \dot{\delta}_i) \cos(\alpha_i) \boldsymbol{I}_{B_i} + (\dot{\beta} + \dot{\delta}_i) \sin(\alpha_i) \boldsymbol{J}_{B_i} + \dot{\alpha}_i \boldsymbol{K}_{B_i}, \quad (2.35)$$

$$i = 3, 4,$$

$$\boldsymbol{\omega}_{B_i r I}^{(I)} = \dot{\alpha}_i \cos(\beta + \delta_i) \boldsymbol{I}_1 + \dot{\alpha}_i \sin(\beta + \delta_i) \boldsymbol{I}_2 + (\dot{\beta} + \dot{\delta}_i) \boldsymbol{I}_3, \quad (2.36)$$

$$i = 3, 4.$$

Let $\boldsymbol{r}_i^{(I)}$ denote the inertial position of the center of mass of wheel i , $i = 1, 2, 3, 4$, respectively, given by

$$\boldsymbol{r}_1^{(I)} = \boldsymbol{r}_O^{(I)} - L_2 \boldsymbol{k}_1, \quad \boldsymbol{r}_2^{(I)} = \boldsymbol{r}_O^{(I)} + L_2 \boldsymbol{k}_1, \quad (2.37)$$

$$\boldsymbol{r}_3^{(I)} = \boldsymbol{r}_O^{(I)} - L_2 \boldsymbol{k}_1 + L_c \boldsymbol{k}_2, \quad \boldsymbol{r}_4^{(I)} = \boldsymbol{r}_O^{(I)} + L_2 \boldsymbol{k}_1 + L_c \boldsymbol{k}_2, \quad (2.38)$$

where

$$\boldsymbol{r}_2^{(I)} - \boldsymbol{r}_1^{(I)} = L_1 \boldsymbol{k}_1, \quad \boldsymbol{r}_4^{(I)} - \boldsymbol{r}_3^{(I)} = L_1 \boldsymbol{k}_1, \quad L_2 = L_1/2,$$

and where L_1 denotes the length of the lines joining the centers of the front wheels, and the centers of the rear wheels, $L_b > 0$, $L_c > 0$.

Denote by $\boldsymbol{r}_i^{(I)}$ the inertial velocity of the center of mass of wheel i given

by

$$(2.39)$$

$$\mathbf{v}_i^{(I)} = \frac{d_I \mathbf{r}_i^{(I)}}{dt}, \quad i = 1, 2, 3, 4.$$

In this case, the variables $\alpha_1, \alpha_1, \alpha_1, \alpha_1, \delta_3$ and δ_3 are part of the generalized co-ordinates of the mobile ADS. Wheel i has a mass Θ_i given by

$$m_i = m_{wr}, \quad i = 1, 2, 3, 4. \quad (2.40)$$

It is assumed that the inertia matrix of wheel i , $\mathcal{J}_i^{(B_i)}$, is diagonal and is given by

$$\mathcal{J}_i^{(B_i)} = \text{diag} (I_{wr1}, I_{wr2}, I_{wr3}), \quad i = 1, 2, 3, 4, \quad (2.41)$$

where $I_{wr1} = I_{wr2}, I_{wr3} > 0$.

2.3.1 Velocity Constraints

It is assumed that each wheel rolls perfectly. This assumption leads to the following nonholonomic velocity constraints at the point of contact of wheel i with the (X, Y) plane ([58, 129]),

$$\mathbf{v}_i^{(I)} + \boldsymbol{\omega}_{B_i I}^{(I)} \times (-a \mathbf{I}_3) = \mathbf{0}_{3 \times 1}, \quad i = 1, 2, 3, 4, \quad (2.42)$$

where $\mathbf{0}_{3 \times 1}$ denotes the 3 by 1 matrix of zeros. Using (2.42), the following constraints are obtained for each wheel.

Wheel 1:

$$\dot{x} + L_2 \sin(\beta) \dot{\beta} - \dot{\alpha}_1 a \sin(\beta) = 0, \quad (2.43)$$

$$\dot{y} - L_2 \cos(\beta) \dot{\beta} + \dot{\alpha}_1 a \cos(\beta) = 0, \quad (2.44)$$

Wheel 2:

$$\dot{x} + L_2 \sin(\beta) \dot{\beta} - \dot{\alpha}_1 a \sin(\beta) = 0, \quad (2.45)$$

$$\dot{y} - L_2 \cos(\beta)\dot{\beta} + \dot{\alpha}_1 a \cos(\beta) = 0, \quad (2.46)$$

Wheel 3:

$$\dot{x} + (L_2 \sin(\beta) - L_c \cos(\beta))\dot{\beta} - a \sin(\beta + \delta_3)\dot{\alpha}_3 = 0, \quad (2.47)$$

$$\dot{y} - (L_2 \cos(\beta) + L_c \sin(\beta))\dot{\beta} + a \cos(\beta + \delta_3)\dot{\alpha}_3 = 0, \quad (2.48)$$

Wheel 4:

$$\dot{x} + (L_2 \sin(\beta) - L_c \cos(\beta))\dot{\beta} - a \sin(\beta + \delta_3)\dot{\alpha}_3 = 0, \quad (2.49)$$

$$\dot{y} - (L_2 \cos(\beta) + L_c \sin(\beta))\dot{\beta} + a \cos(\beta + \delta_3)\dot{\alpha}_3 = 0, \quad (2.50)$$

It is not difficult to show that the inertial velocity vector of the center of wheel i , $\mathbf{v}_i^{(I)} = \boldsymbol{\omega}_{B_i I}^{(I)} \times (a\mathbf{I}_3)$ ((2.42)), lies in the plane of wheel i ,

$i = 1, 2, 3, 4$, respectively.

During the motion of the vehicle, the virtual rectangle that consists of the four corners that coincide with the centers of the four wheels has constant shape and dimensions and moves in a fixed plane parallel to the (X, Y) plane. Thus, the inertial velocities of the four corners of the virtual rectangle are $\mathbf{r}_i^{(I)}$, $i = 1, 2, 3, 4$, respectively, (2.39).

It follows that the instantaneous center of rotation (ICR) of the above-mentioned virtual rectangle lies at the intersection of lines parallel to the (X, Y) plane, that pass through the centers of wheels 4, 3, 2 and 1, and that are perpendicular to the wheel center velocity vectors $\mathbf{r}_4^{(I)}$, $\mathbf{r}_3^{(I)}$, $\mathbf{r}_2^{(I)}$ and $\mathbf{r}_1^{(I)}$, respectively, [172] (Fig. 2.1). The steering

system steers the front wheels such that the above-mentioned relations with respect to the ICR are satisfied and is similar to an Ackermann steering system ([18]).

2.4 Turret (Body 6)

The turret is designated as *Body 6*. The body reference frame B_5 has an associated co-ordinate system $(X_{B_6}, Z_{B_5}, Z_{B_6})$ with unit vectors

$(\mathbf{I}_{B_5}^{(I)}, \mathbf{J}_{B_5}^{(I)}, \mathbf{K}_{B_5}^{(I)})$ defined below, and with origin fixed at the center of

mass of the turret, that is, point T in Fig. 2.1. The relevant rotation matrix is given by

$$\mathbf{R}_{B_5 2I} = [\mathbf{I}_{B_5}^{(I)} : \mathbf{J}_{B_5}^{(I)} : \mathbf{K}_{B_5}^{(I)}]. \quad (2.51)$$

The turret rotates relative to the vehicle body in azimuth via a revolute joint with a circular coupling between the two bodies. The axis of rotation of the turret is a line that passes through the center of the circular coupling and coincides with the Z_{B_5} axis. Thus, the center of mass T of the turret lies on the axis of rotation of the turret. In addition, the Z_{B_5} axis is always parallel to the Z_{B_5} axis of the vehicle body reference frame implying that the (X_{B_5}, Y_{B_5}) plane is always parallel to the (X_{B_5}, Y_{B_5}) plane.

Let γ denote the rotation angle of the turret relative to the vehicle body in azimuth (Fig. 2.1). The unit vectors of the body reference frame B_5 are given by

$$\mathbf{I}_{B_6}^{(I)} = \cos(\beta + \gamma)\mathbf{I}_1 + \sin(\beta + \gamma)\mathbf{I}_2, \quad (2.52)$$

$$\mathbf{J}_{B_6}^{(I)} = -\sin(\beta + \gamma)\mathbf{I}_1 + \cos(\beta + \gamma)\mathbf{I}_2, \quad (2.53)$$

$$\mathbf{K}_{B_6}^{(I)} = \mathbf{I}_3. \quad (2.54)$$

The Euler angles of the turret are obtained from (2.3) and are given by

$$\Psi_6 = (\beta + \gamma), \quad \Theta_6 = 0, \quad \Phi_6 = 0. \quad (2.55)$$

The angular velocity of the turret body reference frame B_5 with respect to the inertial reference frame I is given by

$$\boldsymbol{\omega}_{B_5 I}^{(B_5)} = (\dot{\beta} + \dot{\gamma}) \mathbf{K}_{B_5}. \quad (2.56)$$

Let $\mathbf{r}_i^{(I)}$ denote the inertial position of the center of mass of the turret (point T in Fig. 2.1) given by

$$\mathbf{r}_6^{(I)} = \mathbf{r}_5^{(I)} + \mathbf{R}_{B_5 I} \mathbf{h}_T, \quad \mathbf{h}_T = \mathbf{h}_T^{(B_5)} = [0, h_{Ty}, h_{Tz}]^\top, \quad (2.57)$$

where \mathbf{h}_T is a fixed vector in the body reference frame of the vehicle body B_5 . Let $\mathbf{v}_i^{(I)}$ denote the inertial velocity of the center of mass of the turret given by

$$\mathbf{v}_6^{(I)} = \frac{d_I \mathbf{r}_6^{(I)}}{dt}. \quad (2.58)$$

The variable γ is part of the generalized co-ordinates of the mobile ADS. The mass of the turret m_5 is given by

$$m_6 = m_T. \quad (2.59)$$

It is assumed that the inertia matrix of the turret, $\mathcal{J}_5^{(B_5)}$, is diagonal and is given by

$$\mathcal{J}_6^{(B_6)} = \text{diag}(J_{T1}, J_{T2}, J_{T3}), \quad (2.60)$$

where $Z_{B_5}, Z_{B_5}, J_{T3} > 0$.

2.4.1 Electric Motor EM_{δ_v}

By using the same approach as in Sect. 2.2.1, the following results are obtained with regard to the AA gun electric motor EM_{δ_v} .

1. The stator of the electric motor EM_{δ_v} is rigidly mounted on the turret and thus forms part of the turret.
2. The resultant applied torque acting about the center of mass of the rotor of electric motor EM_{δ_v} (*Body 11*) is given by

$$\mathbf{T}_{A,11}^{(I)} = T_{\zeta_0} \mathbf{I}_{B_{11}}^{(I)} = T_{\zeta_0} \mathbf{I}_{B_6}^{(I)} \quad (2.61)$$

$$(\mathbf{I}_{B_{11}}^{(I)} = \mathbf{I}_{B_6}^{(I)}, (2.52), (2.130)).$$

3. It is assumed that the electric motor EM_{δ_v} satisfies Newton's third law (extended for the case of torques).
4. Thus, it follows from the above that there is a reaction torque $-T_{\zeta_0} \mathbf{I}_{B_{11}}^{(I)}$ acting on the stator of electric motor EM_{δ_v} .
5. The above-mentioned reaction torque acts as a resultant applied torque about the center of mass of the turret (*Body 6*) given by ((2.52))

$$\mathbf{T}_{A,6}^{(I)} = -T_{\zeta_0} \mathbf{I}_{B_6}^{(I)}, \quad \mathbf{T}_{A,6}^{(B_6)} = \mathbf{R}_{I2B_6} \mathbf{T}_{A,6}^{(I)} = -T_{\zeta_0} \mathbf{I}_{B_6}. \quad (2.62)$$

2.5 Anti-Aircraft Gun (Body 7)

The AA gun is designated as *Body 7*. The body reference frame B_5 has an associated co-ordinate system $(X_{B_5}, Z_{B_5}, Z_{B_6})$ with unit vectors

$(\mathbf{I}_{B_5}^{(I)}, \mathbf{J}_{B_5}^{(I)}, \mathbf{K}_{B_5}^{(I)})$ defined below, and with origin fixed at the center of

mass of the AA gun, that is, point G in Fig. 2.1. The relevant rotation matrix is given by

$$(2.63)$$

$$\mathbf{R}_{B_7 2I} = [\mathbf{I}_{B_7}^{(I)} : \mathbf{J}_{B_7}^{(I)} : \mathbf{K}_{B_7}^{(I)}].$$

The AA gun is carried by a mechanical structure that is rigidly attached to the turret such that the following holds.

1. The AA gun rotates relative to the turret in elevation via a revolute joint and about an axis passing through point H (Fig. 2.1). The rotation axis is perpendicular to the longitudinal axis of the AA gun, and is parallel to the (X_{B_5}, Y_{B_5}) plane (and to the (X_{B_5}, Y_{B_5}) plane).
2. Point H lies on the axis of rotation of the turret, that is, the Z_{B_5} axis, and is vertically above point T , the center of mass of the turret. Point H is fixed in the body reference frames of the turret and of the vehicle body. In order to simplify the presentation point H is alternatively referred to as the hinge point H of the AA gun.
3. The AA gun rotates together with the turret relative to the vehicle body in azimuth.
4. Point M lies on the longitudinal axis and at the exit of the AA gun (Fig. 2.1). In order to simplify the presentation point M is alternatively referred to as the AA gun muzzle.

Let ζ denote the rotation angle of the AA gun relative to the turret in elevation. In this work only motions of the mobile ADS are considered such that ζ satisfies the following constraint

$$\zeta \in (-\pi/2, \pi/2). \quad (2.64)$$

The unit vectors of the body reference frame B_5 are given by

$$\mathbf{I}_{B_7}^{(I)} = \cos(\beta + \gamma)\mathbf{I}_1 + \sin(\beta + \gamma)\mathbf{I}_2, \quad (2.65)$$

$$\mathbf{J}_{B_7}^{(I)} = -\sin(\beta + \gamma)\cos(\zeta)\mathbf{I}_1 + \cos(\beta + \gamma)\cos(\zeta)\mathbf{I}_2 + \sin(\zeta)\mathbf{I}_3, \quad (2.66)$$

$$\begin{aligned} \mathbf{K}_{B_7}^{(I)} = & (\sin(\beta + \gamma) \sin(\zeta))\mathbf{I}_1 + (-\cos(\beta + \gamma) \sin(\zeta))\mathbf{I}_2 \\ & + \cos(\zeta)\mathbf{I}_3. \end{aligned} \quad (2.67)$$

The Euler angles of the AA gun are obtained from (2.3), and are given by

$$\Psi_7 = (\beta + \gamma), \quad \Theta_7 = \zeta, \quad \Phi_7 = 0. \quad (2.68)$$

The angular velocity of the body reference frame B_5 with respect to the inertial reference frame I is given by

$$\omega_{B_7rI}^{(B_7)} = \dot{\zeta}\mathbf{I}_{B_7} + (\dot{\beta} + \dot{\gamma}) \sin(\zeta)\mathbf{J}_{B_7} + (\dot{\beta} + \dot{\gamma}) \cos(\zeta)\mathbf{K}_{B_7}. \quad (2.69)$$

The distance from point H to point G is denoted by L_1 , and the distance from point H to point M is denoted by N_p (Fig. 2.1). Let $\mathbf{r}_i^{(I)}$ denote the inertial position of the center of mass of the AA gun (point G in Fig. 2.1) given by

$$\mathbf{r}_7^{(I)} = \mathbf{r}_5^{(I)} + \mathbf{R}_{B_52I}\mathbf{h}_T + \mathbf{R}_{B_62I}\mathbf{h}_m + \mathbf{R}_{B_72I}(L_g\mathbf{J}_{B_7}), \quad (2.70)$$

$$\mathbf{h}_m = \mathbf{h}_m^{(B_6)} = [0, 0, h_{mz}]^\top, \quad (2.71)$$

where \mathbf{h}_m is the vector from point T to point H , and is a fixed vector in the body reference frame of the turret B_5 . Let $\mathbf{r}_i^{(I)}$ denote the inertial

velocity of the center of mass of the AA gun given by

$$\mathbf{v}_7^{(I)} = \frac{d_I \mathbf{r}_7^{(I)}}{dt}. \quad (2.72)$$

For later reference, the inertial position, velocity and acceleration of the hinge point H of the AA gun are given by ((2.16), (2.19))

$$\mathbf{r}_H^{(I)} = \mathbf{r}_5^{(I)} + \mathbf{R}_{B_52I}\mathbf{h}_T + \mathbf{R}_{B_62I}\mathbf{h}_m, \quad (2.73)$$

$$\mathbf{r}_H^{(I)} = \begin{bmatrix} x - \sin(\beta)(L_b + h_{Ty}) \\ y + \cos(\beta)(L_b + h_{Ty}) \\ h_b + h_{Tz} + h_{mz} \end{bmatrix}, \quad (2.74)$$

$$\mathbf{r}_H^{(I)} = \mathbf{r}_{OA}^{(I)} + \begin{bmatrix} -\sin(\beta)(L_b + h_{Ty}) \\ \cos(\beta)(L_b + h_{Ty}) \\ h_b + h_{Tz} + h_{mz} \end{bmatrix}, \quad \mathbf{r}_{OA}^{(I)} = \begin{bmatrix} x \\ y \\ 0 \end{bmatrix}, \quad (2.75)$$

$$\mathbf{v}_H^{(I)} = \frac{d_I \mathbf{r}_H^{(I)}}{dt} = \begin{bmatrix} \dot{x} - \cos(\beta)\dot{\beta}(L_b + h_{Ty}) \\ \dot{y} - \sin(\beta)\dot{\beta}(L_b + h_{Ty}) \\ 0 \end{bmatrix}, \quad (2.76)$$

$$\mathbf{v}_H^{(I)} = \mathbf{v}_{OA}^{(I)} + \begin{bmatrix} -\cos(\beta)\dot{\beta}(L_b + h_{Ty}) \\ -\sin(\beta)\dot{\beta}(L_b + h_{Ty}) \\ 0 \end{bmatrix}, \quad \mathbf{v}_{OA}^{(I)} = \begin{bmatrix} \dot{x} \\ \dot{y} \\ 0 \end{bmatrix}, \quad (2.77)$$

$$\begin{aligned} \mathbf{a}_H^{(I)} &= \frac{d_I \mathbf{v}_H^{(I)}}{dt} \\ &= \begin{bmatrix} \ddot{x} + \sin(\beta)\dot{\beta}^2(L_b + h_{Ty}) - \cos(\beta)\ddot{\beta}(L_b + h_{Ty}) \\ \ddot{y} - \cos(\beta)\dot{\beta}^2(L_b + h_{Ty}) - \sin(\beta)\ddot{\beta}(L_b + h_{Ty}) \\ 0 \end{bmatrix}. \end{aligned} \quad (2.78)$$

The variable ζ is part of the generalized co-ordinates of the mobile ADS. The mass of the AA gun m_5 is given by

$$m_5 = m_b. \quad (2.79)$$

It is assumed that the inertia matrix of the AA gun, $\mathcal{J}_7^{(B7)}$, is diagonal

and is given by

$$(2.80)$$

$$\mathcal{J}_7^{(B_7)} = \text{diag} (J_{g1}, J_{g2}, J_{g3}),$$

where $J_{b1}, J_{b1}, m = 13$.

2.6 Drive System and Differential Gearbox (Body 8)

The drive system is designated as *Body 8*. The body reference frame B_5 has an associated co-ordinate system $(X_{B_6}, Z_{B_5}, Z_{B_6})$ with unit vectors $(\mathbf{I}_{B_5}^{(I)}, \mathbf{J}_{B_5}^{(I)}, \mathbf{K}_{B_5}^{(I)})$ defined below, and with origin fixed at the center of mass of the drive system. The relevant rotation matrix is given by

$$\mathbf{R}_{B_7 2I} = [\mathbf{I}_{B_7}^{(I)} : \mathbf{J}_{B_7}^{(I)} : \mathbf{K}_{B_7}^{(I)}]. \quad (2.81)$$

Let α_s denote the rotation angle of the drive system relative to the vehicle body and about an axis parallel to \mathbf{k}_1 (Fig. 2.1). The unit vectors of the body reference frame B_5 are given by

$$\mathbf{I}_{B_8}^{(I)} = \cos(\alpha_s)\mathbf{I}_3 + \sin(\alpha_s)\mathbf{k}_1, \quad (2.82)$$

$$\mathbf{J}_{B_8}^{(I)} = -\sin(\alpha_s)\mathbf{I}_3 + \cos(\alpha_s)\mathbf{k}_1, \quad (2.83)$$

$$\mathbf{K}_{B_8}^{(I)} = \mathbf{k}_2. \quad (2.84)$$

The angular velocity of the body reference frame B_5 with respect to the inertial reference frame I is given by

$$\boldsymbol{\omega}_{B_8 r I}^{(B_8)} = \dot{\beta} \cos(\alpha_s)\mathbf{I}_{B_8} - \dot{\beta} \sin(\alpha_s)\mathbf{J}_{B_8} + \dot{\alpha}_s \mathbf{K}_{B_8}. \quad (2.85)$$

Let $\mathbf{r}_i^{(I)}$ denote the inertial position of the center of mass of the drive system given by

$$\mathbf{r}_8^{(I)} = x\mathbf{I}_1 + y\mathbf{I}_2 + L_s\mathbf{k}_2 + h_s\mathbf{I}_3, \quad (2.86)$$

where δ_3 denotes the vertical distance of the center of mass above the inertial (X, Y) plane, $h_s > a$, $L_c > 0$. Let $\mathbf{r}_i^{(I)}$ denote the inertial velocity of the center of mass of the drive system given by

$$\mathbf{v}_6^{(I)} = \frac{d_I \mathbf{r}_6^{(I)}}{dt}. \quad (2.87)$$

The variable α_s is part of the generalized co-ordinates of the mobile ADS. The equivalent mass of the drive system is given by

$$m_8 = m_s. \quad (2.88)$$

It is assumed that the inertia matrix of the drive system, $\mathcal{J}_7^{(B_7)}$, is diagonal and is given by

$$\mathcal{J}_8^{(B_8)} = \text{diag}(J_{s1}, J_{s2}, J_{s3}), \quad (2.89)$$

where $J_{s1} = J_{s2}$, $J_{s3} > 0$.

With reference to Sect. 2.2.1, the electric motor EM_{α_s} exerts a torque $T_{\alpha_s}\mathbf{k}_2$ about the center of mass of the drive system. Thus, the resultant applied torque is given by

$$\mathbf{T}_{A,8}^{(I)} = T_{\alpha_s}\mathbf{k}_2, \quad \mathbf{T}_{A,8}^{(B_8)} = T_{\alpha_s}\mathbf{K}_{B_8}. \quad (2.90)$$

2.6.1 Velocity Constraint

The simplified kinematic model of the differential gearbox introduces the following velocity constraint (p. 294, [95]),

$$\dot{\alpha}_1 + \dot{\alpha}_2 - k_d \dot{\alpha}_s = 0, \quad (2.91)$$

where $k_d = 2k_0$, and k_0 denotes the gear ratio of the differential gearbox, $k_0 \neq 0$. In this case $k_0 \neq 0$, implying that

$$k_d = 2. \quad (2.92)$$

2.7 Steering System (Body 9)

A steering system implementing the basic relations of the Ackermann steering system ([18]) is considered. In order to simplify the kinematic and dynamic models of the mobile ADS, the steering system is modelled as a lumped mass and designated as *Body 9*. The body reference frame B_5 has an associated co-ordinate system $(X_{B_6}, Z_{B_5}, Z_{B_6})$ with unit vectors $(\mathbf{I}_{B_5}^{(I)}, \mathbf{J}_{B_5}^{(I)}, \mathbf{K}_{B_5}^{(I)})$ defined below, and with origin fixed at the

center of mass of the steering system. The relevant rotation matrix is given by

$$\mathbf{R}_{B_7 2I} = [\mathbf{I}_{B_7}^{(I)} : \mathbf{J}_{B_7}^{(I)} : \mathbf{K}_{B_7}^{(I)}]. \quad (2.93)$$

Let δ_v denote the rotation angle of the steering system relative to the vehicle body and about the Z_{B_5} axis that is always parallel to the Z_{B_5} axis of the vehicle body reference frame. It is assumed that if the steering system is turned through an angle δ_v then an upright virtual wheel with center located at point T_{δ_v} is steered through an angle δ_v while at the same time wheel 3 is steered through an angle δ_3 and wheel 4 is steered through an angle δ_3 (the line of symmetry of the virtual wheel is shown in Fig. 2.1). The virtual wheel has radius a and is assumed to roll perfectly on the (X, Y) plane.

The unit vectors of the body reference frame B_5 are given by

$$\mathbf{I}_{B_9}^{(I)} = \cos(\beta + \delta_v)\mathbf{I}_1 + \sin(\beta + \delta_v)\mathbf{I}_2, \quad (2.94)$$

$$\mathbf{J}_{B_9}^{(I)} = -\sin(\beta + \delta_v)\mathbf{I}_1 + \cos(\beta + \delta_v)\mathbf{I}_2, \quad (2.95)$$

$$\mathbf{K}_{B_9}^{(I)} = \mathbf{I}_3. \quad (2.96)$$

The angular velocity of the body reference frame B_5 with respect to the inertial reference frame I is given by

$$\boldsymbol{\omega}_{B_9 I}^{(B_9)} = (\dot{\beta} + \dot{\delta}_v)\mathbf{K}_{B_9}. \quad (2.97)$$

Let $\mathbf{r}_i^{(I)}$ denote the inertial position of the center of mass of the steering system given by

$$\mathbf{r}_9^{(I)} = x\mathbf{I}_1 + y\mathbf{I}_2 + L_v\mathbf{k}_2 + h_v\mathbf{I}_3, \quad (2.98)$$

where δ_3 denotes the vertical distance of the center of mass above the inertial (X, Y) plane, $h_s > a$, $L_c > 0$. Let $\mathbf{r}_i^{(I)}$ denote the inertial velocity of the center of mass of the steering system given by

$$\mathbf{v}_6^{(I)} = \frac{d_I \mathbf{r}_6^{(I)}}{dt}. \quad (2.99)$$

The variable δ_v is part of the generalized co-ordinates of the mobile ADS. The equivalent mass of the steering system is given by

$$m_8 = m_s. \quad (2.100)$$

It is assumed that the inertia matrix of the steering system, $\mathcal{J}_9^{(B_9)}$, is

diagonal and is given by

$$\mathcal{J}_9^{(B_9)} = \text{diag}(J_{v1}, J_{v2}, J_{v3}), \quad (2.101)$$

where $J_{v1} = J_{v2}$, $J_{s3} > 0$.

With reference to Sect. 2.2.1, the electric motor EM_{δ_v} exerts a torque $T_{\delta_v} \mathbf{I}_3$ about the center of mass of the steering system. Thus, the resultant applied torque is given by

$$\mathbf{T}_{A,9}^{(I)} = T_{\delta_v} \mathbf{I}_3, \quad \mathbf{T}_{A,9}^{(B_9)} = T_{\delta_v} \mathbf{K}_{B_9}. \quad (2.102)$$

2.7.1 Geometric Constraints

Let $\mathbf{r}_i^{(I)}$ denote the inertial velocity of the center of the virtual wheel,

that is, point T_{δ_v} . Then, the line parallel to the (X, Y) plane, passing through the point T_{δ_v} and perpendicular to the velocity vector $\mathbf{r}_i^{(I)}$,

passes through the ICR (Fig. 2.1).

It follows from the above and Fig. 2.1 that the vehicle steering system results in the following nonlinear geometric constraints between δ_3 and δ_v , and between δ_4 and δ_v ,

$$\delta_3 = \arctan2(L_c \sin(\delta_v), -L_2 \sin(\delta_v) + L_c \cos(\delta_v)), \quad (2.103)$$

$$\delta_4 = \arctan2(L_c \sin(\delta_v), L_2 \sin(\delta_v) + L_c \cos(\delta_v)), \quad (2.104)$$

subject to

$$-L_2 \sin(\delta_v) + L_c \cos(\delta_v) > 0, \quad \delta_3 \in \left(-\frac{\pi}{2}, \frac{\pi}{2}\right), \quad (2.105)$$

$$L_2 \sin(\delta_v) + L_c \cos(\delta_v) > 0, \quad \delta_4 \in \left(-\frac{\pi}{2}, \frac{\pi}{2}\right), \quad (2.106)$$

where

$$\arctan2(y_1, x_1) = \arg(x_1 + j_c y_1) \in (-\pi, \pi], \quad (2.107)$$

denotes the four-quadrant arctangent function, $\arg(x_1 + j_c y_1)$ denotes the principal argument of $(x_1 + j_c y_1)$, $B_i, y_1 \in \mathbb{R}$, $j_c = \sqrt{-1}$, and in this case $h_b > a$, (2.103)–(2.106) ($[1, 4]$). From (2.105), (2.106), it follows that

$$\arctan2(-L_c, L_2) < \delta_v < \arctan2(L_c, L_2), \quad \delta_v \in \left(-\frac{\pi}{2}, \frac{\pi}{2}\right). \quad (2.108)$$

Henceforward, only vehicle motions for which (2.105), (2.106), (2.108), are satisfied will be considered. Using (2.108), (2.103), (2.104), the limits of the front wheel steering angles δ_3 and δ_3 are as follows

$$\arctan2\left(\frac{-L_c^2}{\sqrt{L_c^2 + L_2^2}}, \frac{2L_c L_2}{\sqrt{L_c^2 + L_2^2}}\right) < \delta_3 < \frac{\pi}{2}, \quad (2.109)$$

$$-\frac{\pi}{2} < \delta_4 < \arctan2\left(\frac{L_c^2}{\sqrt{L_c^2 + L_2^2}}, \frac{2L_c L_2}{\sqrt{L_c^2 + L_2^2}}\right). \quad (2.110)$$

In Chap. 4, a methodology is presented for computing the constrained motion of the controlled dynamic model of the mobile ADS. In particular, (2.103)–(2.104) are used to accurately compute the steering angles δ_3 , δ_3 , as functions of time given the computed steering system turning angle δ_v as a function of time. Thus, the geometric constraints (2.103)–(2.104) are not used to eliminate the variables δ_3 , δ_3 , from the generalized co-ordinates. In this instance, the result is that some of the entries of the mass matrix \mathbf{M} of the basic dynamic model of the mobile ADS are relatively simple (Chap. 4).

In [60, 61], a vehicle is considered with a simpler front wheel steering system model. The associated nonlinear geometric constraint

relates δ_3 to δ_v and is similar in form to (2.103). In this case, the geometric constraint is used to eliminate δ_3 from the vehicle generalized co-ordinates. The result is that some of the entries of the mass matrix M in the corresponding basic dynamic model of the vehicle, are more complicated ([60, 61]).

By using (2.108), the lower and upper limits for δ_v are given by

$$\delta_{v,min} = \arctan2(-L_c, L_2), \quad \delta_{v,max} = \arctan2(L_c, L_2). \quad (2.111)$$

The following relations are obtained from (2.103)–(2.106),

$$\begin{aligned} \sin(\delta_3) &= \frac{L_c \sin(\delta_v)}{A_3}, & \cos(\delta_3) &= \frac{-L_2 \sin(\delta_v) + L_c \cos(\delta_v)}{A_3}, \\ \sin(\delta_4) &= \frac{L_c \sin(\delta_v)}{A_4}, & \cos(\delta_4) &= \frac{L_2 \sin(\delta_v) + L_c \cos(\delta_v)}{A_4}, \end{aligned} \quad (2.112)$$

where

$$\begin{aligned} A_3 &= \sqrt{(L_c \sin(\delta_v))^2 + (-L_2 \sin(\delta_v) + L_c \cos(\delta_v))^2}, \\ A_4 &= \sqrt{(L_c \sin(\delta_v))^2 + (L_2 \sin(\delta_v) + L_c \cos(\delta_v))^2}. \end{aligned} \quad (2.113)$$

Since the system motion is assumed to satisfy the constraints (2.105), (2.106), it follows from (2.113) that the following strict inequalities hold,

$$A_3 > 0, \quad A_4 > 0, \quad (2.114)$$

for all δ_v that satisfy (2.105), (2.106). By using (2.103)–(2.108), and assuming that the mobile ADS is moving forward (Fig. 2.1), the following holds.

1. If the steering system turning angle $\Delta_{tofC,k}$ then $\delta_3 = 0$, $\delta_4 = 0$, implying that the mobile ADS moves in a straight line.
2. If the steering system turning angle $\Delta_{tofC,k}$ then $\delta_3 > \delta_v > \delta_4 > 0$,

implying that the mobile ADS turns to the left.

3. If the steering system turning angle $\Delta_{tofC,k}$ then $\delta_3 > \delta_v > \delta_4 > 0$, implying that the mobile ADS turns to the right.

2.7.2 Velocity Constraints

By differentiating the geometric constraints (2.103), (2.104), with respect to time, the following two velocity constraints are obtained

$$\dot{\delta}_3 - \frac{L_c^2 \dot{\delta}_v}{A_3^2} = 0, \quad (2.115)$$

$$\dot{\delta}_4 - \frac{L_c^2 \dot{\delta}_v}{A_4^2} = 0, \quad (2.116)$$

where B_3, B_4 , are given by (2.113).

2.8 Rotor of the Turret Electric Motor EM_{γ_0}

(Body 10)

The rotor of the turret electric motor EM_{γ_0} is designated as *Body 10*.

The body reference frame B_{10} has an associated co-ordinate system

$(X_{B_{10}}, Y_{B_{10}}, Z_{B_{10}})$ with unit vectors $(\mathbf{I}_{B_{10}}^{(I)}, \mathbf{J}_{B_{10}}^{(I)}, \mathbf{K}_{B_{10}}^{(I)})$ defined below,

and with origin fixed at the center of mass of the rotor. The relevant rotation matrix is given by

$$\mathbf{R}_{B_{10}2I} = [\mathbf{I}_{B_{10}}^{(I)} \ ; \ \mathbf{J}_{B_{10}}^{(I)} \ ; \ \mathbf{K}_{B_{10}}^{(I)}]. \quad (2.117)$$

Let γ_0 denote the rotation angle of the rotor relative to the vehicle body in azimuth and about the $Y_{B_{10}}$ axis that is always parallel to the Z_{B_5}

axis of the vehicle body reference frame. The unit vectors of the body reference frame B_{10} are given by

$$\mathbf{I}_{B_{10}}^{(I)} = \cos(\beta + \gamma_0)\mathbf{I}_1 + \sin(\beta + \gamma_0)\mathbf{I}_2, \quad (2.118)$$

$$\mathbf{J}_{B_{10}}^{(I)} = -\sin(\beta + \gamma_0)\mathbf{I}_1 + \cos(\beta + \gamma_0)\mathbf{I}_2, \quad (2.119)$$

$$\mathbf{K}_{B_{10}}^{(I)} = \mathbf{I}_3. \quad (2.120)$$

The angular velocity of the body reference frame B_{10} with respect to the inertial reference frame I is given by

$$\boldsymbol{\omega}_{B_{10}rI}^{(B_{10})} = (\dot{\beta} + \dot{\gamma}_0)\mathbf{K}_{B_{10}}. \quad (2.121)$$

Let $\mathbf{r}_i^{(I)}$ denote the inertial position of the center of mass of the rotor given by

$$\mathbf{r}_{10}^{(I)} = \mathbf{r}_5^{(I)} + \mathbf{R}_{B_5 2I} \mathbf{h}_{mp}, \quad \mathbf{h}_{mp} = \mathbf{h}_{mp}^{(B_5)} = [h_{mpx}, h_{mpy}, h_{mpz}]^\top, \quad (2.122)$$

where \mathbf{h}_{mp} is the vector from the center of mass of the vehicle body to the center of mass of the rotor, and \mathbf{h}_{mp} is fixed in the body reference frame of the vehicle body B_5 . Let $\mathbf{r}_i^{(I)}$ denote the inertial velocity of the center of mass of the rotor given by

$$\mathbf{v}_6^{(I)} = \frac{d_I \mathbf{r}_6^{(I)}}{dt}. \quad (2.123)$$

The variable γ_0 is part of the generalized co-ordinates of the mobile ADS. The mass of the rotor $\zeta(t)$ is given by

$$m_{10} = m_{mp}. \quad (2.124)$$

It is assumed that the inertia matrix of the rotor, $\mathcal{J}_{10}^{(B_{10})}$, is diagonal and is given by

$$\mathcal{J}_{10}^{(B_{10})} = \text{diag} (J_{mp1}, J_{mp2}, J_{mp3}), \quad (2.125)$$

where $J_{mp1} = J_{mp2}, J_{mp3} > 0$.

With reference to Sect. 2.2.1, the turret electric motor EM_{γ_0} exerts a torque $T_{\gamma_0} \mathbf{I}_3$ about the center of mass of its rotor. Thus, the resultant applied torque is given by

$$\mathbf{T}_{A,10}^{(I)} = T_{\gamma_0} \mathbf{I}_3, \quad \mathbf{T}_{A,10}^{(B_{10})} = T_{\gamma_0} \mathbf{K}_{B_{10}}. \quad (2.126)$$

2.8.1 Velocity Constraint

The rotor of the turret electric motor EM_{γ_0} drives a gearbox based mechanism that rotates the turret relative to the vehicle body in azimuth. The above-mentioned gearbox based mechanism results in the following velocity constraint (pp. 286–287, [95])

$$\dot{\gamma}_0 = k_{mp} \dot{\gamma}, \quad (2.127)$$

where k_{mp} denotes the effective gear ratio, $k_{mp} > 1$. It is further assumed that the construction of the gearbox based mechanism is such that the following geometric constraint is obtained from (2.127),

$$\gamma_0(t) = k_{mp} \gamma(t) \quad \text{for all } t \geq 0. \quad (2.128)$$

2.9 Rotor of the AA Gun Electric Motor EM_{δ_v}

(Body 11)

The rotor of the AA gun electric motor EM_{δ_v} is designated as *Body 11*.

The body reference frame B_{10} has an associated co-ordinate system

$(X_{B_{10}}, Y_{B_{10}}, Z_{B_{10}})$ with unit vectors $(\mathbf{I}_{B_{10}}^{(I)}, \mathbf{J}_{B_{10}}^{(I)}, \mathbf{K}_{B_{10}}^{(I)})$ defined below,

and with origin fixed at the center of mass of the rotor. The relevant rotation matrix is given by

$$\mathbf{R}_{B_{10}2I} = [\mathbf{I}_{B_{10}}^{(I)} : \mathbf{J}_{B_{10}}^{(I)} : \mathbf{K}_{B_{10}}^{(I)}]. \quad (2.129)$$

Let ζ_0 denote the rotation angle of the rotor relative to the turret in elevation and about the $X_{B_{11}}$ axis that is always parallel to the X_{B_6} axis of the turret reference frame. The unit vectors of the body reference frame B_{10} are given by

$$\mathbf{I}_{B_{11}}^{(I)} = \cos(\beta + \gamma)\mathbf{I}_1 + \sin(\beta + \gamma)\mathbf{I}_2, \quad (2.130)$$

$$\begin{aligned} \mathbf{J}_{B_{11}}^{(I)} = & -\sin(\beta + \gamma)\cos(\zeta_0)\mathbf{I}_1 + \cos(\beta + \gamma)\cos(\zeta_0)\mathbf{I}_2 \\ & + \sin(\zeta_0)\mathbf{I}_3, \end{aligned} \quad (2.131)$$

$$\begin{aligned} \mathbf{K}_{B_{11}}^{(I)} = & (\sin(\beta + \gamma)\sin(\zeta_0))\mathbf{I}_1 + (-\cos(\beta + \gamma)\sin(\zeta_0))\mathbf{I}_2 \\ & + \cos(\zeta_0)\mathbf{I}_3. \end{aligned} \quad (2.132)$$

The angular velocity of the body reference frame B_{10} with respect to the inertial reference frame I is given by

$$\boldsymbol{\omega}_{B_{11}rI}^{(B_{11})} = \dot{\zeta}_0\mathbf{I}_{B_7} + (\dot{\beta} + \dot{\gamma})\sin(\zeta_0)\mathbf{J}_{B_7} + (\dot{\beta} + \dot{\gamma})\cos(\zeta_0)\mathbf{K}_{B_7}. \quad (2.133)$$

Let $\mathbf{r}_i^{(I)}$ denote the inertial position of the center of mass of the rotor

given by

$$\mathbf{r}_{11}^{(I)} = \mathbf{r}_5^{(I)} + \mathbf{R}_{B_52I}\mathbf{h}_T + \mathbf{R}_{B_62I}\mathbf{h}_{mg}, \quad \mathbf{h}_{mg} = \mathbf{h}_{mg}^{(B_6)} = [0, h_{mgy}, h_{mgz}]^\top, \quad (2.134)$$

where \mathbf{h}_{mg} is the vector from the center of mass of the turret to the center of mass of the rotor, and \mathbf{h}_{mg} is fixed in the body reference frame of the turret B_5 . Let $\mathbf{r}_i^{(I)}$ denote the inertial velocity of the center of mass of the rotor given by

$$\mathbf{v}_7^{(I)} = \frac{d_I \mathbf{r}_7^{(I)}}{dt}. \quad (2.135)$$

The variable ζ_0 is part of the generalized co-ordinates of the mobile ADS. The mass of the rotor $\zeta(t)$ is given by

$$m_{11} = m_{mg}. \quad (2.136)$$

It is assumed that the inertia matrix of the rotor, $\mathcal{J}_{11}^{(B_{11})}$, is diagonal and is given by

$$\mathcal{J}_{11}^{(B_{11})} = \text{diag} (J_{mg1}, J_{mg2}, J_{mg3}), \quad (2.137)$$

where $X_{B_{11}}$, $J_{mg2} = J_{mg3} > 0$.

With reference to Sect. 2.2.1, the AA gun electric motor EM_{δ_v} exerts a torque $T_{\zeta_0} \mathbf{I}_{B_6}^{(I)}$ about the center of mass of its rotor. Thus, the resultant applied torque is given by

$$\mathbf{T}_{A,11}^{(I)} = T_{\zeta_0} \mathbf{I}_{B_{11}}^{(I)}, \quad \mathbf{T}_{A,11}^{(B_{11})} = T_{\zeta_0} \mathbf{I}_{B_{11}} \quad (2.138)$$

2.9.1 Velocity Constraint

The rotor of the AA gun electric motor EM_{δ_v} drives a gearbox based mechanism that rotates the AA gun relative to the turret in elevation. The above-mentioned gearbox based mechanism results in the following velocity constraint (pp. 286–287, [95])

$$\dot{\zeta}_0 = k_{mg}\dot{\zeta}, \quad (2.139)$$

where T_{α_s} denotes the effective gear ratio, $k_{mg} > 1$. It is further assumed that the construction of the gearbox based mechanism is such that the following geometric constraint is obtained from (2.139),

$$\zeta_0(t) = k_{mg}\zeta(t) \quad \text{for all } t \geq 0. \quad (2.140)$$

2.10 Definition of Generalized Co-Ordinates \mathbf{q} and Generalized Velocities $\dot{\mathbf{q}}$

The vector of generalized co-ordinates \mathbf{q} and the vector of generalized velocities $\dot{\mathbf{q}}$ are given by

$$\mathbf{q} = [x, y, \beta, \alpha_1, \alpha_2, \alpha_4, \alpha_3, \delta_4, \delta_3, \delta_v, \alpha_s, \gamma, \zeta, \gamma_0, \zeta_0]^\top, \quad \dot{\mathbf{q}} = \frac{d\mathbf{q}}{dt}. \quad (2.141)$$

Thus, there are $n = 15$ generalized co-ordinates.

The geometric inequality constraints (2.105)–(2.106), (2.108), (2.64), define an admissible region or set, B_5 , for the generalized co-ordinates \mathbf{q} of the mobile ADS as follows (Chap. 3)

$$P_0 = \{\mathbf{q} \in \mathbb{R}^{15} : (2.105)–(2.106), (2.108), (2.64) \text{ are satisfied}\}. \quad (2.142)$$

Henceforward, only admissible motions of the mobile ADS that satisfy $\mathbf{q}(t) \in P_0$ for all $t \geq 0$ are considered. The velocity constraints on the motion of the mobile ADS are discussed further in Chap. 3.

2.11 Inertial Azimuth and Elevation Angles of a Vector

Consider an inertial vector \mathbf{b} specified as follows

$$\mathbf{b} = [b_x, b_y, b_z]^\top \quad \text{such that} \quad \sqrt{b_x^2 + b_y^2} > 0. \quad (2.143)$$

The magnitude or Euclidean norm of the vector \mathbf{b} is denoted by $\|\mathbf{b}\|$ and is given by

$$\|\mathbf{b}\| = \sqrt{b_x^2 + b_y^2 + b_z^2}. \quad (2.144)$$

The inertial azimuth and elevation angles of \mathbf{b} are denoted by \mathbf{a}_b and \mathbf{e}_b , respectively, and are defined as follows ((2.107))

$$\mathbf{a}_b = \arctan2(b_y, b_x) \in (-\pi, \pi], \quad (2.145)$$

$$\mathbf{e}_b = \arctan2(b_z, \sqrt{b_x^2 + b_y^2}) \in (-\pi/2, \pi/2). \quad (2.146)$$

Thus, the inertial vector \mathbf{b} is expressed in terms of \mathbf{a}_b and \mathbf{e}_b as follows

$$\mathbf{b} = \begin{bmatrix} b_x \\ b_y \\ b_z \end{bmatrix} = \|\mathbf{b}\| \begin{bmatrix} \cos(\mathbf{a}_b) \cos(\mathbf{e}_b) \\ \sin(\mathbf{a}_b) \cos(\mathbf{e}_b) \\ \sin(\mathbf{e}_b) \end{bmatrix}. \quad (2.147)$$

The term inertial is used in conjunction with \mathbf{a}_b , \mathbf{e}_b , in order to emphasize that \mathbf{a}_b , \mathbf{e}_b , are the azimuth and elevation angles of an inertial vector \mathbf{b} . In order to simplify the presentation, \mathbf{a}_b , \mathbf{e}_b , are also referred to as the azimuth and elevation angles of \mathbf{b} or as the inertial

angles of \mathbf{b} . The angles α_b, β_b , are related to the spherical co-ordinates of the vector \mathbf{b} ([81, 179]).

2.12 Line-of-Sight Vector from the Mobile ADS to the AAT

The line-of-sight (LOS) vector from the mobile ADS to the AAT, $\mathbf{r}_{los}^{(I)}$, is defined as the inertial vector from the hinge point H of the AA gun (Fig. 2.1) to the center of mass of the AAT and is given by

$$\mathbf{r}_{los}^{(I)} = \mathbf{r}_{targ}^{(I)} - \mathbf{r}_H^{(I)} = [r_{losx}^{(I)}, r_{losy}^{(I)}, r_{losz}^{(I)}]^\top, \quad (2.148)$$

and where it is assumed that

$$s_{los} = \sqrt{(r_{losx}^{(I)})^2 + (r_{losy}^{(I)})^2} > 0, \quad (2.149)$$

and $\mathbf{r}_{targ}^{(I)}$ is the inertial position of the center of mass of the AAT. Given

the following inertial trajectories of the AAT and of the hinge point H of the mobile ADS ((2.73)–(2.78))

$$\begin{aligned} & \mathbf{r}_{targ}^{(I)}(t), \quad \frac{d_I \mathbf{r}_{targ}^{(I)}(t)}{dt}, \quad \frac{d_I^2 \mathbf{r}_{targ}^{(I)}(t)}{dt^2}, \\ & \mathbf{r}_H^{(I)}(t), \quad \frac{d_I \mathbf{r}_H^{(I)}(t)}{dt}, \quad \frac{d_I^2 \mathbf{r}_H^{(I)}(t)}{dt^2}, \quad t \geq 0. \end{aligned} \quad (2.150)$$

Then, by using (2.148), the following LOS vector trajectories are computed

$$\mathbf{v}_{los}^{(I)} = \frac{d_I \mathbf{r}_{los}^{(I)}(t)}{dt} = \frac{d_I \mathbf{r}_{targ}^{(I)}(t)}{dt} - \frac{d_I \mathbf{r}_H^{(I)}(t)}{dt}, \quad t \geq 0, \quad (2.151)$$

$$(2.152)$$

$$\mathbf{a}_{los}^{(I)} = \frac{d_I^2 \mathbf{r}_{los}^{(I)}(t)}{dt^2} = \frac{d_I^2 \mathbf{r}_{targ}^{(I)}(t)}{dt^2} - \frac{d_I^2 \mathbf{r}_H^{(I)}(t)}{dt^2}, \quad t \geq 0.$$

The inertial angles of the LOS vector are given by ((2.145), (2.146), (2.148))

$$\mathbf{a}_{los} = \arctan2(r_{losy}^{(I)}, r_{losx}^{(I)}) \in (-\pi, \pi], \quad (2.153)$$

$$\mathbf{e}_{los} = \arctan2(r_{losz}^{(I)}, s_{los}) \in (-\pi/2, \pi/2). \quad (2.154)$$

Given a trajectory $\mathbf{r}_{los}^{(I)}(t)$, $t \geq 0$, and assume that a suitable scientific computing system is used to compute the term $\arctan2(r_{losy}^{(I)}, r_{losx}^{(I)})$ in (2.153), and thus the trajectory of the azimuth angle $\mathbf{a}_{los}(t)$, $t \geq 0$ (see command line help for the Maple function `arctan`, [16], and the MATLAB function `arctan2`, [110, 112]). If at any time t the trajectory of the actual azimuth angle of the LOS vector increases to a value just greater than γ or decreases to a value less than or equal to $-\pi$ then $\mathbf{a}_{los}(t)$, (2.153), jumps to $-\pi$ or to γ , respectively. The afore-mentioned wrapping of $\mathbf{a}_{los}(t)$, $\mathbf{a}_{los}(t)$, to the interval $k_{mg} > 1$ is not desirable. Smooth trajectories for the LOS inertial angles $\mathbf{a}_{los}(t)$, $\mathbf{a}_{los}(t)$, can be obtained by numerically integrating the LOS inertial angular rates $\dot{\mathbf{a}}_{los}(t)$, $\dot{\mathbf{a}}_{los}(t)$. The steps of the procedure are as follows.

First, compute the first and second time derivatives of $\mathbf{a}_{los}(t)$ and $\mathbf{a}_{los}(t)$, (2.153), (2.154), (2.149), as follows

$$(2.155)$$

$$\begin{aligned}\frac{d\mathbf{a}_{los}}{dt} &= \frac{\dot{r}_{losy}^{(I)}r_{losx}^{(I)} - r_{losy}^{(I)}\dot{r}_{losx}^{(I)}}{(r_{losx}^{(I)})^2 + (r_{losy}^{(I)})^2} \\ &= \frac{\dot{r}_{losy}^{(I)}r_{losx}^{(I)} - r_{losy}^{(I)}\dot{r}_{losx}^{(I)}}{s_{los}^2}, \\ \frac{d\mathbf{e}_{los}}{dt} &= \frac{\dot{r}_{losz}^{(I)}s_{los} - r_{losz}^{(I)}\dot{s}_{los}}{s_{los}^2 + (r_{losz}^{(I)})^2},\end{aligned}\quad (2.156)$$

$$\frac{d^2\mathbf{a}_{los}}{dt^2} = \frac{\ddot{r}_{losy}^{(I)}r_{losx}^{(I)} - r_{losy}^{(I)}\ddot{r}_{losx}^{(I)}}{s_{los}^2} - \frac{2\dot{s}_{los}(\dot{r}_{losy}^{(I)}r_{losx}^{(I)} - r_{losy}^{(I)}\dot{r}_{losx}^{(I)})}{s_{los}^3},\quad (2.157)$$

$$\begin{aligned}\frac{d^2\mathbf{e}_{los}}{dt^2} &= \frac{\ddot{r}_{losz}^{(I)}s_{los} - r_{losz}^{(I)}\ddot{s}_{los}}{s_{los}^2 + (r_{losz}^{(I)})^2} \\ &= \frac{(2s_{los}\dot{s}_{los} + 2r_{losz}^{(I)}\dot{r}_{losz}^{(I)})(\dot{r}_{losz}^{(I)}s_{los} - r_{losz}^{(I)}\dot{s}_{los})}{(s_{los}^2 + (r_{losz}^{(I)})^2)^2}.\end{aligned}\quad (2.158)$$

Second, compute the initial conditions $h_b > a$, $h_b > a$, by using (2.153)–(2.154).

Third, solve numerically the differential equations describing the motion of the mobile ADS and AAT, including (2.155), (2.156), for the inertial angles of the LOS vector $\mathbf{a}_{los}(t)$, $\mathbf{a}_{los}(t)$, by employing, for example, a fourth order Runge-Kutta algorithm with a fixed time-step. Thus, $\mathbf{a}_{los}(t)$, $\mathbf{a}_{los}(t)$, are effectively obtained by using the following equations

$$\mathbf{a}_{los}(t) = \mathbf{a}_{los}(0) + \int_0^t \dot{\mathbf{a}}_{los}(\tau)d\tau, \quad t \geq 0,\quad (2.159)$$

$$(2.160)$$

$$\mathbf{a}_{los}(t) = \mathbf{a}_{los}(0) + \int_0^t \dot{\mathbf{a}}_{los}(\tau) d\tau, \quad t \geq 0,$$

where the integrals are computed numerically and where the right-hand-sides of (2.155), (2.156), are applied for $\dot{\mathbf{a}}_{los}(\tau)$, $\dot{\mathbf{a}}_{los}(\tau)$, respectively. Thus, smooth trajectories are obtained for $\mathbf{a}_{los}(t)$, $\mathbf{a}_{los}(t)$, and for $\dot{\mathbf{a}}_{los}(t)$, $\dot{\mathbf{a}}_{los}(t)$, $\dot{\mathbf{a}}_{los}(t)$, $\dot{\mathbf{a}}_{los}(t)$. For the mobile ADS application considered here, the azimuth angle $\mathbf{a}_{los}(t)$ computed from (2.159) will not necessarily be limited to the interval $k_{mg} > 1$, while the elevation angle $\mathbf{a}_{los}(t)$ computed from (2.160) will be limited to the interval $(-\pi/2, \pi/2)$ due to (2.149).

Consider the case where the vehicle body and wheels of the mobile ADS are completely stationary. Then, it follows that the hinge point H is stationary relative to the inertial reference frame, implying that $\mathbf{v}_H^{(I)} = \mathbf{a}_H^{(I)} = \mathbf{0}_{3 \times 1}$ or $d_I \mathbf{r}_H^{(I)} / dt = d_I^2 \mathbf{r}_H^{(I)} / dt^2 = \mathbf{0}_{3 \times 1}$. This leads to simplifications in the expressions for the LOS vector and its time derivatives, (2.148), (2.151), (2.152).

2.13 Aiming Vector of the AA Gun

The aiming vector of the AA gun is defined as the unit vector $\mathbf{J}_{B_7}^{(I)}$ of the body reference frame B_5 of the AA gun ((2.66)), and is expressed in terms of the generalized co-ordinates n, γ, ζ , as follows

$$\text{Aiming vector of the AA gun} = \mathbf{J}_{B_7}^{(I)}, \quad (2.161)$$

$$(2.162)$$

$$\begin{aligned} \mathbf{J}_{B_7}^{(I)} &= \begin{bmatrix} -\sin(\beta + \gamma) \cos(\zeta) \\ \cos(\beta + \gamma) \cos(\zeta) \\ \sin(\zeta) \end{bmatrix} \\ &= \begin{bmatrix} \cos(\pi/2 + \beta + \gamma) \cos(\zeta) \\ \sin(\pi/2 + \beta + \gamma) \cos(\zeta) \\ \sin(\zeta) \end{bmatrix}. \end{aligned}$$

The aiming vector points in the direction from G to M and along the longitudinal axis of the AA gun (Fig. 2.1). The inertial azimuth and elevation angles of the AA gun aiming vector $\mathbf{J}_{B_7}^{(I)}$ are denoted by \mathbf{a}_{gun}

and \mathbf{a}_{gun} , respectively, and are related to the generalized co-ordinates n , γ , ζ , and to the Euler angles Ψ_7 , m_5 , of the AA gun as follows ((2.145)–(2.146))

$$\mathbf{a}_{gun} = \frac{\pi}{2} + \Psi_7 = \frac{\pi}{2} + \beta + \gamma, \quad (2.163)$$

$$\mathbf{e}_{gun} = \Theta_7 = \zeta \in (-\pi/2, \pi/2). \quad (2.164)$$

The angles \mathbf{a}_{gun} and \mathbf{a}_{gun} will be referred to as the aiming angles of the AA gun, or simply as the azimuth and elevation angles of the AA gun. The angles \mathbf{a}_{gun} and \mathbf{a}_{gun} specify the inertial direction in which the AA gun is aiming.

Thus, by using (2.162), (2.163), (2.164), the aiming vector of the AA gun, $\mathbf{J}_{B_7}^{(I)}$, (2.161), is expressed in terms of the aiming angles, \mathbf{a}_{gun} , \mathbf{a}_{gun} , as follows

$$\mathbf{J}_{B_7}^{(I)} = \begin{bmatrix} \cos(\mathbf{a}_{gun}) \cos(\mathbf{e}_{gun}) \\ \sin(\mathbf{a}_{gun}) \cos(\mathbf{e}_{gun}) \\ \sin(\mathbf{e}_{gun}) \end{bmatrix}. \quad (2.165)$$

Note that the AA gun aiming angles \mathbf{a}_{gun} , \mathbf{e}_{gun} , are not computed by using (2.161), (2.145), (2.146), but are obtained by using (2.163), (2.164), and the given smooth trajectories of the angles n , γ , ζ .

Alternatively, if the AA gun aiming angles \mathbf{a}_{gun} , \mathbf{e}_{gun} , and the angle n are given then the angles γ , ζ , are computed by using (2.163), (2.164).

2.14 Inertial Position and Velocity of the AA Gun Muzzle

The inertial position of the AA gun muzzle is given by (Sect. 2.5)

$$\mathbf{r}_{muz}^{(I)} = \mathbf{r}_5^{(I)} + \mathbf{R}_{B_5 2I} \mathbf{h}_T + \mathbf{R}_{B_6 2I} \mathbf{h}_m + \mathbf{R}_{B_7 2I} (L_m \mathbf{J}_{B_7}), \quad (2.166)$$

$$\Rightarrow \mathbf{r}_{muz}^{(I)} = \begin{bmatrix} x - \sin(\beta)(L_b + h_{Ty}) - \sin(\beta + \gamma) \cos(\zeta) L_m \\ y + \cos(\beta)(L_b + h_{Ty}) + \cos(\beta + \gamma) \cos(\zeta) L_m \\ h_b + h_{Tz} + h_{mz} + \sin(\zeta) L_m \end{bmatrix}. \quad (2.167)$$

In addition, by using (2.73), (2.165), $\mathbf{r}_{muz}^{(I)}$ is expressed in terms of the inertial position of the hinge point H of the AA gun, $\mathbf{r}_i^{(I)}$, and the aiming angles of the AA gun, as follows

$$\mathbf{r}_{muz}^{(I)} = \mathbf{r}_H^{(I)} + L_m \mathbf{J}_{B_7}^{(I)}, \quad (2.168)$$

where

$$\mathbf{J}_{B_7}^{(I)} = \begin{bmatrix} \cos(\mathbf{a}_{gun}) \cos(\mathbf{e}_{gun}) \\ \sin(\mathbf{a}_{gun}) \cos(\mathbf{e}_{gun}) \\ \sin(\mathbf{e}_{gun}) \end{bmatrix}. \quad (2.169)$$

In (2.167), the inertial position $\mathbf{r}_{muz}^{(I)}$ is expressed as a function of the generalized co-ordinates appearing on the right-hand-side of (2.167).

Thus, the inertial velocity $\mathbf{r}_{muz}^{(I)}$ is obtained by computing directly the time derivative of $\mathbf{r}_{muz}^{(I)}$ as follows

$$\mathbf{v}_{muz}^{(I)} = \frac{d_I \mathbf{r}_{muz}^{(I)}}{dt}, \quad (2.170)$$

$$\Rightarrow \mathbf{v}_{muz}^{(I)} =$$

$$\begin{bmatrix} \dot{x} - \cos(\beta)(L_b + h_{Ty})\dot{\beta} + (-\cos(\beta + \gamma)(\dot{\beta} + \dot{\gamma})\cos(\zeta) + \sin(\beta + \gamma)\sin(\zeta)\dot{\zeta})L_m \\ \dot{y} - \sin(\beta)(L_b + h_{Ty})\dot{\beta} + (-\sin(\beta + \gamma)(\dot{\beta} + \dot{\gamma})\cos(\zeta) - \cos(\beta + \gamma)\sin(\zeta)\dot{\zeta})L_m \\ \cos(\zeta)L_m\dot{\zeta} \end{bmatrix}. \quad (2.171)$$

The inertial velocity of the AA gun muzzle can also be obtained by using the kinematic relations given in Appendix A as follows

$$\begin{aligned} \mathbf{v}_{muz}^{(I)} = & \mathbf{v}_5^{(I)} + \mathbf{R}_{B_5 2I}(\boldsymbol{\omega}_{B_5 rI}^{(B_5)} \times \mathbf{h}_T) + \mathbf{R}_{B_6 2I}(\boldsymbol{\omega}_{B_6 rI}^{(B_6)} \times \mathbf{h}_m) \\ & + \mathbf{R}_{B_7 2I}(\boldsymbol{\omega}_{B_7 rI}^{(B_7)} \times (L_m \mathbf{J}_{B_7})). \end{aligned} \quad (2.172)$$

For later use, the inertial velocity of the AA gun muzzle is expressed in terms of the time derivative of the right-hand-side of (2.168), (2.169), as follows


$$\mathbf{v}_{muz}^{(I)} = \mathbf{v}_H^{(I)} + L_m \frac{d_I \mathbf{J}_{B_7}^{(I)}}{dt}, \quad (2.173)$$

where

$$\frac{d_I \mathbf{J}_{B_7}^{(I)}}{dt} =$$

$$\begin{bmatrix} -\sin(\mathbf{a}_{gun})\dot{\mathbf{a}}_{gun} \cos(\mathbf{e}_{gun}) - \cos(\mathbf{a}_{gun})\dot{\mathbf{e}}_{gun} \sin(\mathbf{e}_{gun}) \\ \cos(\mathbf{a}_{gun})\dot{\mathbf{a}}_{gun} \cos(\mathbf{e}_{gun}) - \sin(\mathbf{a}_{gun})\dot{\mathbf{e}}_{gun} \sin(\mathbf{e}_{gun}) \\ \cos(\mathbf{e}_{gun})\dot{\mathbf{e}}_{gun} \end{bmatrix}. \quad (2.174)$$

3. Kinematic Model of the Mobile Air Defence System

Constantinos Frangos¹ 

(1) Electrical Engineer working in Decision and Control, Pretoria, South Africa

This Chapter presents the kinematic model of the mobile ADS. The kinematic model is derived by using all the velocity constraints and describes the generalized velocities in terms of the selected independent generalized velocities.

3.1 Velocity Constraints of the Mobile ADS

The geometric and velocity constraints are as follows.

1. Four Geometric Constraints.
 - a. Turret motor and gearbox based mechanism: one geometric constraint (2.128) obtained from the velocity constraint (2.127).
 - b. AA gun motor and gearbox based mechanism: one geometric constraint (2.140) obtained from the velocity constraint (2.139).
 - c. Front wheel steering system: two geometric constraints (2.103)–(2.104).

2. Thirteen Velocity Constraints.

The velocity constraints include the time derivatives of the two geometric constraints (2.103)–(2.104) and are as follows.

- a. Wheels 1, 2, 3 and 4: eight velocity constraints (2.43)–(2.50).
- b. Drive system and differential gearbox: one velocity constraint (2.91).
- c. Turret motor and gearbox based mechanism: one velocity constraint (2.127).
- d. AA gun motor and gearbox based mechanism: one velocity constraint (2.139).
- e. Front wheel steering system: two velocity constraints, (2.115)–(2.116), obtained by differentiating with respect to time the two geometric constraints (2.103)–(2.104).

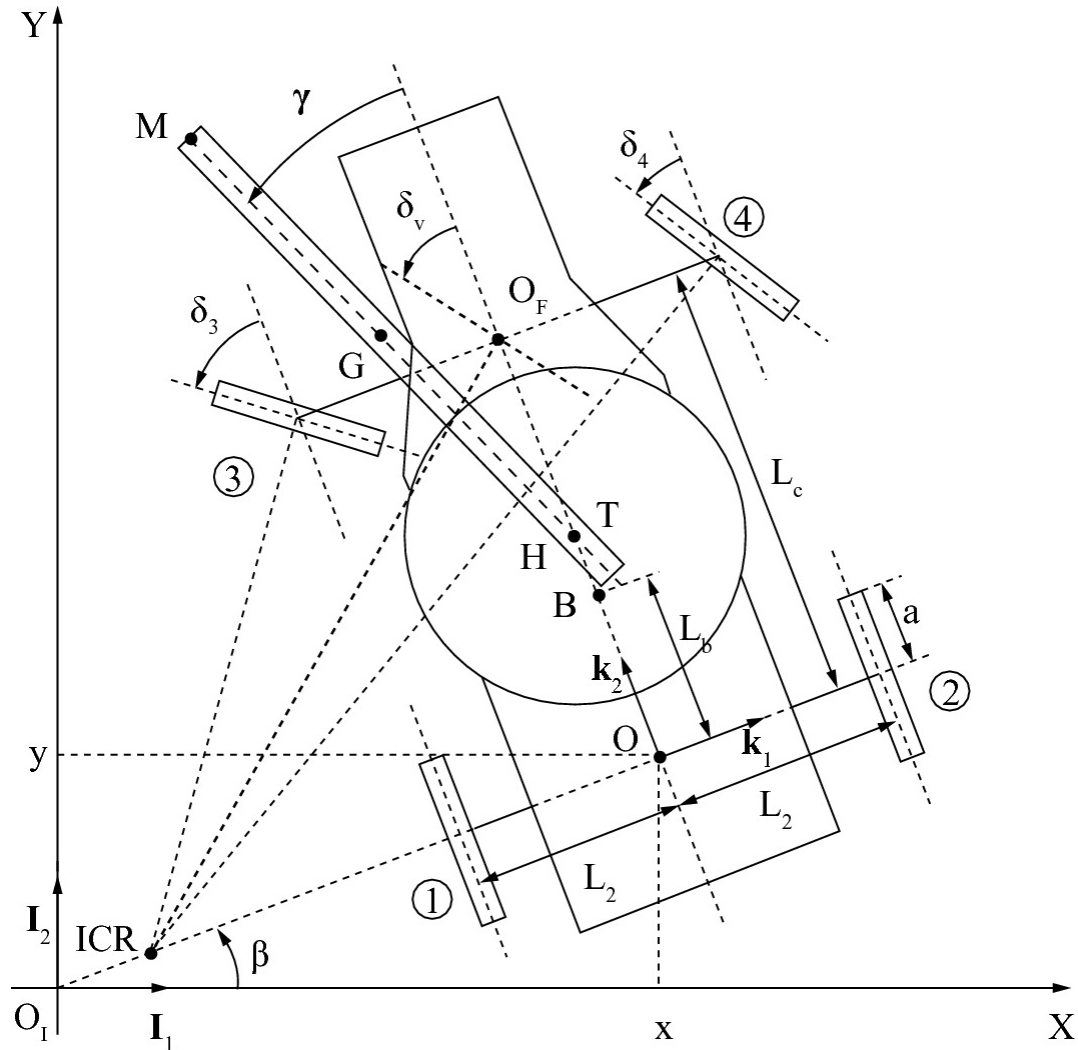


Fig. 3.1 Schematic of the mobile air defence system

The following preliminary steps are applied in order to derive the kinematic model of the mobile ADS (Fig. 3.1).

1. First, note that the eight velocity constraints (2.43)–(2.50) are not independent. Up to seven independent velocity constraints can be obtained from (2.43)–(2.50).

Second, substitute the geometric constraints (2.103)–(2.104) into the velocity constraints (2.43)–(2.50).

In particular, substitute the relations (2.112) in the expanded form of the eight velocity constraints (2.43)–(2.50) (that is, the trigonometric terms in (2.47)–(2.50) containing δ_3 and δ_4 are expanded).

The resulting eight velocity constraints, denoted by (2.43)–(2.50) = (2.112) in order to save space, are not independent. Up to six independent velocity constraints can be obtained from (2.43)–(2.50) = (2.112).

2. The velocity constraints (2.91), (2.127), (2.139), are independent with respect to the velocity constraints (2.43)–(2.50) = (2.112).

3. The velocity constraints (2.115)–(2.116) are independent with respect to the velocity constraints (2.43)–(2.50) = (2.112).

4. It follows that the kinematic model of the mobile ADS is based on a total of thirteen velocity constraints, (2.43)–(2.50) = (2.112), (2.91), (2.127), (2.139), (2.115)–(2.116), that are not independent.

In particular, up to eleven independent velocity constraints can be obtained from the above-mentioned thirteen velocity constraints.

Thus, the thirteen velocity constraints (2.43)–(2.50) = (2.112), (2.91), (2.127), (2.139), (2.115)–(2.116), are represented as follows

$$\mathbf{G}\mathbf{p} = \mathbf{0}_{15 \times 1}, \quad (3.1)$$

where $\mathbf{G} = \mathbf{G}(\mathbf{q}) \in \mathbb{R}^{13 \times 15}$ is the velocity constraints matrix (\mathbf{G} is not given here in order to save space), and

$$\begin{aligned} n &= 15 \text{ generalized co-ordinates,} \\ m &= 13 \text{ velocity constraints,} \end{aligned} \quad (3.2)$$

$$N = 11 \text{ rigid bodies} \quad (3.3)$$

((2.141), (A.5), and (A.123)). Henceforward, the explicit functional dependence on \mathbf{q} , \mathbf{q} and $d\mathbf{p}/dt$, is suppressed in order to simplify the presentation. In addition, it is assumed throughout that $L_b > 0$, (2.142).

The rank of the velocity constraints matrix \mathbf{G} is eleven,¹

$$\text{Rank}(\mathbf{G}) = 11. \quad (3.4)$$

It follows that at least one set of eleven independent velocity constraints can be found from the thirteen velocity constraints, (3.1).

Furthermore, by using the assumptions and derivations in Appendix A, the matrix m_5 , (A.106), is $3N \times n = 33 \times 15$, the matrix U_ρ , (A.113), is $3N \times n = 33 \times 15$, thus leading to a matrix U , (A.119), that is $3N \times n = 33 \times 15$, $U = U(\mathbf{q}) \in \mathbb{R}^{66 \times 15}$. The selected generalized co-ordinates \mathbf{q} , (2.141), are such that the matrix U has full column rank ((A.120)),

$$\text{Rank}(U) = n = 15. \quad (3.5)$$

In this work all thirteen velocity constraints (3.1) are used in the derivation of the kinematic and dynamic models of the mobile ADS (Appendices A and B). However, for completeness, two different methods are presented below for converting the thirteen velocity constraints (3.1) to a set of eleven independent velocity constraints in the following form

$$\mathbf{G}_f \mathbf{p} = \mathbf{0}_{11 \times 1}, \quad (3.6)$$

where $\mathbf{G}_f = \mathbf{G}_f(\mathbf{q}) \in \mathbb{R}^{11 \times 15}$, and $\text{Rank}(\mathbf{G}_f) = 11$.

The first method employs a reduction procedure as follows. Apply elementary row operations ([126]) in order to transform the original velocity constraints (3.1) to an equivalent system of velocity constraints given by

$$\mathbf{G}_r \mathbf{p} = \mathbf{0}_{13 \times 1}, \quad (3.7)$$

where the matrix $\mathbf{G}_r = \mathbf{G}_r(\mathbf{q}) \in \mathbb{R}^{13 \times 15}$ is in reduced row echelon form,

$$(3.8)$$

$$\mathbf{G}_r = \begin{bmatrix} \mathbf{A}_f \\ \mathbf{0}_{2 \times 15} \end{bmatrix}, \quad \mathbf{A}_f = [\mathbf{A}_{f1} : \mathbf{A}_{f2} : \mathbf{A}_{f3}],$$

and where $\mathbf{A}_f = \mathbf{A}_f(\mathbf{q}) \in \mathbb{R}^{11 \times 15}$, $\text{Rank}(\mathbf{A}_f) = 11$, $\mathbf{A}_{f1} \in \mathbb{R}^{11 \times 9}$,

$$\mathbf{A}_{f2} = \mathbf{A}_{f2}(\mathbf{q}) \in \mathbb{R}^{11}, \quad \mathbf{A}_{f3} = \mathbf{A}_{f3}(\mathbf{q}) \in \mathbb{R}^{11 \times 5},$$

$$\mathbf{A}_{f1} = \begin{bmatrix} \mathbf{I}_9 \\ \mathbf{0}_{2 \times 9} \end{bmatrix}, \quad (3.9)$$

\mathbf{I}_9 denotes the 9 by 9 unit matrix,

$$\mathbf{A}_{f2} = [0, 0, 0, 0, 0, 0, 0, 0, -L_c^2/A_4^2, -L_c^2/A_3^2, 0, 0]^\top, \quad (3.10)$$

$$\mathbf{A}_{f3} = \begin{bmatrix} -ak_d \sin(\beta)/2 & 0 & 0 & 0 & 0 \\ ak_d \cos(\beta)/2 & 0 & 0 & 0 & 0 \\ \frac{ak_d \sin(\delta_v)}{(2L_c \cos(\delta_v))} & 0 & 0 & 0 & 0 \\ \frac{k_d(L_2 \sin(\delta_v) - L_c \cos(\delta_v))}{(2L_c \cos(\delta_v))} & 0 & 0 & 0 & 0 \\ \frac{-k_d(L_2 \sin(\delta_v) + L_c \cos(\delta_v))}{(2L_c \cos(\delta_v))} & 0 & 0 & 0 & 0 \\ -k_d A_4 / (2L_c \cos(\delta_v)) & 0 & 0 & 0 & 0 \\ -k_d A_3 / (2L_c \cos(\delta_v)) & 0 & 0 & 0 & 0 \\ 0 & 0 & 0 & 0 & 0 \\ 0 & 0 & 0 & 0 & 0 \\ 0 & 1 & 0 & -1/k_{mp} & 0 \\ 0 & 0 & 1 & 0 & -1/k_{mg} \end{bmatrix}, \quad (3.11)$$

subject to

$$\cos(\delta_v) \neq 0, \quad L_c \neq 0. \quad (3.12)$$

Given that the system motion satisfies $L_b > 0$, (2.142), it follows that

(2.105)–(2.106), and (2.108), are satisfied thus implying that $\cos(\delta_v) \neq 0$, while $L_c > 0$. Thus, conditions (3.12) are met.

From (3.8), it can be seen that the last two rows of the matrix \mathbf{G}_r are zero-rows, indicating that there are two redundant velocity constraints out of the thirteen velocity constraints, (3.1). Thus, a set of eleven independent velocity constraints is obtained directly from (3.7), (3.8), and represented as follows

$$\mathbf{A}_f \mathbf{p} = \mathbf{0}_{11 \times 1}. \quad (3.13)$$

The second method employs deletion of the dependent or redundant velocity constraints as follows. Given that up to six independent velocity constraints can be obtained from the eight velocity constraints (2.43)–(2.50) = (2.112). One possible combination of six independent velocity constraints is ((2.43)–(2.45), (2.47)–(2.49)) = (2.112). These six velocity constraints, together with the five independent velocity constraints (2.91), (2.127), (2.139), (2.115)–(2.116), lead to eleven independent velocity constraints represented as follows

$$\mathbf{A}_{red} \mathbf{p} = \mathbf{0}_{11 \times 1}, \quad (3.14)$$

$$\mathbf{A}_{red} = \mathbf{A}_{red}(\mathbf{q}) \in \mathbb{R}^{11 \times 15}, \text{Rank}(\mathbf{A}_{red}) = 11.$$

3.2 Kinematic Model of the Mobile ADS

Hereafter, the kinematic model of the mobile ADS is derived by using all the velocity constraints (3.1). Firstly, note that the relation between the dimension of the null space of \mathbf{G} , $\mathbf{Q}_A \in \mathbb{R}^n$, and $\text{Rank}(\mathbf{G})$ is given by

(Theorem 31, p. 281, [126]),

$$\begin{aligned} \text{Rank}(\mathbf{G}) + \text{Dim}(\text{Null}(\mathbf{G})) &= \text{number of columns of } \mathbf{G} \\ &= n = 15. \end{aligned} \quad (3.15)$$

Given that $\text{Rank}(\mathbf{G}) = 11$, (3.4), and using (3.15), it follows that

$$\begin{aligned} \text{Dim}(\text{Null}(\mathbf{G})) &= n_s = n - \text{Rank}(\mathbf{G}) \\ &= 15 - 11 = 4. \end{aligned} \quad (3.16)$$

Let \mathbf{p}_s denote the vector of independent generalized velocities, $\mathbf{p}_s \in \mathbb{R}^{n_s}$, $n_s > 4$, (3.16) (Appendix A). In this case, the elements of \mathbf{p}_s are set equal to the following generalized velocities,

$$\mathbf{p}_s = [p_{s1}, p_{s2}, p_{s3}, p_{s4}]^\top = \left[\frac{d\delta_v}{dt}, \frac{d\alpha_s}{dt}, \frac{d\gamma}{dt}, \frac{d\zeta}{dt} \right]^\top, \quad (3.17)$$

$$\Rightarrow \mathbf{p}_s = \mathbf{C}_s \mathbf{p} \text{ or } \mathbf{C}_s \mathbf{p} = \mathbf{p}_s, \quad (3.18)$$

where $\mathbf{C}_s \in \mathbb{R}^{4 \times 15}$, and ((A.132))

$$\mathbf{C}_s = \left[\mathbf{0}_{4 \times 9} : \mathbf{I}_4 : \mathbf{0}_{4 \times 2} \right], \quad (3.19)$$

$$\text{Rank} \left(\begin{bmatrix} \mathbf{G} \\ \mathbf{C}_s \end{bmatrix} \right) = n_s + \text{Rank}(\mathbf{G}) = 4 + 11 = 15.$$

The associated vector of independent generalized co-ordinates \mathbf{p}_s is obtained from (3.17) as follows

$$\begin{aligned} \mathbf{p}_s &= \frac{d\mathbf{q}_s}{dt}, \quad \mathbf{q}_s = [q_{s1}, q_{s2}, q_{s3}, q_{s4}]^\top \\ &= [\delta_v, \alpha_s, \gamma, \zeta]^\top \\ &= \mathbf{C}_s \mathbf{q}. \end{aligned} \quad (3.20)$$

The generalized co-ordinates δ_v , α_s , are actuated by the applied torques T_{δ_v} , T_{α_s} , respectively. In addition, the generalized co-ordinates γ , ζ , are linearly related via the respective gearbox based mechanism ratios to the generalized co-ordinates γ_0 , ζ_0 , that are actuated by the applied torques T_{γ_0} , T_{ζ_0} , respectively.

Equations (3.1) and (3.18), are solved jointly for \mathbf{q} in terms of \mathbf{p}_s , and the solution is expressed as follows ([65] and Sect. B.3.1),

$$\mathbf{p} = \mathbf{S}\mathbf{p}_s, \quad (3.21)$$

where $\mathbf{S} = \mathbf{S}(\mathbf{q}) \in \mathbb{R}^{15 \times 4}$ is the null space matrix given by

$$\mathbf{S} = \begin{bmatrix} 0 & ak_d \sin(\beta)/2 & 0 & 0 \\ 0 & -ak_d \cos(\beta)/2 & 0 & 0 \\ 0 & -ak_d \sin(\delta_v)/(2L_c \cos(\delta_v)) & 0 & 0 \\ 0 & \frac{-k_d(L_2 \sin(\delta_v) - L_c \cos(\delta_v))}{(2L_c \cos(\delta_v))} & 0 & 0 \\ 0 & \frac{k_d(L_2 \sin(\delta_v) + L_c \cos(\delta_v))}{(2L_c \cos(\delta_v))} & 0 & 0 \\ 0 & k_d A_4/(2L_c \cos(\delta_v)) & 0 & 0 \\ 0 & k_d A_3/(2L_c \cos(\delta_v)) & 0 & 0 \\ L_c^2/A_4^2 & 0 & 0 & 0 \\ L_c^2/A_3^2 & 0 & 0 & 0 \\ 1 & 0 & 0 & 0 \\ 0 & 1 & 0 & 0 \\ 0 & 0 & 1 & 0 \\ 0 & 0 & 0 & 1 \\ 0 & 0 & k_{mp} & 0 \\ 0 & 0 & 0 & k_{mg} \end{bmatrix}, \quad (3.22)$$

subject to

$$\cos(\delta_v) \neq 0, \quad A_3 \neq 0, \quad A_4 \neq 0, \quad L_c \neq 0. \quad (3.23)$$

Given that the system motion satisfies $L_b > 0$, (2.142), it follows that

(2.105)–(2.106), and (2.108), are satisfied thus implying that $\cos(\delta_v) \neq 0$, and $-T_{\delta_v} \mathbf{I}_3$, $-T_{\delta_v} \mathbf{I}_3$, (2.114), while $L_c > 0$. Thus,

conditions (3.23) are met.

By using (3.16) it follows that the matrix \mathbf{S} has full column rank,

$$\text{Rank}(\mathbf{S}) = n_s = 4. \quad (3.24)$$

In addition, by substituting the expression for \mathbf{q} , (3.21)–(3.22), in (3.1), (3.7), (3.13), and (3.14), and simplifying, the following is obtained

$$\begin{aligned} \mathbf{GS} &= \mathbf{0}_{13 \times 4}, \quad \mathbf{G}_r \mathbf{S} = \mathbf{0}_{13 \times 4}, \quad \mathbf{A}_f \mathbf{S} = \mathbf{0}_{11 \times 4}, \\ \mathbf{A}_{red} \mathbf{S} &= \mathbf{0}_{11 \times 4}. \end{aligned} \quad (3.25)$$

It follows from (3.25) that the expression for \mathbf{q} , (3.21), (3.22), solves the homogeneous equation representing the original velocity constraints that are not independent, (3.1), as well as homogeneous equations representing the sets of converted velocity constraints that are independent, (3.13), (3.14) ([65]).

Chapter 4 deals with the dynamic model of the mobile ADS, and partitions the vector of generalized co-ordinates \mathbf{q} , (2.141), into the vector of independent generalized co-ordinates \mathbf{p}_s , (3.20), and the following vectors of dependent generalized co-ordinates,

$$\begin{aligned} \mathbf{q}_{d1} &= [x, y, \beta, \alpha_1, \alpha_2, \alpha_4, \alpha_3]^\top, \\ \mathbf{q}_{d2} &= [\delta_4, \delta_3, \gamma_0, \zeta_0]^\top, \text{ and } \mathbf{p}_{d1} = \frac{d\mathbf{q}_{d1}}{dt}. \end{aligned} \quad (3.26)$$

Each generalized co-ordinate in \mathbf{q}_{d2} can be computed directly in terms of the independent generalized co-ordinates in \mathbf{p}_s , by using the geometric constraints (2.104), (2.103), (2.128), (2.140). In addition, note that the matrix $\mathbf{S} = \mathbf{S}(\beta, \delta_v)$, (3.22).

Thus, the kinematic model of the mobile ADS dealt with here is given by (3.21)–(3.22). The mathematical form of the null space matrix \mathbf{S} , (3.22), is generally different for each particular choice of the vector of independent generalized velocities \mathbf{p}_s , (3.17). This implies that the form of the kinematic model is not unique ([82]).

For later use, the following relation is obtained by computing the time derivative of both sides of (3.21) as follows

$$(3.27)$$

$$\frac{d\mathbf{p}}{dt} = \frac{d\mathbf{S}}{dt}\mathbf{p}_s + \mathbf{S}\frac{d\mathbf{p}_s}{dt}.$$

In this work, the scientific computing systems Maple ([16, 186]) and MATLAB/MATLAB Symbolic Toolbox ([110, 112]) are used to do the symbolic computations and manipulations (as well as other systems such as Mathematica, [183], Maxima, [114, 138], Octave/Octave Symbolic Package, [133]; see also [123]). The MATLAB Symbolic Toolbox 2007b ([112]) uses Maple internally to do the symbolic computations. The above-mentioned systems have the required functions to compute the rank of the symbolic matrix \mathbf{G} , (3.1), (3.4); the rank of the symbolic matrix \mathbf{U} , (3.5); the rank of the symbolic matrix \mathbf{A}_f , (3.13); the rank of the symbolic matrix \mathbf{A}_{red} , (3.14); the null space of \mathbf{G} , (3.1), (3.18), that is, effectively the matrix \mathbf{S} , (3.21), (3.22); and the reduced row echelon form of \mathbf{G} , that is, the matrix \mathbf{G}_r , (3.7), (3.8) (Maple also obtains some provisos or conditions for the above computations, [33, 91]).

3.3 Decoupled Kinematic Models of the Vehicle System and of the Turret and AA Gun System

The matrix \mathbf{S} in the kinematic model of the mobile ADS, (3.21)–(3.22), is expressed in terms of matrices \mathbf{S}_1 and \mathbf{S}_2 as follows

$$\mathbf{S} = \begin{bmatrix} \mathbf{S}_1 & \vdots & \mathbf{0}_{11 \times 2} \\ \mathbf{0}_{4 \times 2} & \vdots & \mathbf{S}_2 \end{bmatrix}, \quad (3.28)$$

$$\mathbf{S}_1 = \mathbf{S}_{1:11,1:2}, \quad \mathbf{S}_2 = \mathbf{S}_{12:15,3:4}, \quad (3.29)$$

where $S_1 = S_1(\beta, \delta_v) \in \mathbb{R}^{11 \times 2}$, $S_2 \in \mathbb{R}^{4 \times 2}$ is a constant matrix, and

where MATLAB/Octave style syntax is used in (3.29) to represent the selection of rows and columns of the matrix S in defining the matrices

S_1 and S_2 ([43, 110]).

Thus, by using (3.28), the kinematic model of the mobile ADS, (3.21), is represented as two decoupled kinematic models. In order to simplify the presentation, the first kinematic model is referred to as the kinematic model of the *vehicle system* consisting of the vehicle body, the wheels and the steering and drive systems. The second kinematic model is referred to as the kinematic model of the *turret and AA gun system* consisting of the turret, the AA gun, and the drive systems for the turret and AA gun. The above-mentioned kinematic models are represented as follows

$$\Rightarrow \begin{bmatrix} p_1 \\ p_2 \end{bmatrix} = S \begin{bmatrix} p_{s1} \\ p_{s2} \end{bmatrix}, \quad (3.30)$$

$$\Rightarrow \begin{bmatrix} p_1 \\ p_2 \end{bmatrix} = \begin{bmatrix} S_1 \\ \mathbf{0}_{4 \times 2} \end{bmatrix} p_{s1} + \begin{bmatrix} \mathbf{0}_{11 \times 2} \\ S_2 \end{bmatrix} p_{s2}, \quad (3.31)$$

$$\Rightarrow \begin{bmatrix} p_1 \\ p_2 \end{bmatrix} = \begin{bmatrix} S_1 p_{s1} \\ S_2 p_{s2} \end{bmatrix}, \quad (3.32)$$

\Rightarrow Kinematic Model of the Vehicle System:

$$p_1 = S_1(\beta, \delta_v) p_{s1}, \quad (3.33)$$

$$\frac{dp_1}{dt} = S_1(\beta, \delta_v) \frac{dp_{s1}}{dt} + \frac{dS_1(\beta, \delta_v)}{dt} p_{s1}, \quad (3.34)$$

where

$$\mathbf{p}_1 = \frac{d\mathbf{q}_1}{dt}, \quad (3.35)$$

$$\mathbf{q}_1 = [x, y, \beta, \alpha_1, \alpha_2, \alpha_4, \alpha_3, \delta_4, \delta_3, \delta_v, \alpha_s]^\top,$$

$$\mathbf{p}_{s1} = \frac{d\mathbf{q}_{s1}}{dt} = [\dot{\delta}_v, \dot{\alpha}_s]^\top, \quad \mathbf{q}_{s1} = [\delta_v, \alpha_s]^\top, \quad (3.36)$$

⇒ Kinematic Model of the Turret and AA Gun System:

$$\mathbf{p}_2 = \mathbf{S}_2 \mathbf{p}_{s2}, \quad (3.37)$$

$$\frac{d\mathbf{p}_2}{dt} = \mathbf{S}_2 \frac{d\mathbf{p}_{s2}}{dt} + \frac{d\mathbf{S}_2}{dt} \mathbf{p}_{s2}, \quad (3.38)$$

where

$$\mathbf{p}_2 = \frac{d\mathbf{q}_2}{dt} = [\dot{\gamma}, \dot{\zeta}, \dot{\gamma}_0, \dot{\zeta}_0]^\top, \quad \mathbf{q}_2 = [\gamma, \zeta, \gamma_0, \zeta_0]^\top, \quad (3.39)$$

$$\mathbf{p}_{s2} = \frac{d\mathbf{q}_{s2}}{dt} = [\dot{\gamma}, \dot{\zeta}]^\top, \quad \mathbf{q}_{s2} = [\gamma, \zeta]^\top. \quad (3.40)$$

The vectors \mathbf{q} , \mathbf{p} , (2.141), and \mathbf{p}_s , \mathbf{p}_s , (3.20), are partitioned in terms of the relevant vector quantities given in (3.30)–(3.40) as follows

$$\mathbf{q} = \begin{bmatrix} \mathbf{q}_1 \\ \mathbf{q}_2 \end{bmatrix}, \quad \mathbf{p} = \begin{bmatrix} \mathbf{p}_1 \\ \mathbf{p}_2 \end{bmatrix}, \quad \mathbf{q}_s = \begin{bmatrix} \mathbf{q}_{s1} \\ \mathbf{q}_{s2} \end{bmatrix}, \quad \mathbf{p}_s = \begin{bmatrix} \mathbf{p}_{s1} \\ \mathbf{p}_{s2} \end{bmatrix}. \quad (3.41)$$

The initial conditions $\mathbf{q}(0) = \mathbf{q}_0 \in \mathbb{R}^{15}$ and $\mathbf{p}_s(0) = \mathbf{p}_{s0} \in \mathbb{R}^4$ are partitioned according to (3.41) as follows

$$(3.42)$$

$$\mathbf{q}_0 = \begin{bmatrix} \mathbf{q}_{1,0} \\ \mathbf{q}_{2,0} \end{bmatrix}, \quad \mathbf{p}_{s0} = \begin{bmatrix} \mathbf{p}_{s1,0} \\ \mathbf{p}_{s2,0} \end{bmatrix}.$$

Footnotes

[1](#) At the end of Sect. [3.2](#), a brief summary is given of the symbolic computing software used to obtain some of the results in this work.

4. Dynamic Model and Nonlinear Control of the Mobile Air Defence System

Constantinos Frangos¹ 

(1) Electrical Engineer working in Decision and Control, Pretoria, South Africa

This Chapter deals with the dynamic model and nonlinear control of the mobile ADS as follows.

1. Application of the Lagrange equations (Appendix B) in order to derive the basic dynamic model of the mobile ADS.
2. Application of the kinematic model in order to derive the reduced dynamic model of the mobile ADS.
3. The reduced dynamic model is employed in order to derive a nonlinear feedback control law for the ADS using inverse dynamics transformations.
4. Analysis of the zero dynamics of the controlled dynamic model of the mobile ADS.
5. Methodology for the computation of the constrained motion of the controlled dynamic model of the mobile ADS satisfying all the holonomic and nonholonomic velocity constraints.
6. Methodology for the computation of the vector of generalized

constraint forces and the vector of Lagrange multipliers.

4.1 Basic Dynamic Model of the Mobile ADS

The Lagrange equations are extended in Appendix B for the case of constrained rigid multibody systems subject to velocity constraints that may not be independent. The Lagrange equations employ the total kinetic energy \mathcal{E}_{tot} and total potential energy \mathcal{V}_{tot} of the multibody system. For the case of the mobile ADS, \mathcal{E}_{tot} and \mathcal{V}_{tot} are given by

$$\mathcal{E}_{tot} = \sum_{i=1}^{11} \mathcal{E}_i, \quad \mathcal{V}_{tot} = \sum_{i=1}^{11} \mathcal{V}_i, \quad (4.1)$$

where \mathcal{E}_i , \mathcal{V}_i , $\arg(x_1 + j_c y_1)$, are obtained from (B.22), (B.20). Note that it is assumed throughout that $L_b > 0$, (2.142).

By employing the expressions for \mathcal{E}_{tot} , \mathcal{V}_{tot} , and applying the Lagrange equations, (B.53)–(B.54), (B.57), the following basic dynamic model of the mobile ADS is obtained,

$$\mathbf{M} \frac{d^2 \mathbf{q}}{dt^2} + \mathbf{H} = \mathbf{Q}_A + \mathbf{Q}_C, \quad (4.2)$$

where $\mathbf{M} = \mathbf{M}(\mathbf{q}) \in \mathbb{R}^{15 \times 15}$ is the mass matrix, $\mathbf{M} = \mathbf{M}^\top$, $\det(\mathbf{M}) > 0$,

$\mathbf{H} = \mathbf{H}(\mathbf{q}, \mathbf{p}) \in \mathbb{R}^{15}$, $\mathbf{Q}_A \in \mathbb{R}^{15}$ is the vector of generalized applied forces, and $\mathbf{Q}_C \in \mathbb{R}^{15}$ is the vector of generalized constraint forces

(Appendix B).

The vector of generalized applied forces $\mathbf{Q}_A = [Q_{A1}, \dots, Q_{A15}]^\top$ is given by

$$\begin{aligned} Q_{Aj} &= 0, \quad j = 1, 2, \dots, 9, \quad Q_{A10} = T_{\delta_v}, \quad Q_{A11} = T_{\alpha_s}, \\ Q_{Aj} &= 0, \quad j = 12, 13, \quad Q_{A14} = T_{\gamma_0}, \quad Q_{A15} = T_{\zeta_0}, \end{aligned} \quad (4.3)$$

where Q_{A10} , Q_{A10} , Q_{A10} , Q_{A10} , are generalized applied forces having units of torque (Nm) and are equal to the applied torques T_{δ_v} , T_{α_s} , T_{γ_0} , T_{δ_v} , respectively ((2.141)).

The vector of generalized constraint forces $\mathbf{Q}_C = [Q_{C1}, \dots, Q_{C15}]^T$ is given by ((B.57))

$$\mathbf{Q}_C = \mathbf{G}^T \boldsymbol{\lambda}, \quad (4.4)$$

where $\boldsymbol{\lambda} \in \mathbb{R}^{13}$ is the vector of Langrange multipliers, and \mathbf{G} is the velocity constraints matrix, (3.1). The term generalized applied force or generalized constraint force is used to refer to quantities having units of force or torque.

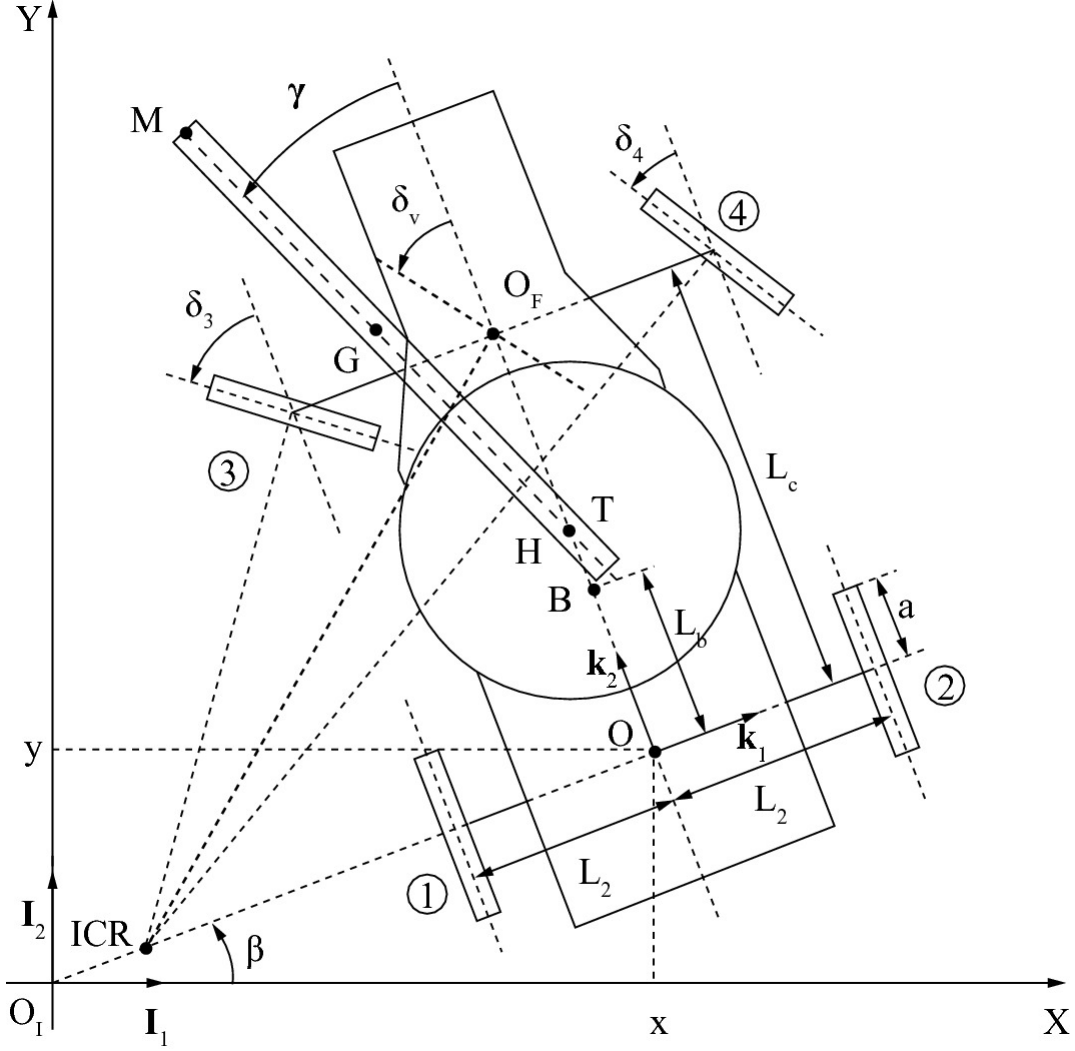


Fig. 4.1 Schematic of the mobile air defence system

The vector of generalized gravitational forces $\mathbf{Q}_{grav} = [Q_{grav1}, \dots, Q_{grav15}]^T$, (B.35), is given by

$$\mathbf{Q}_{grav} = \begin{bmatrix} \mathbf{0}_{12 \times 1} \\ -m_g g L_g \cos(\zeta) \\ \mathbf{0}_{2 \times 1} \end{bmatrix}. \quad (4.5)$$

The element $Q_{grav13} = -m_g g L_g \cos(\zeta)$ in (4.5) represents a torque acting about the hinge point H of the AA gun due to the gravitational

force acting at the center of mass of the AA gun (point G in Fig. 4.1). The vector $-\mathbf{Q}_{grav}$ is part of the vector \mathbf{H} , (4.2).

The nonzero elements of $\mathbf{M} = [M_{i,j}]$, $i, j = 1, \dots, 15$, are given below (lengthy expressions are not given in order to save space and are indicated by three stars * * *)

$$M_{1,1} = m_g + m_{mg} + 4m_{wr} + m_{mp} + m_s + m_b + m_T + m_v, \quad (4.6)$$

$$M_{1,3} = M_{3,1} = * * *, \quad (4.7)$$

$$M_{1,12} = M_{12,1} = -\cos(\beta + \gamma)(m_g \cos(\zeta)L_g + m_{mg}h_{mgy}), \quad (4.8)$$

$$M_{1,13} = M_{13,1} = m_g \sin(\beta + \gamma) \sin(\zeta)L_g, \quad (4.9)$$

$$M_{1,1} = m_g + m_{mg} + 4m_{wr} + m_{mp} + m_s + m_b + m_T + m_v, \quad (4.10)$$

$$M_{1,3} = M_{3,1} = * * *, \quad (4.11)$$

$$M_{2,12} = M_{12,2} = -\sin(\beta + \gamma)(m_g \cos(\zeta)L_g + m_{mg}h_{mgy}), \quad (4.12)$$

$$M_{2,13} = M_{13,2} = -m_g \cos(\beta + \gamma) \sin(\zeta)L_g, \quad (4.13)$$

$$M_{3,3} = * * *, \quad (4.14)$$

$$M_{3,8} = M_{8,3} = I_{wr1}, \quad M_{3,9} = M_{9,3} = I_{wr1}, \quad (4.15)$$

$$M_{3,10} = M_{10,3} = J_{v3}, \quad (4.16)$$

$$M_{3,12} = M_{12,3} = \quad (4.17)$$

$$\begin{aligned}
& m_g \cos^2(\zeta) L_g^2 + \cos^2(\zeta) J_{g3} + m_g h_{Ty} L_g \cos(\gamma) \cos(\zeta) + \\
& m_g L_b L_g \cos(\gamma) \cos(\zeta) + m_{mg} h_{mgy}^2 + J_{mg2} + J_{T3} + \\
& m_{mg} h_{Ty} h_{mgy} \cos(\gamma) + m_{mg} L_b h_{mgy} \cos(\gamma) + \\
& J_{g2} - J_{g2} \cos^2(\zeta),
\end{aligned}$$

$$\begin{aligned}
M_{3,13} = M_{13,3} &= m_g \sin(\zeta) L_g (\cos(\beta + \gamma) \sin(\beta) - \\
& \sin(\beta + \gamma) \cos(\beta)) (L_b + h_{Ty}) \\
&= -m_g \sin(\zeta) L_g \sin(\gamma) (L_b + h_{Ty}),
\end{aligned} \tag{4.18}$$

$$M_{3,14} = M_{14,3} = J_{mp3}, \tag{4.19}$$

$$\begin{aligned}
M_{4,4} &= I_{wr3}, & M_{5,5} &= I_{wr3}, \\
M_{6,6} &= I_{wr3}, & M_{7,7} &= I_{wr3},
\end{aligned} \tag{4.20}$$

$$\begin{aligned}
M_{8,8} &= I_{wr1}, & M_{9,9} &= I_{wr1}, \\
M_{10,10} &= J_{v3}, & M_{11,11} &= J_{s3},
\end{aligned} \tag{4.21}$$

$$\begin{aligned}
M_{12,12} &= m_g L_g^2 \cos^2(\zeta) + m_{mg} h_{mgy}^2 + J_{g2} - J_{g2} \cos^2(\zeta) + \\
& J_{g3} \cos^2(\zeta) + J_{T3} + J_{mg2},
\end{aligned} \tag{4.22}$$

$$M_{13,13} = m_g L_g^2 + J_{g1}, \tag{4.23}$$

$$M_{14,14} = J_{mp3}, \quad M_{15,15} = J_{mg1}. \tag{4.24}$$

The nonzero elements of $\mathbf{H} = [H_1, \dots, H_{15}]^\top$ are given below (lengthy expressions are not given in order to save space and are indicated by three stars ***)

$$H_1 = ***, \quad H_2 = ***, \quad H_3 = ***, \tag{4.25}$$

$$\tag{4.26}$$

$$H_{12} = ***, \quad H_{13} = ***.$$

With reference to the vector of Lagrange multipliers $\lambda = [\lambda_1, \dots, \lambda_{13}]^\top$, each Lagrange multiplier N , $\arg(x_1 + j_c y_1)$, is associated with the corresponding velocity constraint in (3.1) as follows.

1. N , $i = 1, 2, \dots, 8$, are associated with the eight velocity constraints, (2.43)–(2.50) = (2.112), respectively.
2. a_b is associated with (2.91).
3. λ_{10} is associated with (2.127).
4. λ_{10} is associated with (2.139).
5. λ_{10} is associated with (2.115).
6. λ_{10} is associated with (2.116).

In [63, 64], by using the d'Alembert principle ([81]), the Newton-Euler equations are extended for the case of constrained rigid multibody systems subject to velocity constraints that may not be independent. The Newton-Euler equations are applied to the mobile ADS and the following basic dynamic model is obtained

$$\mathbf{M}_{NE} \frac{d^2 \mathbf{q}}{dt^2} + \mathbf{H}_{NE} = \mathbf{Q}_{grav} + \mathbf{Q}_A + \mathbf{G}^\top \lambda, \quad (4.27)$$

and where it is verified that $\mathbf{M}_{NE} = \mathbf{M}$ ((4.6)–(4.24)),

$\mathbf{H}_{NE} = \mathbf{H} + \mathbf{Q}_{grav}$ ((4.25)–(4.26), (4.5)). Thus, the basic dynamic

model of the mobile ADS, (4.2), (4.4), obtained by using the Lagrange equations (Appendix B) is identical to the basic dynamic model, (4.27), obtained by applying the Newton-Euler equations ([63, 64]).

By using (4.2)–(4.3), (4.4), the basic dynamic model of the mobile ADS is expressed as follows

$$\mathbf{M} \frac{d\mathbf{p}}{dt} + \mathbf{H} = \mathbf{D}\mathbf{T}_d + \mathbf{G}^\top \boldsymbol{\lambda}, \quad (4.28)$$

where

$$\mathbf{D} = \begin{bmatrix} \mathbf{0}_{9 \times 2} & \mathbf{0}_{9 \times 2} \\ \mathbf{I}_2 & \mathbf{0}_{2 \times 2} \\ \mathbf{0}_{2 \times 2} & \mathbf{0}_{2 \times 2} \\ \mathbf{0}_{2 \times 2} & \mathbf{I}_2 \end{bmatrix}, \quad \mathbf{T}_d = [T_{\delta_v}, T_{\alpha_s}, T_{\gamma_0}, T_{\zeta_0}]^\top, \quad (4.29)$$

and \mathbf{T}_d is the vector of applied torques also referred to as the vector of control inputs. There are four control inputs, $m_c = 4$, (B.11), that are used to control the motion of the mobile ADS.

By using (4.28)–(4.29), (4.4), the detailed equations describing the basic dynamic model of the mobile ADS are given by

$$M_{1,1} \frac{d^2 x}{dt^2} + M_{1,3} \frac{d^2 \beta}{dt^2} + M_{1,12} \frac{d^2 \gamma}{dt^2} + M_{1,13} \frac{d^2 \zeta}{dt^2} + H_1 = Q_{C1}, \quad (4.30)$$

$$M_{2,2} \frac{d^2 y}{dt^2} + M_{2,3} \frac{d^2 \beta}{dt^2} + M_{2,12} \frac{d^2 \gamma}{dt^2} + M_{2,13} \frac{d^2 \zeta}{dt^2} + H_2 = Q_{C2}, \quad (4.31)$$

$$\mathbf{M}_{\text{row3}} \frac{d^2 \mathbf{q}}{dt^2} + H_3 = Q_{C3}, \quad (4.32)$$

$$M_{4,4} \frac{d^2 \alpha_1}{dt^2} = Q_{C4}, \quad (4.33)$$

$$M_{4,4} \frac{d^2 \alpha_1}{dt^2} = Q_{C4}, \quad (4.34)$$

$$(4.35)$$

$$M_{4,4} \frac{d^2 \alpha_1}{dt^2} = Q_{C4},$$

$$M_{4,4} \frac{d^2 \alpha_1}{dt^2} = Q_{C4}, \quad (4.36)$$

$$M_{8,8} \frac{d^2 \delta_4}{dt^2} + M_{8,3} \frac{d^2 \beta}{dt^2} = Q_{C8}, \quad (4.37)$$

$$M_{8,8} \frac{d^2 \delta_4}{dt^2} + M_{8,3} \frac{d^2 \beta}{dt^2} = Q_{C8}, \quad (4.38)$$

$$M_{10,10} \frac{d^2 \delta_v}{dt^2} + M_{10,3} \frac{d^2 \beta}{dt^2} = T_{\delta_v} + Q_{C10}, \quad (4.39)$$

$$M_{11,11} \frac{d^2 \alpha_s}{dt^2} = T_{\alpha_s} + Q_{C11}, \quad (4.40)$$

$$\begin{aligned} M_{12,12} \frac{d^2 \gamma}{dt^2} + M_{12,1} \frac{d^2 x}{dt^2} + M_{12,2} \frac{d^2 y}{dt^2} \\ + M_{12,3} \frac{d^2 \beta}{dt^2} + H_{12} = Q_{C12}, \end{aligned} \quad (4.41)$$

$$\begin{aligned} M_{13,13} \frac{d^2 \zeta}{dt^2} + M_{13,1} \frac{d^2 x}{dt^2} + M_{13,2} \frac{d^2 y}{dt^2} \\ + M_{13,3} \frac{d^2 \beta}{dt^2} + H_{13} = Q_{C13}, \end{aligned} \quad (4.42)$$

$$M_{14,14} \frac{d^2 \gamma_0}{dt^2} + M_{14,3} \frac{d^2 \beta}{dt^2} = T_{\gamma_0} + Q_{C14}, \quad (4.43)$$

$$M_{15,15} \frac{d^2 \zeta_0}{dt^2} = T_{\zeta_0} + Q_{C15}, \quad (4.44)$$

where M_{row3} denotes a row vector containing the elements of row three of the mass matrix M . The generalized constraint force Q_{Cj} is equal to the sum of several terms as follows ((4.4))

$$Q_{Cj} = G_{1,j}\lambda_1 + G_{2,j}\lambda_2 + \cdots + G_{13,j}\lambda_{13} = \sum_{i=1}^{13} G_{i,j}\lambda_i, \quad (4.45)$$

$$j = 1, 2, \dots, 15,$$

$(G_f) = 11, \arg(x_1 + j_c y_1), j = 1, 2, \dots, 15, (3.1)$. By using (4.4), (3.1), the generalized constraint forces are given by

$$Q_{C1} = \lambda_1 + \lambda_3 + \lambda_5 + \lambda_7, \quad (4.46)$$

$$Q_{C1} = \lambda_1 + \lambda_3 + \lambda_5 + \lambda_7, \quad (4.47)$$

$$\begin{aligned} Q_{C3} = & L_2 \sin(\beta)\lambda_1 - L_2 \cos(\beta)\lambda_2 - L_2 \sin(\beta)\lambda_3 + L_2 \cos(\beta)\lambda_4 \\ & + (-L_c \cos(\beta) + L_2 \sin(\beta))\lambda_5 \\ & + (-L_c \sin(\beta) - L_2 \cos(\beta))\lambda_6 \\ & + (-L_c \cos(\beta) - L_2 \sin(\beta))\lambda_7 \\ & + (-L_c \sin(\beta) + L_2 \cos(\beta))\lambda_8, \end{aligned} \quad (4.48)$$

$$\Psi_7 = (\beta + \gamma), \quad \Theta_7 = \zeta, \quad \Phi_7 = 0. \quad (4.49)$$

$$\Psi_7 = (\beta + \gamma), \quad \Theta_7 = \zeta, \quad \Phi_7 = 0. \quad (4.50)$$

$$Q_{C6} = -a \sin(\beta + \delta_4)\lambda_7 + a \cos(\beta + \delta_4)\lambda_8, \quad (4.51)$$

$$Q_{C6} = -a \sin(\beta + \delta_4)\lambda_7 + a \cos(\beta + \delta_4)\lambda_8, \quad (4.52)$$

$$Q_{C8} = \lambda_{13}, \quad (4.53)$$

$$Q_{C8} = \lambda_{13}, \quad (4.54)$$

$$Q_{C10} = -(L_c^2/A_3^2)\lambda_{12} - (L_c^2/A_4^2)\lambda_{13}, \quad (4.55)$$

$$Q_{C11} = -k_d\lambda_9, \quad (4.56)$$

$$Q_{C12} = -k_{mp}\lambda_{10}, \quad (4.57)$$

$$Q_{C13} = -k_{mg}\lambda_{11}, \quad (4.58)$$

$$Q_{C14} = \lambda_{10}, \quad (4.59)$$

$$Q_{C14} = \lambda_{10}, \quad (4.60)$$

4.2 Reduced Dynamic Model of the Mobile ADS

The reduced dynamic model of the mobile ADS is derived as follows. The independent generalized co-ordinates and velocities \mathbf{p}_s and $\dot{\mathbf{p}}_s$ are given by

$$\mathbf{q}_s = [\delta_v, \alpha_s, \gamma, \zeta]^\top, \quad \dot{\mathbf{p}}_s = [\dot{\delta}_v, \dot{\alpha}_s, \dot{\gamma}, \dot{\zeta}]^\top. \quad (4.61)$$

Thus, for the mobile ADS it holds that $n_s = m_c = 4$ ((B.11)).

Differentiate with respect to time both sides of (3.21), yielding

$$\frac{d\mathbf{p}}{dt} = \mathbf{S} \frac{d\mathbf{p}_s}{dt} + \frac{d\mathbf{S}}{dt} \mathbf{p}_s. \quad (4.62)$$

Then, insert the expression for $d\mathbf{p}/dt$, (4.62), in (4.28) and multiply both sides of the resulting equation from the left by \mathbf{S}^\top to obtain the following

$$(4.63)$$

$$\mathbf{S}^\top \left(\mathbf{M} \mathbf{S} \frac{d\mathbf{p}_s}{dt} + \mathbf{M} \frac{d\mathbf{S}}{dt} \mathbf{p}_s + \mathbf{H} \right) = \mathbf{S}^\top \mathbf{D} \mathbf{T}_d + \mathbf{S}^\top \mathbf{G}^\top \boldsymbol{\lambda}.$$

From (3.25) it follows that

$$\mathbf{S}^\top \mathbf{G}^\top = (\mathbf{G}\mathbf{S})^\top = \mathbf{0}_{4 \times 13}.$$

Thus, Eq. 4.63 simplifies to the reduced dynamic model of the mobile ADS in terms of $d\mathbf{p}_s/dt$,

$$\mathbf{M}_s \frac{d\mathbf{p}_s}{dt} + \mathbf{H}_s = \mathbf{D}_s \mathbf{T}_d, \quad (4.64)$$

where

$$\mathbf{M}_s = \mathbf{S}^\top \mathbf{M} \mathbf{S}, \quad \mathbf{H}_s = \mathbf{S}^\top \mathbf{M} \frac{d\mathbf{S}}{dt} \mathbf{p}_s + \mathbf{S}^\top \mathbf{H}, \quad (4.65)$$

$$\mathbf{D}_s = \mathbf{S}^\top \mathbf{D} = \begin{bmatrix} 1 & 0 & 0 & 0 \\ 0 & 1 & 0 & 0 \\ 0 & 0 & k_{mp} & 0 \\ 0 & 0 & 0 & k_{mg} \end{bmatrix}, \quad (4.66)$$

$\mathbf{M}_s = \mathbf{M}_s(\mathbf{q}) \in \mathbb{R}^{4 \times 4}$, $\mathbf{H}_s = \mathbf{H}_s(\mathbf{q}, \mathbf{p}) \in \mathbb{R}^4$, $\mathbf{D}_s \in \mathbb{R}^{4 \times 4}$. Using (4.65), (4.66), and the mathematical forms of \mathbf{M} , \mathbf{H} , \mathbf{p}_s , \mathbf{S} , and $d\mathbf{S}/dt$, the matrices \mathbf{T}_{α_s} , \mathbf{H}_s and $-\boldsymbol{\pi}$, are computed analytically and/or numerically.

Given that the mass matrix \mathbf{M} is symmetric and positive definite. Furthermore, given that the matrix \mathbf{S} has full column rank, that is,

$\text{Rank}(\mathbf{S}) = 4$, (3.24). Then, it follows that the matrix $\mathbf{M}_s = \mathbf{S}^\top \mathbf{M} \mathbf{S}$ is also symmetric and positive definite, that is,

$$\mathbf{M}_s = \mathbf{M}_s^\top, \quad \det(\mathbf{M}_s) > 0 \quad (4.67)$$

(Theorem 14.2.9, p. 213, [80], and Theorem 4.2.1, p. 140, [71]). One of the main advantages of the reduced dynamic model (4.64)–(4.66), is that the vector of Lagrange multipliers λ does not appear there.

Thus, the reduced dynamic model of the mobile ADS considered here is given by Eqs. (4.64)–(4.66). As mentioned previously, the null space matrix S generally depends on the selected vector of independent generalized velocities p_s , (3.17). This implies that the reduced dynamic model of the mobile ADS is not unique in form ([82]).

4.3 Nonlinear Feedback Control of the Reduced Dynamic Model of the Mobile ADS

A methodology is presented for deriving a nonlinear feedback control law for the vector of applied torques T_d appearing in the reduced dynamic model of the mobile ADS, (4.64),

$$T_d(\mathcal{X}) = [T_{\delta_v}(\mathcal{X}), T_{\alpha_s}(\mathcal{X}), T_{\gamma_0}(\mathcal{X}), T_{\zeta_0}(\mathcal{X})]^\top, \quad (4.68)$$

where the array \mathcal{X} of feedback variables is defined later. The control objective is that the following four variables should asymptotically track specified reference trajectories.

1. The steering system azimuth angle relative to the vehicle body, $\delta_v(t)$, $t \geq 0$.
2. The drive system rotational velocity relative to the vehicle body, $\dot{\alpha}_s(t)$, $t \geq 0$.
3. The turret azimuth angle relative to the vehicle body, $\gamma(t)$, $t \geq 0$.
4. The AA gun elevation angle relative to the turret, $\zeta(t)$, $t \geq 0$.

In particular, let $\boldsymbol{\eta}_i(t)$, $t \geq 0$, $\boldsymbol{\eta}_{i,ref}(t)$, be vectors that group the four variables of the mobile ADS and their time derivatives as follows

$$\boldsymbol{\eta}_1(t) = \left[\delta_v(t), \frac{d\delta_v(t)}{dt}, \frac{d^2\delta_v(t)}{dt^2}, \frac{d\alpha_s(t)}{dt}, \frac{d^2\alpha_s(t)}{dt^2} \right]^\top, \quad (4.69)$$

$$\boldsymbol{\eta}_2(t) = \left[\gamma(t), \frac{d\gamma(t)}{dt}, \frac{d^2\gamma(t)}{dt^2}, \zeta(t), \frac{d\zeta(t)}{dt}, \frac{d^2\zeta(t)}{dt^2} \right]^\top. \quad (4.70)$$

Let $\boldsymbol{\eta}_{i,ref}(t)$, $t \geq 0$, denote the vector reference trajectory for $\boldsymbol{\eta}_i(t)$, $t \geq 0$, $\boldsymbol{\eta}_{i,ref}(t)$,

$$\boldsymbol{\eta}_{1,ref}(t) = \left[\delta_{v,ref}(t), \frac{d\delta_{v,ref}(t)}{dt}, \frac{d^2\delta_{v,ref}(t)}{dt^2}, \frac{d\alpha_{s,ref}(t)}{dt}, \frac{d^2\alpha_{s,ref}(t)}{dt^2} \right]^\top, \quad (4.71)$$

$$\boldsymbol{\eta}_{2,ref}(t) = \left[\gamma_{ref}(t), \frac{d\gamma_{ref}(t)}{dt}, \frac{d^2\gamma_{ref}(t)}{dt^2}, \zeta_{ref}(t), \frac{d\zeta_{ref}(t)}{dt}, \frac{d^2\zeta_{ref}(t)}{dt^2} \right]^\top. \quad (4.72)$$

Thus, the nonlinear feedback control law should ensure that $\boldsymbol{\eta}_i(t)$, $t \geq 0$, asymptotically tracks the reference trajectory $\boldsymbol{\eta}_{i,ref}(t)$, $t \geq 0$, $\boldsymbol{\eta}_{i,ref}(t)$, as follows,

$$\begin{aligned} \lim_{t \rightarrow \infty} (\boldsymbol{\eta}_1(t) - \boldsymbol{\eta}_{1,ref}(t)) &= \mathbf{0}_{5 \times 1}, \\ \lim_{t \rightarrow \infty} (\boldsymbol{\eta}_2(t) - \boldsymbol{\eta}_{2,ref}(t)) &= \mathbf{0}_{6 \times 1}. \end{aligned} \quad (4.73)$$

First, define the following inverse dynamics transformation for the reduced dynamic model of the mobile ADS, (4.64) ([35, 99, 124, 153,

167])

$$\mathbf{T}_d = \mathbf{D}_s^{-1}(\mathbf{M}_s \mathbf{u} + \mathbf{H}_s), \quad (4.74)$$

where $\mathbf{u} \in \mathbb{R}^4$. By inserting (4.74) in (4.64), the following equation is obtained,

$$\begin{bmatrix} d^2\delta_v/dt^2 \\ d^2\alpha_s/dt^2 \\ d^2\gamma/dt^2 \\ d^2\zeta/dt^2 \end{bmatrix} = \mathbf{u} = \begin{bmatrix} u_1 \\ u_2 \\ u_3 \\ u_4 \end{bmatrix}. \quad (4.75)$$

Second, the functions \mathbf{p}_s , \mathbf{p}_s , \mathbf{p}_s and \mathbf{p}_s are specified as follows

$$u_1 = \frac{d^2\delta_{v,ref}}{dt^2} - c_{1,1} \left(\frac{d\delta_v}{dt} - \frac{d\delta_{v,ref}}{dt} \right) - c_{1,2} (\delta_v - \delta_{v,ref}), \quad (4.76)$$

$$u_2 = \frac{d^2\alpha_{s,ref}}{dt^2} - c_{2,1} \left(\frac{d\alpha_s}{dt} - \frac{d\alpha_{s,ref}}{dt} \right), \quad (4.77)$$

$$u_3 = \frac{d^2\gamma_{ref}}{dt^2} - c_{3,1} \left(\frac{d\gamma}{dt} - \frac{d\gamma_{ref}}{dt} \right) - c_{3,2} (\gamma - \gamma_{ref}), \quad (4.78)$$

$$u_4 = \frac{d^2\zeta_{ref}}{dt^2} - c_{4,1} \left(\frac{d\zeta}{dt} - \frac{d\zeta_{ref}}{dt} \right) - c_{4,2} (\zeta - \zeta_{ref}), \quad (4.79)$$

where the constants $c_{i,j}$, $i = 1, 3, 4$, $j = 1, 2$, and Z_{B_5} , are chosen such that the following polynomials in s are Hurwitz ([35, 99, 124, 153, 167])

$$f_1(s) = s^2 + c_{1,1}s + c_{1,2}, \quad f_2(s) = s + c_{2,1}, \quad (4.80)$$

$$f_3(s) = s^2 + c_{3,1}s + c_{3,2}, \quad f_4(s) = s^2 + c_{4,1}s + c_{4,2}. \quad (4.81)$$

Then, it follows from (4.75)–(4.79) that ([35, 99, 124, 153, 167])

$$\left(\frac{d^i \delta_v(t)}{dt^i} - \frac{d^i \delta_{v,ref}(t)}{dt^i} \right) \rightarrow 0 \quad \text{as } t \rightarrow \infty, \quad i = 0, 1, 2, \quad (4.82)$$

$$\left(\frac{d^i \alpha_s(t)}{dt^i} - \frac{d^i \alpha_{s,ref}(t)}{dt^i} \right) \rightarrow 0 \quad \text{as } t \rightarrow \infty, \quad i = 1, 2, \quad (4.83)$$

$$\left(\frac{d^i \gamma(t)}{dt^i} - \frac{d^i \gamma_{ref}(t)}{dt^i} \right) \rightarrow 0 \quad \text{as } t \rightarrow \infty, \quad i = 0, 1, 2, \quad (4.84)$$

$$\left(\frac{d^i \zeta(t)}{dt^i} - \frac{d^i \zeta_{ref}(t)}{dt^i} \right) \rightarrow 0 \quad \text{as } t \rightarrow \infty, \quad i = 0, 1, 2. \quad (4.85)$$

Third, the required applied torques T_{δ_v} , T_{α_s} , T_{γ_0} , T_{δ_v} , are computed from (4.74). Thus, the nonlinear feedback control law for the vector of applied torques, (4.68), employs the array of feedback variables \mathcal{X} ,

$$\mathcal{X} = \left(\mathbf{q}, \mathbf{p}, e_1, \frac{de_1}{dt}, e_{c2}, e_3, \frac{de_3}{dt}, e_4, \frac{de_4}{dt}, \frac{d^2 \delta_{v,ref}}{dt^2}, \frac{d^2 \alpha_{s,ref}}{dt^2}, \frac{d^2 \gamma_{ref}}{dt^2}, \frac{d^2 \zeta_{ref}}{dt^2} \right), \quad (4.86)$$

where $e_1 = \delta_v - \delta_{v,ref}$, $e_{c2} = d\alpha_s/dt - d\alpha_{s,ref}/dt$, $e_3 = \gamma - \gamma_{ref}$, $e_4 = \zeta - \zeta_{ref}$. The derived nonlinear feedback control law is valid for all motions of the mobile ADS that satisfy $L_b > 0$, (2.142).

4.3.1 Analysis of the Zero Dynamics

The analysis of the zero dynamics involves the kinematic and reduced dynamic models of the mobile ADS as used in the derivation of the nonlinear feedback control law ((4.74) and Sect. 4.3), and follows the methodology described on pp. 280–289, [109].

The relevant equations are obtained from Chap. 3, and Sects. 4.2 and 4.3, and are repeated here for convenience as follows

$$\mathbf{p}_s = \left[\frac{d\delta_v}{dt}, \frac{d\alpha_s}{dt}, \frac{d\gamma}{dt}, \frac{d\zeta}{dt} \right]^\top, \quad \mathbf{q}_s = [\delta_v, \alpha_s, \gamma, \zeta]^\top, \quad (4.87)$$

$$\frac{d\mathbf{q}_s}{dt} = \mathbf{p}_s, \quad (4.88)$$

$$\mathbf{M}_s \frac{d\mathbf{p}_s}{dt} + \mathbf{H}_s = \mathbf{D}_s \mathbf{T}_d, \quad (4.89)$$

$$\mathbf{p} = \mathbf{S} \mathbf{p}_s, \quad (4.90)$$

$$\frac{d\mathbf{q}}{dt} = \mathbf{p}, \quad (4.91)$$

$$\frac{d\mathbf{p}}{dt} = \mathbf{S} \frac{d\mathbf{p}_s}{dt} + \frac{d\mathbf{S}}{dt} \mathbf{p}_s. \quad (4.92)$$

The input of the reduced dynamic model of the mobile ADS is \mathbf{T}_d , (4.89), while the output is denoted by δ_3 and is given by (Sect. 4.3)

$$\mathbf{y}_c = [\delta_v, d\alpha_s/dt, \gamma, \zeta]^\top. \quad (4.93)$$

Thus, the zero dynamics will be determined with respect to the input \mathbf{T}_d and the output δ_3 . The specific methodology described on pp. 285–286, [109] is applied in the following steps.

First, given that the output δ_3 is set equal to $\mathbf{0}_{3 \times 1}$, (4.93). Then the following relations are obtained from (4.87), (4.90), (4.92), (4.93),

$$\begin{aligned} \mathbf{y}_c = \mathbf{0}_{4 \times 1} \Rightarrow \delta_v = \dot{\delta}_v = \ddot{\delta}_v = 0, \quad \dot{\alpha}_s = \ddot{\alpha}_s = 0, \\ \gamma = \dot{\gamma} = \ddot{\gamma} = 0, \quad \zeta = \dot{\zeta} = \ddot{\zeta} = 0, \end{aligned} \quad (4.94)$$

$$\Rightarrow \mathbf{p}_s = \mathbf{0}_{4 \times 1}, \quad \dot{\mathbf{p}}_s = \mathbf{0}_{4 \times 1}, \quad (4.95)$$

$$H_{12} = ***, \quad H_{13} = ***. \quad (4.96)$$

Second, the input \mathbf{T}_d is computed from (4.89) as follows

$$\mathbf{D}_s \mathbf{T}_d = \mathbf{H}_s \Rightarrow \mathbf{T}_d = \mathbf{D}_s^{-1} \mathbf{H}_s. \quad (4.97)$$

The form of \mathbf{T}_d in (4.97) is identical to the nonlinear feedback control law (4.74) with $\mathbf{u} = \mathbf{0}_{4 \times 1}$. By substituting $\mathbf{p} = \mathbf{0}_{15 \times 1}$, (4.96), in (4.25)–(4.26), the expression for \mathbf{H} simplifies to the following ((4.5))

$$\mathbf{H} = -\mathbf{Q}_{grav}. \quad (4.98)$$

In addition, by substituting $\mathbf{p}_s = \mathbf{0}_{4 \times 1}$, (4.95), and $\mathbf{H} = -\mathbf{Q}_{grav}$ in (4.65) it follows that

$$\begin{aligned} \mathbf{H}_s &= \mathbf{S}^\top \mathbf{H} \\ &= -\mathbf{S}^\top \mathbf{Q}_{grav} \\ &= [0, 0, 0, m_g g L_g \cos(\zeta)]^\top \quad (\zeta = 0) \\ &= [0, 0, 0, m_g g L_g]^\top. \end{aligned} \quad (4.99)$$

Thus, the input \mathbf{T}_d , (4.97), is given by

$$\begin{aligned} \mathbf{T}_d &= \mathbf{D}_s^{-1} \mathbf{H}_s \\ &= [0, 0, 0, m_g g L_g \cos(\zeta)/k_{mg}]^\top \quad (\zeta = 0) \\ &= [0, 0, 0, m_g g L_g/k_{mg}]^\top. \end{aligned} \quad (4.100)$$

The vector of applied torques \mathbf{T}_d , (4.100), perfectly counteracts the generalized gravitational force \mathbf{Q}_{grav} , (4.5), that is, $\mathbf{D}_s \mathbf{T}_d = \mathbf{H}_s$ in (4.89), thus ensuring that the AA gun remains completely stationary. By using (4.96) and (4.91) it follows that

$$(4.101)$$

$$\dot{\mathbf{q}} = \mathbf{0}_{15 \times 1}, \quad \mathbf{p} = \mathbf{0}_{15 \times 1}, \quad \dot{\mathbf{p}} = \mathbf{0}_{15 \times 1} \quad \text{for all } t \geq 0.$$

From (4.94), (4.101), it follows that

$$\delta_v(t) = 0, \quad \gamma(t) = 0, \quad \zeta(t) = 0, \quad \alpha_s(t) = \alpha_s(0) \quad \text{for all } t \geq 0. \quad (4.102)$$

Let the vector \mathbf{q}_z consist of the first nine and the last two generalized co-ordinates in \mathbf{q} , (2.141), \mathbf{p}_s consists of the remaining four generalized co-ordinates $\delta_v, \alpha_s, \gamma, \zeta$, (4.87), and let $\mathbf{p}_z = d\mathbf{q}_z/dt$.

Third, it follows from the above and (4.101) that the zero dynamics are given by

$$\dot{\mathbf{q}}_z = \mathbf{0}_{11 \times 1}, \quad \mathbf{p}_z = \mathbf{0}_{11 \times 1}, \quad \dot{\mathbf{p}}_z = \mathbf{0}_{11 \times 1} \quad \text{for all } t \geq 0. \quad (4.103)$$

Thus, the zero dynamics are neutrally stable since the mobile ADS remains stationary and retains its initial position and orientation for all time, that is,

$$\mathbf{q}_z(t) = \mathbf{q}_z(0) \quad \text{for all } t \geq 0. \quad (4.104)$$

More general methods for the investigation of the zero dynamics are given in Chaps. 3 and 4, [154], Chap. 6, [88, 99].

4.4 Constrained Motion of the Controlled Dynamic Model of the Mobile ADS

The constrained motion of the controlled dynamic model of the mobile ADS that satisfies the geometric constraints (2.103)–(2.104), (2.128), (2.140), and the velocity constraints (3.1), is computed over a finite time horizon \mathcal{T}_F ,

$$\mathcal{T}_F = [t_0, t_{FIN}], \quad t_0 < t_{FIN}, \quad (4.105)$$

by applying the reduced dynamic model (4.64)–(4.66) as follows.

1. Given the initial conditions for \mathbf{q} , $\mathbf{q}(t_0) = \mathbf{q}_0 \in P_0$, (2.142),

satisfying the geometric constraints (2.103)–(2.104), (2.128), (2.140), and given the initial conditions for \mathbf{p}_s , $\mathbf{p}_s(t_0) = \mathbf{p}_{s0}$, it follows that

$$\mathbf{p}(t_0) = \mathbf{p}_0 = \mathbf{S}(\mathbf{q}_0)\mathbf{p}_{s0}, \quad (4.106)$$

where α_s satisfies the velocity constraints (3.1).

2. Given the vectors of reference trajectories $\boldsymbol{\eta}_{i,ref}(t)$, $t \in \mathcal{T}_F$, $i = 1, 2$, (4.71), (4.72).
3. Solve the following Eqs. ((4.74)–(4.79), (4.64)–(4.66), (3.17)–(3.21), (3.26)) jointly for \mathbf{p}_s , \mathbf{q}_{d2} , \mathbf{q}_{d2} , \mathbf{p}_s , \mathbf{q} , $d\mathbf{p}_s/dt$, for all $t \in \mathcal{T}_F$, in cases where the solution exists and is unique,

$$\delta_v = q_{s1}, \quad \gamma = q_{s3}, \quad \zeta = q_{s4}, \quad (4.107)$$

$$\beta = q_{d1(3)}, \quad (4.108)$$

$$\delta_3 = \arctan2(L_c \sin(\delta_v), -L_2 \sin(\delta_v) + L_c \cos(\delta_v)), \quad (4.109)$$

$$\delta_4 = \arctan2(L_c \sin(\delta_v), L_2 \sin(\delta_v) + L_c \cos(\delta_v)), \quad (4.110)$$

$$\gamma_0 = k_{mp}\gamma, \quad \zeta_0 = k_{mg}\zeta, \quad (4.111)$$

$$\mathbf{p} = \mathbf{S}\mathbf{p}_s, \quad (4.112)$$

$$\frac{d\mathbf{q}_{d1}}{dt} = \mathbf{p}_{d1}, \quad (4.113)$$

$$u_1 = \frac{d^2\delta_{v,ref}}{dt^2} - c_{1,1} \left(\frac{d\delta_v}{dt} - \frac{d\delta_{v,ref}}{dt} \right) - c_{1,2} (\delta_v - \delta_{v,ref}), \quad (4.114)$$

$$(4.115)$$

$$u_2 = \frac{d^2\alpha_{s,ref}}{dt^2} - c_{2,1} \left(\frac{d\alpha_s}{dt} - \frac{d\alpha_{s,ref}}{dt} \right),$$

$$u_3 = \frac{d^2\gamma_{ref}}{dt^2} - c_{3,1} \left(\frac{d\gamma}{dt} - \frac{d\gamma_{ref}}{dt} \right) - c_{3,2} (\gamma - \gamma_{ref}), \quad (4.116)$$

$$u_4 = \frac{d^2\zeta_{ref}}{dt^2} - c_{4,1} \left(\frac{d\zeta}{dt} - \frac{d\zeta_{ref}}{dt} \right) - c_{4,2} (\zeta - \zeta_{ref}), \quad (4.117)$$

$$\mathbf{u} = [u_1, u_2, u_3, u_4]^\top, \quad (4.118)$$

$$\mathbf{T}_d = \mathbf{D}_s^{-1}(\mathbf{M}_s\mathbf{u} + \mathbf{H}_s), \quad (4.119)$$

$$\frac{d\mathbf{q}_s}{dt} = \mathbf{p}_s, \quad (4.120)$$

$$\frac{d\mathbf{p}_s}{dt} = \mathbf{M}_s^{-1}(\mathbf{D}_s\mathbf{T}_d - \mathbf{H}_s), \quad (4.121)$$

$$\mathbf{M}_s = \mathbf{S}^\top \mathbf{M} \mathbf{S}, \quad \mathbf{H}_s = \mathbf{S}^\top \mathbf{M} \frac{d\mathbf{S}}{dt} \mathbf{p}_s + \mathbf{S}^\top \mathbf{H}, \quad (4.122)$$

$$\mathbf{D}_s = \mathbf{S}^\top \mathbf{D}.$$

4. In addition, using $d\mathbf{p}_s/dt$, \mathbf{p}_s , \mathbf{q} , \mathbf{q} , and (4.62), compute the vector of the generalized accelerations $d\mathbf{p}/dt$ as follows

$$\frac{d\mathbf{p}}{dt} = \mathbf{S} \frac{d\mathbf{p}_s}{dt} + \frac{d\mathbf{S}}{dt} \mathbf{p}_s. \quad (4.123)$$

5. In summary, the constrained motion of the controlled dynamic model of the mobile ADS consists of the following computed trajectories

(4.124)

$$(\mathbf{q}(t), \mathbf{p}(t), d\mathbf{p}(t)/dt), \quad t \in \mathcal{T}_F,$$

and satisfies the geometric constraints (2.103)–(2.104), (2.128), (2.140), and the velocity constraints (3.1).

Equations (4.107)–(4.122) are based on the kinematic and dynamic models of the mobile ADS as derived from the Lagrange equations, and on the nonlinear feedback control law. The complete system of equations is solved jointly subject to given initial conditions. Hence, the computed solution (4.124) is the predicted motion trajectory of the actual controlled mobile ADS.

4.5 Generalized Constraint Forces

The vector of generalized constraint forces \mathbf{Q}_C is computed as follows (Appendix B). Using (4.4), (4.28), the vector of generalized constraint forces \mathbf{Q}_C is given by

$$\mathbf{Q}_C = \mathbf{M} \frac{d\mathbf{p}}{dt} + \mathbf{H} - \mathbf{D}\mathbf{T}_d. \quad (4.125)$$

By substituting the constrained motion of the controlled dynamic model of the mobile ADS, (4.124), and the computed vector of applied torques \mathbf{T}_d , (4.119), in the expression on the right-hand-side of (4.125), a unique vector of generalized constraint forces \mathbf{Q}_C is obtained.

4.6 Lagrange Multipliers

The vector of Lagrange multipliers $\boldsymbol{\lambda}$ is computed as follows

(Appendix B). Given the constrained motion of the controlled dynamic model of the mobile ADS, (4.124), and the resulting vector of

generalized constraint forces \mathbf{Q}_C computed by using (4.125).

Substitute (4.124) and \mathbf{Q}_C in (4.4), and re-arrange Eq. (4.4) as follows

$$\mathbf{G}^\top \boldsymbol{\lambda} = \mathbf{Q}_C. \quad (4.126)$$

The vector of Lagrange multipliers $\boldsymbol{\lambda}$ that satisfies Eq. (4.126) is not

unique since the velocity constraints (3.1) are not independent,

$\text{Rank}(\mathbf{G}) = 11 < 13$. The exact solution of (4.126) that has minimum Euclidean norm is given by (Appendix B, Case P4)

$$\boldsymbol{\lambda} = (\mathbf{G}^\top)^{MP} \mathbf{Q}_C, \quad (4.127)$$

where $(\mathbf{G}^\top)^{MP} \in \mathbb{R}^{13 \times 15}$ denotes the Moore-Penrose generalized

inverse of the matrix \mathbf{G}^\top , and $\|\boldsymbol{\lambda}\| \leq \|\boldsymbol{\lambda}_e\|$ where $\boldsymbol{\lambda}_e$ is any given exact solution of (4.126).

5. Operational Modes of the Mobile Air Defence System

Constantinos Frangos¹ 

(1) Electrical Engineer working in Decision and Control, Pretoria, South Africa

This Chapter deals with the operational modes of the mobile ADS. The operational modes consist of various combinations of the tracking modes of the vehicle body and of the AA gun. The afore-mentioned tracking modes are based on the nonlinear feedback control law developed in Chap. 4. In addition, some results based on the firing rate of the AA gun are presented.

5.1 Asymptotic Tracking Results

The reference trajectories for δ_v , γ , ζ , for \mathbf{p}_s , and for $d\mathbf{p}_s/dt$, $t \geq 0$, are denoted as follows (Chap. 4)

$$\dot{y} - L_2 \cos(\beta)\dot{\beta} + \dot{\alpha}_1 a \cos(\beta) = 0, \quad (5.1)$$

$$\mathbf{p}_{s,ref}(t) = \begin{bmatrix} \dot{\delta}_{v,ref}(t) \\ \dot{\alpha}_{s,ref}(t) \\ \dot{\gamma}_{ref}(t) \\ \dot{\zeta}_{ref}(t) \end{bmatrix}, \quad t \geq 0, \quad (5.2)$$

$$(5.3)$$

$$\mathbf{p}_{s1,ref}(t) = \begin{bmatrix} \dot{\delta}_{v,ref}(t) \\ \dot{\alpha}_{s,ref}(t) \end{bmatrix}, \quad t \geq 0,$$

$$\mathbf{p}_{s2,ref}(t) = \begin{bmatrix} \dot{\gamma}_{ref}(t) \\ \dot{\zeta}_{ref}(t) \end{bmatrix}, \quad t \geq 0, \quad (5.4)$$

$$\frac{d\mathbf{p}_{s,ref}(t)}{dt} = \begin{bmatrix} \ddot{\delta}_{v,ref}(t) \\ \ddot{\alpha}_{s,ref}(t) \\ \ddot{\gamma}_{ref}(t) \\ \ddot{\zeta}_{ref}(t) \end{bmatrix}, \quad t \geq 0, \quad (5.5)$$

$$\frac{d\mathbf{p}_{s1,ref}(t)}{dt} = \begin{bmatrix} \ddot{\delta}_{v,ref}(t) \\ \ddot{\alpha}_{s,ref}(t) \end{bmatrix}, \quad t \geq 0, \quad (5.6)$$

$$\frac{d\mathbf{p}_{s2,ref}(t)}{dt} = \begin{bmatrix} \ddot{\gamma}_{ref}(t) \\ \ddot{\zeta}_{ref}(t) \end{bmatrix}, \quad t \geq 0. \quad (5.7)$$

In Chap. 4 a nonlinear feedback control law is derived for the mobile ADS such that the following asymptotic tracking results are obtained ((4.82)–(4.85)),

$$\delta_v(t) \rightarrow \delta_{v,ref}(t), \quad \gamma(t) \rightarrow \gamma_{ref}(t), \quad \zeta(t) \rightarrow \zeta_{ref}(t) \quad \text{as } t \rightarrow \infty, \quad (5.8)$$

$$\mathbf{p}_s(t) \rightarrow \mathbf{p}_{s,ref}(t), \quad \text{as } t \rightarrow \infty, \quad (5.9)$$

$$\frac{d\mathbf{p}_s(t)}{dt} \rightarrow \frac{d\mathbf{p}_{s,ref}(t)}{dt} \quad \text{as } t \rightarrow \infty. \quad (5.10)$$

With reference to (5.1)–(5.10) and the kinematic model of the vehicle system, (3.33)–(3.36), the asymptotic tracking results for the variables related to the motion of the vehicle body are as follows

$$(5.11)$$

$$\delta_v(t) \rightarrow \delta_{v,ref}(t) \text{ as } t \rightarrow \infty,$$

$$\mathbf{p}_{s1}(t) \rightarrow \mathbf{p}_{s1,ref}(t) \text{ as } t \rightarrow \infty, \quad (5.12)$$

$$\frac{d\mathbf{p}_{s1}(t)}{dt} \rightarrow \frac{d\mathbf{p}_{s1,ref}(t)}{dt} \text{ as } t \rightarrow \infty. \quad (5.13)$$

With reference to (5.1)–(5.10) and the kinematic model of the turret and AA gun system, (3.37)–(3.40), the asymptotic tracking results for the variables related to the motion of the turret and the AA gun are as follows

$$\gamma(t) \rightarrow \gamma_{ref}(t), \quad \zeta(t) \rightarrow \zeta_{ref}(t) \text{ as } t \rightarrow \infty, \quad (5.14)$$

$$\mathbf{p}_{s1}(t) \rightarrow \mathbf{p}_{s1,ref}(t) \text{ as } t \rightarrow \infty, \quad (5.15)$$

$$\frac{d\mathbf{p}_{s1}(t)}{dt} \rightarrow \frac{d\mathbf{p}_{s1,ref}(t)}{dt} \text{ as } t \rightarrow \infty. \quad (5.16)$$

Given the initial conditions ((3.41), (3.42))

$$\begin{aligned} \mathbf{q}_1(0) = \mathbf{q}_{1,0}, \quad \mathbf{q}_2(0) = \mathbf{q}_{2,0}, \quad \mathbf{p}_{s1}(0) = \mathbf{p}_{s1,0}, \\ \mathbf{p}_{s2}(0) = \mathbf{p}_{s2,0}. \end{aligned} \quad (5.17)$$

Then, the following holds.

Firstly, for the case of the variables related to the motion of the vehicle body, consider the relevant reference trajectories from (5.1)–(5.7). The resulting closed-loop trajectories of the independent generalized co-ordinates, velocities and accelerations, $\mathbf{q}_{s1}(t)$, $\dot{\mathbf{q}}_{s1}(t)$, $d\mathbf{p}_{s1}(t)/dt$, $t \geq 0$, are computed via (3.36), (4.75)–(4.79) (Chap. 4).

Furthermore, the resulting motion trajectories of the vehicle system, $\mathbf{q}_1(t)$, $\mathbf{q}_2(t)$, $d\mathbf{p}_1(t)/dt$, $t \geq 0$, are computed via (3.33)–(3.35), (5.17).

Secondly, for the case of the variables related to the motion of the turret and the AA gun, consider the relevant reference trajectories from (5.1)–(5.7). The resulting closed-loop trajectories of the independent

generalized co-ordinates, velocities and accelerations, $\mathbf{q}_{s1}(t)$, $\mathbf{q}_{s1}(t)$, $d\mathbf{p}_{s1}(t)/dt$, $t \geq 0$, are computed via (3.40), (4.75)–(4.79) (Chap. 4).

Furthermore, the resulting motion trajectories of the turret and AA gun system, $\mathbf{q}_1(t)$, $\mathbf{q}_1(t)$, $d\mathbf{p}_1(t)/dt$, $t \geq 0$, are computed via (3.37)–(3.39), (5.17). The rotation of the turret in azimuth relative to the vehicle body rotates the AA gun in azimuth relative to the vehicle body.

Thus, control of the vehicle body and of the AA gun is obtained as follows.

1. If proper reference trajectories $\delta_{v,ref}(t)$, $d\alpha_{s,ref}(t)/dt$, together with the relevant first and second order time derivatives, $t \geq 0$, are specified then maneuvering control of the vehicle body in a plane parallel to the inertial (X, Y) plane is obtained.
2. If proper reference trajectories $\Delta_{tofC,k}$, $\zeta_{ref}(t)$, together with their first and second order time derivatives, $t \geq 0$, are specified then directional control of the AA gun aiming vector relative to the vehicle body is obtained.

By using the above-mentioned asymptotic tracking results, various tracking modes of the vehicle body and of the AA gun are considered and the required reference trajectories, (5.1)–(5.7), are presented in each case.

In addition, given the kinematic model of the mobile ADS, (3.21), or equivalently the decoupled kinematic models of the vehicle system, (3.33)–(3.36), and of the turret and AA gun system, (3.37)–(3.40), and the reference trajectories (5.1)–(5.7). Then, the asymptotic tracking results (5.8)–(5.16) and the kinematic model of the mobile ADS are used to compute steady state values of some elements of the vector of generalized velocities \mathbf{q} and the vector of generalized co-ordinates \mathbf{q} .

5.2 Vehicle Body Tracking Mode VM1: Vehicle Body is Maneuvering

In this configuration, the vehicle body of the mobile ADS is both translating and rotating relative to the inertial reference frame. It is assumed that the reference trajectories $\delta_{v,ref}(t)$ and $\dot{\alpha}_{s,ref}(t)$, and the relevant first and second order time derivatives are chosen such that the vehicle body is performing the desired maneuver. In the sequel, a particular steady state motion trajectory for the vehicle body is considered.

5.3 Vehicle Body Tracking Mode VM1A: Vehicle Body is Moving in a Straight Line

It is assumed that the vehicle body is in steady state motion. In particular, the vehicle body is not rotating relative to the inertial reference frame and its center of mass is moving forward at a constant speed k_0 and in a straight line that coincides with the Z_{B_5} axis (with direction the unit vector k_1 , Fig. 5.1).

$$\Rightarrow \mathbf{v}_5^{(I)} = \begin{bmatrix} \dot{x} \\ \dot{y} \\ 0 \end{bmatrix} = \begin{bmatrix} -v_b \sin(\beta) \\ v_b \cos(\beta) \\ 0 \end{bmatrix} = \begin{bmatrix} -v_b \sin(\beta_b) \\ v_b \cos(\beta_b) \\ 0 \end{bmatrix}, \quad (5.21)$$

$$\Rightarrow \mathbf{v}_O^{(I)} = \mathbf{v}_{OA}^{(I)} = \mathbf{v}_H^{(I)} = \mathbf{v}_5^{(I)}. \quad (5.22)$$

5.4 Vehicle Body Tracking Mode VM2: Vehicle Body is Stationary

In this configuration, the wheels and vehicle body are in a stationary steady state relative to the inertial reference frame. It follows from (3.33)–(3.36), (5.8)–(5.16), that the reference trajectories are given by

$$\delta_{v,ref} = \dot{\delta}_{v,ref} = \ddot{\delta}_{v,ref} = 0, \quad \dot{\alpha}_{s,ref} = 0, \quad (5.23)$$

and that

$$\delta_v = \dot{\delta}_v = \ddot{\delta}_v = 0, \quad \dot{\alpha}_s = 0 \Rightarrow \dot{\beta} = 0, \quad \beta = \beta_b, \quad (5.24)$$

$$\Rightarrow \boldsymbol{\omega}_{B_5rI}^{(B_5)} = \mathbf{0}_{3 \times 1}, \quad \mathbf{v}_5^{(B_5)} = \mathbf{0}_{3 \times 1}, \quad (5.25)$$

$$\Rightarrow \mathbf{v}_O^{(I)} = \mathbf{v}_{OA}^{(I)} = \mathbf{v}_H^{(I)} = \mathbf{v}_5^{(I)} = \mathbf{0}_{3 \times 1}. \quad (5.26)$$

5.5 AA Gun Tracking Mode GM1: AA Gun is Rotating Relative to the Vehicle Body

The AA gun is rotating relative to the vehicle body if it is rotating in elevation relative to the turret and/or if the turret is rotating in azimuth relative to the vehicle body. The reference trajectories $\Delta_{tofC,k}$ and

$\zeta_{ref}(t)$, and their higher order time derivatives are required for the

directional control of the AA gun relative to the vehicle body and are determined as follows.

Given reference trajectories of the AA gun aiming angles,

$$\mathbf{a}_{gun,ref}(t), d\mathbf{a}_{gun,ref}(t)/dt, d^2\mathbf{a}_{gun,ref}(t)/dt^2, \quad t \geq 0, \quad (5.27)$$

$$\mathbf{a}_{gun,ref}(t), d\mathbf{a}_{gun,ref}(t)/dt, d^2\mathbf{a}_{gun,ref}(t)/dt^2, \quad t \geq 0, \quad (5.28)$$

and the trajectories of the mobile ADS angle $\beta(t)$ (Fig. 5.1),

$$\beta(t), d\beta(t)/dt, d^2\beta(t)/dt^2, \quad t \geq 0. \quad (5.29)$$

It follows that the required reference values for the turret azimuth angle, $\Delta_{tofC,k}$, the AA gun elevation angle, $\zeta_{ref}(t)$, and their higher order time derivatives, are computed at each time t by using (2.163)–(2.164) as follows,

$$\gamma_{ref}(t) = \mathbf{a}_{gun,ref}(t) - \frac{\pi}{2} - \beta(t), \quad (5.30)$$

$$d\gamma_{ref}(t)/dt = d\mathbf{a}_{gun,ref}(t)/dt - d\beta(t)/dt, \quad (5.31)$$

$$d^2\gamma_{ref}(t)/dt^2 = d^2\mathbf{a}_{gun,ref}(t)/dt^2 - d^2\beta(t)/dt^2, \quad (5.32)$$

$$\zeta_{ref}(t) = \mathbf{e}_{gun,ref}(t), \quad (5.33)$$

$$d\zeta_{ref}(t)/dt = d\mathbf{e}_{gun,ref}(t)/dt, \quad (5.34)$$

$$d^2\zeta_{ref}(t)/dt^2 = d^2\mathbf{e}_{gun,ref}(t)/dt^2. \quad (5.35)$$

5.6 AA Gun Tracking Mode GM1A: AA Gun Aiming Vector is Tracking the LOS Vector

In this case, the aiming vector of the AA gun should asymptotically track the LOS vector. For the given configuration of the mobile ADS it follows that the aiming vector of the AA gun should asymptotically

become parallel with the LOS vector. Conceptually, both of these vectors point from point H outwards in certain directions (Fig. 5.1). Note that during the initial stage of engaging an AAT it is generally required that the AA gun should be tracking the center of mass of the AAT, that is, the LOS vector.

Practically, the above means that the reference values for the AA gun aiming angles $\mathbf{a}_{gun,ref}(t)$, $\mathbf{a}_{gun,ref}(t)$, and their time derivatives in

(5.27)–(5.28), are set equal to the inertial angles of the LOS vector, $\mathbf{a}_{los}(t)$, $\mathbf{a}_{los}(t)$, and their time derivatives, (2.155)–(2.160), as follows

$$\mathbf{a}_{gun,ref}(t) = \mathbf{a}_{los}(t), \quad \frac{d\mathbf{a}_{gun,ref}(t)}{dt} = \frac{d\mathbf{a}_{los}(t)}{dt}, \quad (5.36)$$

$$\frac{d^2\mathbf{a}_{gun,ref}(t)}{dt^2} = \frac{d^2\mathbf{a}_{los}(t)}{dt^2},$$

$$\mathbf{a}_{gun,ref}(t) = \mathbf{a}_{los}(t), \quad \frac{d\mathbf{a}_{gun,ref}(t)}{dt} = \frac{d\mathbf{a}_{los}(t)}{dt}, \quad (5.37)$$

$$\frac{d^2\mathbf{a}_{gun,ref}(t)}{dt^2} = \frac{d^2\mathbf{a}_{los}(t)}{dt^2},$$

Consider the case of an AA laser gun that is tracking the LOS vector. It is assumed that the laser beam travels close to the speed of light in vacuum ($\approx 3 \times 10^8$ m/s) and in a straight line. In addition, assume a set

of engagement scenarios where the AAT velocities and AAT distances to point H of the mobile ADS are such that the center of mass of the AAT moves less than 1 cm over the time of travel of the laser beam to the AAT. Thus, if the AA laser gun is tracking the LOS vector and the laser beam is activated then it will intercept the AAT within a distance of approximately 1 cm from its center of mass (and ignoring the body of the AAT).

5.7 AA Gun Tracking Mode GM1B: AA Gun Aiming Vector is Tracking the Fire Control

Vector

However, for the case of an AA gun firing a projectile with a finite initial velocity as considered here, the AA gun aiming vector must actually track the fire control vector. The fire control vector is calculated by solving a relevant fire control problem.¹

5.8 AA Gun Tracking Mode GM2: AA Gun is not Rotating Relative to the Vehicle Body

In this configuration, the AA gun is not rotating relative to the vehicle body. That is, the turret and the AA gun are in a stationary steady state relative to the vehicle body. It follows from (3.37)–(3.40), (5.8)–(5.16), that the reference trajectories are given by

$$\begin{aligned} \gamma_{ref} = \gamma_{refc}, \quad \dot{\gamma}_{ref} = \ddot{\gamma}_{ref} = 0, \quad \zeta_{ref} = \zeta_{refc}, \\ \dot{\zeta}_{ref} = \ddot{\zeta}_{ref} = 0, \end{aligned} \quad (5.38)$$

where B_{targ} , $(X_{B_6}$ are given real numbers, and

$$\gamma = \gamma_{refc}, \quad \dot{\gamma} = \ddot{\gamma} = 0, \quad \zeta = \zeta_{refc}, \quad \dot{\zeta} = \ddot{\zeta} = 0. \quad (5.39)$$

5.9 Main Operational Modes of the Mobile ADS

The main operational modes of the mobile ADS are summarized in Table 5.1 and are defined by considering various combinations of tracking modes of the vehicle body and of the AA gun.

Table 5.1 Table of the main operational modes of the mobile ADS

	AA gun is not rotating relative to vehicle body (GM2)	AA gun is rotating relative to vehicle body (GM1)
Vehicle body is stationary relative to inertial reference frame (VM2)	OM3	OM2
Vehicle body is moving in a straight line (VM1A)	OM1B	OM1A

5.10 Operational Mode OM1: Mobile ADS is Maneuvering

In this configuration, the vehicle body is in tracking mode VM1 and the AA gun is in any tracking mode. Two subsidiary operational modes that are of interest are OM1A and OM1B and are described next.

5.11 Operational Mode OM1A: Vehicle Body is Moving in a Straight Line (VM1A) and the AA Gun is Rotating Relative to the Vehicle Body (GM1)

The vehicle body is in tracking mode VM1A leading to (5.18)–(5.22), and the AA gun is in tracking mode GM1 leading to (5.27)–(5.35). In this case, the inertial velocity of the AA gun muzzle, (2.172), simplifies to the following

$$\begin{aligned} \mathbf{v}_{muz}^{(I)} = & \mathbf{v}_5^{(I)} + \mathbf{R}_{B_6 2I}(\boldsymbol{\omega}_{B_6 r I}^{(B_6)} \times \mathbf{h}_m) \\ & + \mathbf{R}_{B_7 2I}(\boldsymbol{\omega}_{B_7 r I}^{(B_7)} \times (L_m \mathbf{J}_{B_7})). \end{aligned} \quad (5.40)$$

5.12 Operational Mode OM1B: Vehicle Body is Moving in a Straight Line (VM1A) and the AA Gun is not Rotating Relative to the Vehicle Body (GM2)

The vehicle body is in tracking mode VM1A leading to (5.18)–(5.22), and the AA gun is in tracking mode GM2 leading to (5.38)–(5.39). Thus, based on the above, and using (3.33)–(3.36), (5.8)–(5.16), it follows that

$$\begin{aligned} \dot{\gamma} = 0, \dot{\zeta} = 0, \dot{\beta} = 0 \Rightarrow \gamma = \gamma_{refc}, \zeta = \zeta_{refc}, \\ \beta = \beta_b, \end{aligned} \quad (5.41)$$

$$\Rightarrow \omega_{B_6rI}^{(B_6)} = \omega_{B_7rI}^{(B_7)} = \mathbf{0}_{3 \times 1}. \quad (5.42)$$

In this case, the inertial velocity of the AA gun muzzle, (5.40), further simplifies to the following

$$\mathbf{v}_{muzz}^{(I)} = \mathbf{v}_5^{(I)} = \begin{bmatrix} -v_b \sin(\beta) \\ v_b \cos(\beta) \\ 0 \end{bmatrix} = \begin{bmatrix} -v_b \sin(\beta_b) \\ v_b \cos(\beta_b) \\ 0 \end{bmatrix}. \quad (5.43)$$

5.13 Operational Mode OM2: Vehicle Body is Stationary (VM2) and the AA Gun is Rotating Relative to the Vehicle Body (GM1)

In this configuration, the vehicle body is in tracking mode VM2 leading to (5.23)–(5.26), and the AA gun is in tracking mode GM1. For this case, the inertial velocity of the AA gun muzzle, (2.172), simplifies to the following

$$\mathbf{v}_{muzz}^{(I)} = \mathbf{R}_{B_62I}(\omega_{B_6rI}^{(B_6)} \times \mathbf{h}_m) + \mathbf{R}_{B_72I}(\omega_{B_7rI}^{(B_7)} \times (L_m \mathbf{J}_{B_7})). \quad (5.44)$$

5.14 Operational Mode OM3: Vehicle Body is Stationary (VM2) and the AA Gun is not Rotating Relative to the Vehicle Body (GM2)

In this configuration, all bodies comprising the mobile ADS are completely stationary relative to the inertial reference frame. Thus, the vehicle body is in tracking mode VM2 leading to (5.23)–(5.26), and the AA gun is in tracking mode GM2 leading to (5.38)–(5.39). In this case, the inertial velocity of the AA gun muzzle, (2.172), simplifies to the following

$$\mathbf{A}_f \mathbf{p} = \mathbf{0}_{11 \times 1}. \quad (5.45)$$

5.15 Firing Rate of the AA Gun and Firing Times of the AA Projectiles

The following simplifying assumptions are made with regard to the firing of AA projectiles.

1. The firing of the AA projectile generates significant forces on the AA gun that generally disturb the motion of the mobile ADS. These effects are not taken into consideration in the present work.
2. If the firing button of the mobile ADS is pressed at any given time $\gamma(t)$ then the AA gun fires the first projectile instantaneously at time $\gamma(t)$.
3. It is assumed that at the time of release of the firing button, the AA gun immediately stops firing. Thus, no AA projectile is fired at the time of release of the firing button.
4. It is further assumed that the center of mass of the projectile moves in zero time from the breach of the AA gun to the AA gun muzzle.
5. The motion of the AA gun muzzle directly influences the inertial velocity of the AA projectile at the firing time (Chap. 6).
6. If the AA gun fires then it fires at the maximum firing rate denoted by Ψ_7 ,

$$\text{maximum firing rate} = N_0 \text{ projectiles per second.} \quad (5.46)$$

Thus, the time period between the firing of consecutive AA projectiles is

$$\Delta_0 = \frac{1}{N_0}. \quad (5.47)$$

7. In order to prevent overheating of the AA gun barrel and maximize its operational lifespan, the AA gun cannot be fired continuously for

more than EM_{δ_v} seconds followed by a suitable time period of no firing,

(5.48)

Δ_{fmax} = maximum time period of continuous firing of the AA gun in seconds .

8. The number of projectiles that the AA gun fires over a time period of length EM_{δ_v} is denoted by N_{fmax} and is given by the following ((5.46), (5.48))

$$N_{fmax} = \text{ceil}(N_0 \Delta_{fmax}), \quad (5.49)$$

where

$$\text{ceil}(x_a) = \text{smallest integer} \geq x_a, \quad x_a \in \mathbb{R}. \quad (5.50)$$

Given that the firing button is pressed at time $\gamma(t)$ and released at time $t_{fire} + \Delta_f$ where

$$0 < \Delta_f \leq \Delta_{fmax}. \quad (5.51)$$

Then, the AA gun immediately stops firing at time $t_{fire} + \Delta_f$.

Furthermore, the number of projectiles fired by the AA gun during the time interval $[t_{fire}, t_{fire} + \Delta_f]$ is given by

$$N_f = \text{ceil}(N_0 \Delta_f). \quad (5.52)$$

It follows that the sequence of firing times of the N_p projectiles,

$N_f \geq 1$, are given by

(5.53)

$$t_{fire} + k\Delta_0, \quad k = 0, 1, \dots, N_f - 1, \quad \Delta_0 = \frac{1}{N_0},$$

$$\Rightarrow t_{fire}, t_{fire} + \Delta_0, t_{fire} + 2\Delta_0, \dots, t_{fire} + (N_f - 1)\Delta_0. \quad (5.54)$$

Assume that it is given that the AA gun must fire a burst of Ψ_7 projectiles starting at a given time $\gamma(t)$, $1 \leq N_a \leq N_{fmax}$. Then, the firing button must be released at time $J_{s1} = J_{s2}$, where L_1 is computed by using (5.52), (5.50), as follows

$$\Delta_a = \text{sat} \left((N_a - 1)\Delta_0 + \frac{\Delta_0}{2}, 0, \Delta_{fmax} \right), \quad (5.55)$$

where the saturation function sat is defined as follows


$$\text{sat} (x_a, x_{min}, x_{max}) = \begin{cases} x_{max} & \text{if } x_a > x_{max} \\ x_a & \text{if } x_{min} \leq x_a \leq x_{max} , \\ x_{min} & \text{if } x_a < x_{min} \end{cases}, \quad (5.56)$$

$x_{min} < x_{max}$, B_i , J_{b23} , $x_{max} \in \mathbb{R}$. The time Q_{A10} is added in (5.55) in order to (conservatively) ensure that the resulting L_1 , (5.55), produces the specified Ψ_7 via (5.52), that is, $N_a = \text{ceil} (N_0\Delta_a)$.

Footnotes

1 A conceptual fire control problem is formulated and solved numerically in Chap. 7.

6. Point Mass Flight Dynamics Model of the Anti-Aircraft Projectile

Constantinos Frangos¹ 

(1) Electrical Engineer working in Decision and Control, Pretoria, South Africa

This Chapter deals with the point mass flight dynamics model of the AA projectile ([79, 115]) as follows.

1. The AA projectile is considered to be a point mass and the flight dynamics model describes the inertial motion of the point mass ([79, 115]). Thus, the rotational motion of the actual AA projectile is not considered.
2. The differential equations of the point mass flight dynamics model together with the specified initial condition define an initial value problem. The final time of the initial value problem is equal to the ground impact time ([44, 119]).
3. The AA gun fires a single projectile at a sequence of increasing elevation angles and at a fixed azimuth angle. The case of zero wind velocity and the case of a given cross wind velocity are considered.
4. In all cases, the trajectory of the AA projectile is computed by solving numerically the initial value problem using a fourth order Runge-Kutta algorithm with a fixed time-step ([44]).

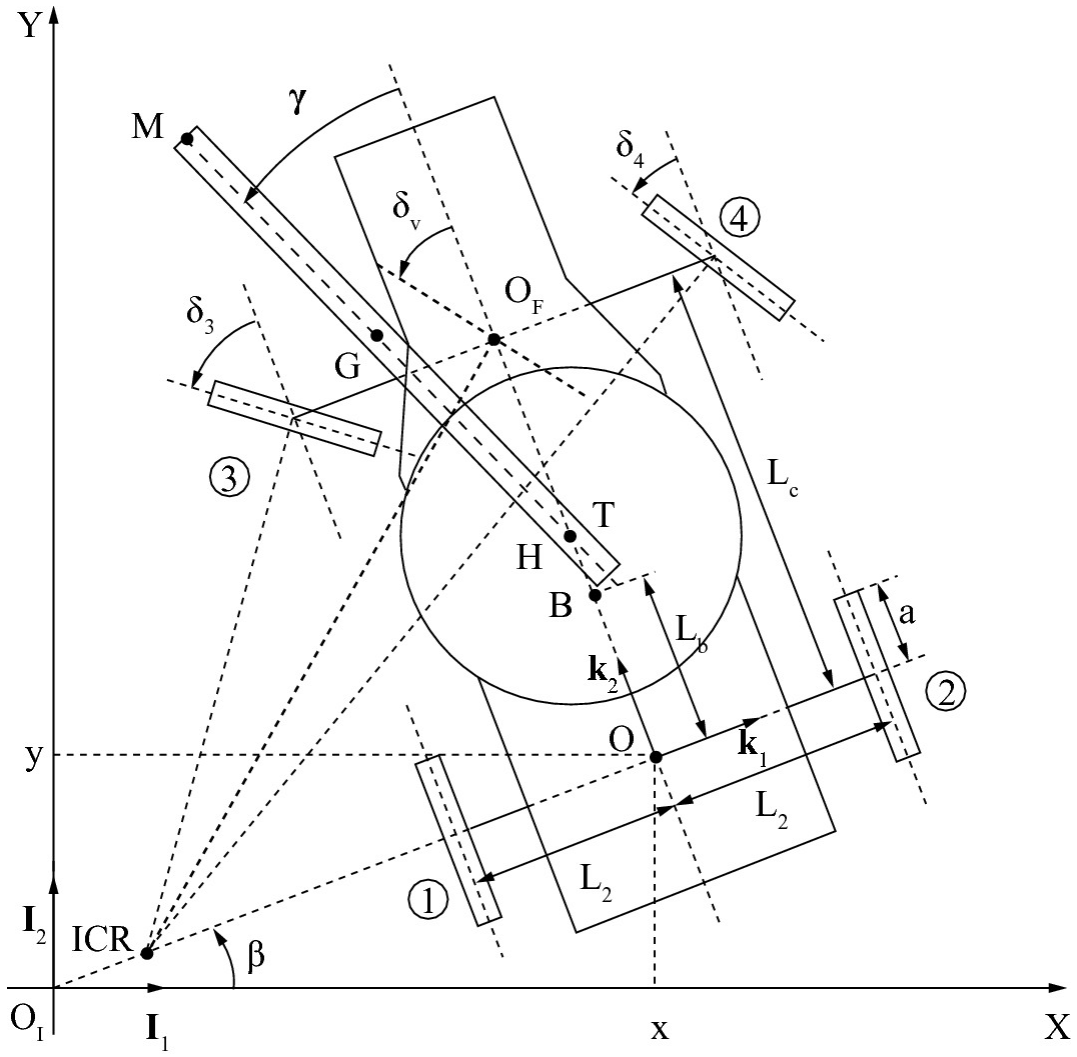


Fig. 6.1 Schematic of the mobile air defence system

6.1 Inertial Position and Velocity of the AA Projectile

The point mass flight dynamics model of the AA projectile is based on the following assumptions and methods.

1. The following group of assumptions holds.
 - a. The earth is spherical and is not rotating ([12]).
 - b. The motions of the mobile ADS and AA projectile take place on and just above a small area on the surface of the earth.

- c. The above-mentioned small area on the surface of the earth is considered to be locally flat.
- d. The origin of the inertial co-ordinate system is fixed on the locally flat surface of the earth (Appendix B).
2. The actual AA projectile is a symmetrical solid body of revolution having cylindrical shape with an ogive-like front end ([24, 78, 116, 122, 180]). The symmetry axis is the longitudinal axis and the projectile is spin-stabilized.
3. In this work, the AA projectile is considered to be a point mass. A flight dynamics model is used to describe the inertial motion of the point mass ([46, 79, 115, 116, 169]). Thus, the rotational motion is not considered. The point mass flight dynamics model consists of a set of nonlinear differential equations that include the gravitational force, the aerodynamic drag force and the effect of a wind velocity ([115]). In the sequel, the term AA projectile refers to a point mass.
4. The inertial position $\mathbf{r}_{proj}^{(I)}(t)$ and the inertial velocity $\mathbf{v}_{proj}^{(I)}(t)$ of

the AA projectile (Chap. 2) are denoted as follows

$$\mathbf{r}_{proj}^{(I)}(t) = [r_{projx}^{(I)}(t), r_{projy}^{(I)}(t), r_{projz}^{(I)}(t)]^\top, t \in [t_{fire}, t_{hitG}], \quad (6.1)$$

$$\mathbf{v}_{proj}^{(I)}(t) = [v_{projx}^{(I)}(t), v_{projy}^{(I)}(t), v_{projz}^{(I)}(t)]^\top = \frac{d_I \mathbf{r}_{proj}^{(I)}(t)}{dt}, \quad (6.2)$$

$$t \in [t_{fire}, t_{hitG}],$$

where $\gamma(t)$ denotes the firing time, Q_{Cj} denotes the ground impact time (where the ground is represented by the inertial (X, Y) plane). The ground impact time Q_{Cj} is defined in terms of an event as follows ([77, 120])

$$t_{hitG} = \inf A_{hitG}, \quad (6.3)$$

where

$$A_{hitG} = \{\tau \in (t_{fire}, \infty) : r_{projz}^{(I)}(\tau) \leq 0, v_{projz}^{(I)}(\tau) < 0\}. \quad (6.4)$$

The fired AA projectile will impact the ground in a finite time implying that the set Q_{A10} is not empty. Hereafter, it is assumed that time $t \in [t_{fire}, t_{hitG}]$, unless otherwise stated.

5. The time of flight to ground impact, $T_{\delta_v} \mathbf{I}_3$, is defined as follows

$$\Delta_{tofG} = t_{hitG} - t_{fire}. \quad (6.5)$$

6. It is assumed that the AA projectile moves in zero time from the breach of the AA gun to the AA gun muzzle (Fig. 6.1).
7. Given the above assumption, the inertial position of the AA projectile at the firing time $\gamma(t)$ coincides with the inertial position of the AA gun muzzle ((2.168))

$$\mathbf{r}_{proj}^{(I)}(t_{fire}) = \mathbf{r}_{muz}^{(I)}(t_{fire}), \quad (6.6)$$

$$\Rightarrow \mathbf{r}_{proj}^{(I)}(t_{fire}) = \mathbf{r}_H^{(I)}(t) + L_m \mathbf{J}_{B_7}^{(I)}(t), \quad t = t_{fire}, \quad (6.7)$$

where

$$\mathbf{r}_H^{(I)}(t_{fire}) = \mathbf{r}_{OA}^{(I)}(t) + \begin{bmatrix} -\sin(\beta(t))(L_b + h_{Ty}) \\ \cos(\beta(t))(L_b + h_{Ty}) \\ h_b + h_{Tz} + h_{mz} \end{bmatrix}, \quad (6.8)$$

$$\mathbf{r}_{OA}^{(I)}(t) = \begin{bmatrix} x(t) \\ y(t) \\ 0 \end{bmatrix}, \quad t = t_{fire},$$

$$\mathbf{J}_{B_7}^{(I)}(t_{fire}) = \begin{bmatrix} \cos(\mathbf{a}_{gun}(t)) \cos(\mathbf{e}_{gun}(t)) \\ \sin(\mathbf{a}_{gun}(t)) \cos(\mathbf{e}_{gun}(t)) \end{bmatrix}, \quad t = t_{fire}. \quad (6.9)$$

$$\left[\sin(\mathbf{e}_{gun}(t)) \right]$$

8.

The generic firing velocity of the AA projectile at time $\gamma(t)$,

$\mathbf{v}_P^{(I)}(t_{fire})$, is defined as follows

$$\mathbf{v}_P^{(I)}(t_{fire}) = V_0 \mathbf{J}_{B_7}^{(I)}(t_{fire}), \quad \|\mathbf{v}_P^{(I)}(t_{fire})\| = V_0, \quad (6.10)$$

where Φ_i is referred to as the generic firing speed.

9. It is assumed that the inertial velocity of the AA projectile at the firing time $\gamma(t)$, $\mathbf{v}_{proj}^{(I)}(t_{fire})$, is equal to the vector sum of the generic firing velocity, $\mathbf{v}_P^{(I)}(t_{fire})$, and the inertial velocity of the AA gun muzzle, as follows

$$\mathbf{v}_{proj}^{(I)}(t_{fire}) = \mathbf{v}_{muz}^{(I)}(t_{fire}) + \mathbf{v}_P^{(I)}(t_{fire}), \quad (6.11)$$

where

$$\mathbf{v}_{muz}^{(I)}(t_{fire}) = \mathbf{v}_H^{(I)}(t) + L_m d_I \mathbf{J}_{B_7}^{(I)}(t)/dt, \quad t = t_{fire}, \quad (6.12)$$

$$\mathbf{v}_H^{(I)}(t_{fire}) = \mathbf{v}_{OA}^{(I)}(t) + \begin{bmatrix} -\cos(\beta(t))\dot{\beta}(t)(L_b + h_{Ty}) \\ -\sin(\beta(t))\dot{\beta}(t)(L_b + h_{Ty}) \\ 0 \end{bmatrix}, \quad (6.13)$$

$$\mathbf{v}_{OA}^{(I)}(t) = \begin{bmatrix} \dot{x}(t) \\ \dot{y}(t) \\ 0 \end{bmatrix}, \quad t = t_{fire},$$

$$\frac{d_I \mathbf{J}_{B_7}^{(I)}(t)}{dt} =$$

$$\begin{bmatrix} -\sin(\mathbf{a}_{gun})\dot{\mathbf{a}}_{gun} \cos(\mathbf{e}_{gun}) - \cos(\mathbf{a}_{gun})\dot{\mathbf{e}}_{gun} \sin(\mathbf{e}_{gun}) \\ \cos(\mathbf{a}_{gun})\dot{\mathbf{a}}_{gun} \cos(\mathbf{e}_{gun}) - \sin(\mathbf{a}_{gun})\dot{\mathbf{e}}_{gun} \sin(\mathbf{e}_{gun}) \\ \cos(\mathbf{e}_{gun})\dot{\mathbf{e}}_{gun} \end{bmatrix}, t = t_{fire}. \quad (6.14)$$

10.

It follows from (6.12), (6.10), (5.45), that if the mobile ADS is completely stationary (operational mode OM3) then $\mathbf{v}_{proj}^{(I)}(t_{fire})$ is

given by

$$\mathbf{v}_{proj}^{(I)}(t_{fire}) = \mathbf{v}_P^{(I)}(t_{fire}) = V_0 \mathbf{J}_{B_7}^{(I)}(t_{fire}). \quad (6.15)$$

11.

It is assumed that there is a wind acting on the AA projectile. The wind velocity, $\mathbf{V}_{wind}^{(I)}$, is generally a function of time t and of the

inertial position $\mathbf{r}_{proj}^{(I)}(t)$ ([46]),

$$\mathbf{V}_{wind}^{(I)} = \mathbf{V}_{wind}^{(I)}(t; \mathbf{r}_{proj}^{(I)}(t)). \quad (6.16)$$

However, in this work it is assumed that for the time horizon under consideration, the wind velocity, $\mathbf{V}_{wind}^{(I)}$, is a constant vector

([46]).

12.

The inertial velocity of the AA projectile relative to the wind, $\mathbf{v}_{rel2w}^{(I)}(t)$, also referred to as the relative velocity, is defined as

follows ([46])

$$\mathbf{v}_{rel2w}^{(I)}(t) = \mathbf{v}_{proj}^{(I)}(t) - \mathbf{V}_{wind}^{(I)}. \quad (6.17)$$

13. Let $\mathbf{u}_{rel2w}^{(I)}(t)$ denote a unit vector in the direction of $\mathbf{v}_{rel2w}^{(I)}(t)$, and

given by

$$\mathbf{u}_{rel2w}^{(I)}(t) = \frac{\mathbf{v}_{rel2w}^{(I)}(t)}{\|\mathbf{v}_{rel2w}^{(I)}(t)\|}, \quad \|\mathbf{v}_{rel2w}^{(I)}(t)\| \neq 0, \quad (6.18)$$

where $\|\mathbf{v}_{rel2w}^{(I)}(t)\|$ is referred to as the relative speed of the AA projectile.

14. The Mach number of the relative speed is given by

$$MachN_{rel2w}(t) = \frac{\|\mathbf{v}_{rel2w}^{(I)}(t)\|}{v_{sound}(t)}, \quad (6.19)$$

where $v_{sound}(t)$ denotes the speed of sound computed by using the International Standard Atmosphere (ISA) model, and is a function of several variables at time t , including the altitude, $r_{projz}^{(I)}(t)$ ([46, 113, 116, 169]).

15. In this Chapter, the presentation of the material and the computation of the AA projectile trajectories are simplified by setting the firing time $\gamma(t)$ equal to a fixed value for all AA projectiles fired by the AA gun.

6.2 Point Mass Flight Dynamics Model of the AA Projectile

By applying Newton's second law ([5, 10, 12, 13, 70, 75, 81]), the point mass flight dynamics model describing the inertial motion of the AA projectile is given by ([79, 115])

(6.20)

$$\begin{bmatrix} \frac{d_I \mathbf{r}_{proj}^{(I)}(t)}{dt} \\ \frac{d_I \mathbf{v}_{proj}^{(I)}(t)}{dt} \end{bmatrix} = \begin{bmatrix} \mathbf{v}_{proj}^{(I)}(t) \\ (\mathbf{F}_{aero}^{(I)}(t) + \mathbf{F}_{grav}^{(I)}) / m_{proj} \end{bmatrix},$$

$$t \in [t_{fire}, t_{hitG}],$$

where the following holds.

1. $m_{proj}(0)$ is the mass.
2. $\mathbf{F}_{aero}^{(I)}(t)$ is the resultant aerodynamic force.
3. $\mathbf{F}_{grav}^{(I)}$ is the gravitational force and is given by (Appendix B)

$$\mathbf{F}_{grav}^{(I)} = -m_{proj} g \mathbf{I}_3, \quad (6.21)$$

where g denotes the gravitational acceleration, $g = 9.81 \text{ m/s}^2$.

Henceforth, in order to simplify the presentation the explicit functional dependence on time t is mostly suppressed. It is assumed that the resultant aerodynamic force $\mathbf{F}_{aero}^{(I)}$ in (6.20) consists of an

aerodynamic drag force $\mathbf{F}_{drag}^{(I)}$ acting in a direction that is opposite to

the relative velocity $\mathbf{v}_{rel2w}^{(I)}$ and is given by ([24, 46, 115, 116])

$$\begin{aligned} \mathbf{F}_{aero}^{(I)} &= \mathbf{F}_{drag}^{(I)} = -0.5 \rho A_b C_{drag} \|\mathbf{v}_{rel2w}^{(I)}\|^2 \mathbf{u}_{rel2w}^{(I)} \\ &= -0.5 \rho A_b C_{drag} \|\mathbf{v}_{rel2w}^{(I)}\| \mathbf{v}_{rel2w}^{(I)}, \end{aligned} \quad (6.22)$$

where the following holds.

- 1.

($X_{B_{10}}$ is the drag coefficient and is a nonlinear function of $\mathbf{p}_z = d\mathbf{q}_z/dt$, (6.19), and thus of the relative speed $\|\mathbf{v}_{rel2w}^{(I)}\|$ and of the speed of sound $\mathbf{q}_{s1}(t)$ ([24, 116]),

$$C_{drag} = C_{drag}(\|\mathbf{v}_{rel2w}^{(I)}\|/v_{sound}). \quad (6.23)$$

2. n denotes the air-density computed using the ISA model ([113]).
3. B_5 is a reference area assumed to be given by $A_b = \pi a_b^2$ where \mathbf{p}_s is the radius of the AA projectile.

The wind velocity $\mathbf{v}_{wind}^{(I)}$ influences the relative velocity $\mathbf{v}_{rel2w}^{(I)}$, (6.17), the aerodynamic drag force \mathbf{F}_{drag} , (6.22), and thus the AA projectile trajectory ([115]).

It follows that (6.20), (6.7), (6.11), define an initial value problem (Chap. 2, [44, 119]). The state vector \mathbf{X} of the point mass flight dynamics model, (6.20), is defined as follows

$$\mathbf{X} = \begin{bmatrix} \mathbf{r}_{proj}^{(I)} \\ \mathbf{v}_{proj}^{(I)} \end{bmatrix}, \quad (6.24)$$

$\mathbf{X} \in \mathbb{R}^6$. The elements of \mathbf{X} are given by

$$\mathbf{X} = [X_1, X_2, X_3, X_4, X_5, X_6]^T = [r_{projx}^{(I)}, r_{projy}^{(I)}, r_{projz}^{(I)}, v_{projx}^{(I)}, v_{projy}^{(I)}, v_{projz}^{(I)}]^T. \quad (6.25)$$

By using (6.20), (6.25), the point mass flight dynamics model is expressed in state space form as follows

$$(6.26)$$

$$\frac{d\mathbf{X}(t)}{dt} = \mathbf{f}_{proj}(\mathbf{X}(t)), \quad \mathbf{X}(t_{fire}) = \mathbf{X}_0, \quad t \in [t_{fire}, t_{hitG}],$$

$$\mathbf{X}_0 = \begin{bmatrix} \mathbf{r}_{proj,0}^{(I)} \\ \mathbf{v}_{proj,0}^{(I)} \end{bmatrix}, \quad (6.27)$$

where the vector function $\mathbf{Q}_C \in \mathbb{R}^n$ maps a vector in \mathbb{R}^6 to a vector in \mathbb{R}^6 , and is obtained by using (6.25) and the right-hand-side of (6.20).

The initial position $\mathbf{r}_{proj,0}^{(I)}$ is given by the right-hand-side of (6.7), and

the initial velocity $\mathbf{v}_{proj,0}^{(I)}$ is given by the right-hand-side of (6.11). Thus,

$\mathbf{r}_{proj,0}^{(I)}$, $\mathbf{v}_{proj,0}^{(I)}$, are functions of the generalized co-ordinates \mathbf{q} and the generalized velocities $d\mathbf{p}/dt$ of the mobile ADS at time $\gamma(t)$, and of the generic firing speed Φ_i ((6.10)).

The solution of the initial value problem (6.26), in cases where it exists and is unique (Chap. 2, [44, 119]), is denoted by \mathbf{A}_{red} and satisfies the following equation

$$\mathbf{X}(t) = \mathbf{X}_0 + \int_{t_{fire}}^t \mathbf{f}_{proj}(\mathbf{X}(\tau))d\tau, \quad t \in [t_{fire}, t_{hitG}]. \quad (6.28)$$

The solution of the initial value problem is a function of time t , the firing time $\gamma(t)$, and the initial condition N_p , and can be denoted as

follows

$$\begin{aligned} \mathbf{X}(t) &= \mathbf{X}(t; t_{fire}) = \mathbf{X}(t; t_{fire}, \mathbf{X}_0), \\ t &\in [t_{fire}, t_{hitG}], \quad \mathbf{X}(t_{fire}) = \mathbf{X}_0. \end{aligned} \quad (6.29)$$

It follows from the above that the ground impact time Q_{Cj} is a function of the initial condition N_p , and thus of the AA gun aiming angles at the firing time, $\mathbf{a}_{gun}(t_{fire})$, $\mathbf{a}_{gun}(t_{fire})$. Similarly, the ground impact inertial position $\mathbf{r}_{proj}^{(I)}(t_{hitG})$ and ground impact inertial velocity $\mathbf{v}_{proj}^{(I)}(t_{hitG})$ are also functions of the AA gun aiming angles at the firing time, $\mathbf{a}_{gun}(t_{fire})$, $\mathbf{a}_{gun}(t_{fire})$.

The ground impact range r_d is defined relative to the inertial (X, Y) co-ordinates of the AA projectile position at the firing time as follows

$$r_d = \|\mathbf{r}_d\| \quad \text{where} \quad \mathbf{r}_d = \begin{bmatrix} r_{projx}^{(I)}(t_{hitG}) \\ r_{projy}^{(I)}(t_{hitG}) \end{bmatrix} - \begin{bmatrix} r_{projx}^{(I)}(t_{fire}) \\ r_{projy}^{(I)}(t_{fire}) \end{bmatrix}. \quad (6.30)$$

The inertial speed $v_{proj}^{(I)}$ and kinetic energy \mathcal{E}_{proj} of the AA projectile are given by

$$v_{proj}^{(I)} = \|\mathbf{v}_{proj}^{(I)}\| = \sqrt{(v_{projx}^{(I)})^2 + (v_{projy}^{(I)})^2 + (v_{projz}^{(I)})^2}, \quad (6.31)$$

$$\mathcal{E}_{proj} = \frac{1}{2} m_{proj} \|\mathbf{v}_{proj}^{(I)}\|^2. \quad (6.32)$$

Assume that the trajectory $\mathbf{r}_{proj}^{(I)}(t)$, $t \in [t_{fire}, t_{hitG}]$, is a regular curve in

three dimensional space ([104]). Then, it follows that the distance travelled along the trajectory over the time interval $[t_{fire}, t]$, also

referred to as the length of the trajectory or arc length, $s(t)$, is given by ([104])

$$(6.33)$$

$$s(t) = \int_{t_{fire}}^t \|\mathbf{v}_{proj}^{(t)}(\tau)\| d\tau, \quad t \in [t_{fire}, t_{hitG}],$$

$$s(t_{fire}) = 0,$$

\Rightarrow Total length of the AA projectile trajectory = $s(t_{hitG})$. (6.34)

The initial value problem (6.26) does not have a closed-form solution. It follows that there is no closed-form expression available for the vector function $\mathbf{X}(t; t_{fire}, \mathbf{X}_0)$, (6.29), in terms of time t , the firing time $\gamma(t)$,

the initial condition N_p , and the AA projectile parameters ((6.27),

(6.22)).

Thus, a numerical solution to the initial value problem (6.26) is computed using appropriate numerical methods ([6, 22, 27, 32, 44, 68, 77, 152, 156, 175]). Furthermore, all quantities given in (6.30)–(6.33) are computed numerically.

Table 6.1 Table of values of the drag coefficient ($X_{B_{10}}$ of the AA projectile and the corresponding Mach number $p_z = dq_z/dt$

$p_z = dq_z/dt$	$(X_{B_{10}})$
0	0.182
0.01	0.182
0.4	0.186
0.6	0.187
0.7	0.187
0.8	0.196
0.9	0.232
0.95	0.29
0.975	0.331
1	0.374
1.025	0.398
1.05	0.414

$p_z = dq_z/dt$	$(X_{B_{10}}$
1.1	0.407
1.2	0.389
1.35	0.365
1.5	0.347
2	0.287
2.5	0.239
3	0.204
3.5015	0.1773
4.0121	0.1652

6.3 Parameter Values for the Anti-Aircraft Projectile

The parameter values for a given 35 mm AA projectile are obtained ([8, 9]) and used in this work as follows.

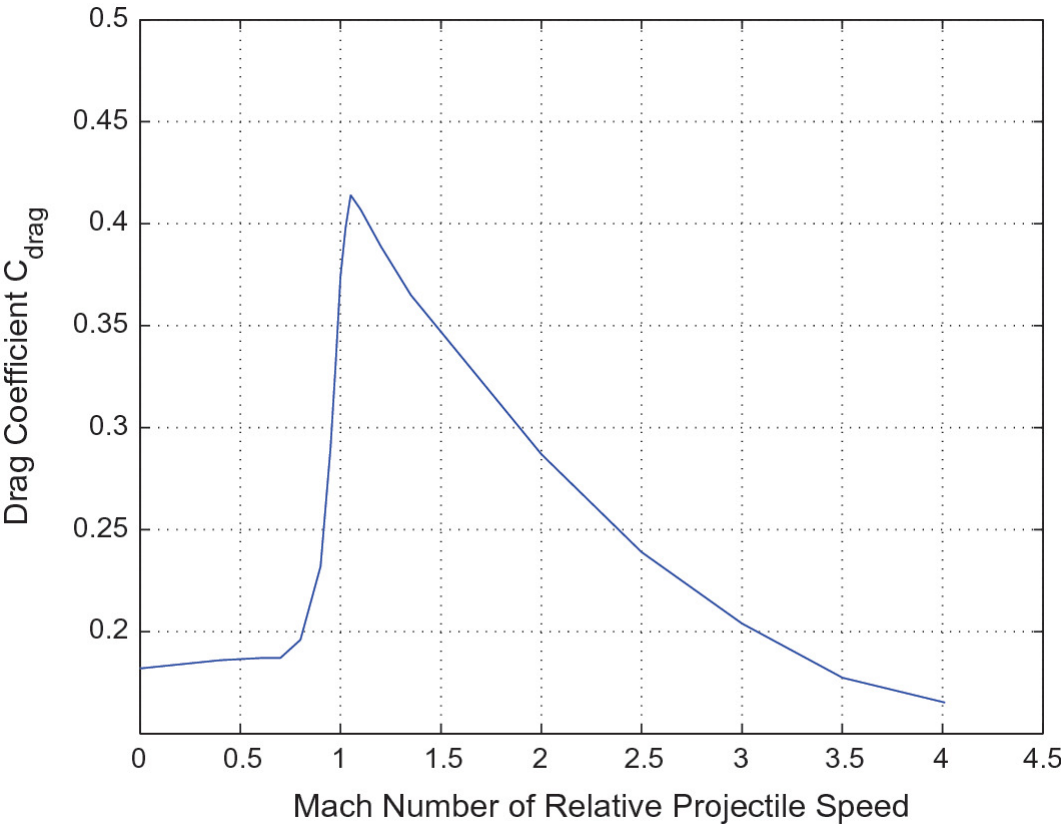


Fig. 6.2 Plot of the drag coefficient of the AA projectile, $(X_{B_{10}}$, versus Mach number,

$$p_z = dq_z/dt$$

1. The mass, (6.20), is

$$m_{proj} = 0.550 \text{ kg} . \quad (6.35)$$

2. The generic firing speed, (6.10), is

$$V_0 = 1180 \text{ m/s} . \quad (6.36)$$

3. The radius p_s and reference area B_5 , (6.22), are

$$a_b = \frac{35 \times 10^{-3}}{2} \text{ m} , \quad (6.37)$$
$$A_b = \pi a_b^2 = \pi(35 \times 10^{-3}/2)^2 \text{ m}^2 .$$

4. The numerical values of the drag coefficient, $(X_{B_{10}}$, at various Mach numbers, $p_z = dq_z/dt$, are given in Table 6.1. The afore-mentioned numerical values were obtained from data given in Table 2 of [9], and from the discrete data points plotted in Fig. 1(a) of [8]. A plot of the drag coefficient, $(X_{B_{10}}$, versus the Mach number, $p_z = dq_z/dt$, is shown in Fig. 6.2.

5. Linear interpolation is used to compute the value of the drag coefficient $(X_{B_{10}}$ for Mach numbers $p_z = dq_z/dt$ lying inbetween the data values given in Table 6.1.

6.4 Parameter Values for the Mobile ADS

The relevant parameter values for the mobile ADS are as follows.

1. The geometric parameters are given by (Chap. 3 and Fig. 6.1)

$$\mathbf{a}_{gun,ref}(t), d\mathbf{a}_{gun,ref}(t)/dt, d^2\mathbf{a}_{gun,ref}(t)/dt^2, \quad t \geq 0, \quad (6.38)$$

$$L_b = 1.6 \text{ m}, \quad h_b = 1.4 \text{ m}, \quad (6.39)$$

$$L_c = 3.3 \text{ m}, \quad \mathbf{h}_T = [0, 0.2, 1.3]^T \text{ m}, \quad (6.40)$$

$$\mathbf{h}_m = [0, 0, 0.2]^T \text{ m},$$

$$L_m = 2.8 \text{ m}, \quad L_g = 1.2 \text{ m}. \quad (6.41)$$

2. The AA gun fires a single AA projectile at a sequence of increasing elevation angles and at a fixed azimuth angle as follows

$$\mathbf{e}_{gun}(t_{fire}) \in \mathbf{A}_0, \quad \mathbf{a}_{gun}(t_{fire}) = \pi/2, \quad (6.42)$$

$$\mathbf{A}_0 = \{100 \text{ mils}, 200 \text{ mils}, \dots, 1500 \text{ mils}\},$$

where

$$6400 \text{ mils} = 2\pi \text{ radians}. \quad (6.43)$$

3. The mils firing time is $I_{wr3} > 0$ for all $\mathbf{e}_{gun}(t_{fire}) \in \mathbf{A}_0$, implying that the time of flight to ground impact is given by

$$\Delta_{tofG} = t_{hitG} - t_{fire} = t_{hitG}. \quad (6.44)$$

4. The mobile ADS is completely stationary for all times $t \in [t_{fire}, t_{hitG}]$, that is, it is in operational mode OM3 throughout the flight of the AA projectile implying that

$$\frac{d\mathbf{q}(t)}{dt} = \mathbf{0}_{15 \times 1} \Rightarrow \mathbf{q}(t) = \mathbf{q}(t_{fire}), \quad t \in [t_{fire}, t_{hitG}]. \quad (6.45)$$

5. It is assumed that the mobile ADS is positioned such that (see Fig 6.1)

$$(6.46)$$

$$x = y = 0, \quad \beta = 0, \quad \alpha_i = 0, \quad i = 1, 2, 3, 4, \\ \delta_j = 0, \quad j = 3, 4, v, \quad \alpha_s = 0.$$

It follows that the inertial position and velocity of the hinge point H of the AA gun are given by ((6.8), (6.13))

$$\mathbf{r}_H^{(I)}(t) = [0, 1.8, 2.9]^\top \text{ m}, \quad \mathbf{v}_H^{(I)}(t) = \mathbf{0}_{3 \times 1}, \\ t \in [t_{fire}, t_{hitG}]. \quad (6.47)$$

6. Using (2.163), (2.164), it follows that the AA gun azimuth and elevation angles γ and ζ are as follows

$$\gamma(t_{fire}) = 0, \quad \zeta(t_{fire}) = \mathbf{e}_{gun}(t_{fire}) \in \mathbf{A}_0. \quad (6.48)$$

7. It follows that the inertial position and velocity of the AA gun muzzle are given by

$$\mathbf{r}_{muz}^{(I)}(t) = \mathbf{r}_H^{(I)}(t_{fire}) + L_m \mathbf{J}_{B_7}^{(I)}(t_{fire}), \\ \mathbf{v}_{muz}^{(I)}(t) = \mathbf{0}_{3 \times 1}, \quad t \in [t_{fire}, t_{hitG}], \quad (6.49)$$

and that the initial inertial position and velocity of the AA projectile are given by ((6.27), (6.7), (6.11))

$$\mathbf{r}_{proj,0}^{(I)} = \mathbf{r}_H^{(I)}(t_{fire}) + L_m \mathbf{J}_{B_7}^{(I)}(t_{fire}), \\ \mathbf{v}_{proj,0}^{(I)} = V_0 \mathbf{J}_{B_7}^{(I)}(t_{fire}), \quad (6.50)$$

where

$$\mathbf{J}_{B_7}^{(I)}(t_{fire}) = \begin{bmatrix} 0 \\ \cos(\mathbf{e}_{gun}(t_{fire})) \\ \sin(\mathbf{e}_{gun}(t_{fire})) \end{bmatrix}. \quad (6.51)$$

At time $\gamma(t)$ all the generalized co-ordinates in \mathbf{q} are equal to zero

except for ζ , (6.48), ζ_0 , (2.140).

8.

For each AA gun elevation angle $\mathbf{e}_{gun}(t_{fire}) \in \mathbf{A}_0$, the corresponding initial inertial position and velocity, $\mathbf{r}_{proj,0}^{(I)}$, $\mathbf{v}_{proj,0}^{(I)}$, are computed.

Some of the computed values are as follows.

$\zeta(t_{fire}) = \mathbf{e}_{gun}(t_{fire}) = 100$ mils :

$$\begin{aligned}\mathbf{r}_{proj,0}^{(I)} &= [0, 4.58652, 3.17445]^\top \text{ m}, \\ \mathbf{v}_{proj,0}^{(I)} &= [0, 1174.32, 115.66]^\top \text{ m/s},\end{aligned}\tag{6.52}$$

$\zeta(t_{fire}) = \mathbf{e}_{gun}(t_{fire}) = 100$ mils :

$$\begin{aligned}\mathbf{r}_{proj,0}^{(I)} &= [0, 3.7799, 4.8799]^\top \text{ m}, \\ \mathbf{v}_{proj,0}^{(I)} &= [0, 834.386, 834.386]^\top \text{ m/s},\end{aligned}\tag{6.53}$$

$\zeta(t_{fire}) = \mathbf{e}_{gun}(t_{fire}) = 1500$ mils :

$$\begin{aligned}\mathbf{r}_{proj,0}^{(I)} &= [0, 4.58652, 3.17445]^\top \text{ m}, \\ \mathbf{v}_{proj,0}^{(I)} &= [0, 1174.32, 115.66]^\top \text{ m/s},\end{aligned}\tag{6.54}$$

6.5 Computation of the AA Projectile Trajectory with No Wind

In this case it is assumed that there is no wind,

$$\mathbf{V}_{wind}^{(I)} = \mathbf{0}_{3 \times 1}.\tag{6.55}$$

Since there is no wind, it follows that for each AA gun elevation angle the AA projectile trajectory will lie in the inertial (Y, Z) plane. The trajectory is computed by solving the initial value problem (6.26)

numerically for A_{red} , $t \in [t_{fire}, t_{hitG}]$, using a fourth order Runge-Kutta algorithm with a fixed time-step $(A_{red}) = 11$ s ([27, 44, 68, 77, 156]).

The numerical solution of the initial value problem is sequentially computed at discrete times in the following set

$$\begin{aligned}\mathcal{T}_c &= \{t_{fire}, t_{fire} + \Delta_{sim}, t_{fire} + 2\Delta_{sim}, \dots, t_{max}\}, \\ t_{max} &= t_{fire} + N_{sim}\Delta_{sim},\end{aligned}\tag{6.56}$$

where t_{max} is chosen such that it is greater than the largest possible

value of Q_{Cj} , (6.3), (6.4), for all $e_{gun}(t_{fire}) \in A_0$, and such that

$t_{max} - t_{fire}$ is an integer multiple X_{B11} of Δ_{sim} . In this case, $(x_1 + j_c y_1)$

s.

In particular, the computations are performed as follows. Consider the time interval $\mathcal{T}_{c,i}$ defined by the i th consecutive pair of times in \mathcal{T}_c ,

(6.56),

$$\begin{aligned}\mathcal{T}_{c,i} &= (t_{fire} + i\Delta_{sim}, t_{fire} + (i + 1)\Delta_{sim}], \\ i &= 0, 1, 2, \dots, N_{sim} - 1.\end{aligned}\tag{6.57}$$

At the end of each time interval $\mathcal{T}_{c,i}$, $i = 0, 1, 2, \dots, N_{sim} - 1$, and having

computed $r_{proj}^{(I)}(t_{fire} + (i + 1)\Delta_{sim})$ and other variables of interest at

time $t_{fire} + (i + 1)\Delta_{sim}$, the Runge-Kutta algorithm programmatically

calls a suitable algorithm (in this case, an advanced regula falsi based algorithm implemented in the MATLAB function `odezero`, [32, 110,

120]) in order to find the first time $t \in \mathcal{T}_{c,i}$ where $r_{projz}^{(I)}(t) \leq 0$,

$v_{projz}^{(I)}(t) < 0$. If such a time t can be found then the ground impact time

is $j = 1, 2$. The trajectory of the AA projectile is stopped at time Q_{Cj} .

Thus, the numerical solution of the initial value problem is actually computed on the following set of times

$$\{t_{fire}, t_{fire} + \Delta_{sim}, t_{fire} + 2\Delta_{sim}, \dots, t_{fire} + N_e\Delta_{sim}, t_{hitG}\}, \quad (6.58)$$

$$N_e = \text{ceil}((t_{hitG} - t_{fire})/\Delta_{sim}) - 1.$$

In general, the length of the time horizon $(t_{hitG} - t_{fire})$ is not an integer multiple of the time-step Δ_{sim} with the result that the last time-step is less than Δ_{sim} .

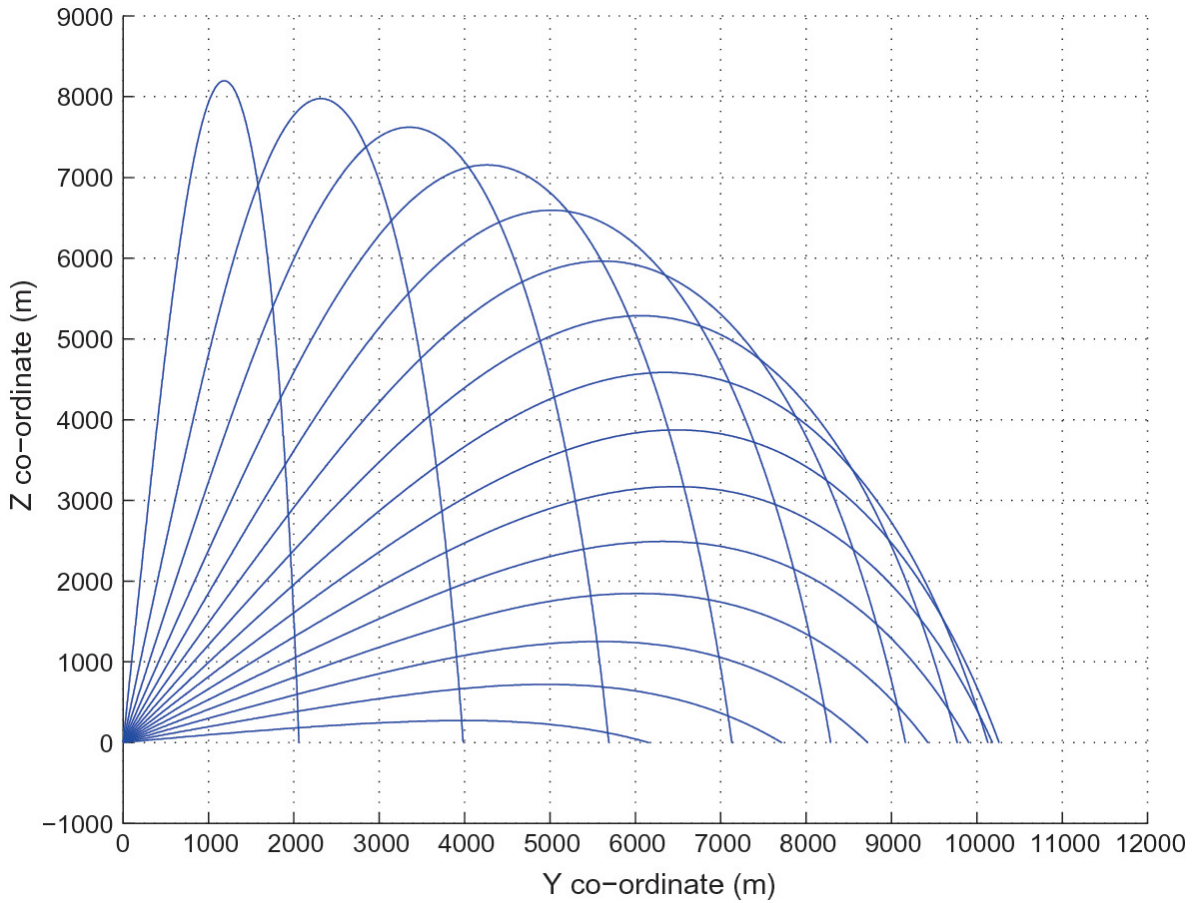


Fig. 6.3 Plot of the AA projectile trajectories, that is, $r_{projz}^{(l)}(t)$ versus $r_{projy}^{(l)}(t)$, $t \in [t_{fire}, t_{hitG}]$, for AA gun elevation angle $e_{gun}(t_{fire}) \in A_0$: with no wind

Table 6.2 Table of values of the AA gun elevation angle $a_{gun}(t_{fire})$ (mils) and the variables $T_{\delta_v} \mathbf{I}_3$ (s), r_d (m), $s(t_{hitG})$ (m), $\mathbf{v}_{proj}^{(I)}(t_{hitG})$ (m/s), $\mathcal{E}_{proj}(t_{hitG})$ (J), $\max_t r_{projz}^{(I)}(t)$ (m), $r_{projx}^{(I)}(t_{hitG})$ (m) (abridged headings shown below): with no wind

a_{gun} (mils)	$T_{\delta_v} \mathbf{I}_3$ (s)	r_d (m)	s (m)	$\mathbf{v}_{proj}^{(I)}$ (m/s)	\mathcal{E}_{proj} (J)	$\max_t r_{projz}^{(I)}$ (m)	$F_{drag}^{(I)}$ (m)
100.0	14.03	6155.70	6191.29	224.81	13898.43	273.50	0.00
200.0	22.38	7712.13	7903.52	188.13	9733.50	721.71	0.00
300.0	29.51	8719.59	9213.11	181.59	9068.54	1253.35	0.00
400.0	36.02	9424.58	10372.89	185.12	9423.63	1847.94	0.00
500.0	42.10	9903.14	11456.28	192.01	10138.46	2491.27	0.00
600.0	47.86	10180.30	12482.83	199.60	10956.32	3170.62	0.00
700.0	53.31	10258.36	13448.76	206.82	11763.25	3872.94	0.00
800.0	58.45	10127.05	14337.72	213.29	12510.03	4583.87	0.00
900.0	63.24	9768.63	15125.87	218.87	13174.09	5287.10	0.00
1000.0	67.63	9161.94	15785.85	223.59	13748.12	5964.03	0.00
1100.0	71.53	8287.02	16291.33	227.49	14231.78	6593.88	0.00
1200.0	74.88	7129.69	16622.41	230.63	14627.01	7154.26	0.00
1300.0	77.60	5688.62	16773.49	232.90	14916.18	7622.24	0.00
1400.0	79.60	3982.85	16762.69	234.40	15108.83	7976.03	0.00
1500.0	80.83	2059.08	16644.19	235.27	15222.23	8197.07	0.00

In subsequent Chapters the Runge-Kutta algorithm is applied in order to solve numerically sets of nonlinear ODEs over time horizons whose lengths are not an integer multiple of the fixed time-step. Thus, the numerical solutions are computed on sets of times that have a structure that is equivalent to (6.58). In order to simplify the presentation the sets of times will be represented in a form analogous to the following

$$\{t_{fire}, t_{fire} + \Delta_{sim}, \dots, t_{hitG}\}, \quad (6.59)$$

and reference will be made to (6.59).

The computed AA projectile trajectories are shown in Fig. 6.3. The ground distance from the AA gun muzzle to the ground impact point, r_d , (6.30), is given in Table 6.2 and shown in Fig. 6.4. Additional results of interest are shown in Figs. 6.4, 6.5, 6.6, 6.7, 6.8, 6.9, 6.10 and 6.11.

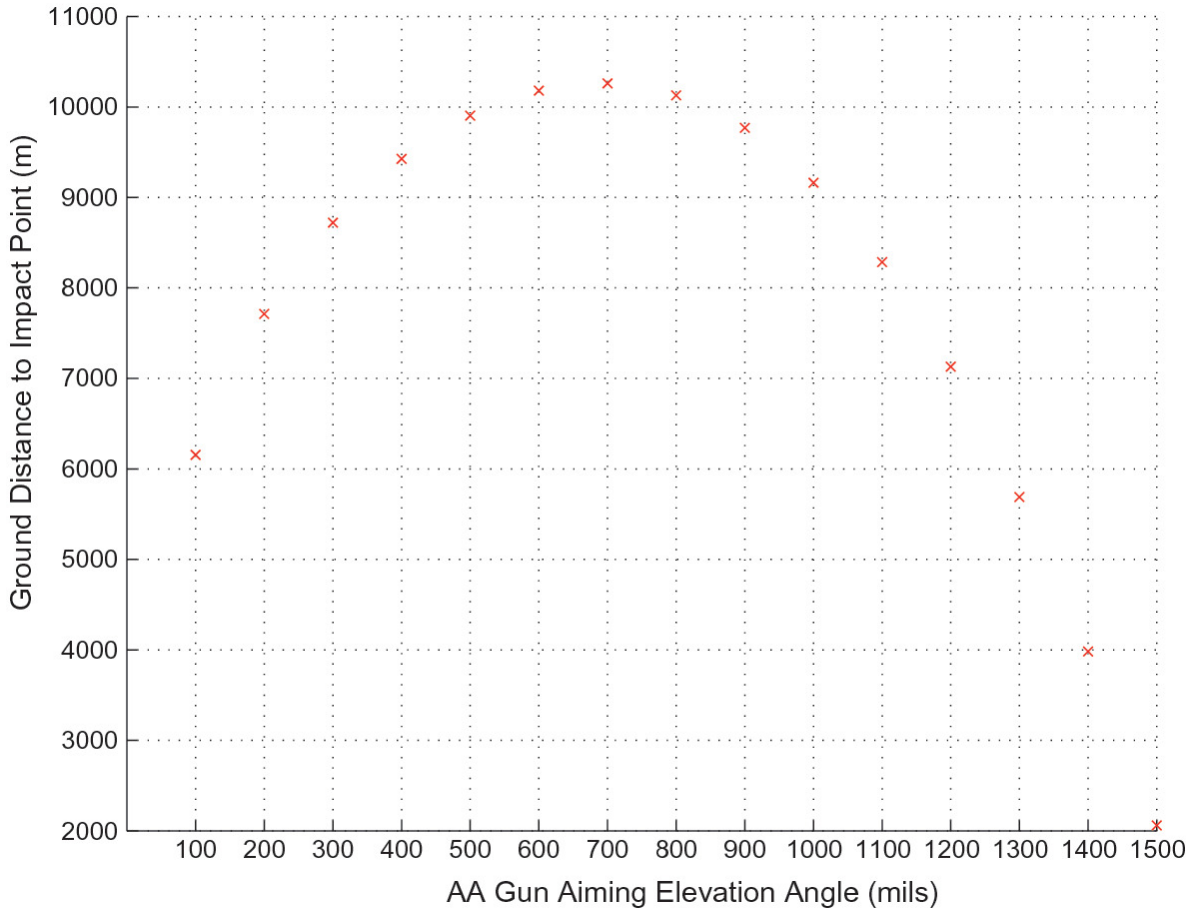


Fig. 6.4 Plot of ground distance to AA projectile ground impact point r_d versus AA gun elevation angle $e_{gun}(t_{fire}) \in A_0$: with no wind

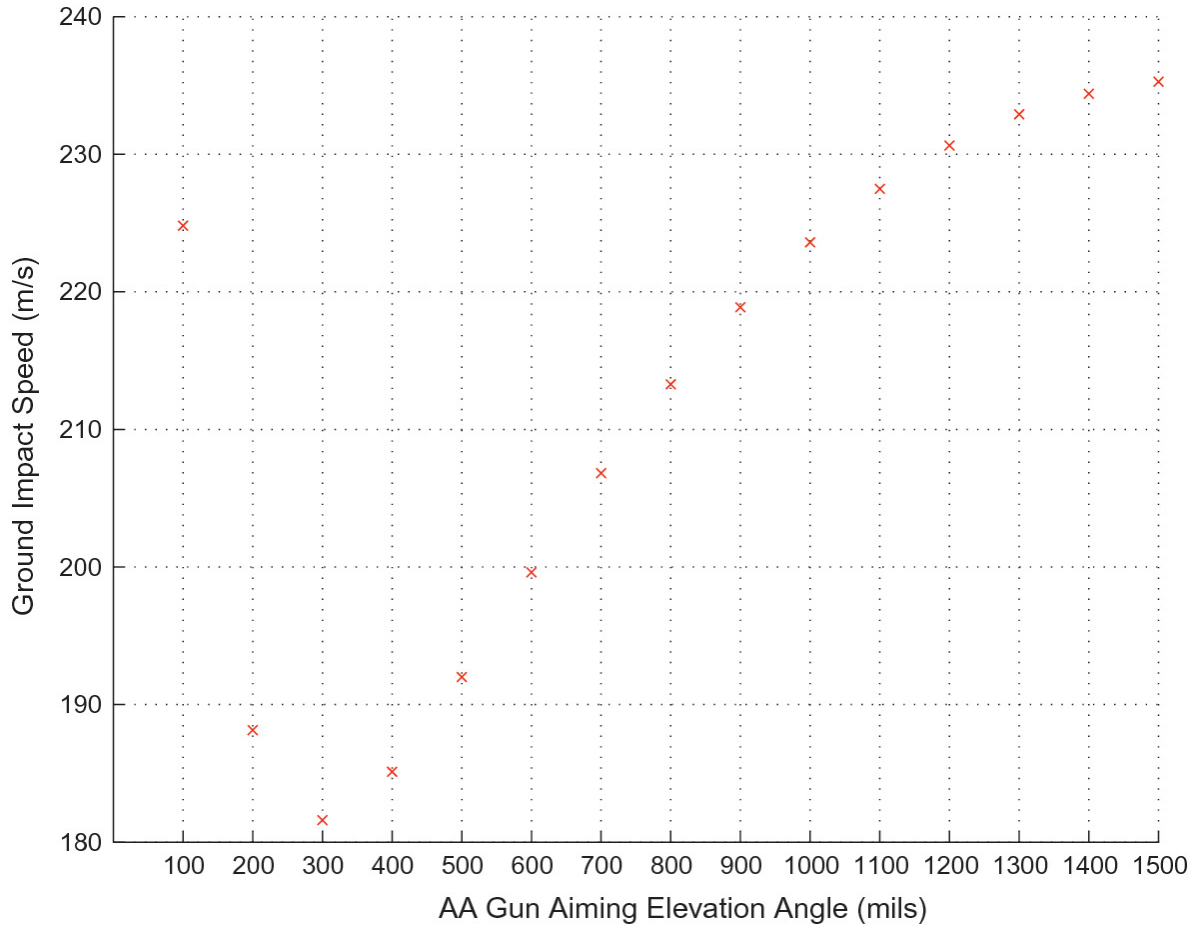


Fig. 6.5 Plot of AA projectile ground impact speed $\|\mathbf{v}_{proj}^{(I)}(t_{hitG})\|$ versus AA gun elevation angle

$\mathbf{e}_{gun}(t_{fire}) \in A_0$: with no wind

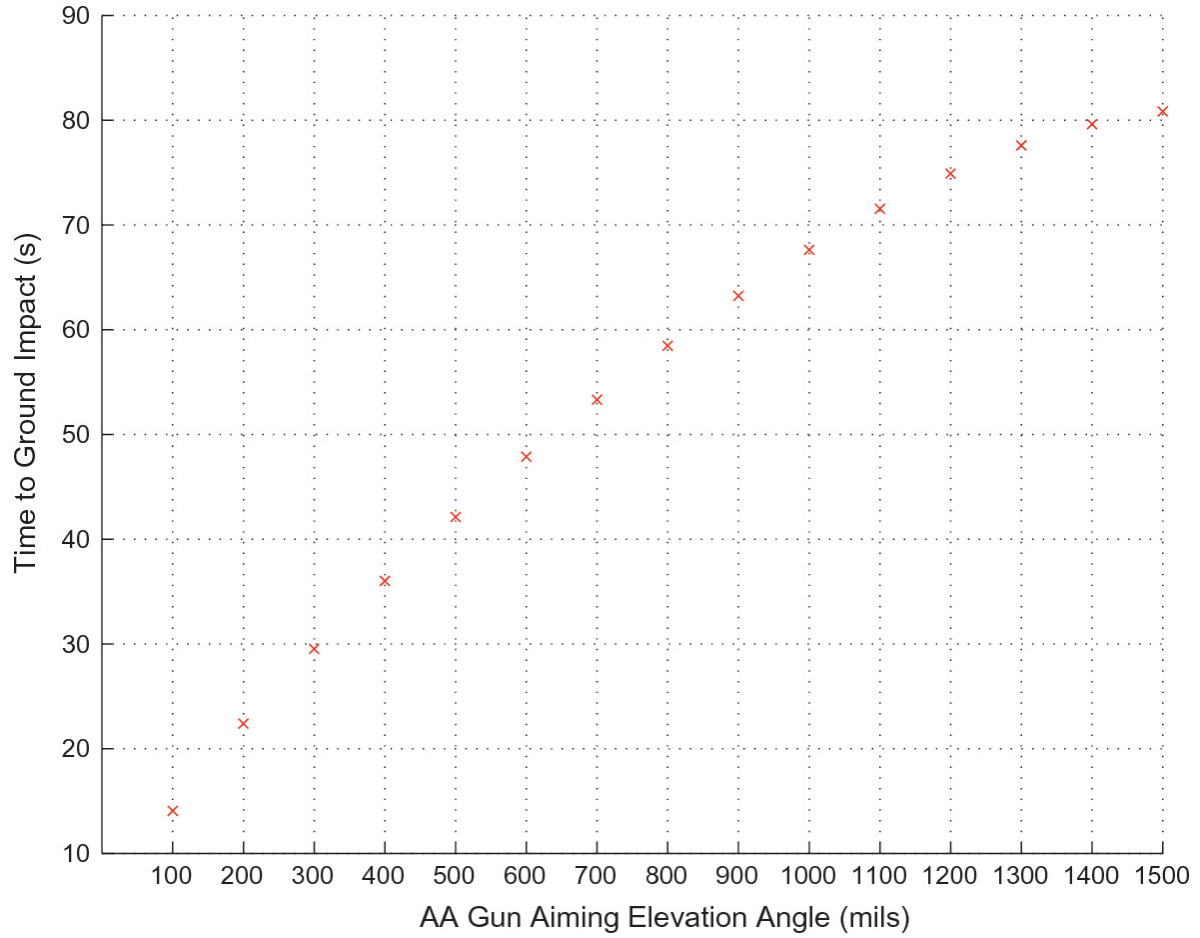


Fig. 6.6 Plot of AA projectile time of flight to ground impact $\Delta_{tofG} = t_{hitG} - t_{fire} = t_{hitG}$ versus AA gun elevation angle $e_{gun}(t_{fire}) \in A_0$: with no wind

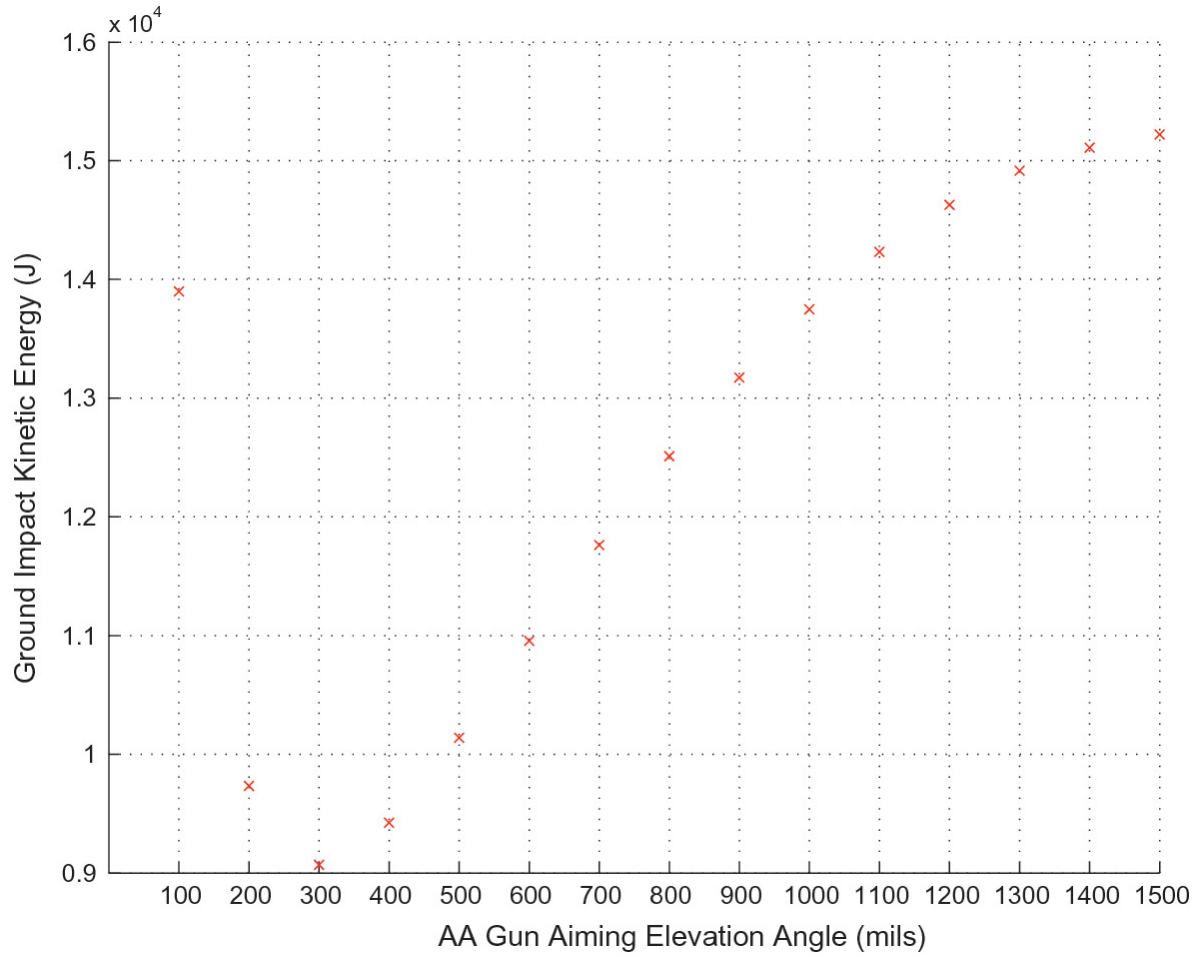


Fig. 6.7 Plot of AA projectile kinetic energy at ground impact $\mathcal{E}_{proj}(t_{hitG})$ versus AA gun elevation angle $e_{gun}(t_{fire}) \in A_0$: with no wind

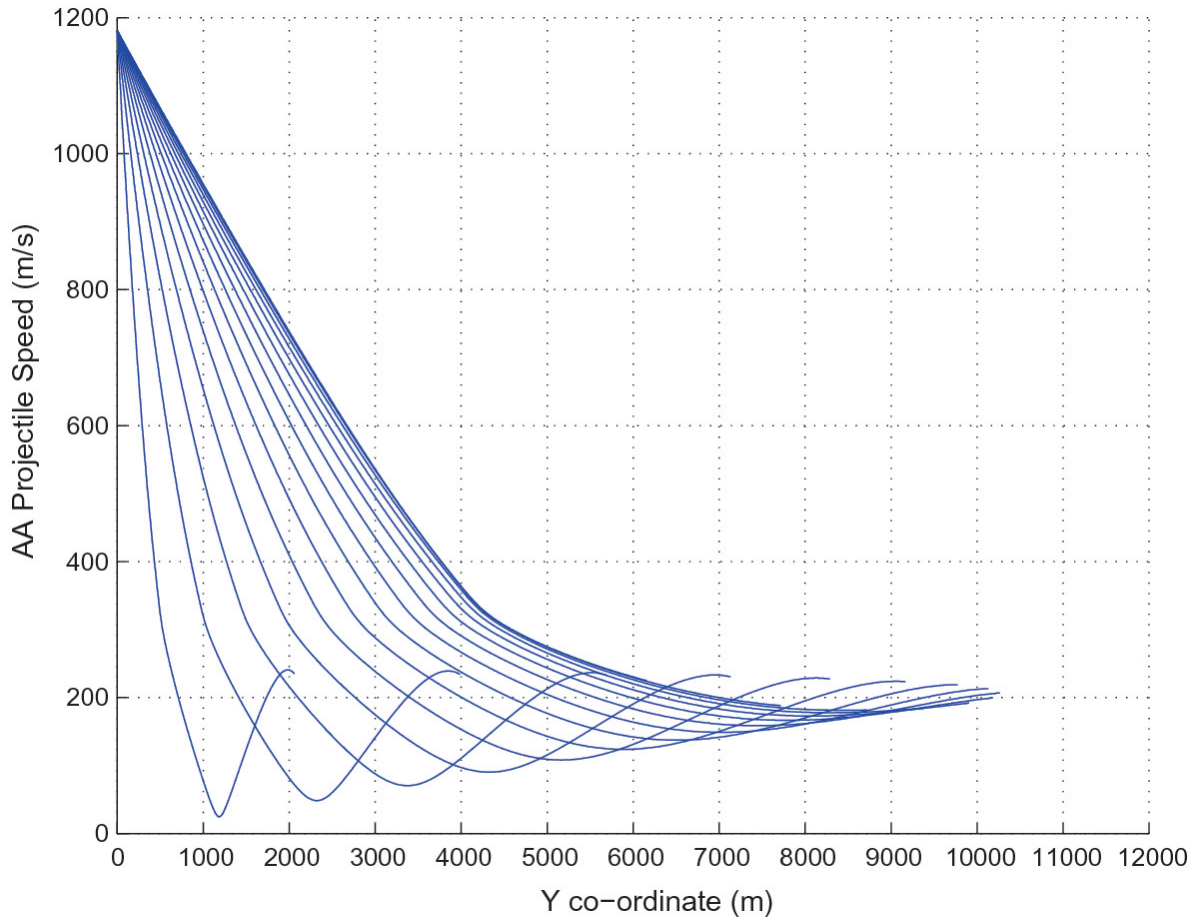


Fig. 6.8 Plot of AA projectile speed $\|\mathbf{v}_{proj}^{(I)}(t)\|$ versus $r_{proj}^{(I)}(t)$, $t \in [t_{fire}, t_{hitG}]$, for AA gun elevation angle $e_{gun}(t_{fire}) \in A_0$ (plots for increasing $a_{gun}(t_{fire})$ are towards lower left): with no wind

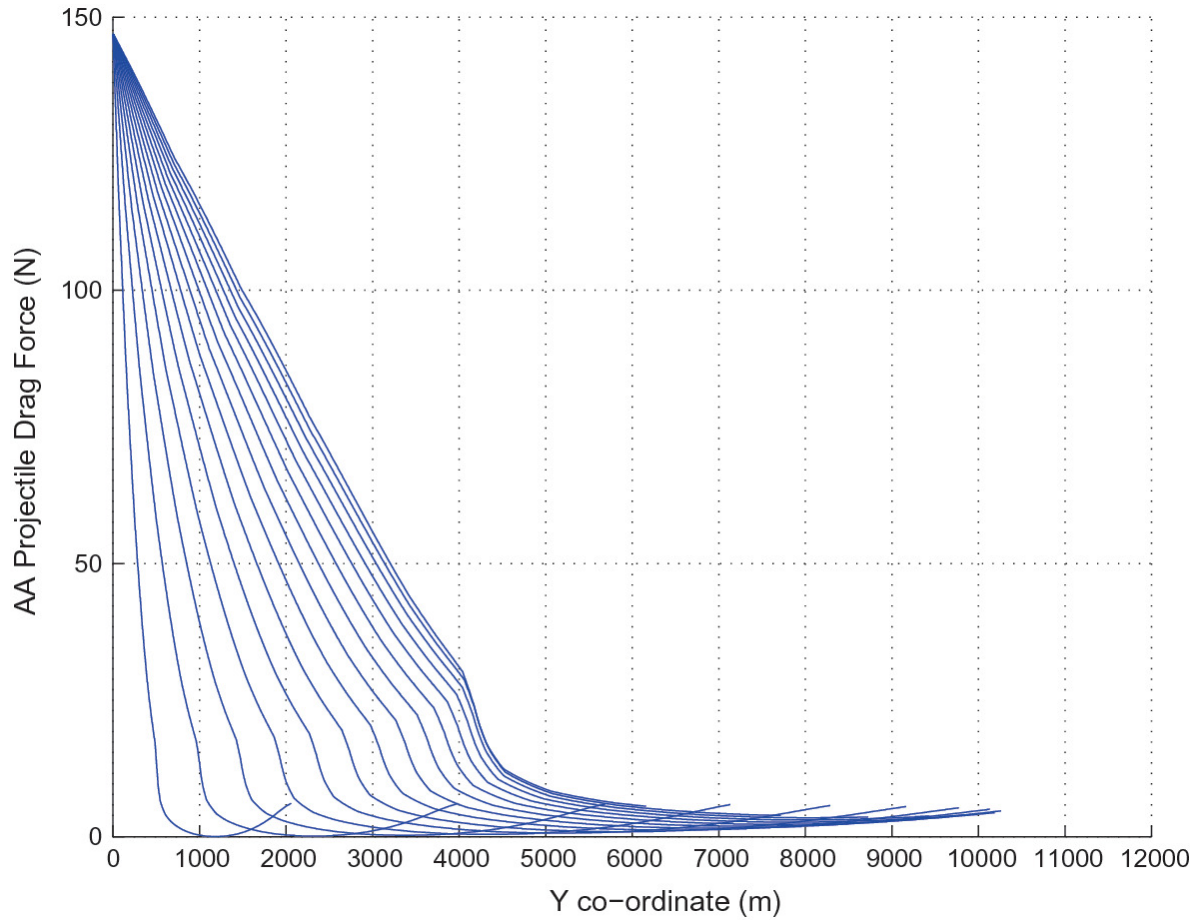


Fig. 6.9 Plot of AA projectile aerodynamic drag force magnitude $\|F_{drag}(t)\|$ versus $r_{proj}^{(l)}(t)$, $t \in [t_{fire}, t_{hitG}]$, for AA gun elevation angle $\alpha_{gun}(t_{fire}) \in A_0$ (plots for increasing $\alpha_{gun}(t_{fire})$ are towards lower left): with no wind

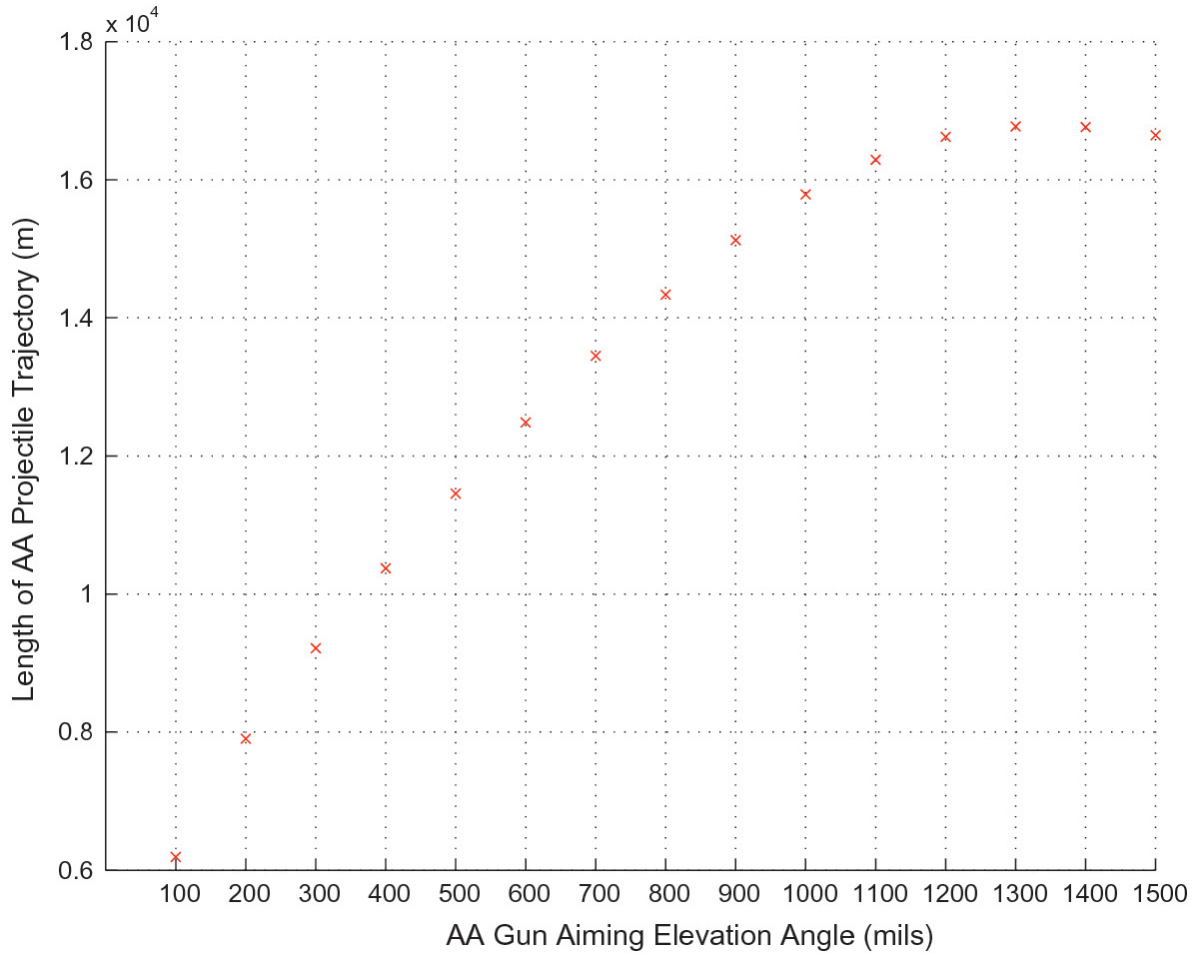


Fig. 6.10 Plot of the total length of the AA projectile trajectory $s(t_{hitG})$ versus the AA gun elevation angle $e_{gun}(t_{fire}) \in A_0$: with no wind

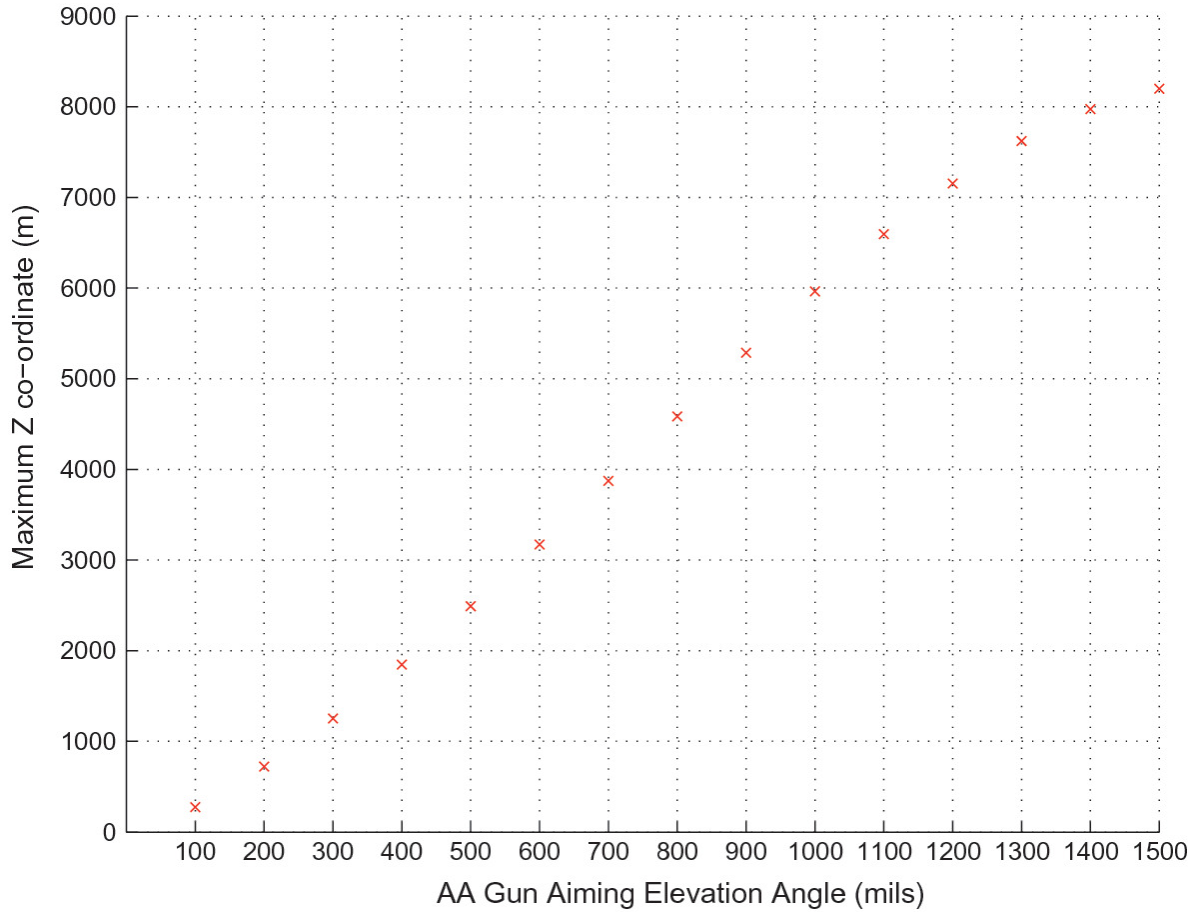


Fig. 6.11 Plot of the maximum of the AA projectile Z co-ordinate $r_{projz}^{(t)}(t)$ over time t ,

$t \in [t_{fire}, t_{hitG}]$, versus the AA gun elevation angle $e_{gun}(t_{fire}) \in A_0$: with no wind

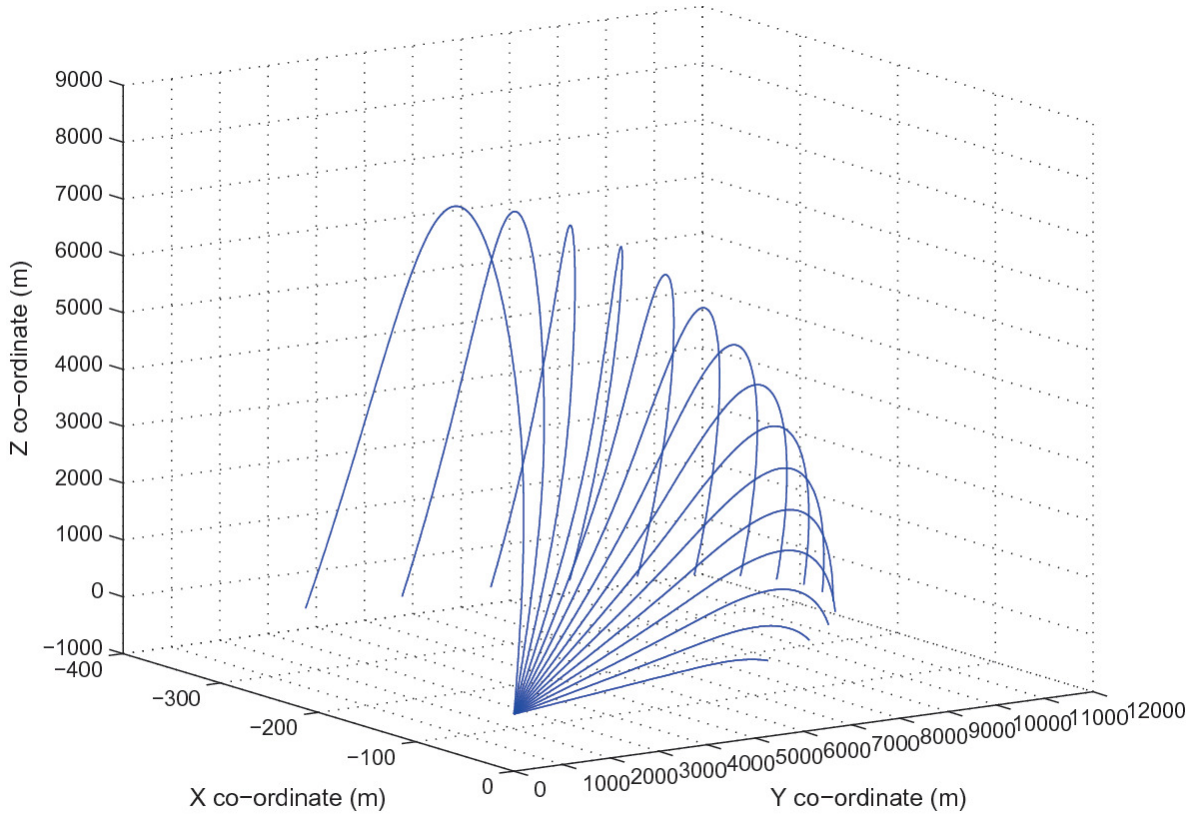


Fig. 6.12 Plot of the three-dimensional AA projectile trajectories, that is, $r_{projz}^{(I)}(t)$ versus $r_{projx}^{(I)}(t)$ and $r_{projy}^{(I)}(t)$, $t \in [t_{fire}, t_{hitG}]$, for AA gun elevation angle $e_{gun}(t_{fire}) \in A_0$: with a cross wind

6.6 Computation of the AA Projectile Trajectory with a Cross Wind

In this case it is assumed that there is a cross wind given by

$$\mathbf{V}_{wind}^{(I)} = [-5, 0, 0]^T \text{ m/s} . \quad (6.60)$$

Due to the direction of the cross wind, the AA projectile moves to the left of the inertial (Y, Z) plane (when looking in the direction of the positive Y axis) and impacts the second quadrant of the inertial (X, Y) plane. The computed trajectories are plotted in Fig. 6.12. The inertial (X, Y) plane co-ordinates of the ground impact points are shown in Fig. 6.14.

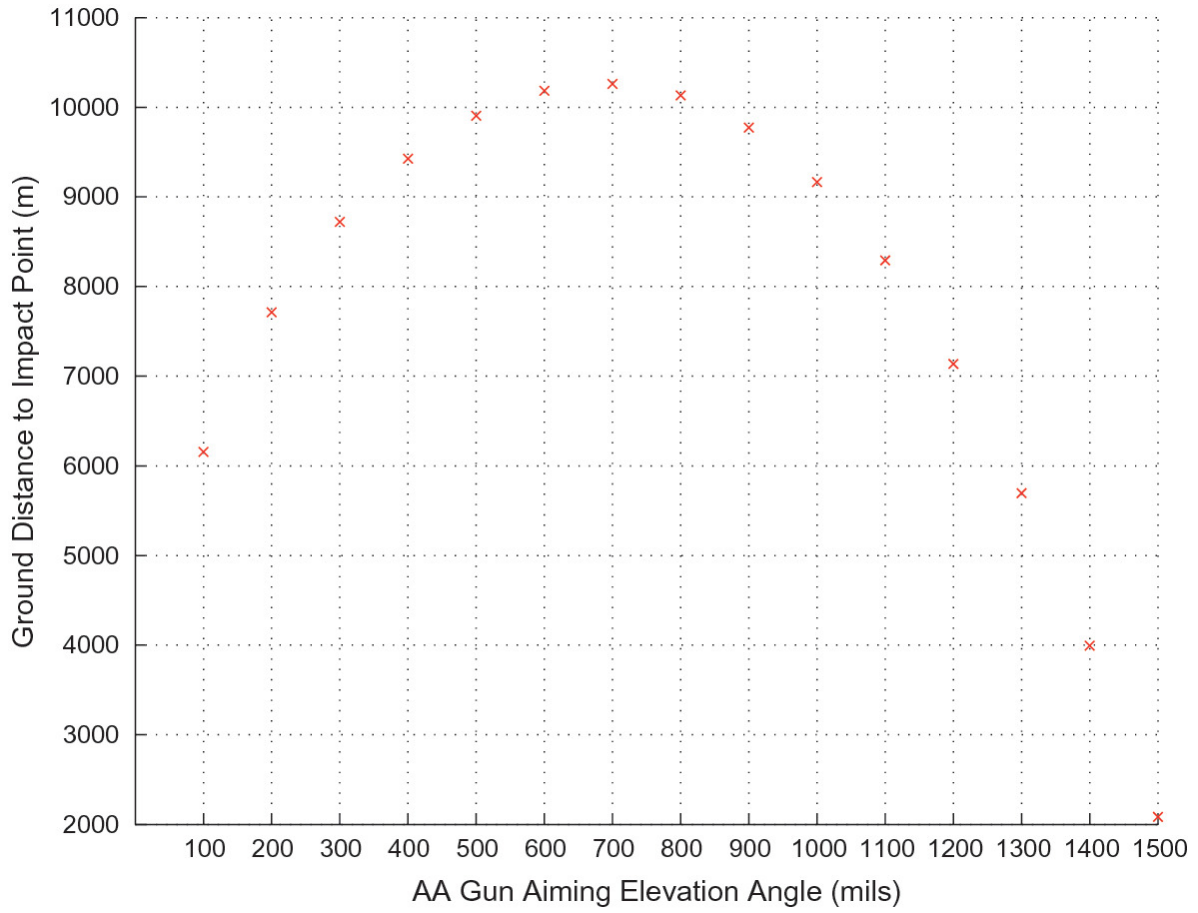


Fig. 6.13 Plot of ground distance to AA projectile ground impact point r_d versus AA gun elevation angle $e_{gun}(t_{fire}) \in A_0$: with a cross wind

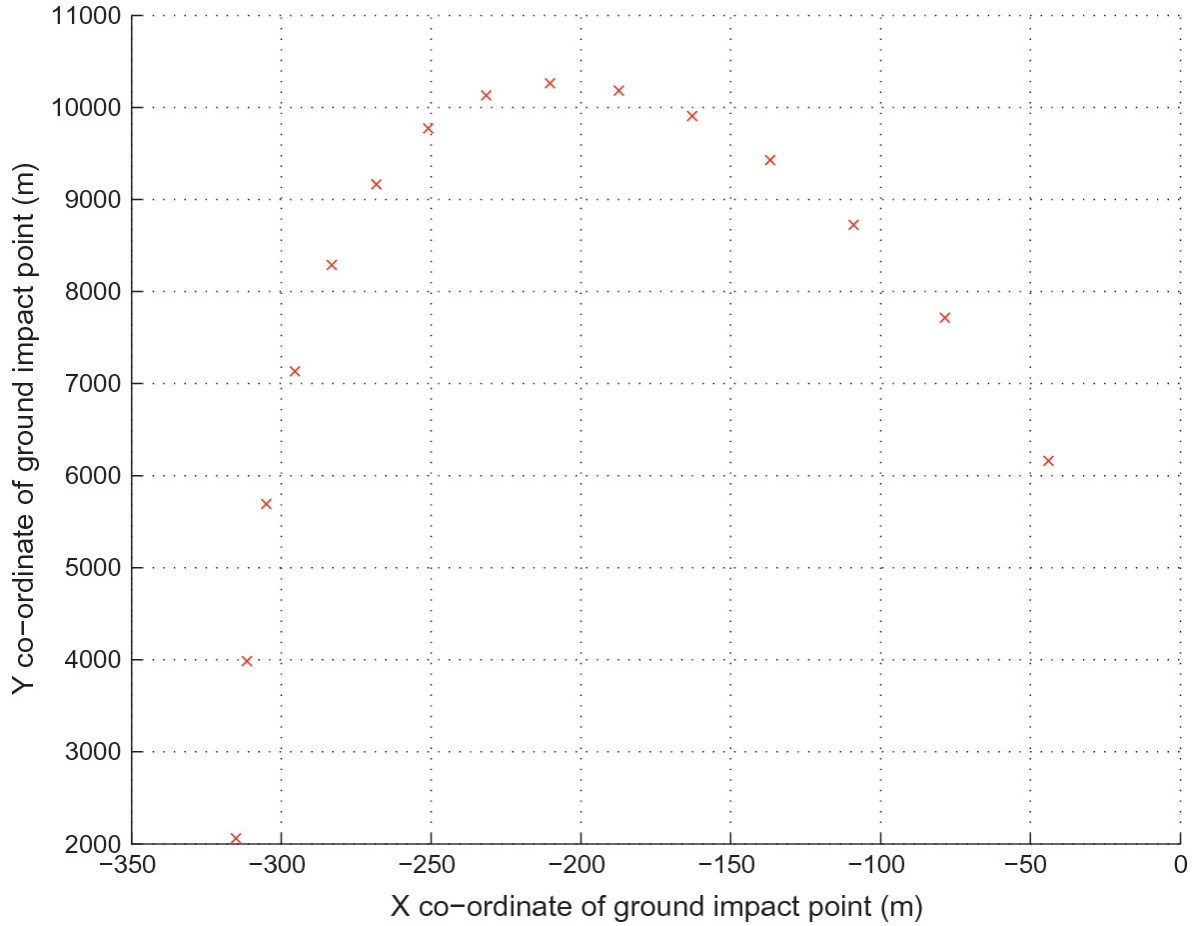


Fig. 6.14 Plot of Y co-ordinate $r_{projy}^{(I)}(t_{hitG})$ versus X co-ordinate $r_{projx}^{(I)}(t_{hitG})$ of the AA projectile ground impact inertial position for AA gun elevation angle $e_{gun}(t_{fire}) \in A_0$ (impact points for increasing $a_{gun}(t_{fire})$ are towards the left): with a cross wind

Table 6.3 Table of values of the AA gun elevation angle $a_{gun}(t_{fire})$ (mils) and the variables $T_{\delta_v} I_3$ (s), r_d (m), $s(t_{hitG})$ (m), $v_{proj}^{(I)}(t_{hitG})$ (m/s), $\mathcal{E}_{proj}(t_{hitG})$ (J), $\max_t r_{projz}^{(I)}(t)$ (m), $r_{projx}^{(I)}(t_{hitG})$ (m) (abridged headings shown below): with a cross wind

a_{gun} (mils)	$T_{\delta_v} I_3$ (s)	r_d (m)	s (m)	$v_{proj}^{(I)}$ (m/s)	\mathcal{E}_{proj} (J)	$\max_t r_{projz}^{(I)}$ (m)	$F_{drag}^{(I)}$ (m)
100.0	14.03	6155.84	6191.53	224.85	13902.83	273.50	-43.96
200.0	22.38	7712.50	7904.11	188.18	9738.51	721.70	-43.96

a_{gun} (mils)	$T_{\delta_v} I_3$ (s)	r_d (m)	s (m)	$v_{proj}^{(I)}$ (m/s)	\mathcal{E}_{proj} (J)	$\max_t r_{projz}^{(I)}$ (m)	$F_{drag}^{(I)}$ (m)
300.0	29.51	8720.23	9214.05	181.65	9073.87	1253.35	-108.96
400.0	36.02	9425.52	10374.16	185.17	9429.16	1847.93	-108.96
500.0	42.10	9904.42	11457.87	192.06	10144.13	2491.26	-108.96
600.0	47.85	10181.95	12484.71	199.66	10962.08	3170.61	-187.39
700.0	53.31	10260.43	13450.92	206.87	11769.09	3872.92	-187.39
800.0	58.45	10129.61	14340.14	213.34	12515.92	4583.85	-108.96
900.0	63.24	9771.76	15128.55	218.92	13180.02	5287.07	-108.96
1000.0	67.63	9165.77	15788.79	223.64	13754.06	5963.99	-108.96
1100.0	71.53	8291.76	16294.56	227.54	14237.72	6593.84	-187.39
1200.0	74.88	7135.72	16625.96	230.67	14632.95	7154.21	-108.96
1300.0	77.60	5696.70	16777.45	232.94	14922.10	7622.19	-108.96
1400.0	79.60	3994.94	16767.23	234.44	15114.74	7975.97	-108.96
1500.0	80.83	2083.01	16649.77	235.32	15228.11	8197.01	-108.96

The ground distance to the ground impact point, r_d , is shown in Fig. 6.13. It turns out that for AA gun elevation angles of approximately 400 mils and larger the ground distance to the ground impact point gradually increases relative to the case with no wind, see Table 6.3. The rest of the results are broadly similar to the results obtained for the case with no wind and are not shown here in order to save space.

7. The Fire Control Problem

Constantinos Frangos¹ 

(1) Electrical Engineer working in Decision and Control, Pretoria,
South Africa

 **Constantinos Frangos**

Email: cfrangos123@gmail.com

This Chapter deals with the formulation and numerical solution of a conceptual fire control problem FCA as follows.

1. Fire control problem FCA involves the specification of a finite number of intercept times of the AA projectile with the CM of the AAT, $t \geq 0$, $k = 1, 2, \dots, n_f$. The associated firing times $t \geq 0$, $k = 1, 2, \dots, n_f$, are obtained as shown below.
2. For each given intercept time $t \geq 0$ the following quantities are computed.
 - a. The inertial azimuth and elevation angles of the fire control vector, $\mathbf{a}_{FC}(t_{fire,k})$, $\mathbf{a}_{FC}(t_{fire,k})$. At time $t \geq 0$, the aiming azimuth and elevation angles of the AA gun are equal to $\mathbf{a}_{FC}(t_{fire,k})$ and $\mathbf{a}_{FC}(t_{fire,k})$, respectively.
 - b. The time of flight of the AA projectile to the CM of the AAT, $\Delta_{tofC,k}$.

c. It follows that the firing time of the AA projectile is

$$t_{fire,k} = t_{hitC,k} - \Delta_{tofC,k}.$$

The fire control problem is also formulated using feasible control.

7.1 Fire Control Problem FCA

The mobile ADS engages the AAT over a finite time horizon \mathcal{T}_F ,

$$\mathcal{T}_F = [t_0, t_{FIN}], \quad t_0 < t_{FIN}, \quad (7.1)$$

In order to establish an upper limit on the performance of the mobile ADS an ideal case is assumed. In particular, it is assumed that the inertial trajectories of the CM of the AAT and the inertial trajectories of the hinge point H of the AA gun are given. In practical applications, error-prone estimation algorithms and noisy sensors are employed in order to estimate the motion of the AAT relative to the mobile ADS. This will inevitably lead to reduced performance compared to the ideal case considered here.

The position, velocity and acceleration trajectories of the center of mass of the AAT are denoted as follows

$$\mathbf{r}_{targ}^{(I)}(t), \quad \frac{d_I \mathbf{r}_{targ}^{(I)}(t)}{dt}, \quad \frac{d_I^2 \mathbf{r}_{targ}^{(I)}(t)}{dt^2}, \quad t \in \mathcal{T}_F. \quad (7.2)$$

Given the reference trajectories for the mobile ADS, (5.1)–(5.7). Then, the closed loop trajectories of the vehicle system $\mathbf{q}_1(t)$, $\mathbf{q}_1(t)$, $d\mathbf{p}_1(t)/dt$, are computed by using (4.75)–(4.79), (3.33)–(3.34), leading to the computation of the trajectories

$$x(t), y(t), \beta(t), \dot{x}(t), \dot{y}(t), \dot{\beta}(t), \ddot{x}(t), \ddot{y}(t), \ddot{\beta}(t), \quad t \in \mathcal{T}_F. \quad (7.3)$$

Using the above, it is possible to compute the trajectory of the hinge point H of the AA gun, together with the first and second order time derivatives, given by

$$\mathbf{r}_H^{(I)}(t), \quad \frac{d_I \mathbf{r}_H^{(I)}(t)}{dt}, \quad \frac{d_I^2 \mathbf{r}_H^{(I)}(t)}{dt^2}, \quad t \in \mathcal{T}_F, \quad (7.4)$$

and to compute various other quantities of interest (Chaps. 2 and 3).

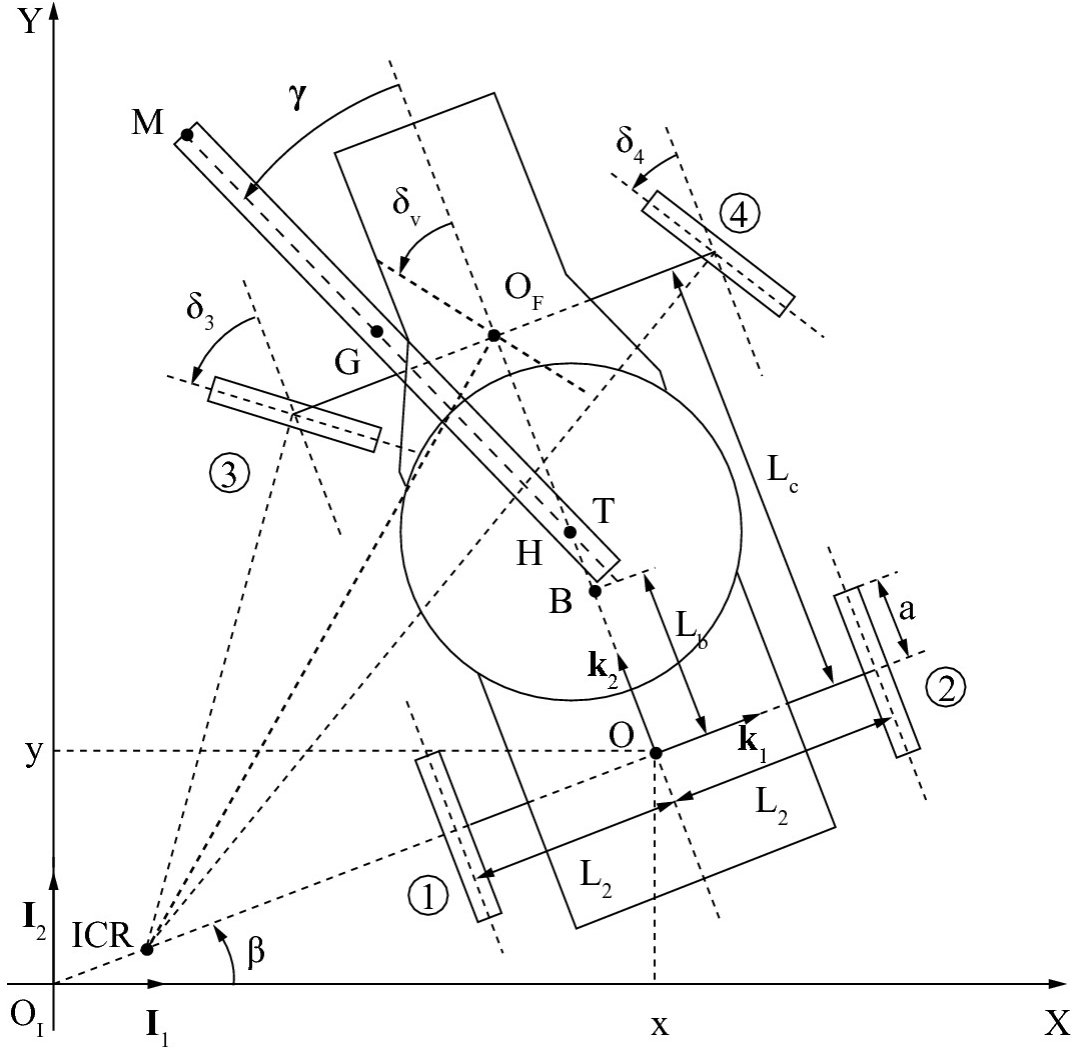


Fig. 7.1 Schematic of the mobile air defence system

It is assumed throughout that the vehicle body of the mobile ADS is not rotating relative to the inertial reference frame I and that it is in either one of the following two states.

1. The vehicle body is completely stationary implying that

$$(7.5)$$

$$\mathbf{r}_H^{(I)}(t) = \mathbf{r}_H^{(I)}(t_0), \quad \frac{d_I \mathbf{r}_H^{(I)}(t)}{dt} = \frac{d_I^2 \mathbf{r}_H^{(I)}(t)}{dt^2} = \mathbf{0}_{3 \times 1},$$

$$t \in \mathcal{T}_F.$$

2. The vehicle body is moving forward at a constant speed k_0 and in a straight line that coincides with the longitudinal axis (Z_{B_5} axis) of the vehicle body, Fig. 7.1, implying that

$$\frac{d_I^2 \mathbf{r}_H^{(I)}(t)}{dt^2} = \mathbf{0}_{3 \times 1}, \quad \frac{d_I \mathbf{r}_H^{(I)}(t)}{dt} = \mathbf{v}_H^{(I)} = \begin{bmatrix} v_b \cos(\beta_b + \pi/2) \\ v_b \sin(\beta_b + \pi/2) \\ 0 \end{bmatrix}, \quad (7.6)$$

$$t \in \mathcal{T}_F,$$

and where $\beta(t) = \beta_b =$ a fixed angle, $t \in \mathcal{T}_F$.

The formulation of fire control problem FCA is based on the following assumptions and methods.

1. Given a finite number n_f of intercept times of the AA projectile with the center of mass of the AAT, $t \geq 0$, $k = 1, 2, \dots, n_f$,

$$t_0 \leq t_{hitC,1} < t_{hitC,2} < \dots < t_{hitC,n_f-1} < t_{hitC,n_f} \leq t_{FIN}. \quad (7.7)$$

In this work the first and final intercept times are chosen as follows

$$t_{hitC,1} = 0, \quad t_{hitC,n_f} = t_{FIN}. \quad (7.8)$$

2. Given the intercept times, (7.7), (7.8), the firing time of the AA projectile, $t \geq 0$, is obtained as follows

$$t_{fire,k} = t_{hitC,k} - \Delta_{tofC,k}, \quad t_{fire,k} < t_{hitC,k},$$

$$k = 1, 2, \dots, n_f, \quad (7.9)$$

where $\Delta_{tofC,k}$ is the time of flight of the AA projectile to the intercept point $\mathbf{r}_{targI,k}$, (7.12), and must be computed as part of the solution to fire control problem FCA.

3. It follows that the first firing time R_{B_i2I} will be a negative number given by

$$t_{fire,1} = 0 - \Delta_{tofC,1} = -\Delta_{tofC,1}. \quad (7.10)$$

The initial time j_i of the time horizon \mathcal{T}_F , (7.1), is set equal to R_{B_i2I} as follows

$$t_0 = t_{fire,1} = -\Delta_{tofC,1} \Rightarrow \mathcal{T}_F = [t_{fire,1}, t_{FIN}]. \quad (7.11)$$

Thus, the initial time j_i is not known beforehand and the values of variables at time j_i cannot be specified beforehand. In order to circumvent this difficulty certain assumptions are made such that once R_{B_i2I} is computed, (7.10), the values of variables at time

$t_0 = t_{fire,1}$ can also be computed.

4. By using (7.7), (7.2), the n_f intercept points on the inertial trajectory of the center of mass of the AAT are computed as follows

$$\mathbf{r}_{targI,k} = \mathbf{r}_{targ}^{(I)}(t_{hitC,k}), \quad k = 1, 2, \dots, n_f. \quad (7.12)$$

5. In the sequel, the index k refers to the k th intercept time, (7.7). Thus, all variables can be indexed in terms of k or they can equivalently be expressed as a function of the k th intercept time $t \geq 0$, or the k th firing time $t \geq 0$, $k = 1, 2, \dots, n_f$.

6. It is assumed that at each firing time $t \geq 0$ the AA gun is

completely stationary relative to the vehicle body of the mobile ADS.

7.

The FC vector, $\mathbf{D}_{FC}^{(I)}(t_{fire,k})$, is a unit vector pointing from the hinge point H of the AA gun outwards, and is given by

$$\mathbf{D}_{FC}^{(I)}(t_{fire,k}) = \begin{bmatrix} \cos(\mathbf{a}_{FC}(t_{fire,k})) \cos(\mathbf{e}_{FC}(t_{fire,k})) \\ \sin(\mathbf{a}_{FC}(t_{fire,k})) \cos(\mathbf{e}_{FC}(t_{fire,k})) \\ \sin(\mathbf{e}_{FC}(t_{fire,k})) \end{bmatrix}, \quad (7.13)$$

where $\mathbf{a}_{FC}(t_{fire,k})$ is the azimuth angle and $\mathbf{e}_{FC}(t_{fire,k})$ is the elevation angle of the FC vector, and must be computed as part of the solution to fire control problem FCA.

8.

In fire control problem FCA, the AA gun can only fire at the times defined in (7.9). It is assumed that at each firing time $t \geq 0$ the AA gun aiming vector, $\mathbf{J}_{B_7}^{(I)}(t_{fire,k})$, is equal to the FC vector,

$\mathbf{D}_{FC}^{(I)}(t_{fire,k})$, implying that

$$\mathbf{J}_{B_7}^{(I)}(t_{fire,k}) = \mathbf{D}_{FC}^{(I)}(t_{fire,k}), \quad (7.14)$$

and

$$\mathbf{a}_{gun}(t) = \mathbf{a}_{FC}(t), \quad \mathbf{e}_{gun}(t) = \mathbf{e}_{FC}(t), \quad t = t_{fire,k}, \quad (7.15)$$

$$k = 1, 2, \dots, n_f.$$

9.

Given the above assumptions that at each firing time $t \geq 0$ the AA gun is completely stationary relative to the vehicle body and that the vehicle body is not rotating relative to the inertial reference frame throughout the engagement. Then, it follows that at each firing time $t \geq 0$ both the FC vector and the AA gun aiming vector

are not rotating with respect to the inertial reference frame I . This implies that

$$(7.16)$$

$$\dot{\mathbf{a}}_{FC}(t) = \ddot{\mathbf{a}}_{FC}(t) = 0, \quad \dot{\mathbf{e}}_{FC}(t) = \ddot{\mathbf{e}}_{FC}(t) = 0, \\ t = t_{fire,k},$$

$$\dot{\mathbf{a}}_{gun}(t) = \ddot{\mathbf{a}}_{gun}(t) = 0, \quad \dot{\mathbf{e}}_{gun}(t) = \ddot{\mathbf{e}}_{gun}(t) = 0, \\ t = t_{fire,k}, \quad (7.17)$$

$$k = 1, 2, \dots, n_f.$$

10.

It is assumed that the nonlinear feedback control law of the mobile ADS will precisely rotate the AA gun from one stationary firing position relative to the vehicle body at time $t \geq 0$, to the next stationary firing position relative to the vehicle body at time $-T_{\gamma_0} \mathbf{I}_3$, such that constraints (7.15)–(7.17) are satisfied,

$$k = 1, 2, \dots, n_f - 1.$$

11.

The initial conditions of the AA projectile that is fired at time $t \geq 0$ depend on the values of the inertial angles of the FC vector,

$$\mathbf{a}_{FC}(t_{fire,k}), \mathbf{a}_{FC}(t_{fire,k}), k = 1, 2, \dots, n_f.$$

12.

Furthermore, the inertial position and velocity trajectories of the AA projectile that is fired at time $t \geq 0$ are denoted as functions of $t \geq 0$ and of a different time variable τ used to describe the motion of the AA projectile over the time horizon $[t_{fire,k}, t_{hitC,k}]$, as follows

$$\mathbf{r}_{proj}^{(I)}(\tau; t_{fire,k}), \quad \mathbf{v}_{proj}^{(I)}(\tau; t_{fire,k}), \\ \dots, \quad \left[\mathbf{r}_{proj}^{(I)}(\tau; t_{fire,k}) \right]$$

$$\mathbf{X}(\tau; t_{fire,k}) = \begin{bmatrix} \mathbf{v}_{proj}^{(I)}(\tau; t_{fire,k}) \end{bmatrix}, \quad (7.18)$$

$$\tau \in [t_{fire,k}, t_{hitC,k}],$$

$k = 1, 2, \dots, n_f$. Thus, $t \geq 0$ is used as an index variable in order to associate $\mathbf{X}(\tau; t_{fire,k})$ to the AA projectile that is fired at time $t \geq 0, k = 1, 2, \dots, n_f$.

13. For each given intercept time $t \geq 0, k = 1, 2, \dots, n_f$, the above-mentioned trajectories of the AA projectile are computed by solving an initial value problem involving the point mass flight dynamics model ((6.26)) expressed in terms of time τ as follows

$$\frac{d\mathbf{X}(\tau; t)}{d\tau} = \mathbf{f}_{proj}(\mathbf{X}(\tau; t)), \quad \mathbf{X}(t; t) = \mathbf{X}_0(t), \quad (7.19)$$

$$\tau \in [t, t_{hitC,k}], \quad t = t_{fire,k},$$

$$\mathbf{X}_0(t_{fire,k}) = \begin{bmatrix} \mathbf{r}_{proj,0}^{(I)}(t_{fire,k}) \\ \mathbf{v}_{proj,0}^{(I)}(t_{fire,k}) \end{bmatrix}, \quad (7.20)$$

where the initial conditions $\mathbf{r}_{proj,0}^{(I)}(t_{fire,k}), \mathbf{v}_{proj,0}^{(I)}(t_{fire,k})$, in (7.20)

are computed by using (2.168), (2.173), respectively, as follows

$$\mathbf{r}_{proj,0}^{(I)}(t_{fire,k}) = \mathbf{r}_H^{(I)}(t_{fire,k}) + L_m \mathbf{J}_{B7}^{(I)}(t_{fire,k}), \quad (7.21)$$

where

$$\mathbf{r}_H^{(I)}(t_{fire,k}) = \mathbf{r}_{OA}^{(I)}(t_{fire,k}) + \begin{bmatrix} -\sin(\beta_b)(L_b + h_{Ty}) \\ \cos(\beta_b)(L_b + h_{Ty}) \\ h_b + h_{Tz} + h_{mz} \\ x(t_{fire,k}) \end{bmatrix}, \quad (7.22)$$

$$r_{OA}^{(I)}(t_{fire,k}) = \begin{bmatrix} y(t_{fire,k}) \\ 0 \end{bmatrix}, \quad (7.23)$$

$$\mathbf{J}_{B_7}^{(I)}(t_{fire,k}) = \begin{bmatrix} \cos(\mathbf{a}_{FC}(t_{fire,k})) \cos(\mathbf{e}_{FC}(t_{fire,k})) \\ \sin(\mathbf{a}_{FC}(t_{fire,k})) \cos(\mathbf{e}_{FC}(t_{fire,k})) \\ \sin(\mathbf{e}_{FC}(t_{fire,k})) \end{bmatrix},$$

and

$$\begin{aligned} \mathbf{v}_{proj,0}^{(I)}(t_{fire,k}) &= \mathbf{v}_H^{(I)}(t_{fire,k}) + \mathbf{v}_P^{(I)}(t_{fire,k}) \\ &= \mathbf{v}_{OA}^{(I)}(t_{fire,k}) + \mathbf{v}_P^{(I)}(t_{fire,k}) \\ &= \begin{bmatrix} v_b \cos(\beta_b + \pi/2) \\ v_b \sin(\beta_b + \pi/2) \\ 0 \end{bmatrix} + V_0 \mathbf{J}_{B_7}^{(I)}(t_{fire,k}), \end{aligned} \quad (7.24)$$

$k = 1, 2, \dots, n_f$. It has been assumed that either the vehicle body of the mobile ADS is moving forward at a constant speed k_0 and in a straight line implying that $d\beta(t)/dt = 0$, $J_{s1} = J_{s2}$, or that the vehicle body is stationary implying that $k_0 \neq 0$ in (7.24).

14. The fire control problem FCA is defined as follows.

For each given intercept time $t \geq 0$ compute the parameters $-\pi, i = 1, 2, 3u$, that is, the inertial angles of the FC vector and the time-of-flight of the AA projectile,

$$\begin{aligned} \mathbf{a}_{FC}(t_{fire,k}) &= c_{1,k}, \quad \mathbf{e}_{FC}(t_{fire,k}) = c_{2,k}, \\ \Delta_{tofC,k} &= c_{3,k} = c_{3u,k}^2, \end{aligned} \quad (7.25)$$

where

$$t_{fire,k} = t_{fire,k} - \Delta_{tofC,k} \quad (7.26)$$

$$t_{fire,k} = t_{hitC,k} - \Delta_{tofC,k}, \quad (7.26)$$

such that the following holds. The AA projectile that is fired at time $t \geq 0$ will intercept the center of mass of the AAT at the specified intercept time $t \geq 0$, that is,

$$\mathbf{r}_{proj}^{(I)}(t_{hitC,k}; t_{fire,k}) = \mathbf{r}_{targ}^{(I)}(t_{hitC,k}), \quad (7.27)$$

$$d\zeta_{ref}(t)/dt = d\mathbf{e}_{gun,ref}(t)/dt, \quad (7.28)$$

$$\mathbf{p}_{s1}(t) \rightarrow \mathbf{p}_{s1,ref}(t) \quad \text{as } t \rightarrow \infty, \quad (7.29)$$

where $n_s = m_c = 4$, $I_{wr1} = I_{wr2}$ are given positive real numbers representing the minimum and maximum permissible times of flight, respectively, and where $-\pi/2 < \mathbf{e}_{FCmin} < \mathbf{e}_{FCmax} < \pi/2$ are given lower and upper bounds for the elevation angle of the FC vector. The above computation is repeated in sequence for each intercept time $t \geq 0$, $k = 1, 2, \dots, n_f$.

15. At each time $t \geq 0$ the FC vector points ahead of the LOS vector due to the finite time of flight $\Delta_{tofC,k}$.

The following should be noted with regard to fire control problem FCA, (7.25)–(7.29).

1. It has been implicitly assumed that fire control problem FCA has a solution, that is, the sequence of values $\mathbf{a}_{FC}(t_{fire,k})$, $\mathbf{a}_{FC}(t_{fire,k})$, $\Delta_{tofC,k}$, $k = 1, 2, \dots, n_f$, exist. However, for various reasons fire control problem FCA may not have a solution.
2. For example, if an intercept point between the AA projectile trajectory and the trajectory of the AAT at the specified intercept

time $t \geq 0$ does not exist then fire control problem FCA does not have a solution for the given $t \geq 0$.

3. For the case where the AA gun must engage a stationary target lying on the (X, Y) plane, fire control problem FCA may have two solutions. One solution represents a “low trajectory” and corresponds to the minimum time of flight and is the desirable solution. The other solution represents a “high trajectory” and corresponds to a longer time of flight.
4. There is no closed-form expression available for $\mathbf{r}_{proj}^{(I)}(t_{hitC,k}; t_{fire,k})$ appearing in the equality constraint (7.27), in terms of the variables T_{γ_0} , T_{γ_0} , $c_{3u,k}$, (7.25), and other given parameters (Chap. 6).
5. In the application of an iterative constrained minimization algorithm to compute $\mathbf{a}_{FC}(t_{fire,k})$, $\mathbf{a}_{FC}(t_{fire,k})$, $\Delta_{tofC,k}$, and solve fire control problem FCA, it may happen that at some intermediate iteration the computed values T_{γ_0} , T_{γ_0} , $c_{3u,k}$, are such that the AA projectile impacts the ground, (6.3), (6.4), before the final time $t_{fire,k} + \Delta_{tofC,k}$. In this case, the trajectory of the AA projectile will be stopped at time Q_{Cj} , (6.3).
6. Fire control problem FCA deals with the conceptual problem of the AA projectile intercepting the center of mass of the AAT. Thus, the following aspects are not taken into account.
 - a. The fact that the AA projectile will practically first impact the body of the AAT before reaching the center of mass.
 - b. The geometric shape of the body of the AAT.
 - c. The material properties of the body of the AAT and of the AA

the material properties of the body of the AA and of the AA projectile.

The above-mentioned points 6a, 6b, are taken into account in Chap. 8.

7.

Assume that the sequence of values $\mathbf{a}_{FC}(t_{fire,k})$, $\mathbf{e}_{FC}(t_{fire,k})$, $\Delta_{tofC,k}$, $k = 1, 2, \dots, n_f$, solve fire control problem FCA. Then, the following sequence of values also solve fire control problem FCA

$$\begin{aligned} \mathbf{a}_{FC}(t_{fire,k}) \pm i2\pi, \quad \mathbf{e}_{FC}(t_{fire,k}), \quad \Delta_{tofC,k}, \\ k = 1, 2, \dots, n_f, \quad i = 0, 1, 2, \dots \end{aligned} \quad (7.30)$$

If needed, constraints can be added to $\mathbf{a}_{FC}(t_{fire,k})$ in order to exclude periodic solutions, (7.30).

8.

The following constraints limit the deviation of the inertial angles of the FC vector from the inertial angles of the LOS vector at time $t \geq 0$, and can be included in the formulation of fire control problem FCA as follows

$$\begin{aligned} |\mathbf{a}_{FC}(t_{fire,k}) - \mathbf{a}_{los}(t_{fire,k})| &\leq \epsilon_1, \\ |\mathbf{e}_{FC}(t_{fire,k}) - \mathbf{e}_{los}(t_{fire,k})| &\leq \epsilon_2, \\ k &= 1, 2, \dots, n_f, \end{aligned} \quad (7.31)$$

where the bounds $\epsilon_1, \epsilon_2 > 0$, are chosen appropriately, for example, $(X_{B_5}, Y_{B_5}, Z_{B_5}), (X_{B_5}, Y_{B_5}, Z_{B_5})$.

9. The miss distance $\cos(\delta_v) \neq 0$ between the AA projectile fired at time $t \geq 0$, and the center of mass of the AAT at time $t_{fire,k} + \Delta_{tofC,k}$, is given by ((7.27))

$$d_{miss}(t_{fire,k}) = \|\mathbf{r}_{proj}^{(I)}(t + \Delta_{tofC,k}; t) - \mathbf{r}_{targ}^{(I)}(t + \Delta_{tofC,k})\|, \quad (7.27)$$

$$t = t_{fire,k}, \quad k = 1, 2, \dots, n_f. \quad (7.32)$$

By using (7.32), the vector equality constraint (7.27) can be replaced by an equivalent scalar equality constraint given by

$$d_{miss}^2(t_{fire,k}) = 0. \quad (7.33)$$

10.

The following single equality constraint is equivalent to (7.33) and also to (7.27), for all $k = 1, 2, \dots, n_f$,

$$\sum_{k=1}^{n_f} d_{miss}^2(t_{fire,k}) = 0. \quad (7.34)$$

11. It is possible to express the inertial angles of the FC vector as the sum of the known inertial angles of the LOS vector and an unknown lead azimuth angle $\mathbf{a}_{lead}(t_{fire,k})$ and unknown lead elevation angle $\mathbf{a}_{lead}(t_{fire,k})$, respectively, that must be determined, as follows

$$\begin{aligned} \mathbf{a}_{FC}(t) &= \mathbf{a}_{los}(t) + \mathbf{a}_{lead}(t), \\ \mathbf{e}_{FC}(t) &= \mathbf{e}_{los}(t) + \mathbf{e}_{lead}(t), \quad t = t_{fire,k}, \end{aligned} \quad (7.35)$$

$k = 1, 2, \dots, n_f$. The angles $\mathbf{a}_{lead}(t_{fire,k})$, $\mathbf{a}_{lead}(t_{fire,k})$, are referred to as the lead angles of the FC vector. Thus, fire control problem FCA is reformulated as follows. For each given intercept time $t \geq 0$, compute the parameters T_{γ_0} , T_{γ_0} , $c_{3u,k}$, determining the variable values $\mathbf{a}_{lead}(t_{fire,k}) = c_{1,k}$, $\mathbf{a}_{lead}(t_{fire,k}) = c_{1,k}$,

$\Delta_{tofC,k} = c_{3u,k}^2$, such that the constraints (7.27)–(7.29) are

satisfied. The following inequality constraints are equivalent to (7.31), and can be added to the reformulated fire control problem FCA as follows

$$|\mathbf{a}_{lead}(t_{fire,k})| \leq c_{1,k}, \quad |\mathbf{a}_{lead}(t_{fire,k})| \leq c_{1,k}$$

$$\begin{aligned} |\alpha_{lead}(fire,k)| &\geq c_1, \quad |\sigma_{lead}(fire,k)| \geq c_2, \\ k &= 1, 2, \dots, n_f. \end{aligned} \quad (7.36)$$

7.2 Fire Control Problem Formulation Using Feasible Control

Feasible control was co-developed with Prof. Yaakov Yavin (1935–2006) at the Laboratory for Decision and Control, Dept. of Electrical, Electronic and Computer Engineering, University of Pretoria. Feasible control circumvents certain difficulties that arise with optimal control and related methods ([14, 15, 21, 37, 89, 96, 102, 143, 166]).

Feasible control facilitates the design of control strategies for linear and nonlinear dynamic systems such that a wide range of practical performance specifications and constraints are satisfied. Feasible control has been applied to the following problems.

1. In [212] feasible control is applied in order to compute an open-loop control strategy for the rudder of a super tanker ship such that it maneuvers safely through constrained waters, in this case, a narrow zigzag channel. The open loop control strategy is assumed to be a piecewise constant or a piecewise linear function of time and is parameterized by a finite number of parameters grouped in a vector \mathbf{b} . The feasible control problem consists of determining the vector \mathbf{b} such that a number of practical specifications and constraints are satisfied. The specifications and constraints are expressed as inequalities in the time domain, and there is no objective function that must be minimized or maximized. Thus, the emphasis of feasible control is on feasibility and not on optimality.

Given the complicated form of the hydrodynamic model of the super tanker ship, and of the specifications and constraints that have to be satisfied. If an approach based on optimal control is attempted then application of the Pontryagin minimum principle will result in a two-point-boundary-value-problem (TPBVP) representing necessary conditions for an optimal control. In this

case, the TPBVP will have a very complicated form and be difficult to solve numerically.

2. In [55, 56], feasible control is applied in order to compute the vector \mathbf{b} parameterizing a closed loop dynamic controller for a linear model of an aerial vehicle such that a wide range of specifications and constraints are satisfied. The dynamic controller has the structure of a linear quadratic Gaussian (LQG) controller. The vector \mathbf{b} parameterizes the state weighting matrix and the state noise covariance matrix of an auxiliary LQG control problem. The linear model of the aerial vehicle is subject to random initial conditions, while the addition of white state noise and white measurement noise is considered in [56]. The constraints and specifications are expressed as inequalities in the time domain, s -domain, and frequency domain.
3. In [59] feasible control is applied in order to compute the vector \mathbf{b} parameterizing a portfolio control strategy for an insurance company such that a range of specifications and constraints are satisfied. A nonlinear discrete-time state space model of the asset/liability structure is used. The state space model describes the evolution over time of all the asset accounts and all the liability accounts on the balance sheet of the insurance company, and incorporates the effects of various types of financial transactions.
4. In [210, 211], feasible control is applied in order to compute the vector \mathbf{b} parameterizing open-loop control strategies for mechanical systems, for example, a disk rolling on a stationary or moving horizontal plane.

In this Section, the fire control problem is formulated using feasible control as follows.

1. As in fire control problem FCA, for each given intercept time $t \geq 0$, the parameters T_{γ_0} , T_{γ_0} , $c_{3u,k}$ in (7.25) determining $\mathbf{a}_{FC}(t_{fire,k})$,

$\mathbf{a}_{FC}(t_{fire,k})$, $\Delta_{tofC,k}$, must be computed such that certain inequality constraints are satisfied. For convenience, the parameters T_{γ_0} , T_{γ_0} , $c_{3u,k}$ in (7.25) are grouped in a vector $\mathbf{b}_k \in \mathbb{R}^3$ as follows

$$\mathbf{b}_k = [c_{1,k}, c_{2,k}, c_{3u,k}]^\top. \quad (7.37)$$

The application of feasible control deals with the satisfaction of the following inequality constraints.

2. Firstly, it is assumed that the equality constraint (7.33) must be satisfied within an error tolerance $\mathbf{p}_s \in \mathbb{R}^{n_s}$, as follows,

$$0 \leq d_{miss}^2(t_{fire,k}) \leq \epsilon_{max}. \quad (7.38)$$

3. Secondly, it is required that a number of inequality constraints are satisfied, as follows

$$a_{min,i} \leq g_i(\mathbf{b}_k) \leq a_{max,i}, \quad i = 1, 2, \dots, n_{con}, \quad (7.39)$$

where $g_i = g_i(\mathbf{b}_k) \in \mathbb{R}$, $i = 1, 2, 3, 4$, $i = 1, 2, \dots, n_{con}$. The functions m represent practical performance specifications and constraints, including, for example, the constraints (7.27)–(7.29), (7.31).

4. Define the function \mathbf{H}_s as follows

$$W_k = w_0 \text{pen}_s(d_{miss}^2(t_{fire,k}), 0, \epsilon_{max}) + \sum_{i=1}^{n_{con}} w_i \text{pen}_s(g_i, a_{min,i}, a_{max,i}), \quad (7.40)$$

where the penalty weights $y_1 \in \mathbb{R}$, $i = 0, 1, 2, \dots, n_{con}$,

$W_k = W_k(\mathbf{b}_k) \in \mathbb{R}$, and pen_s is a quadratic penalty function defined as follows ([11, 30, 140, 164])

(7.41)

$$\text{pen}_s(x_a, x_{min}, x_{max}) = \begin{cases} (x_a - x_{max})^2 & \text{if } x_a > x_{max} \\ 0 & \text{if } x_{min} \leq x_a \leq x_{max} \\ (x_a - x_{min})^2 & \text{if } x_a < x_{min} \end{cases},$$

$x_{min} < x_{max}$, J_{b23} , X_{B11} , $m_i > 0$. The function $J_{s3} > 0$ for all vectors $\mathbf{b}_k \in \mathbb{R}^3$. Note that there is no closed-form expression available for the miss distance $\cos(\delta_v) \neq 0$, (7.32), and generally for the functions m , and thus for the function H_s , (7.40), in terms of the vector \mathbf{b}_k and other given parameters.

5. The objective is to find a vector $\mathbf{b}_k \in \mathbb{R}^3$ such that the constraints, (7.38), (7.39), are satisfied. The constraints (7.38), (7.39), are satisfied if and only if the equation $J_{s3} > 0$ is satisfied. Thus, a vector $\mathbf{b}_k \in \mathbb{R}^3$ is feasible if and only if it satisfies the equation $J_{s3} > 0$, that is,

$$\mathbf{G}^\top \boldsymbol{\lambda} = \mathbf{Q}_C. \quad (7.42)$$

Equation (7.42) may have more than one solution, that is, a feasible vector \mathbf{b}_k is not necessarily unique.

6. A formulation of the fire control problem using feasible control is as follows. Compute a vector $\mathbf{b}_k \in \mathbb{R}^3$ such that the Eq. (7.42) is satisfied. Given an initial guess for the vector $\mathbf{b}_k \in \mathbb{R}^3$, an iterative minimization algorithm is applied in order to gradually reduce H_s to zero in double precision ([11, 30, 140, 149, 164]).

7. If a vector \mathbf{b}_k is obtained such that Eq. (7.42) is satisfied then \mathbf{b}_k is feasible. By applying (7.25) feasible variable values $\mathbf{a}_{FC}(t_{fire,k})$, $\mathbf{a}_{FC}(t_{fire,k})$, $\Delta_{tofC,k}$, are obtained. The above procedure is repeated in order to compute a feasible vector \mathbf{b}_k for each intercept time $t \geq 0$, $k = 1, 2, \dots, n_f$. The question of existence and uniqueness of solutions to the equation $J_{s3} > 0$ is beyond the scope of existing works on feasible control ([55, 56, 59, 212]).

7.3 Air Defence System Deployment and Attacking Aerial Target Engagement Scenario

The deployment of the mobile ADS is shown in Fig. 7.2. It is assumed that the defended location is fixed at the origin O_I of the inertial coordinate system (X, Y, Z) with unit vectors $(\mathbf{I}_1, \mathbf{I}_2, \mathbf{I}_3)$.

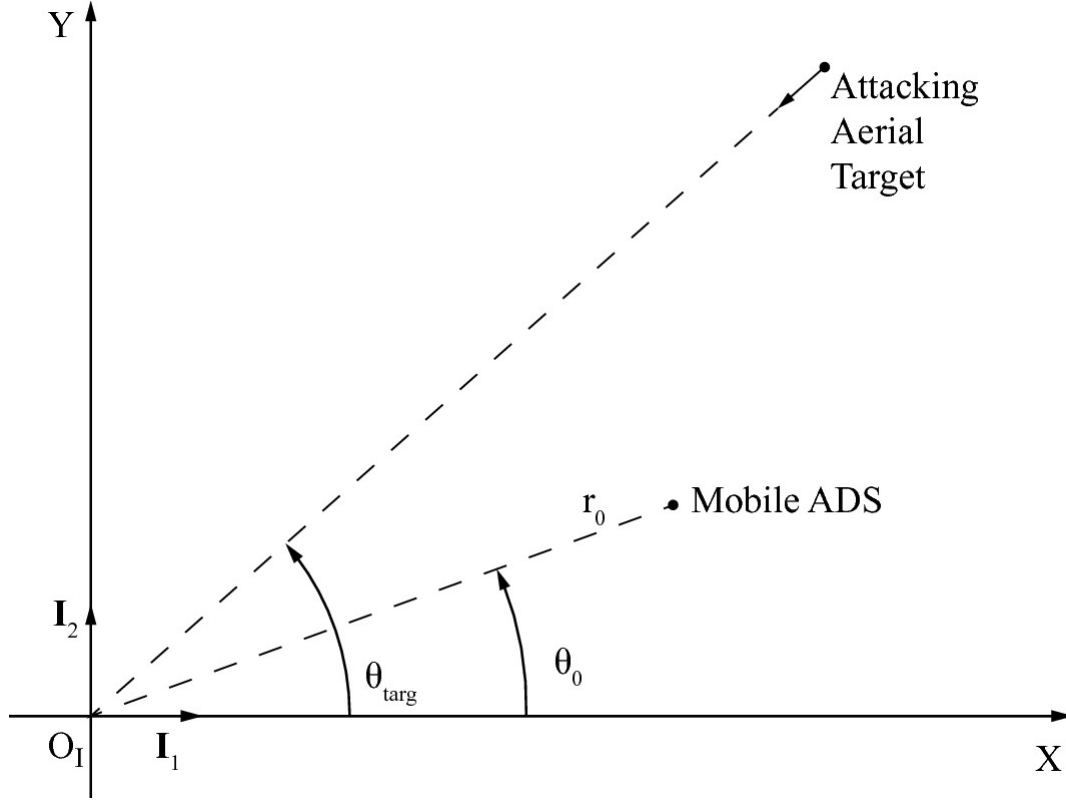


Fig. 7.2 Schematic of the deployment of the mobile ADS and the attacking aerial target; the defended location is at the origin O_I

The mobile ADS is at a distance ϵ_1 from the origin O_I and at an angle δ_v relative to the X axis.¹ The projection of the trajectory of the AAT onto the (X, Y) plane is also shown in Fig. 7.2.

In order to simplify the computations the following assumptions and methods are employed.

1. It is assumed that the AAT is moving in a straight line, at a constant height and at a constant velocity.
2. As stated earlier in this Chapter, the vehicle body of the mobile ADS is assumed to be either completely stationary or moving forward in a straight line and at a constant speed.
3. The values of the position vectors $\mathbf{r}_{OA}^{(I)}(t)$, $\mathbf{r}_{targ}^{(I)}(t)$, are specified at the first given intercept time, that is, at time $t = t_{hitC,1} = 0$, (7.8),

and are denoted as follows $\mathbf{r}_{OA}^{(I)}(t_{hitC,1}) = \mathbf{r}_{OA}^{(I)}(0)$,

$$\mathbf{r}_{targ}^{(I)}(t_{hitC,1}) = \mathbf{r}_{targ}^{(I)}(0).$$

4.

Based on the assumed motion trajectories of the mobile ADS and the AAT it follows that $\mathbf{r}_{OA}^{(I)}(t)$ and $\mathbf{r}_{targ}^{(I)}(t)$ can be computed for any

$t \in \mathcal{T}_F$ by using forward in time extrapolation if $t \geq 0$, and backward in time extrapolation if $t \leq 0$.

In the case of the mobile ADS the position vector $\mathbf{r}_{OA}^{(I)}(0)$ is given by

(Fig. 7.2)

$$\mathbf{r}_{OA}^{(I)}(0) = r_0 \cos(\theta_0) \mathbf{I}_1 + r_0 \sin(\theta_0) \mathbf{I}_2, \quad (7.43)$$

where

$$r_0 = 1995 \text{ m}, \theta_0 = 195 \text{ mils}. \quad (7.44)$$

The position vector $\mathbf{r}_H^{(I)}(0)$ is computed by using $\mathbf{r}_{OA}^{(I)}(0)$ and (7.22).

The vehicle body of the mobile ADS is moving forward in a straight line at a constant speed k_0 , and the inertial velocity $\mathbf{v}_H^{(I)}(0)$ is given by

((7.24))

$$\mathbf{v}_{OA}^{(I)}(t) = \mathbf{v}_{OA}^{(I)} = \begin{bmatrix} v_b \cos(\beta_b + \pi/2) \\ v_b \sin(\beta_b + \pi/2) \\ 0 \end{bmatrix}, \quad t \in \mathcal{T}_F. \quad (7.45)$$

If the vehicle body is actually stationary throughout the engagement of the AAT then $k_0 \neq 0$ m/s implying that $\mathbf{v}_{OA}^{(I)} = \mathbf{0}_{3 \times 1}$, (7.45). Thus, the

initial velocity of the AA projectile $\mathbf{r}_{proj,0}^{(I)}(t_{fire,k})$ is obtained by using (7.45), (7.24).

The inertial position vector $\mathbf{r}_{OA}^{(I)}(t)$ is given by

$$\mathbf{r}_{OA}^{(I)}(t) = \mathbf{r}_{OA}^{(I)}(0) + \mathbf{v}_{OA}^{(I)} t, \quad t \in \mathcal{T}_F. \quad (7.46)$$

For any computed firing time $t \geq 0$, (7.9), the position vector

$\mathbf{r}_{OA}^{(I)}(t_{fire,k})$ is obtained by using (7.46) as follows

$$\mathbf{r}_{OA}^{(I)}(t_{fire,k}) = \mathbf{r}_{OA}^{(I)}(0) + \mathbf{v}_{OA}^{(I)} t_{fire,k}, \quad k = 1, 2, \dots, n_f. \quad (7.47)$$

Thus, the initial position of the AA projectile $\mathbf{r}_{proj,0}^{(I)}(t_{fire,k})$ is obtained by using (7.47), (7.21)–(7.23).

In the case of the AAT the position vector $\mathbf{r}_{targ}^{(I)}(0)$ is given by

$$\mathbf{r}_{targ}^{(I)}(0) = r_0 \mathbf{e}_{targ} + r_{0,targ} \mathbf{e}_{targ} + h_{targ} \mathbf{I}_3, \quad (7.48)$$

where $r_{0,targ} = 3500$ m, $h_{targ} = 301$ m. The AAT is flying towards the defended location in a straight line, at constant altitude $X_{B_{11}}$ and at a constant speed $c_{3u,k}$. The inertial velocity of the center of mass of the AAT is given by

$$\begin{aligned} \mathbf{v}_{targ}^{(I)}(t) &= \mathbf{v}_{targ}^{(I)} = -v_{targ} \mathbf{e}_{targ}, \\ \mathbf{e}_{targ} &= \cos(\theta_{targ}) \mathbf{I}_1 + \sin(\theta_{targ}) \mathbf{I}_2, \quad t \in \mathcal{T}_F, \end{aligned} \quad (7.49)$$

where $v_{targ} = 251$ m/s, $\theta_{targ} = 800$ mils $= \pi/4$ rad. The inertial position of the center of mass of the AAT $\mathbf{r}_{targ}^{(I)}(t)$ is given by

$$(7.50)$$

$$\mathbf{r}_{targ}^{(I)}(t) = \mathbf{r}_{targ}^{(I)}(0) + \mathbf{v}_{targ}^{(I)} t, \quad t \in \mathcal{T}_F.$$

For any computed firing time $t \geq 0$, (7.9), the position vector

$\mathbf{r}_{projx}^{(I)}(t_{hitG})$ is obtained by using (7.50) as follows

$$\begin{aligned} \mathbf{r}_{targ}^{(I)}(t_{fire,k}) &= \mathbf{r}_{targ}^{(I)}(0) + \mathbf{v}_{targ}^{(I)} t_{fire,k}, \\ k &= 1, 2, \dots, n_f. \end{aligned} \quad (7.51)$$

7.4 Computational Results for Fire Control Problem FCA: Vehicle Body of Mobile ADS is Completely Stationary

The vehicle body of the mobile ADS is completely stationary throughout the engagement of the AAT implying that ((7.24))

$$v_b = 0 \Rightarrow \mathbf{v}_H^{(I)}(t) = \mathbf{v}_{OA}^{(I)}(t) = \mathbf{0}_{3 \times 1}, \quad t \in \mathcal{T}_F. \quad (7.52)$$

The following numerical data is used in the computations.

1. The angle β_s of the mobile ADS is given by

$$\beta_b = -\pi/2. \quad (7.53)$$

2. The initial and final times are given by

$$t_0 = t_{fire,1} = -\Delta_{tofC,1}, \quad t_{FIN} = 20 \text{ s}, \quad (7.54)$$

where $h_s > a$ must be computed. The computations below yield

$$\Delta_{tofC,1} = 5.99701 \text{ s}.$$

3. The sequence of intercept times is equally spaced and is given by

$$\begin{aligned} t_{hitC,k} &= (k-1)\Delta_{hitC}, \quad k = 1, 2, \dots, n_f = 101, \\ \Delta_{hitC} &= 0.2 \text{ s}, \quad t_{hitC,1} = 0, \quad t_{hitC,101} = t_{FIN} = 20 \text{ s}. \end{aligned} \quad (7.55)$$

$$\Delta_{hitC} = 0.2 \text{ s}, \quad t_{hitC,1} = 0, \quad t_{hitC,n_f} = t_{FIN} = 20 \text{ s}.$$

Thus, the set of specified intercept times (in seconds) is given by

$$\begin{aligned} & \{t_{hitC,k}, k = 1, 2, \dots, n_f = 101\} \\ & = \{0, 0.2, 0.4, \dots, 19.6, 19.8, 20\}. \end{aligned} \quad (7.56)$$

4.

A fourth order Runge-Kutta algorithm is used in order to solve numerically the point mass flight dynamics model of the AA projectile with a fixed time-step

$$\Delta_{sim} = 0.01 \text{ s} \quad (7.57)$$

on the set of times ((6.59))

$$\{t_{fire,k}, t_{fire,k} + \Delta_{sim}, \dots, t_{hitC,k}\}, \quad k = 1, 2, \dots, n_f. \quad (7.58)$$

where $t_{fire,k} = t_{hitC,k} - \Delta_{tofC,k}$.

5.

The bounds used in the constraints (7.28)–(7.29) are as follows

$$\begin{aligned} \Delta_{tofCmin} &= 10^{-4} \text{ s}, \quad \Delta_{tofCmax} = 10 \text{ s}, \\ e_{FCmin} &= -45\pi/180, \quad e_{FCmax} = 80\pi/180. \end{aligned} \quad (7.59)$$

6.

For each k , a constrained minimization algorithm implemented by the MATLAB Optimization Toolbox function `fmincon` ([111]) is employed in order to compute the three variables T_{γ_0} , T_{γ_0} , $c_{3u,k}$,

(7.25), such that the three equations (7.27) are satisfied subject to the constraints (7.28)–(7.29). Each of the three equations (7.27) is satisfied within a specified absolute error tolerance of 10^{-6} . The

function `fmincon` requires the user to specify a cost function, J_{cost}

. In this case the cost function is specified as a fixed value, $J_{cost} = 0$.

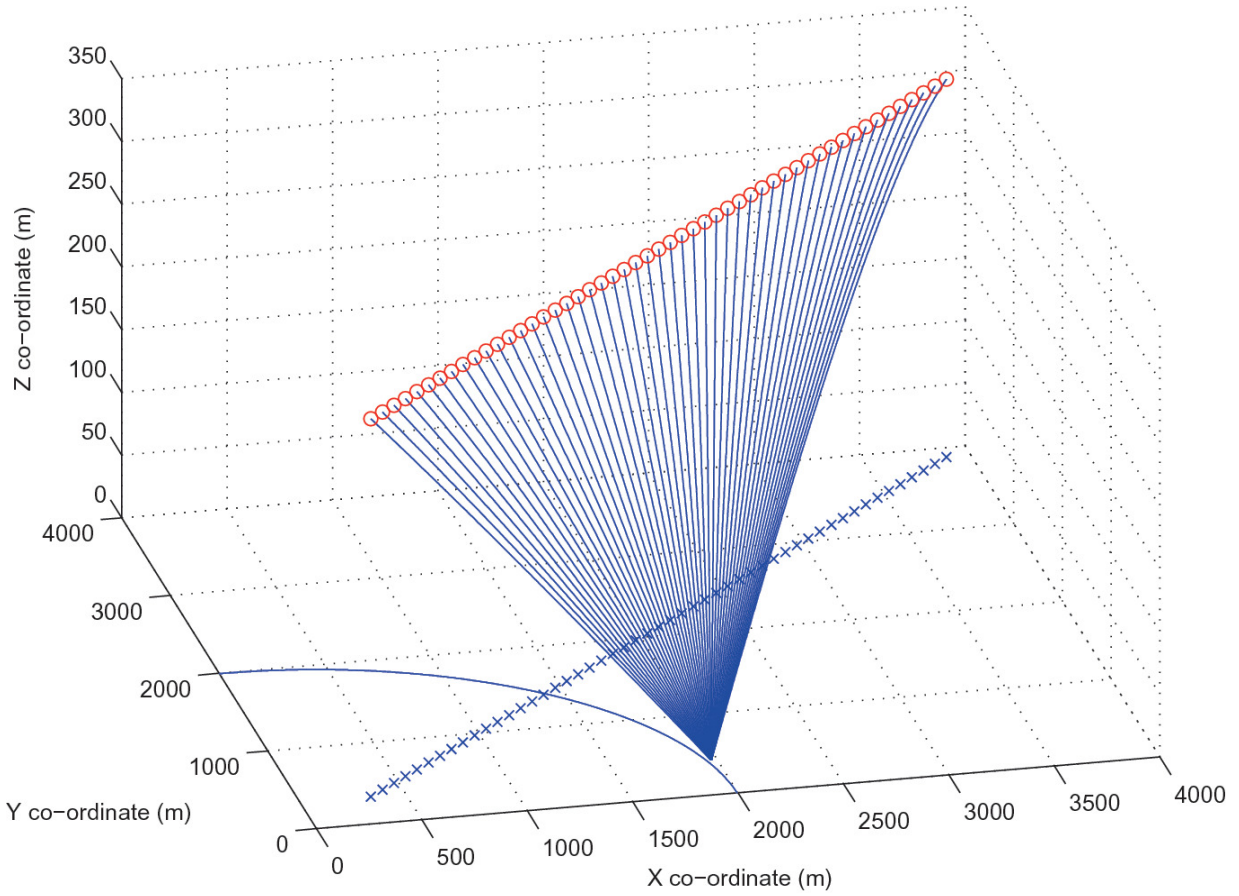


Fig. 7.3 Plot of the inertial X, Y, Z , co-ordinates of the AA projectile trajectory $\mathbf{r}_{proj}^{(I)}(\tau; t_{fire,k})$, $\tau \in [t_{fire,k}, t_{hitC,k}]$, for $k = 1, 3, 5, \dots, n_f$, and of points on the AAT trajectory $\mathbf{r}_{projx}^{(I)}(t_{hitG}), (o)$, $k = 1, 3, 5, \dots, n_f$: vehicle body of mobile ADS is stationary

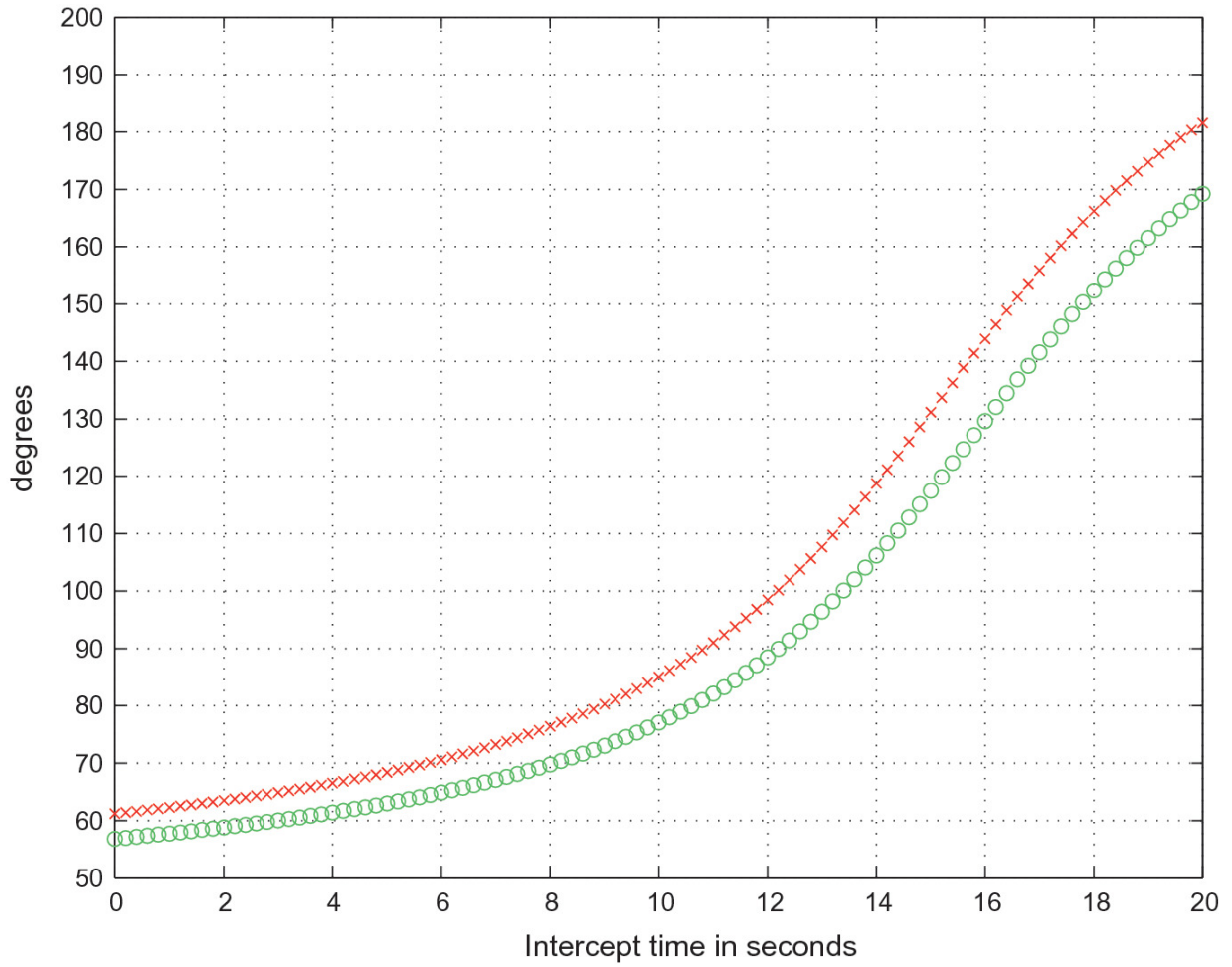


Fig. 7.4 Plot of the inertial azimuth angle of the FC vector $a_{FC}(t_{fire,k})$, (x), and the inertial azimuth angle of the LOS vector $(A_f) = 11$, (o), versus the intercept time $t \geq 0$, $k = 1, 2, \dots, n_f$: vehicle body of mobile ADS is stationary

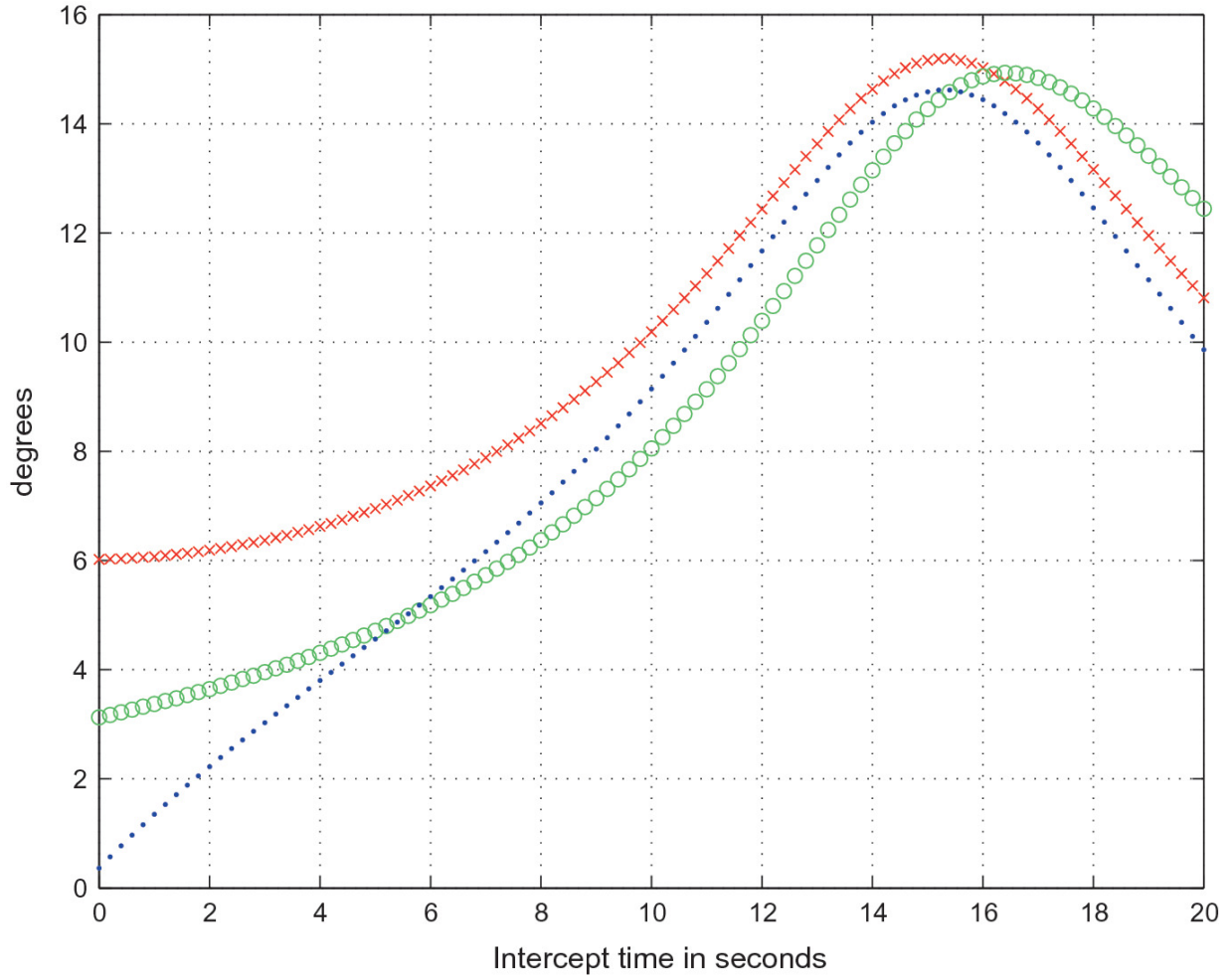


Fig. 7.5 Plot of the inertial elevation angle of the FC vector $\mathbf{a}_{FC}(t_{fire,k})$, (x), the inertial elevation angle of the LOS vector $(A_f) = 11$, (o), and the inertial elevation angle of the projectile velocity vector $\mathbf{e}_{proj}(t_{hitC,k}; t_{fire,k})$, (·), versus the intercept time $t \geq 0$.

$k = 1, 2, \dots, n_f$: vehicle body of mobile ADS is stationary

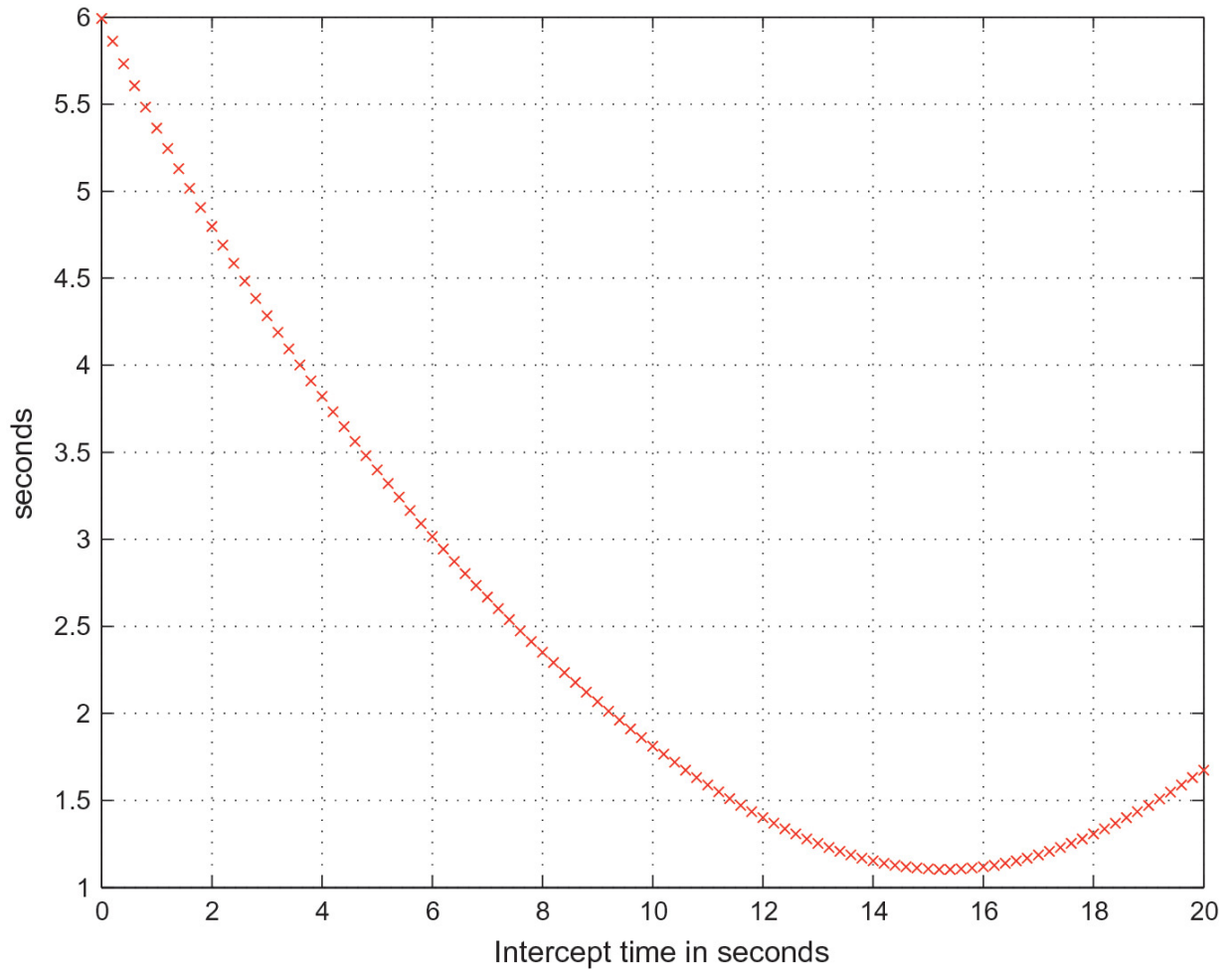


Fig. 7.6 Plot of the time of flight of the AA projectile $\Delta_{tofC,k}$ versus the intercept time $t \geq 0$, $k = 1, 2, \dots, n_f$: vehicle body of mobile ADS is stationary

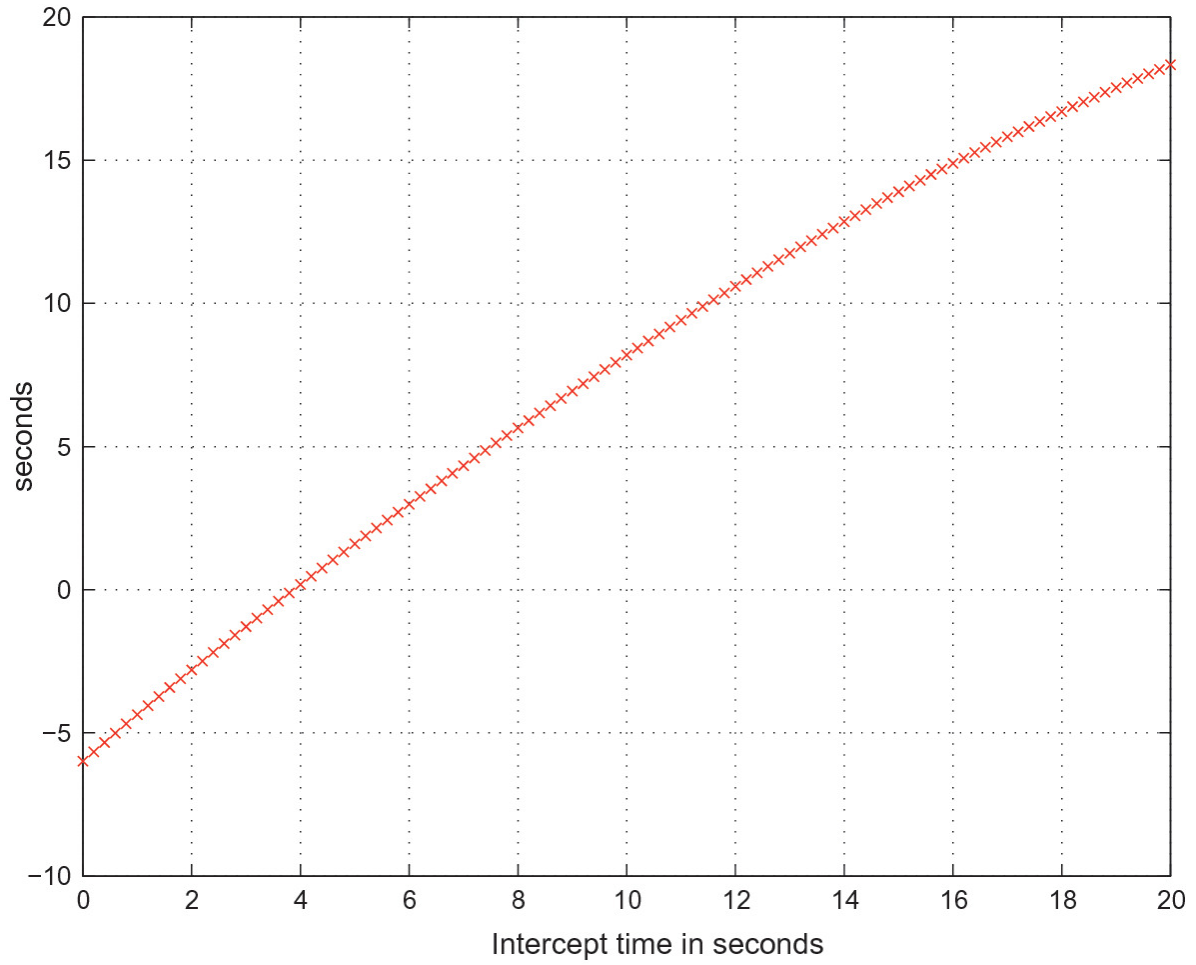


Fig. 7.7 Plot of the firing time of the AA projectile $t \geq 0$ versus the intercept time $t \geq 0$,
 $k = 1, 2, \dots, n_f$: vehicle body of mobile ADS is stationary

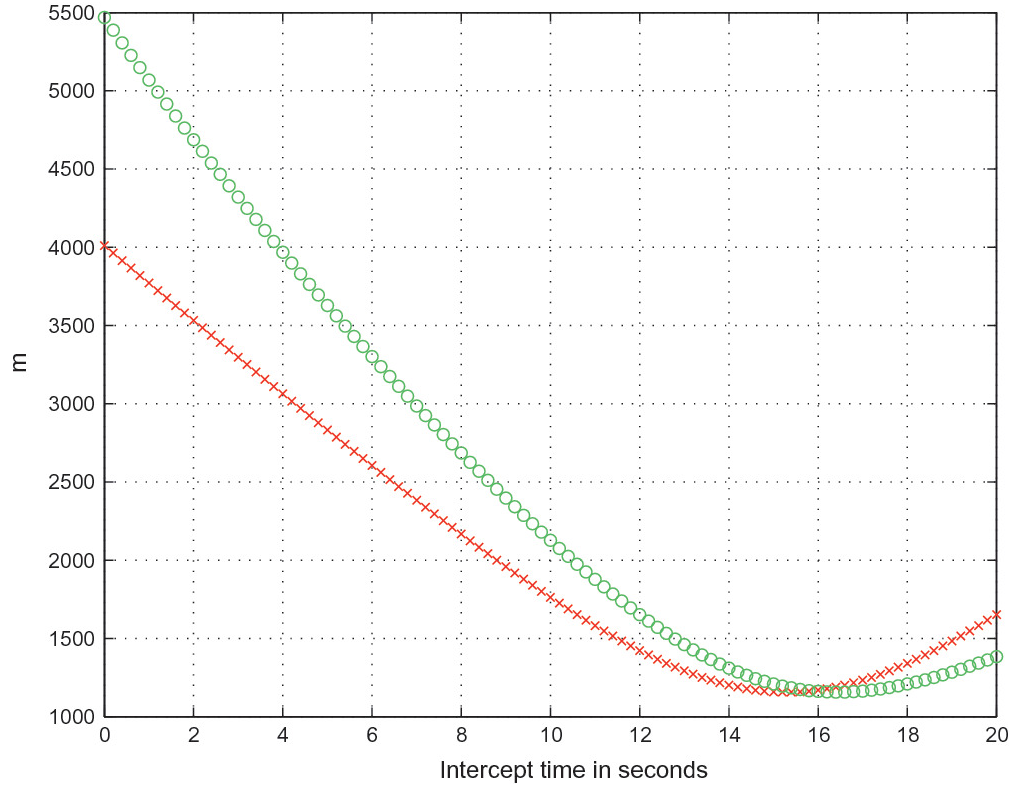


Fig. 7.8 Plot of the LOS distance $\|\mathbf{r}_{los}^{(I)}(t_{hitC,k})\|$, (x), and the LOS distance $\|\mathbf{r}_{los}^{(I)}(t_{hitC,k})\|$, (o), versus the intercept time $t \geq 0$, $k = 1, 2, \dots, n_f$: vehicle body of mobile ADS is stationary

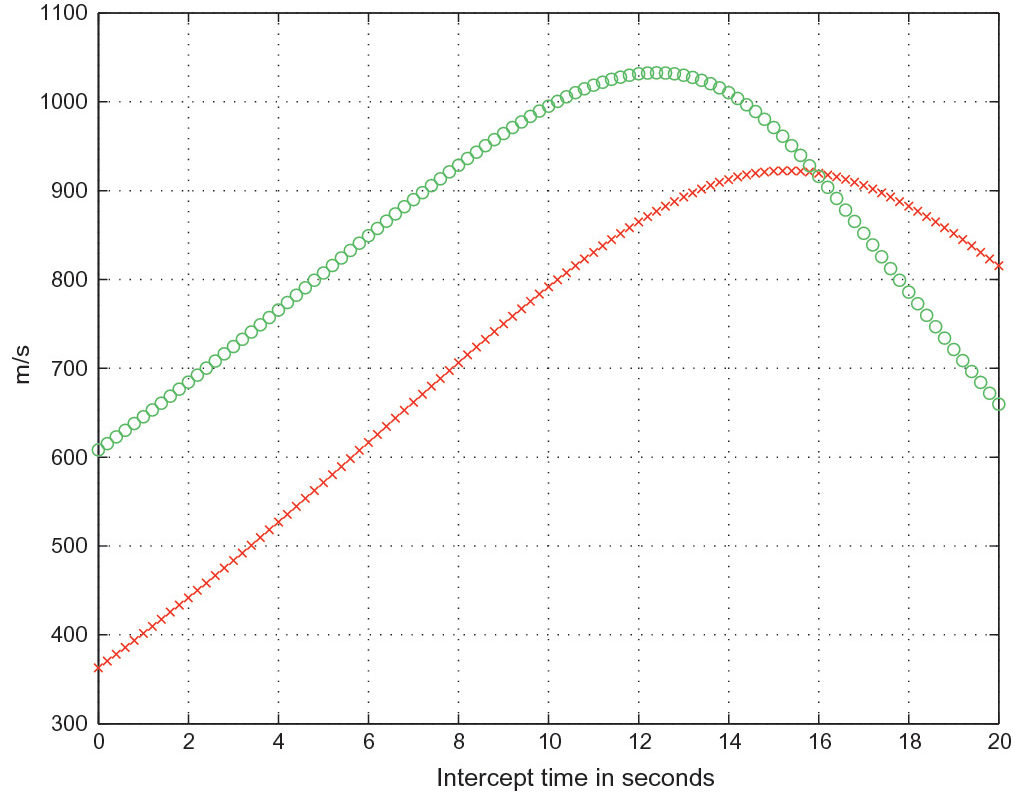


Fig. 7.9 Plot of the intercept speed of the AA projectile $\|\mathbf{v}_{proj}^{(I)}(t_{hitC,k}; t_{fire,k})\|$, (x), and the relative intercept speed of the AA projectile $\|\mathbf{v}_{proj}^{(I)}(t_{hitC,k}; t_{fire,k}) - \mathbf{v}_{targ}^{(I)}(t_{hitC,k})\|$, (o), versus the intercept time $t \geq 0$, $k = 1, 2, \dots, n_f$: vehicle body of mobile ADS is stationary

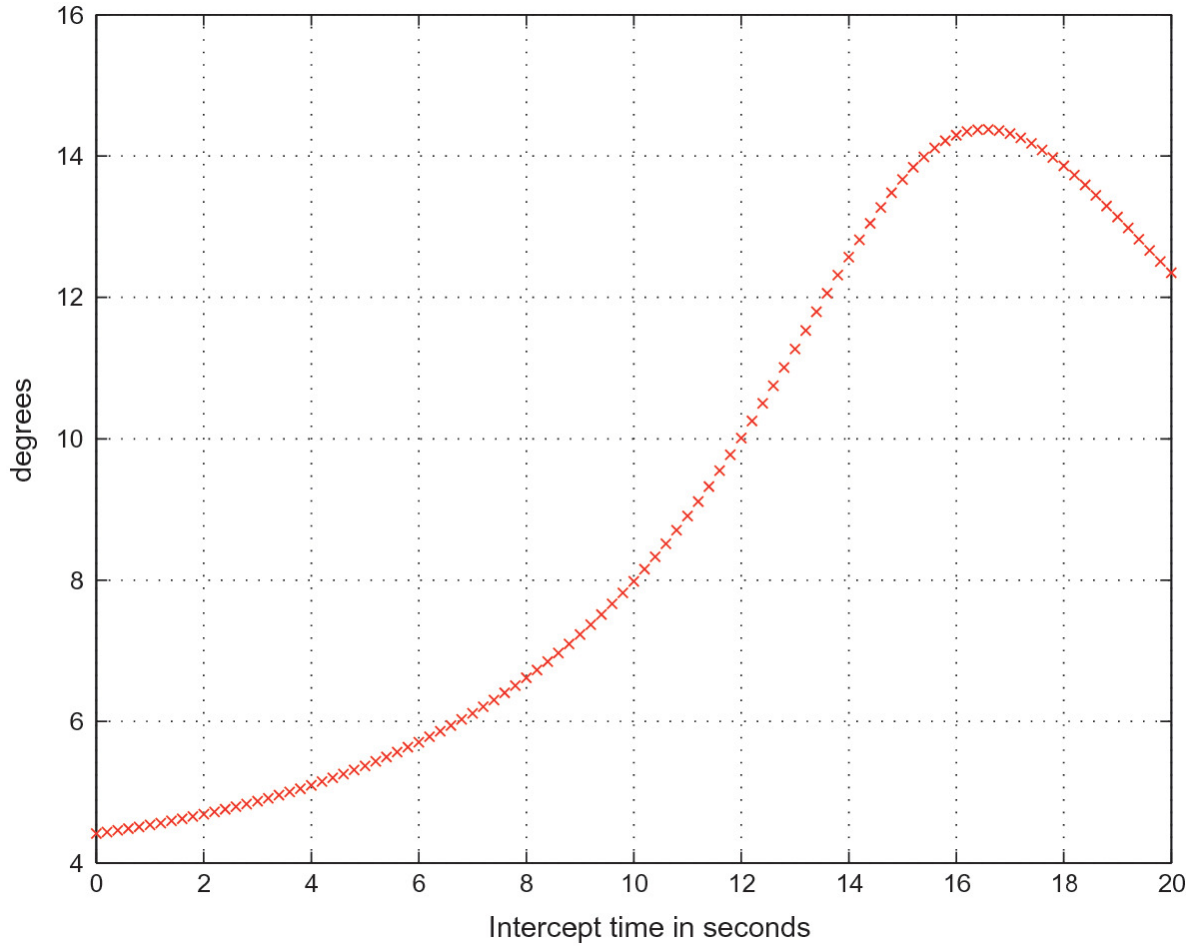


Fig. 7.10 Plot of the lead azimuth angle $a_{lead}(t_{fire,k})$ versus the intercept time $t \geq 0$,
 $k = 1, 2, \dots, n_f$: vehicle body of mobile ADS is stationary

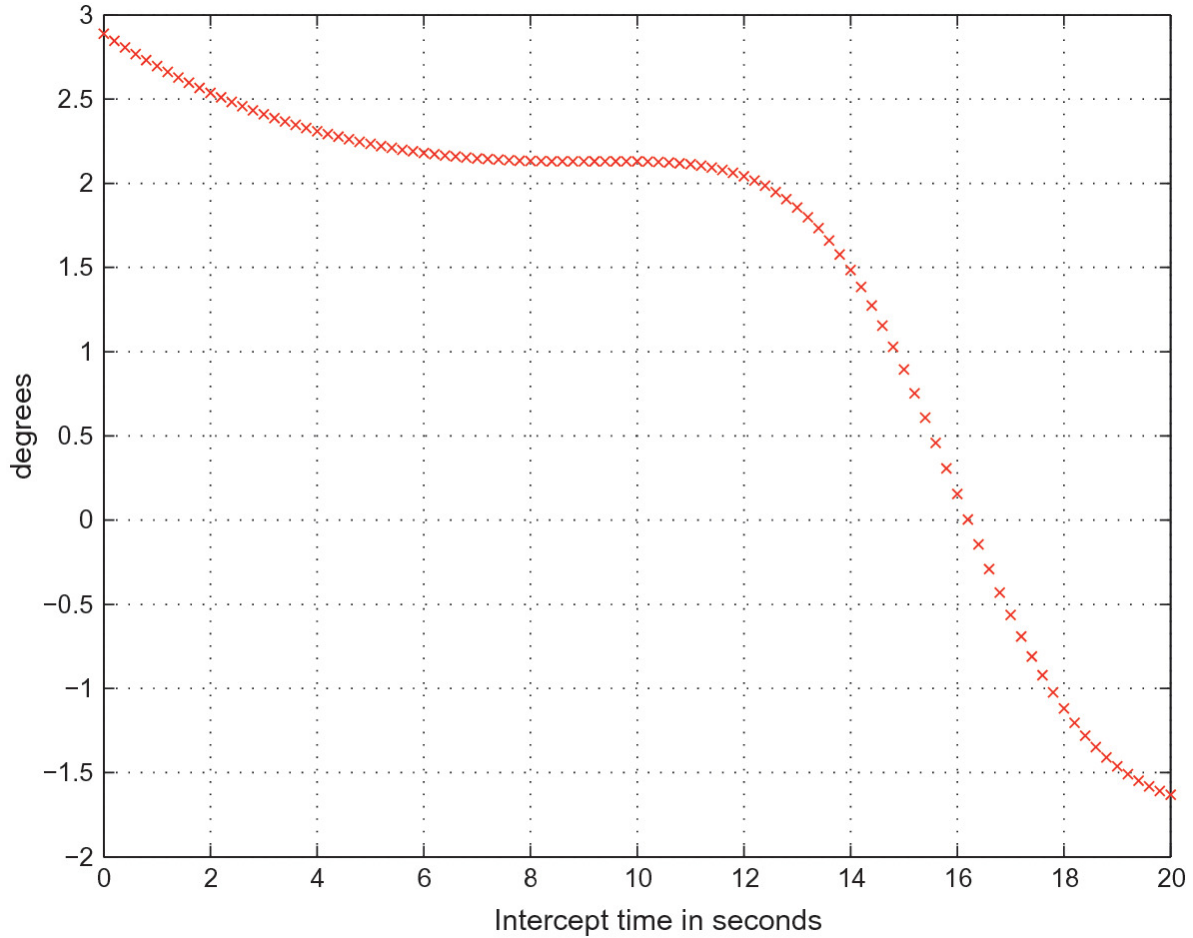


Fig. 7.11 Plot of the lead elevation angle $a_{lead}(t_{fire,k})$ versus the intercept time $t \geq 0$,
 $k = 1, 2, \dots, n_f$: vehicle body of mobile ADS is stationary

With reference to the computational results presented in Figs. 7.3, 7.4, 7.5, 7.6, 7.7, 7.8, 7.9, 7.10 and 7.11, note the following.

1. The results are plotted versus the discrete intercept times $t \geq 0$, $k = 1, 2, \dots, n_f$, (7.55), on the horizontal axis in Figs. 7.4, 7.5, 7.6, 7.7, 7.8, 7.9, 7.10 and 7.11. Variables that are indicated as being functions of the firing time $t \geq 0$ are also plotted versus the discrete intercept times $t \geq 0$, $k = 1, 2, \dots, n_f$.
2. It can be seen from Fig. 7.5 that the inertial elevation angle of the velocity vector of the AA projectile at the intercept time with the

CM of the AAT, $t \geq 0$, is positive for all $k = 1, 2, \dots, n_f$,

$$\mathbf{e}_{proj}(t_{hitC,k}; t_{fire,k}) > 0, \quad k = 1, 2, \dots, n_f. \quad (7.60)$$

In this work it will be assumed throughout that condition (7.60) holds. Thus, engagement scenarios where $\mathbf{e}_{proj}(t_{hitC,k}; t_{fire,k}) \leq 0$

are not considered, that is, scenarios where the AA projectile at the intercept time $t \geq 0$ is moving parallel to or falling towards the

(X, Y) plane.

3. The minimum distance $\|\mathbf{r}_{los}^{(I)}(t_{hitC,k})\|$ is 1157.1 m and occurs at time $t_{hitC,k} = 15.4$ s. This particular AAT position is known as the closest point of approach (CPA).

4. The intercept speed of the AA projectile is given by

$$\|\mathbf{v}_{proj}^{(I)}(t_{hitC,k}; t_{fire,k})\|. \quad (7.61)$$

The relative intercept speed of the AA projectile is defined as follows

$$\|\mathbf{v}_{proj}^{(I)}(t_{hitC,k}; t_{fire,k}) - \mathbf{v}_{targ}^{(I)}(t_{hitC,k})\|. \quad (7.62)$$

Figure 7.3 shows plots of the AA projectile trajectories intercepting the center of mass of the AAT for the following selection of intercept times $t \geq 0$, $k = 1, 3, 5, \dots, n_f = 101$. The projection of the trajectory of the AAT onto the (X, Y) plane is also shown, as well as part of a circle with center the origin O_I and with radius ϵ_1 .

As shown in Fig. 7.4, the inertial azimuth angle of the FC vector is always larger than the inertial azimuth angle of the LOS vector at the firing time $t \geq 0$, see also Fig. 7.10. The above is true for the case of the

inertial elevation angles, except when the AAT is moving away from the mobile ADS, see Figs. 7.5, 7.11 and 7.6.

The maximum intercept speed, (7.61), is 922.3 m/s and occurs at time $t_{hitC,k} = 15.4$ s (see Fig. 7.9), that is, at the CPA. The maximum relative intercept speed, (7.62), is 1032.7 m/s and occurs at time $t_{hitC,k} = 12.4$ s (see Fig. 7.9).

7.5 Computational Results for Fire Control Problem FCA: Vehicle Body of Mobile ADS is Moving in a Straight Line at Constant Speed

In this case the vehicle body of the mobile ADS is moving forward in a straight line at constant speed k_0 throughout the engagement of the

AAT. If the following parameter values are assumed ((7.24))

$$v_b = 20 \text{ m/s}, \quad \beta_b = -\pi/2, \quad (7.63)$$

then it follows that

$$\mathbf{v}_H^{(I)}(t) = \mathbf{v}_{OA}^{(I)}(t) = \begin{bmatrix} 20 \\ 0 \\ 0 \end{bmatrix} \text{ m/s}, \quad t \in \mathcal{T}_F. \quad (7.64)$$

The computational results are presented in Figs. 7.12, 7.13, 7.14, 7.15, 7.16, 7.17, 7.18, 7.19 and 7.20. In this case $\Delta_{tofC,1} = 5.99701$ s, (7.54).

The CPA is 1354.0 m and occurs at time $t_{hitC,k} = 12.4$ s, see Fig. 7.17.

In Fig. 7.12, the AA projectile trajectory intercepts the center of mass of the AAT at each given intercept time $t \geq 0$, while the inertial position of the muzzle of the AA gun during the motion of the mobile ADS is also depicted, for $k = 1, 3, 5, \dots, n_f = 101$.

As shown in Fig. 7.19 the lead azimuth angle $\mathbf{a}_{lead}(t_{fire,k})$ is in this case larger than the case where the mobile ADS is stationary (see Fig.

7.10) due to the forward motion of the mobile ADS at a constant speed and in a straight line that is parallel to δ_3 .

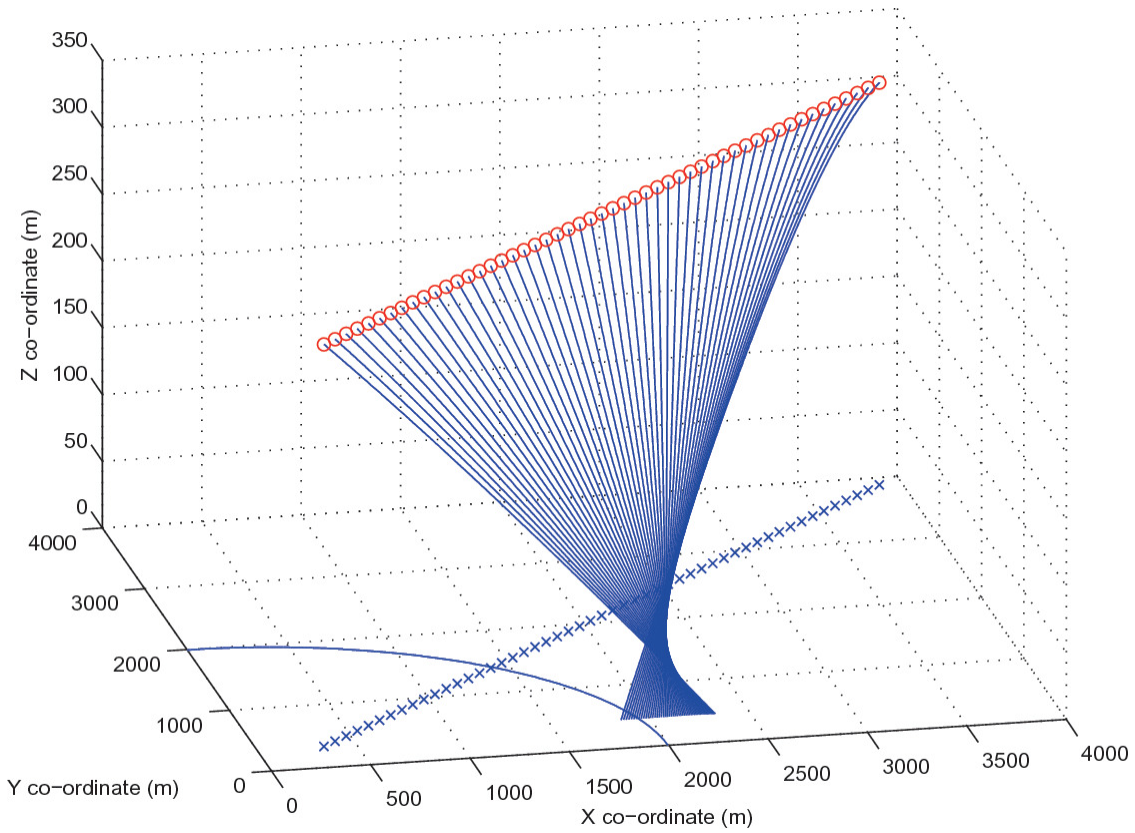


Fig. 7.12 Plot of the inertial X, Y, Z, co-ordinates of the AA projectile trajectory $\mathbf{r}_{proj}^{(I)}(\tau; t_{fire,k})$, $\tau \in [t_{fire,k}, t_{hitC,k}]$, for $k = 1, 3, 5, \dots, n_f$, and of points on the AAT trajectory $\mathbf{r}_{projx}^{(I)}(t_{hitG})$, (o), $k = 1, 3, 5, \dots, n_f$: vehicle body of mobile ADS is moving

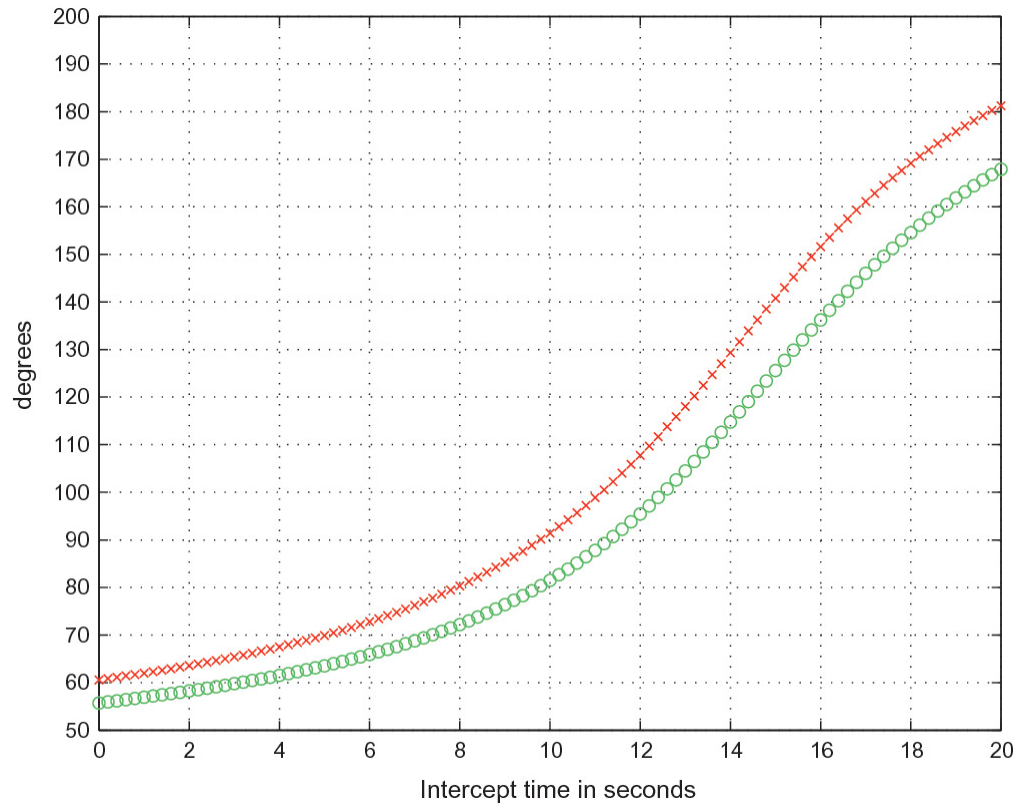


Fig. 7.13 Plot of the inertial azimuth angle of the FC vector $\mathbf{a}_{FC}(t_{fire,k})$, (x), and the inertial azimuth angle of the LOS vector $(A_f) = 11$, (o), versus the intercept time $t \geq 0$, $k = 1, 2, \dots, n_f$: vehicle body of mobile ADS is moving

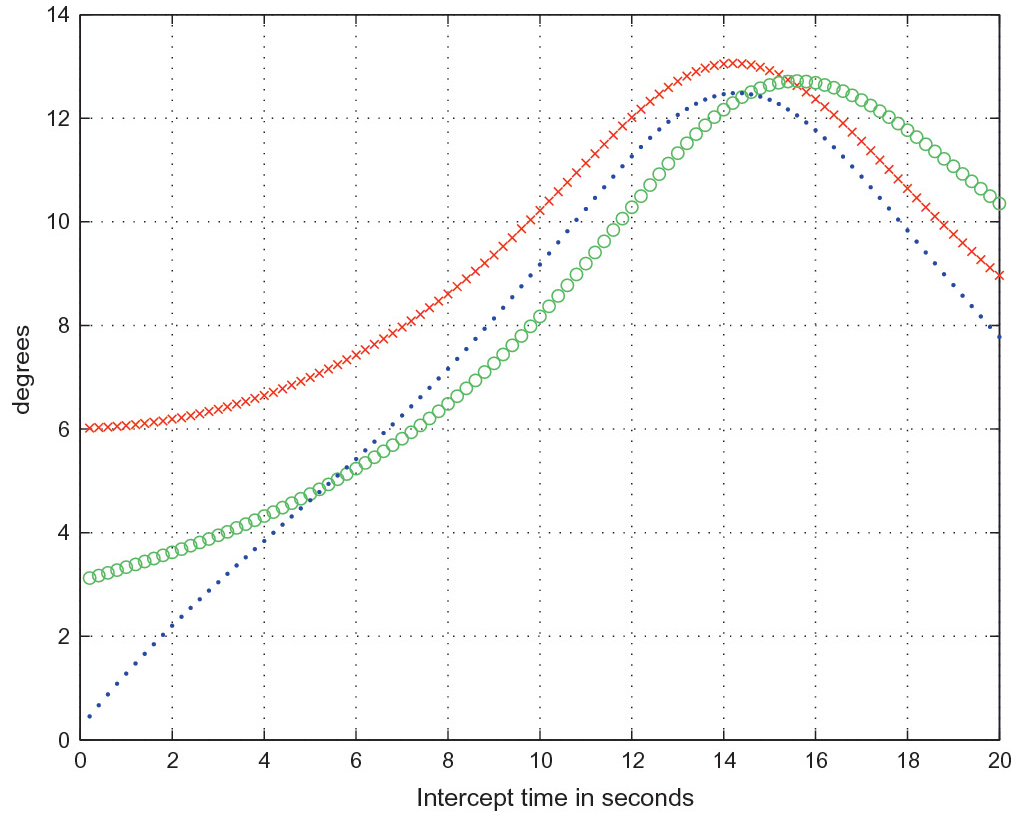


Fig. 7.14 Plot of the inertial elevation angle of the FC vector $\mathbf{a}_{FC}(t_{fire,k})$, (x), the inertial elevation angle of the LOS vector $(A_f) = 11$, (o), and the inertial elevation angle of the projectile velocity vector $\mathbf{e}_{proj}(t_{hitC,k}; t_{fire,k})$, (·), versus the intercept time $t \geq 0$, $k = 1, 2, \dots, n_f$: vehicle body of mobile ADS is moving

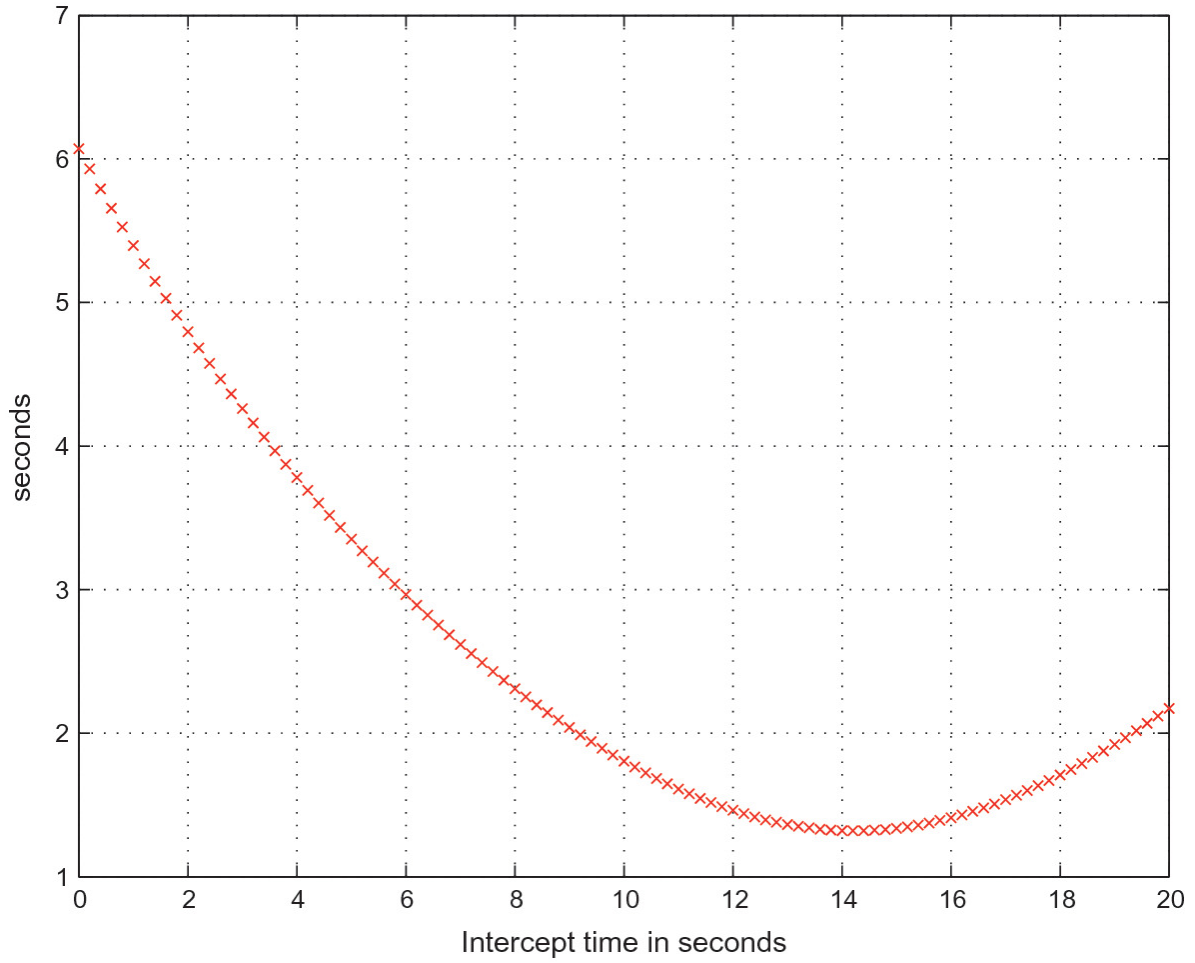


Fig. 7.15 Plot of the time of flight of the AA projectile $\Delta_{tofC,k}$ versus the intercept time $t \geq 0$, $k = 1, 2, \dots, n_f$: vehicle body of mobile ADS is moving

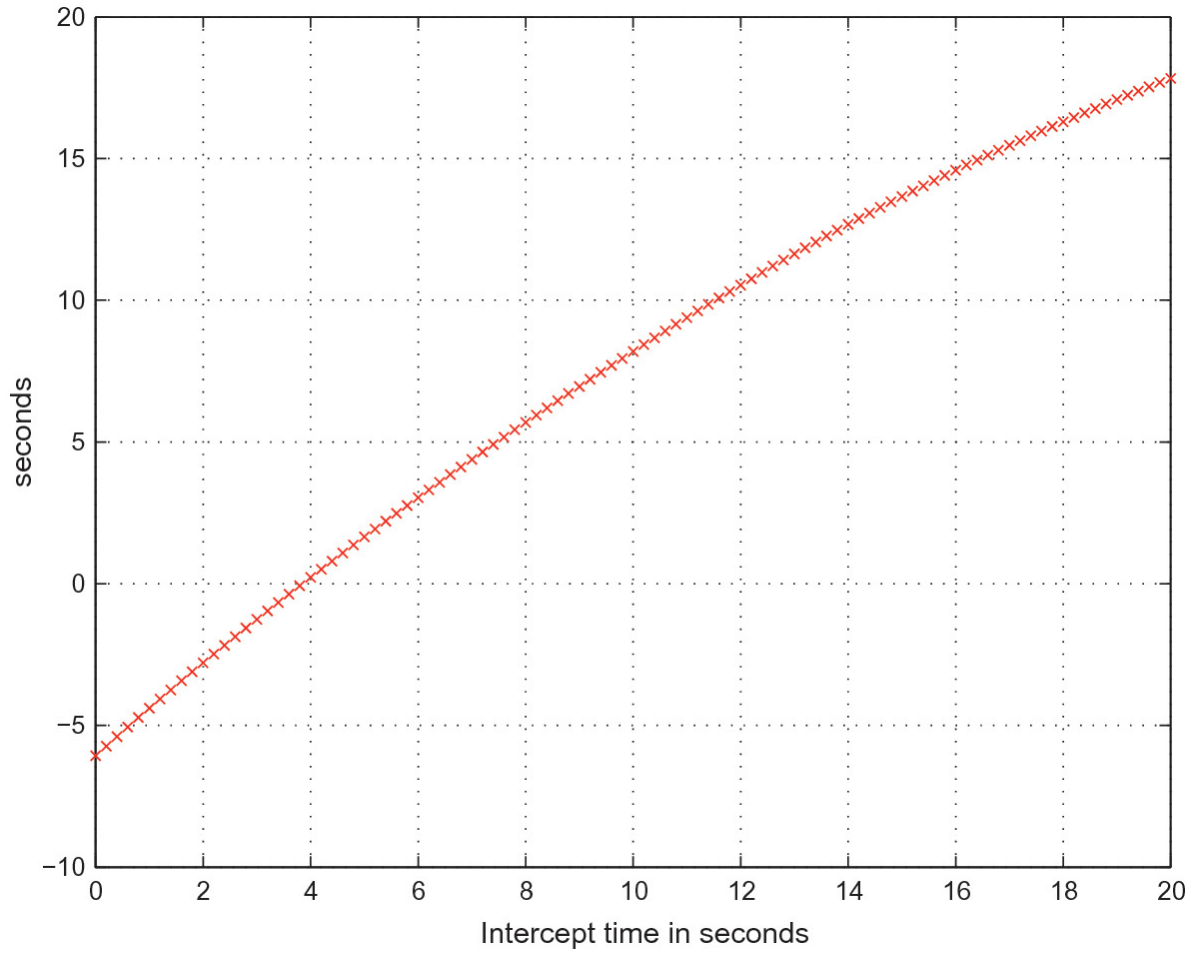


Fig. 7.16 Plot of the firing time of the AA projectile $t \geq 0$ versus the intercept time $t \geq 0$,

$k = 1, 2, \dots, n_f$: vehicle body of mobile ADS is moving

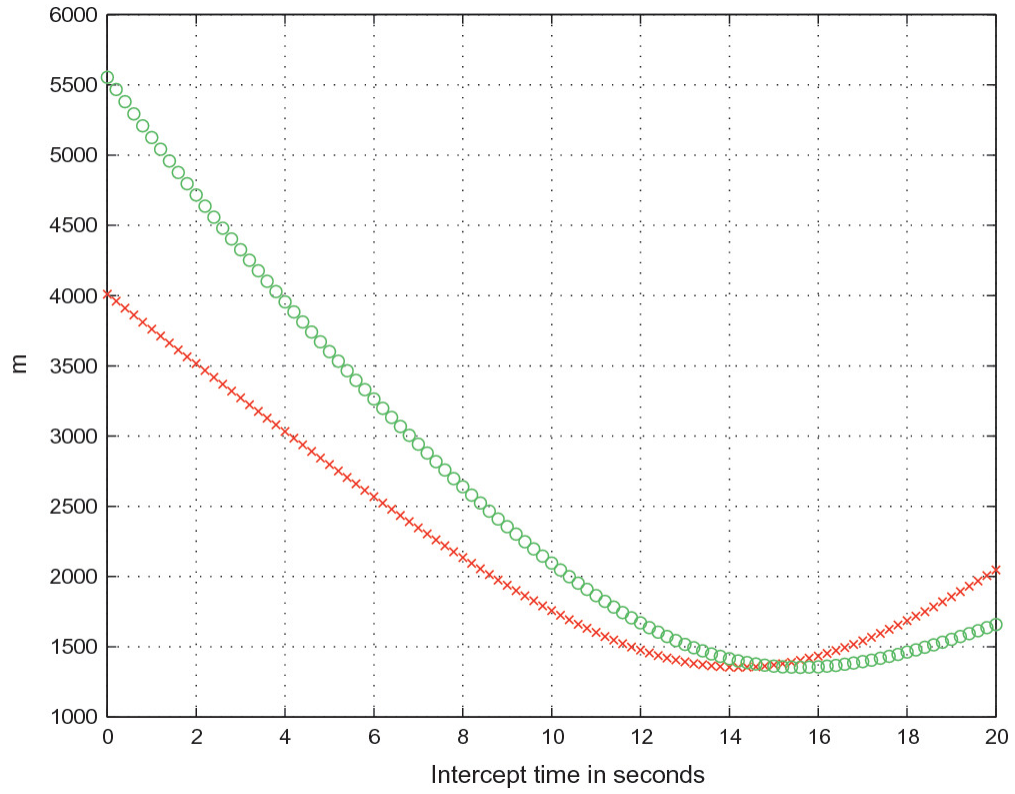


Fig. 7.17 Plot of the LOS distance $\|\mathbf{r}_{los}^{(I)}(t_{hitC,k})\|$, (x), and the LOS distance $\|\mathbf{r}_{los}^{(I)}(t_{hitC,k})\|$, (o), versus the intercept time $t \geq 0$, $k = 1, 2, \dots, n_f$: vehicle body of mobile ADS is moving

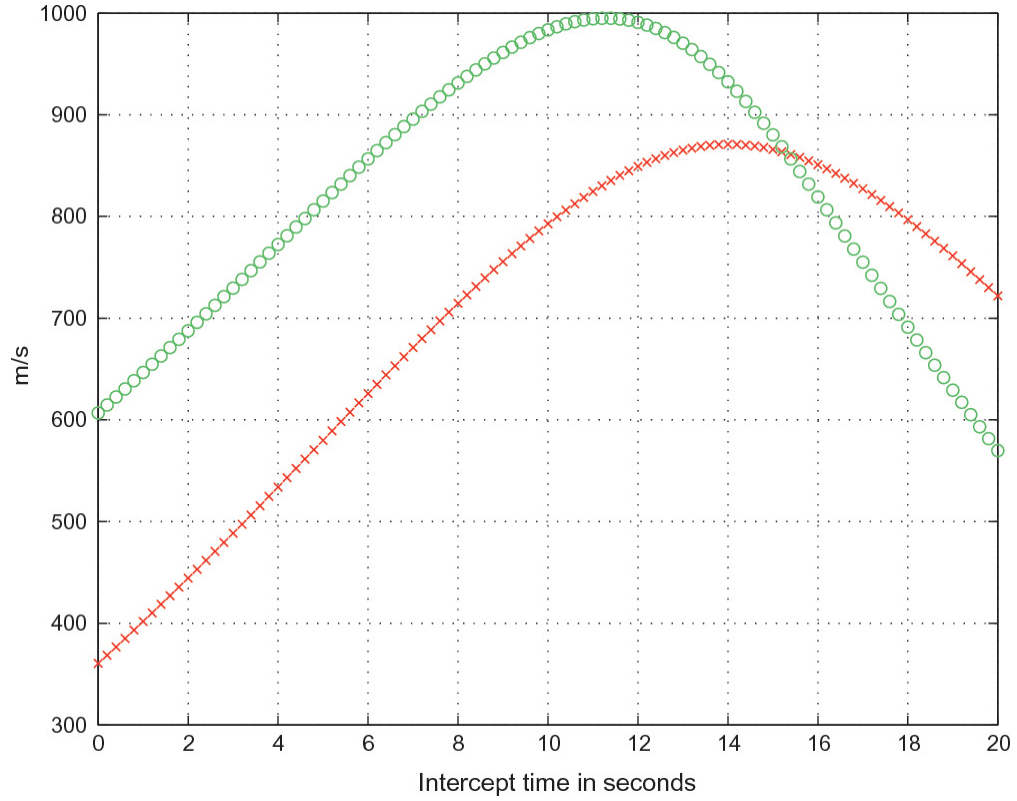


Fig. 7.18 Plot of the intercept speed of the AA projectile $\|\mathbf{v}_{proj}^{(l)}(t_{hitC,k}; t_{fire,k})\|$, (x), and the relative intercept speed of the AA projectile $\|\mathbf{v}_{proj}^{(l)}(t_{hitC,k}; t_{fire,k}) - \mathbf{v}_{targ}^{(l)}(t_{hitC,k})\|$, (o), versus the intercept time $t \geq 0$, $k = 1, 2, \dots, n_f$: vehicle body of mobile ADS is moving

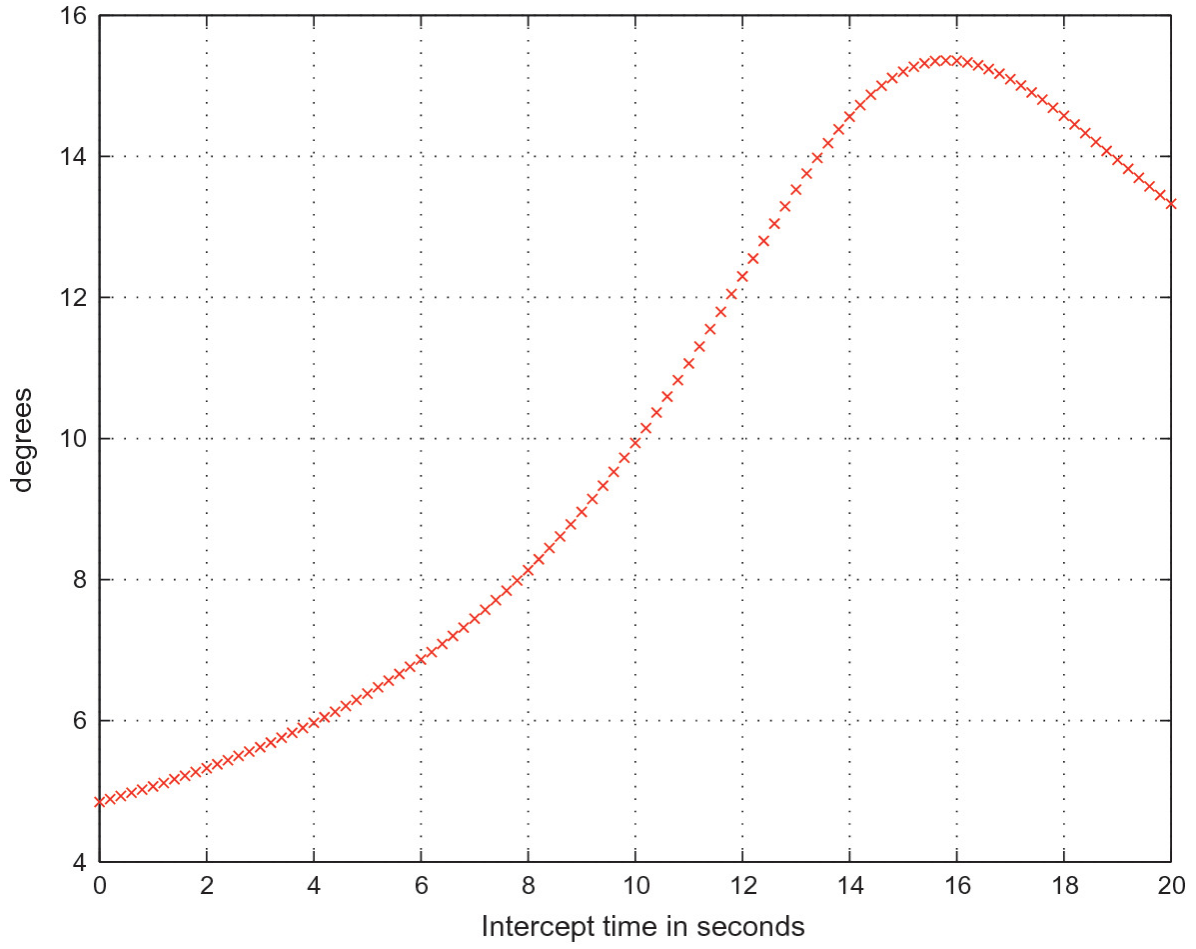


Fig. 7.19 Plot of the lead azimuth angle $a_{lead}(t_{fire,k})$ versus the intercept time $t \geq 0$,
 $k = 1, 2, \dots, n_f$: vehicle body of mobile ADS is moving

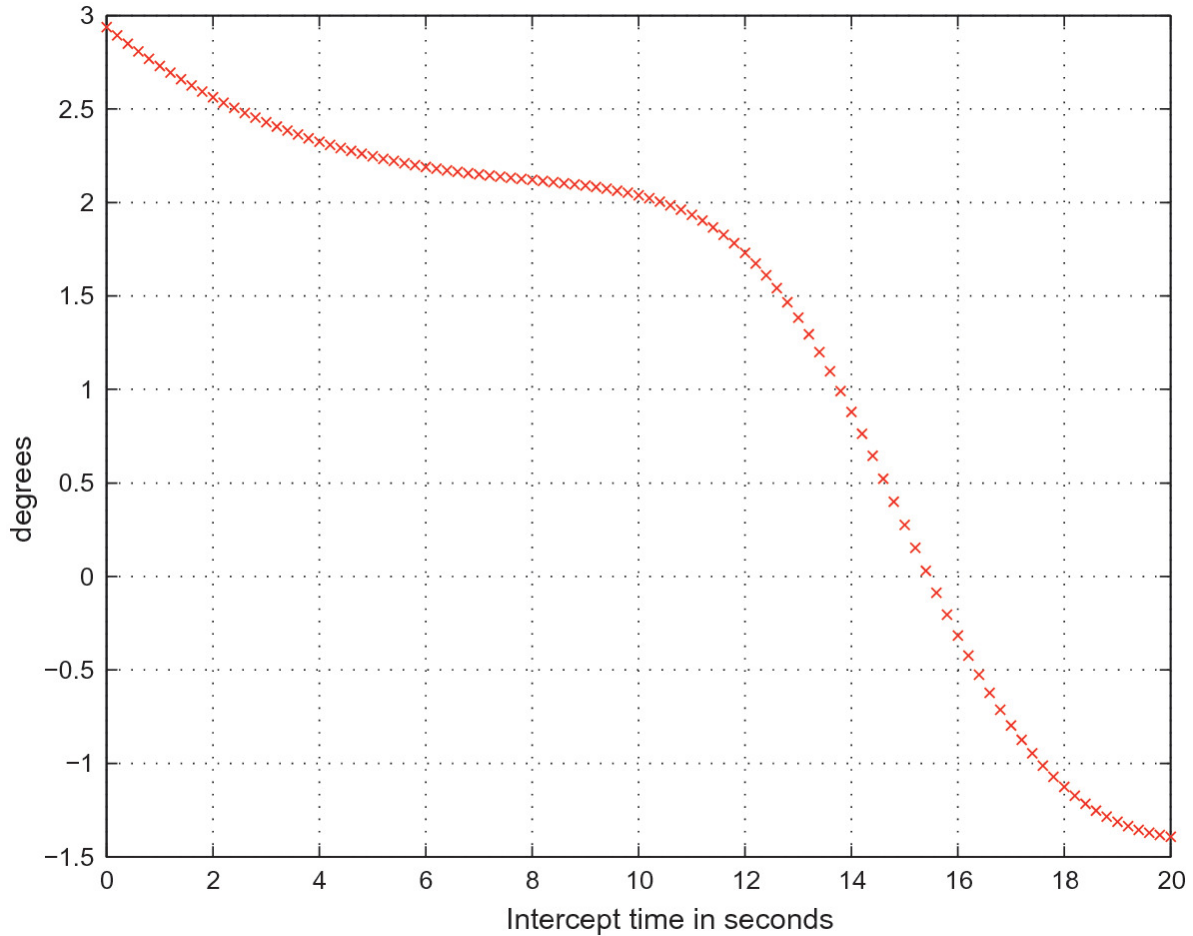


Fig. 7.20 Plot of the lead elevation angle $a_{lead}(t_{fire,k})$ versus the intercept time $t \geq 0$, $k = 1, 2, \dots, n_f$: vehicle body of mobile ADS is moving

The maximum intercept speed, (7.61), is 870.9 m/s and occurs at time $t_{hitC,k} = 14$ s (see Fig. 7.18), that is, close to the CPA. The maximum relative intercept speed, (7.62), is 995 m/s and occurs at time $t_{hitC,k} = 12.4$ s (see Fig. 7.18). The intercept speed and relative intercept speed values are lower than the corresponding values for the case of the stationary mobile ADS. The main reason is that the mobile ADS is moving parallel to δ_3 , and after some point is effectively moving away from the AAT.

Footnotes

¹ In practice, there will be several mobile ADSs deployed and suitably positioned in order to jointly engage one or more AATs.

8. Computation of the Impact Point of the AA Projectile on the Body of the Attacking Aerial Target

Constantinos Frangos¹ 

(1) Electrical Engineer working in Decision and Control, Pretoria, South Africa

This Chapter deals with the computation of the impact point of the AA projectile on the body of the AAT as follows.

1. The geometry of the three-dimensional body of the AAT is given in Fig. 8.1. A body reference frame B_{targ} is defined with origin fixed at the center of mass of the AAT.
 2. A computational method is presented for computing the impact point of the AA projectile on the body of the AAT relative to the origin of the body reference frame B_{targ} and expressed in B_{targ} .
-

8.1 Geometry of the Attacking Aerial Target

In this work the AAT is assumed to have the geometry shown in Fig. 8.1. The body of the AAT consists of a half-sphere of radius p_s mounted on a cylinder of length L_1 and radius p_s , $-m_g g L_g \cos(\zeta)$, p_s ,

$T_{\gamma_0}, L_{a2} > 0$. The surfaces of the half-sphere and cylinder are closed.

The longitudinal axis of the AAT coincides with the longitudinal axis of the cylinder.

It is assumed that there is a body reference frame B_{targ} and an associated co-ordinate system $-T_{\delta_v} I_3 Y_{B_{targ}}, = \pi/4$ with unit vectors $h_s > a = \pi/4 y_1 \in \mathbb{R}$ and with origin fixed at the center of mass of the AAT (Fig. 8.1).

It is assumed that the CM lies on the longitudinal axis of the AAT and that the $(X_{B_{10}}$ axis points forward and coincides with the longitudinal axis of the AAT. The $X_{B_{targ}}$ axis is perpendicular to the $(X_{B_{10}}$ axis and is parallel to the inertial (X, Y) plane during level flight. The $(X_{B_{10}}$ axis points up and is perpendicular to the $(X_{B_{targ}}, Y_{B_{targ}})$ plane.

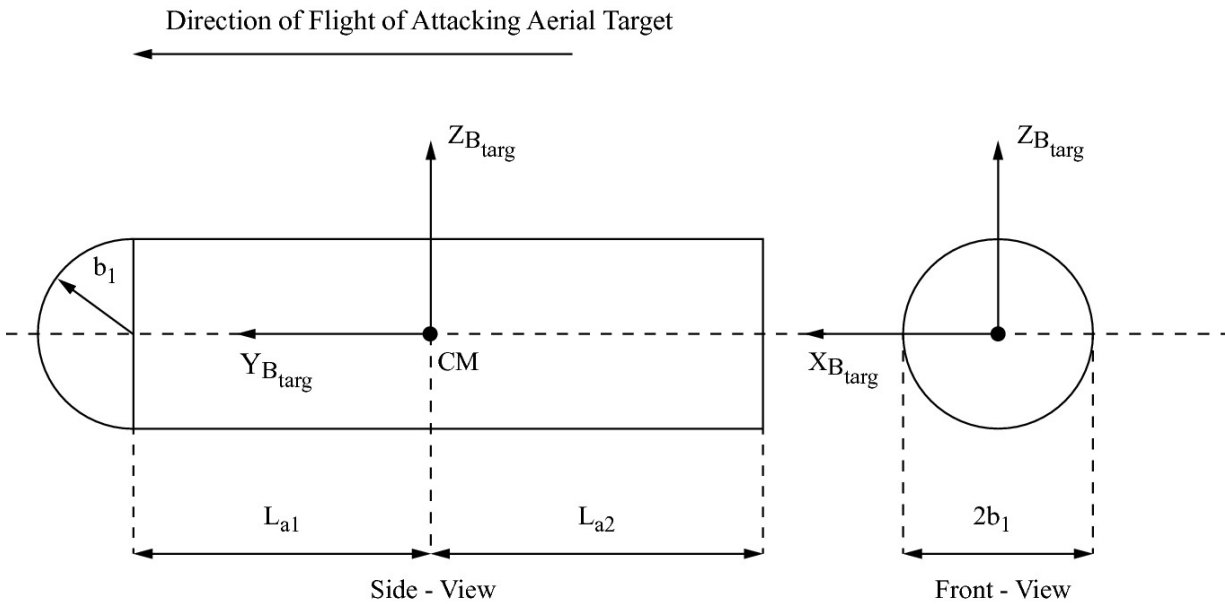


Fig. 8.1 Schematic of attacking aerial target

The AA projectile impacts the body of the AAT if it enters the space occupied by the half-sphere or the space occupied by the cylinder.¹ The

above-mentioned spaces are sets of position vectors $[x_0, y_0, z_0]^\top$ defined relative to the origin of the body reference frame B_{targ} and expressed in B_{targ} , as follows

$$\begin{aligned} \mathbf{V}_{hs} = \{ [x_0, y_0, z_0]^\top \in \mathbb{R}^3 : x_0^2 + z_0^2 + (y_0 - L_{a1})^2 \leq b_1^2, \\ L_{a1} \leq y_0 \leq L_{a1} + b_1 \}, \end{aligned} \quad (8.1)$$

$$\delta_4 = \arctan2 (L_c \sin(\delta_v), L_2 \sin(\delta_v) + L_c \cos(\delta_v)), \quad (8.2)$$

The sets T_{γ_0} and \mathbf{V}_{cyl} have common elements, that is, the disk shaped surface on the right part of the half-sphere coincides with the disk shaped surface on the left part of the cylinder (Fig. 8.1). It follows that the set $\mathbf{V}_{hs} \cap \mathbf{V}_{cyl}$ is not empty.

The sets T_{γ_0} and \mathbf{V}_{cyl} are defined by inequalities, (8.1), (8.2). By using penalty functions, the sets T_{γ_0} and \mathbf{V}_{cyl} can each be defined by a single equality as follows

$$\mathbf{V}_{hs} = \{ [x_0, y_0, z_0]^\top \in \mathbb{R}^3 : C_{hs}(x_0, y_0, z_0) = 0 \}, \quad (8.3)$$

$$\begin{aligned} C_{hs} = \text{pen}_a(\sqrt{x_0^2 + z_0^2 + (y_0 - L_{a1})^2}, 0, b_1) \\ + \text{pen}_a(y_0, L_{a1}, L_{a1} + b_1), \end{aligned} \quad (8.4)$$

$$\mathbf{V}_{cyl} = \{ [x_0, y_0, z_0]^\top \in \mathbb{R}^3 : C_{cyl}(x_0, y_0, z_0) = 0 \}, \quad (8.5)$$

$$C_{cyl} = \text{pen}_a(\sqrt{x_0^2 + z_0^2}, 0, b_1) + \text{pen}_a(y_0, -L_{a2}, L_{a1}), \quad (8.6)$$

where pen_a is an absolute value penalty function given by ([11, 30, 140, 164])

$$(8.7)$$

$$\text{pen}_a(x_b, x_{min}, x_{max}) = \begin{cases} x_b - x_{max} & \text{if } x_b > x_{max} \\ 0 & \text{if } x_{min} \leq x_b \leq x_{max} \\ x_{min} - x_b & \text{if } x_b < x_{min} \end{cases},$$

$x_{min} < x_{max}$, B_i , J_{b23} , $x_{max} \in \mathbb{R}$. In the sequel the impact of the AA projectile on the body of the AAT will be described by using the set B_{targ} given by

$$\begin{aligned} V_{targ} &= \{[x_0, y_0, z_0]^\top \in \mathbb{R}^3 : [x_0, y_0, z_0]^\top \in V_{hs} \text{ or } [x_0, y_0, z_0]^\top \in V_{cyl}\} \\ &= V_{hs} \cup V_{cyl}. \end{aligned} \quad (8.8)$$

By using (8.3)–(8.7) the set B_{targ} is equivalently defined as follows

$$\begin{aligned} V_{targ} &= \{[x_0, y_0, z_0]^\top \in \mathbb{R}^3 : C_{hs}(x_0, y_0, z_0) = 0 \text{ or} \\ &C_{cyl}(x_0, y_0, z_0) = 0\}. \end{aligned} \quad (8.9)$$

Attacking aerial targets can have a more complicated geometry and incorporate, for example, wings, tail planes, fins, canards, etc. The set B_{targ} for such AATs can be defined in a manner analogous to that given above.

8.2 Inertial Trajectory of the Attacking Aerial Target

The following assumptions are applicable with regard to the inertial trajectory of the AAT.

1. The inertial trajectory of the center of mass of the AAT, $\mathbf{r}_{targ}^{(I)}(t)$, as

well as the Euler angles and Euler angular rates are specified as follows

$$\mathbf{r}_{targ}^{(I)}(t), \quad \frac{d_I \mathbf{r}_{targ}^{(I)}(t)}{dt}, \quad \frac{d_I^2 \mathbf{r}_{targ}^{(I)}(t)}{dt^2}, \quad t \in \mathcal{T}_F. \quad (8.10)$$

$$\Psi_{targ}(t), \Theta_{targ}(t), \Phi_{targ}(t), \quad \dot{\Psi}_{targ}(t), \dot{\Theta}_{targ}(t), \dot{\Phi}_{targ}(t), \quad t \in \mathcal{T}_F. \quad (8.11)$$

The dynamic model of the AAT and the feedback control law required to produce the specified motion of the AAT, (8.10), (8.11), are not considered in this work.

2. The rotation matrix from the inertial reference frame I to the body reference frame B_{targ} of the AAT is given by (Appendix A)

$$\begin{aligned} \mathbf{R}_{I2B_{targ}} &= \mathbf{R}_Y(\Phi_{targ})\mathbf{R}_X(\Theta_{targ})\mathbf{R}_Z(\Psi_{targ}), \\ \mathbf{R}_{B_{targ}2I} &= \mathbf{R}_{I2B_{targ}}^\top. \end{aligned} \quad (8.12)$$

3. Consider the AAT motion trajectory presented in Chap. 7. The AAT is flying towards the defended location in a straight line, without rolling or pitching, at constant altitude $X_{B_{11}}$ and at a constant speed $c_{3u,k}$ (Fig. 7.2). Thus, it follows that the inertial velocity vector of the center of mass of the AAT is parallel to $\mathbf{J}_{B_{targ}}^{(I)}$ and is given by ((7.49))

$$\begin{aligned} \mathbf{v}_{targ}^{(I)}(t) &= -v_{targ}\mathbf{e}_{targ}, \\ \mathbf{e}_{targ} &= \cos(\theta_{targ})\mathbf{I}_1 + \sin(\theta_{targ})\mathbf{I}_2, t \in \mathcal{T}_F. \end{aligned} \quad (8.13)$$

The above implies that the inertial azimuth angle of the velocity vector is $\alpha_{targ} = \pi + \theta_{targ}$, and that the Euler azimuth angle of the body reference frame B_{targ} is constant and is given by

$$\Psi_{targ} = \pi + \theta_{targ} - \pi/2 = \theta_{targ} + \pi/2, \quad \dot{\Psi}_{targ} = 0, \quad t \in \mathcal{T}_F. \quad (8.14)$$

All the other Euler angles and Euler angular rates are zero ((8.11)).

4. It follows that the associated rotation matrix is given by ((8.12), Appendix A)

$$\mathbf{R}_{I2B_{targ}} = \mathbf{R}_Z(\Psi_{targ}), \quad \mathbf{R}_{B_{targ}2I} = \mathbf{R}_{I2B_{targ}}^\top, \quad t \in \mathcal{T}_F. \quad (8.15)$$

8.3 Computation of the Impact Point of the AA Projectile on the Body of the Attacking Aerial Target

The computational results for fire control problem FCA are employed for the case of a completely stationary vehicle body of the mobile ADS as obtained in Chap. 7. Thus, for each given intercept time of the AA projectile with the CM of the AAT, $t \geq 0$, the following have been

computed for $k = 1, 2, \dots, n_f$.

1. The inertial azimuth and elevation angles of the FC vector $\mathbf{a}_{FC}(t_{fire,k})$, $\mathbf{a}_{FC}(t_{fire,k})$.
2. The time of flight of the AA projectile to the CM of the AAT, $\Delta_{tofC,k}$.
3. The firing time of the AA projectile is thus $t_{fire,k} = t_{hitC,k} - \Delta_{tofC,k}$.
4. In Chap. 7 the geometry of the body of the AAT is ignored. Thus, the AA projectile that is fired at time $t \geq 0$, travels over the time interval

$$\mathcal{T}_{FL,k} = [t_{fire,k}, t_{hitC,k}], \quad (8.16)$$

until intercept with the CM of the AAT at time $t \geq 0$.

5. In this Chapter the geometry of the body of the AAT is taken into account. Thus, the AA projectile will actually impact the body of the AAT at some time $t_{hitT,k}$ slightly before the intercept time with the CM, $t \geq 0$, and $t_{hitT,k} \in \mathcal{T}_{FL,k}$.

The position vector of the AA projectile fired at time $t \geq 0$ relative to the CM of the AAT at time t is given by

$$\mathbf{r}_{rel}^{(I)}(t; t_{fire,k}) = \mathbf{r}_{proj}^{(I)}(t; t_{fire,k}) - \mathbf{r}_{targ}^{(I)}(t), \quad t \in \mathcal{T}_{FL,k}, \quad (8.17)$$

where $\mathbf{r}_{proj}^{(I)}(t; t_{fire,k})$ is obtained by solving the point mass flight dynamics model of the AA projectile (7.19). The vector $\mathbf{r}_{rel}^{(I)}(t; t_{fire,k})$ is expressed in the body reference frame B_{targ} as follows ((8.12))

$$\mathbf{r}_{rel}^{(B_{targ})}(t; t_{fire,k}) = \mathbf{R}_{I2B_{targ}} \mathbf{r}_{rel}^{(I)}(t; t_{fire,k}), \quad t \in \mathcal{T}_{FL,k}. \quad (8.18)$$

In order to simplify the presentation, $t \geq 0$ is replaced by k and the superscript $h_s > a$ is suppressed, as follows

$$\begin{aligned} \mathbf{r}_{rel}(t; k) &= \mathbf{r}_{rel}^{(B_{targ})}(t; t_{fire,k}), \\ \mathbf{r}_{rel}(t; k) &= [r_{relx}(t; k), r_{rely}(t; k), r_{relz}(t; k)]^\top, \quad t \in \mathcal{T}_{FL,k}. \end{aligned} \quad (8.19)$$

The AA projectile impacts the body of the AAT at time $t_{hitT,k}$ implying that $\mathbf{r}_{rel}(t_{hitT,k}; k) \in V_{targ}$, (8.9). Thus, the impact point of the AA projectile on the body of the AAT is $\mathbf{r}_{rel}(t_{hitT,k}; k)$.

In order to accurately compute the impact time and the impact point of the AA projectile on the body of the AAT the following approach is applied. Consider a sphere with radius k_0 and with center fixed to the CM of the AAT. This sphere completely encloses the AAT and is referred to as the target bounding sphere (TBS). It follows that k_0 must be larger than the radius of the sphere that just encloses the body of the AAT. The space of the TBS is defined by the following set

$$\Rightarrow \text{Kinematic Model of the Vehicle System:} \quad (8.20)$$

The set V_{TBS} is equivalently defined as follows

$$V_{TBS} = \{[x_0, y_0, z_0]^T \in \mathbb{R}^3 : C_{TBS}(x_0, y_0, z_0) = 0\}, \quad (8.21)$$

where

$$C_{TBS} = \text{pen}_a(\sqrt{x_0^2 + y_0^2 + z_0^2}, 0, c_0). \quad (8.22)$$

As soon as the incoming AA projectile enters the space of the TBS then a much smaller time-step Δ_{fine} is used in the numerical computation of the trajectory of the AA projectile and of the AAT,

$$\mathbf{A}_f \mathbf{p} = \mathbf{0}_{11 \times 1}. \quad (8.23)$$

In this manner the final approach of the AA projectile towards the AAT is computed more accurately thus leading to a more accurate computation of the impact time and the impact point of the AA projectile on the body of the AAT. If the values of the time-steps Δ_{sim} , Δ_{fine} , are decreased and the value of the TBS radius k_0 is increased then this will generally result in a more accurate computation of the impact time and impact point. However, a longer computation time will be required.

The details of the computational procedure are as follows.

1. A suitable numerical integration algorithm (for example, a fourth order Runge-Kutta algorithm) with a fixed time-step Δ_{sim} is applied in order to compute all variables of interest at discrete times in the set $\mathcal{T}_{comp,k}$ given by ((6.59))

$$\begin{aligned} \mathcal{T}_{comp,k} &= \{t_{a,k,1}, t_{a,k,2}, \dots, t_{a,k,N_{c1,k}}\} \\ &= \{t_{fire,k}, t_{fire,k} + \Delta_{sim}, \dots, t_{hitC,k}\}, \end{aligned} \quad (8.24)$$

where $N_{c1,k} = N_{set}(\mathcal{T}_{comp,k})$, $N_{set}(x_a)$ denotes the number of elements in the set B_i , and $t_{a,k,1}, t_{a,k,2}, \dots, t_{a,k,N_{c1,k}}$ are used as

auxiliary variables.

2.

In particular, the computations are performed as follows. Consider the time interval $\mathcal{T}_{comp,k,i}$ defined by the i th consecutive pair of times in $\mathcal{T}_{comp,k}$, (8.24),

$$\mathcal{T}_{comp,k,i} = (t_{a,k,i}, t_{a,k,i+1}], \quad i = 1, 2, \dots, N_{c1,k} - 1. \quad (8.25)$$

At the end of each time interval $\mathcal{T}_{comp,k,i}$, $i = 1, 2, \dots, N_{c1,k} - 1$, and having computed $\mathbf{p}_s(t_0) = \mathbf{p}_{s0}$ and other variables of interest at time $Y_{B_{targ}}$, the numerical integration algorithm programmatically calls a suitable algorithm (in this case, an advanced regula falsi based algorithm implemented in the MATLAB function `odezero`, [32, 110, 120]) in order to find the first time $t \in \mathcal{T}_{comp,k,i}$ where $[t_{fire}, t]$ is an element of the set V_{TBS} , (8.21),

$$\mathbf{r}_{rel}(t; k) \in V_{TBS} \Rightarrow$$

$$C_{TBS}(r_{relx}(t; k), r_{rely}(t; k), r_{relz}(t; k)) = 0. \quad (8.26)$$

3. If such a time t can be found then the intercept time of the AA projectile with the TBS is $\mathbf{q}(t) \in P_0$. The same numerical integration algorithm using a fixed time-step Δ_{fine} is applied in order to compute all variables of interest from the time $T_{\gamma_0} \mathbf{I}_3$ to the specified intercept time $t \geq 0$ at discrete times in the set $\mathcal{T}_{TBS,k}$ given by ((6.59))

$$\begin{aligned} \mathcal{T}_{TBS,k} &= \{t_{b,k,1}, t_{b,k,2}, \dots, t_{b,k,N_{c2,k}}\}, \\ &= \{t_{TBS,k}, t_{TBS,k} + \Delta_{fine}, \dots, t_{hitC,k}\}, \end{aligned} \quad (8.27)$$

where $N_{c2,k} = N_{set}(\mathcal{T}_{TBS,k})$, and $t_{a,k,1}, t_{a,k,2}, \dots, t_{a,k,N_{c1,k}}$ are used as auxiliary variables.

4. In particular, the computations are performed as follows. Consider the time interval $\mathcal{T}_{TBS,k,i}$ defined by the i th consecutive pair of times in $\mathcal{T}_{TBS,k}$, (8.27),

$$\mathcal{T}_{TBS,k,i} = (t_{b,k,i}, t_{b,k,i+1}], \quad i = 1, 2, \dots, N_{c2,k} - 1. \quad (8.28)$$

At the end of each time interval $\mathcal{T}_{TBS,k,i}$, $i = 1, 2, \dots, N_{c1,k} - 1$, and having computed $\mathbf{p}_s(t_0) = \mathbf{p}_{s0}$ and other variables of interest at time $Y_{B_{targ}}$, the numerical integration algorithm programmatically calls a suitable algorithm (in this case, an advanced regula falsi based algorithm implemented in the MATLAB function `odezero`, [32, 110, 120]) in order to find the first time $t \in \mathcal{T}_{TBS,k,i}$ where $[t_{fire}, t]$ is an element of the set B_{targ} , (8.9),

$$\mathbf{r}_{rel}(t; k) \in V_{targ} \Rightarrow$$

$$C_{hs}(r_{relx}(t; k), r_{rely}(t; k), r_{relz}(t; k)) = 0 \quad \text{or}$$

$$C_{cyl}(r_{relx}(t; k), r_{rely}(t; k), r_{relz}(t; k)) = 0. \quad (8.29)$$

5. If such a time t can be found then the following holds.
- a. The impact time of the AA projectile with the body of the AAT is $J_{mp3} > 0$.
 - b. The impact point of the AA projectile on the body of the AAT is $\mathbf{r}_{rel}(t_{hitT,k}; k)$.
 - c. The trajectories of the AA projectile and of the AAT are stopped

at time $t_{hitT,k}$.

In summary, a numerical integration algorithm with a fixed time-step is used to compute the motion trajectories of the AA projectile and the AAT. Furthermore, the numerical integration algorithm programmatically calls at the end of each time-step ((8.25), (8.28)) a suitable algorithm ([120]) in order to firstly detect the impact of the AA projectile with the TBS, (8.26), and thereafter to compute the impact time and impact point of the AA projectile on the body of the AAT, (8.29).

8.4 Vulnerability Model of the Attacking Aerial Target

In this work it is assumed that if one AA projectile impacts any point on the body of the AAT then the AA projectile detonates and the AAT is destroyed.

Advanced vulnerability models of AATs include additional refinements and features. For example, one refinement is to divide the body of the AAT into a number of compartments. Each given compartment contains particular types of systems and requires a specified minimum number of AA projectile impacts before it is destroyed. The complete AAT is destroyed if given combinations of compartments are destroyed ([40]).

Another feature of advanced vulnerability models is the possibility of taking into account the material properties of the body of the AAT and of the AA projectile. For example, some vulnerability models consider the detonation and fragmentation of the AA projectile and the subsequent fragment motion and impact with systems located inside the AAT ([40]).

8.5 Computational Results

The numerical solution of fire control problem FCA for the case of a completely stationary vehicle body of the mobile ADS is employed (Sect. 7.4). Some of the relevant data is repeated here for convenience.

The initial and final times are given by

$$t_0 = t_{fire,1} = -\Delta_{tofC,1}, \quad t_{FIN} = 20 \text{ s}, \quad (8.30)$$

The sequence of intercept times, (7.7), is equally spaced and is given by

$$\begin{aligned} t_{hitC,k} &= (k-1)\Delta_{hitC}, \quad k = 1, 2, \dots, n_f = 101, \\ \Delta_{hitC} &= 0.2 \text{ s}, \quad t_{hitC,1} = 0, \quad t_{hitC,n_f} = t_{FIN} = 20 \text{ s}. \end{aligned} \quad (8.31)$$

Thus, the set of specified intercept times (in seconds) is given by

$$\begin{aligned} \{t_{hitC,k}, k = 1, 2, \dots, n_f = 101\} &= \\ \{0, 0.2, 0.4, \dots, 19.6, 19.8, 20\}. \end{aligned} \quad (8.32)$$

A fourth order Runge-Kutta algorithm is used in order to solve numerically the point mass flight dynamics model of the AA projectile with a fixed time-step

$$\Delta_{sim} = 0.01 \text{ s}. \quad (8.33)$$

For each specified intercept time $t \geq 0$, the time of flight $\Delta_{tofC,k}$ has been computed, implying that the firing time is $t_{fire,k} = t_{hitC,k} - \Delta_{tofC,k}$, $k = 1, 2, \dots, n_f = 101$.

In addition, the inertial azimuth and elevation angles of the FC vector have been computed, $\mathbf{a}_{FC}(t_{fire,k})$, $\mathbf{a}_{FC}(t_{fire,k})$, $k = 1, 2, \dots, n_f = 101$. The dimensions of the AAT are $b_1 = 0.15 \text{ m}$, $L_{a1} = 1.75 \text{ m}$, $L_{a2} = 1.75 \text{ m}$, $L_a = L_{a1} + L_{a2} = 3.6 \text{ m}$. The radius of the TBS is $k_0 \neq 0 \text{ m}$, and the finer fixed time-step used within the TBS is $\Delta_{fine} = 10^{-4} \text{ s}$. Hereafter, the following notations are used.

1. $t_{hitC,k} - t_{hitT,k}$ is the difference between the specified intercept time of the AA projectile with the CM of the AAT and the impact time of the AA projectile with the body of the AAT.

2. $\|\mathbf{r}_{rel}(t_{hitT,k}; k)\|$ is the distance from the CM of the AAT to the impact point of the AA projectile on the body of the AAT.

The computed results are analyzed with respect to the following main cases. Firstly, the case where the AAT is furthest away from the mobile ADS and secondly, the case where the AAT is closest to the mobile ADS.

When the AAT is furthest from the mobile ADS, that is, for $k = 1$, $dp_1(t)/dt$, $\|\mathbf{r}_{los}^{(I)}(t_{hitC,k})\| \approx 4000$ m, then the following can be seen from Figs. 8.2, 8.3, 8.4, 8.5, 8.6 and 8.7.

1. The maximum value of $(t_{hitC,k} - t_{hitT,k})$ is approximately 1.5 ms, occurs at $k = 1$, and $dp_1(t)/dt$ s, $\|\mathbf{r}_{los}^{(I)}(t_{hitC,k})\| \approx 4000$ m, see Fig. 8.2.
2. The maximum value of $\|\mathbf{r}_{rel}(t_{hitT,k}; k)\|$ is 0.9 m, occurs at $k = 1$, and $dp_1(t)/dt$ s, $\|\mathbf{r}_{los}^{(I)}(t_{hitC,k})\| \approx 4000$ m, see Fig. 8.3.
3. The AA projectile impacts the body of the AAT on the left side and towards the front of the cylindrical section, see Figs. 8.4, 8.5, 8.6 and 8.7.
4. The velocity vector of the AA projectile on impact with the body of the AAT is almost horizontal having a small positive inertial elevation angle, see Figs. 8.6 and 8.7.

When the AAT is in the vicinity of the closest point of approach to the mobile ADS, that is, for $L_b > 0$, $t_{hitC,k} = 15.4$ s,

$\|\mathbf{r}_{los}^{(I)}(t_{hitC,k})\| \approx 1157.1$ m (Chap. 7), then the following can be seen from

Figs. 8.2, 8.3, 8.4, 8.5, 8.6 and 8.7.

1. The minimum value of $(t_{hitC,k} - t_{hitT,k})$ is 0.159 ms, occurs at $L_b > 0$, and $t_{hitC,k} = 15.4$ s, $\|\mathbf{r}_{los}^{(I)}(t_{hitC,k})\| \approx 1157.1$ m, see Fig. 8.2.
2. The minimum value of $\|\mathbf{r}_{rel}(t_{hitT,k}; k)\|$ is 0.15 m, occurs at $L_b > 0$, and $t_{hitC,k} = 15.4$ s, $\|\mathbf{r}_{los}^{(I)}(t_{hitC,k})\| \approx 1157.1$ m, see Fig. 8.3.
3. The AA projectile impacts the body of the AAT on the left side and at a point that is quite close to the CM of the AAT, see Figs. 8.4, 8.5, 8.6 and 8.7.
4. The velocity vector of the AA projectile on impact with the body of the AAT has a visibly greater inertial elevation angle than the case above, see Figs. 8.6 and 8.7.

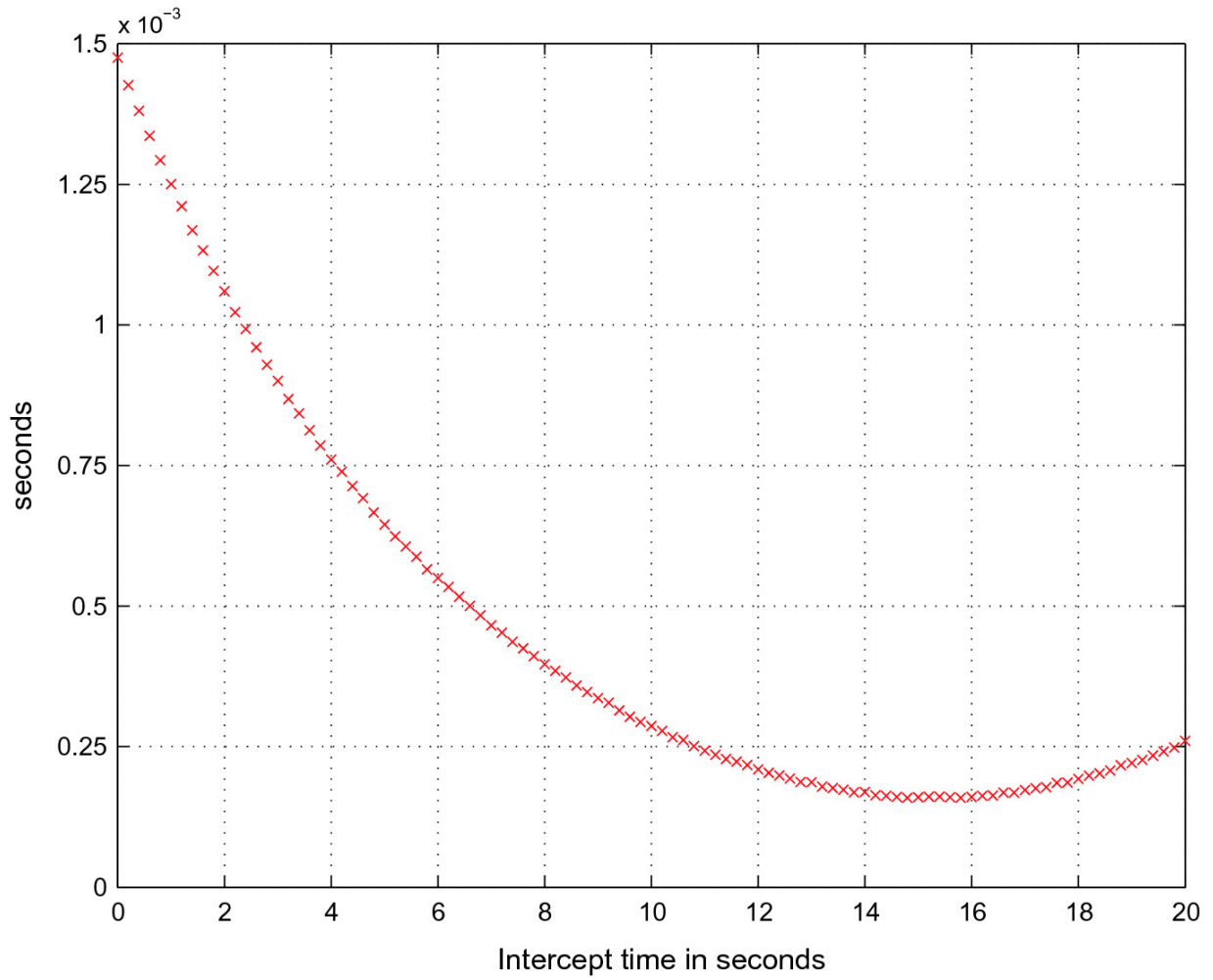


Fig. 8.2 Plot of $t_{hitC,k} - t_{hitT,k}$ versus the intercept time $t \geq 0$, $k = 1, 2, \dots, n_f$: vehicle body of mobile ADS is stationary

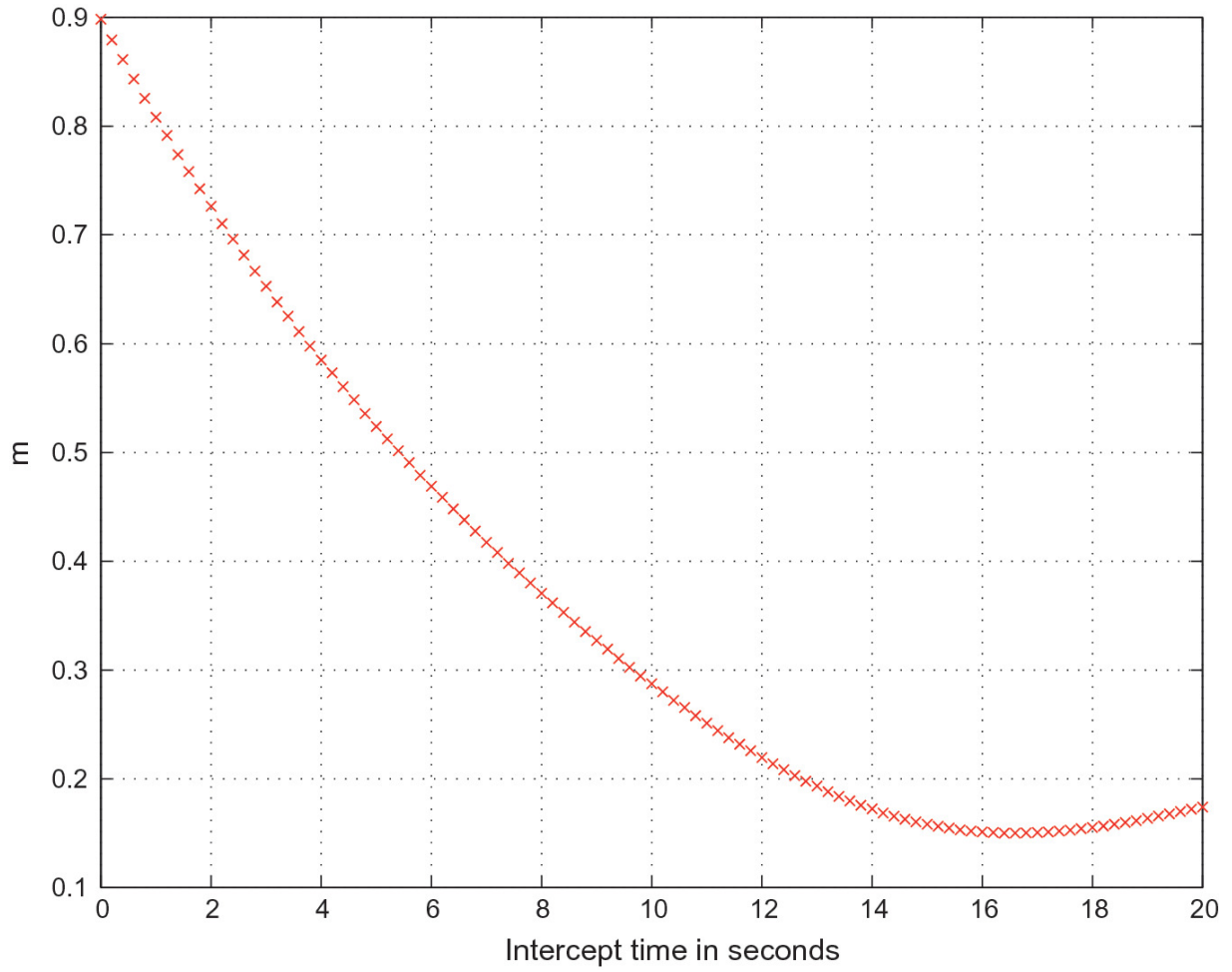


Fig. 8.3 Plot of $\|r_{rel}(t_{hitT,k};k)\|$ versus the intercept time $t \geq 0$, $k = 1, 2, \dots, n_f$: vehicle body of mobile ADS is stationary

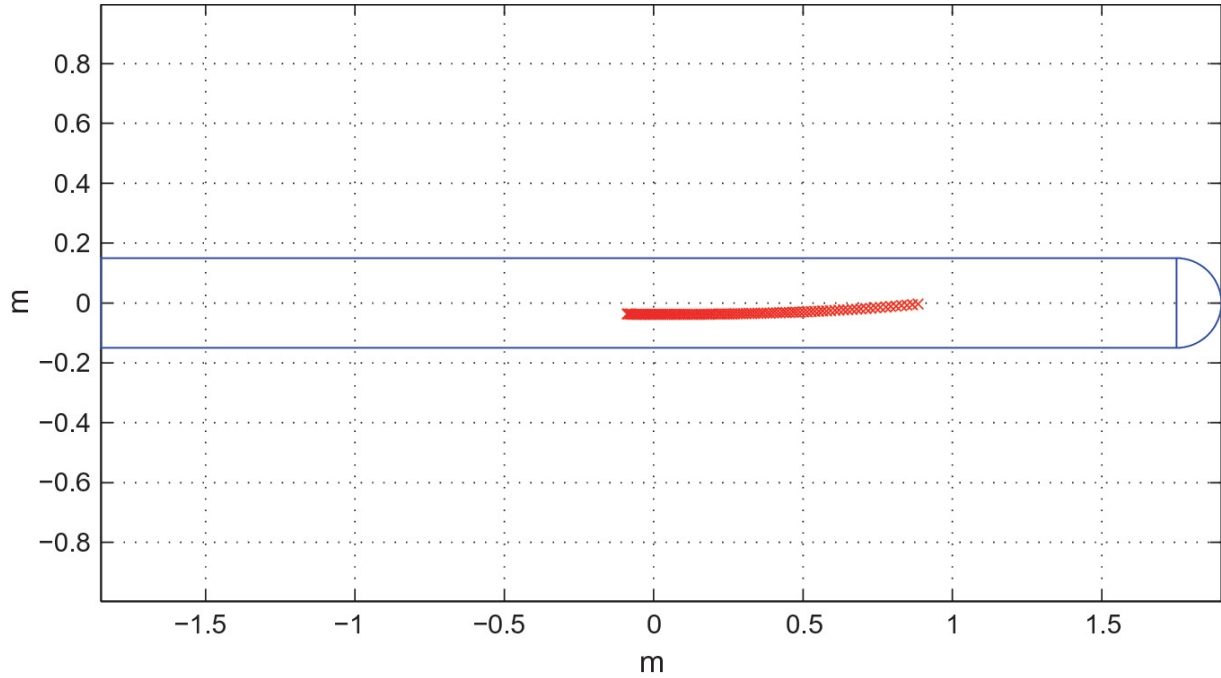


Fig. 8.4 Plot of the co-ordinates of the impact point of the AA projectile on the body of the AAT, $r_{relz}(t_{hitT,k};k)$ versus $r_{rely}(t_{hitT,k};k)$, as observed when looking in the direction of the negative $X_{B_{targ}}$ axis, for $k = 1, 2, \dots, n_f$: vehicle body of mobile ADS is stationary

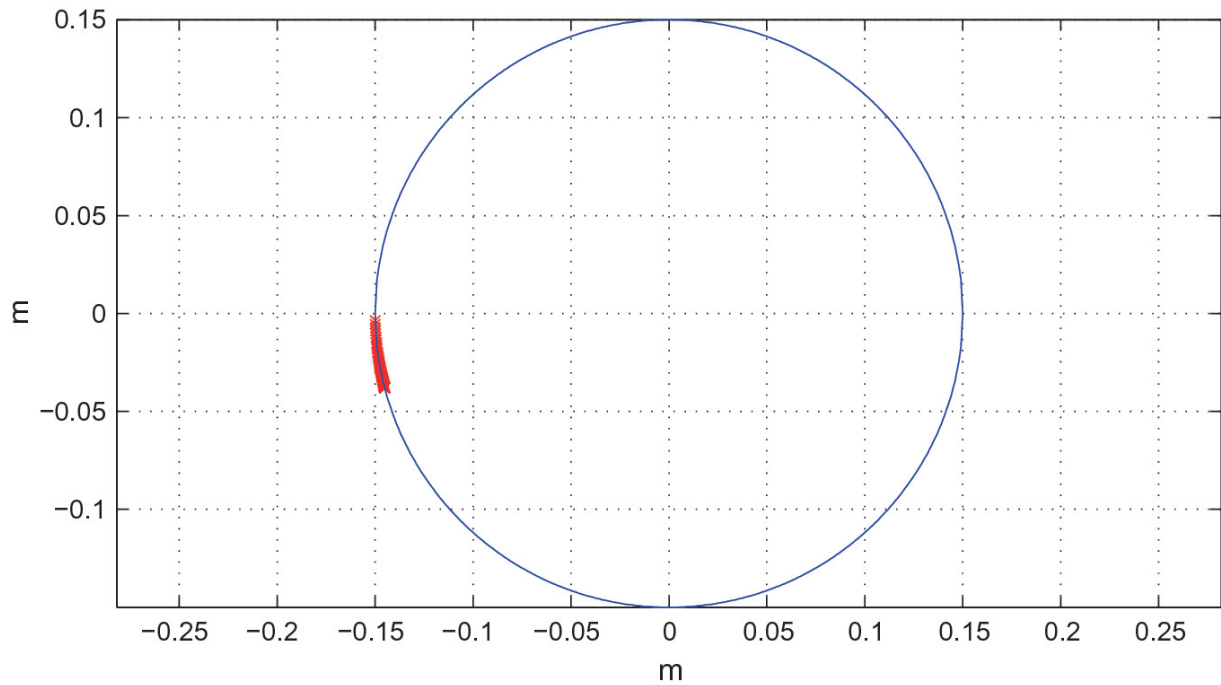


Fig. 8.5 Plot of the co-ordinates of the impact point of the AA projectile on the body of the AAT, $r_{relz}(t_{hitT,k};k)$ versus $r_{relx}(t_{hitT,k};k)$, as observed when looking in the direction of the positive

($X_{B_{10}}$ axis, for $k = 1, 2, \dots, n_f$: vehicle body of mobile ADS is stationary

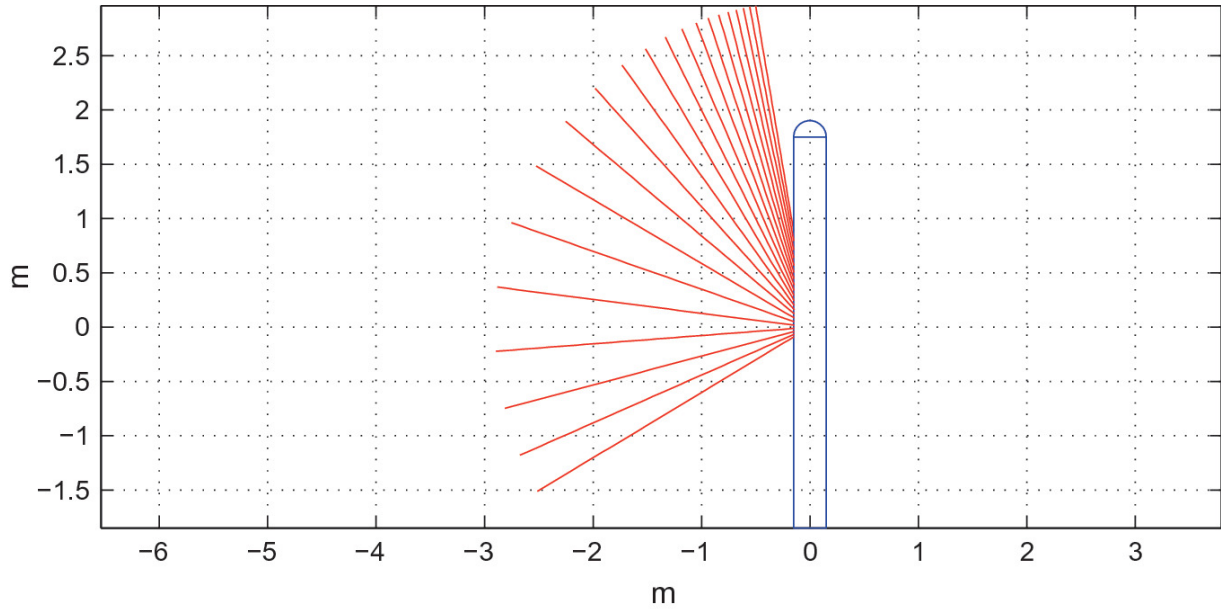


Fig. 8.6 Plot of the co-ordinates -187.39 versus $r_{relx}(t;k)$ of the trajectory of the AA projectile just before impact with the body of the AAT, $t \in [t_{TBS,k}, t_{hitT,k}]$, as observed when looking in the direction of the negative ($X_{B_{10}}$ axis, for $k = 1, 6, 11, \dots, n_f$: vehicle body of mobile ADS is stationary

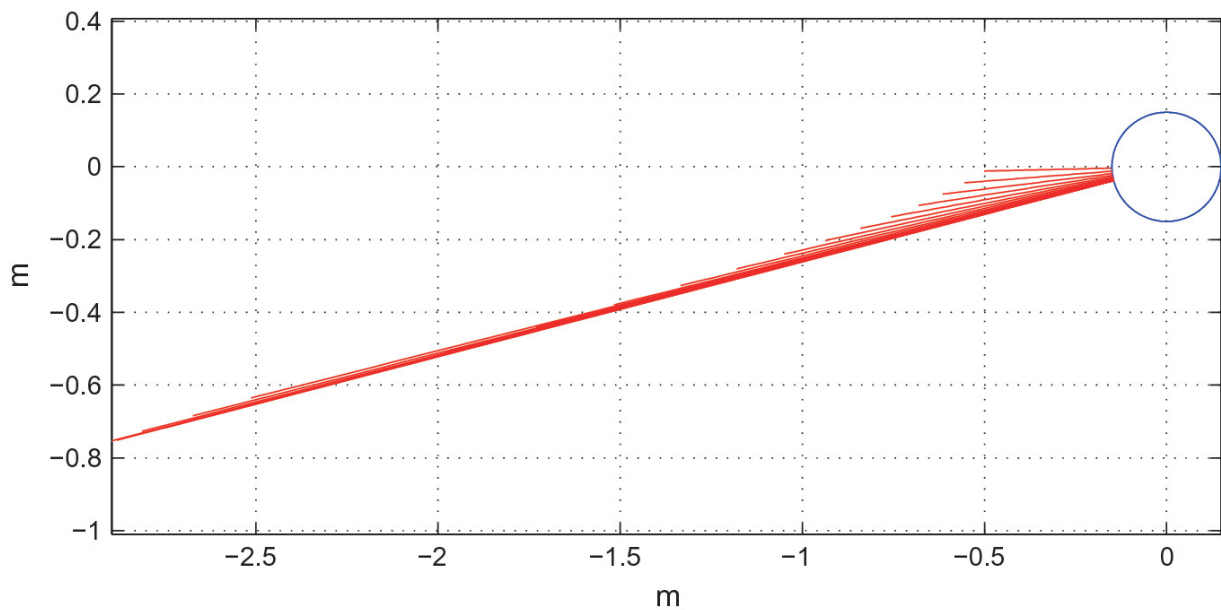


Fig. 8.7 Plot of the co-ordinates $k_d = 2k_0$ versus $r_{relx}(t; k)$ of the trajectory of the AA projectile just before impact with the body of the AAT, $t \in [t_{TBS,k}, t_{hitT,k}]$, as observed when looking in the direction of the positive $(X_{B_{10}}$ axis, for $k = 1, 6, 11, \dots, n_f$: vehicle body of mobile ADS is stationary

Footnotes

- 1 Also referred to as the space of the half-sphere or the space of the cylinder.

9. Computation of the Probability that the AA Projectile Will Impact the Body of the Attacking Aerial Target

Constantinos Frangos¹ 

(1) Electrical Engineer working in Decision and Control, Pretoria, South Africa

This Chapter deals with the computation of the probability that the AA projectile will impact the body of the AAT as follows.

1. Derivation of the stochastic model describing the dispersion of the AA projectiles fired by the AA gun.
2. Computation of the probability that the AA projectile fired at time $t \geq 0$ will impact any point on the body of the AAT, $P_{hitT,k}$.
3. The vulnerability model of the AAT assumes that if one or more AA projectiles impact the body of the AAT then the AAT is destroyed (Chap. 8). Thus, if one AA projectile is fired then the probability of destroying the AAT is $P_{hitT,k}$ ([40, 108, 142]).
4. Computation of the probability that a burst of N_p AA projectiles will destroy the AAT, and the accumulative probability that a burst of N_p AA projectiles will destroy the AAT.
5. A verification method is applied in order to verify the

computational method used to obtain $P_{hitT,k}$.

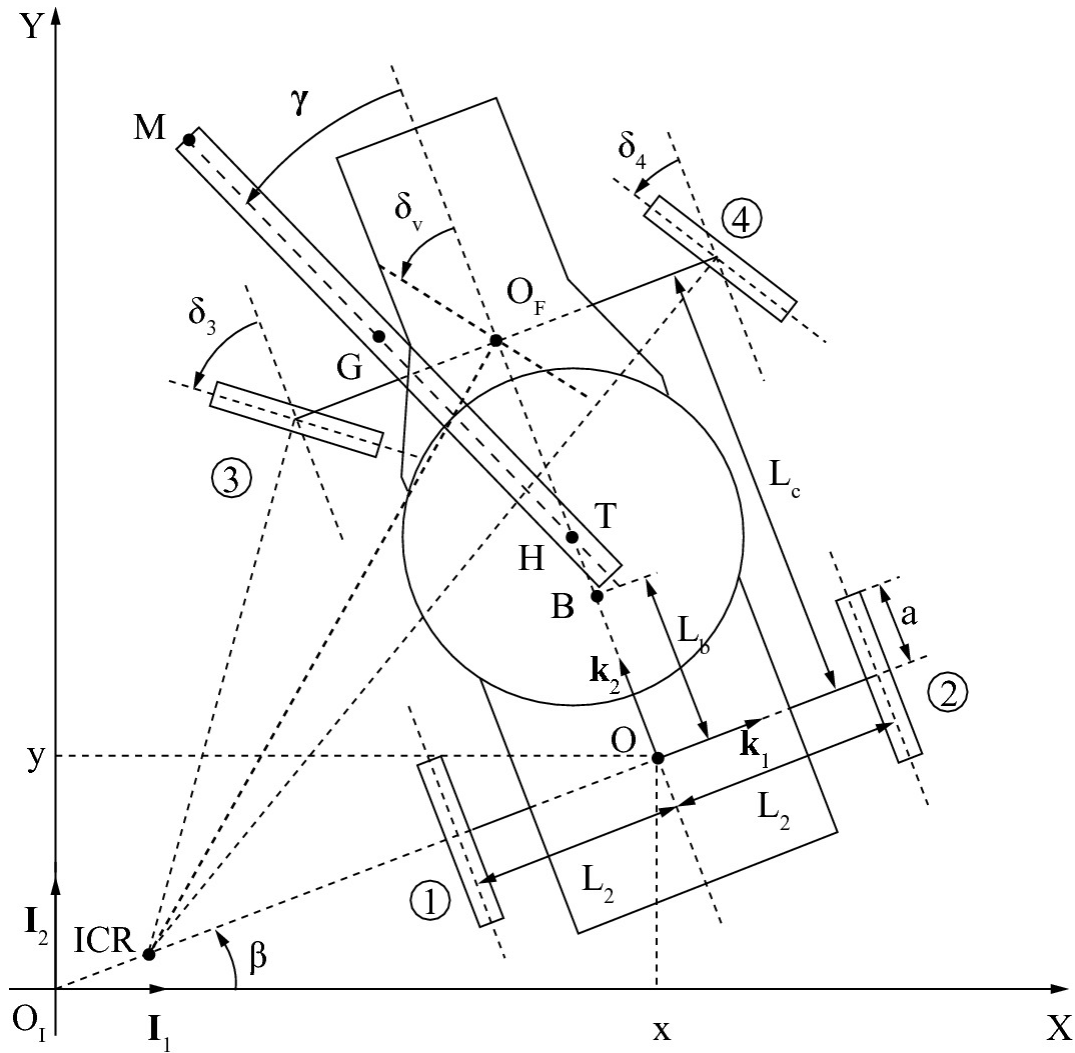


Fig. 9.1 Schematic of the mobile air defence system

9.1 Stochastic Model of the Dispersion of the AA Projectiles Fired by the AA Gun

The stochastic model describing the dispersion of the AA projectiles fired by the AA gun is derived by using the following assumptions and methods.

1. The computational results as obtained in Chap. 7 for fire control problem FCA for the case of a completely stationary vehicle body

of the mobile ADS (Fig. 9.1) are employed. Thus, for each given intercept time of the AA projectile with the CM of the AAT, $t \geq 0$, the following quantities have been computed for $k = 1, 2, \dots, n_f$.

a. The inertial azimuth and elevation angles of the FC vector $\mathbf{a}_{FC}(k) = \mathbf{a}_{FC}(t_{fire,k})$, $\mathbf{a}_{FC}(k) = \mathbf{a}_{FC}(t_{fire,k})$.

b. The time of flight of the AA projectile to the CM of the AAT, $\Delta_{tofC,k}$.

c. The firing time of the AA projectile is thus $t_{fire,k} = t_{hitC,k} - \Delta_{tofC,k}$.

2. In Chap. 7 the geometry of the AAT body has been ignored. The AA projectile that is fired at time $t \geq 0$ travels over the time interval $[t_{fire,k}, t_{hitC,k}]$ until intercept with the CM of the AAT at time $t \geq 0$.

In Chap. 8, the geometry of the body of the AAT is taken into account. Thus, the AA projectile will actually impact the body of the AAT at some time $t_{hitT,k}$ slightly before the intercept time with the CM, $t \geq 0$.

In this Chapter, the geometry of the body of the AAT is also taken into account. However, due to the fact that the initial velocity of the AA projectile is a random vector, the AA projectile will either miss the AAT or it will impact the body of the AAT. In the latter case, there may be a possibility that the impact time will be a little greater than $t \geq 0$. Thus, the trajectory of the AA

projectile is computed over an extended time horizon $[t_{fire,k}, t_{hitC,k} + \Delta_d]$, $d\mathbf{p}_s/dt$.

3. Consider the AA projectile that is fired at time $t \geq 0$. If there are

no disturbances acting on the AA projectile at the firing time then the generic firing velocity vector of the AA projectile $\mathbf{v}_P^{(B_7)}(t_{fire,k})$

is parallel to \mathbf{J}_{B_7} and is given by ((6.10))

$$\begin{aligned}\mathbf{v}_P^{(B_7)}(t_{fire,k}) &= V_0 \mathbf{J}_{B_7} = [0, V_0, 0]^\top, \\ \mathbf{v}_P^{(I)}(t_{fire,k}) &= V_0 \mathbf{J}_{B_7}^{(I)}(t_{fire,k}).\end{aligned}\tag{9.1}$$

Conceptually, the generic firing velocity vector of the AA projectile $\mathbf{v}_P^{(B_7)}(t_{fire,k})$ points from the muzzle of the AA gun (point M in Fig.

9.1) outwards. In the sequel, point M is alternatively referred to as the muzzle M of the AA gun.

4.

Let $\varepsilon_\psi(t_{fire,k}), x_{max} \in \mathbb{R}$, be continuous random variables

denoting the azimuth and elevation error angles applicable to the AA projectile that is fired at time $t \geq 0$. In order to simplify the

presentation, the following notation is used

$$\varepsilon_{\psi,k} = \varepsilon_\psi(t_{fire,k}), \quad \varepsilon_{\theta,k} = \varepsilon_\theta(t_{fire,k}), \quad k = 1, 2, \dots, n_f.\tag{9.2}$$

In addition, define the random vector B_i as follows

$$\boldsymbol{\varepsilon}_k = \begin{bmatrix} \varepsilon_{\psi,k} \\ \varepsilon_{\theta,k} \end{bmatrix}, \quad k = 1, \dots, n_f.\tag{9.3}$$

It is assumed that the sequence of random vectors B_i ,

$k = 1, 2, \dots, n_f$, are stochastically independent and identically

distributed (IID) with the random vector $\boldsymbol{\varepsilon} = [\varepsilon_\psi, \varepsilon_\theta]^\top$.

5. The joint probability density function (PDF) of the random vector $\boldsymbol{\varepsilon}$ is specified as follows

$$\tag{9.4}$$

$$f_{\varepsilon_k}(y_1, y_2) = f_{\varepsilon}(y_1, y_2) = f_{\varepsilon_\psi, \varepsilon_\theta}(y_1, y_2), \quad \mathbf{y} = [y_1, y_2]^\top \in \mathbb{R}^2, \\ k = 1, \dots, n_f, \quad 0 < \sigma(\varepsilon_\psi), \sigma(\varepsilon_\theta) < \infty,$$

where $\sigma(x_a)$ denotes the standard deviation of the random variable B_i . The standard deviations of n_f , k_0 , are bounded, (9.4), implying that the second moments of n_f , k_0 , are bounded. In many practical applications the sample values or realizations of the random vector B_i will be physically constrained to a bounded set $\mathbf{B}_0 \subset \mathbb{R}^2$, and $f_{\varepsilon_\psi, \varepsilon_\theta}(y_1, y_2) \geq 0$, $\mathbf{y} \in \mathbf{B}_0$, $f_{\varepsilon_\psi, \varepsilon_\theta}(y_1, y_2) \geq 0$, $\mathbf{y} \in \mathbf{B}_0$.

6.

The motion trajectory of the AA projectile fired at time $t \geq 0$ depends on the initial conditions. The initial conditions of the AA projectile depend partly on the realization of the random vector B_i denoted by $h_b > a$,

$$\boldsymbol{\varepsilon}_k(\omega_k) = \begin{bmatrix} \varepsilon_{\psi, k}(\omega_k) \\ \varepsilon_{\theta, k}(\omega_k) \end{bmatrix}, \quad (9.5)$$

where \mathbf{T}_d denotes some element of the sample space Ω_{ε_k} of the random vector B_i , and $\Omega_{\varepsilon_k} = \mathbb{R}^2$ (Chap. 4, [2], Chap. 2, [19, 67, 90, 97, 98, 135, 161, 165, 173, 184]).¹ Note that in the case of \mathbf{T}_d the convention of using bold letters to denote vector and matrix quantities is not applied.

7.

The azimuth and elevation error angles, \mathbf{J}_{B_7} , T_{α_s} , are used to represent the effect of random disturbances on the generic firing velocity vector of the AA projectile $\mathbf{v}_P^{(B_7)}(t_{fire, k})$ as follows.

- a. Rotate the body reference frame of the AA gun, B_5 , about the Z_{B_5} axis through the azimuth error angle J_{B_7} .
- b. Rotate the resulting reference frame B_7 about the X_{B_6} axis through the elevation error angle T_{α_s} , thus leading to a reference frame Q_{Cj} , with unit vectors $(\mathbf{I}_{B_{err}}, \mathbf{q}_1(t), N_{fmax})$. The origin of the reference frame Q_{Cj} is fixed at the muzzle M of the AA gun (Fig. 9.1).
- c. Thus, if there are disturbances acting on the AA projectile then the generic firing velocity vector is no longer parallel to the Z_{B_5} axis of the AA gun reference frame B_5 , and thus no longer parallel to the longitudinal axis of the AA gun.
- d. The generic firing velocity vector of the AA projectile is now parallel to the $Y_{B_{err}}$ axis of reference frame Q_{Cj} and is given by

$$\mathbf{v}_P^{(B_{err})}(t_{fire,k}) = V_0 \mathbf{J}_{B_{err}} = [0, V_0, 0]^T. \quad (9.6)$$

8. The rotation matrix from the body reference frame B_5 of the AA gun to the reference frame Q_{Cj} is given by (Appendix A)

$$\mathbf{R}_{B_7 2 B_{err}} = \mathbf{R}_X(\varepsilon_{\theta,k}) \mathbf{R}_Z(\varepsilon_{\psi,k}), \quad \mathbf{R}_{B_{err} 2 B_7} = \mathbf{R}_{B_7 2 B_{err}}^T. \quad (9.7)$$

9. It follows that the generic firing velocity vector of the AA projectile expressed in reference frame B_5 is given by

$$\mathbf{v}_P^{(B_7)}(t_{fire,k}) = \mathbf{R}_{B_7 2 B_{err}} \mathbf{v}_P^{(B_{err})}(t_{fire,k}) = V_0 \mathbf{I}_{B_{err}} = V_0 \begin{bmatrix} -\cos(\varepsilon_{\theta,k}) \sin(\varepsilon_{\psi,k}) \\ \cos(\varepsilon_{\theta,k}) \cos(\varepsilon_{\psi,k}) \\ \sin(\varepsilon_{\theta,k}) \end{bmatrix} \quad (9.8)$$

$$\mathbf{v}_P(t_{fire,k}) = \mathbf{R}_{B_{err}2B_7} \mathbf{v}_0 \mathbf{J}_{B_{err}} = v_0 \begin{bmatrix} \cos(\varepsilon_{\theta,k}) \cos(\varepsilon_{\psi,k}) \\ \sin(\varepsilon_{\theta,k}) \end{bmatrix}. \quad (9.8)$$

The generic firing velocity $\mathbf{v}_P^{(B_7)}(t_{fire,k})$ expressed in the inertial reference frame is given by ((6.10))

$$\begin{aligned} \mathbf{v}_P^{(I)}(t_{fire,k}) &= \mathbf{R}_{B_72I} \mathbf{v}_P^{(B_7)}(t_{fire,k}), \\ \mathbf{R}_{B_72I} &= \mathbf{R}_{B_72I}(\mathbf{a}_{FC}(k), \mathbf{e}_{FC}(k)). \end{aligned} \quad (9.9)$$

If the azimuth and elevation error angles are zero, $\varepsilon_{\psi,k} = \varepsilon_{\theta,k} = 0$, then reference frame Q_{Cj} is parallel to the body reference frame B_5 , and

$$\mathbf{v}_P^{(B_7)}(t_{fire,k}) = \mathbf{v}_P^{(B_{err})}(t_{fire,k}) = [0, V_0, 0]^T. \quad (9.10)$$

10. Since the generic firing velocity $\mathbf{v}_P^{(I)}(t_{fire,k})$, (9.9), is a function of the random vector B_i , it follows from (6.11), that the initial velocity of the AA projectile is a function of the random vector B_i .
11. Hence, the point mass flight dynamics model of the AA projectile, (7.19), is subject to random initial conditions that are a function of the random vector B_i ([34, 127, 128, 165]), and is given by

$$\begin{aligned} \frac{d\mathbf{X}(\tau; t)}{d\tau} &= \mathbf{f}_{proj}(\mathbf{X}(\tau; t)), \quad \mathbf{X}(t; t) = \mathbf{X}_0(t, \boldsymbol{\varepsilon}_k), \\ \tau &\in [t, t_{hitC,k} + \Delta_d], \quad t = t_{fire,k}, \end{aligned} \quad (9.11)$$

$$\mathbf{X}_0(t_{fire,k}, \boldsymbol{\varepsilon}_k) = \begin{bmatrix} \mathbf{r}_{proj,0}^{(I)}(t_{fire,k}, \boldsymbol{\varepsilon}_k) \\ \mathbf{v}_{proj,0}^{(I)}(t_{fire,k}, \boldsymbol{\varepsilon}_k) \end{bmatrix}. \quad (9.12)$$

In the literature, (9.11) is referred to as a random differential equation ([34, 127, 128, 165]) or as a pseudo-deterministic

equation ([64, 127, 128, 165]) or as a crypto-deterministic

system ([67, 165]). The initial conditions $(\mathbf{I}_{B_5}^{(I)}, \mathbf{J}_{B_5}^{(I)}, \mathbf{K}_{B_5}^{(I)})$,

$(\mathbf{I}_{B_5}^{(I)}, \mathbf{J}_{B_5}^{(I)}, \mathbf{K}_{B_5}^{(I)})$, (9.12), are computed as follows.

12.

The initial position $(\mathbf{I}_{B_5}^{(I)}, \mathbf{J}_{B_5}^{(I)}, \mathbf{K}_{B_5}^{(I)})$ is computed from (7.21)–(7.

23) and is given by

$$\mathbf{r}_{proj,0}^{(I)}(t_{fire,k}, \boldsymbol{\varepsilon}_k) = \mathbf{r}_H^{(I)}(t) + L_m \mathbf{J}_{B_7}^{(I)}(t), \quad t = t_{fire,k}, \quad (9.13)$$

where

$$\mathbf{r}_H^{(I)}(t) = \mathbf{r}_{OA}^{(I)}(t) + \begin{bmatrix} -\sin(\beta_b)(L_b + h_{Ty}) \\ \cos(\beta_b)(L_b + h_{Ty}) \\ h_b + h_{Tz} + h_{mz} \end{bmatrix}, \quad (9.14)$$

$$\mathbf{r}_{OA}^{(I)}(t) = \begin{bmatrix} x(t) \\ y(t) \\ 0 \end{bmatrix}, \quad t = t_{fire,k},$$

$$\mathbf{J}_{B_7}^{(I)}(t) = \begin{bmatrix} \cos(\mathbf{a}_{FC}(t)) \cos(\mathbf{e}_{FC}(t)) \\ \sin(\mathbf{a}_{FC}(t)) \cos(\mathbf{e}_{FC}(t)) \\ \sin(\mathbf{e}_{FC}(t)) \end{bmatrix}, \quad t = t_{fire,k}. \quad (9.15)$$

Based on the assumptions in Sect. 9.1, the random vector B_i

affects the initial velocity $(\mathbf{I}_{B_5}^{(I)}, \mathbf{J}_{B_5}^{(I)}, \mathbf{K}_{B_5}^{(I)})$ but does not affect the

initial position. Thus, the initial position $(\mathbf{I}_{B_5}^{(I)}, \mathbf{J}_{B_5}^{(I)}, \mathbf{K}_{B_5}^{(I)})$ is

actually not a function of B_i ((9.13)–(9.15)).

The initial velocity $(\mathbf{I}_{B_5}^{(I)}, \mathbf{J}_{B_5}^{(I)}, \mathbf{K}_{B_5}^{(I)})$ is computed from (7.24) and

13.

(9.8)–(9.9), and is given by

(9.16)

$$\begin{aligned}
\mathbf{v}_{proj,0}^{(I)}(t_{fire,k}, \boldsymbol{\varepsilon}_k) &= \mathbf{v}_H^{(I)}(t_{fire,k}) + \mathbf{v}_P^{(I)}(t_{fire,k}) \\
&= \mathbf{v}_{OA}^{(I)}(t_{fire,k}) + \mathbf{v}_P^{(I)}(t_{fire,k}) \\
&= \begin{bmatrix} v_b \cos(\beta_b + \pi/2) \\ v_b \sin(\beta_b + \pi/2) \\ 0 \end{bmatrix} + \mathbf{v}_P^{(I)}(t_{fire,k}) \\
&= \mathbf{v}_P^{(I)}(t_{fire,k}) \\
&= \mathbf{R}_{B_7 2I} \mathbf{v}_P^{(B_7)}(t_{fire,k}),
\end{aligned}$$

$$\Rightarrow \mathbf{v}_{proj,0}^{(I)}(t_{fire,k}, \boldsymbol{\varepsilon}_k) = \mathbf{R}_{B_7 2I} V_0 \begin{bmatrix} -\cos(\varepsilon_{\theta,k}) \sin(\varepsilon_{\psi,k}) \\ \cos(\varepsilon_{\theta,k}) \cos(\varepsilon_{\psi,k}) \\ \sin(\varepsilon_{\theta,k}) \end{bmatrix}. \quad (9.17)$$

It has been assumed above that the vehicle body of the mobile ADS is stationary implying that $d\beta(t)/dt = 0$, $J_{s1} = J_{s2}$, $k_0 \neq 0$

(Fig. 9.1).

14.

It follows from (9.17), (9.9), (9.13), (9.12), that each element of the initial conditions $t_{hitC,k} - t_{hitT,k}$ is a smooth and bounded

function of trigonometric functions of the elements of the random vector B_i . Thus, by using (9.4), it follows that the second moment

and hence standard deviation of each element of the initial conditions $t_{hitC,k} - t_{hitT,k}$ is bounded.

15.

Using the same approach as in [34], and given k , consider a realization $h_b > a$, (9.5). Then it follows that the point mass flight

dynamics model is subject to deterministic initial conditions that are a function of $h_b > a$ ((9.11)–(9.12), and [34, 128, 165]), and is

given by

$$\frac{d\mathbf{x}_{\omega_k}(\tau; t)}{d\tau} = \mathbf{f}_{proj}(\mathbf{x}_{\omega_k}(\tau; t)), \quad \mathbf{x}_{\omega_k}(t; t) = \mathbf{x}_{\omega_k,0}(t), \quad (9.18)$$

$$\tau \in [t, t_{hitC,k} + \Delta_d], \quad t = t_{fire,k},$$

$$\mathbf{x}_{\omega_k,0}(t_{fire,k}) = \mathbf{X}_0(t_{fire,k}, \boldsymbol{\varepsilon}_k(\omega_k)) \quad (9.19)$$

$$= \begin{bmatrix} \mathbf{r}_{proj,0}^{(I)}(t_{fire,k}, \boldsymbol{\varepsilon}_k(\omega_k)) \\ \mathbf{v}_{proj,0}^{(I)}(t_{fire,k}, \boldsymbol{\varepsilon}_k(\omega_k)) \end{bmatrix}.$$

This work deals with the case where the initial value problem (9.18) has a unique solution $\mathbf{x}_{\omega_k}(\tau; t_{fire,k})$ that satisfies the following equation ([34, 119, 128, 165])

$$\mathbf{x}_{\omega_k}(\tau; t) = \mathbf{x}_{\omega_k,0}(t) + \int_t^\tau \mathbf{f}_{proj}(\mathbf{x}_{\omega_k}(s; t)) ds, \quad (9.20)$$

$$\tau \in [t, t_{hitC,k} + \Delta_d], \quad t = t_{fire,k}.$$

16. Furthermore, this work deals with the case where the point mass flight dynamics model subject to random initial conditions, (9.11), (9.12), has a unique mean square solution $\mathbf{X}(\tau; t_{fire,k})$ that satisfies the following equation ([34, 127, 128, 165])²

$$\mathbf{X}(\tau; t_{fire,k}) = \mathbf{X}_0(t_{fire,k}, \boldsymbol{\varepsilon}_k) + \int_{t_{fire,k}}^\tau \mathbf{f}_{proj}(\mathbf{X}(s; t_{fire,k})) ds, \quad (9.21)$$

$$\tau \in [t_{fire,k}, t_{hitC,k} + \Delta_d],$$

where $\mathbf{X}(\tau; t_{fire,k})$ is a function of B_i , (9.21) ([165]),

$$\mathbf{X}(\tau; t_{fire,k}) = \mathbf{X}(\tau; t_{fire,k}, \boldsymbol{\varepsilon}_k) = \begin{bmatrix} \mathbf{r}_{proj}^{(I)}(\tau; t_{fire,k}, \boldsymbol{\varepsilon}_k) \\ \mathbf{v}_{proj}^{(I)}(\tau; t_{fire,k}, \boldsymbol{\varepsilon}_k) \end{bmatrix}, \quad (9.22)$$

and where for each \mathbf{T}_d , (9.5), the realization of the random process $\mathbf{X}(\tau; t_{fire,k}, \boldsymbol{\varepsilon}_k)$ is equal to the deterministic motion

trajectory of the AA projectile (9.20), that is,

$$\begin{aligned} X(\tau; t, \boldsymbol{\varepsilon}_k(\omega_k)) &= \mathbf{x}_{\omega_k}(\tau; t), \quad \tau \in [t, t_{hitC,k} + \Delta_d], \\ t &= t_{fire,k}. \end{aligned} \quad (9.23)$$

17.

For each k and for each time $\tau \in [t_{fire,k}, t_{hitC,k} + \Delta_d]$,

$X(\tau; t_{fire,k}, \boldsymbol{\varepsilon}_k)$ is a random vector in \mathbb{R}^6 that is a function of the random vector B_i , (9.22) ([165]). However, there is no closed-form expression available for the random vector $X(\tau; t_{fire,k}, \boldsymbol{\varepsilon}_k)$ nor for its joint PDF, in terms of τ , $t \geq 0$, B_i and other given parameters.

18.

The second moment and thus standard deviation of each element of the random vector $X(\tau; t_{fire,k}, \boldsymbol{\varepsilon}_k)$, is bounded ([34, 128, 165])

$$\begin{aligned} \sigma(X_i(\tau; t_{fire,k}, \boldsymbol{\varepsilon}_k)) &< \infty, \quad i = 1, 2, \dots, 6, \\ \text{for all } \tau &\in [t_{fire,k}, t_{hitC,k} + \Delta_d]. \end{aligned} \quad (9.24)$$

19. A fixed time α_1 is added to the specified intercept time $t \geq 0$. The value of α_1 is chosen by taking the following into account.

a.

It is assumed that for any given realization $h_b > a$, the AA projectile will either miss the AAT, or it will impact the body of the AAT within the time interval $[t_{fire,k}, t_{hitC,k} + \Delta_d]$. Thus, it is assumed that the probability that the AA projectile will impact the body of the AAT after the time $t_{hitC,k} + \Delta_d$ is 0.

b.

In order to reduce computation time, and considering the relative speed of the AA projectile and the engagement

scenario used in Chaps. 7 and 8, it was found that $0 < \Delta_d \ll \Delta_{tofC,k}$.

9.1.1 Remarks on Applications of Stochastic Optimal Control

The formulation and numerical solution of problems dealing with the stochastic optimal control and state estimation of nonlinear dynamic systems subject to random initial conditions, white state noise and white measurement noise, and subject to complicated performance requirements, control constraints and state constraints, are presented in [52, 97, 98, 187–209].

Stochastic optimal control problems involve the numerical solution of the Hamilton-Jacobi-Bellman (HJB) partial differential equation (PDE) for the optimal objective function and optimal feedback control function on a discretized set or grid in B_5 (where k_{mp} number of state variables in the dynamic model of the system). The HJB PDE represents sufficient conditions for the optimal objective function and optimal feedback control function ([52, 97, 98]).

The HJB PDE is discretized by using a unique numerical approximation method developed by Prof. Harold J. Kushner, Division of Applied Mathematics, Brown University, USA ([97, 98]). Convergence of the above-mentioned numerical approximations is proved via the probabilistic methods of weak convergence theory ([98]).

If each state variable is discretized into γ values then the grid in B_5 consists of a total of p_s points. Taking into account the boundary conditions, this results in a potentially large number (somewhat less than p_s) of nonlinear equations that have to be solved iteratively for an equal number of unknowns representing the values of the optimal objective function on the grid. Thus, a potentially large scale scientific computing problem must be solved (for example, $\mu = 21$, $\nu = 6$, $k = 1$, $k = 1$, etc).

The numerical solution of the HJB PDE yields approximations of the optimal objective function and the optimal feedback control function or strategy on the chosen grid in B_5 . Practically, the computed optimal feedback control strategy is difficult to implement.

Prof. Yavin developed a methodology whereby the above-mentioned computational framework is applied in order to systematically evaluate the performance of a given feedback control strategy relative to the optimal feedback control strategy for all initial conditions of the system on the chosen grid in B_5 (for advanced applications see the research monographs [192, 193]).

Assume that the given feedback control strategy has been determined by some method, for example, based on experience/knowledge of the system, and that it is relatively straightforward to implement. An approximation of the suboptimal objective function for the given feedback control strategy is computed by solving the relevant functional PDE on the same grid in B_5 (using the above-mentioned numerical approximation method).

If the computed suboptimal objective function is sufficiently close to the optimal objective function (as defined by a suitable measure) then the given feedback control strategy is a candidate for controlling the system. In some cases the suboptimal objective function is very close or almost identical to the optimal objective function.

The research collaboration with Prof. Yavin in this field includes the following applications.

1. Optimal feedback control strategies and parameter selection for an electromagnetic actuator ([200]).
2. Optimal and suboptimal feedback guidance and control strategies for a projectile ([201, 202, 206]).
3. Optimal and suboptimal feedback control strategies for manufacturing systems consisting of networks of finite capacity buffers, flexible manufacturing systems (FMSs), dedicated manufacturing machines, assembly machines, and finite capacity inventories ([203–205, 209]). The manufacturing systems are modelled by using continuous time Markov chains. The optimal

modeled by using continuous time Markov chains. The optimal objective function and the optimal feedback control strategy are obtained by solving a HJB differential difference type equation ([20]).

4. Optimal and suboptimal feedback control strategies for a nonlinear discrete-time stochastic state space model of a manufacturing system ([57]). The optimal objective function and optimal feedback control strategy are obtained by solving the Bellman dynamic programming equation ([17, 100, 163]).

9.2 Computation of the Probability that the AA Projectile Will Impact the Body of the Attacking Aerial Target, $P_{hitT,k}$

A methodology is presented for computing the probability that the AA projectile will impact the body of the attacking aerial target, $P_{hitT,k}$, for any given intercept time $t \geq 0$, $k = 1, 2, \dots, n_f$.

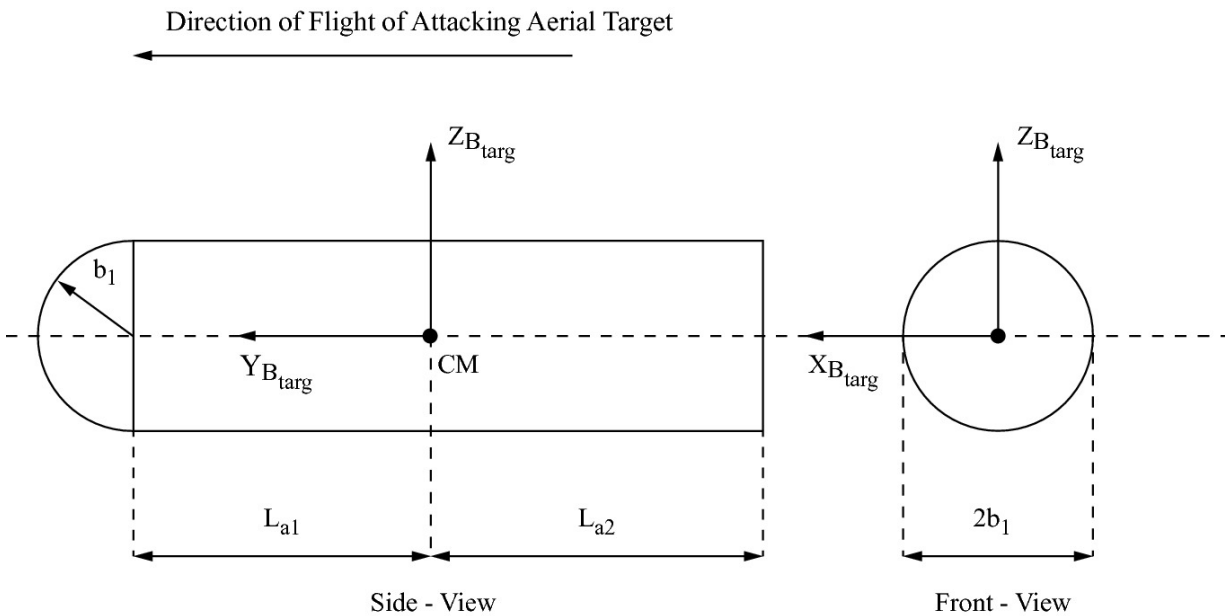


Fig. 9.2 Schematic of attacking aerial target

Consider the AA projectile that is fired at time $t \geq 0$. The variables given below are formally defined for time t in the continuous interval

$$\mathcal{T}_{FL,k} = [t_{fire,k}, t_{hitC,k} + \Delta_d]. \quad (9.25)$$

The position vector of the AA projectile relative to the CM of the AAT at time t is given by ((9.22))

$$\mathbf{r}_{rel}^{(I)}(t; t_{fire,k}, \boldsymbol{\varepsilon}_k) = \mathbf{r}_{proj}^{(I)}(t; t_{fire,k}, \boldsymbol{\varepsilon}_k) - \mathbf{r}_{targ}^{(I)}(t), \quad t \in \mathcal{T}_{FL,k}. \quad (9.26)$$

This vector is expressed in the body reference frame B_{targ} as follows ((8.12))

$$\mathbf{r}_{rel}^{(B_{targ})}(t; t_{fire,k}, \boldsymbol{\varepsilon}_k) = \mathbf{R}_{I2B_{targ}} \mathbf{r}_{rel}^{(I)}(t; t_{fire,k}, \boldsymbol{\varepsilon}_k), \quad t \in \mathcal{T}_{FL,k}. \quad (9.27)$$

In order to simplify the presentation, $t \geq 0$ is replaced by k and the superscript $h_s > a$ is suppressed as follows

$$\begin{aligned} \mathbf{r}_{rel}(t; k, \boldsymbol{\varepsilon}_k) &= \mathbf{r}_{rel}^{(B_{targ})}(t; t_{fire,k}, \boldsymbol{\varepsilon}_k), \\ \mathbf{r}_{rel}(t; k, \boldsymbol{\varepsilon}_k) &= [r_{relx}(t; k, \boldsymbol{\varepsilon}_k), r_{rely}(t; k, \boldsymbol{\varepsilon}_k), r_{relz}(t; k, \boldsymbol{\varepsilon}_k)]^\top, \\ &t \in \mathcal{T}_{FL,k}. \end{aligned} \quad (9.28)$$

For a given realization $h_b > a$, (9.5), the computational procedure given in Sect. 8.3 is applied by taking the following into account.

1. All the relevant variables are computed at discrete times in the following set ((6.59))

$$\begin{aligned} \mathcal{T}_{comp,k} &= \{t_{fire,k}, t_{fire,k} + \Delta_{sim}, \dots, t_{hitC,k}, \\ &t_{hitC,k} + \Delta_{sim}, \dots, t_{hitC,k} + \Delta_d\}. \end{aligned} \quad (9.29)$$

2. If the AA projectile impacts the TBS then all the relevant variables are computed at discrete times in the following set ((6.59))

$$\mathcal{T}_{TBS,k} = \{t_{TBS,k}, t_{TBS,k} + \Delta_{fine}, \dots, t_{hitC,k} + \Delta_d\}. \quad (9.30)$$

3. The AA projectile either impacts the body of the AAT or it does not impact the body of the AAT as follows.
 - a. The AA projectile impacts the body of the AAT if it impacts the TBS and thereafter impacts the body of the AAT.
 - b. The AA projectile does not impact the body of the AAT if it does not impact the TBS or if it impacts the TBS and thereafter does not impact the body of the AAT.

Thus, the methods in Sect. 8.3 are used together with (9.29), (9.30), in order to determine if and at what point the AA projectile will impact the body of the AAT. In order to compute the probability that the AA projectile will impact the body of the AAT the following approach is applied.

Define the set $J_{hitT,k}$ as follows

$$J_{hitT,k} = J_{hitT,k}(\boldsymbol{\varepsilon}_k) = \{t \in (t_{fire,k}, t_{hitC,k} + \Delta_d) : \mathbf{r}_{rel}(t; k, \boldsymbol{\varepsilon}_k) \in V_{targ}\}. \quad (9.31)$$

Thus, if the AA projectile does not impact the body of the AAT then $J_{hitT,k} = \emptyset$ while if it does impact the body of the AAT then $J_{hitT,k} \neq \emptyset$. It has been assumed above that the probability that the AA projectile will impact the body of the AAT after the time $t_{hitC,k} + \Delta_d$ is 0.

Define the impact time of the AA projectile with the body of the AAT, $t_{hitT,k}$, as follows ([98, 161, 184])

$$t_{hitT,k} = t_{hitT,k}(\boldsymbol{\varepsilon}_k) = \begin{cases} \inf J_{hitT,k}(\boldsymbol{\varepsilon}_k) & \text{if } J_{hitT,k}(\boldsymbol{\varepsilon}_k) \neq \emptyset \\ \infty & \text{if } J_{hitT,k}(\boldsymbol{\varepsilon}_k) = \emptyset \end{cases}. \quad (9.32)$$

The stopping time $T_{\delta_v} I_3$ is defined as follows ([98])

$$(9.33)$$

$$t_{stop,k} = t_{stop,k}(\boldsymbol{\varepsilon}_k) = \min(t_{hitC,k} + \Delta_d, t_{hitT,k}(\boldsymbol{\varepsilon}_k)).$$

Given a realization $h_b > a$, (9.5). The resulting realizations of the random quantities in (9.31)–(9.33) are described as follows.

1. If the AA projectile impacts the body of the AAT then the set $J_{hitT,k}(\boldsymbol{\varepsilon}_k(\omega_k))$ is not empty otherwise it is empty.
2. If the AA projectile impacts the body of the AAT then $i = 1, 2, 3, 4$ is the first time $t \in (t_{fire,k}, t_{hitC,k} + \Delta_d]$ that $\mathbf{r}_{rel}(t; k, \boldsymbol{\varepsilon}_k(\omega_k)) \in V_{targ}$. The time $i = 1, 2, 3, 4$ is computed by using the methods presented in Sect. 8.3.
3. If the AA projectile does not impact the body of the AAT then the stopping time is $t_{stop,k}(\boldsymbol{\varepsilon}_k(\omega_k)) = t_{hitC,k} + \Delta_d$. If the AA projectile does impact the body of the AAT then the stopping time is $t_{stop,k}(\boldsymbol{\varepsilon}_k(\omega_k)) = i = 1, 2, 3, 4$. At the stopping time $t_{stop,k}(\boldsymbol{\varepsilon}_k(\omega_k))$, the motion trajectories of the AA projectile and the AAT are stopped.
4. If the AA projectile impacts the body of the AAT then $\lambda_{10}(t_{stop,k}(\boldsymbol{\varepsilon}_k(\omega_k)); k, \boldsymbol{\varepsilon}_k(\omega_k)) s(t_{hitG})$. If the AA projectile does not impact the body of the AAT then $\lambda_{10}(t_{stop,k}(\boldsymbol{\varepsilon}_k(\omega_k)); k, \boldsymbol{\varepsilon}_k(\omega_k)) s(t_{hitG})$.

For a given k , $\mathbf{r}_{rel}(t_{stop,k}(\boldsymbol{\varepsilon}_k); k, \boldsymbol{\varepsilon}_k)$ is a random vector in \mathbb{R}^3 that is a function of the random vector B_i . However, there is no closed-form

expression available for $\mathbf{r}_{rel}(t_{stop,k}(\boldsymbol{\varepsilon}_k); k, \boldsymbol{\varepsilon}_k)$ nor for its joint PDF, in terms of B_i and other given parameters.

Define the function Ind as follows ([161, 165, 184])

$$\text{Ind} = \text{Ind}(k; y_1, y_2) = \begin{cases} 1 & \text{if } \mathbf{r}_{rel}(t_{stop,k}(\mathbf{y}); k, \mathbf{y}) \in \mathbf{V}_{targ} \\ 0 & \text{if } \mathbf{r}_{rel}(t_{stop,k}(\mathbf{y}); k, \mathbf{y}) \notin \mathbf{V}_{targ} \end{cases}, \quad (9.34)$$

$$\mathbf{y} = [y_1, y_2]^\top \in \mathbb{R}^2, \quad k = 1, 2, \dots, n_f.$$

Define the following set ((9.34)),

$$\mathbf{y}_c = \mathbf{0}_{4 \times 1} \Rightarrow \delta_v = \dot{\delta}_v = \ddot{\delta}_v = 0, \quad \dot{\alpha}_s = \ddot{\alpha}_s = 0, \quad (9.35)$$

$$\gamma = \dot{\gamma} = \ddot{\gamma} = 0, \quad \zeta = \dot{\zeta} = \ddot{\zeta} = 0,$$

It is assumed that the set $= \pi/4$ represents a solid region in \mathbb{R}^3

without any openings or holes ([105]). Chapter 8 deals with the case where there are no disturbances acting on the AA projectile, that is, the azimuth and elevation error angles are always zero, $\boldsymbol{\varepsilon}_k = \mathbf{0}_{2 \times 1}$ for all

$k = 1, 2, \dots, n_f$. For this case, the AA projectile impacts the body of the AAT, that is, $\text{Ind}(k; 0, 0) = 1$, (9.34), for all $k = 1, 2, \dots, n_f$. It follows that the point $\mathbf{0}_{2 \times 1} \in \mathcal{A}_{Ind,k}$, (9.35), $k = 1, 2, \dots, n_f$.

By using (9.4), (9.31)–(9.34), (9.35), the probability that the AA projectile fired at time $t \geq 0$ will impact the body of the AAT is equal to the expected value of the function Ind, (9.34), as follows ([2, 67, 83, 161, 171, 184])

$$(9.36)$$

$$\begin{aligned}
P_{hitT,k} &= \text{Prob} (\mathbf{r}_{rel}(t_{stop,k}(\boldsymbol{\varepsilon}_k); k, \boldsymbol{\varepsilon}_k) \in \mathbf{V}_{targ}) \\
&= \text{E} (\text{Ind} (k; \boldsymbol{\varepsilon}_{\psi,k}, \boldsymbol{\varepsilon}_{\theta,k})) \\
&= \int \int_{\mathbb{R}^2} \text{Ind} (k; y_1, y_2) f_{\boldsymbol{\varepsilon}_k}(y_1, y_2) dy_1 dy_2 \\
&= \int \int_{\mathbb{R}^2} \text{Ind} (k; y_1, y_2) f_{\boldsymbol{\varepsilon}}(y_1, y_2) dy_1 dy_2 \\
&= \int \int_{\mathbb{R}^2} \text{Ind} (k; y_1, y_2) f_{\boldsymbol{\varepsilon}_{\psi}, \boldsymbol{\varepsilon}_{\theta}}(y_1, y_2) dy_1 dy_2 \\
&= \int \int_{\mathcal{A}_{Ind,k}} f_{\boldsymbol{\varepsilon}_{\psi}, \boldsymbol{\varepsilon}_{\theta}}(y_1, y_2) dy_1 dy_2, \\
\Rightarrow P_{hitT,k} &= \int \int_{\mathcal{A}_{Ind,k}} f_{\boldsymbol{\varepsilon}_{\psi}, \boldsymbol{\varepsilon}_{\theta}}(y_1, y_2) dy_1 dy_2, \tag{9.37}
\end{aligned}$$

where $\text{E}(B_i)$ denotes the expected value of the random variable B_i . In (9.36), the variables k_0 and k_0 are associated with the random variables n_f and k_0 , and represent the azimuth and elevation error angles, respectively. Thus, the units of k_0 and k_0 are radians (rad).

Based on the vulnerability model of the AAT (Chap. 8), if one or more AA projectiles impact any point on the body of the AAT then the AAT is destroyed. Thus, if one AA projectile is fired then the probability of destroying the AAT, also referred to as the kill probability ([40]), is given by

$$P_{kill,k} = P_{hitT,k}. \tag{9.38}$$

There are no closed-form expressions available for $P_{hitT,k}$, Ind , $T_{\delta_v} \mathbf{I}_3$, $t_{hitT,k}$, $\mathbf{J}_{hitT,k}$ and $= \pi/4$ in terms of B_i and other given parameters. Thus, the probability $P_{hitT,k}$ cannot be computed directly by using (9.37). The approach used in this work is to first find a bounding set

$\mathbf{q}_{s1}(t)$ that is a subset of \mathbb{R}^3 and that includes all the elements of the set $= \pi/4$, (9.35), as follows

$$\begin{aligned}\mathcal{A}_{Ind,k} \subset \mathbf{D}_0(k), \quad \mathbf{D}_0(k) &= \mathcal{A}_{Ind,k} \cup (\mathbf{D}_0(k) - \mathcal{A}_{Ind,k}), \\ \mathcal{A}_{Ind,k} \cap (\mathbf{D}_0(k) - \mathcal{A}_{Ind,k}) &= \emptyset,\end{aligned}\tag{9.39}$$

where $(\mathbf{D}_0(k) - \mathcal{A}_{Ind,k})$ denotes the set of all the elements in $\mathbf{q}_{s1}(t)$ that are not in $= \pi/4$. It follows from (9.34)–(9.35), (9.39), that

$$\begin{aligned}\text{Ind}(k; y_1, y_2) &= 1 \quad \text{if } \mathbf{y} \in \mathcal{A}_{Ind,k}, \\ \text{Ind}(k; y_1, y_2) &= 0 \quad \text{if } \mathbf{y} \in (\mathbf{D}_0(k) - \mathcal{A}_{Ind,k}), \\ \text{Ind}(k; y_1, y_2) &= 0 \quad \text{if } \mathbf{y} \notin \mathbf{D}_0(k).\end{aligned}\tag{9.40}$$

In this work, the bounding set $\mathbf{q}_{s1}(t)$ is assumed to be a box or rectangle centered at the origin. By using $\mathbf{q}_{s1}(t)$ and (9.34)–(9.40), the probability $P_{hitT,k}$ is computed as follows

$$\begin{aligned}& \int \int_{\mathbf{D}_0(k)} \text{Ind}(k; y_1, y_2) f_{\varepsilon_\psi, \varepsilon_\theta}(y_1, y_2) dy_1 dy_2 \\ &= \int \int_{\mathcal{A}_{Ind,k}} \text{Ind}(k; y_1, y_2) f_{\varepsilon_\psi, \varepsilon_\theta}(y_1, y_2) dy_1 dy_2 + \\ & \int \int_{\mathbf{D}_0(k) - \mathcal{A}_{Ind,k}} \text{Ind}(k; y_1, y_2) f_{\varepsilon_\psi, \varepsilon_\theta}(y_1, y_2) dy_1 dy_2\end{aligned}\tag{9.41}$$

$$\begin{aligned}
&= \int \int_{\mathcal{A}_{Ind,k}} \text{Ind}(k; y_1, y_2) f_{\varepsilon_\psi, \varepsilon_\theta}(y_1, y_2) dy_1 dy_2 + 0 \\
&= \int \int_{\mathcal{A}_{Ind,k}} f_{\varepsilon_\psi, \varepsilon_\theta}(y_1, y_2) dy_1 dy_2 \\
&= P_{hitT,k}, \\
\Rightarrow P_{hitT,k} &= \int \int_{D_0(k)} \text{Ind}(k; y_1, y_2) f_{\varepsilon_\psi, \varepsilon_\theta}(y_1, y_2) dy_1 dy_2. \tag{9.42}
\end{aligned}$$

In the following Sections, computational methods NM1 and NM2 are presented for computing increasingly tighter bounding sets $D(k)$ and $D_f(k)$, respectively, for the set $\mathcal{A}_{Ind,k} = \pi/4$. The sets $D(k)$ and $D_f(k)$ are used separately in the place of $\mathcal{A}_{Ind,k}$ as domains of integration in the numerical computation of the double integral in (9.42), thus yielding approximations of the probability $P_{hitT,k}$ in each case.

9.3 Computational Method NM1 for the Computation of $P_{hitT,k}$

Computational method NM1 computes $P_{hitT,k}$ and is summarized as follows.

1. Given the intercept time $t \geq 0$, that is, given k .
2. Let $r_{proj}^{(t)}(t_{hitG})$ denote the line-of-intercept (LOI) vector, that is, the inertial vector pointing from the hinge point H of the AA gun at time $t \geq 0$ (Fig. 9.1) to the center of mass of the AAT at time $t \geq 0$, and given by

$$(9.43)$$

$$\mathbf{r}_{LOI}^{(I)}(t_{hitC,k}) = \mathbf{r}_{targ}^{(I)}(t_{hitC,k}) - \mathbf{r}_H^{(I)}(t_{fire,k}).$$

In the case considered here, the vehicle body of the ADS is completely stationary implying that $\mathbf{r}_H^{(I)}(t_{fire,k}) = \mathbf{r}_H^{(I)}(t_{hitC,k})$. Thus,

in this case, the LOI vector equals the LOS vector at time $t \geq 0$,

$$\mathbf{r}_{LOI}^{(I)}(t_{hitC,k}) = \mathbf{r}_{los}^{(I)}(t_{hitC,k}), \quad (2.148).$$

3. For each k , an appropriate bounding set $D(k)$ for the set $= \pi/4$, (9.35), is computed,

$$\mathcal{A}_{Ind,k} \subset D(k), \quad k = 1, 2, \dots, n_f, \quad (9.44)$$

Note that the basic assumption, (7.60), applies throughout. The set $D(k)$ is used as domain of integration for the double integral in (9.42).

4. The bounding set $D(k)$ has a rectangular shape as follows

$$D(k) = \{[y_1, y_2]^T \in \mathbb{R}^2 : |y_1| \leq y_{1m,k}, |y_2| \leq y_{2m,k}\}, \quad (9.45)$$

where the bounds $D(k)$, $D(k)$, are computed such that (9.44)

holds. In this work the bounds in (9.45) are computed as follows

$$\begin{aligned} y_{1m,k} &= \arctan2(d_1, \|\mathbf{r}_{LOI}^{(I)}(t_{hitC,k})\|), \\ y_{2m,k} &= \arctan2(d_1, \|\mathbf{r}_{LOI}^{(I)}(t_{hitC,k})\|), \end{aligned} \quad (9.46)$$

where p_s is the radius of a sphere with center fixed to the CM of the AAT. This sphere is referred to as the integration limits bounding sphere (ILBS). The radius p_s is selected such that the

ILBS is somewhat larger than the sphere that just encloses the AAT. It was found that for the AAT considered here, the resulting bounding set $D(k)$ satisfies (9.44) (see computational results).

5.

Thus, by using (9.44), (9.42), the probability Q_{A10} , (9.36), is given by

$$\begin{aligned} P_{hitT,k} &= \int \int_{\mathcal{A}_{Ind,k}} f_{\varepsilon_\psi, \varepsilon_\theta}(y_1, y_2) dy_1 dy_2 \\ &= \int \int_{D(k)} \text{Ind}(k; y_1, y_2) f_{\varepsilon_\psi, \varepsilon_\theta}(y_1, y_2) dy_1 dy_2. \end{aligned} \quad (9.47)$$

In principle, a suitable numerical integration algorithm, for example, adaptive quadrature ([43, 72, 92, 110]), can be applied in order to compute the double integral in (9.47). However, in the numerical computation of the double integral it was found that the direct computation of the function $\arg(x_1 + j_c y_1)$ for any given $\mathbf{y} = [y_1, y_2]^\top$ leads to a lengthy total computation time. The computation time is substantially reduced by pre-computing and storing the function $\arg(x_1 + j_c y_1)$ for all vectors $\mathbf{y} = [y_1, y_2]^\top$ that belong to a discretized version of the set $D(k)$.

6. The bounding set $D(k)$ is discretized into a set $j = 1, 2$ as follows

$$\begin{aligned} D_{grid}(k) = \{ [y_1, y_2]^\top \in \mathbb{R}^2 : y_1 = i_1 \Delta_{1,k}, i_1 = 0, \pm 1, \pm 2, \dots, \pm n_1, \\ y_2 = i_2 \Delta_{2,k}, i_2 = 0, \pm 1, \pm 2, \dots, \pm n_2 \}, \end{aligned} \quad (9.48)$$

where

$$\begin{aligned} \Delta_{1,k} &= \frac{y_{1m,k}}{n_1}, \quad \Delta_{2,k} = \frac{y_{2m,k}}{n_2}, \\ N_{set}(D_{grid}(k)) &= n_{tot} = (2n_1 + 1)(2n_2 + 1), \end{aligned} \quad (9.49)$$

and where $(2n_1 + 1)$ and $(2n_2 + 1)$ are the specified number of discretization points for the intervals $[-y_{1m,k}, y_{1m,k}]$ and

$[-y_{1m,k}, y_{1m,k}]$, respectively.

7.

Thus, for each vector $\mathbf{y} = [y_1, y_2]^T$ in the discrete set $j = 1, 2$, the function value $z = \text{Ind}(k; y_1, y_2)$, (9.34), is computed by using the methods presented in Sect. 8.3. The pair of values $Z_{B_{10}}$ is stored in the set B_I as follows

$$B_I(k) = \{(z, \mathbf{y}) : z = \text{Ind}(k; y_1, y_2), \mathbf{y} = [y_1, y_2]^T \in D_{grid}(k)\}. \quad (9.50)$$

8.

For any $\mathbf{y} = [y_1, y_2]^T \in D(k)$, the function value $\arg(x_1 + j_c y_1)$ in (9.47) is computed by applying two-dimensional linear interpolation using the values stored in the set $B_I(k)$, (9.50) ([43, 110]).

9.

Let $C_1(k)$ denote the subset of $j = 1, 2$ for which the function Ind is equal to 1,

$$C_1(k) = \{[y_1, y_2]^T \in D_{grid}(k) : \text{Ind}(k; y_1, y_2) = 1\}. \quad (9.51)$$

The ratio of the number of points in the set $C_1(k)$ to the total number of points $EM_{\delta_v} e_4 = \zeta - \zeta_{ref}$, expressed as a percentage, is as follows

$$h_{NM1,k} = \frac{N_{set}(C_1(k))}{n_{tot}} \times 100\%. \quad (9.52)$$

10. The slender cylindrical-type shape of the AAT versus the spherical shape and size of the enclosing ILBS leads to the following. The function Ind , (9.34), is equal to 1 for a small fraction of the

points in the discrete set $j = 1, 2$, and is equal to 0 for the majority of the points in $j = 1, 2$. The result is that a low value is obtained for $\delta_3 = 0$. This problem is addressed by computational method NM2.

9.4 Computational Method NM2 for the Computation of $P_{hitT,k}$

Computational method NM2 computes $P_{hitT,k}$ by employing the results of computational method NM1 and is summarized as follows.

1. Compute the minimum and maximum values of the k_0 element and of the k_0 element of all the vectors $\mathbf{y} = [y_1, y_2]^T \in \mathbf{C}_1(k)$,

$$x_{1min,k} = \inf\{x_a \in \mathbb{R} : \text{the vector } [x_a, y_2]^T \in \mathbf{C}_1(k), y_2 \in \mathbb{R}\}, \quad (9.53)$$

$$x_{1max,k} = \sup\{x_a \in \mathbb{R} : \text{the vector } [x_a, y_2]^T \in \mathbf{C}_1(k), y_2 \in \mathbb{R}\}, \quad (9.54)$$

$$x_{1min,k} = \inf\{x_a \in \mathbb{R} : \text{the vector } [x_a, y_2]^T \in \mathbf{C}_1(k), y_2 \in \mathbb{R}\}, \quad (9.55)$$

$$x_{1max,k} = \sup\{x_a \in \mathbb{R} : \text{the vector } [x_a, y_2]^T \in \mathbf{C}_1(k), y_2 \in \mathbb{R}\}, \quad (9.56)$$

2. The symmetrical bounds $\mathbf{D}(k)$ and $\mathbf{D}(k)$ on the variables k_0 and k_0 , respectively, are obtained as follows

$$y_{1m,k} = \chi_{1m,k} + g_1 \Delta_{1,k}, \quad \chi_{1m,k} = \max(|x_{1min,k}|, |x_{1max,k}|), \quad (9.57)$$

$$y_{1m,k} = \chi_{1m,k} + g_1 \Delta_{1,k}, \quad \chi_{1m,k} = \max(|x_{1min,k}|, |x_{1max,k}|), \quad (9.58)$$

where $\beta(t)$, $\beta(t)$, are as obtained by using computational method NM1, (9.49), and $p_s, h_b > a$ are integers used to set the bounds on the variables k_0 and k_0 , (9.59). The bounding set $D_f(k)$ is given by

$$\dot{y} - (L_2 \cos(\beta) + L_c \sin(\beta))\dot{\beta} + a \cos(\beta + \delta_3)\dot{\alpha}_3 = 0, \quad (9.59)$$

The integers $p_s, h_b > a$ are chosen such that a part of the region in \mathbb{R}^3 where $\text{Ind}(k; y_1, y_2) = 0$ is included in the bounding set $D_f(k)$. It follows that the set $D_f(k)$ has generally tighter bounds on the variables k_0 and k_0 than the bounding set $D(k)$, and that

$$\mathcal{A}_{Ind,k} \subset D_f(k), \quad k = 1, 2, \dots, n_f. \quad (9.60)$$

3. Thus, by using (9.60), (9.42), the probability Q_{A10} , (9.36), is given by

$$\begin{aligned} P_{hitT,k} &= \int \int_{\mathcal{A}_{Ind,k}} f_{\varepsilon_\psi, \varepsilon_\theta}(y_1, y_2) dy_1 dy_2 \\ &= \int \int_{D_f(k)} \text{Ind}(k; y_1, y_2) f_{\varepsilon_\psi, \varepsilon_\theta}(y_1, y_2) dy_1 dy_2. \end{aligned} \quad (9.61)$$

4. The number of discretization points $(2n_{1,k} + 1)$ and $(2n_{2,k} + 1)$ for the intervals $[-y_{1m,k}, y_{1m,k}]$ and $[-y_{2m,k}, y_{2m,k}]$, respectively, are computed as follows

$$(2n_{2,k} + 1) = \text{number2odd}(\text{ceil}(\sqrt{n_{tot}/r_{0,k}})), \quad (9.62)$$

$$(2n_{1,k} + 1) = \text{number2odd}(\text{ceil}(r_{0,k}(2n_{2,k} + 1))), \quad (9.63)$$

where n_{tot} is the total number of discretization points that was

originally specified for numerical method NM1,

$$r_{0,k} = \frac{y_{1m,k}}{y_{2m,k}}, \quad (9.64)$$

ceil α_s is given by (5.50), and

$$\text{number2odd}(x_a) = \begin{cases} x_a & \text{if } x_a \text{ is an odd integer } > 0 \\ x_a + 1 & \text{if } x_a \text{ is an even integer } > 0 \end{cases}. \quad (9.65)$$

5. The set $\mathbf{D}_{fgrid}(k)$ is the discretized version of the bounding set

$\mathbf{D}_f(k)$ as follows

$$\mathbf{D}_{fgrid}(k) = \{[y_1, y_2]^\top \in \mathbb{R}^2 : y_1 = i_1 \Delta_{1,k}, i_1 = 0, \pm 1, \pm 2, \dots, \pm n_{1,k}, y_2 = i_2 \Delta_{2,k}, i_2 = 0, \pm 1, \pm 2, \dots, \pm n_{2,k}\}, \quad (9.66)$$

where

$$\Delta_{1,k} = \frac{y_{1m,k}}{n_{1,k}}, \quad \Delta_{2,k} = \frac{y_{2m,k}}{n_{2,k}}, \quad (9.67)$$

$$N_{set}(\mathbf{D}_{fgrid}(k)) = n_{tot,k} = (2n_{1,k} + 1)(2n_{2,k} + 1) \geq n_{tot},$$

and where $(2n_{1,k} + 1)$ is obtained from (9.62), and $(2n_{2,k} + 1)$ is obtained from (9.63).

6. Thus, for each vector $\mathbf{y} = [y_1, y_2]^\top$ in the discrete set $\mathbf{D}_{fgrid}(k)$, (9.66), the function value $z = \text{Ind}(k; y_1, y_2)$, (9.34), is computed by using the methods presented in Sect. 8.3. The pair of values $Z_{B_{10}}$ is stored in the set $Y_{B_{10}}$ as follows

$$\mathbf{B}_{fI}(k) = \{(z, \mathbf{y}) : z = \text{Ind}(k; y_1, y_2), \mathbf{y} = [y_1, y_2]^\top \in \mathbf{D}_{fgrid}(k)\}. \quad (9.68)$$

7. For any $\mathbf{y} = [y_1, y_2]^\top \in \mathbf{D}_f(k)$, the function value $\arg(x_1 + j_c y_1)$ in (9.61) is computed by applying two-dimensional linear

(9.68) is computed by applying two-dimensional linear interpolation using the values stored in the set Q_{grav13} ([43, 110]).

8. Let $C_{f1}(k)$ denote the subset of $D_{fgrid}(k)$ for which the function Ind is equal to 1,

$$C_{f1}(k) = \{[y_1, y_2]^T \in D_{fgrid}(k) : \text{Ind}(k; y_1, y_2) = 1\}. \quad (9.69)$$

The ratio of the number of points in the set $C_{f1}(k)$ to the total number of points $q \in \mathbb{R}^n \cap N_{set}(D_{fgrid}(k))$, expressed as a percentage, is as follows

$$h_{NM2,k} = \frac{N_{set}(C_{f1}(k))}{n_{tot,k}} \times 100\%. \quad (9.70)$$

9.5 Probability of Destroying the AAT for the Case Where a Burst of AA Projectiles is Fired

Assume that a burst of N_p AA projectiles is fired instantaneously against the AAT at time $t \geq 0$. The probability that i out of N_p AA projectiles will impact the body of the AAT is computed for $\text{Ind}(k; 0, 0) = 1$, using the following assumptions and methods.

1. At each of p_s predefined times t_{fire,j_v} , $v = 1, 2, \dots, n_0$, the AA gun fires a burst of N_p AA projectiles instantaneously where the index $j_v \in \mathcal{T}_{burst}$,

$$\mathcal{T}_{burst} = \{j_1, j_2, \dots, j_{n_0}\} \subset \{1, 2, 3, \dots, n_f\}, \quad N_{set}(\mathcal{T}_{burst}) = n_0. \quad (9.71)$$

At times t_{fire,j_ν} , $j_\nu \in \mathcal{T}_{burst}$, the AA gun does not fire any AA projectiles.

2. It is further assumed that the N_p AA projectiles fired in a burst at time t_{fire,j_ν} are stochastically independent, and that the probability that any given AA projectile will impact the body of the AAT is the same, that is, $L_c > 0$, $\nu = 1, 2, \dots, n_0$, (9.37).

3. Let \mathbf{H}_s denote the number of AA projectiles that impact the body of the AAT out of the burst of N_p projectiles fired at time t_{fire,j_ν} , $\nu = 1, 2, \dots, n_0$. Then, it follows that the random variable \mathbf{H}_s has a binomial probability mass function (PMF) given by

$$\begin{aligned} \text{Prob}(Y_{j_\nu} = i) &= C_i^{N_p} (P_{hitT,j_\nu})^i (1 - P_{hitT,j_\nu})^{N_p - i}, \\ i &= 0, 1, 2, \dots, N_p, \quad \nu = 1, 2, \dots, n_0, \end{aligned} \quad (9.72)$$

where

$$C_i^{N_p} = \frac{N_p!}{i!(N_p - i)!}, \quad i = 0, 1, 2, \dots, N_p. \quad (9.73)$$

4. The probability of destroying the AAT for the case where a burst of N_p AA projectiles is fired at time t_{fire,j_ν} is given by

$$\begin{aligned} P_{Bkill,j_\nu} &= \text{Prob}(Y_{j_\nu} \geq 1) = \sum_{i=1}^{N_p} \text{Prob}(Y_{j_\nu} = i), \\ &\nu = 1, 2, \dots, n_0. \end{aligned} \quad (9.74)$$

5. The discrete random variable \mathbf{H}_s takes on the following consecutive integer values, $0, 1, 2, \dots, N_p$, for each $\nu = 1, 2, \dots, n_0$. Let $\mathbf{P}(Y_{j_\nu})$ denote the whole PMF of the random variable \mathbf{H}_s and

let $P(Y_{j\nu}; i)$ denote the probability that $L_b > 0$, as follows ((9.72))

$$P(Y_{j\nu}) = \text{PMF of } Y_{j\nu}, \quad \nu = 1, 2, \dots, n_0, \quad (9.75)$$

$$P(Y_{j\nu}; i) = \text{Prob}(Y_{j\nu} = i), \quad i = 0, 1, 2, \dots, N_p, \quad (9.76)$$

$$\nu = 1, 2, \dots, n_0.$$

6. It is convenient to represent each PMF $P(Y_{j\nu})$, $\nu = 1, 2, \dots, n_0$, as a row vector in $\mathbb{R}^{1 \times (N_p+1)}$ as follows

$$P(Y_{j\nu}) = [P(Y_{j\nu}; 0), P(Y_{j\nu}; 1), P(Y_{j\nu}; 2), \dots, P(Y_{j\nu}; N_p)], \quad (9.77)$$

$$\nu = 1, 2, \dots, n_0.$$

7. It follows from the above that the sequence of random variables H_s , $\nu = 1, 2, \dots, n_0$, are stochastically independent but not identically distributed (pp. 122–125, [136, 139]). In addition, the random variable H_s is stochastically independent with respect to the sum of the previous ($X_{B_{10}}$ random variables, $Y_{j_1} + Y_{j_2} + \dots + Y_{j_{\nu-1}}$ (pp. 122–125, [136, 139]).

9.6 Accumulative Probability of Destroying the AAT for the Case Where a Burst of AA Projectiles is Fired

Given that the AA gun fires a burst of N_p projectiles at each time $t_{fire, j\nu}$, $\nu = 1, 2, \dots, n_0$, starting with EM_{α_s} . Intuitively, the probability of destroying the AAT after ν bursts of N_p AA projectiles each have

been fired, should increase or accumulate as the index ν increases, $\nu = 1, 2, \dots, n_0$. This probability is called the accumulative probability of destroying the AAT and is computed by using the following assumptions and methods.

1. Let \mathcal{E}_{j_ν} be a random variable denoting the sum total of the AA projectiles that have impacted the body of the AAT after ν bursts of N_p AA projectiles each have been fired, as follows

$$\mathcal{E}_{j_\nu} = \sum_{i=1}^{\nu} Y_{ji}, \quad \nu = 1, 2, \dots, n_0, \quad (9.78)$$

where $t_{hitC,k} = 14$.

2. The discrete random variable \mathcal{E}_{j_ν} takes on the following consecutive integer values $0, 1, 2, \dots, \nu N_p$, for each $k_{mp} > 1, \dots, p_s$. Since ν bursts of N_p AA projectiles each have been fired, it follows that the maximum possible value of \mathcal{E}_{j_ν} is νN_p .
3. Let $h_b > a$ denote the whole PMF of the random variable \mathcal{E}_{j_ν} and let $P(\mathcal{E}_{j_\nu}; i)$ denote the probability that $\mu = 21$, as follows

$$M_{1,13} = M_{13,1} = m_g \sin(\beta + \gamma) \sin(\zeta) L_g, \quad (9.79)$$

$$P(\mathcal{E}_{j_\nu}; i) = \text{Prob}(\mathcal{E}_{j_\nu} = i), \quad i = 0, 1, \dots, \nu N_p, \quad (9.80)$$

$$\nu = 1, 2, \dots, n_0.$$

4. It is convenient to represent each PMF $h_b > a$, $\nu = 1, 2, \dots, n_0$, as a row vector in $\mathbb{R}^{1 \times (\nu N_p + 1)}$ as follows ((9.80))

(9.81)

$$P(\mathcal{E}_{j_\nu}) = [P(\mathcal{E}_{j_\nu}; 0), P(\mathcal{E}_{j_\nu}; 1), P(\mathcal{E}_{j_\nu}; 2), \dots, P(\mathcal{E}_{j_\nu}; \nu N_p)],$$

$$\nu = 1, 2, \dots, n_0.$$

The method used to compute each PMF $h_b > a$, $\nu = 1, 2, \dots, n_0$, is given below.

5. By using the facts given in point 7, Sect. 9.5, it can be shown (pp. 122–125, [136, 139]) that since the sequence of random variables Ψ_7 , $t_{hitC,k} = 12.4$, are stochastically independent, the PMF of \mathcal{E}_{j_ν} is the convolution of the individual PMFs, $\mathbf{a}_{los}(t)$, $t_{hitC,k} = 12.4$, as follows

$$P(\mathcal{E}_{j_\nu}) = P(Y_{j_1}) * P(Y_{j_2}) * P(Y_{j_3}) * \dots * P(Y_{j_\nu}),$$

$$\nu = 1, 2, \dots, n_0, \quad (9.82)$$

where $P(\mathcal{E}_{j_1}) = P(Y_{j_1})$, $P(Y_{j_\nu}) \in \mathbb{R}^{1 \times (N_p+1)}$, (9.77),

$P(\mathcal{E}_{j_\nu}) \in \mathbb{R}^{1 \times (\nu N_p+1)}$, (9.81), $\nu = 1, 2, \dots, n_0$, and where $-T_{\gamma_0} \mathbf{I}_3$

denotes the convolution of two finite row vectors $\mathbf{x}_1 \in \mathbb{R}^{1 \times n_1}$ and

$\mathbf{x}_2 \in \mathbb{R}^{1 \times n_2}$, and $(\mathbf{x}_1 * \mathbf{x}_2) \in \mathbb{R}^{1 \times (n_1+n_2-1)}$ ([136, 139]).

6. Practically, (9.82) is implemented by applying the following recursive equation (point 7, Sect. 9.5)

$$P(\mathcal{E}_{j_\nu}) = P(Y_{j_\nu}) * P(\mathcal{E}_{j_{\nu-1}}), \quad P(\mathcal{E}_{j_1}) = P(Y_{j_1}),$$

$$\nu = 2, 3, \dots, n_0. \quad (9.83)$$

7. Thus, the accumulative probability of destroying the AAT after ν bursts of N_p AA projectiles each have been fired, is given by

 νN_n νN_n

$$P_{Akill,j_v} = \text{Prob} (\mathcal{E}_{j_v} \geq 1) = \sum_{i=1}^r \text{Prob} (\mathcal{E}_{j_v} = i) = \sum_{i=1}^r P(\mathcal{E}_{j_v}; i), \quad (9.84)$$

$v = 1, 2, \dots, n_0.$

9.7 Computational Results

The numerical solution of fire control problem FCA for the case of a completely stationary vehicle body of the mobile ADS is employed (Sect. 7.4). Some of the relevant data is repeated here for convenience.

The initial and final times are given by

$$t_0 = t_{fire,1} = -\Delta_{tofC,1}, \quad t_{FIN} = 20 \text{ s}, \quad (9.85)$$

The sequence of intercept times is equally spaced and is given by

$$\begin{aligned} t_{hitC,k} &= (k-1)\Delta_{hitC}, \quad k = 1, 2, \dots, n_f = 101, \\ \Delta_{hitC} &= 0.2 \text{ s}, \quad t_{hitC,1} = 0, \quad t_{hitC,n_f} = t_{FIN} = 20 \text{ s}. \end{aligned} \quad (9.86)$$

Thus, the set of specified intercept times (in seconds) is given by

$$\{t_{hitC,k}, k = 1, 2, \dots, n_f\} = \{0, 0.2, 0.4, \dots, 19.6, 19.8, 20\}. \quad (9.87)$$

For each specified intercept time $t \geq 0$, the time of flight $\Delta_{tofC,k}$ has been computed implying that the firing time is $t_{fire,k} = t_{hitC,k} - \Delta_{tofC,k}$, $k = 1, 2, \dots, n_f = 101$. In addition, the inertial azimuth and elevation angles of the FC vector have been computed, $\mathbf{a}_{FC}(t_{fire,k})$, $\mathbf{a}_{FC}(t_{fire,k})$, $k = 1, 2, \dots, n_f = 101$. A fourth order Runge-Kutta algorithm is used in order to solve numerically the point mass flight dynamics model of the AA projectile, with a fixed time-step

$$\Delta_{sim} = 0.01 \text{ s}. \quad (9.88)$$

The dimensions of the AAT are given in Sect. 8.5 and are repeated here for convenience. The dimensions of the AAT are $b_1 = 0.15 \text{ m}$,

$L_{a1} = 1.75$ m, $L_{a1} = 1.75$ m, $L_a = L_{a1} + L_{a2} = 3.6$ m (Fig. 9.2). In this case, the radius of the TBS is $k_0 \neq 0$ m, the finer fixed time-step used within the TBS is $\Delta_{fine} = 10^{-4}$ s, and $\Delta_d = 0.05$ s.

It is assumed that the azimuth and elevation error angles are stochastically independent and that they each have a Gaussian PDF as follows ([136, 139])

$$x(t), y(t), \beta(t), \dot{x}(t), \dot{y}(t), \dot{\beta}(t), \ddot{x}(t), \ddot{y}(t), \ddot{\beta}(t), t \in \mathcal{T}_F. \quad (9.89)$$

$$f_{\varepsilon_\psi}(y_1) = \mathcal{N}(y_1; \mu_1, \sigma_1), \quad f_{\varepsilon_\theta}(y_2) = \mathcal{N}(y_2; \mu_2, \sigma_2), \quad (9.90)$$

where

$$\delta_v = \dot{\delta}_v = \ddot{\delta}_v = 0, \quad \dot{\alpha}_s = 0 \Rightarrow \dot{\beta} = 0, \quad \beta = \beta_b, \quad (9.91)$$

$$\mu_2 = \text{E}(\varepsilon_\theta) = 0, \quad \sigma_2 = \sigma(\varepsilon_\theta) = 10^{-3} \text{ rad}, \quad (9.92)$$

$$\mathcal{N}(w; \mu_w, \sigma_w) = \frac{1}{\sqrt{2\pi\sigma_w^2}} \exp(-(w - \mu_w)^2 / (2\sigma_w^2)). \quad (9.93)$$

The double integrals in computational methods NM1 and NM2 are computed numerically by applying the MATLAB functions `dblquad`, `quadgk` that implement adaptive quadrature using the Gauss-Kronrod rules (see for example [92]), with an absolute error tolerance of 10^{-8}

([110]). Hereafter, the above-mentioned algorithm is referred to as the AQUADGK algorithm.

In addition, the following data and parameter values are employed.

1. The probability that the AA projectile will impact the body of the AAT, $P_{hitT,k}$, is computed for every fourth value of the time index k , that is, $k \in \mathcal{T}_{red}$ as follows

$$(9.94)$$

$$\mathcal{T}_{red} = \{1, 5, 9, 13, \dots, 93, 97, n_f\}, \quad N_{set}(\mathcal{T}_{red}) = 26.$$

The associated set of intercept times $t \geq 0$ (in seconds) is given by

$$\{t_{hitC,k}, k \in \mathcal{T}_{red}\} = \{0, 0.8, 1.6, \dots, 18.4, 19.2, 20\}. \quad (9.95)$$

2. The radius of the ILBS is $d_1 = 2.2$ m.
3. For computational method NM1, the number of discretization points for the variables k_0 and k_1 are $2n_1 + 1 = 151$ and $2n_2 + 1 = 151$, respectively. Thus, the total number of points in the set $j = 1, 2$ is $n_{tot} = (2n_1 + 1)(2n_2 + 1) = 22801$.
4. The integers used in computational method NM2 are $h_b > a$, $h_b > a$.
5. The number of AA projectiles fired in each burst is $N_p = 15$.
6. A burst of N_p AA projectiles is fired instantaneously at each time $t \geq 0$ with index $\mathbf{p} = \mathbf{0}_{15 \times 1}$ given by

$$\begin{aligned} \mathcal{T}_{burst} = \{j_1, j_2, \dots, j_7\} &= \{1, 17, 33, 49, 65, 81, 101\}, \\ N_{set}(\mathcal{T}_{burst}) &= n_0 = 7. \end{aligned} \quad (9.96)$$

The associated set of intercept times $t \geq 0$ (in seconds) is given by

$$\{t_{hitC,k}, k \in \mathcal{T}_{burst}\} = \{0, 3.2, 6.4, 9.6, 12.8, 16, 20\}. \quad (9.97)$$

A plot of the LOS distance $\|\mathbf{r}_{los}^{(I)}(t_{hitC,k})\|$ versus $t \geq 0$ is shown in Fig.

9.3. Most of the results are plotted against the intercept time $t \geq 0$ and some are also plotted against the LOS distance $\|\mathbf{r}_{los}^{(I)}(t_{hitC,k})\|$.

The probability that the AA projectile will impact the body of the AAT, $P_{hitT,k}$, is computed by using computational method NM2. Note that computational method NM2 employs the results of computational method NM1.

The computed values are given in Table 9.1, and plotted versus $t \geq 0$ and versus $\|\mathbf{r}_{los}^{(I)}(t_{hitC,k})\|$ in Figs. 9.4 and 9.5, respectively. It can be seen that the probability $P_{hitT,k}$ gradually increases as the AAT approaches the mobile ADS, and reaches its maximum value when the AAT is approximately at the CPA (Chap. 7).

Plots of some of the variables used in computational methods NM1 and NM2 versus $t \geq 0$, namely, $D(k)$, $D(k)$, are shown in Fig. 9.6,

$\delta_3 = 0$, $\delta_3 = 0$, are shown in Fig. 9.7, $(n_{tot,k} - n_{tot}) \times 100\% / n_{tot}$, is shown in Fig. 9.8, and $(2n_{1,k} + 1)$, $(2n_{1,k} + 1)$, and $2n_1 + 1 = 2n_2 + 1$, are shown in Fig. 9.9.

In addition, contour plots of the function $\arg(x_1 + j_c y_1)$, for computational method NM1, where $\mathbf{y} = [y_1, y_2]^T \in D_{grid}(k)$, $k = 1$, and computational method NM2, where $\mathbf{y} = [y_1, y_2]^T \in D_{fgrid}(k)$, $k = 1$, are shown in Fig. 9.10 and Fig. 9.11, respectively.

For the case where the AA gun fires bursts of $N_p = 15$ projectiles against the AAT, the probability of destroying the AAT, $\Delta_{tofC,k}$, where $P_{Bkill,k} = \text{Prob}(Y_k \geq 1)$, is significantly higher than for the case where

one AA projectile is fired, $X(\tau; t_{fire,k}, \boldsymbol{\varepsilon}_k)$, $k \in \mathcal{T}_{red}$, see Table 9.2 and the plots shown in Figs. 9.12 and 9.13.

The accumulative probability of destroying the AAT, $-T_{\gamma_0} \mathbf{I}_3$, where $P_{Akill,j_\nu} = \text{Prob}(\Xi_{j_\nu} \geq 1)$, $\nu = 1, 2, \dots, n_0 = 7$, increases as expected with increasing values of ν , see Table 9.3 and the plots shown in Figs. 9.14 and 9.15.

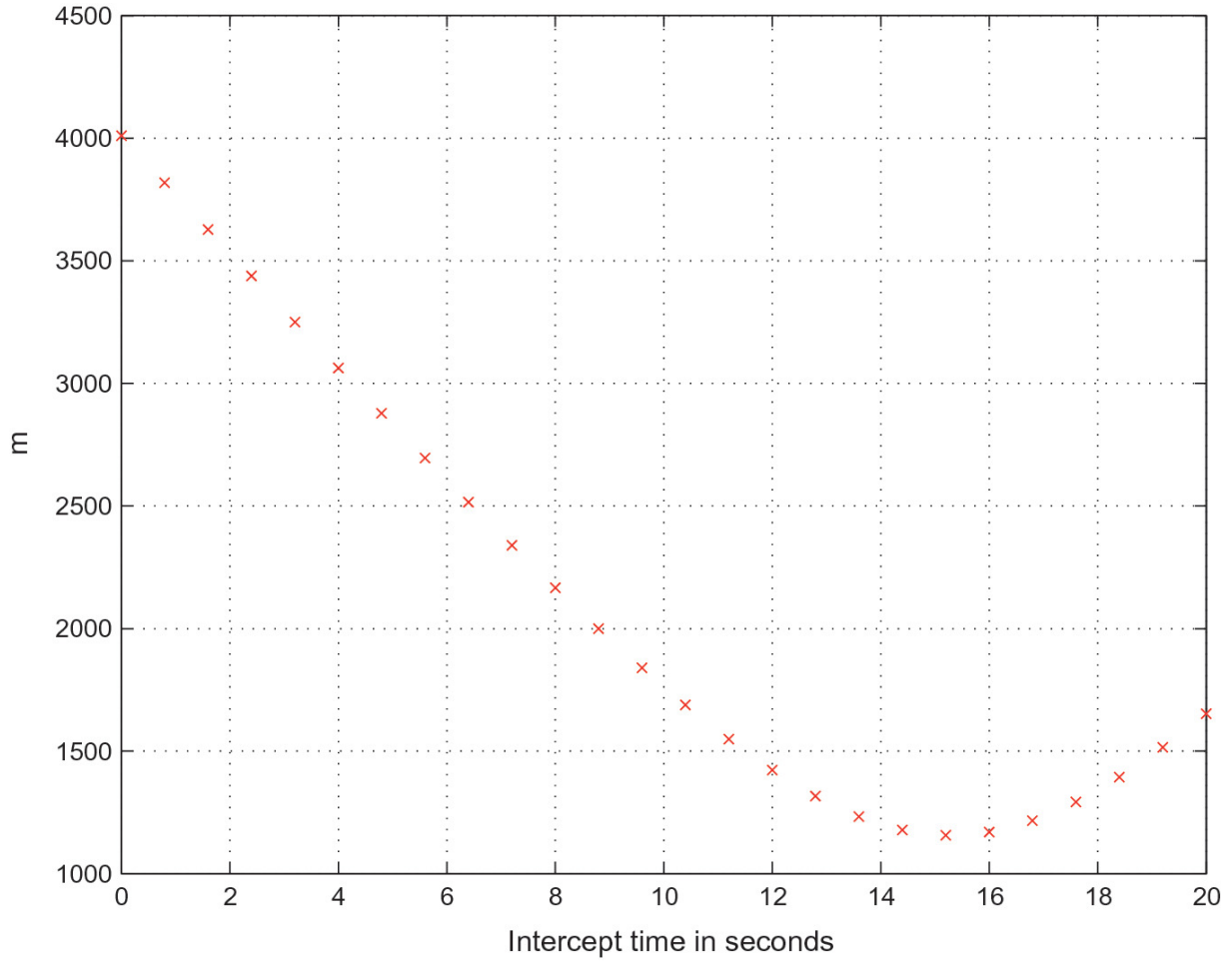


Fig. 9.3 Plot of $\|\mathbf{r}_{los}^{(I)}(t_{hitC,k})\|$ versus the intercept time $t \geq 0$, $k \in \mathcal{T}_{red}$

Table 9.1 Table of values of the probability that an AA projectile will impact the body of the AAT, $P_{hitT,k}$, the intercept time $t \geq 0$, LOS distance $\|\mathbf{r}_{los}^{(I)}(t_{hitC,k})\|$, $k \in \mathcal{T}_{red}$, (9.94)

k	$t \geq 0$ (s)	$\ r_{los}^{(T)}(t_{hitC,k})\$ (m)	$P_{hitT,k}$
1	0.00	4010.86	0.002460
5	0.80	3819.03	0.002888
9	1.60	3628.17	0.003413
13	2.40	3438.45	0.004031
17	3.20	3250.06	0.004825
21	4.00	3063.24	0.005834
25	4.80	2878.31	0.007023
29	5.60	2695.65	0.008598
33	6.40	2515.76	0.010586
37	7.20	2339.27	0.013196
41	8.00	2167.02	0.016588
45	8.80	2000.10	0.020895
49	9.60	1839.96	0.026777
53	10.40	1688.54	0.034131
57	11.20	1548.39	0.043521
61	12.00	1422.86	0.054455
65	12.80	1316.11	0.066460
69	13.60	1233.05	0.077563
73	14.40	1178.70	0.086588
77	15.20	1157.11	0.090758
81	16.00	1170.08	0.090493
85	16.80	1216.53	0.085914
89	17.60	1292.83	0.078658
93	18.40	1394.11	0.069307
97	19.20	1515.35	0.059449
101	20.00	1652.18	0.050083

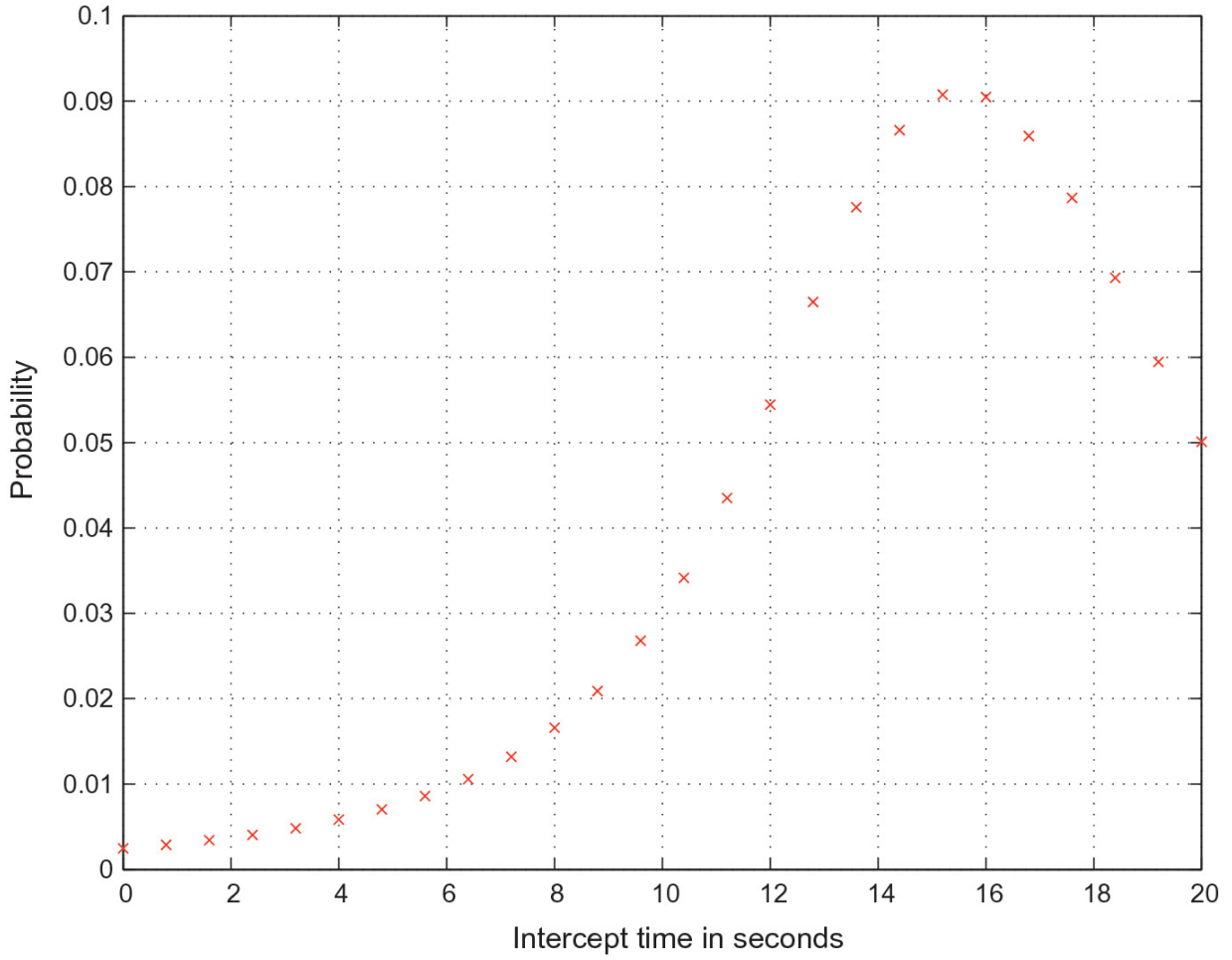


Fig. 9.4 Plot of $P_{hitT,k}$ versus the intercept time $t \geq 0$, $k \in \mathcal{T}_{red}$

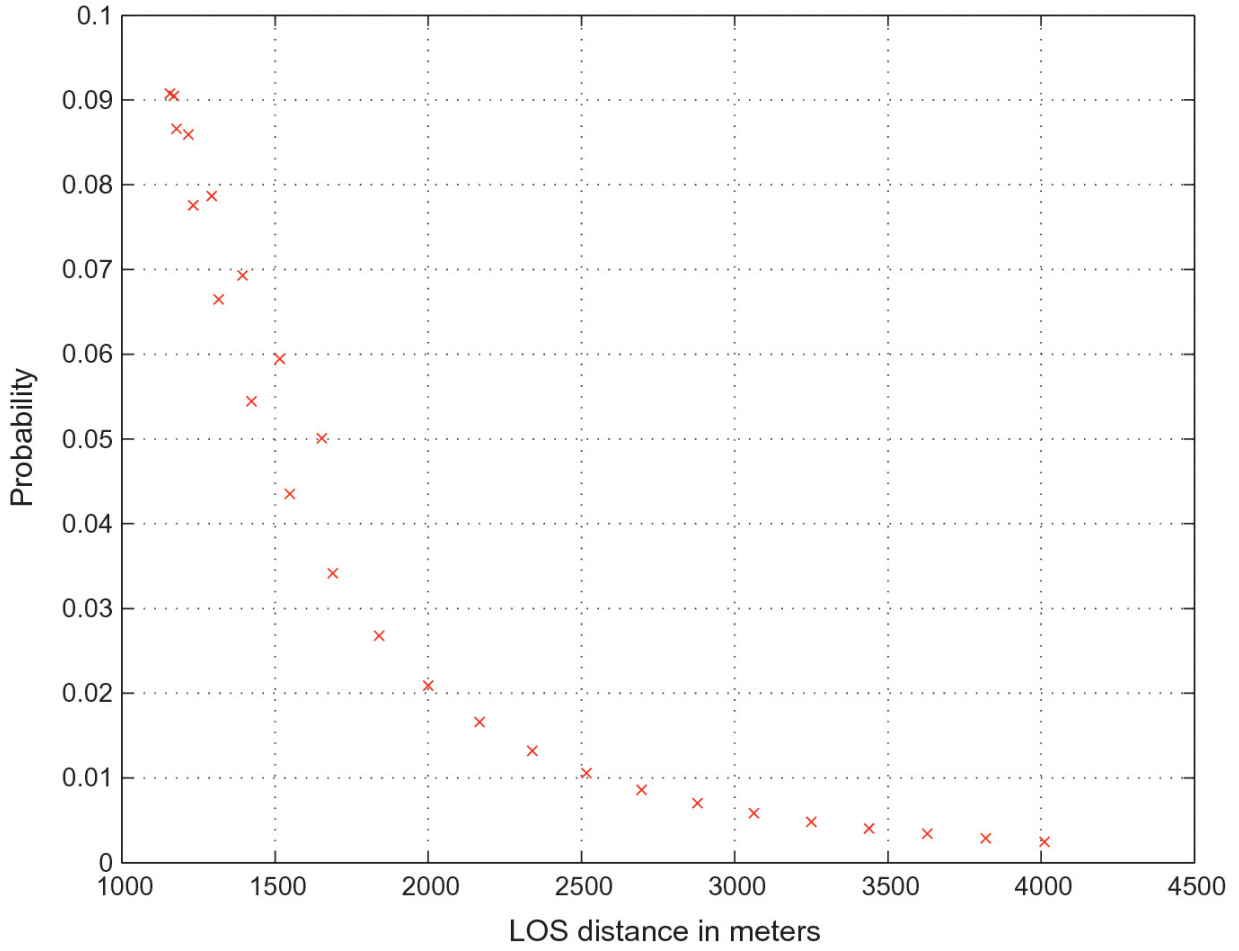


Fig. 9.5 Plot of $P_{hitT,k}$ versus $\|r_{los}^{(I)}(t_{hitC,k})\|$, $k \in \mathcal{T}_{red}$

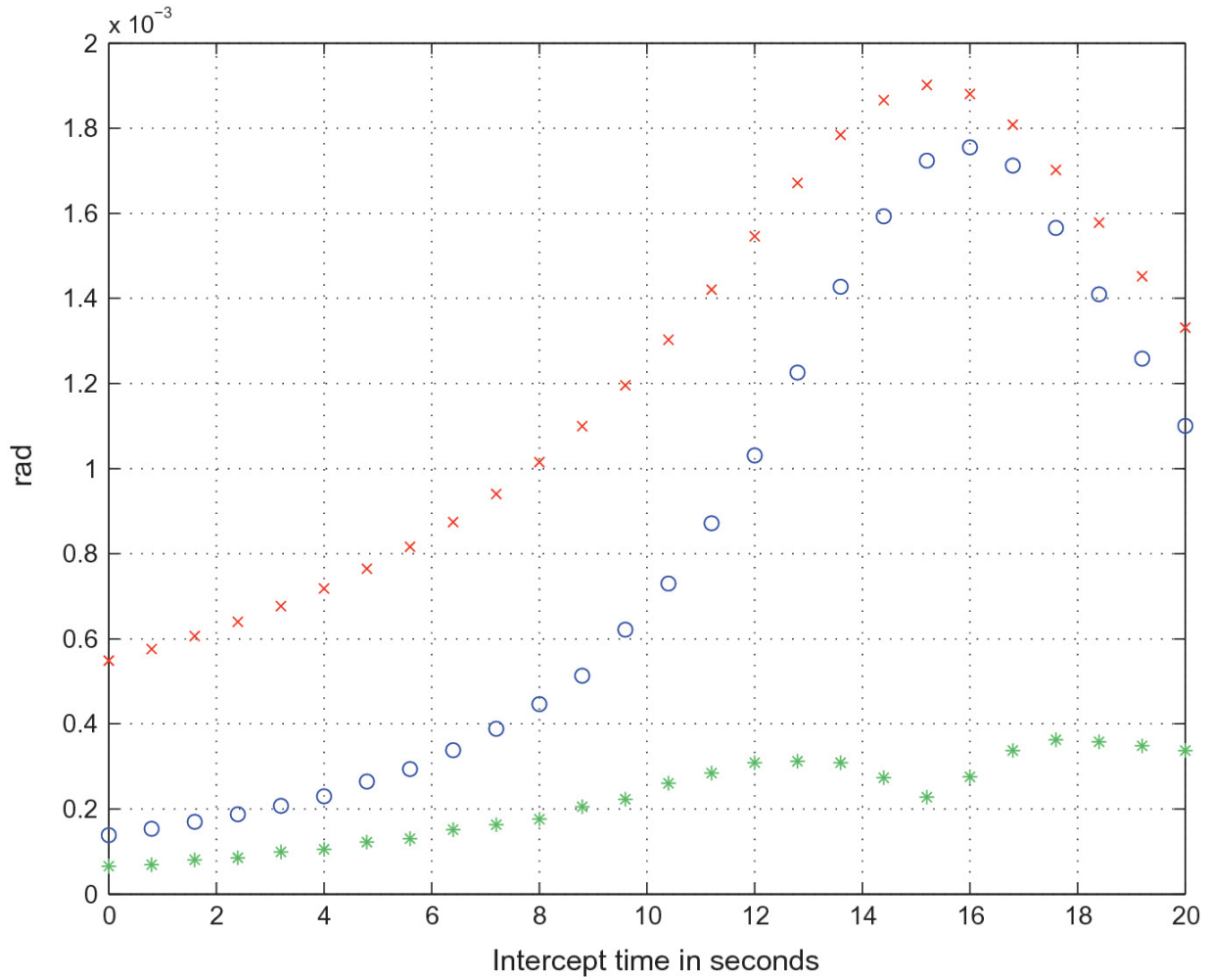


Fig. 9.6 Plot of $D(k), (o), D(k), (*)$, for computational method NM2, and $y_{1m,k} = y_{2m,k}, (x)$, for computational method NM1, versus the intercept time $t \geq 0, k \in \mathcal{T}_{red}$

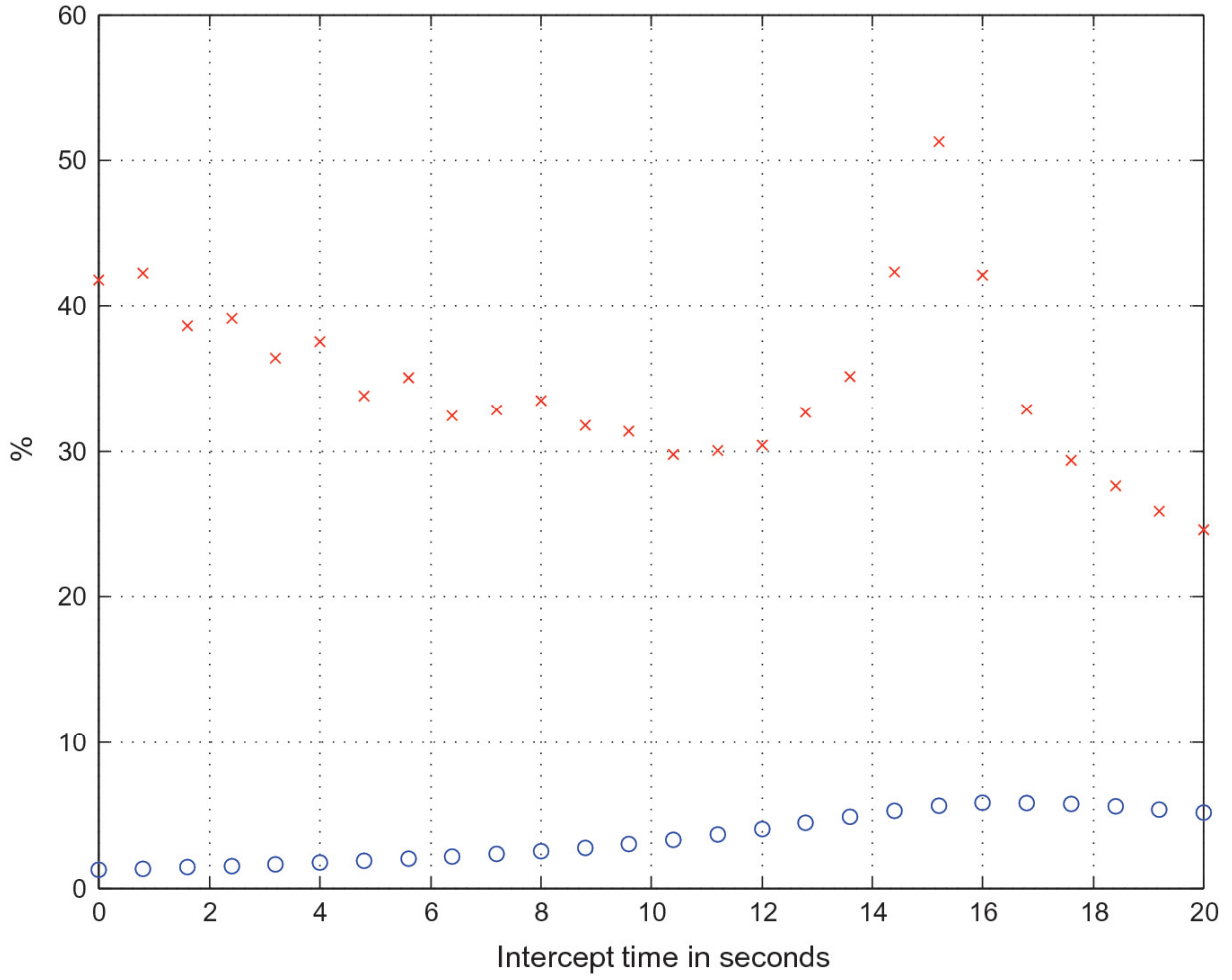


Fig. 9.7 Plot of $\delta_3 = 0$, (o), and $\delta_3 = 0$, (x), versus the intercept time $t \geq 0$, $k \in \mathcal{T}_{red}$

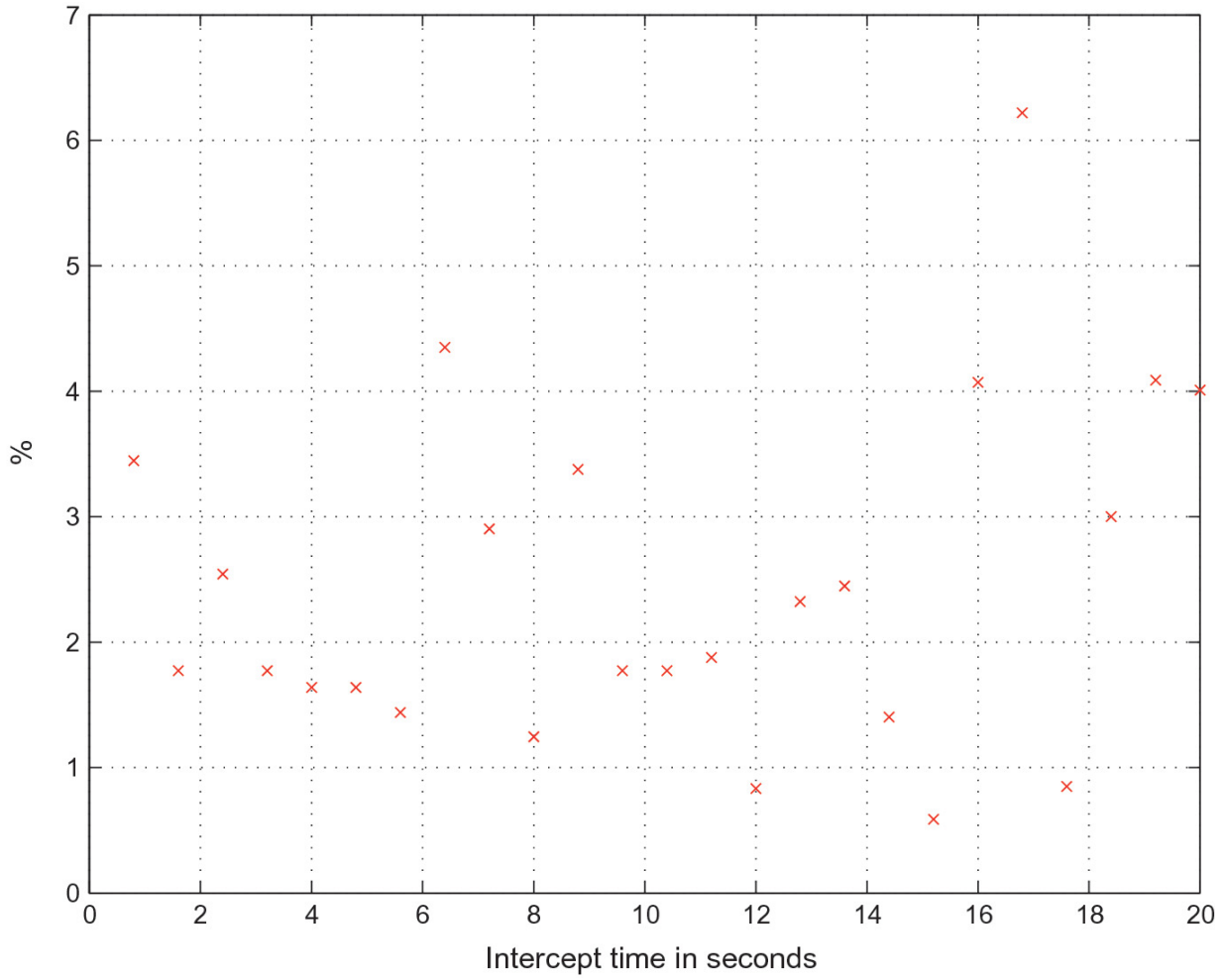


Fig. 9.8 Plot of $(n_{tot,k} - n_{tot}) \times 100\% / n_{tot}$ versus the intercept time $t \geq 0$, $k \in \mathcal{T}_{red}$

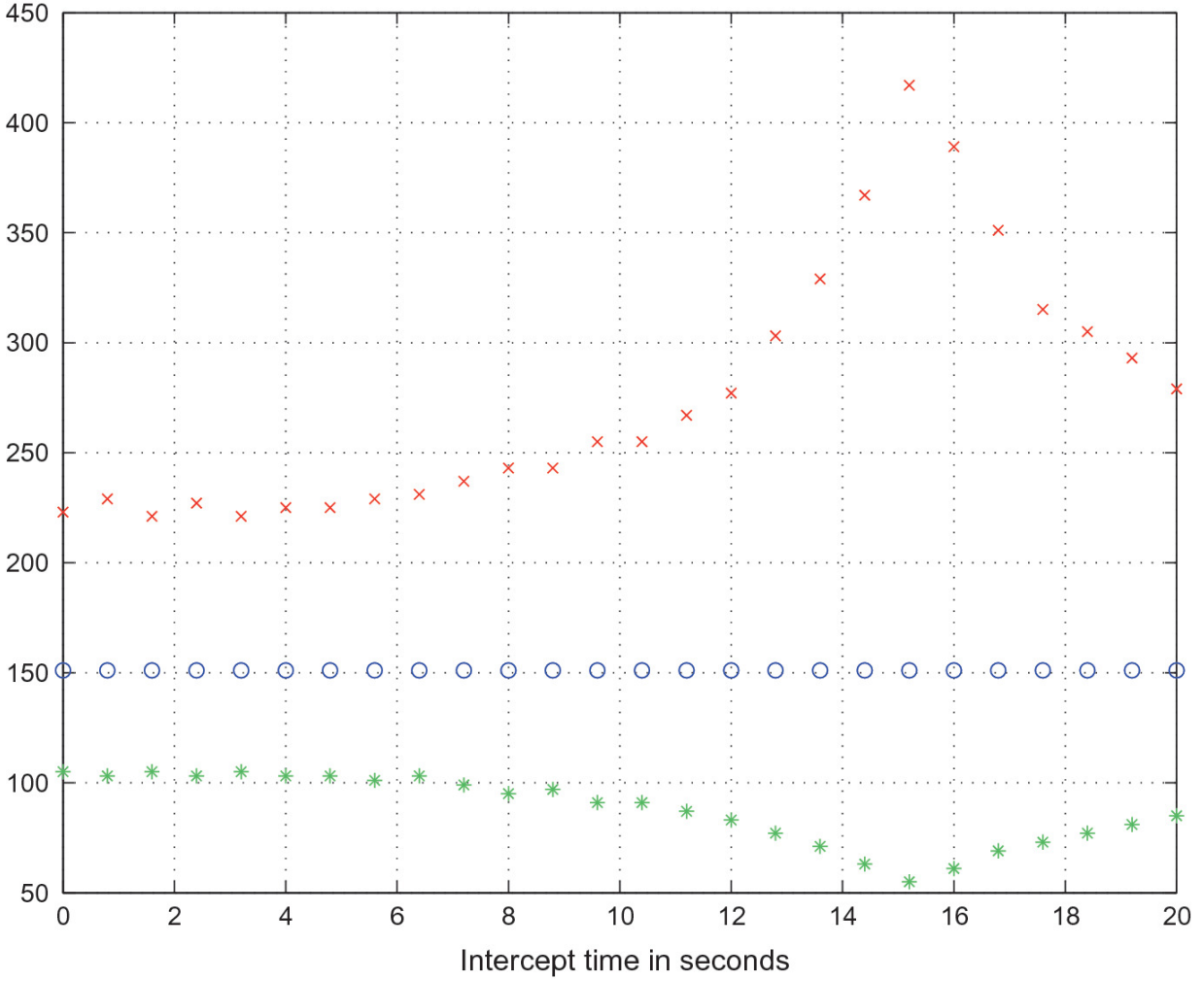


Fig. 9.9 Plot of $(2n_{1,k} + 1)$, (x), and $(2n_{1,k} + 1)$, (*), for computational method NM2, and $2n_1 + 1 = 2n_2 + 1$, (o), for computational method NM1, versus the intercept time $t \geq 0$, $k \in \mathcal{T}_{red}$

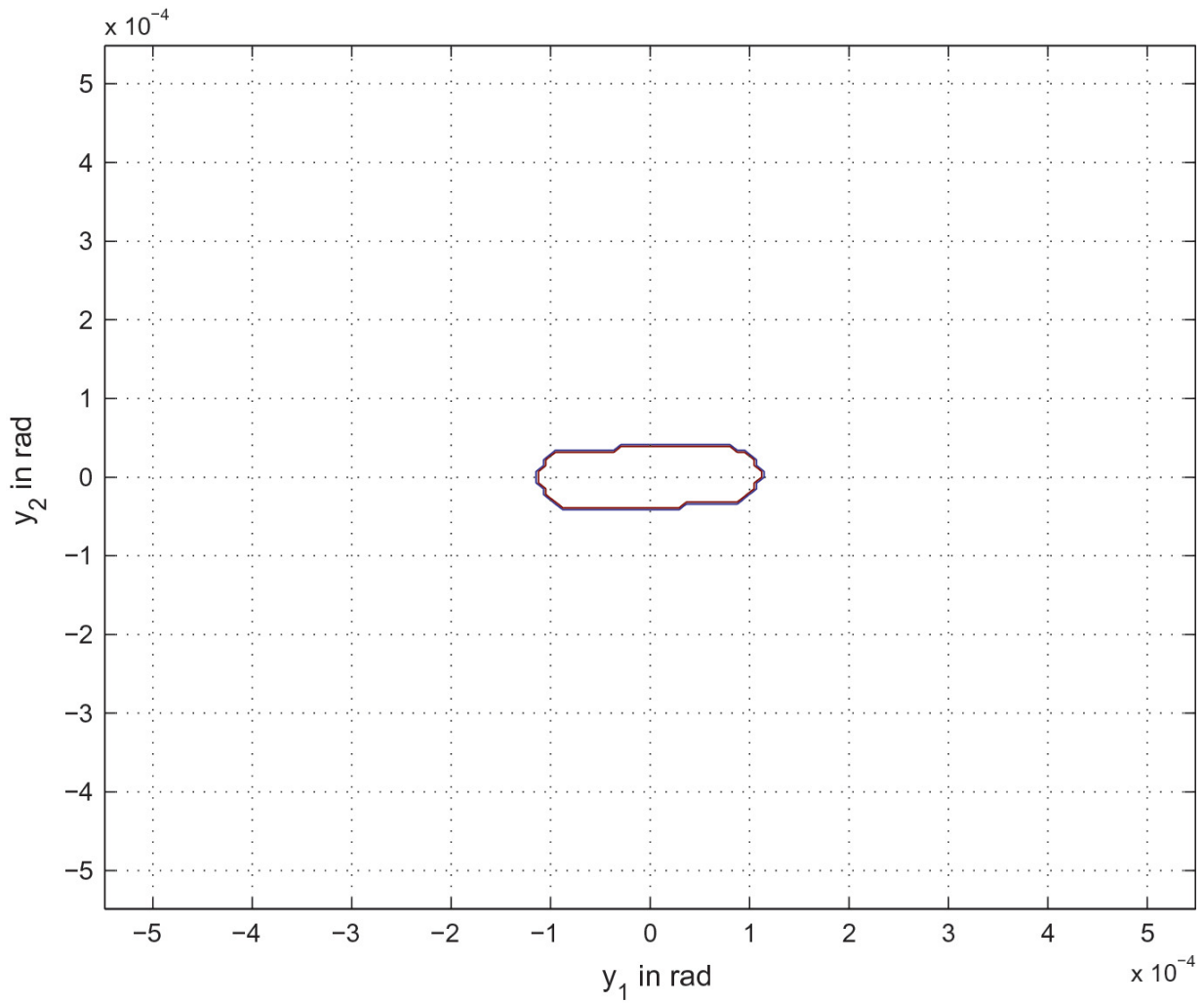


Fig. 9.10 Contour plot of the function $\arg(x_1 + jcy_1)$, for computational method NM1,
 $\mathbf{y} = [y_1, y_2]^T \in D_{grid}(k)$, $k = 1$; $\text{Ind} = 1$ for ζ inside the enclosed region around the origin,
and $\text{Ind} = g$ for ζ outside this region

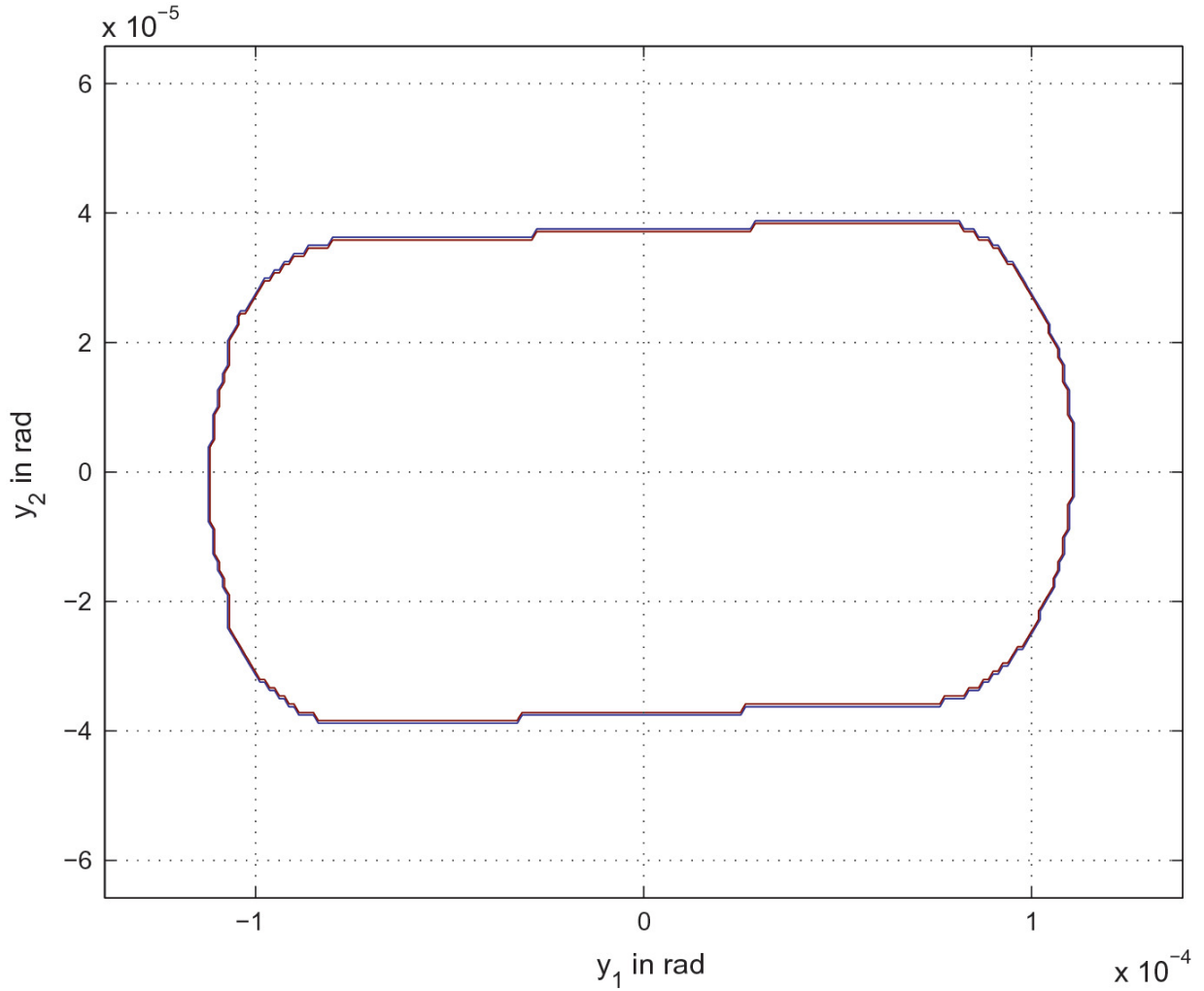


Fig. 9.11 Contour plot of the function $\arg(x_1 + jcy_1)$, for computational method NM2, $y = [y_1, y_2]^T \in D_{fgrid}(k)$, $k = 1$; $\text{Ind} = 1$ for ζ inside the enclosed region around the origin, and $\text{Ind} = g$ for ζ outside this region

Table 9.2 Table of values of the probability that at least one AA projectile out of a burst of N_p AA projectiles will impact the body of the AAT, $\text{Prob}(Y_k \geq 1)$, the intercept time $t \geq 0$, LOS distance $\|\mathbf{r}_{los}^{(l)}(t_{hitC,k})\|$, $k \in \mathcal{T}_{red}$, (9.94)

k	$t \geq 0$ (s)	$\ \mathbf{r}_{los}^{(l)}(t_{hitC,k})\ $ (m)	$\text{Prob}(Y_k \geq 1)$
1	0.00	4010.86	0.036277
5	0.80	3819.03	0.042455

k	$t \geq 0$ (s)	$\ r_{los}^{(t)}(t_{hitC,k})\ $ (m)	Prob ($Y_k \geq 1$)
9	1.60	3628.17	0.049983
13	2.40	3438.45	0.058789
17	3.20	3250.06	0.069974
21	4.00	3063.24	0.084022
25	4.80	2878.31	0.100320
29	5.60	2695.65	0.121492
33	6.40	2515.76	0.147541
37	7.20	2339.27	0.180659
41	8.00	2167.02	0.221907
45	8.80	2000.10	0.271485
49	9.60	1839.96	0.334446
53	10.40	1688.54	0.406020
57	11.20	1548.39	0.486981
61	12.00	1422.86	0.568251
65	12.80	1316.11	0.643555
69	13.60	1233.05	0.702112
73	14.40	1178.70	0.742960
77	15.20	1157.11	0.760011
81	16.00	1170.08	0.758958
85	16.80	1216.53	0.740099
89	17.60	1292.83	0.707376
93	18.40	1394.11	0.659516
97	19.20	1515.35	0.601218
101	20.00	1652.18	0.537317

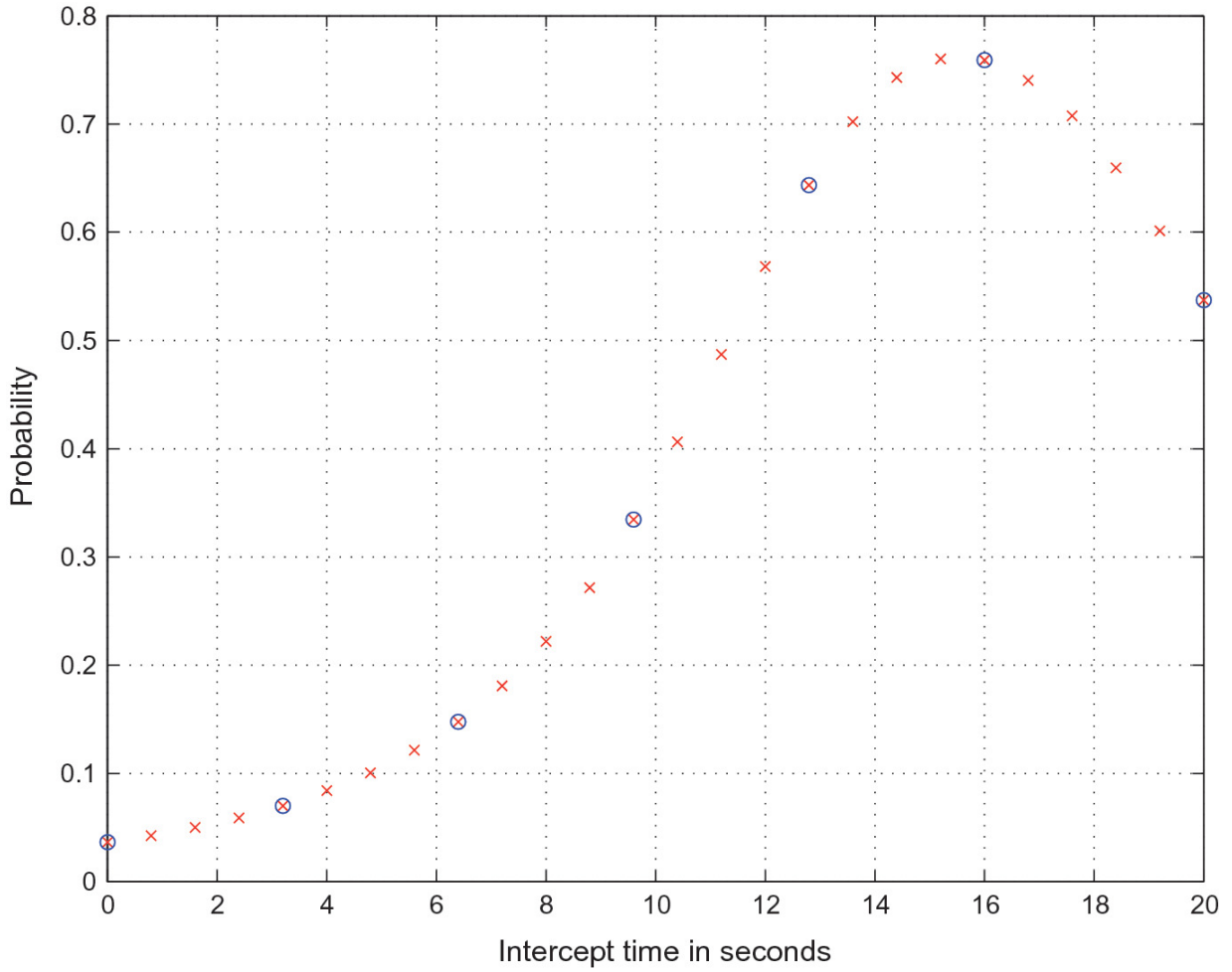


Fig. 9.12 Plot of $\Delta_{tofC,k}$ versus the intercept time $t \geq 0$, $k \in \mathcal{T}_{red}$, (x), $\mathbf{p} = \mathbf{0}_{15 \times 1}$, (o)

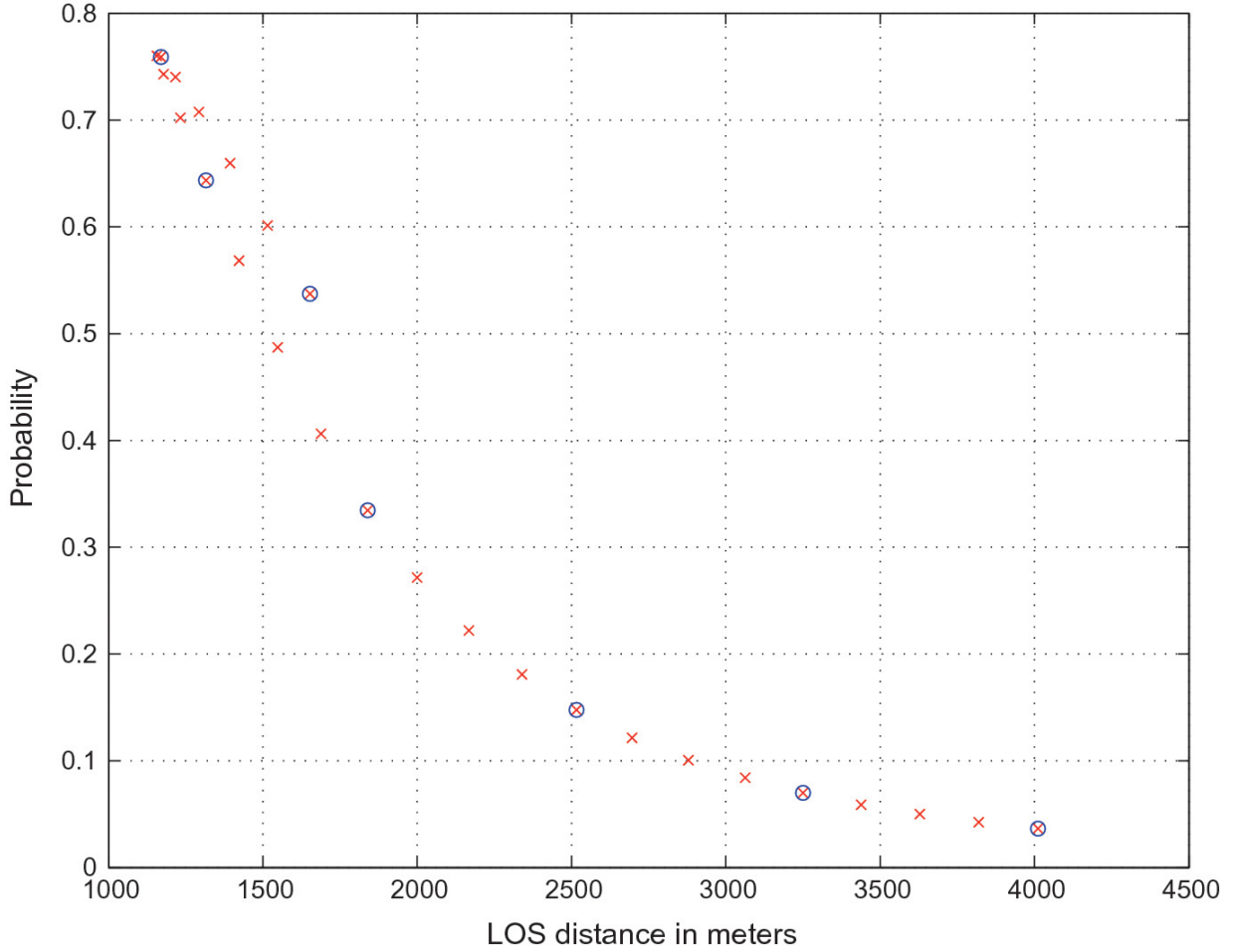


Fig. 9.13 Plot of $\Delta_{tofC,k}$ versus $\|\mathbf{r}_{los}^{(I)}(t_{hitC,k})\|$, $k \in \mathcal{T}_{red}$, (x), $\mathbf{p} = \mathbf{0}_{15 \times 1}$, (o)

Table 9.3 Table of values of the probability that at least one AA projectile will impact the body of the AAT after ν bursts of N_p AA projectiles each have been fired, $\text{Prob}(\bar{\mathcal{E}}_{j_\nu} \geq 1)$, the intercept time t_{fire,j_ν} , LOS distance $\|\mathbf{r}_{los}^{(I)}(t_{hitC,j_\nu})\|$, for $\nu = 1, 2, \dots, n_0 = 7$, (9.96)

ν	r_d	t_{fire,j_ν} (s)	$\ \mathbf{r}_{los}^{(I)}(t_{hitC,j_\nu})\ $ (m)	$\text{Prob}(\bar{\mathcal{E}}_{j_\nu} \geq 1)$
1	1	0.00	4010.86	0.036277
2	17	3.20	3250.06	0.103713
3	33	6.40	2515.76	0.235953
4	49	9.60	1839.96	0.491485
5	65	12.80	1316.11	0.818742
6	81	16.00	1170.08	0.956309

v	r_d	$t_{fire,jv}$ (s)	$\ r_{los}^{(t)}(t_{hitC,jv})\ $ (m)	Prob ($\Xi_{jv} \geq 1$)
7	101	20.00	1652.18	0.979785

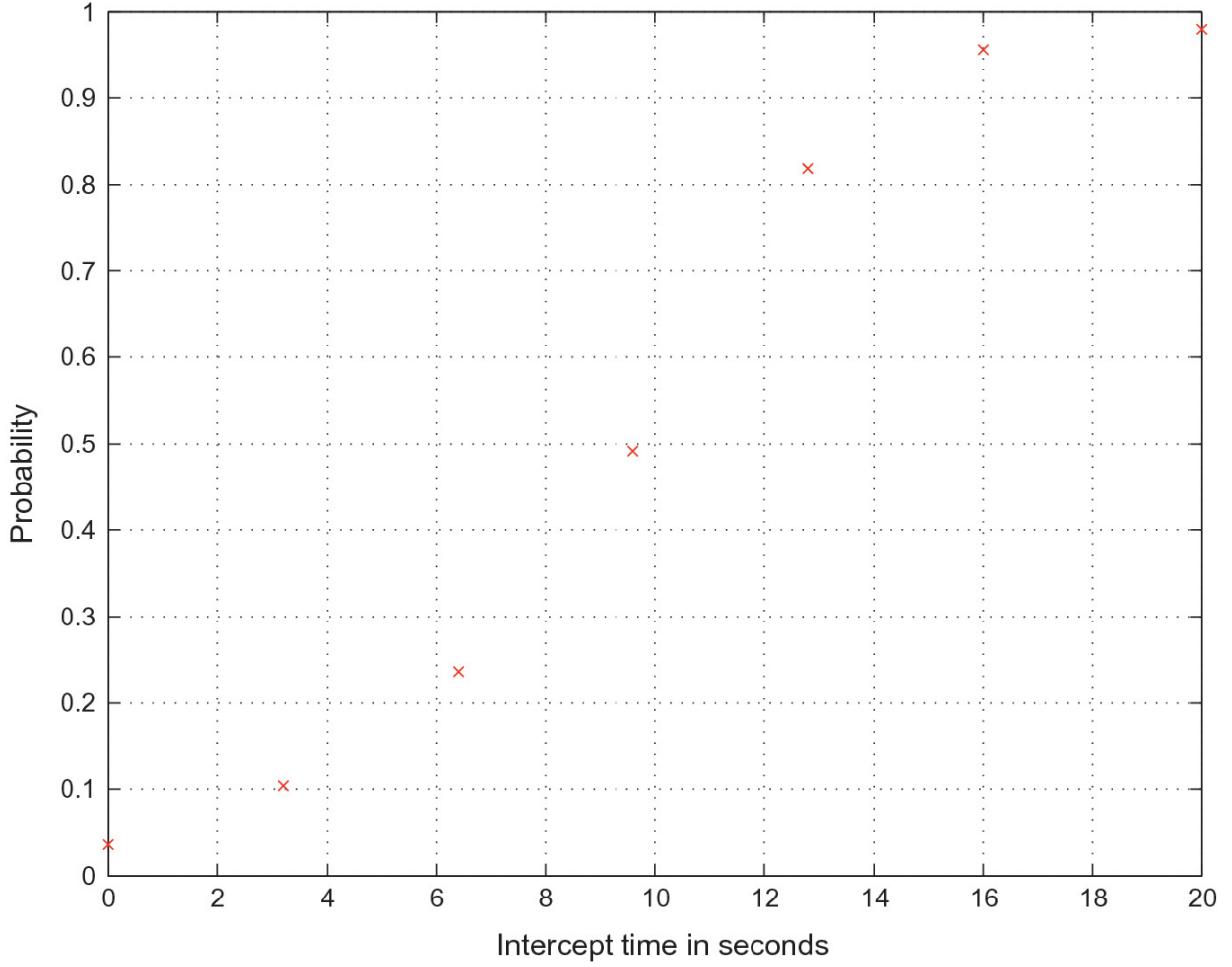


Fig. 9.14 Plot of $\Delta_{tofC,k}$ versus the intercept time $t \geq 0$, $p = \mathbf{0}_{15 \times 1}$

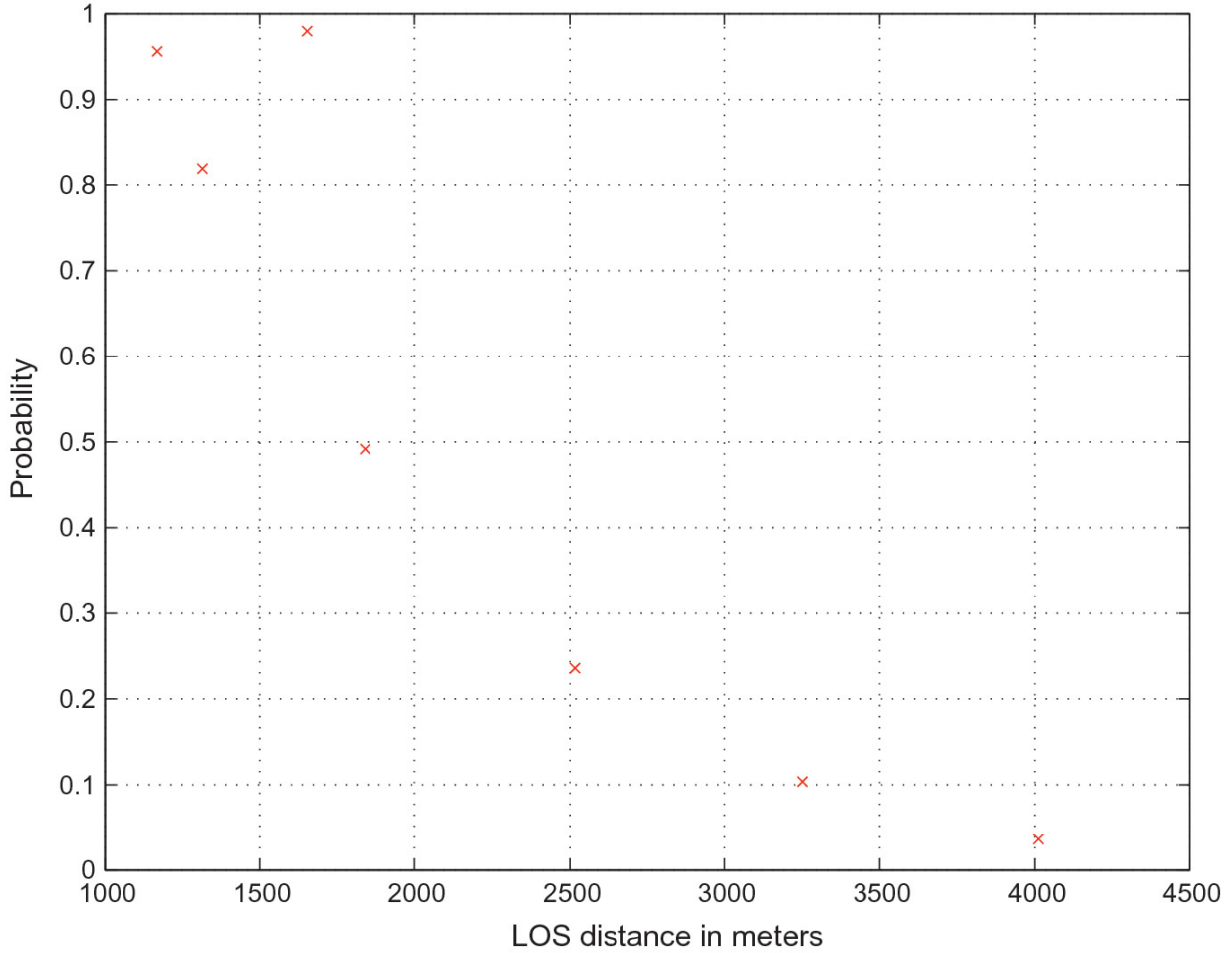


Fig. 9.15 Plot of $\Delta_{tofC,k}$ versus $\|r_{los}^{(l)}(t_{hitC,k})\|$, $p = \mathbf{0}_{15 \times 1}$

9.8 Verification Method VMB for the Computation of the Probability $P_{hitT,k}$

Verification method VMB ([132]) proposes a special engagement scenario whereby the mobile ADS fires an ideal AA projectile at time $t \geq 0$ against a stationary target k that has the shape of a sphere. The

ideal AA projectile is assumed to travel at a constant speed and in a straight line.³ In the sequel, target k is referred to as stationary sphere k .

Using the assumptions of the special engagement scenario, expressions are derived for a number of quantities. The afore-

mentioned expressions facilitate the direct and accurate computation of the probability that the ideal AA projectile will impact the body of stationary sphere k , denoted by $N_f \geq 1$. The value $N_f \geq 1$ is compared with $P_{hitT,k}$, that is, the probability that the ideal AA projectile will impact the body of stationary sphere k as obtained by applying computational method NM2 to the special engagement scenario, for $k = 1, 2, \dots, n_f$.

The CM of a uniform stationary sphere k with radius $\eta_1(0)$ is fixed at each specified inertial position of the original AAT denoted by $\mathbf{r}_{targI,k}$ ((7.12)). Thus, at each time $t \in \mathcal{T}_{FL,k}$, (9.25), the inertial position and velocity of stationary sphere k , denoted by $\mathbf{r}_{targ,k}^{(I)}(t)$ and $\mathbf{v}_{targ,k}^{(I)}(t)$, respectively, are given by

$$\begin{aligned} \mathbf{r}_{targ,k}^{(I)}(t) &= \mathbf{r}_{targI,k}, \quad \mathbf{v}_{targ,k}^{(I)}(t) = \mathbf{0}_{3 \times 1} \quad \forall t \in \mathcal{T}_{FL,k}, \\ \mathcal{T}_{FL,k} &= [t_{fire,k}, t_{hitC,k} + \Delta_d]. \end{aligned} \quad (9.98)$$

The body reference frame B_{targ} , (8.15), is fixed at the CM of stationary sphere k , and the $(X_{B_{10}}$ axis points in the direction of the constant forward velocity vector of the original AAT that is moving in a straight line (Fig. 9.2, Fig. 7.2, Sect. 7.3).

At time $t_{fire,k} = t_{hitC,k} - \Delta_{tofC,k}$ the AA gun is aimed at the CM of stationary sphere k and fires an ideal AA projectile. It follows that at time $t \geq 0$ the AA gun is aligned with the LOS vector $\mathbf{r}_{los}(t_{fire,k})$, (2.148), and that the inertial angles of the fire control vector (Chap. 7) are in this case equal to the inertial angles of the LOS vector, $\mathbf{r}_{los}^{(I)}(t_{fire,k})$, (2.153)–(2.154), as follows

$$\mathbf{a}_{FC}(t_{fire,k}) = \mathbf{a}_{los}(t_{fire,k}), \quad \mathbf{e}_{FC}(t_{fire,k}) = \mathbf{e}_{los}(t_{fire,k}), \quad (9.99)$$

where

$$\mathbf{r}_{los}^{(I)}(t_{fire,k}) = \mathbf{r}_{targI,k} - \mathbf{r}_H^{(I)}(t_{fire,k}). \quad (9.100)$$

The vector from the muzzle M of the AA gun to the CM of stationary sphere k is denoted by $\mathbf{r}_{M2targ,k}$ and is given by

$$\mathbf{r}_{M2targ,k} = \mathbf{r}_{targI,k} - \mathbf{r}_{muz}^{(I)}(t_{fire,k}). \quad (9.101)$$

It follows from the above that the inertial angles of $\mathbf{r}_{M2targ,k}$ are identical to $(A_f) = 11$ and $(A_f) = 11$.

In the computation of $\Delta_{tofC,k}$, $t \geq 0$, in Chap. 7, it is assumed that the azimuth and elevation error angles are zero, $\varepsilon_{\psi,k} = \varepsilon_{\theta,k} = 0$. Hence, the ideal AA projectile travels along a straight line from the muzzle M of the AA gun to the CM of stationary sphere k in a time $\Delta_{tofC,k}$, and at an assumed constant speed $L_b > 0$. Since the ideal AA projectile covers a distance $\|\mathbf{r}_{M2targ,k}\|$ in a time $\Delta_{tofC,k}$ it follows that the constant speed $L_b > 0$ is given by

$$V_{const,k} = \frac{\|\mathbf{r}_{M2targ,k}\|}{\Delta_{tofC,k}}. \quad (9.102)$$

The straight line path of the ideal AA projectile is parallel to the longitudinal axis of the AA gun, that is, the line from the hinge point H to the muzzle M of the AA gun (Fig. 9.1).

With regard to the application of computational method NM2 to the special engagement scenario, the following assumptions and methods are employed.

1. The set B_{targ} associated with the AAT in Sect. 9.2 is replaced by the set dp/dt associated with stationary sphere k with radius $\eta_1(0)$ and given by ((8.9))

$$\delta_v = \dot{\delta}_v = \ddot{\delta}_v = 0, \dot{\alpha}_s = -v_b/a, \Rightarrow \dot{\beta} = 0, \beta = \beta_b, \quad (9.103)$$

$$C_{sph,k} = \text{pen}_a(\sqrt{x_0^2 + y_0^2 + z_0^2}, 0, \rho_{sph,k}). \quad (9.104)$$

2. The generic firing velocity vector of the ideal AA projectile expressed in body reference frame B_5 is given by ((9.8), (9.102))

$$\mathbf{v}_P^{(B_7)}(t_{fire,k}) = V_{const,k} \begin{bmatrix} -\cos(\varepsilon_{\theta,k}) \sin(\varepsilon_{\psi,k}) \\ \cos(\varepsilon_{\theta,k}) \cos(\varepsilon_{\psi,k}) \\ \sin(\varepsilon_{\theta,k}) \end{bmatrix}. \quad (9.105)$$

As mentioned earlier in this Chapter, conceptually, the vector $\mathbf{v}_P^{(B_7)}(t_{fire,k})$ points from the muzzle M of the AA gun outwards.

3. The point mass flight dynamics model of the ideal AA projectile is subject to random initial conditions that are a function of the random vector B_i , and is given by ((9.11)–(9.17))

$$\frac{d\mathbf{X}(\tau; t)}{d\tau} = \mathbf{f}_{proj}(\mathbf{X}(\tau; t)) = \begin{bmatrix} \mathbf{v}_{proj}^{(I)}(\tau; t) \\ \mathbf{0}_{3 \times 1} \end{bmatrix},$$

$$\mathbf{X}(t; t) = \mathbf{X}_0(t, \boldsymbol{\varepsilon}_k), \quad \tau \in [t, t_{hitC,k} + \Delta_d], \quad t = t_{fire,k}, \quad (9.106)$$

$$\mathbf{X}_0(t_{fire,k}, \boldsymbol{\varepsilon}_k) = \begin{bmatrix} \mathbf{r}_{proj,0}^{(I)}(t_{fire,k}, \boldsymbol{\varepsilon}_k) \\ \mathbf{v}_{proj,0}^{(I)}(t_{fire,k}, \boldsymbol{\varepsilon}_k) \end{bmatrix}, \quad (9.107)$$

where the initial conditions are obtained as follows.

4. The initial position $(\mathbf{I}_{B_5}^{(I)}, \mathbf{J}_{B_5}^{(I)}, \mathbf{K}_{B_5}^{(I)})$ is given by

$$\mathbf{r}_{proj,0}^{(I)}(t_{fire,k}, \boldsymbol{\varepsilon}_k) = \mathbf{r}_H^{(I)}(t) + L_m \mathbf{J}_{B_7}^{(I)}(t), \quad t = t_{fire,k}, \quad (9.108)$$

where

(9.109)

$$\mathbf{r}_H^{(I)}(t) = \mathbf{r}_{OA}^{(I)}(t) + \begin{bmatrix} -\sin(\beta_b)(L_b + h_{Ty}) \\ \cos(\beta_b)(L_b + h_{Ty}) \\ h_b + h_{Tz} + h_{mz} \end{bmatrix},$$

$$\mathbf{r}_{OA}^{(I)}(t) = \begin{bmatrix} x(t) \\ y(t) \\ 0 \end{bmatrix}, \quad t = t_{fire,k},$$

$$\mathbf{J}_{B7}^{(I)}(t) = \begin{bmatrix} \cos(\mathbf{a}_{FC}(t)) \cos(\mathbf{e}_{FC}(t)) \\ \sin(\mathbf{a}_{FC}(t)) \cos(\mathbf{e}_{FC}(t)) \\ \sin(\mathbf{e}_{FC}(t)) \end{bmatrix}, \quad t = t_{fire,k}. \quad (9.110)$$

5.

The initial velocity $(\mathbf{I}_{B5}^{(I)}, \mathbf{J}_{B5}^{(I)}, \mathbf{K}_{B5}^{(I)})$ is given by ((9.105), (9.102))

$$\begin{aligned} \mathbf{v}_{proj,0}^{(I)}(t_{fire,k}, \boldsymbol{\varepsilon}_k) &= \mathbf{v}_P^{(I)}(t_{fire,k}) \\ &= \mathbf{R}_{B72I} \mathbf{v}_P^{(B7)}(t_{fire,k}), \end{aligned} \quad (9.111)$$

$$\Rightarrow \mathbf{v}_{proj,0}^{(I)}(t_{fire,k}, \boldsymbol{\varepsilon}_k) = \mathbf{R}_{B72I} V_{const,k} \begin{bmatrix} -\cos(\varepsilon_{\theta,k}) \sin(\varepsilon_{\psi,k}) \\ \cos(\varepsilon_{\theta,k}) \cos(\varepsilon_{\psi,k}) \\ \sin(\varepsilon_{\theta,k}) \end{bmatrix}. \quad (9.112)$$

In the derivation of an expression for $N_f \geq 1$ the following assumptions and methods are applied.

1. With reference to the generic firing velocity vector $\mathbf{v}_P^{(B7)}(t_{fire,k})$,

(9.105), it follows that the actual direction of flight of the ideal AA projectile depends on the realization $h_b > a$, (9.5). Thus, in order to simplify the presentation let δ_v be a vector denoting the realization $h_b > a$ as follows

$$\mathbf{z}_k = \begin{bmatrix} z_{1,k} \\ z_{2,k} \end{bmatrix} = \boldsymbol{\varepsilon}_k(\omega_k) = \begin{bmatrix} \varepsilon_{\psi,k}(\omega_k) \\ \varepsilon_{\theta,k}(\omega_k) \end{bmatrix}. \quad (9.113)$$

2. Let $\zeta(t)$ denote a unit vector in the direction of the realization of $\mathbf{v}_P^{(B_7)}(t_{fire,k})$ expressed in body reference frame B_5 and given by ((9.105), (9.113))

$$\mathbf{u}_{P,k} = \mathbf{u}_{P,k}^{(B_7)} = \begin{bmatrix} u_{P,kx} \\ u_{P,ky} \\ u_{P,kz} \end{bmatrix} = \begin{bmatrix} -\cos(z_{2,k}) \sin(z_{1,k}) \\ \cos(z_{2,k}) \cos(z_{1,k}) \\ \sin(z_{2,k}) \end{bmatrix}. \quad (9.114)$$

Conceptually, the unit vector $\zeta(t)$ points from the muzzle M of the AA gun outwards.

3. In this work, the feasible values of δ_v are constrained to the set $B_0 \subset \mathbb{R}^2$ centered at the origin and given by

$$\mathbf{A}_a = (-a_0, a_0) \times (-a_0, a_0), \quad a_0 = \pi/2. \quad (9.115)$$

4. The angle between the unit vector $\zeta(t)$ and the Z_{B_5} axis is denoted by $\phi_{Y,k}$ and is given by the following relation ((9.114))

$$\cos(\phi_{Y,k}) = u_{P,ky}, \quad (9.116)$$

$$\Rightarrow \cos(\phi_{Y,k}) = \cos(z_{2,k}) \cos(z_{1,k}). \quad (9.117)$$

It follows that the RHS of (9.117) is positive for all $m = 13$ and that the angle $\phi_{Y,k}$ is computed from (9.117) as follows

$$\phi_{Y,k} = \arccos(\cos(z_{2,k}) \cos(z_{1,k})). \quad (9.118)$$

With reference to (9.118), it is assumed that $\phi_{Y,k}$ lies in the interval $\mathbf{p}_s \in \mathbb{R}^{n_s}$,

$$\phi_{Y,k} \in [0, \pi/2). \quad (9.119)$$

In addition, it follows from (9.117) that

$$\cos^2(\phi_{Y,k}) = \cos^2(z_{2,k}) \cos^2(z_{1,k}). \quad (9.120)$$

5. An expression needs to be derived for the set $A_{cone,k} \subset \mathbf{A}_a$, (9.129), such that if δ_v lies in the set \mathbf{M}_{row3} then the ideal AA projectile fired at time $t \geq 0$ will impact the body of stationary sphere k . If the value of δ_v does not lie in the set \mathbf{M}_{row3} then the ideal AA projectile fired at time $t \geq 0$ will not impact the body of stationary sphere k .
6. With reference to Fig. 9.1, consider a plane \mathbf{VP}_k at time $t \geq 0$ that is vertical to the inertial (X, Y) plane and that includes the $k, \boldsymbol{\varepsilon}_k(\omega_k)$ plane of the body reference frame B_5 fixed to point G , the center of mass of the AA gun (Fig. 9.16). Given that the Z_{B_5} axis coincides with the line from the hinge point H of the AA gun to the CM of stationary sphere k (Fig. 9.16). It follows that the vertical plane \mathbf{VP}_k also passes through the CM of stationary sphere k . The cross-sections of the AA gun and stationary sphere k that lie on vertical plane \mathbf{VP}_k are shown in Fig. 9.16.
7. Consider a cone \mathbf{CN}_k with axis that coincides with the Z_{B_5} axis and with apex fixed at the muzzle M of the AA gun (Fig. 9.16). The inner surface of the cone touches tangentially the surface of

stationary sphere k as shown in Fig. 9.16. The cone CN_k has half-cone angle $= \pi/4$ that is computed as follows

$$\sin(\phi_{cone,k}) = \frac{\rho_{sph,k}}{\|\mathbf{r}_{M2targ,k}\|} \Rightarrow \phi_{cone,k} = \arcsin\left(\frac{\rho_{sph,k}}{\|\mathbf{r}_{M2targ,k}\|}\right), \quad (9.121)$$

where $0 < \rho_{sph,k} < \|\mathbf{r}_{M2targ,k}\| < \infty$. In many cases

$\rho_{sph,k} \ll \|\mathbf{r}_{M2targ,k}\|$. The value of $= \pi/4$ depends on the positive finite values $\eta_1(0)$ and $\|\mathbf{r}_{M2targ,k}\|$. Thus, the value of $= \pi/4$ is positive and lies in the interval $\mathbf{p}_s \in \mathbb{R}^{n_s}$,

$$\cos(\phi_{Y,k}) = u_{P,ky}, \quad (9.122)$$

8.

Assume that $\phi_{Y,k} = \phi_{cone,k}$. Then, it follows from (9.117) that δ_v takes on appropriate values such that the following relation is satisfied

$$\cos(z_{2,k}) \cos(z_{1,k}) = \cos(\phi_{cone,k}), \quad (9.123)$$

and implying that ((9.116), (9.120))

$$m_{proj} = 0.550 \text{ kg} . \quad (9.124)$$

$$\cos^2(z_{2,k}) \cos^2(z_{1,k}) = \cos^2(\phi_{cone,k}). \quad (9.125)$$

9. Thus, assume that δ_v lies in the set $\beta(t) = \beta_b =$, representing the equality constraint (9.123), as follows

$$A_{circ,k} = \{[y_1, y_2]^T \in \mathbf{A}_a : \cos(y_2) \cos(y_1) = \cos(\phi_{cone,k})\}. \quad (9.126)$$

By using (9.114), (9.123)–(9.125), and standard trigonometric identities, the following relations are derived for the elements of the unit vector $\zeta(t)$

$$(9.127)$$

$$\begin{aligned}
u_{P,kx}^2 + u_{P,kz}^2 &= \cos^2(z_{2,k}) \sin^2(z_{1,k}) + \sin^2(z_{2,k}) \\
&= \cos^2(z_{2,k}) \sin^2(z_{1,k}) + 1 - \cos^2(z_{2,k}) \\
&= \cos^2(z_{2,k})(\sin^2(z_{1,k}) - 1) + 1 \\
&= -\cos^2(z_{2,k}) \cos^2(z_{1,k}) + 1 \\
&= -\cos^2(\phi_{cone,k}) + 1 \\
&= \sin^2(\phi_{cone,k}),
\end{aligned}$$

$$u_{P,ky} = \cos(\phi_{cone,k}). \quad (9.128)$$

It follows from (9.127)–(9.128) that the unit vector $\zeta(t)$ lies on the surface of cone CN_k while its end-point touches a circle with radius $\sin(\phi_{cone,k})$. The center of the circle is fixed on the Z_{B_5} axis at a distance $\cos(\phi_{cone,k})$ from the muzzle M of the AA gun

(towards the CM of stationary sphere k , Fig. 9.16). The plane of the circle is perpendicular to the Z_{B_5} axis. It follows that if

assumption 9 is satisfied then the direction of the realization of the generic firing velocity vector $\mathbf{v}_P^{(B_7)}(t_{fire,k})$, (9.105), is such that

the ideal AA projectile just impacts the body of stationary sphere k .

10. Thus, the ideal AA projectile fired at time $t \geq 0$ will impact the body of stationary sphere k if the angle $\phi_{Y,k}$ of the unit vector $\zeta(t)$ lies in the interval $M_{NE} = M$, that is, if δ_v lies in the set

$$A_{cone,k} \subset A_a \text{ given by ((9.118))}$$

$$A_{cone,k} = \{[y_1, y_2]^T \in A_a : 0 \leq \arccos(\cos(y_2) \cos(y_1)) \leq \phi_{cone,k}\}, \dots$$

$$k = 1, 2, \dots, n_f. \quad (9.129)$$

Define the function $\text{Ind } Z_{B_5}$ as follows

$$\text{Ind}_{cone} = \text{Ind}_{cone}(k; y_1, y_2) = \begin{cases} 1 & \text{if } \mathbf{y} \in A_{cone,k} \\ 0 & \text{if } \mathbf{y} \notin A_{cone,k} \end{cases}, \quad (9.130)$$

$$\mathbf{y} = [y_1, y_2]^\top \in \mathbb{R}^2, \quad k = 1, 2, \dots, n_f.$$

Thus, the probability that the ideal AA projectile fired at time $t \geq 0$ will impact the body of stationary sphere k is equal to the probability that $B_i \text{ P}(\Xi_{j_v}; i)$, and is given by

$$\begin{aligned} P_{VhitT,k} &= \text{Prob}(\boldsymbol{\varepsilon}_k \in A_{cone,k}) \\ &= \text{E}(\text{Ind}_{cone}(k; \boldsymbol{\varepsilon}_{\psi,k}, \boldsymbol{\varepsilon}_{\theta,k})) \\ &= \int \int_{\mathbb{R}^2} \text{Ind}_{cone}(k; y_1, y_2) f_{\boldsymbol{\varepsilon}_{\psi}, \boldsymbol{\varepsilon}_{\theta}}(y_1, y_2) dy_1 dy_2, \end{aligned} \quad (9.131)$$

$$\Rightarrow P_{VhitT,k} = \int \int_{A_{cone,k}} f_{\boldsymbol{\varepsilon}_{\psi}, \boldsymbol{\varepsilon}_{\theta}}(y_1, y_2) dy_1 dy_2. \quad (9.132)$$

Following the procedure presented in Sect. 9.2, a bounding set N_{fmax} for the set M_{row3} is employed, $A_{cone,k} \subset D_V(k)$. The bounding set N_{fmax} is a rectangle centered at the origin. Thus, the probability $N_f \geq 1$ is computed as follows

$$P_{VhitT,k} = \int \int_{D_V(k)} \text{Ind}_{cone}(k; y_1, y_2) f_{\boldsymbol{\varepsilon}_{\psi}, \boldsymbol{\varepsilon}_{\theta}}(y_1, y_2) dy_1 dy_2. \quad (9.133)$$

11.

The computation of $P_{hitT,k}$ is based on the application of computational method NM2 (Sect. 9.4) to the special engagement scenario.

12. The percentage difference between the probability $P_{hitT,k}$ and the

probability $N_f \geq 1$, is given by

(9.134)

$$e_{VhitT,k} = \frac{P_{hitT,k} - P_{VhitT,k}}{P_{VhitT,k}} \times 100\%.$$

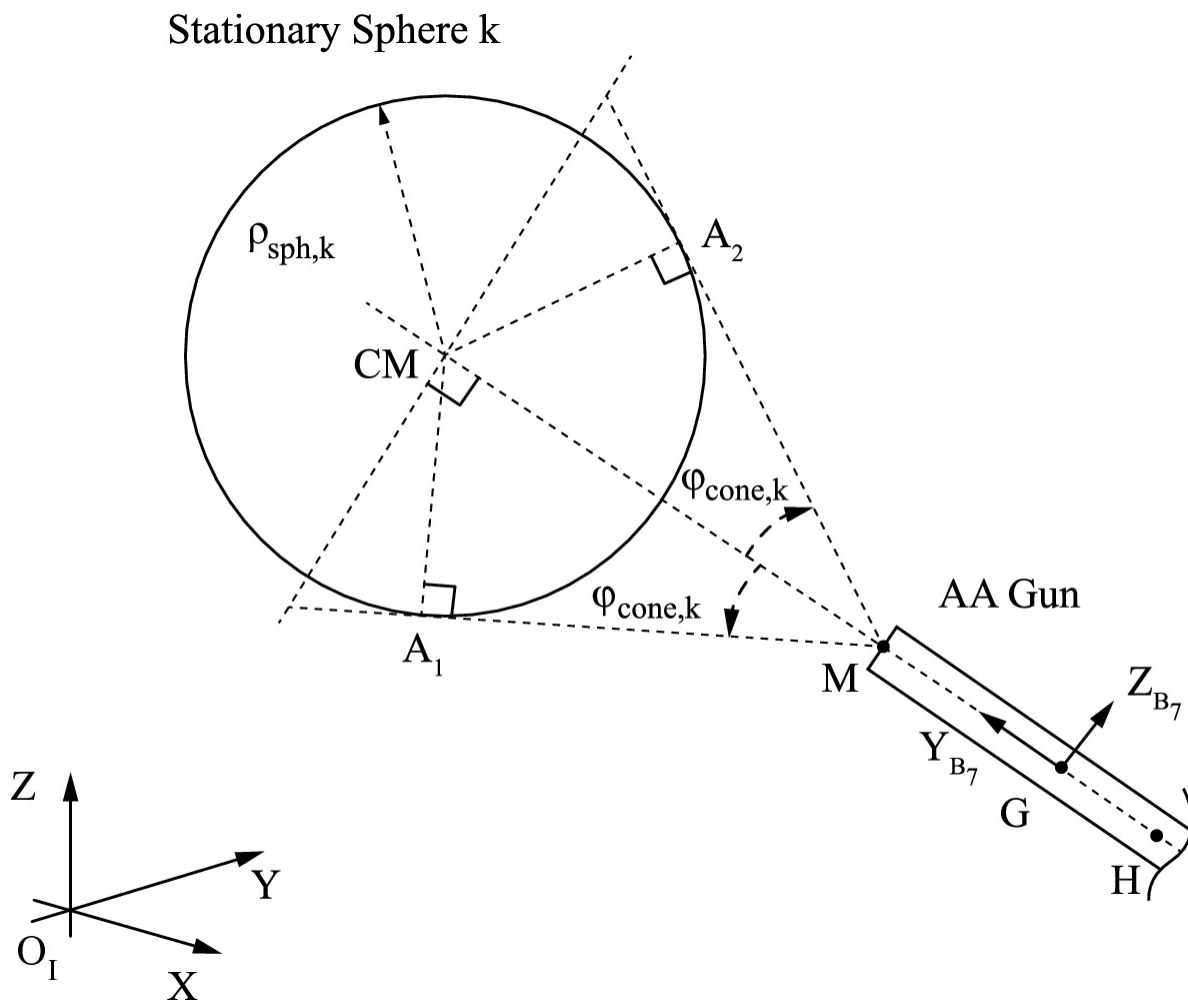


Fig. 9.16 Schematic of the AA gun engaging stationary sphere k

Two separate cases of the special engagement scenario are considered as follows.

1. Case 1: Stationary spheres with different radii.

In this case the half-cone angle $= \pi/4$ is fixed for all k as follows

$$\mathcal{A}_{Ind,k} \subset \mathbf{D}_f(k), \quad k = 1, 2, \dots, n_f. \quad (9.135)$$

By using (9.121), the radius $\eta_1(0)$ of stationary sphere k is computed such that the constraint (9.135) is satisfied,

$$\rho_{sph,k} = \|\mathbf{r}_{M2targ,k}\| \sin(\phi_{cone0}), \quad k = 1, 2, \dots, n_f. \quad (9.136)$$

It follows from (9.135), (9.129), that the set \mathbf{M}_{row3} is fixed for all k ,

$$A_{cone,k} = A_{cone0}, \quad k = 1, 2, \dots, n_f, \quad (9.137)$$

where

$$\dot{\mathbf{q}} = \mathbf{0}_{15 \times 1}, \quad \mathbf{p} = \mathbf{0}_{15 \times 1}, \quad \dot{\mathbf{p}} = \mathbf{0}_{15 \times 1} \quad \text{for all } t \geq 0. \quad (9.138)$$

The bounding set N_{fmax} is also fixed as follows

$$\dot{x} + L_2 \sin(\beta)\dot{\beta} - \dot{\alpha}_1 a \sin(\beta) = 0, \quad (9.139)$$

$r_{rely}(t_{hitT,k}; k)$. Thus, the probability $N_f \geq 1$ is fixed and is given by

$$\begin{aligned} P_{VhitT,k} &= P_{VhitT0} \\ &= \int \int_{\mathbf{D}_{V0}} \text{Ind}_{cone}(k; y_1, y_2) f_{\varepsilon_\psi, \varepsilon_\theta}(y_1, y_2) dy_1 dy_2, \end{aligned} \quad (9.140)$$

$$k = 1, 2, \dots, n_f.$$

2. Case 2: Stationary spheres with identical radii.

In this case the radius $\eta_1(0)$ of stationary sphere k is constant for all k as follows

$$\rho_{sph,k} = \rho_{sph0}, \quad k = 1, 2, \dots, n_f. \quad (9.141)$$

The half-cone angle $= \pi/4$ is computed by using (9.121), that is,

$$(9.142)$$

$$\phi_{cone,k} = \arcsin\left(\frac{\rho_{sph0}}{\|\mathbf{r}_{M2targ,k}\|}\right), \quad k = 1, 2, \dots, n_f.$$

The probability $N_f \geq 1$ is computed by using (9.133), for $k = 1, 2, \dots, n_f$.

9.8.1 Computational Results

The data given in Sect. 9.7 is used with some extensions and additions as specified below.

In the computation of $N_f \geq 1$ the following data is employed.

1. For Case 2 (stationary spheres with identical radii) the bounding set N_{fmax} , (9.133), is given by

$$\mathbf{D}_V(k) = \{[y_1, y_2]^\top \in \mathbf{A}_a : -a_{1max,k} \leq y_1 \leq a_{1max,k}, \quad (9.143)$$

$$-a_{2max,k} \leq y_2 \leq a_{2max,k}\},$$

$$a_{1max,k} = 1.2\phi_{cone,k}, \quad a_{2max,k} = 1.2\phi_{cone,k}, \quad (9.144)$$

$$k \in \mathcal{T}_{red}.$$

2. For Case 1 (stationary spheres with different radii) the bounding set \mathbf{D}_{V0} , (9.139), is given by

$$\mathbf{D}_{V0} = \{[y_1, y_2]^\top \in \mathbf{A}_a : -a_{1max0} \leq y_1 \leq a_{1max0}, \quad (9.145)$$

$$-a_{2max0} \leq y_2 \leq a_{2max0}\},$$

$$a_{1max0} = 1.2\phi_{cone0}, \quad a_{2max0} = 1.2\phi_{cone0}. \quad (9.146)$$

In the application of computational method NM2 to compute $P_{hitT,k}$, the following data is employed for Cases 1 and 2.

1. The parameter p_s , (9.46), is replaced by B_{10} given by

$$d_{1,k} = 1.2\rho_{sph,k}, \quad k \in \mathcal{T}_{red}. \quad (9.147)$$

2. The radius of the TBS is $k_0 \neq 0$ m.

The double integrals in computational method NM2 and verification method VMB are computed numerically by applying the MATLAB functions `dblquad`, `quadgk`, implementing the AQUADGK algorithm and using an absolute error tolerance of 10^{-8} ([110]).

In Case 1, $p_s \in \mathbb{R}^{n_s}$ $\phi_{cone0} = 10^{-3}$ rad, $k \in \mathcal{T}_{red}$, and each stationary sphere has a different radius. Part of the computational results are shown in Table 9.4. It can be seen that the absolute percentage difference $|e_{VhitT,k}|$ lies approximately between 0.0022% and 0.091% for all $k \in \mathcal{T}_{red}$.

In Case 2, $L_{a2} > 0$ ($2n_1 + 1$) m, $k \in \mathcal{T}_{red}$, and each stationary sphere has an identical radius. Part of the computational results are shown in Table 9.5. It can be seen that the absolute percentage difference $|e_{VhitT,k}|$ lies approximately between 0.0053% and 0.23% for all $k \in \mathcal{T}_{red}$.

Table 9.4 Verification method VMB, Case 1: Stationary spheres with different radii. Table of values of k , the intercept time $t \geq 0$, $\|\mathbf{r}_{M2target,k}\|$, $\Delta_{tofC,k}$, $= \pi/4$, $\eta_1(0)$, $P_{hitT,k}$, $N_f \geq 1$,

$$J_{s1} = J_{s2} ((P_{hitT,k} - P_{VhitT,k})/P_{VhitT,k}) \times 100\%$$

k	$t \geq 0$ (s)	$\ \mathbf{r}_{M2target,k}\ $ (m)	$\Delta_{tofC,k}$ (s)	$= \pi/4$ (rad)	$\eta_1(0)$ (m)	$P_{hitT,k}$	$N_f \geq 1$	$e_{VhitT,k}$ (%)
1	0.00	4008.06	5.99701	0.001	4.00806	0.393609	0.393469	0.0354779
5	0.80	3816.23	5.48804	0.001	3.81623	0.393588	0.393469	0.0300678
9	1.60	3625.37	5.02039	0.001	3.62537	0.393564	0.393469	0.0241173
13	2.40	3435.65	4.58962	0.001	3.43565	0.393538	0.393469	0.0175474

k	$t \geq 0$ (s)	$\ \mathbf{r}_{M2targ,k}\ $ (m)	$\Delta_{tofC,k}$ (s)	$= \pi/4$ (rad)	$\eta_1(0)$ (m)	$P_{hitT,k}$	$N_f \geq 1$	$e_{VhitT,k}$ (%)
17	3.20	3247.26	4.19193	0.001	3.24726	0.39351	0.393469	0.0102646
21	4.00	3060.44	3.8242	0.001	3.06044	0.393478	0.393469	0.00215824
25	4.80	2875.51	3.48377	0.001	2.87551	0.393442	0.393469	- 0.00690282
29	5.60	2692.85	3.16832	0.001	2.69285	0.393402	0.393469	-0.017073
33	6.40	2512.96	2.87592	0.001	2.51296	0.393357	0.393469	-0.0285326
37	7.20	2336.47	2.605	0.001	2.33647	0.393306	0.393469	-0.0414881
41	8.00	2164.22	2.3544	0.001	2.16422	0.393248	0.393469	-0.0561675
45	8.80	1997.3	2.12347	0.001	1.9973	0.393183	0.393469	-0.0728047
49	9.60	1837.16	1.91205	0.001	1.83716	0.393567	0.393469	0.0248002
53	10.40	1685.74	1.72056	0.001	1.68574	0.393484	0.393469	0.00372934
57	11.20	1545.59	1.55007	0.001	1.54559	0.393393	0.393469	-0.0194451
61	12.00	1420.06	1.4025	0.001	1.42006	0.393296	0.393469	-0.0440801
65	12.80	1313.31	1.28062	0.001	1.31331	0.393504	0.393469	0.00876414
69	13.60	1230.25	1.18798	0.001	1.23025	0.393112	0.393469	-0.0908504
73	14.40	1175.9	1.12835	0.001	1.1759	0.393658	0.393469	0.0479133
77	15.20	1154.31	1.10488	0.001	1.15431	0.393631	0.393469	0.0410609
81	16.00	1167.28	1.11897	0.001	1.16728	0.393647	0.393469	0.0452086
85	16.80	1213.73	1.16976	0.001	1.21373	0.393398	0.393469	-0.0181401
89	17.60	1290.03	1.25447	0.001	1.29003	0.393176	0.393469	-0.0746388
93	18.40	1391.31	1.36936	0.001	1.39131	0.393271	0.393469	-0.0503457
97	19.20	1512.55	1.51078	0.001	1.51255	0.393369	0.393469	-0.0255329
101	20.00	1649.38	1.67572	0.001	1.64938	0.393309	0.393469	-0.0406937

Table 9.5 Verification method VMB, Case 2: Stationary spheres with identical radii. Table of values of k , the intercept time $t \geq 0$, $\|\mathbf{r}_{M2targ,k}\|$, $\Delta_{tofC,k}$, $= \pi/4$, $\eta_1(0)$, $P_{hitT,k}$, $N_f \geq 1$,

$$J_{s1} = J_{s2} ((P_{hitT,k} - P_{VhitT,k})/P_{VhitT,k}) \times 100\%$$

k	$t \geq 0$ (s)	$\ \mathbf{r}_{M2targ,k}\ $ (m)	$\Delta_{tofC,k}$ (s)	$= \pi/4$ (rad)	$\eta_1(0)$ (m)	$P_{hitT,k}$	$N_f \geq 1$	$e_{VhitT,k}$ (%)
1	0.00	4008.06	5.99701	0.000249497	1	0.0306145	0.0306451	-0.0998415
5	0.80	3816.23	5.48804	0.000262039	1	0.0337637	0.0337495	0.0420494

k	$t \geq 0$ (s)	$\ r_{M2targ,k}\ $ (m)	$\Delta_{tofC,k}$ (s)	$= \pi/4$ (rad)	$\eta_1(0)$ (m)	$P_{hitT,k}$	$N_f \geq 1$	$e_{VhitT,k}$ (%)
9	1.60	3625.37	5.02039	0.000275834	1	0.0373404	0.0373276	0.0343698
13	2.40	3435.65	4.58962	0.000291066	1	0.0414857	0.041475	0.0259201
17	3.20	3247.26	4.19193	0.000307952	1	0.0462499	0.0463106	-0.131048
21	4.00	3060.44	3.8242	0.00032675	1	0.0519862	0.051983	0.00625438
25	4.80	2875.51	3.48377	0.000347764	1	0.0586749	0.058678	- 0.00522186
29	5.60	2692.85	3.16832	0.000371353	1	0.066519	0.0666282	-0.163994
33	6.40	2512.96	2.87592	0.000397937	1	0.0760991	0.0761236	-0.0322653
37	7.20	2336.47	2.605	0.000427996	1	0.0873526	0.0875211	-0.192485
41	8.00	2164.22	2.3544	0.00046206	1	0.101183	0.10125	-0.0659867
45	8.80	1997.3	2.12347	0.000500676	1	0.117701	0.117802	-0.0857436
49	9.60	1837.16	1.91205	0.000544317	1	0.137542	0.13769	-0.107521
53	10.40	1685.74	1.72056	0.00059321	1	0.161351	0.16134	0.00692177
57	11.20	1545.59	1.55007	0.000647	1	0.188557	0.188852	-0.156135
61	12.00	1420.06	1.4025	0.000704198	1	0.219201	0.219599	-0.181413
65	12.80	1313.31	1.28062	0.000761434	1	0.251356	0.251655	-0.118564
69	13.60	1230.25	1.18798	0.00081284	1	0.281054	0.281331	-0.098449
73	14.40	1175.9	1.12835	0.000850411	1	0.303598	0.303438	0.0524141
77	15.20	1154.31	1.10488	0.000866321	1	0.313026	0.312887	0.0446287
81	16.00	1167.28	1.11897	0.00085669	1	0.307314	0.307162	0.049328
85	16.80	1213.73	1.16976	0.00082391	1	0.28715	0.287812	-0.229925
89	17.60	1290.03	1.25447	0.000775175	1	0.259301	0.259514	-0.081798
93	18.40	1391.31	1.36936	0.000718748	1	0.22751	0.227636	-0.0553723
97	19.20	1512.55	1.51078	0.000661133	1	0.196262	0.196316	-0.0274719
101	20.00	1649.38	1.67572	0.000606288	1	0.167661	0.167892	-0.137332

Footnotes

1 An alternative notation is to use upper-case letters to denote random variables or random vectors (for example, Y , Z) and the corresponding lower-case letters to denote the realizations of the random variables or random vectors (for example, $(2n_1 + 1)$, $a_{gun,ref}(t)$), [83, 121, 136, 139, 148, 157, 171].

2 The formal verification of the conditions for this result would, in principle, follow a methodology similar to that given on pp. 1098–1101, [34], pp. 57–59, [127], pp. 116–119, [165], and in Chap. 4, [128].

3 The effects of the gravitational force and the aerodynamic drag force are not taken into account.

Appendix A

Kinematics of Constrained Rigid Multibody Systems Subject to Velocity Constraints That May Not be Independent

This Appendix presents some elements of the kinematics of constrained rigid multibody systems. The relevant results are obtained mainly from [10, 63, 64, 70, 73, 81, 84, 94, 107, 125, 147, 153–155, 168, 215]. The assumptions, results and methods employed are as follows.

1. It is assumed that right-handed Cartesian co-ordinate systems are used throughout.
2. There is an inertial reference frame I and an associated co-ordinate system (X, Y, Z) with unit vectors $(\mathbf{I}_1, \mathbf{I}_2, \mathbf{I}_3)$ and with origin fixed in the inertial reference frame I (bold letters are used to denote vector and matrix quantities).
3. The unit vectors of the inertial reference frame I , $(\mathbf{I}_1, \mathbf{I}_2, \mathbf{I}_3)$, are given by

$$\mathbf{I}_1 = \begin{bmatrix} 1 \\ 0 \\ 0 \end{bmatrix}, \quad \mathbf{I}_2 = \begin{bmatrix} 0 \\ 1 \\ 0 \end{bmatrix}, \quad \mathbf{I}_3 = \begin{bmatrix} 0 \\ 0 \\ 1 \end{bmatrix}, \quad (\text{A.1})$$

and

$$[\mathbf{I}_1 : \mathbf{I}_2 : \mathbf{I}_3] = \mathbf{I}_3, \quad (\text{A.2})$$

where \mathbf{I}_3 denotes the 3 by 3 unit matrix. The unit vectors

$(\mathbf{I}_1, \mathbf{I}_2, \mathbf{I}_3)$ are expressed directly in the inertial reference frame I .

This can be explicitly indicated by using a superscript (I) as follows $(\mathbf{I}_1^{(I)}, \mathbf{I}_2^{(I)}, \mathbf{I}_3^{(I)})$, where $\mathbf{I}_1^{(I)} = \mathbf{I}_1$, $\mathbf{I}_1^{(I)} = \mathbf{I}_1$, $\mathbf{I}_1^{(I)} = \mathbf{I}_1$, (A.1).

4. Consider a constrained rigid multibody system consisting of N rigid bodies and subject to a total of m nonholonomic and holonomic velocity constraints that may not be independent.
5. For each rigid body i , there is a body reference frame B_i and an associated co-ordinate system $(X_{B_i}, Y_{B_i}, Z_{B_i})$ with unit vectors $(\mathbf{I}_{B_i}, \mathbf{J}_{B_i}, \mathbf{K}_{B_i})$ and with origin fixed at the center of mass of rigid body i , $(X_{B_i}, Y_{B_i}, Z_{B_i})$. Thus, body reference frame B_i translates and rotates together with rigid body i .
6. The unit vectors of the body reference frame B_i , $(\mathbf{I}_{B_i}, \mathbf{J}_{B_i}, \mathbf{K}_{B_i})$, are given by

$$\mathbf{I}_{B_i} = \begin{bmatrix} 1 \\ 0 \\ 0 \end{bmatrix}, \quad \mathbf{J}_{B_i} = \begin{bmatrix} 0 \\ 1 \\ 0 \end{bmatrix}, \quad \mathbf{K}_{B_i} = \begin{bmatrix} 0 \\ 0 \\ 1 \end{bmatrix}, \quad (\text{A.3})$$

and

$$[\mathbf{I}_{B_i} \vdots \mathbf{J}_{B_i} \vdots \mathbf{K}_{B_i}] = \mathbf{I}_3. \quad (\text{A.4})$$

The unit vectors $(\mathbf{I}_{B_i}, \mathbf{J}_{B_i}, \mathbf{K}_{B_i})$ are expressed directly in the body reference frame B_i . This can be explicitly indicated by using a superscript (B_i) as follows $(\mathbf{I}_{B_i}^{(B_i)}, \mathbf{J}_{B_i}^{(B_i)}, \mathbf{K}_{B_i}^{(B_i)})$, where $\mathbf{I}_{B_i}^{(B_i)} = \mathbf{I}_{B_i}$,

$$\mathbf{J}_{B_i}^{(B_i)} = \mathbf{J}_{B_i}, \quad \mathbf{K}_{B_i}^{(B_i)} = \mathbf{K}_{B_i}, \quad (\text{A.3}).$$

7. Let \mathbf{q} denote the vector of generalized co-ordinates and \mathbf{q} the

vector of generalized velocities describing the motion of the multibody system relative to the inertial reference frame I where (A.5)

$$\mathbf{q} = [q_1, q_2, \dots, q_n]^\top,$$

$$\mathbf{p} = [p_1, p_2, \dots, p_n]^\top = \frac{d\mathbf{q}}{dt} = \dot{\mathbf{q}}, \quad (\text{A.6})$$

$$\frac{d\mathbf{p}}{dt} = \frac{d^2\mathbf{q}}{dt^2} = \ddot{\mathbf{q}}, \quad (\text{A.7})$$

$\mathbf{q} = \mathbf{q}(t) \in \mathbb{R}^n$, $\dot{\mathbf{q}} = \dot{\mathbf{q}}(t) \in \mathbb{R}^n$, and t denotes time. The selected generalized co-ordinates \mathbf{q} are suitable for describing the inertial position and orientation of the multibody system.

In this work, the generalized co-ordinates \mathbf{q} are generally dependent ([10, 60–62, 70, 73, 81, 84, 107]).

8. The translational motion of each rigid body can be described by three generalized co-ordinates and the rotational motion can be described by three generalized co-ordinates. In particular, a vector of generalized co-ordinates ϵ_i can be selected for each rigid body

i. An appropriate selection is $\mathbf{q}_i = [x_i, y_i, z_i, \Psi_i, \Theta_i, \Phi_i]^\top \in \mathbb{R}^6$,

$(X_{B_i}, Y_{B_i}, Z_{B_i})$, where the following holds.

- a. x_i, y_i, z_i denote the co-ordinates of the center of mass of rigid body i with respect to the inertial co-ordinate system (X, Y, Z) , $(X_{B_i}, Y_{B_i}, Z_{B_i})$.
- b. $\alpha_s, \Theta_i, \Phi_i$ denote the Euler rotation angles required to bring the inertial co-ordinate system (X, Y, Z) into alignment with the body co-ordinate system $\mathbf{q}_1(t) \beta(t) Q_{Cj}$ (using, for

example, the rotation axis sequence $\mathcal{Z} \rightarrow \mathcal{X} \rightarrow \mathcal{Y}$),

$(X_{B_i}, Y_{B_i}, Z_{B_i})$ ([10, 70, 73, 81, 94, 107, 147, 155]).

In this case, the vector of generalized co-ordinates for the constrained rigid multibody system is given by $\mathbf{q} = [\mathbf{q}_1^\top, \mathbf{S}^\top, \dots,$

$$\mathbf{q}_N^\top]^\top \in \mathbb{R}^{6N}.$$

9.

Consider the case of a rigid body moving in three-dimensional space and assume that there are no constraints on its motion. Then it follows that the rigid body has three translational degrees of freedom and three rotational degrees of freedom, for a total of six degrees of freedom ([10, 70, 73, 81, 107, 147, 155]).

10.

Hereafter, the time variable t and the rigid body index i appearing in the body reference frame label B_i and also in other subscripts, take on the following values, unless stated otherwise,

$$t \geq 0, \quad i = 1, 2, \dots, N. \quad (\text{A.8})$$

11.

Let $\mathbf{r}_i^{(I)}$ denote the inertial position of the center of mass of rigid body i expressed in the inertial reference frame I ([10, 147]),

$$\mathbf{r}_i^{(I)} = \mathbf{r}_i^{(I)}(\mathbf{q}) \in \mathbb{R}^3. \quad (\text{A.9})$$

12. In order to describe the orientation of body reference frame B_i

with respect to the inertial reference frame I some preliminary results are needed. Let $\mathbf{y}^{(I)}$ denote a given vector $\mathbf{y} \in \mathbb{R}^3$

expressed in the inertial reference frame I , and $\mathbf{y}^{(B_i)}$ denote the

same vector expressed in the body reference frame B_i . The

relationship between $\mathbf{y}^{(I)}$ and $\mathbf{y}^{(B_i)}$ is given by

$$\mathbf{y}^{(B_i)} = \mathbf{R}_{I2B_i} \mathbf{y}^{(I)}, \quad \mathbf{y}^{(I)} = \mathbf{R}_{B_i2I} \mathbf{y}^{(B_i)} = \mathbf{R}_{I2B_i}^{-1} \mathbf{y}^{(B_i)}, \quad (\text{A.10})$$

where \mathbf{R}_{B_i2I} is the rotation matrix *from* the inertial reference frame I to the body reference frame B_i ([10, 73, 81, 147]),

$$\mathbf{R}_{I2B_i} = \mathbf{R}_{I2B_i}(\mathbf{q}) \in \mathbb{R}^{3 \times 3}. \quad (\text{A.11})$$

13.

Thus, the orientation of body reference frame B_i with respect to the inertial reference frame I is represented by the rotation matrix \mathbf{R}_{B_i2I} ([94]). The rotation matrix \mathbf{R}_{B_i2I} is given by ([10, 73, 81, 94])

$$\mathbf{R}_{I2B_i} = \begin{bmatrix} c_{X_{B_i},X} & c_{X_{B_i},Y} & c_{X_{B_i},Z} \\ c_{Y_{B_i},X} & c_{Y_{B_i},Y} & c_{Y_{B_i},Z} \\ c_{Z_{B_i},X} & c_{Z_{B_i},Y} & c_{Z_{B_i},Z} \end{bmatrix}, \quad (\text{A.12})$$

where $\bar{\varepsilon}_{jv}$ is equal to the cosine of the angle between the positive k axis of body reference frame B_i and the positive j axis of the inertial reference frame I , $n_s = n - r_G = 4$, $I_{wr1} = I_{wr2}$.

14. Given the rotation matrix \mathbf{R}_{B_i2I} . Then, by using (A.2), (A.10), it follows that the unit vectors of the inertial reference frame I expressed in the body reference frame B_i , $(\mathbf{I}_1^{(B_i)}, \mathbf{I}_2^{(B_i)}, \mathbf{I}_3^{(B_i)})$, form the columns of the rotation matrix \mathbf{R}_{B_i2I} as follows

$$\mathbf{I}_1^{(B_i)} = \mathbf{R}_{I2B_i} \mathbf{I}_1, \quad \mathbf{I}_2^{(B_i)} = \mathbf{R}_{I2B_i} \mathbf{I}_2, \quad \mathbf{I}_3^{(B_i)} = \mathbf{R}_{I2B_i} \mathbf{I}_3, \quad (\text{A.13})$$

$$\Rightarrow [\mathbf{I}_1^{(B_i)} : \mathbf{I}_2^{(B_i)} : \mathbf{I}_3^{(B_i)}] = \mathbf{R}_{I2B_i}, \quad (\text{A.14})$$

where $\mathbf{I}_1^{(B_i)} = \mathbf{I}_1^{(B_i)}(\mathbf{q})$, $\mathbf{I}_2^{(B_i)} = \mathbf{I}_2^{(B_i)}(\mathbf{q})$, $\mathbf{I}_3^{(B_i)} = \mathbf{I}_3^{(B_i)}(\mathbf{q})$, (A.11). The

unit vectors $(\mathbf{I}_1^{(B_i)}, \mathbf{I}_2^{(B_i)}, \mathbf{I}_3^{(B_i)})$ are expressed as follows

$$\begin{aligned}\mathbf{I}_1^{(B_i)} &= I_{1x}^{(B_i)} \mathbf{I}_{B_i} + I_{1y}^{(B_i)} \mathbf{J}_{B_i} + I_{1z}^{(B_i)} \mathbf{K}_{B_i} \\ &= [I_{1x}^{(B_i)}, I_{1y}^{(B_i)}, I_{1z}^{(B_i)}]^\top,\end{aligned}\quad (\text{A.15})$$

$$\begin{aligned}\mathbf{I}_1^{(B_i)} &= I_{1x}^{(B_i)} \mathbf{I}_{B_i} + I_{1y}^{(B_i)} \mathbf{J}_{B_i} + I_{1z}^{(B_i)} \mathbf{K}_{B_i} \\ &= [I_{1x}^{(B_i)}, I_{1y}^{(B_i)}, I_{1z}^{(B_i)}]^\top,\end{aligned}\quad (\text{A.16})$$

$$\begin{aligned}\mathbf{I}_1^{(B_i)} &= I_{1x}^{(B_i)} \mathbf{I}_{B_i} + I_{1y}^{(B_i)} \mathbf{J}_{B_i} + I_{1z}^{(B_i)} \mathbf{K}_{B_i} \\ &= [I_{1x}^{(B_i)}, I_{1y}^{(B_i)}, I_{1z}^{(B_i)}]^\top,\end{aligned}\quad (\text{A.17})$$

15. Given the rotation matrix \mathbf{R}_{B_i2I} . Then, by using (A.4), (A.10), it follows that the unit vectors of the body reference frame B_i expressed in the inertial reference frame I , $(\mathbf{I}_{B_i}^{(I)}, \mathbf{J}_{B_i}^{(I)}, \mathbf{K}_{B_i}^{(I)})$, form the columns of the rotation matrix \mathbf{R}_{B_i2I} as follows

$$\mathbf{I}_{B_i}^{(I)} = \mathbf{R}_{B_i2I} \mathbf{I}_{B_i}, \quad \mathbf{J}_{B_i}^{(I)} = \mathbf{R}_{B_i2I} \mathbf{J}_{B_i}, \quad \mathbf{K}_{B_i}^{(I)} = \mathbf{R}_{B_i2I} \mathbf{K}_{B_i}, \quad (\text{A.18})$$

$$\Rightarrow [\mathbf{I}_{B_i}^{(I)} : \mathbf{J}_{B_i}^{(I)} : \mathbf{K}_{B_i}^{(I)}] = \mathbf{R}_{B_i2I}, \quad (\text{A.19})$$

where $\mathbf{I}_{B_i}^{(I)} = \mathbf{I}_{B_i}^{(I)}(\mathbf{q})$, $\mathbf{J}_{B_i}^{(I)} = \mathbf{J}_{B_i}^{(I)}(\mathbf{q})$, $\mathbf{K}_{B_i}^{(I)} = \mathbf{K}_{B_i}^{(I)}(\mathbf{q})$, (A.11). The

unit vectors $(\mathbf{I}_{B_i}^{(I)}, \mathbf{J}_{B_i}^{(I)}, \mathbf{K}_{B_i}^{(I)})$ are expressed as follows

$$\begin{aligned}\mathbf{I}_{B_i}^{(I)} &= I_{B_ix}^{(I)} \mathbf{I}_1 + I_{B_iy}^{(I)} \mathbf{I}_2 + I_{B_iz}^{(I)} \mathbf{I}_3 \\ &= [I_{B_ix}^{(I)}, I_{B_iy}^{(I)}, I_{B_iz}^{(I)}]^\top,\end{aligned}\quad (\text{A.20})$$

$$\mathbf{J}_{B_i}^{(I)} = J_{B_ix}^{(I)} \mathbf{I}_1 + J_{B_iy}^{(I)} \mathbf{I}_2 + J_{B_iz}^{(I)} \mathbf{I}_3$$

$$= [J_{B_i x}^{(I)}, J_{B_i y}^{(I)}, J_{B_i z}^{(I)}]^\top, \quad (\text{A.21})$$

$$\begin{aligned} \mathbf{K}_{B_i}^{(I)} &= K_{B_i x}^{(I)} \mathbf{I}_1 + K_{B_i y}^{(I)} \mathbf{I}_2 + K_{B_i z}^{(I)} \mathbf{I}_3 \\ &= [K_{B_i x}^{(I)}, K_{B_i y}^{(I)}, K_{B_i z}^{(I)}]^\top. \end{aligned} \quad (\text{A.22})$$

16.

If the unit vectors of the body reference frame B_i expressed in the inertial reference frame I , $(\mathbf{I}_{B_i}^{(I)}, \mathbf{J}_{B_i}^{(I)}, \mathbf{K}_{B_i}^{(I)})$, are given then the

rotation matrix $\mathbf{R}_{B_i 2I}$ is constructed by using (A.19), that is,

$$\mathbf{R}_{B_i 2I} = [\mathbf{I}_{B_i}^{(I)} : \mathbf{J}_{B_i}^{(I)} : \mathbf{K}_{B_i}^{(I)}] \quad (\text{see Chap. 2 for practical examples}).$$

17.

By using the unit vectors $(\mathbf{I}_1, \mathbf{I}_2, \mathbf{I}_3)$ and the unit vectors

$(\mathbf{I}_{B_i}^{(I)}, \mathbf{J}_{B_i}^{(I)}, \mathbf{K}_{B_i}^{(I)})$ the rotation matrix $\mathbf{R}_{B_i 2I}$, (A.12), is represented as

follows

$$\mathbf{R}_{I 2B_i} = \begin{bmatrix} \mathbf{I}_1^\top \mathbf{I}_{B_i}^{(I)} & \mathbf{I}_2^\top \mathbf{I}_{B_i}^{(I)} & \mathbf{I}_3^\top \mathbf{I}_{B_i}^{(I)} \\ \mathbf{I}_1^\top \mathbf{J}_{B_i}^{(I)} & \mathbf{I}_2^\top \mathbf{J}_{B_i}^{(I)} & \mathbf{I}_3^\top \mathbf{J}_{B_i}^{(I)} \\ \mathbf{I}_1^\top \mathbf{K}_{B_i}^{(I)} & \mathbf{I}_2^\top \mathbf{K}_{B_i}^{(I)} & \mathbf{I}_3^\top \mathbf{K}_{B_i}^{(I)} \end{bmatrix}. \quad (\text{A.23})$$

18. From (A.10), (A.12), (A.23), it follows that

$$\mathbf{R}_{B_i 2I} = \mathbf{R}_{I 2B_i}^{-1} = \mathbf{R}_{I 2B_i}^\top, \quad (\text{A.24})$$

$$\mathbf{R}_{I 2B_i}^\top \mathbf{R}_{I 2B_i} = \mathbf{R}_{I 2B_i} \mathbf{R}_{I 2B_i}^\top = \mathbf{I}_3, \quad (\text{A.25})$$

$$\Rightarrow \mathbf{R}_{B_i 2I} \mathbf{R}_{I 2B_i} = \mathbf{R}_{I 2B_i} \mathbf{R}_{B_i 2I} = \mathbf{I}_3. \quad (\text{A.26})$$

Thus, it follows from the above that the rotation matrices $\mathbf{K}_{B_i 2I}$, $\mathbf{R}_{B_i 2I}$, are all orthogonal matrices .

19.

By taking the time derivative of both sides of (A.26), the following relation is obtained

$$\mathbf{R}_{I2B_i} \frac{d\mathbf{R}_{B_i 2I}}{dt} + \frac{d\mathbf{R}_{I2B_i}}{dt} \mathbf{R}_{B_i 2I} = \mathbf{0}_{3 \times 3}, \quad (\text{A.27})$$

$$\Rightarrow \mathbf{R}_{I2B_i} \frac{d\mathbf{R}_{B_i 2I}}{dt} = -\frac{d\mathbf{R}_{I2B_i}}{dt} \mathbf{R}_{B_i 2I} = -\left(\mathbf{R}_{I2B_i} \frac{d\mathbf{R}_{B_i 2I}}{dt} \right)^\top, \quad (\text{A.28})$$

where the time derivative of the rotation matrix is obtained by computing the time derivative of each element of the rotation matrix, $d\mathbf{R}_{B_i 2I}/dt = [dR_{B_i 2I,j,k}/dt]$, $n_s = m_c = 4$, $d\mathbf{R}_{B_i 2I}/dt =$

$[dR_{B_i 2I,j,k}/dt]$, $n_s = m_c = 4$. From (A.28) it follows that

$\mathbf{R}_{I2B_i} d\mathbf{R}_{B_i 2I}/dt$ is a 3 by 3 skew-symmetric matrix ([10, 73, 81]).

20.

The rotation matrix from body reference frame B_i to body reference frame L_1 is obtained from (A.24) as follows

$$\mathbf{R}_{B_i 2B_j} = \mathbf{R}_{I2B_j} \mathbf{R}_{B_i 2I} = \mathbf{R}_{B_j 2I}^\top \mathbf{R}_{B_i 2I}, \quad i, j = 1, 2, \dots, N. \quad (\text{A.29})$$

21.

In order to simplify the presentation, it is assumed that the rotation matrix $\mathbf{R}_{B_i 2I}$ of rigid body i is parameterized by using \mathbf{p}_s

generalized co-ordinates, where $n_\rho \in \{1, 2, 3\}$. For example, for

three dimensional motion the rotation matrix can be

parameterized by using $y_1 \in \mathbb{R}$ Euler angles , while for planar

motion the rotation matrix can be parameterized by using $y_1 \in \mathbb{R}$

Euler angle ([10, 81, 94]).

It is possible to parameterize the rotation matrix by using $v_1 \in \mathbb{R}$

22. It is possible to parameterize the rotation matrix by using $y_1 \in \mathbb{R}^3$ as generalized co-ordinates. In this case, there will be $m_\rho = n_\rho - 3$ independent equality constraints involving the selected generalized co-ordinates. For example, if the rotation matrix is parameterized by using $y_1 \in \mathbb{R}^3$ Euler parameters then $m_\rho = 1$, implying that a single equation constrains the four Euler parameters (Chaps. 7, 8, [10], Chaps. 4, 5, [81]).

23. Consider the case where the rotation matrix \mathbf{R}_{B_i2I} is parameterized by using three Euler angles. Then, the rotation matrix \mathbf{R}_{B_i2I} is determined as a function of the Euler angles as follows ([10, 81, 94]).

24. First, assume that the inertial co-ordinate system (X, Y, Z) is rotated about *one* of its axes X, Y or Z , through a positive angle ν resulting in a co-ordinate system $(X_{B_5}, Y_{B_5}, Z_{B_5})$ ([10, 81, 94]). The three possible single rotations and the associated rotation matrices are as follows ([10, 73, 81, 94]).

a. Single rotation about the Z axis through a positive angle ν .

The rotation matrix is denoted by $\mathbf{P}(Y_{j\nu})$ and is given by

$$\mathbf{R}_Z(\xi) = \begin{bmatrix} \cos(\xi) & \sin(\xi) & 0 \\ -\sin(\xi) & \cos(\xi) & 0 \\ 0 & 0 & 1 \end{bmatrix}. \quad (\text{A.30})$$

b. Single rotation about the X axis through a positive angle ν .

The rotation matrix is denoted by $\mathbf{P}(X_{j\nu})$ and is given by

$$\mathbf{R}_X(\xi) = \begin{bmatrix} 1 & 0 & 0 \\ 0 & \cos(\xi) & \sin(\xi) \\ 0 & -\sin(\xi) & \cos(\xi) \end{bmatrix}. \quad (\text{A.31})$$

$$\begin{bmatrix} 0 & -\sin(\xi) & \cos(\xi) \end{bmatrix}$$

c.

Single rotation about the Y axis through a positive angle ν .

The rotation matrix is denoted by $\mathbf{R}_{\mathcal{Y}}(\xi)$ and is given by

$$\mathbf{R}_{\mathcal{Y}}(\xi) = \begin{bmatrix} \cos(\xi) & 0 & -\sin(\xi) \\ 0 & 1 & 0 \\ \sin(\xi) & 0 & \cos(\xi) \end{bmatrix}. \quad (\text{A.32})$$

25. Second, assume that the inertial co-ordinate system (X, Y, Z) is successively rotated about three valid rotation axes such that the resulting co-ordinate system is parallel to the body co-ordinate system $(X_{B_i}, Y_{B_i}, Z_{B_i})$. The rotation angle about the first axis is denoted by α_s , the rotation angle about the second axis is denoted by Θ_i and the rotation angle about the third axis is denoted by Φ_i . The rotation matrix $\mathbf{R}_{B_i 2I}$ is determined by computing the product of three rotation matrices, (A.30)–(A.32), in the correct order ([10, 94]). There are twelve valid rotation axis sequences ([10, 94]). For example, for the valid rotation axis sequence $\mathcal{Z} \rightarrow \mathcal{X} \rightarrow \mathcal{Y}$, the rotation matrix $\mathbf{R}_{B_i 2I}$ is determined as follows.

a.

Rotation angle about first axis is α_s : The inertial co-ordinate system (X, Y, Z) is rotated about the \mathcal{Z} axis, in this case the Z axis, through a positive angle α_s , resulting in a co-ordinate system $(X_{B_5}, Y_{B_5}, Z_{B_5})$. The rotation matrix after one rotation is given by

$$\mathbf{R}_{I 2A_1} = \mathbf{R}_{\mathcal{Z}}(\Psi_i). \quad (\text{A.33})$$

- b. *Rotation angle about second axis is Θ_i* : The co-ordinate system $(X_{B_5}, Y_{B_5}, Z_{B_5})$ is rotated about the \mathcal{X} axis, in this case the X_{B_6} axis, through a positive angle Θ_i , resulting in a co-ordinate system $(X_{B_5}, Y_{B_5}, Z_{B_5})$. The rotation matrix after two rotations is given by

$$\mathbf{R}_{I2A_2} = \mathbf{R}_{\mathcal{X}}(\Theta_i)\mathbf{R}_{\mathcal{Z}}(\Psi_i). \quad (\text{A.34})$$

- c. *Rotation angle about third axis is Φ_i* : The co-ordinate system $(X_{B_5}, Y_{B_5}, Z_{B_5})$ is rotated about the \mathcal{Y} axis, in this case the Z_{B_5} axis, through a positive angle Φ_i , resulting in a co-ordinate system $(X_{B_5}, Y_{B_5}, Z_{B_5})$, that is parallel to the body co-ordinate system $\mathbf{q}_1(t) \beta(t) Q_{Cj}$. The rotation matrix after three rotations is given by

$$M_{1,13} = M_{13,1} = m_g \sin(\beta + \gamma) \sin(\zeta)L_g, \quad (\text{A.35})$$

By using (A.30)–(A.32), the rotation matrix \mathbf{R}_{B_i2I} for several other valid rotation axis sequences (given in brackets below), is computed as follows ([10, 94])

$$a_{1max0} = 1.2\phi_{cone0}, \quad a_{2max0} = 1.2\phi_{cone0}. \quad (\text{A.36})$$

$$\mathbf{R}_{I2B_i} = \mathbf{R}_{\mathcal{X}}(\Phi_i)\mathbf{R}_{\mathcal{Y}}(\Theta_i)\mathbf{R}_{\mathcal{Z}}(\Psi_i) \quad (\mathcal{Z} \rightarrow \mathcal{Y} \rightarrow \mathcal{X}), \quad (\text{A.37})$$

$$\mathbf{R}_{I2B_i} = \mathbf{R}_{\mathcal{Z}}(\Phi_i)\mathbf{R}_{\mathcal{X}}(\Theta_i)\mathbf{R}_{\mathcal{Z}}(\Psi_i) \quad (\mathcal{Z} \rightarrow \mathcal{X} \rightarrow \mathcal{Z}). \quad (\text{A.38})$$

26. The time derivative of the unit vectors $(\mathbf{I}_{B_i}^{(I)}, \mathbf{J}_{B_i}^{(I)}, \mathbf{K}_{B_i}^{(I)})$ in

reference frame I is denoted by $(d_I \mathbf{I}_{B_i}^{(I)}/dt, d_I \mathbf{J}_{B_i}^{(I)}/dt, d_I \mathbf{K}_{B_i}^{(I)}/dt)$, and is directly related to the angular velocity $\omega_{B_i r I}^{(B_i)}$ of reference frame B_i with respect to reference frame I , and expressed in reference frame B_i , as follows (Chap. 2, [10], Chap. 4, [81])

$$\frac{d_I \mathbf{I}_{B_i}^{(I)}}{dt} = \mathbf{R}_{B_i 2I}(\omega_{B_i r I}^{(B_i)} \times \mathbf{I}_{B_i}), \quad (\text{A.39})$$

$$(\text{A.40})$$

$$\frac{d_I \mathbf{J}_{B_i}^{(I)}}{dt} = \mathbf{R}_{B_i 2I}(\omega_{B_i r I}^{(B_i)} \times \mathbf{J}_{B_i}),$$

$$\frac{d_I \mathbf{K}_{B_i}^{(I)}}{dt} = \mathbf{R}_{B_i 2I}(\omega_{B_i r I}^{(B_i)} \times \mathbf{K}_{B_i}), \quad (\text{A.41})$$

where $\omega_{B_i r I}^{(B_i)} = \omega_{B_i r I}^{(B_i)}(\mathbf{q}, d\mathbf{q}/dt) \in \mathbb{R}^3$, and

$$\begin{aligned} \omega_{B_i r I}^{(B_i)} &= \omega_{B_i r Ix}^{(B_i)} \mathbf{I}_{B_i} + \omega_{B_i r Iy}^{(B_i)} \mathbf{J}_{B_i} + \omega_{B_i r Iz}^{(B_i)} \mathbf{K}_{B_i} \\ &= \left[\omega_{B_i r Ix}^{(B_i)}, \omega_{B_i r Iy}^{(B_i)}, \omega_{B_i r Iz}^{(B_i)} \right]^\top. \end{aligned} \quad (\text{A.42})$$

Both sides of Eqs. (A.39)–(A.41) are expressed in reference frame I . If the unit vectors $(\mathbf{I}_{B_i}^{(I)}, \mathbf{J}_{B_i}^{(I)}, \mathbf{K}_{B_i}^{(I)})$ are given (that is, the rotation matrix $\mathbf{R}_{B_i 2I}$ is given), and the time derivatives of the unit vectors in reference frame I denoted by $(d_I \mathbf{I}_{B_i}^{(I)}/dt, d_I \mathbf{J}_{B_i}^{(I)}/dt, d_I \mathbf{K}_{B_i}^{(I)}/dt)$ are given, then the angular velocity $\omega_{B_i r I}^{(B_i)}$ is obtained directly from

(A.39)–(A.41).

27. The following relations hold for the angular velocity

$$(\text{B:}) \quad (\text{B:})$$

$$\omega_{IrB_i}^{\sim\sim} = -\omega_{B_i r I}^{\sim\sim}, \quad (\text{A.43})$$

$$\omega_{B_i r I}^{(I)} = \mathbf{R}_{B_i 2 I} \omega_{B_i r I}^{(B_i)}, \quad (\text{A.44})$$

$$\omega_{IrB_i}^{(I)} = -\omega_{B_i r I}^{(I)}. \quad (\text{A.45})$$

In addition, by using (A.45), (A.29), it follows that

$$(\text{A.46})$$

$$\begin{aligned} \omega_{B_i r B_j}^{(B_i)} &= \omega_{B_i r I}^{(B_i)} + \omega_{I r B_j}^{(B_i)} \\ &= \omega_{B_i r I}^{(B_i)} - \omega_{B_j r I}^{(B_i)} \\ &= \omega_{B_i r I}^{(B_i)} - \mathbf{R}_{B_j 2 B_i} \omega_{B_j r I}^{(B_j)}. \end{aligned}$$

28. The time derivatives of the unit vectors $(\mathbf{I}_{B_i}^{(B_i)}, \mathbf{J}_{B_i}^{(B_i)}, \mathbf{K}_{B_i}^{(B_i)})$ in reference frame I are denoted by $(d_I \mathbf{I}_{B_i}^{(B_i)})/dt$, $d_I \mathbf{J}_{B_i}^{(B_i)}/dt$,

$\mathbf{J}_{B_i}^{(B_i)} = \mathbf{J}_{B_i}$, they are expressed in reference frame B_i and are

obtained by multiplying both sides of (A.39)–(A.41) from the left by $\mathbf{R}_{B_i 2 I}$ as follows

$$\frac{d_I \mathbf{I}_{B_i}^{(B_i)}}{dt} = \left(\frac{d_I \mathbf{I}_{B_i}^{(I)}}{dt} \right)^{(B_i)} = \mathbf{R}_{I 2 B_i} \frac{d_I \mathbf{I}_{B_i}^{(I)}}{dt} = \omega_{B_i r I}^{(B_i)} \times \mathbf{I}_{B_i}, \quad (\text{A.47})$$

$$\frac{d_I \mathbf{J}_{B_i}^{(B_i)}}{dt} = \left(\frac{d_I \mathbf{J}_{B_i}^{(I)}}{dt} \right)^{(B_i)} = \mathbf{R}_{I 2 B_i} \frac{d_I \mathbf{J}_{B_i}^{(I)}}{dt} = \omega_{B_i r I}^{(B_i)} \times \mathbf{J}_{B_i}, \quad (\text{A.48})$$

$$d_I \mathbf{K}_{B_i}^{(B_i)} = \left(d_I \mathbf{K}_{B_i}^{(I)} \right)^{(B_i)} = d_I \mathbf{K}_{B_i}^{(I)} \quad (\text{A.49})$$

$$\frac{d\nu_l}{dt} = \left(\frac{d\nu_l}{dt} \right) = \mathbf{R}_{I2B_i} \frac{d\nu_l}{dt} = \boldsymbol{\omega}_{B_i r I}^{(D_i)} \times \mathbf{K}_{B_i}. \quad (\text{A.49})$$

29. Let $\mathbf{x}^{(B_i)}$ denote a given vector $\mathbf{u} \in \mathbb{R}^4$ expressed in reference frame B_i ,

$$\begin{aligned} \mathbf{x}^{(B_i)} &= x_1^{(B_i)} \mathbf{I}_{B_i} + x_2^{(B_i)} \mathbf{J}_{B_i} + x_3^{(B_i)} \mathbf{K}_{B_i} \\ &= [x_1^{(B_i)}, x_2^{(B_i)}, x_3^{(B_i)}]^\top, \end{aligned} \quad (\text{A.50})$$

where $x_1^{(B_i)} = x_1^{(B_i)}(\mathbf{q})$, $x_2^{(B_i)} = x_2^{(B_i)}(\mathbf{q})$, $x_3^{(B_i)} = x_3^{(B_i)}(\mathbf{q})$, and

$\mathbf{x}^{(B_i)} = \mathbf{x}^{(B_i)}(\mathbf{q})$. Since \mathbf{q} generally varies with time t it follows that $\mathbf{x}^{(B_i)}$ will also generally vary with time t . A typical example is where $\mathbf{x}^{(B_i)}$ is the position vector of a point relative to the origin of reference frame B_i .

30. The time derivative of the vector $\mathbf{x}^{(B_i)}$ in reference frame B_i is given by the time derivative of each element of $\mathbf{x}^{(B_i)}$, (A.50), as follows (Chap. 2, [10])

$$\begin{aligned} \frac{d_{B_i} \mathbf{x}^{(B_i)}}{dt} &= \frac{d_{B_i} \mathbf{x}^{(B_i)}(\mathbf{q})}{dt} \\ &= \frac{dx_1^{(B_i)}(\mathbf{q})}{dt} \mathbf{I}_{B_i} + \frac{dx_2^{(B_i)}(\mathbf{q})}{dt} \mathbf{J}_{B_i} + \frac{dx_3^{(B_i)}(\mathbf{q})}{dt} \mathbf{K}_{B_i} \\ &= \frac{\partial \mathbf{x}^{(B_i)}(\mathbf{q})}{\partial \mathbf{q}} \frac{d\mathbf{q}}{dt}, \end{aligned} \quad (\text{A.51})$$

31. where $\partial \mathbf{x}^{(B_i)}(\mathbf{q})/\partial \mathbf{q} \in \mathbb{R}^{3 \times n}$.
 Let $\mathbf{x}^{(I)}$ denote the given vector \mathbf{q} expressed in reference frame I as follows

$$\begin{aligned}
 \mathbf{x}^{(I)} &= \mathbf{R}_{B_i 2 I} \mathbf{x}^{(B_i)} \\
 &= x_1^{(B_i)} \mathbf{I}_{B_i}^{(I)} + x_2^{(B_i)} \mathbf{J}_{B_i}^{(I)} + x_3^{(B_i)} \mathbf{K}_{B_i}^{(I)} \\
 &= x_1^{(I)} \mathbf{I}_1 + x_2^{(I)} \mathbf{I}_2 + x_3^{(I)} \mathbf{I}_3, \\
 &= [x_1^{(I)}, x_2^{(I)}, x_3^{(I)}]^\top,
 \end{aligned} \tag{A.52}$$

where $x_1^{(I)} = x_1^{(I)}(\mathbf{q})$, $x_2^{(I)} = x_2^{(I)}(\mathbf{q})$, $x_3^{(I)} = x_3^{(I)}(\mathbf{q})$, and
 $\mathbf{x}^{(I)} = \mathbf{x}^{(I)}(\mathbf{q})$.

32. The time derivative of the vector $\mathbf{x}^{(I)}$ in reference frame I is given by the time derivative of each element of $\mathbf{x}^{(I)}$, (A.52), as follows

$$\begin{aligned}
 \frac{d_I \mathbf{x}^{(I)}}{dt} &= \frac{d_I \mathbf{x}^{(I)}(\mathbf{q})}{dt} \\
 &= \frac{dx_1^{(I)}(\mathbf{q})}{dt} \mathbf{I}_1 + \frac{dx_2^{(I)}(\mathbf{q})}{dt} \mathbf{I}_2 + \frac{dx_3^{(I)}(\mathbf{q})}{dt} \mathbf{I}_3 \\
 &= \frac{\partial \mathbf{x}^{(I)}(\mathbf{q})}{\partial \mathbf{q}} \frac{d\mathbf{q}}{dt},
 \end{aligned} \tag{A.53}$$

where $\partial \mathbf{x}^{(I)}(\mathbf{q})/\partial \mathbf{q} \in \mathbb{R}^{3 \times n}$.

33. By using (A.39)–(A.41), (A.52), (A.50), the time derivative in reference frame I , $d_I \mathbf{x}^{(I)}/dt$, is *related* to the time derivative in reference frame B_i , $d_{B_i} \mathbf{x}^{(B_i)}/dt$, and the angular velocity $\boldsymbol{\omega}_{n \dots}^{(B_i)}$, as

follows (Chap. 2, [10], Chap. 4, [81])

$$\begin{aligned}
\frac{d_I \mathbf{x}^{(I)}}{dt} &= \frac{d_I (\mathbf{R}_{B_i 2I} \mathbf{x}^{(B_i)})}{dt} \\
&= \frac{d_I}{dt} \left(x_1^{(B_i)} \mathbf{I}_{B_i}^{(I)} + x_2^{(B_i)} \mathbf{J}_{B_i}^{(I)} + x_3^{(B_i)} \mathbf{K}_{B_i}^{(I)} \right) \\
&= \frac{dx_1^{(B_i)}}{dt} \mathbf{I}_{B_i}^{(I)} + \frac{dx_2^{(B_i)}}{dt} \mathbf{J}_{B_i}^{(I)} + \frac{dx_3^{(B_i)}}{dt} \mathbf{K}_{B_i}^{(I)} + \\
&\quad x_1^{(B_i)} \frac{d_I \mathbf{I}_{B_i}^{(I)}}{dt} + x_2^{(B_i)} \frac{d_I \mathbf{J}_{B_i}^{(I)}}{dt} + x_3^{(B_i)} \frac{d_I \mathbf{K}_{B_i}^{(I)}}{dt} \\
&= \mathbf{R}_{B_i 2I} \frac{d_{B_i} \mathbf{x}^{(B_i)}}{dt} + x_1^{(B_i)} \frac{d_I \mathbf{I}_{B_i}^{(I)}}{dt} + x_2^{(B_i)} \frac{d_I \mathbf{J}_{B_i}^{(I)}}{dt} + x_3^{(B_i)} \frac{d_I \mathbf{K}_{B_i}^{(I)}}{dt},
\end{aligned}$$

and

$$\begin{aligned}
&x_1^{(B_i)} \frac{d_I \mathbf{I}_{B_i}^{(I)}}{dt} + x_2^{(B_i)} \frac{d_I \mathbf{J}_{B_i}^{(I)}}{dt} + x_3^{(B_i)} \frac{d_I \mathbf{K}_{B_i}^{(I)}}{dt} \\
&= \mathbf{R}_{B_i 2I} (\boldsymbol{\omega}_{B_i r I}^{(B_i)} \times (x_1^{(B_i)} \mathbf{I}_{B_i} + x_2^{(B_i)} \mathbf{J}_{B_i} + x_3^{(B_i)} \mathbf{K}_{B_i})) \\
&= \mathbf{R}_{B_i 2I} (\boldsymbol{\omega}_{B_i r I}^{(B_i)} \times (x_1^{(B_i)} \mathbf{I}_{B_i} + x_2^{(B_i)} \mathbf{J}_{B_i} + x_3^{(B_i)} \mathbf{K}_{B_i})) \\
&= \mathbf{R}_{B_i 2I} (\boldsymbol{\omega}_{B_i r I}^{(B_i)} \times \mathbf{x}^{(B_i)}), \\
\Rightarrow \frac{d_I \mathbf{x}^{(I)}}{dt} &= \frac{d_I (\mathbf{R}_{B_i 2I} \mathbf{x}^{(B_i)})}{dt} \\
&= \mathbf{R}_{B_i 2I} \frac{d_{B_i} \mathbf{x}^{(B_i)}}{dt} + \mathbf{R}_{B_i 2I} (\boldsymbol{\omega}_{B_i r I}^{(B_i)} \times \mathbf{x}^{(B_i)}). \tag{A.54}
\end{aligned}$$

Both sides of Eq. (A.54) are expressed in reference frame I .

34. Relation (A.54) can be expressed in reference frame B_i by

multiplying both sides of (A.54) from the left by $\mathbf{R}_{B_i 2I}$, as follows

$$(d_I \mathbf{x}^{(I)})^{(B_i)} = d_I \mathbf{x}^{(I)}$$

$$\begin{aligned}
\left(\frac{\cdot}{dt} \right) &= \mathbf{R}_{I2B_i} \frac{\cdot}{dt} \\
&= \frac{d_{B_i} \mathbf{x}^{(B_i)}}{dt} + \boldsymbol{\omega}_{B_i I}^{(B_i)} \times \mathbf{x}^{(B_i)}, \\
\Rightarrow \left(\frac{d_I \mathbf{x}^{(I)}}{dt} \right)^{(B_i)} &= \frac{d_{B_i} \mathbf{x}^{(B_i)}}{dt} + \boldsymbol{\omega}_{B_i I}^{(B_i)} \times \mathbf{x}^{(B_i)}. \tag{A.55}
\end{aligned}$$

35.

The time derivative of the vector $\mathbf{x}^{(B_i)}$ in reference frame I , and expressed in reference frame B_i , is denoted by $d_I \mathbf{x}^{(B_i)} / dt$ and is computed by using (A.55) as follows

$$\frac{d_I \mathbf{x}^{(B_i)}}{dt} = \left(\frac{d_I \mathbf{x}^{(I)}}{dt} \right)^{(B_i)} = \frac{d_{B_i} \mathbf{x}^{(B_i)}}{dt} + \boldsymbol{\omega}_{B_i I}^{(B_i)} \times \mathbf{x}^{(B_i)}. \tag{A.56}$$

36.

In direct analogy to the relation (A.54), the time derivative in reference frame B_i , $d_{B_i} \mathbf{x}^{(B_i)} / dt$, is related to the time derivative in reference frame I , $d_I \mathbf{x}^{(I)} / dt$, and the angular velocity $\boldsymbol{\omega}_{I B_i}^{(I)}$, as

follows

$$\begin{aligned}
\frac{d_{B_i} \mathbf{x}^{(B_i)}}{dt} &= \frac{d_{B_i} (\mathbf{R}_{I2B_i} \mathbf{x}^{(I)})}{dt} \\
&= \mathbf{R}_{I2B_i} \frac{d_I \mathbf{x}^{(I)}}{dt} + \mathbf{R}_{I2B_i} (\boldsymbol{\omega}_{I B_i}^{(I)} \times \mathbf{x}^{(I)}). \tag{A.57}
\end{aligned}$$

37. By substituting the expression on the right-hand-side of (A.57) for $d_{B_i} \mathbf{x}^{(B_i)} / dt$ in (A.54), and using (A.43), the following relation is

obtained,

$$\boldsymbol{\omega}_{I B_i}^{(I)} \times \mathbf{x}^{(I)} = \mathbf{R}_{I2B_i} (\boldsymbol{\omega}_{I B_i}^{(B_i)} \times \mathbf{x}^{(B_i)}). \tag{A.58}$$

$$\frac{d_{B_i} \mathbf{x}^{(I)}}{dt} = \mathbf{R}_{B_i I} \frac{d_{B_i} \mathbf{x}^{(B_i)}}{dt} \mathbf{R}_{B_i I}^T + \boldsymbol{\omega}_{I r B_i}^{(I)} \times \mathbf{x}^{(I)} \quad (\text{A.58})$$

38. Similarly, the time derivative of the vector $\mathbf{x}^{(I)}$ in reference frame B_i , and expressed in reference frame I , is denoted by $d_I \mathbf{x}^{(B_i)}/dt$ and is computed by using (A.57) as follows

$$\frac{d_{B_i} \mathbf{x}^{(I)}}{dt} = \left(\frac{d_{B_i} \mathbf{x}^{(B_i)}}{dt} \right)^{(I)} = \frac{d_I \mathbf{x}^{(I)}}{dt} + \boldsymbol{\omega}_{I r B_i}^{(I)} \times \mathbf{x}^{(I)}. \quad (\text{A.59})$$

39. For any two vectors $\alpha_s, \mathbf{b}_0 \in \mathbb{R}^3$, $\mathbf{a}_0 = [a_{0x}, a_{0y}, a_{0z}]^\top$, $\mathbf{a}_0 = [a_{0x}, a_{0y}, a_{0z}]^\top$, the following relations hold (Chap. 2, [81]),
- $$\mathbf{a}_0 \times \mathbf{b}_0 = -(\mathbf{b}_0 \times \mathbf{a}_0), \quad \mathbf{a}_0 \times \mathbf{b}_0 = \tilde{\mathbf{a}}_0 \mathbf{b}_0, \quad \mathbf{b}_0 \times \mathbf{a}_0 = \tilde{\mathbf{b}}_0 \mathbf{a}_0, \quad (\text{A.60})$$

where $\alpha_s, \tilde{\mathbf{b}}_0$ are skew-symmetric matrices given by

$$\tilde{\mathbf{a}}_0 = \begin{bmatrix} 0 & -a_{0z} & a_{0y} \\ a_{0z} & 0 & -a_{0x} \\ -a_{0y} & a_{0x} & 0 \end{bmatrix}, \quad \tilde{\mathbf{b}}_0 = \begin{bmatrix} 0 & -b_{0z} & b_{0y} \\ b_{0z} & 0 & -b_{0x} \\ -b_{0y} & b_{0x} & 0 \end{bmatrix}. \quad (\text{A.61})$$

Thus, using (A.60)–(A.61), Eq. (A.54) can be expressed as follows

$$\frac{d_I \mathbf{x}^{(I)}}{dt} = \mathbf{R}_{B_i 2I} \frac{d_{B_i} \mathbf{x}^{(B_i)}}{dt} + \mathbf{R}_{B_i 2I} (\tilde{\boldsymbol{\omega}}_{B_i r I}^{(B_i)} \mathbf{x}^{(B_i)}), \quad (\text{A.62})$$

$$\Rightarrow \frac{d_I \mathbf{x}^{(I)}}{dt} = \mathbf{R}_{B_i 2I} \frac{d_{B_i} \mathbf{x}^{(B_i)}}{dt} - \mathbf{R}_{B_i 2I} (\tilde{\boldsymbol{\chi}}^{(B_i)} \boldsymbol{\omega}_{B_i r I}^{(B_i)}), \quad (\text{A.63})$$

where $\boldsymbol{\omega}_{B_i r I}^{(B_i)}$ and $\tilde{\boldsymbol{\chi}}^{(B_i)}$ are skew-symmetric matrices given by

$$\tilde{\boldsymbol{\omega}}_{B_i r I}^{(B_i)} = \begin{bmatrix} 0 & -\omega_{B_i r I z}^{(B_i)} & \omega_{B_i r I y}^{(B_i)} \\ \omega_{B_i r I z}^{(B_i)} & 0 & -\omega_{B_i r I x}^{(B_i)} \\ -\omega_{B_i r I y}^{(B_i)} & \omega_{B_i r I x}^{(B_i)} & 0 \end{bmatrix} \quad (\text{A.64})$$

$$\tilde{\omega}_{B_i r I} = \begin{bmatrix} \tilde{\omega}_{B_i r I z}^{(B_i)} & \tilde{\omega}_{B_i r I x}^{(B_i)} & \tilde{\omega}_{B_i r I y}^{(B_i)} \\ -\omega_{B_i r I y}^{(B_i)} & \omega_{B_i r I x}^{(B_i)} & 0 \end{bmatrix}, \quad (\text{A.64})$$

$$\tilde{\mathbf{x}}^{(B_i)} = \begin{bmatrix} 0 & -x_3^{(B_i)} & x_2^{(B_i)} \\ x_3^{(B_i)} & 0 & -x_1^{(B_i)} \\ -x_2^{(B_i)} & x_1^{(B_i)} & 0 \end{bmatrix}. \quad (\text{A.65})$$

40. A relation for the second time derivative of $\mathbf{x}^{(I)}$ in reference frame I , $d_I^2 \mathbf{x}^{(I)} / dt^2$, is obtained as follows.

First, compute the time derivative of both sides of Eq. (A.54) in reference frame I ,

$$\frac{d_I^2 \mathbf{x}^{(I)}}{dt^2} = \frac{d_I}{dt} (\mathbf{R}_{B_i 2I} \frac{d_{B_i} \mathbf{x}^{(B_i)}}{dt}) + \frac{d_I}{dt} (\mathbf{R}_{B_i 2I} (\boldsymbol{\omega}_{B_i r I}^{(B_i)} \times \mathbf{x}^{(B_i)})). \quad (\text{A.66})$$

The structure of each of the terms on the right-hand-side of (A.66) matches the structure of the term on the left-hand-side of (A.54).

Second, apply relation (A.54) to each of the two terms on the right-hand-side of (A.66),

$$\frac{d_I}{dt} (\mathbf{R}_{B_i 2I} \frac{d_{B_i} \mathbf{x}^{(B_i)}}{dt}) = \mathbf{R}_{B_i 2I} \frac{d_{B_i}^2 \mathbf{x}^{(B_i)}}{dt^2} + \mathbf{R}_{B_i 2I} (\boldsymbol{\omega}_{B_i r I}^{(B_i)} \times \frac{d_{B_i} \mathbf{x}^{(B_i)}}{dt}), \quad (\text{A.67})$$

$$\begin{aligned} \frac{d_I}{dt} (\mathbf{R}_{B_i 2I} (\boldsymbol{\omega}_{B_i r I}^{(B_i)} \times \mathbf{x}^{(B_i)})) &= \mathbf{R}_{B_i 2I} \frac{d_{B_i}}{dt} (\boldsymbol{\omega}_{B_i r I}^{(B_i)} \times \mathbf{x}^{(B_i)}) + \\ &\quad \mathbf{R}_{B_i 2I} (\boldsymbol{\omega}_{B_i r I}^{(B_i)} \times (\boldsymbol{\omega}_{B_i r I}^{(B_i)} \times \mathbf{x}^{(B_i)})) \\ &= \mathbf{R}_{B_i 2I} (\frac{d_{B_i} \boldsymbol{\omega}_{B_i r I}^{(B_i)}}{dt} \times \mathbf{x}^{(B_i)}) + \\ &\quad \mathbf{R}_{B_i 2I} (\boldsymbol{\omega}_{B_i r I}^{(B_i)} \times \frac{d_{B_i} \mathbf{x}^{(B_i)}}{dt}) + \\ &\quad \mathbf{R}_{B_i 2I} (\boldsymbol{\omega}_{B_i r I}^{(B_i)} \times (\boldsymbol{\omega}_{B_i r I}^{(B_i)} \times \mathbf{x}^{(B_i)})). \end{aligned} \quad (\text{A.68})$$

Third, by using (A.66)–(A.68) it follows that

Thus, by using (A.60)–(A.65), it follows that

$$\begin{aligned} \frac{d_I^2 \mathbf{x}^{(I)}}{dt^2} &= \mathbf{R}_{B_i 2I} \frac{d_{B_i}^2 \mathbf{x}^{(B_i)}}{dt^2} + 2\mathbf{R}_{B_i 2I} (\boldsymbol{\omega}_{B_i rI}^{(B_i)} \times \frac{d_{B_i} \mathbf{x}^{(B_i)}}{dt}) + \\ &\mathbf{R}_{B_i 2I} \left(\frac{d_{B_i} \boldsymbol{\omega}_{B_i rI}^{(B_i)}}{dt} \times \mathbf{x}^{(B_i)} \right) + \mathbf{R}_{B_i 2I} (\boldsymbol{\omega}_{B_i rI}^{(B_i)} \times (\boldsymbol{\omega}_{B_i rI}^{(B_i)} \times \mathbf{x}^{(B_i)})). \end{aligned} \quad (\text{A.69})$$

In the sequel two practical applications of the above derivations are considered.

41. First, without loss of generality, consider the inertial position vector of a point P fixed in rigid body 1 and given by

$$\mathbf{r}_P^{(I)} = \mathbf{r}_1^{(I)} + \mathbf{R}_{B_1 2I} \mathbf{s}_P^{(B_1)}, \quad (\text{A.70})$$

where $\mathbf{s}_P^{(B_1)}$ is the position vector of point P relative to the origin

of body reference frame B_5 , $\mathbf{R}_{B_i 2I} = [\mathbf{I}_{B_i}^{(I)} : \mathbf{J}_{B_i}^{(I)} : \mathbf{K}_{B_i}^{(I)}]$. Since the

vector $\mathbf{s}_P^{(B_1)}$ is fixed in body reference frame B_5 , it follows that

$$\frac{d_{B_1} \mathbf{s}_P^{(B_1)}}{dt} = \mathbf{0}_{3 \times 1}, \quad \frac{d_{B_1}^2 \mathbf{s}_P^{(B_1)}}{dt^2} = \mathbf{0}_{3 \times 1}. \quad (\text{A.71})$$

The inertial velocity of point P is obtained by using (A.54), (A.63), (A.71), as follows

$$\frac{d_I \mathbf{r}_P^{(I)}}{dt} = \frac{d_I \mathbf{r}_1^{(I)}}{dt} + \mathbf{R}_{B_1 2I} (\boldsymbol{\omega}_{B_1 rI}^{(B_1)} \times \mathbf{s}_P^{(B_1)}), \quad (\text{A.72})$$

$$\Rightarrow \frac{d_I \mathbf{r}_P^{(I)}}{dt} = \frac{d_I \mathbf{r}_1^{(I)}}{dt} - \mathbf{R}_{B_1 2I} (\tilde{\mathbf{s}}_P^{(B_1)} \boldsymbol{\omega}_{B_1 rI}^{(B_1)}), \quad (\text{A.73})$$

where

$$\tilde{\mathbf{s}}_P^{(B_1)} = \begin{bmatrix} 0 & -s_{Pz}^{(B_1)} & s_{Py}^{(B_1)} \\ s_{Pz}^{(B_1)} & 0 & -s_{Px}^{(B_1)} \\ \hat{} & \hat{} & \hat{} \end{bmatrix}. \quad (\text{A.74})$$

$$\begin{bmatrix} -s_{Py}^{(I)} & s_{Px}^{(I)} & 0 \end{bmatrix}$$

By using (A.72), (A.69), (A.71), the inertial acceleration of point P is given by

$$\begin{aligned} \frac{d_I^2 \mathbf{r}_P^{(I)}}{dt^2} = & \frac{d_I^2 \mathbf{r}_1^{(I)}}{dt^2} + \mathbf{R}_{B_1 2I} \left(\frac{d_{B_1} \boldsymbol{\omega}_{B_1 r I}^{(B_1)}}{dt} \times \mathbf{s}_P^{(B_1)} \right) + \\ & \mathbf{R}_{B_1 2I} \left(\boldsymbol{\omega}_{B_1 r I}^{(B_1)} \times \left(\boldsymbol{\omega}_{B_1 r I}^{(B_1)} \times \mathbf{s}_P^{(B_1)} \right) \right). \end{aligned} \quad (\text{A.75})$$

42. Second, without loss of generality, consider the case of a point mass d whose motion is specified relative to the body reference frame B_5 as follows

$$\mathbf{s}_d^{(B_1)}, \quad \frac{d_{B_1} \mathbf{s}_d^{(B_1)}}{dt}, \quad \frac{d_{B_1}^2 \mathbf{s}_d^{(B_1)}}{dt^2}, \quad (\text{A.76})$$

where $\mathbf{s}_d^{(B_1)} = \mathbf{s}_d^{(B_1)}(\mathbf{q}) \in \mathbb{R}^3$ is the position vector of the point

mass relative to the origin of body reference frame B_5 . Then, by

using (A.76) and (A.72), (A.75), (A.69), the position of the point mass relative to the origin of the inertial reference frame is given by

$$\mathbf{r}_P^{(I)} = \mathbf{r}_1^{(I)} + \mathbf{R}_{B_1 2I} \mathbf{s}_P^{(B_1)}, \quad (\text{A.77})$$

and the velocity and acceleration are given by

$$\frac{d_I \mathbf{r}_d^{(I)}}{dt} = \frac{d_I \mathbf{r}_1^{(I)}}{dt} + \mathbf{R}_{B_1 2I} \frac{d_{B_1} \mathbf{s}_d^{(B_1)}}{dt} + \mathbf{R}_{B_1 2I} \left(\boldsymbol{\omega}_{B_1 r I}^{(B_1)} \times \mathbf{s}_d^{(B_1)} \right), \quad (\text{A.78})$$

$$\begin{aligned} \frac{d_I^2 \mathbf{r}_d^{(I)}}{dt^2} = & \frac{d_I^2 \mathbf{r}_1^{(I)}}{dt^2} + \mathbf{R}_{B_1 2I} \frac{d_{B_1}^2 \mathbf{s}_d^{(B_1)}}{dt^2} + 2\mathbf{R}_{B_1 2I} \left(\boldsymbol{\omega}_{B_1 r I}^{(B_1)} \times \frac{d_{B_1} \mathbf{s}_d^{(B_1)}}{dt} \right) + \\ & \mathbf{R}_{B_1 2I} \left(\frac{d_{B_1} \boldsymbol{\omega}_{B_1 r I}^{(B_1)}}{dt} \times \mathbf{s}_d^{(B_1)} \right) + \mathbf{R}_{B_1 2I} \left(\boldsymbol{\omega}_{B_1 r I}^{(B_1)} \times \left(\boldsymbol{\omega}_{B_1 r I}^{(B_1)} \times \mathbf{s}_d^{(B_1)} \right) \right). \end{aligned} \quad (\text{A.79})$$

43. By using (A.4), (A.51), it follows that

$$\frac{d_{B_i} \mathbf{I}_{B_i}}{dt} = \mathbf{0}_{3 \times 1}, \quad \frac{d_{B_i} \mathbf{J}_{B_i}}{dt} = \mathbf{0}_{3 \times 1}, \quad \frac{d_{B_i} \mathbf{K}_{B_i}}{dt} = \mathbf{0}_{3 \times 1}. \quad (\text{A.80})$$

44. Thus, given the rotation matrix $\mathbf{R}_{B_i 2I}$, expressions for the unit vectors $(\mathbf{I}_{B_i}^{(I)}, \mathbf{J}_{B_i}^{(I)}, \mathbf{K}_{B_i}^{(I)})$ and their time derivatives in the inertial reference frame I are computed by using (A.19) or (A.53) as follows

$$\left[\frac{d_I \mathbf{I}_{B_i}^{(I)}}{dt} \ ; \ \frac{d_I \mathbf{J}_{B_i}^{(I)}}{dt} \ ; \ \frac{d_I \mathbf{K}_{B_i}^{(I)}}{dt} \right] = \frac{d \mathbf{R}_{B_i 2I}}{dt}, \quad (\text{A.81})$$

or

$$\frac{d_I \mathbf{I}_{B_i}^{(I)}}{dt} = \frac{\partial \mathbf{I}_{B_i}^{(I)}(\mathbf{q})}{\partial \mathbf{q}} \frac{d \mathbf{q}}{dt}, \quad (\text{A.82})$$

$$\frac{d_I \mathbf{J}_{B_i}^{(I)}}{dt} = \frac{\partial \mathbf{J}_{B_i}^{(I)}(\mathbf{q})}{\partial \mathbf{q}} \frac{d \mathbf{q}}{dt}, \quad (\text{A.83})$$

$$\frac{d_I \mathbf{K}_{B_i}^{(I)}}{dt} = \frac{\partial \mathbf{K}_{B_i}^{(I)}(\mathbf{q})}{\partial \mathbf{q}} \frac{d \mathbf{q}}{dt}, \quad (\text{A.84})$$

where $\partial j(\mathbf{q})/\partial \mathbf{q} \in \mathbb{R}^{3 \times n}$, $j = \mathbf{I}_{B_i}^{(I)}, \mathbf{J}_{B_i}^{(I)}, \mathbf{K}_{B_i}^{(I)}$.

45. By using (A.54), (A.80)–(A.84), the following equations are obtained

$$\frac{d_I \mathbf{I}_{B_i}^{(I)}}{\mathcal{A}^*} = \mathbf{R}_{B_i 2I}(\boldsymbol{\omega}_{B_i r I}^{(B_i)} \times \mathbf{I}_{B_i}), \quad \frac{d_I \mathbf{J}_{B_i}^{(I)}}{\mathcal{A}^*} = \mathbf{R}_{B_i 2I}(\boldsymbol{\omega}_{B_i r I}^{(B_i)} \times \mathbf{J}_{B_i}),$$

u u

$$\frac{d_I \mathbf{K}_{B_i}^{(I)}}{dt} = \mathbf{R}_{B_i 2I} (\boldsymbol{\omega}_{B_i r I}^{(B_i)} \times \mathbf{K}_{B_i}), \quad (\text{A.85})$$

implying that

$$\mathbf{R}_{I 2B_i} \frac{d_I \mathbf{I}_{B_i}^{(I)}}{dt} = \boldsymbol{\omega}_{B_i r I}^{(B_i)} \times \mathbf{I}_{B_i} = \begin{bmatrix} 0 \\ \omega_{B_i r I z}^{(B_i)} \\ -\omega_{B_i r I y}^{(B_i)} \end{bmatrix}, \quad (\text{A.86})$$

$$\mathbf{R}_{I 2B_i} \frac{d_I \mathbf{J}_{B_i}^{(I)}}{dt} = \boldsymbol{\omega}_{B_i r I}^{(B_i)} \times \mathbf{J}_{B_i} = \begin{bmatrix} -\omega_{B_i r I z}^{(B_i)} \\ 0 \\ \omega_{B_i r I x}^{(B_i)} \end{bmatrix}, \quad (\text{A.87})$$

$$(\text{A.88})$$

$$\mathbf{R}_{I 2B_i} \frac{d_I \mathbf{K}_{B_i}^{(I)}}{dt} = \boldsymbol{\omega}_{B_i r I}^{(B_i)} \times \mathbf{K}_{B_i} = \begin{bmatrix} \omega_{B_i r I y}^{(B_i)} \\ -\omega_{B_i r I x}^{(B_i)} \\ 0 \end{bmatrix}.$$

Thus, given expressions for the left-hand-sides of (A.86)–(A.88) in terms of $\mathbf{R}_{I 2B_i} = \mathbf{R}_{B_i 2I}^\top$, and in terms of the time derivatives of the

unit vectors $(\mathbf{I}_{B_i}^{(I)}, \mathbf{J}_{B_i}^{(I)}, \mathbf{K}_{B_i}^{(I)})$ in the inertial reference frame I ,

(A.81)–(A.84), the three elements of the angular velocity vector $\boldsymbol{\omega}_{B_i r I}^{(B_i)}$ are obtained by using any two of the three Eqs. (A.86)–

(A.88).

46. Equations (A.86)–(A.88) are expressed in condensed form as follows (Chap. 4, [10, 81])

$$\mathbf{R}_{I 2B_i} \frac{d \mathbf{R}_{B_i 2I}}{dt} = \tilde{\boldsymbol{\omega}}_{B_i r I}^{(B_i)}, \quad (\text{A.89})$$

$$\frac{d}{dt} \mathbf{v}_i$$

where

$$\tilde{\boldsymbol{\omega}}_{B_i r I}^{(B_i)} = \begin{bmatrix} 0 & -\omega_{B_i r I z}^{(B_i)} & \omega_{B_i r I y}^{(B_i)} \\ \omega_{B_i r I z}^{(B_i)} & 0 & -\omega_{B_i r I x}^{(B_i)} \\ -\omega_{B_i r I y}^{(B_i)} & \omega_{B_i r I x}^{(B_i)} & 0 \end{bmatrix} \quad (\text{A.90})$$

((A.28)).

47.

The following results, (A.91)–(A.99), are analogous to (A.80)–(A.88), for the rotation matrix $\mathbf{R}_{B_i 2I}$. Using (A.2), it follows that

$$\frac{d_I \mathbf{I}_1}{dt} = \mathbf{0}_{3 \times 1}, \quad \frac{d_I \mathbf{I}_2}{dt} = \mathbf{0}_{3 \times 1}, \quad \frac{d_I \mathbf{I}_3}{dt} = \mathbf{0}_{3 \times 1}. \quad (\text{A.91})$$

48.

Thus, given the rotation matrix $\mathbf{R}_{B_i 2I}$, expressions for the unit vectors $(\mathbf{I}_1^{(B_i)}, \mathbf{I}_2^{(B_i)}, \mathbf{I}_3^{(B_i)})$ and their time derivatives in the body

reference frame B_i are computed by using (A.14) or (A.51) as follows

$$\left[\frac{d_{B_i} \mathbf{I}_1^{(B_i)}}{dt} \ ; \ \frac{d_{B_i} \mathbf{I}_2^{(B_i)}}{dt} \ ; \ \frac{d_{B_i} \mathbf{I}_3^{(B_i)}}{dt} \right] = \frac{d \mathbf{R}_{I 2 B_i}}{dt}, \quad (\text{A.92})$$

or

$$\frac{d_{B_i} \mathbf{I}_1^{(B_i)}}{dt} = \frac{\partial \mathbf{I}_1^{(B_i)}(\mathbf{q})}{\partial \mathbf{q}} \frac{d \mathbf{q}}{dt}, \quad (\text{A.93})$$

$$\frac{d_{B_i} \mathbf{I}_2^{(B_i)}}{dt} = \frac{\partial \mathbf{I}_2^{(B_i)}(\mathbf{q})}{\partial \mathbf{q}} \frac{d \mathbf{q}}{dt}, \quad (\text{A.94})$$

$$\frac{d_{B_i} \mathbf{I}_3^{(B_i)}}{dt} = \frac{\partial \mathbf{I}_3^{(B_i)}(\mathbf{q})}{\partial \mathbf{q}} \frac{d \mathbf{q}}{dt} \quad (\text{A.95})$$

$$\frac{d}{dt} = \frac{\partial}{\partial \mathbf{q}} \frac{d}{dt}, \quad (\text{A.95})$$

where $\partial j(\mathbf{q})/\partial \mathbf{q} \in \mathbb{R}^{3 \times n}$, $j = I_1^{(B_i)}, I_2^{(B_i)}, I_3^{(B_i)}$.

49.

By using (A.57) and (A.91)–(A.95), the following equations are obtained

$$\frac{d_{B_i} \mathbf{I}_1^{(B_i)}}{dt} = \mathbf{R}_{I_2 B_i} (\boldsymbol{\omega}_{I_r B_i}^{(I)} \times \mathbf{I}_1), \quad \frac{d_{B_i} \mathbf{I}_2^{(B_i)}}{dt} = \mathbf{R}_{I_2 B_i} (\boldsymbol{\omega}_{I_r B_i}^{(I)} \times \mathbf{I}_2),$$

$$\frac{d_{B_i} \mathbf{I}_3^{(B_i)}}{dt} = \mathbf{R}_{I_2 B_i} (\boldsymbol{\omega}_{I_r B_i}^{(I)} \times \mathbf{I}_3), \quad (\text{A.96})$$

implying that

$$\mathbf{R}_{B_i 2I} \frac{d_{B_i} \mathbf{I}_1^{(B_i)}}{dt} = -\boldsymbol{\omega}_{B_i r I}^{(I)} \times \mathbf{I}_1, \quad (\text{A.97})$$

$$\mathbf{R}_{B_i 2I} \frac{d_{B_i} \mathbf{I}_2^{(B_i)}}{dt} = -\boldsymbol{\omega}_{B_i r I}^{(I)} \times \mathbf{I}_2, \quad (\text{A.98})$$

$$\mathbf{R}_{B_i 2I} \frac{d_{B_i} \mathbf{I}_3^{(B_i)}}{dt} = -\boldsymbol{\omega}_{B_i r I}^{(I)} \times \mathbf{I}_3, \quad (\text{A.99})$$

where $\boldsymbol{\omega}_{B_i r I}^{(I)} = \boldsymbol{\omega}_{B_i r I}^{(I)}(\mathbf{q}, d\mathbf{q}/dt)$ denotes the angular velocity of the body reference frame B_i with respect to the inertial reference frame I , expressed in the inertial reference frame I .

50. The angular velocity $\boldsymbol{\omega}_{B_i r I}^{(B_i)}$ is represented as follows ((A.86)–

(A.88), (A.81)–(A.84))

$$\boldsymbol{\omega}_{B_i r I}^{(B_i)} = \mathbf{I}^{-1} \frac{d\mathbf{q}}{dt} \quad (\text{A.100})$$

$$\omega_{B_i r I} = \omega_{\rho, i} \overline{dt}, \quad (\text{A.100})$$

where $U_{\rho, i} = U_{\rho, i}(\mathbf{q}) \in \mathbb{R}^{3 \times n}$. From (A.100) it follows that

$$U_{\rho, i} = \frac{\partial \omega_{B_i r I}^{(B_i)}}{\partial \dot{\mathbf{q}}}. \quad (\text{A.101})$$

51.

The inertial velocity and acceleration of the center of mass of rigid body i is obtained from (A.9),

$$\mathbf{v}_i^{(I)} = \frac{d_I \mathbf{r}_i^{(I)}}{dt} = \frac{\partial \mathbf{r}_i^{(I)}}{\partial \mathbf{q}} \frac{d\mathbf{q}}{dt} = U_{\tau, i} \frac{d\mathbf{q}}{dt}, \quad (\text{A.102})$$

$$\mathbf{a}_i^{(I)} = \frac{d_I \mathbf{v}_i^{(I)}}{dt} = \frac{d_I^2 \mathbf{r}_i^{(I)}}{dt^2} = U_{\tau, i} \frac{d^2 \mathbf{q}}{dt^2} + \bar{\mathbf{a}}_i, \quad (\text{A.103})$$

where $\mathbf{v}_i^{(I)} = \mathbf{v}_i^{(I)}(\mathbf{q}, d\mathbf{q}/dt) \in \mathbb{R}^3$, $U_{\tau, i} = U_{\tau, i}(\mathbf{q}) \in \mathbb{R}^{3 \times n}$,

$\mathbf{a}_i^{(I)} = \mathbf{a}_i^{(I)}(\mathbf{q}, d\mathbf{q}/dt, d^2\mathbf{q}/dt^2) \in \mathbb{R}^3$, $\bar{\mathbf{a}}_i = \bar{\mathbf{a}}_i(\mathbf{q}, d\mathbf{q}/dt) \in \mathbb{R}^3$. From

(A.102) it follows that

$$U_{\tau, i} = \frac{\partial \mathbf{r}_i^{(I)}}{\partial \mathbf{q}} = \frac{\partial \mathbf{v}_i^{(I)}}{\partial \dot{\mathbf{q}}}. \quad (\text{A.104})$$

52. For the multibody system consisting of N rigid bodies, Eq. (A.9) and Eqs. (A.102), (A.103), are represented as follows

$$\mathbf{r} = \mathbf{r}(\mathbf{q}), \quad (\text{A.105})$$

$$\mathbf{v} = U_{\tau} \frac{d\mathbf{q}}{dt}, \quad (\text{A.106})$$

$$\mathbf{a} = U_{\tau} \frac{d^2 \mathbf{q}}{dt^2} + \bar{\mathbf{a}}, \quad (\text{A.107})$$

where

$$\mathbf{r} = \begin{bmatrix} \mathbf{r}_1^{(I)} \\ \vdots \\ \mathbf{r}_N^{(I)} \end{bmatrix}, \quad (\text{A.108})$$

$$\mathbf{v} = \begin{bmatrix} \mathbf{v}_1^{(I)} \\ \vdots \\ \mathbf{v}_N^{(I)} \end{bmatrix}, \quad \mathbf{U}_\tau = \begin{bmatrix} \mathbf{U}_{\tau,1} \\ \vdots \\ \mathbf{U}_{\tau,N} \end{bmatrix}, \quad (\text{A.109})$$

$$\mathbf{a} = \begin{bmatrix} \mathbf{a}_1^{(I)} \\ \vdots \\ \mathbf{a}_N^{(I)} \end{bmatrix}, \quad \bar{\mathbf{a}} = \begin{bmatrix} \bar{\mathbf{a}}_1 \\ \vdots \\ \bar{\mathbf{a}}_N \end{bmatrix}, \quad (\text{A.110})$$

$$\mathbf{r} \in \mathbb{R}^{3N}, \quad \mathbf{v} \in \mathbb{R}^{3N}, \quad \mathbf{U}_\tau \in \mathbb{R}^{3N \times n}, \quad \mathbf{a} \in \mathbb{R}^{3N}, \quad \bar{\mathbf{a}} \in \mathbb{R}^{3N}.$$

53. By using (A.54), the angular acceleration of body reference frame B_i is defined as the time derivative of the angular velocity $\omega_{IrB_i}^{(I)}$,

(A.100), in the inertial reference frame I as follows ([10])

$$\begin{aligned} \alpha_i^{(I)} &= \frac{d_I \omega_{B_i r I}^{(I)}}{dt} \\ &= \frac{d_I (\mathbf{R}_{B_i 2 I} \omega_{B_i r I}^{(B_i)})}{dt} \\ &= \mathbf{R}_{B_i 2 I} \frac{d_{B_i} \omega_{B_i r I}^{(B_i)}}{dt} + \mathbf{R}_{B_i 2 I} (\omega_{B_i r I}^{(B_i)} \times \omega_{B_i r I}^{(B_i)}) \\ &= \mathbf{R}_{B_i 2 I} \frac{d_{B_i} \omega_{B_i r I}^{(B_i)}}{dt}, \\ \Rightarrow \alpha_i^{(B_i)} &= \mathbf{R}_{I 2 B_i} \alpha_i^{(I)} = \frac{d_{B_i} \omega_{B_i r I}^{(B_i)}}{dt}, \end{aligned} \quad (\text{A.111})$$

$$\Rightarrow \alpha_i^{(B_i)} = U_{\rho,i} \frac{d^2 \mathbf{q}}{dt^2} + \bar{\alpha}_i, \quad (\text{A.112})$$

where $\alpha_i^{(B_i)} = \alpha_i^{(B_i)}(\mathbf{q}, d\mathbf{q}/dt, d^2\mathbf{q}/dt^2) \in \mathbb{R}^3$,

$$\bar{\alpha}_i = \bar{\alpha}_i(\mathbf{q}, d\mathbf{q}/dt) \in \mathbb{R}^3.$$

54.

For the multibody system consisting of N rigid bodies, Eqs. (A.100), (A.112), are expressed as follows

$$\omega = U_\rho \frac{d\mathbf{q}}{dt}, \quad (\text{A.113})$$

$$\alpha = U_\rho \frac{d^2 \mathbf{q}}{dt^2} + \bar{\alpha}, \quad (\text{A.114})$$

where

$$\omega = \begin{bmatrix} \omega_{B_1 r l}^{(B_1)} \\ \vdots \\ \omega_{B_N r l}^{(B_N)} \end{bmatrix}, \quad U_\rho = \begin{bmatrix} U_{\rho,1} \\ \vdots \\ U_{\rho,N} \end{bmatrix}, \quad (\text{A.115})$$

$$\alpha = \begin{bmatrix} \alpha_1^{(B_1)} \\ \vdots \\ \alpha_N^{(B_N)} \end{bmatrix}, \quad \bar{\alpha} = \begin{bmatrix} \bar{\alpha}_1 \\ \vdots \\ \bar{\alpha}_N \end{bmatrix}, \quad (\text{A.116})$$

$$\omega \in \mathbb{R}^{3N}, \quad U_\rho \in \mathbb{R}^{3N \times n}, \quad \alpha \in \mathbb{R}^{3N}, \quad \bar{\alpha} \in \mathbb{R}^{3N}.$$

55. It is assumed throughout that

$$Q_{C14} = \lambda_{10}, \quad (\text{A.117})$$

where B_5 denotes an open set containing the admissible values for the vector of generalized co-ordinates \mathbf{q} (see Chap. 2 for practical example).

56. Equations (A.106), (A.113), are expressed as follows

$$\begin{bmatrix} \mathbf{v} \\ \boldsymbol{\omega} \end{bmatrix} = \mathbf{U} \frac{d\mathbf{q}}{dt}, \quad (\text{A.118})$$

where

$$\mathbf{U} = \begin{bmatrix} \mathbf{U}_\tau \\ \mathbf{U}_\rho \end{bmatrix}, \quad (\text{A.119})$$

$\mathbf{U} = \mathbf{U}(\mathbf{q}) \in \mathbb{R}^{6N \times n}$. In this work, it is assumed that the generalized co-ordinates \mathbf{q} , (A.5), are selected such that $n \leq 6N$ and the matrix \mathbf{U} , (A.119), has full column rank, that is,

$$n \leq 6N \quad \text{and} \quad \text{Rank}(\mathbf{U}) = n. \quad (\text{A.120})$$

Since the matrix \mathbf{U} has full column rank, (A.120), it follows that the linear transformation (A.118) is one-to-one (pp. 583–584, [80]).

57. Thus, given a value for the left-hand-side of (A.118). It follows that the inverse transformation yields a unique vector $d\mathbf{p}/dt$ given by

$$\frac{d\mathbf{q}}{dt} = (\mathbf{U}^\top \mathbf{U})^{-1} \mathbf{U}^\top \begin{bmatrix} \mathbf{v} \\ \boldsymbol{\omega} \end{bmatrix} \quad (\text{A.121})$$

(Theorem 11.5.1, pp. 144–145, Lemmas 9.2.8, 9.2.9, pp. 116–117, [80]).

58. By using (A.120) it follows that $(\mathbf{U}^\top \mathbf{U})^{-1}$ is a $\boldsymbol{\eta}_1(0)$ symmetric positive definite and invertible matrix that has rank n (Corollary 14.2.14, pp. 214–215, Eqs. (2.4), (2.5), p. 82, Theorem 13.3.7, p. 188, [80]). From the above it follows that $(\mathbf{U}^\top \mathbf{U})^{-1} \mathbf{U}^\top$ is a $n \times 6N$ rectangular matrix that has full row rank,

$$\text{Rank}((\mathbf{U}^\top \mathbf{U})^{-1} \mathbf{U}^\top) = \text{Rank}(\mathbf{U}^\top) = \text{Rank}(\mathbf{U}) = n \quad (\text{A.122})$$

(Lemma 8.3.2, p. 83, [80]). However, the matrix $(\mathbf{U}^\top \mathbf{U})^{-1} \mathbf{U}^\top$ does not have full column rank (except in the case where $n \leq 6N$).

Thus, the linear transformation (A.121) is in general not one-to-one.

59.

The motion of the multibody system is subject to a total of m nonholonomic and holonomic velocity constraints (or kinematic constraints). It is assumed that all the velocity constraints are not explicit functions of time and that they are ideal ([10, 51, 73, 81, 107, 124, 129, 137, 147, 155]). By using (A.5), (A.6), and (A.105), (A.106), (A.113), the velocity constraints are expressed from the outset in terms of the vector of generalized co-ordinates \mathbf{q} , and the vector of generalized velocities $\dot{\mathbf{q}}$, (A.6), as follows

$$m_{10} = m_{mp}. \quad (\text{A.123})$$

where $\mathbf{G} = \mathbf{G}(\mathbf{q}) \in \mathbb{R}^{m \times n}$ is the velocity constraints matrix,

$\zeta_{ref}(t)$. Note that the time derivative of each geometric constraint results in a holonomic velocity constraint that is part of the velocity constraints (A.123).

60.

It is assumed that each element of the matrix \mathbf{G} is a smooth function of \mathbf{q} , $L_b > 0$, (A.117). The initial conditions of the multibody system $X_{B_{11}}$ and $X_{B_{11}}$ satisfy the velocity constraints (A.123), and $\mathbf{q}(0) \in P_0$, (A.117). Henceforward, only admissible motions of the system that satisfy $\mathbf{q}(t) \in P_0$ for all $t \geq 0$, are considered.

61. It is assumed that $(\mathbf{G}_f) = 11$ is equal to a constant value α_s , that

is,

$$\text{Rank}(\mathbf{G}) = r_G = \text{fixed integer} \in \{1, 2, \dots, m\}. \quad (\text{A.124})$$

It follows from (A.124) that the velocity constraints (A.123) may not be independent,

$$r_G \leq m. \quad (\text{A.125})$$

The velocity constraints (A.123) are independent if

$$r_G = m. \quad (\text{A.126})$$

The velocity constraints (A.123) are not independent if

$$r_G < m. \quad (\text{A.127})$$

62.

The relation between the dimension of the null space of \mathbf{G} ,

$\text{Rank}(\mathbf{G})$, and $(\mathbf{G}_f) = 11$ is given by (Theorem 31, p. 281, [126])

$$\text{Rank}(\mathbf{G}) + \text{Dim}(\text{Null}(\mathbf{G})) = \text{number of columns of } \mathbf{G} = n. \quad (\text{A.128})$$

Using (A.124), (A.128), it follows that

$$\text{Dim}(\text{Null}(\mathbf{G})) = n_s = n - r_G. \quad (\text{A.129})$$

63. The kinematic model of the constrained rigid multibody system is derived by using the velocity constraints (A.123). Let \mathbf{p}_s denote

the vector of δ_3 independent generalized velocities ((A.129))

given by

$$\mathbf{p}_s = [p_{s1}, p_{s2}, \dots, p_{sn_s}]^T, \quad (\text{A.130})$$

$\mathbf{p}_s \in \mathbb{R}^{n_s}$. Each element of \mathbf{p}_s is set equal to an appropriately

chosen unique element of \mathbf{q} as follows (Sect. B.3.1)

$$\mathbf{n} = [n_1, n_2, \dots, n_{n_s}]^T = \mathbf{C}_s \mathbf{n} \quad \mathbf{C}_s \in \mathbb{R}^{n_s \times n} \quad (\text{A.131})$$

$$\mathbf{p}_s = [p_{s1}, p_{s2}, \dots, p_{sn_s}]^T = \mathbf{S}\mathbf{p}, \quad \mathbf{S} \in \mathbb{R}^{n \times n_s}, \quad (\text{A.131})$$

such that

$$\text{Rank} \left(\begin{bmatrix} \mathbf{G} \\ \mathbf{C}_s \end{bmatrix} \right) = r_G + n_s = n. \quad (\text{A.132})$$

64. One possible approach for selecting the elements of \mathbf{p}_s is to set them equal to the elements of \mathbf{q} that are directly associated with or directly actuated by the applied forces and torques, and such that (A.132) holds (see Chap. 3 for practical example).

65. Let \mathbf{p}_s denote the associated vector of δ_3 independent generalized co-ordinates obtained from (A.131) as follows

$$\mathbf{p}_s = \frac{d\mathbf{q}_s}{dt}, \quad \mathbf{q}_s = [q_{s1}, q_{s2}, \dots, q_{sn_s}]^T = \mathbf{C}_s \mathbf{q}. \quad (\text{A.133})$$

66. Equations (A.123), (A.131), are solved for \mathbf{q} in terms of \mathbf{p}_s , and the solution is expressed as follows ([65], Sect. B.3.1)

$$\mathbf{p} = \mathbf{S}\mathbf{p}_s, \quad (\text{A.134})$$

where $\mathbf{S} = \mathbf{S}(\mathbf{q}) \in \mathbb{R}^{n \times n_s}$ is the null space matrix and satisfies the following equation

$$\mathbf{G}\mathbf{S} = \mathbf{0}_{m \times n_s}. \quad (\text{A.135})$$

It follows that the expression for \mathbf{q} , (A.134), solves the homogeneous equation (A.123) representing the velocity constraints ([65]). It is assumed that the derived expression for \mathbf{q} , (A.134), is valid for all $L_b > 0$, (A.117). Thus, the kinematic model of the constrained rigid multibody system is given by (A.134).

67. The vectors corresponding to the columns of the matrix \mathbf{S} span the null space $\text{Rank}(\mathbf{G})$. By using (A.129), it follows that the matrix \mathbf{S} has full column rank ,

$$\text{Rank}(\mathbf{S}) = n_s. \quad (\text{A.136})$$

The mathematical form of the null space matrix \mathbf{S} is generally different for each particular choice of the vector of independent generalized velocities \mathbf{p}_s , (A.131). This implies that the form of the kinematic model, (A.134), is not unique ([82, 99, 107]).

68. The acceleration kinematic model is obtained by taking the derivative with respect to time t of (A.134),

$$\frac{d\mathbf{p}}{dt} = \mathbf{S} \frac{d\mathbf{p}_s}{dt} + \frac{d\mathbf{S}}{dt} \mathbf{p}_s. \quad (\text{A.137})$$

69. For later use, the velocity constraints (A.123) are converted to acceleration constraints by differentiating with respect to time t the left-hand-side of (A.123),

$$\mathbf{G} \frac{d\mathbf{p}}{dt} + \frac{d\mathbf{G}}{dt} \mathbf{p} = \mathbf{0}_{m \times 1}. \quad (\text{A.138})$$

70. The vector of generalized accelerations $d\mathbf{p}/dt$ given by (A.137), and the vector of generalized velocities \mathbf{q} given by (A.134), jointly satisfy the acceleration constraints, (A.138), as follows (and using (A.135))

$$\begin{aligned} \mathbf{G} \frac{d\mathbf{p}}{dt} + \frac{d\mathbf{G}}{dt} \mathbf{p} &= \mathbf{G} \mathbf{S} \frac{d\mathbf{p}_s}{dt} + \mathbf{G} \frac{d\mathbf{S}}{dt} \mathbf{p}_s + \frac{d\mathbf{G}}{dt} \mathbf{S} \mathbf{p}_s \\ &= \left(\mathbf{G} \frac{d\mathbf{S}}{dt} + \frac{d\mathbf{G}}{dt} \mathbf{S} \right) \mathbf{p}_s \\ &\quad d\mathbf{G}\mathbf{S} \end{aligned} \quad (\text{A.139})$$

$$\begin{aligned}
&= \frac{d}{dt} \mathbf{p}_s \\
&= \mathbf{0}_{m \times 1}.
\end{aligned}$$

71.

The virtual displacement B_5 associated with the velocity constraints (A.123) satisfies the following equation ([10, 51, 73, 81, 107, 124, 147, 155, 168])

$$\mathbf{G}\delta\mathbf{q} = \mathbf{0}_{m \times 1}, \quad (\text{A.140})$$

where $v_{sound}(t)$. It follows from (A.140) that B_5 is constrained to lie in the null space of the velocity constraints matrix \mathbf{G} .

72.

By using the kinematic model (A.134) an expression for the virtual displacement B_5 is obtained as follows ([51, 73, 107])

$$\delta\mathbf{q} = \mathbf{S}\delta\mathbf{q}_s, \quad (\text{A.141})$$

where $\delta\mathbf{q}_s$ is the independent virtual displacement associated with \mathbf{p}_s , (A.133), $\delta\mathbf{q}_s$ is not constrained, $\mathbf{a}_{gun}(t_{fire})$. Since the matrix \mathbf{S} has full column rank, (A.136), it follows that the linear transformation (A.141) is one-to-one (pp. 583–584, [80]). By employing (A.141), (A.135), Eq. (A.140) can be obtained as follows

$$\mathbf{G}\delta\mathbf{q} = \mathbf{G}\mathbf{S}\delta\mathbf{q}_s = \mathbf{0}_{m \times n_s}\delta\mathbf{q}_s = \mathbf{0}_{m \times 1} \Rightarrow \mathbf{G}\delta\mathbf{q} = \mathbf{0}_{m \times 1}. \quad (\text{A.142})$$

73. The virtual inertial position change of the center of mass of rigid body i , \mathbf{U}_ρ , and the vector of virtual infinitesimal rotations of the

body reference frame B_i , \mathbf{Q}_C , are related to the virtual displacement B_5 as follows ((A.104), (A.101), p. 476, [10], Chap.

4, [01])

$$\delta \mathbf{r}_i = \frac{\partial \mathbf{r}_i^{(I)}}{\partial \mathbf{q}} \delta \mathbf{q} = \frac{\partial \mathbf{v}_i^{(I)}}{\partial \dot{\mathbf{q}}} \delta \mathbf{q} = \mathbf{U}_{\tau,i} \delta \mathbf{q}, \quad (\text{A.143})$$

$$\delta \boldsymbol{\theta}_i = \frac{\partial \boldsymbol{\omega}_{B_i r I}^{(B_i)}}{\partial \dot{\mathbf{q}}} \delta \mathbf{q} = \mathbf{U}_{\rho,i} \delta \mathbf{q}, \quad (\text{A.144})$$

where $\delta \mathbf{r}_i \in \mathbb{R}^3$, $\delta \boldsymbol{\theta}_i \in \mathbb{R}^3$. Note that \mathbf{U}_ρ is expressed in the inertial reference frame I , and \mathbf{Q}_C is expressed in the body reference frame B_i .

74. For the multibody system consisting of N rigid bodies, Eqs. (A.143), (A.144), are expressed as follows

$$\delta \mathbf{r} = \mathbf{U}_\tau \delta \mathbf{q}, \quad (\text{A.145})$$

$$\delta \boldsymbol{\theta} = \mathbf{U}_\rho \delta \mathbf{q}, \quad (\text{A.146})$$

where

$$\delta \mathbf{r} = \begin{bmatrix} \delta \mathbf{r}_1 \\ \vdots \\ \delta \mathbf{r}_N \end{bmatrix}, \quad \delta \boldsymbol{\theta} = \begin{bmatrix} \delta \boldsymbol{\theta}_1 \\ \vdots \\ \delta \boldsymbol{\theta}_N \end{bmatrix}, \quad (\text{A.147})$$

$\delta \mathbf{r} \in \mathbb{R}^{3N}$, $\boldsymbol{\Omega}_{\boldsymbol{\varepsilon}_k} = \mathbb{R}^2$, and m_5 , \mathbf{U}_ρ , are given by (A.109), (A.115), respectively. Equations (A.145), (A.146), are expressed as follows

$$\begin{bmatrix} \delta \mathbf{r} \\ \delta \boldsymbol{\theta} \end{bmatrix} = \mathbf{U} \delta \mathbf{q}, \quad (\text{A.148})$$

where \mathbf{U} is given by (A.119). Since the matrix \mathbf{U} has full column rank, (A.120), it follows that the linear transformation (A.148) is one-to-one (pp. 583–584, [80]).

75.

Thus, given a value for the left-hand-side of (A.148). It follows that the inverse transformation yields a unique virtual displacement B_5 given by

$$\delta \mathbf{q} = (\mathbf{U}^\top \mathbf{U})^{-1} \mathbf{U}^\top \begin{bmatrix} \delta \mathbf{r} \\ \delta \boldsymbol{\theta} \end{bmatrix} \quad (\text{A.149})$$

(Theorem 11.5.1, pp. 144–145, Lemmas 9.2.8, 9.2.9, pp. 116–117, [80]). However, as mentioned above, the linear transformation (A.149) is in general not one-to-one.

76.

The velocity constraints of the multibody system expressed in terms of the variables \mathbf{v} and m are as follows ([81])

$$\mathbf{G}_1 \begin{bmatrix} \mathbf{v} \\ \boldsymbol{\omega} \end{bmatrix} = \mathbf{0}_{m \times 1}, \quad (\text{A.150})$$

where $\mathbf{G}_1 = \mathbf{G}_1(\mathbf{q}) \in \mathbb{R}^{m \times 6N}$. Equation (A.123) expresses the velocity constraints in terms of the variables \mathbf{q} and $\mathbf{p} = d\mathbf{q}/dt$, and can, in principle, be obtained by applying the one-to-one linear transformation (A.118) to Eq. (A.150) as follows ([81])

$$\mathbf{G}_1 \mathbf{U} \frac{d\mathbf{q}}{dt} = \mathbf{0}_{m \times 1}, \quad (\text{A.151})$$

$$\Rightarrow \mathbf{G} \mathbf{p} = \mathbf{0}_{m \times 1}, \quad (\text{A.152})$$

where $\mathbf{p} = \mathbf{0}_{15 \times 1}$.

77. Furthermore, it follows from (A.150) that $\mathbf{a}_b, \delta \boldsymbol{\theta}$, satisfy the following equation ([81])

$$(\text{A.153})$$

$$\mathbf{C} \begin{bmatrix} \delta \mathbf{r} \\ \delta \boldsymbol{\theta} \end{bmatrix} = \mathbf{0}$$

$$\mathbf{U}^T [\delta\theta] = \mathbf{0}_{m \times 1}.$$

Equation (A.140) expresses the constraints on the virtual displacement B_5 , and can, in principle, be obtained by applying the one-to-one linear transformation (A.148) to Eq. (A.153) as follows ([81])

$$\mathbf{G}_1 \mathbf{U} \delta \mathbf{q} = \mathbf{0}_{m \times 1}, \quad (\text{A.154})$$

$$\Rightarrow \mathbf{G} \delta \mathbf{q} = \mathbf{0}_{m \times 1}. \quad (\text{A.155})$$

Appendix B

Lagrange Equations for Constrained Rigid Multibody Systems Subject to Velocity Constraints that May Not be Independent

This Appendix presents some elements of the dynamics of constrained rigid multibody systems. The d'Alembert-Lagrange principle is applied in order to extend the Lagrange equations for the case of constrained rigid multibody systems subject to velocity constraints that may not be independent.

B.1 Dynamics of Constrained Rigid Multibody Systems

This Section summarizes some elements of the dynamics of constrained rigid multibody systems and builds upon the material on kinematics presented in Appendix A. The results are obtained mainly from [5, 7, 10, 13, 38, 51, 63, 64, 66, 73, 81, 94, 107, 125, 137, 147, 153, 168, 178, 181, 215]. Some related results and applications are given in [36, 39, 50, 74–76, 93, 117, 129, 150, 154, 167, 172, 179, 214]. The assumptions, results and methods employed are as follows.

1. The earth is a sphere with a uniform mass distribution, is non-rotating and is considered to be an inertial reference frame I with

an associated co-ordinate system (X, Y, Z) .

2.

A very small part of the surface of the earth is assumed to be locally flat and all rigid bodies move on or very close to this part of the surface of the earth. The origin of the inertial co-ordinate system (X, Y, Z) is fixed on the locally flat surface of the earth, the inertial (X, Y) plane is parallel to the surface of the earth and the Z axis is pointing upwards.

3.

The gravitational acceleration is constant and is given by ([12])

$$\mathbf{a}_{grav}^{(I)} = -g\mathbf{I}_3, \quad (\text{B.1})$$

where $g = 9.81 \text{ m/s}^2$.

4.

As stated in Appendix A, it is assumed throughout that $L_b > 0$, (A.117).

5.

It is assumed that the constrained rigid multibody system is disassembled into separate rigid bodies by removing all the constraining joints and contacts, and by replacing them with the relevant constraint forces and constraint torques acting on each separate rigid body ([10, 81, 107, 131, 144]). Some texts refer to the above process as the principle of constraint release (p. 267, [107]).

6.

In addition, the elements exerting applied forces and applied torques on the rigid bodies are removed and replaced with the relevant applied forces and applied torques acting on each separate rigid body. The applied forces and torques are exerted by actuators, springs, dampers, etc, and are assumed to be specified as functions of \mathbf{q} and $d\mathbf{p}/dt$ ([10, 81]).

7.

Lastly, the earth's (resultant) gravitational force acting at the center of mass of separate rigid body i is given by ([12])

$$\mathbf{F}_{grav,i}^{(I)} = -m_i g \mathbf{I}_3, \quad (\text{B.2})$$

where m_i is the constant mass of rigid body i , $m_i > 0$

where \mathcal{U}_i is the constant mass of rigid body i , $m_i \neq 0$.

8. Thus, all the forces and torques acting on each separate rigid body are classified as constraint forces and torques or as applied forces and torques or as the gravitational force. The above-mentioned collection of separate rigid bodies together with the forces and torques acting on each separate rigid body is referred to as the free-body diagram of the constrained rigid multibody system ([10, 131, 144]).
9. The resultant applied force and torque, and the resultant constraint force and torque acting on separate rigid body i are equal to the vector sum of the individual applied forces and torques, and to the vector sum of the individual constraint forces and torques acting on separate rigid body i , respectively, and are denoted as follows.
10. $\mathbf{F}_{A,i}^{(I)}$ denotes the resultant applied force acting at the center of mass of separate rigid body i , and $\mathbf{T}_{A,i}^{(B_i)}$ denotes the resultant applied torque acting about the center of mass of separate rigid body i .
11. $\mathbf{F}_{C,i}^{(I)}$ denotes the resultant constraint force acting at the center of mass of separate rigid body i , and $\mathbf{T}_{A,i}^{(B_i)}$ denotes the resultant constraint torque acting about the center of mass of separate rigid body i .
12. The resultant constraint force and torque $\mathbf{F}_{C,i}^{(I)}$ and $\mathbf{T}_{A,i}^{(B_i)}$ are such that the motion of each separate rigid body i is identical to its motion when it is part of the constrained rigid multibody system satisfying all the velocity constraints (A.123).
13. The resultant constraint force and torque $\mathbf{F}_{C,i}^{(I)}$ and $\mathbf{T}_{A,i}^{(B_i)}$ are not

known.

14.

It is assumed that the resultant applied force $\mathbf{F}_{A,i}^{(I)}$ and the resultant applied torque $\mathbf{T}_{A,i}^{(B_i)}$ are sufficiently smooth functions of \mathbf{q} , $d\mathbf{p}/dt$,

$$\mathbf{F}_{A,i}^{(I)} = \mathbf{F}_{A,i}^{(I)}(\mathbf{q}, d\mathbf{q}/dt) \in \mathbb{R}^3, \quad (\text{B.3})$$

$$\mathbf{T}_{A,i}^{(B_i)} = \mathbf{T}_{A,i}^{(B_i)}(\mathbf{q}, d\mathbf{q}/dt) \in \mathbb{R}^3. \quad (\text{B.4})$$

The resultant applied torque $\mathbf{T}_{A,i}^{(B_i)}$ is equal to the sum of the following torques.

a.

The sum of the torques about the center of mass of separate rigid body i resulting from the applied forces acting on separate rigid body i .

b.

The sum of the pure applied torques acting about the center of mass of separate rigid body i .

15. The free-body diagram is useful in determining expressions for the resultant applied force $\mathbf{F}_{A,i}^{(I)}$ and the resultant applied torque

$\mathbf{T}_{A,i}^{(B_i)}$ in terms of specified applied forces and torques acting on

separate rigid body i (see [10, 81, 147, 181], and example in Chap. 2). The resultant applied force $\mathbf{F}_{A,i}^{(I)}$ and the resultant applied

torque $\mathbf{T}_{A,i}^{(B_i)}$ are required in the computation of the vector of

generalized applied forces \mathbf{Q}_A that appears in the d'Alembert-Lagrange principle and in the Lagrange equations.

16.

In order to simplify the presentation the following notation is introduced

$$\mathbf{F}_A = \begin{bmatrix} \mathbf{F}_{A,1}^{(I)} \\ \vdots \\ \mathbf{F}_{A,N}^{(I)} \end{bmatrix}, \quad \mathbf{T}_A = \begin{bmatrix} \mathbf{T}_{A,1}^{(B_1)} \\ \vdots \\ \mathbf{T}_{A,N}^{(B_N)} \end{bmatrix}, \quad \mathbf{F}_{grav} = \begin{bmatrix} \mathbf{F}_{grav,1}^{(I)} \\ \vdots \\ \mathbf{F}_{grav,N}^{(I)} \end{bmatrix}, \quad (\text{B.5})$$

where $\mathbf{F}_A \in \mathbb{R}^{3N}$, $\mathbf{T}_A \in \mathbb{R}^{3N}$, $\mathbf{F}_{grav} = \mathbf{F}_{grav}(\mathbf{q}) \in \mathbb{R}^{3N}$.

17.

It can be shown that the virtual work of the applied forces and torques acting on separate rigid body i is given by ([10, 81, 147, 181])

$$\delta W_{A,i} = (\delta \mathbf{r}_i)^\top \mathbf{F}_{A,i}^{(I)} + (\delta \boldsymbol{\theta}_i)^\top \mathbf{T}_{A,i}^{(B_i)}, \quad i = 1, 2, \dots, N, \quad (\text{B.6})$$

where the \mathbf{U}_ρ , \mathbf{Q}_C , $(X_{B_i}, Y_{B_i}, Z_{B_i})$, satisfy Eq. (A.153), and using (A.147).

18.

By applying (A.143), (A.144), the virtual work $T_{\gamma_0} \mathbf{I}_3$, (B.6), is expressed in terms of B_5 as follows

$$\begin{aligned} \delta W_{A,i} &= (\delta \mathbf{q})^\top \mathbf{U}_{\tau,i}^\top \mathbf{F}_{A,i}^{(I)} + (\delta \mathbf{q})^\top \mathbf{U}_{\rho,i}^\top \mathbf{T}_{A,i}^{(B_i)} \\ &= (\delta \mathbf{q})^\top (\mathbf{U}_{\tau,i}^\top \mathbf{F}_{A,i}^{(I)} + \mathbf{U}_{\rho,i}^\top \mathbf{T}_{A,i}^{(B_i)}), \quad i = 1, 2, \dots, N, \end{aligned} \quad (\text{B.7})$$

where B_5 satisfies (A.140).

19. By using (A.145)–(A.147), and (B.5), the total virtual work of all the applied forces and torques acting on the N separate rigid bodies is given by ((B.7))

$$\begin{aligned} \delta W_A &= \sum_{i=1}^N \delta W_{A,i} \\ &= (\delta \mathbf{q})^\top \sum_{i=1}^N (\mathbf{U}_{\tau,i}^\top \mathbf{F}_{A,i}^{(I)} + \mathbf{U}_{\rho,i}^\top \mathbf{T}_{A,i}^{(B_i)}) \end{aligned} \quad (\text{B.8})$$

$$\begin{aligned}
& -(\delta \mathbf{q})^\top \sum_{i=1}^n (\mathbf{U}_{\tau,i}^\top \mathbf{F}_{A,i} + \mathbf{U}_{\rho,i}^\top \mathbf{T}_{A,i}) \quad (\text{B.8}) \\
& = (\delta \mathbf{q})^\top (\mathbf{U}_\tau^\top \mathbf{F}_A + \mathbf{U}_\rho^\top \mathbf{T}_A) \\
& = (\delta \mathbf{q})^\top \mathbf{Q}_A,
\end{aligned}$$

where B_5 satisfies (A.140), and \mathbf{Q}_A is the vector of generalized applied forces. Thus, it follows from (B.8) that \mathbf{Q}_A is given by

$$\mathbf{Q}_A = \mathbf{U}_\tau^\top \mathbf{F}_A + \mathbf{U}_\rho^\top \mathbf{T}_A, \quad (\text{B.9})$$

$$\mathbf{Q}_A = \mathbf{Q}_A(\mathbf{q}, d\mathbf{q}/dt) \in \mathbb{R}^n, \quad (\text{B.3})-(\text{B.4}).$$

20.

The vector of generalized applied forces \mathbf{Q}_A , (B.9), can generally be expressed as the sum of two terms as follows ([154])

$$\mathbf{Q}_A = \mathbf{Q}_{A_s} + \mathbf{B}_A \mathbf{u}_{control} \quad (\text{B.10})$$

where $\mathbf{Q}_{A_s} = \mathbf{Q}_{A_s}(\mathbf{q}, d\mathbf{q}/dt) \in \mathbb{R}^n$ is given as a function of \mathbf{q} and $d\mathbf{p}/dt$, $\mathbf{B}_A = \mathbf{B}_A(\mathbf{q}) \in \mathbb{R}^{n \times m_c}$ is given as a function of \mathbf{q} , $m_c = 4$, and $\mathbf{t} = \mathbf{t}_{hitC,1} = \mathbf{0}$ is the vector of applied forces and torques. The vector $e_{VhitT,k}$ is also referred to as the vector of control inputs and is used to control the constrained rigid multibody system. In some practical applications the number of control inputs, m_c , is equal to the number of independent generalized velocities, δ_3 ,

$$r_G \leq m. \quad (\text{B.11})$$

(see (A.130), (A.131), and the derivations for the mobile ADS in Chap. 4).

21. The angular momentum of separate rigid body i about its center of mass and expressed in body reference frame B_i , $\mathbf{L}_i^{(B_i)}$, is given

by (p. 423, [10], Chap. 5, [81])

$$\mathbf{L}_i^{(B_i)} = \mathcal{J}_i^{(B_i)} \boldsymbol{\omega}_{B_i I}^{(B_i)}, \quad (\text{B.12})$$

where $\mathbf{L}_i^{(B_i)} = \mathbf{L}_i^{(B_i)}(\mathbf{q}, d\mathbf{q}/dt) \in \mathbb{R}^3$, and $\mathcal{J}_i^{(B_i)} \in \mathbb{R}^{3 \times 3}$ denotes the constant inertia matrix of separate rigid body i about its center of mass and expressed in the body reference frame B_i . The inertia matrix $\mathcal{J}_i^{(B_i)}$ is symmetric, $\mathcal{J}_i^{(B_i)} = (\mathcal{J}_i^{(B_i)})^\top$, and positive definite, $\mathbf{I}_1^{(B_i)} = \mathbf{I}_1^{(B_i)}(\mathbf{q})$ (p. 328, [10]).

22.

By using (A.56), the time derivative of the angular momentum of separate rigid body i , $\mathbf{L}_i^{(B_i)}$, in the inertial reference frame I , and

expressed in the body reference frame B_i , is given by

$$\frac{d_I \mathbf{L}_i^{(B_i)}}{dt} = \frac{d_I \mathcal{J}_i^{(B_i)} \boldsymbol{\omega}_{B_i I}^{(B_i)}}{dt}, \quad (\text{B.13})$$

$$\Rightarrow \frac{d_I \mathbf{L}_i^{(B_i)}}{dt} = \mathcal{J}_i^{(B_i)} \frac{d_{B_i} \boldsymbol{\omega}_{B_i I}^{(B_i)}}{dt} + \boldsymbol{\omega}_{B_i I}^{(B_i)} \times (\mathcal{J}_i^{(B_i)} \boldsymbol{\omega}_{B_i I}^{(B_i)}). \quad (\text{B.14})$$

23.

For later use, define the following block-diagonal matrices

$$\mathbf{m} = \text{diag} (m_1 \mathbf{I}_3, \dots, m_N \mathbf{I}_3), \quad (\text{B.15})$$

$$\mathcal{J} = \text{diag} (\mathcal{J}_1^{(B_1)}, \dots, \mathcal{J}_N^{(B_N)}), \quad (\text{B.16})$$

where $\mathbf{m} \in \mathbb{R}^{3N \times 3N}$, $\mathcal{J} \in \mathbb{R}^{3N \times 3N}$.

24. Since the matrices $m_i \mathbf{I}_3$ and $\mathcal{J}_i^{(B_i)}$, $(X_{B_i}, Y_{B_i}, Z_{B_i})$, are all

symmetric and positive definite, it follows that the block-diagonal matrices r_d , (B.15), and \mathcal{J} , (B.16), are also symmetric and

positive definite

$$\mathbf{m} = \mathbf{m}^\top, \quad \det(\mathbf{m}) > 0, \quad \mathcal{J} = \mathcal{J}^\top, \quad \det(\mathcal{J}) > 0 \quad (\text{B.17})$$

(equations (3.3), (3.5), pp. 186–187, [80]).

25.

Let k_{mp} denote the following block-diagonal matrix

$$\mathbf{M}_0 = \begin{bmatrix} \mathbf{m} & \mathbf{0}_{3N \times 3N} \\ \mathbf{0}_{3N \times 3N} & \mathcal{J} \end{bmatrix}, \quad (\text{B.18})$$

$\mathbf{M}_0 \in \mathbb{R}^{6N \times 6N}$. Then it follows from the above that the block-diagonal matrix k_{mp} is symmetric and positive definite

$$\mathbf{M}_0 = \mathbf{M}_0^\top, \quad \det(\mathbf{M}_0) > 0. \quad (\text{B.19})$$

26.

The gravitational force given by (B.2) is conservative. It follows that the (gravitational) potential energy of separate rigid body i , \mathcal{V}_i , is given by ([12])

$$\mathcal{V}_i = m_i g r_{iz}^{(I)}. \quad (\text{B.20})$$

where $r_{iz}^{(I)}$ denotes the vertical or Z co-ordinate of the inertial position of the center of mass of separate rigid body i .

27.

The sum total of the potential energies of the N separate rigid bodies is given by

$$\mathcal{V}_{tot} = \sum_{i=1}^N \mathcal{V}_i. \quad (\text{B.21})$$

28. The kinetic energy of separate rigid body i is equal to the sum of the translational kinetic energy and the rotational kinetic energy

the translational kinetic energy and the rotational kinetic energy , and is given by ([10, 73, 81, 107, 147, 155, 168])

$$\mathcal{E}_i = \frac{1}{2}(\mathbf{v}_i^{(I)})^\top m_i \mathbf{I}_3 \mathbf{v}_i^{(I)} + \frac{1}{2}(\boldsymbol{\omega}_{B_i r I}^{(B_i)})^\top \mathcal{J}_i^{(B_i)} \boldsymbol{\omega}_{B_i r I}^{(B_i)}. \quad (\text{B.22})$$

29. The sum total of the kinetic energies of the N separate rigid bodies is given by ((B.22), (B.15)–(B.18))

$$(\text{B.23})$$

$$\begin{aligned} \mathcal{E}_{tot} &= \sum_{i=1}^N \mathcal{E}_i \\ &= \sum_{i=1}^N \left(\frac{1}{2}(\mathbf{v}_i^{(I)})^\top m_i \mathbf{I}_3 \mathbf{v}_i^{(I)} + \frac{1}{2}(\boldsymbol{\omega}_{B_i r I}^{(B_i)})^\top \mathcal{J}_i^{(B_i)} \boldsymbol{\omega}_{B_i r I}^{(B_i)} \right) \\ &= \frac{1}{2} \left(\mathbf{v}^\top \mathbf{m} \mathbf{v} + \boldsymbol{\omega}^\top \mathcal{J} \boldsymbol{\omega} \right) \\ &= \frac{1}{2} [\mathbf{v}^\top \ ; \ \boldsymbol{\omega}^\top] \begin{bmatrix} \mathbf{m} & \mathbf{0}_{3N \times 3N} \\ \mathbf{0}_{3N \times 3N} & \mathcal{J} \end{bmatrix} \begin{bmatrix} \mathbf{v} \\ \boldsymbol{\omega} \end{bmatrix} \\ &= \frac{1}{2} [\mathbf{v}^\top \ ; \ \boldsymbol{\omega}^\top] \mathbf{M}_0 \begin{bmatrix} \mathbf{v} \\ \boldsymbol{\omega} \end{bmatrix}, \end{aligned}$$

$\mathcal{E}_{tot} = \mathcal{E}_{tot}(\mathbf{v}, \boldsymbol{\omega}) \in \mathbb{R}$. Since the matrix k_{mp} is positive definite , (B.19), it follows that the total kinetic energy \mathcal{E}_{tot} of the multibody system, (B.23), is always positive, that is,

$$\mathcal{E}_{tot} > 0 \quad \text{for all} \quad \begin{bmatrix} \mathbf{v} \\ \boldsymbol{\omega} \end{bmatrix} \neq \mathbf{0}_{6N \times 1}. \quad (\text{B.24})$$

30. The total kinetic energy \mathcal{E}_{tot} , (B.23), is expressed in terms of \mathbf{q} , $d\mathbf{p}/dt$, by using (A.106), (A.113), as follows

$$\begin{aligned} \mathcal{E}_{tot} &= \frac{1}{2} \left(\frac{d\mathbf{q}}{dt} \right)^\top \left(\mathbf{U}_\tau^\top \mathbf{m} \mathbf{U}_\tau + \mathbf{U}_\rho^\top \mathcal{J} \mathbf{U}_\rho \right) \left(\frac{d\mathbf{q}}{dt} \right) \\ &= \frac{1}{2} \left(\frac{d\mathbf{q}}{dt} \right)^\top \left(\mathbf{U}^\top \mathbf{M}_0 \mathbf{U} \right) \left(\frac{d\mathbf{q}}{dt} \right), \end{aligned} \quad (\text{B.25})$$

$$\Rightarrow \mathcal{E}_{tot} = \frac{1}{2} \left(\frac{d\mathbf{q}}{dt} \right)^\top \mathbf{M} \left(\frac{d\mathbf{q}}{dt} \right) = \frac{1}{2} \mathbf{p}^\top \mathbf{M} \mathbf{p}, \quad (\text{B.26})$$

where

$$\mathbf{M} = \mathbf{U}_\tau^\top \mathbf{m} \mathbf{U}_\tau + \mathbf{U}_\rho^\top \mathcal{J} \mathbf{U}_\rho = \mathbf{U}^\top \mathbf{M}_0 \mathbf{U}, \quad (\text{B.27})$$

$\mathbf{M} = \mathbf{M}(\mathbf{q}) \in \mathbb{R}^{n \times n}$ is the mass matrix, $\mathcal{E}_{tot} = \mathcal{E}_{tot}(\mathbf{q}, d\mathbf{q}/dt) \in \mathbb{R}$.

31. The matrix k_{mp} is symmetric and positive definite, (B.19).

Furthermore, since it is assumed that the matrix \mathbf{U} has full column rank, (A.120), it follows that the matrix $\mathbf{M} = \mathbf{U}^\top \mathbf{M}_0 \mathbf{U}$, (B.27), is also symmetric and positive definite, that is,

$$\mathbf{M} = \mathbf{M}^\top, \quad \det(\mathbf{M}) > 0 \quad \text{and} \quad \mathbf{M}^{-1} \text{ exists} \quad (\text{B.28})$$

(Theorem 14.2.9, p. 213, [80], and Theorem 4.2.1, p. 140, [71]).

32. Since the mass matrix \mathbf{M} is symmetric and positive definite, (B.28), it follows that the inverse of the mass matrix, \mathbf{M}^{-1} , is

symmetric and positive definite, that is,

$$\rho_{sph,k} = \|\mathbf{r}_{M2targ,k}\| \sin(\phi_{cone0}), \quad k = 1, 2, \dots, n_f. \quad (\text{B.29})$$

(equations (2.4), (2.5), p. 82, and Theorem 13.3.7, p. 188, [80]).

33.

It follows from (B.26), (B.27), (B.28), that the total kinetic energy \mathcal{E}_{tot} expressed in terms of \mathbf{q} , $d\mathbf{p}/dt$, is always positive, that is,

$$\mathcal{E}_{tot} > 0 \quad \text{for all} \quad \frac{d\mathbf{q}}{dt} \neq \mathbf{0}_{n \times 1}. \quad (\text{B.30})$$

34.

Let \mathbf{q}_{d2} and \mathbf{q}_{d2} denote the following vectors ([10, 41, 73, 107, 129, 147, 155, 168])

$$\begin{aligned} \mathbf{W}_1 &= \left[\frac{d_I}{dt} \left(\frac{\partial \mathcal{E}_{tot}}{\partial \dot{q}_1} \right) - \frac{\partial \mathcal{E}_{tot}}{\partial q_1}, \dots, \frac{d_I}{dt} \left(\frac{\partial \mathcal{E}_{tot}}{\partial \dot{q}_n} \right) - \frac{\partial \mathcal{E}_{tot}}{\partial q_n} \right]^\top \\ &= \left[\frac{d_I}{dt} \left(\frac{\partial \mathcal{E}_{tot}}{\partial p_1} \right) - \frac{\partial \mathcal{E}_{tot}}{\partial q_1}, \dots, \frac{d_I}{dt} \left(\frac{\partial \mathcal{E}_{tot}}{\partial p_n} \right) - \frac{\partial \mathcal{E}_{tot}}{\partial q_n} \right]^\top, \end{aligned} \quad (\text{B.31})$$

$$\mathbf{W}_2 = \left[\frac{\partial \mathcal{V}_{tot}}{\partial q_1}, \dots, \frac{\partial \mathcal{V}_{tot}}{\partial q_n} \right]^\top, \quad (\text{B.32})$$

where $\mathbf{W}_1 = \mathbf{W}_1(\mathbf{q}, d\mathbf{q}/dt, d^2\mathbf{q}/dt^2) \in \mathbb{R}^n$, $\mathbf{W}_2 = \mathbf{W}_2(\mathbf{q}) \in \mathbb{R}^n$, and

\mathcal{E}_{tot} , \mathcal{V}_{tot} , are given by (B.26), (B.21). It follows from (B.31),

(B.32), (B.26), (B.21), that $\mathbf{W}_1 + \mathbf{W}_2$ simplifies to the following

form

$$\mathbf{W}_1 + \mathbf{W}_2 = \mathbf{M} \frac{d^2\mathbf{q}}{dt^2} + \mathbf{H} = \mathbf{M} \frac{d\mathbf{p}}{dt} + \mathbf{H}, \quad (\text{B.33})$$

where \mathbf{M} is given by (B.27), and $\mathbf{H} = \mathbf{H}(\mathbf{q}, d\mathbf{q}/dt) \in \mathbb{R}^n$.

35. It is assumed that the d'Alembert-Lagrange principle holds and is

given by ([5, 7, 10, 13, 35, 36, 38, 41, 51, 66, 73, 81, 99, 107, 124, 129, 137, 147, 153, 168])

$$(\delta \mathbf{q})^\top (\mathbf{W}_1 + \mathbf{W}_2 - \mathbf{Q}_A) = 0, \quad (\text{B.34})$$

where B_5 satisfies (A.140), and \mathbf{Q}_A is the vector of generalized applied forces given by (B.9).

36. Using the same methodology that was applied to obtain (B.9), the vector of generalized gravitational forces \mathbf{Q}_{grav} is given by

$$\mathbf{Q}_{grav} = \mathbf{U}_\tau^\top \mathbf{F}_{grav}, \quad (\text{B.35})$$

where \mathbf{V}_{TBS} is given by (B.5), and $\mathbf{Q}_{grav} = \mathbf{Q}_{grav}(\mathbf{q}) \in \mathbb{R}^n$. Note that in (B.33), the term \mathbf{H} includes the term $-\mathbf{Q}_{grav}$.

37. By using (B.33), (B.34), the d'Alembert-Lagrange principle is expressed in the following form

$$(\delta \mathbf{q})^\top \left(\mathbf{M} \frac{d^2 \mathbf{q}}{dt^2} + \mathbf{H} - \mathbf{Q}_A \right) = 0, \quad (\text{B.36})$$

where B_5 satisfies (A.140).

38. By using the relation (A.141), the d'Alembert-Lagrange principle (B.36) is expressed in terms of the independent virtual displacement $\delta \mathbf{q}_s$ as follows ([73, 107, 129])

$$(\delta \mathbf{q}_s)^\top \mathbf{S}^\top \left(\mathbf{M} \frac{d^2 \mathbf{q}}{dt^2} + \mathbf{H} - \mathbf{Q}_A \right) = 0. \quad (\text{B.37})$$

Since $\delta \mathbf{q}_s$ is not constrained, Eq. (B.37) must hold for all $\mathbf{a}_{gun}(t_{fire})$. Thus, the following equation must hold at each time t

$$\mathbf{S}^\top \left(\mathbf{M} \frac{d^2 \mathbf{q}}{dt^2} + \mathbf{H} - \mathbf{Q}_A \right) = \mathbf{0}. \quad (\text{B.38})$$

$$\mathbf{S}^T \left(\mathbf{M} \frac{d^2 \mathbf{q}}{dt^2} + \mathbf{H} - \mathbf{Q}_A \right) = \mathbf{0}_{n_s \times 1}. \quad (\text{B.30})$$

39. In [51], the d'Alembert-Lagrange principle is developed for the cases of nonlinear nonholonomic velocity constraints and acceleration constraints. The approach in reference [51] is to differentiate with respect to time in order to convert velocity constraints to acceleration constraints, and acceleration constraints to third order constraints. It is stated in [51] that the derivation of the above-mentioned results constitutes a proof of the Chetaev principle that was previously applied in the literature as an axiom (that is, without formal proof).
40. Consider the case where the actual motion trajectory of the constrained rigid multibody system is obtained via precise experimental measurements over a finite time horizon $t_{fire} + \Delta_f$ and denoted by

$$\left(\mathbf{q}(t), \frac{d\mathbf{q}(t)}{dt}, \frac{d^2\mathbf{q}(t)}{dt^2} \right), \quad t \in [t_0, t_{FIN}], \quad t_0 < t_{FIN}. \quad (\text{B.39})$$

Then, the measured motion trajectory (B.39) satisfies the following at each time t .

- a. The d'Alembert-Lagrange principle (B.36), (A.140), or equivalently Eq. (B.38), that is,

$$\mathbf{S}^T (\mathbf{M} d^2 \mathbf{q} / dt^2 + \mathbf{H} - \mathbf{Q}_A) = \mathbf{0}_{n_s \times 1}.$$

- b. The velocity constraints $\mathbf{G} d\mathbf{q} / dt = \mathbf{0}_{m \times 1}$, (A.123) (that is, the expression on the left-hand-side of (A.123) evaluates to the zero vector $\mathbf{0}_{m \times 1}$), and thus the acceleration constraints

$$\mathbf{G} d^2 \mathbf{q} / dt^2 + (d\mathbf{G} / dt) d\mathbf{q} / dt = \mathbf{0}_{m \times 1}, \quad (\text{A.138}).$$

- c. The kinematic model $d\mathbf{q} / dt = \mathbf{S} d\mathbf{q}_s / dt$, (A.134), and thus the acceleration kinematic model,

$$d^2 \mathbf{q} / dt^2 = \mathbf{S} d^2 \mathbf{q}_s / dt^2 + (d\mathbf{S} / dt) d\mathbf{q}_s / dt \quad (\text{A.137})$$

$$\frac{\partial \mathcal{L}}{\partial \mathbf{q}} - \frac{\partial \mathcal{L}}{\partial \mathbf{q}_s} + \left(\frac{\partial \mathcal{L}}{\partial \mathbf{v}} \right) \frac{\partial \mathbf{q}_s}{\partial \mathbf{v}}, \quad (\text{A.117})$$

- d. The conditions $L_b > 0$, (A.117), $\text{Rank}(\mathbf{G}) = r_G$, (A.124),
 $\text{Rank}(\mathbf{G}) = 11$, (A.136).

B.2 Lagrange Equations for Constrained Rigid Multibody Systems Subject to Velocity Constraints that May Not be Independent

A number of references ([10, 36, 107, 129, 147, 172, 179]) deal with the dynamic modelling of constrained rigid multibody systems whose motion is subject to independent velocity constraints in the form of (A.123), where $r_G = m$, (A.124).

In [62], the Lagrange equations are extended for constrained rigid multibody systems subject to velocity constraints that may not be independent. The derived Lagrange equations are given by

$$\mathbf{M} \frac{d^2 \mathbf{q}}{dt^2} + \mathbf{H} = \mathbf{Q}_A + \mathbf{G}^\top \boldsymbol{\lambda}, \quad (\text{B.40})$$

and by the velocity constraints (A.123), where $\boldsymbol{\lambda}$ is the vector of Lagrange multipliers, $\boldsymbol{\lambda} \in \mathbb{R}^m$.

Theorem B.1 Lagrange Equations for Constrained Rigid Multibody Systems Subject to Velocity Constraints That May Not be Independent Given a constrained rigid multibody system satisfying the assumptions and properties presented in Appendix A and Appendix B.

The measured motion trajectory of the constrained rigid multibody system denoted by $\mathbf{F}_{drag} \mathbf{J}_{v1} = \mathbf{J}_{v2} \frac{d^2 \mathbf{q}(t)}{dt^2}$, $\phi_{Y,k} = \phi_{cone,k}$, satisfies

at each time t the d'Alembert-Lagrange principle, that is,

$$\left(\mathbf{M} \frac{d^2 \mathbf{q}}{dt^2} + \mathbf{H} - \mathbf{Q}_A \right)^\top \delta \mathbf{q} = 0, \quad (\text{B.41})$$

where B_5 satisfies (A.140), if and only if there exists a vector λ called the vector of Lagrange multipliers, $\lambda \in \mathbb{R}^m$, such that

$$M \frac{d^2 \mathbf{q}}{dt^2} + \mathbf{H} = \mathbf{Q}_A + \mathbf{G}^\top \lambda, \quad (\text{B.42})$$

Proof The Proof of Theorem B.1 consists of two parts.

Part 1: Equations (B.42) and (A.140) imply Eq. (B.41).

By substituting the expression for the vector $M d^2 \mathbf{q} / dt^2 + \mathbf{H} - \mathbf{Q}_A$,

(B.42), into (B.41), and by using (A.140), it follows that

$$\begin{aligned} \left(M \frac{d^2 \mathbf{q}}{dt^2} + \mathbf{H} - \mathbf{Q}_A \right)^\top \delta \mathbf{q} &= (\mathbf{G}^\top \lambda)^\top \delta \mathbf{q} \\ &= \lambda^\top \mathbf{G} \delta \mathbf{q} \\ &= \lambda^\top \mathbf{0}_{m \times 1} \\ &= 0. \end{aligned} \quad (\text{B.43})$$

Part 2: Equations (B.41) and (A.140) imply Eq. (B.42).

The Proof of Part 2 is given in the following steps. Certain results from linear algebra are included for greater clarity.

1.

Let $J_{cost} = 0$ denote a column vector containing the elements of the i th row of the matrix \mathbf{G} , (A.123), $\mathbf{X}(t; t_{fire}, \mathbf{X}_0)$. Then the row space of the matrix \mathbf{G} is given by ([126])

$$\begin{aligned} \text{Row}(\mathbf{G}) = \{ \mathbf{x} \in \mathbb{R}^n : \mathbf{x} = w_1 \mathbf{g}_{r,1} + w_2 \mathbf{g}_{r,2} + \dots \\ + w_m \mathbf{g}_{r,m}, w_i \in \mathbb{R}, i = 1, 2, \dots, m \}. \end{aligned} \quad (\text{B.44})$$

2. Since the column vector $J_{cost} = 0$ contains the elements of the i th column of the matrix \mathbf{G}^\top , $\mathbf{X}(t; t_{fire}, \mathbf{X}_0)$, it follows that the column space of \mathbf{G}^\top equals the row space of \mathbf{G} ([126])

$$\text{Col}(\mathbf{G}^\top) = \text{Row}(\mathbf{G}). \quad (\text{B.45})$$

3. It further follows that (Corollary 30, p. 281, [126])

$$\gamma_0 = k_{mp}\gamma, \quad \zeta_0 = k_{mg}\zeta, \quad (\text{B.46})$$

4. In addition, it can be shown that (Theorem 21, p. 537, [126])

$$\text{Rank}(\mathbf{G}\mathbf{G}^\top) = \text{Rank}(\mathbf{G}^\top) = \text{Rank}(\mathbf{G}). \quad (\text{B.47})$$

5. The column vectors $J_{cost} = 0, i = 1, 2, \dots, m$, span the row space $\mathbf{p} = \mathbf{0}_{1 \times 1}$ and the column space $\text{Col}(\mathbf{G}^\top)$ ([126]), and are in general not linearly independent since $\text{Rank}(\mathbf{G}^\top) = \text{Rank}(\mathbf{G}) = r_G \leq m$, (A.124).

6. Given a vector $\mathbf{q} \in \mathbb{R}^n$ that lies in the column space $\text{Col}(\mathbf{G}^\top)$. Then it follows from (B.44), (B.45), that there exists a vector $\mathbf{w} \in \mathbb{R}^m$ such that ([126])

$$\mathbf{G}^\top \mathbf{w} = \mathbf{x}. \quad (\text{B.48})$$

- The vector y_i that satisfies (B.48) is in general not unique since $\text{Rank}(\mathbf{G}^\top) = \text{Rank}(\mathbf{G}) = r_G \leq m$, (A.124).

7. The null space of \mathbf{G} is given by ([126])

$$\text{Null}(\mathbf{G}) = \{\mathbf{y} \in \mathbb{R}^n : \mathbf{G}\mathbf{y} = \mathbf{0}_{m \times 1}\}. \quad (\text{B.49})$$

8. From (B.49), (B.44), (B.45), it follows that all the vectors in the null space $\text{Null}(\mathbf{G})$ are orthogonal to all the vectors in the

column space $\text{Col}(\mathbf{G}^T)$.

9. Thus, the orthogonal complement of the null space $\text{Null}(\mathbf{G})$ equals the column space $\text{Col}(\mathbf{G}^T)$, and is denoted as follows (Theorem 14, p. 516, [126])

$$(\text{Null}(\mathbf{G}))^\perp = \text{Col}(\mathbf{G}^T). \quad (\text{B.50})$$

10. From (A.140), (B.49), it follows that B_5 lies in the null space $\text{Null}(\mathbf{G})$. Furthermore, Eq. (B.41) implies that the vector $(M d^2 \mathbf{q}/dt^2 + \mathbf{H} - \mathbf{Q}_A)$ is orthogonal to B_5 . Thus, from the above it follows that the vector $(M d^2 \mathbf{q}/dt^2 + \mathbf{H} - \mathbf{Q}_A)$ lies in $(\text{Null}(\mathbf{G}))^\perp$ and hence in the column space $\text{Col}(\mathbf{G}^T)$, (B.50).

11. Thus, given the vector $(M d^2 \mathbf{q}/dt^2 + \mathbf{H} - \mathbf{Q}_A) \in \mathbb{R}^n$, there exists a vector $\boldsymbol{\lambda}$ called the vector of Lagrange multipliers, $\boldsymbol{\lambda} \in \mathbb{R}^m$, such that ((B.48))

$$M \frac{d^2 \mathbf{q}}{dt^2} + \mathbf{H} = \mathbf{Q}_A + \mathbf{G}^T \boldsymbol{\lambda}, \quad (\text{B.51})$$

The vector of Lagrange multipliers $\boldsymbol{\lambda}$ that satisfies (B.51) is in general not unique since $\text{Rank}(\mathbf{G}^T) = \text{Rank}(\mathbf{G}) = r_G \leq m$, (A.124).

12. If the velocity constraints are independent, that is, $r_G = m$, then the vector of Lagrange multipliers $\boldsymbol{\lambda}$ that satisfies (B.51) is unique

and is given by

$$\lambda = (\mathbf{G}\mathbf{G}^\top)^{-1}\mathbf{G}\left(\mathbf{M}\frac{d^2\mathbf{q}}{dt^2} + \mathbf{H} - \mathbf{Q}_A\right) \quad (\text{B.52})$$

(Theorem 11.5.1, pp. 144–145, Lemmas 9.2.8, 9.2.9, pp. 116–117, [80]).

13.

If the velocity constraints are not independent, that is, $r_G = m$ then the vector of Lagrange multipliers λ that satisfies (B.51) is not unique. =

Thus, the Lagrange equations are given by

$$\mathbf{M}\frac{d^2\mathbf{q}}{dt^2} + \mathbf{H} = \mathbf{Q}_A + \mathbf{G}^\top \lambda, \quad (\text{B.53})$$

and the velocity constraints ((A.123))

$$\mathbf{G}\frac{d\mathbf{q}}{dt} = \mathbf{0}_{m \times 1}. \quad (\text{B.54})$$

The vector of generalized constraint forces \mathbf{Q}_C is defined as follows ([147])

$$\mathbf{M}\frac{d^2\mathbf{q}}{dt^2} + \mathbf{H} = \mathbf{Q}_A + \mathbf{Q}_C, \quad (\text{B.55})$$

where $\mathbf{Q}_C = [Q_{C1}, Q_{C2}, \dots, Q_{Cn}]^\top \in \mathbb{R}^n$. By using (B.33), (B.27), (B.9), a unique vector of expressions is derived for the right-hand-side of (B.55) as a function of \mathbf{q} , $d\mathbf{p}/dt$, $\mathbf{r} \in \mathbb{R}^{3N}$. Thus, the vector of generalized constraint forces \mathbf{Q}_C is equal to a unique vector of expressions, implying that

$$\mathbf{Q}_C \text{ is unique.} \quad (\text{B.56})$$

From (B.51), (B.55), it follows that

$$\mathbf{Q}_C = \mathbf{G}^\top \boldsymbol{\lambda}, \quad (\text{B.57})$$

As mentioned above, given \mathbf{G} and \mathbf{Q}_C in (B.57), the vector of Lagrange multipliers $\boldsymbol{\lambda}$ that satisfies (B.57) is in general not unique since

$\text{Rank}(\mathbf{G}^\top) = \text{Rank}(\mathbf{G}) = r_G \leq m$, (A.124). However, since the vector of generalized constraint forces \mathbf{Q}_C is unique, (B.56), it follows from (B.57) that

$$\text{the product } \mathbf{G}^\top \boldsymbol{\lambda} \text{ is unique.} \quad (\text{B.58})$$

If the measured motion trajectory of the constrained rigid multibody system, (B.39), is substituted in the expressions on the right-hand-side of (B.55) then at each time t the expression $\mathbf{M}d^2\mathbf{q}/dt^2 + \mathbf{H} - \mathbf{Q}_A$

evaluates to a unique real vector in \mathbf{T}_d representing the vector of generalized constraint forces \mathbf{Q}_C . Thus, a total of n generalized constraint force components are obtained at each time t .

If there are no velocity constraints, (A.123), on the motion of the multibody system then it follows from (B.41), (A.140), that the Lagrange equations are given by

$$\mathbf{M} \frac{d^2\mathbf{q}}{dt^2} + \mathbf{H} = \mathbf{Q}_A. \quad (\text{B.59})$$

B.3 On the Solution of Consistent Simultaneous Linear Equations

Consider the following problem. Compute the vector $m_i > 0$ satisfying the following set of consistent simultaneous linear equations (SLEs)

$$\mathbf{E}\mathbf{y} = \mathbf{x}, \quad (\text{B.60})$$

where the matrix $\mathbf{E} \in \mathbb{R}^{m \times n}$ and the vector $\mathbf{x} \in \mathbb{R}^m$ are specified. Note that the variables m, n, δ_3 , are used in this Section generically.¹ The given SLEs, (B.60), are consistent implying that ([126])

$$\text{Rank}([\mathbf{E} : \mathbf{x}]) = \text{Rank}(\mathbf{E}). \quad (\text{B.61})$$

The matrix \mathbf{Z} does not necessarily have full rank, that is,

$$\text{Rank}(\mathbf{E}) = r_E \in \{1, 2, \dots, \min(m, n)\}. \quad (\text{B.62})$$

The homogeneous system associated with (B.60) is given by

$$\mathbf{Q}_C = \mathbf{G}^\top \boldsymbol{\lambda}, \quad (\text{B.63})$$

where $\mathbf{y} \in \mathbf{B}_0$. The null space of \mathbf{Z} is the solution set of the homogeneous system (B.63) ([65]). The relation between the dimension of the null space of \mathbf{Z} , $\text{Dim}(\text{Null}(\mathbf{E}))$, and $(\mathbf{I}_1, \mathbf{I}_2, \mathbf{I}_3)$ is given by (Theorem 31, p. 281, [126])

$$\text{Rank}(\mathbf{E}) + \text{Dim}(\text{Null}(\mathbf{E})) = \text{number of columns of } \mathbf{E} = n. \quad (\text{B.64})$$

Using (B.62), (B.64), it follows that

$$\text{Dim}(\text{Null}(\mathbf{E})) = n_s = n - r_E. \quad (\text{B.65})$$

If $\zeta_{ref}(t)$ and $\text{Rank} \mathbf{P}(\boldsymbol{\Xi}_{j_v}; i)$ then the SLEs, (B.60), have a unique solution. In addition, if $\zeta_{ref}(t)$ and $\text{Rank}(\mathbf{E}) = n$ then the SLEs have a unique solution. In the following cases the SLEs have an infinite number of solutions ([65]).

1. $\zeta_{ref}(t)$ and $m_\rho = 1$.
2. $\zeta_{ref}(t)$ and $m_\rho = 1$.
3. $\zeta_{ref}(t)$ and $m_\rho = 1$.

4. $\zeta_{ref}(t)$ and $y_1 \in \mathbb{R}$.

In the above-mentioned cases the solution set of (B.60) consists of a general solution given by ([65, 80])

$$\mathbf{y}_{sol} = \mathbf{y}_p + \mathbf{y}_h, \quad (\text{B.66})$$

where α_s denotes a particular solution of (B.60), $\dot{\alpha}_{s,ref}(t)$, and B_i denotes a general solution of the homogeneous system (B.63), $k_{mg} > 1$ ([65, 126]). In order to simplify the presentation, B_i will be referred to as a homogeneous solution, (B.63). In the sequel, two alternative methods are presented for determining a general solution of (B.60).

B.3.1 On the Solution of Consistent SLEs by Partitioning the Variables into Independent and Dependent Variables

The basic methodology for computing a general solution of (B.60) is as follows.

First, select δ_3 , (B.65), of the elements of ζ to be independent variables and group them into a vector δ_v as follows

$$\mathbf{y}_I = \mathbf{C}_I \mathbf{y} \in \mathbb{R}^{n_s}, \quad (\text{B.67})$$

where $\mathbf{C}_I \in \mathbb{R}^{n_s \times n}$, and such that

$$\text{Rank} \left(\begin{bmatrix} \mathbf{E} \\ \mathbf{C}_I \end{bmatrix} \right) = n_s + r_E = n. \quad (\text{B.68})$$

The remaining $(\mathbf{E}) = n$ elements of ζ are the dependent variables and are grouped into a vector \mathbf{T}_d as follows

$$\mathbf{y}_D = \mathbf{C}_D \mathbf{y} \in \mathbb{R}^{n-n_s}, \quad (\text{B.69})$$

where $\mathbf{C}_D \in \mathbb{R}^{(n-n_s) \times n}$. Thus, each element of δ_v and of \mathbf{T}_d is equal to a unique element of ζ .

Second, set the above-mentioned independent variables δ_v equal to δ_3 parameters $\mathbf{J}_{hitT,k}(\boldsymbol{\varepsilon}_k(\omega_k))$, leading to the following linear system in ζ

$$\mathbf{C}_I \mathbf{y} = \mathbf{w} = \begin{bmatrix} w_1 \\ w_2 \\ \vdots \\ w_{n_s} \end{bmatrix} \in \mathbb{R}^{n_s}. \quad (\text{B.70})$$

Third, construct the augmented matrix $\mathbf{D}(k)$ associated with the joint linear systems (B.60) and (B.70) in ζ , consisting of a total of $\mathbf{p}_s \in \mathbb{R}^{n_s}$ SLEs, as follows ([65])

$$\mathbf{X}_{aug} = \begin{bmatrix} \mathbf{E} & \vdots & \mathbf{x} \\ \mathbf{C}_I & \vdots & \mathbf{w} \end{bmatrix} \in \mathbb{R}^{(m+n_s) \times (n+1)}. \quad (\text{B.71})$$

Fourth, by applying elementary row operations, transform the matrix $\mathbf{D}(k)$ to reduced row echelon form given by ([65])

$$\mathbf{X}_{rref} = \begin{bmatrix} \mathbf{I}_n \in \mathbb{R}^{(r_E+n_s) \times n} & \vdots & \mathbf{y}_{sol} \in \mathbb{R}^{n \times 1} \\ \mathbf{0}_{(m-r_E) \times n} & \vdots & \mathbf{0}_{(m-r_E) \times 1} \end{bmatrix} \in \mathbb{R}^{(m+n_s) \times (n+1)}. \quad (\text{B.72})$$

Fifth, the expression for B_{10} is obtained from the last column of the matrix $(X_{B_{10}}$ and is assumed to be in the following parametric form ([65], (B.66))

$$\mathbf{y}_{sol} = \mathbf{y}_p + \mathbf{S}\mathbf{w} \Rightarrow \mathbf{y}_h = \mathbf{S}\mathbf{w}, \quad (\text{B.73})$$

where $\mathbf{S} \in \mathbb{R}^{n \times n_s}$ is the null space matrix and $\det(\mathbf{M}) > 0$, and where

$$E\mathbf{y}_p = \mathbf{x}, \quad (\text{B.74})$$

$$E\mathbf{y}_h = E\mathbf{S}\mathbf{w} = \mathbf{0}_{m \times n_s}\mathbf{w} = \mathbf{0}_{m \times 1}. \quad (\text{B.75})$$

The null space matrix \mathbf{S} has full column rank and the δ_3 columns of \mathbf{S} are a basis for the null space of the matrix \mathbf{Z} ([65, 126])

$$\text{Null}(\mathbf{E}) = \text{Col}(\mathbf{S}), \quad \text{Rank}(\mathbf{S}) = n_s = n - r_E. \quad (\text{B.76})$$

The solution set of (B.60) is expressed in terms of (B.73) as follows ([65])

$$H_{12} = ***, \quad H_{13} = ***. \quad (\text{B.77})$$

It follows from (B.67), (B.70), (B.69) and (B.73), that the solution for the dependent variables \mathbf{T}_d can be expressed in terms of the solution for the independent variables δ_v and thus in terms of the vector of parameters y_i as follows

$$\mathbf{y}_{Isol} = \mathbf{w}, \quad \mathbf{y}_{Dsol} = \mathbf{C}_D\mathbf{y}_{sol} = \mathbf{C}_D\mathbf{y}_p + \mathbf{C}_D\mathbf{S}\mathbf{w}. \quad (\text{B.78})$$

The particular solution α_s and the null space matrix \mathbf{S} have a specific form or structure that depends on which elements of ζ have been chosen to be independent variables, (B.67), (B.70).

For example, assume that the i th element of the vector ζ is selected to be the first independent variable which is then set equal to \mathbf{T}_d , (B.67), (B.70). It follows that the i th element of α_s will be equal to 0, and the i th element of B_i will be equal to \mathbf{T}_d . Thus, the null space matrix \mathbf{S} will have an i th row whose first element is 1 and all the remaining elements are zeros.

In order to illustrate the above, and without loss of generality, consider the case where the last δ_3 elements of ζ are selected as the independent variables as follows

$$\mathbf{y} = \begin{bmatrix} \mathbf{y}_D \\ \mathbf{y}_I \end{bmatrix}, \quad \mathbf{y}_D = \begin{bmatrix} y_1 \\ y_2 \\ \vdots \\ y_{n-n_s} \end{bmatrix} \in \mathbb{R}^{n-n_s}, \quad \mathbf{y}_I = \begin{bmatrix} y_{n-n_s+1} \\ y_{n-n_s+2} \\ \vdots \\ y_n \end{bmatrix} \in \mathbb{R}^{n_s}, \quad (\text{B.79})$$

$$\mathbf{y}_I = \mathbf{C}_I \mathbf{y} = \mathbf{w}, \quad \mathbf{C}_I = [\mathbf{0}_{n_s \times (n-n_s)} \vdots \mathbf{I}_{n_s}], \quad (\text{B.80})$$

$$\mathbf{y}_D = \mathbf{C}_D \mathbf{y}, \quad \mathbf{C}_D = [\mathbf{I}_{n-n_s} \vdots \mathbf{0}_{(n-n_s) \times n_s}] \quad (\text{B.81})$$

(and assuming that (B.68) holds). In this case, the resulting structures of α_s , B_i and \mathbf{S} are as follows

$$\mathbf{y}_p = \begin{bmatrix} \mathbf{y}_{p1} \\ \mathbf{0}_{n_s \times 1} \end{bmatrix}, \quad \mathbf{y}_h = \begin{bmatrix} \mathbf{y}_{h1} \\ \mathbf{w} \end{bmatrix} = \mathbf{S} \mathbf{w} = \begin{bmatrix} \mathbf{S}_1 \\ \mathbf{I}_{n_s} \end{bmatrix} \mathbf{w}, \quad (\text{B.82})$$

where $\mathbf{y}_{p1} \in \mathbb{R}^{n-n_s}$, $\mathbf{y}_{h1} \in \mathbb{R}^{n-n_s}$, and $\mathbf{S}_1 \in \mathbb{R}^{(n-n_s) \times n_s}$. Thus, it follows

that

$$\begin{aligned} \mathbf{y}_{sol} &= \mathbf{y}_p + \mathbf{y}_h \\ &= \begin{bmatrix} \mathbf{y}_{p1} \\ \mathbf{0}_{n_s \times 1} \end{bmatrix} + \begin{bmatrix} \mathbf{S}_1 \\ \mathbf{I}_{n_s} \end{bmatrix} \mathbf{w} \\ &= \begin{bmatrix} \mathbf{y}_{p1} + \mathbf{S}_1 \mathbf{w} \\ \mathbf{w} \end{bmatrix}, \end{aligned} \quad (\text{B.83})$$

$$\Rightarrow \mathbf{y}_{Isol} = \mathbf{w}, \quad \mathbf{y}_{Dsol} = \mathbf{y}_{p1} + \mathbf{S}_1 \mathbf{w}. \quad (\text{B.84})$$

If $\mathbf{x} = \mathbf{0}_{m \times 1}$ in (B.60) then a homogeneous system is obtained. In this

case, $\mathbf{y}_p = \mathbf{0}_{n \times 1}$, (B.73), and a general solution of (B.60) is given by

$$\mathbf{y}_{sol} = \mathbf{S}\mathbf{w}. \quad (\text{B.85})$$

If $\zeta_{ref}(t)$ and $\text{Rank } \mathbf{P}(\mathcal{E}_{j_v}; i)$, (B.60), then the SLEs have a unique solution given by

$$\mathbf{y}_{sol} = \mathbf{E}^{-1}\mathbf{x}. \quad (\text{B.86})$$

The matrix inverse \mathbf{E}^{-1} in (B.86) can be computed by first forming the following special augmented matrix ([65])

$$\mathbf{Y}_{aug} = [\mathbf{E} : \mathbf{I}_m] \in \mathbb{R}^{m \times 2m}. \quad (\text{B.87})$$

Then, the reduced row echelon form of $\boldsymbol{\eta}_i(t)$ is obtained and is given by

$$\mathbf{Y}_{rref} = [\mathbf{I}_m : \mathbf{E}_{sol}] \in \mathbb{R}^{m \times 2m}. \quad (\text{B.88})$$

The expression for the matrix inverse \mathbf{E}^{-1} is obtained from the matrix $\mathbf{Z}_{B_{10}}$, (B.88), $\mathbf{E}^{-1} = \mathbf{E}_{sol}$.

If $\zeta_{ref}(t)$ and $\text{Rank } (\mathbf{E}) = n$, (B.60), then the SLEs have a unique solution given by

$$\mathbf{y}_{sol} = (\mathbf{E}^\top \mathbf{E})^{-1} \mathbf{E}^\top \mathbf{x}. \quad (\text{B.89})$$

The matrix inverse in (B.89) is computed by applying the methodology described by (B.87), (B.88).

The scientific computing systems Maple ([16]), MATLAB/MATLAB Symbolic Toolbox ([110, 112]) can be used to practically perform the above computations for cases where the elements of \mathbf{Z} , \mathbf{q} , in (B.60) are numerical and/or symbolic expressions ([33, 91]).

B.3.2 On the Solution of Consistent SLEs by using the Moore-Penrose Generalized Inverse

A particular solution of (B.60) having a specific property is presented first. Thereafter, a general solution of (B.60) is given.

The particular solution of (B.60) that has minimum Euclidean norm for any value of $(\mathbf{I}_1, \mathbf{I}_2, \mathbf{I}_3)$, (B.62), is given by ([80], pp. 568–570, [126])

$$\mathbf{y}_p = \mathbf{E}^{MP} \mathbf{x} = \text{unique vector in } \mathbb{R}^n, \quad (\text{B.90})$$

where \mathbf{E}^{MP} denotes the Moore-Penrose generalized inverse of the matrix \mathbf{Z} , $\mathbf{E}^{MP} \in \mathbb{R}^{n \times m}$, $\|\mathbf{E}^{MP} \mathbf{x}\| \leq \|\mathbf{y}_e\|$ where δ_3 is any given exact solution of (B.60), and $\|\mathbf{c}\|$ denotes the magnitude or Euclidean norm of $m_i > 0$ given by

$$\|\mathbf{c}\| = \sqrt{c_1^2 + \dots + c_n^2}. \quad (\text{B.91})$$

The Moore-Penrose generalized inverse \mathbf{E}^{MP} is unique and satisfies the four Moore-Penrose conditions ([80], p. 570, [126]) as follows

$$1. \quad \mathbf{E}\mathbf{E}^{MP}\mathbf{E} = \mathbf{E} \quad (\text{B.92})$$

$$2. \quad \mathbf{E}^{MP}\mathbf{E}\mathbf{E}^{MP} = \mathbf{E}^{MP} \quad (\text{B.93})$$

$$3. \quad (\mathbf{E}\mathbf{E}^{MP})^\top = \mathbf{E}\mathbf{E}^{MP} \quad (\text{B.94})$$

$$3. \quad (\mathbf{E}\mathbf{E}^{MP})^\top = \mathbf{E}\mathbf{E}^{MP} \quad (\text{B.95})$$

A generalized inverse of \mathbf{Z} that satisfies only some of the Moore-Penrose conditions 1. to 4., (B.92)–(B.95), for example, conditions 1., 2. and 3., is denoted by $\mathbf{E}^{\{1,2,3\}}$, and similarly for other combinations of the Moore-Penrose conditions ([80]). All such generalized inverses are not unique, except for $\mathbf{E}^{\{1,2,3,4\}} = \mathbf{E}^{MP}$.

A generalized inverse $\mathbf{E}^{\{1,4\}}$ is called a minimum Euclidean norm generalized inverse of \mathbf{Z} , and is not unique. However, the product $\mathbf{E}^{\{1,4\}} \mathbf{x}$ is the minimum Euclidean norm solution of (B.60) (Theorem

20.3.6, pp. 497–498, [80]), and is unique, that is,

$$\mathbf{E}^{(1,4)} \mathbf{x} = \mathbf{E}^{MP} \mathbf{x}. \quad (\text{B.96})$$

If the matrix \mathbf{Z} is square, $\zeta_{ref}(t)$, and $\text{Rank}(\mathbf{E}) = m$, then \mathbf{E}^{MP} equals the ordinary inverse of \mathbf{Z} , $\mathbf{E}^{MP} = \mathbf{E}^{-1}$.

One method for computing numerically the Moore-Penrose generalized inverse \mathbf{E}^{MP} is the following.

1. Compute the singular value decomposition of the matrix \mathbf{Z} , (B.60), given by (Theorem 30, pp. 567–568, [126])

$$\mathbf{E} = \mathbf{V}_2 \boldsymbol{\Sigma} \mathbf{V}_1^\top, \quad (\text{B.97})$$

where $\mathbf{V}_2 \in \mathbb{R}^{m \times m}$, $\mathbf{V}_1 \in \mathbb{R}^{n \times n}$ are orthogonal matrices, the matrix $\boldsymbol{\Sigma} \in \mathbb{R}^{m \times n}$, is given by

$$\boldsymbol{\Sigma} = \begin{bmatrix} \mathbf{D}_0 & \vdots & \mathbf{0}_{r_E \times (n-r_E)} \\ \mathbf{0}_{(m-r_E) \times r_E} & \vdots & \mathbf{0}_{(m-r_E) \times (n-r_E)} \end{bmatrix}, \quad (\text{B.98})$$

$\mathbf{D}_0 \in \mathbb{R}^{r_E \times r_E}$ is a diagonal matrix given by

$$\mathbf{D}_0 = \text{diag}(\sigma_1, \dots, \sigma_{r_E}), \quad (\text{B.99})$$

and where $\sigma_1 \geq \sigma_2 \geq \dots \geq \sigma_{r_E} > 0$ are the positive singular values of \mathbf{Z} , (B.60), $y_1 \in \mathbb{R}$, (B.62).

2. Compute the Moore-Penrose generalized inverse $\mathbf{E}^{MP} \in \mathbb{R}^{n \times m}$ as follows

$$\mathbf{E}^{MP} = \mathbf{V}_1 \boldsymbol{\Sigma}^{MP} \mathbf{V}_2^\top, \quad (\text{B.100})$$

where the matrix $\boldsymbol{\Sigma}^{MP} \in \mathbb{R}^{n \times m}$ is given by

$$\boldsymbol{\Sigma}^{MP} = \begin{bmatrix} \mathbf{D}_0^{-1} & \vdots & \mathbf{0}_{r_E \times (m-r_E)} \\ \mathbf{0}_{(n-r_E) \times r_E} & \vdots & \mathbf{0}_{(n-r_E) \times (m-r_E)} \end{bmatrix}, \quad (\text{B.101})$$

and \mathbf{A}_f is the diagonal matrix specified in (B.99).

An alternative definition of the Moore-Penrose generalized inverse \mathbf{E}^{MP} is given by ([80])

$$\begin{aligned}\mathbf{E}^{MP} &= \lim_{\epsilon \rightarrow 0} \left((\mathbf{E}^\top \mathbf{E} + \epsilon^2 \mathbf{I}_n)^{-1} \mathbf{E}^\top \right) \\ &= \lim_{\epsilon \rightarrow 0} \left(\mathbf{E}^\top (\mathbf{E} \mathbf{E}^\top + \epsilon^2 \mathbf{I}_m)^{-1} \right).\end{aligned}\tag{B.102}$$

If the elements of the matrix \mathbf{Z} are rational numbers then the Moore-Penrose generalized inverse \mathbf{E}^{MP} is computed analytically by applying (B.102) as follows

$$\mathbf{E}^{MP} = \begin{cases} \lim_{\epsilon \rightarrow 0} \left((\mathbf{E}^\top \mathbf{E} + \epsilon^2 \mathbf{I}_n)^{-1} \mathbf{E}^\top \right) & \text{if } m > n \\ \lim_{\epsilon \rightarrow 0} \left(\mathbf{E}^\top (\mathbf{E} \mathbf{E}^\top + \epsilon^2 \mathbf{I}_m)^{-1} \right) & \text{if } m \leq n \end{cases}.\tag{B.103}$$

If the elements of \mathbf{Z} contain symbolic expressions then \mathbf{E}^{MP} is computed by using (B.103), and where the matrix inverse in (B.103) is computed by using the methodology described by (B.87), (B.88).

However, these computations can potentially become impractical due to increasing computation time and increasing complexity of the resulting symbolic expressions. For the special case where $\boldsymbol{\varepsilon}_k = \mathbf{0}_{2 \times 1}$,

$\mathbf{x} = \mathbf{0}_{m \times 1}$, $\text{Rank}(\mathbf{E}) = 0$, it follows that $\mathbf{E}^{MP} = \mathbf{0}_{n \times m}$, $\mathbf{y}_p = \mathbf{0}_{n \times 1}$,

(B.90).

In summary, the six main cases of the SLEs, (B.60), and the corresponding properties of the particular solution α_s , (B.90), are as follows.

1. **Case P1:** The number of SLEs, (B.60), equals the number of variables, $\zeta_{ref}(t)$, and the matrix \mathbf{Z} has full rank, $\text{Rank}(\mathbf{E}) = m$.
 - a. The SLEs, (B.60), have a unique solution.
 - b. The inverse of \mathbf{Z} exists.

- c. α_s , (B.90), is the unique solution of (B.60) and $E^{MP} = E^{-1}$.
2. **Case P2:** The number of SLEs, (B.60), equals the number of variables, $\zeta_{ref}(t)$, and the matrix Z does not have full rank, $\text{Rank}(E) = m$.
- a. The SLEs, (B.60), do not have a unique solution.
- b. The inverse of Z does not exist.
- c. α_s , (B.90), is the exact solution of (B.60) having minimum Euclidean norm.
3. **Case P3:** The number of SLEs, (B.60), is less than the number of variables, $\zeta_{ref}(t)$, and the matrix Z has full rank, $\text{Rank}(E) = m$.
- a. The SLEs, (B.60), do not have a unique solution.
- b. It follows that $\text{Rank}(EE^T) = \text{Rank}(E) = m$, (B.47), and the square matrix $EE^T \in \mathbb{R}^{m \times m}$ is invertible.
- c. α_s , (B.90), is the exact solution of (B.60) having minimum Euclidean norm and $E^{MP} = E^T(EE^T)^{-1}$.
4. **Case P4:** The number of SLEs, (B.60), is less than the number of variables, $\zeta_{ref}(t)$, and the matrix Z does not have full rank, $\text{Rank}(E) = m$.
- a. The SLEs, (B.60), do not have a unique solution.

- , (B.47), as the unique solution.
- b. The inverse of $(\mathbf{E}\mathbf{E}^\top)$ does not exist.
 - c. α_s , (B.90), is the exact solution of (B.60) having minimum Euclidean norm.
5. **Case P5:** The number of SLEs, (B.60), is greater than the number of variables, $\zeta_{ref}(t)$, and the matrix \mathbf{Z} has full rank, $\text{Rank}(\mathbf{E}) = n$.
- a. The SLEs, (B.60), have a unique solution.
 - b. It follows that $\text{Rank}(\mathbf{E}^\top \mathbf{E}) = \text{Rank}(\mathbf{E}) = n$, (B.47), and the square matrix $\mathbf{E}^\top \mathbf{E} \in \mathbb{R}^{n \times n}$ is invertible.
 - c. α_s , (B.90), is the unique solution of (B.60) and
$$\mathbf{E}^{MP} = \mathbf{E}^\top (\mathbf{E}\mathbf{E}^\top)^{-1}.$$
6. **Case P6:** The number of SLEs, (B.60), is greater than the number of variables, $\zeta_{ref}(t)$, and the matrix \mathbf{Z} does not have full rank, $\text{Rank}(\mathbf{E}) = 0$.
- a. The SLEs, (B.60), do not have a unique solution.
 - b. The inverse of $(\mathbf{E}\mathbf{E}^\top)$ does not exist.
 - c. α_s , (B.90), is the exact solution of (B.60) having minimum Euclidean norm.

A general solution of (B.60) is given by (p. 141, [80])

$$\mathcal{A}_{Ind,k} \subset \mathbf{D}(k), \quad k = 1, 2, \dots, n_f, \quad (\text{B.104})$$

where the vector of parameters $\beta(t) [u_1, \dots, u_n]^\top \in \mathbb{R}^n$. With reference to (B.66), (B.104), a particular solution α_s and a homogeneous solution B_i are given by

$$\mathbf{y}_{sol} = \mathbf{y}_p + \mathbf{y}_h \Rightarrow \mathbf{y}_p = \mathbf{E}^{MP} \mathbf{x}, \quad \mathbf{y}_h = (\mathbf{I}_n - \mathbf{E}^{MP} \mathbf{E}) \mathbf{u}. \quad (\text{B.105})$$

It follows that (by using (B.92))

$$\mathbf{E} \mathbf{y}_p = \mathbf{E} \mathbf{E}^{MP} \mathbf{x} = \mathbf{x}, \quad (\text{B.106})$$

$$\mathbf{E} \mathbf{y}_h = \mathbf{E} (\mathbf{I}_n - \mathbf{E}^{MP} \mathbf{E}) \mathbf{u} = \mathbf{0}_{m \times n} \mathbf{u} = \mathbf{0}_{m \times 1}. \quad (\text{B.107})$$

By using (B.105), (B.93), (B.95), it can be shown that α_s is perpendicular to B_i , that is, $t_{hitC,k} = 14$, as follows

$$\begin{aligned} \mathbf{y}_p \cdot \mathbf{y}_h &= \mathbf{y}_p^\top \mathbf{y}_h = \mathbf{x}^\top ((\mathbf{E}^{MP})^\top - (\mathbf{E}^{MP})^\top \mathbf{E}^\top (\mathbf{E}^{MP})^\top) \mathbf{u} \\ &= \mathbf{x}^\top \mathbf{0}_{m \times n} \mathbf{u} \\ &= 0, \end{aligned} \quad (\text{B.108})$$

for all $\mathbf{q} \in \mathbb{R}^n$. It follows from (B.108) that

$$\|\mathbf{y}_{sol}\| = \|\mathbf{y}_p + \mathbf{y}_h\| \geq \|\mathbf{y}_p\|. \quad (\text{B.109})$$

Thus, the Euclidean norm of the general solution B_{10} will be greater than or equal to $\|\mathbf{y}_p\|$, (B.105).

Given the fact that (Corollary 11.2.2, pp. 140–141, [80], and (B.65))

$$L_m = 2.8 \text{ m}, \quad L_g = 1.2 \text{ m}. \quad (\text{B.110})$$

$$(\text{B.111})$$

$$\text{Dim} (\text{Null} (\mathbf{E})) = \text{Rank} (\mathbf{I}_n - \mathbf{E}^{MP} \mathbf{E}) = n_s < n.$$

It follows from (B.110), (B.111), that the n columns of the matrix $(\mathbf{I}_n - \mathbf{E}^{MP} \mathbf{E})$ span the null space of \mathbf{Z} , and that only δ_3 of the n columns are linearly independent. Thus, the n columns of the matrix $(\mathbf{I}_n - \mathbf{E}^{MP} \mathbf{E})$ are a spanning set but not a basis for the null space of \mathbf{Z} .

References

1. Abramowitz, M., Stegun, I.A.: Handbook of Mathematical Functions. Dover Publications, Mineola, New York (1965)
[zbMATH]
2. Ash, R.B., Doleans-Dade, C.A.: Probability and Measure Theory, 2nd edn. Academic Press, San Diego (2000)
3. Adamiec-Wojcik, I.: Modelling Dynamics of Multibody Systems: Use of Homogeneous Transformations and Joint Coordinates. Lambert Academic Publishing, Köln, Germany (2009)
4. Apostol, T.M.: Mathematical Analysis, 2nd edn. Addison-Wesley, Reading, Massachusetts (1974)
5. Arnold, V.I.: Mathematical Methods of Classical Mechanics, 2nd edn. Springer, New York (1989)
6. Atkinson, K.E.: An Introduction to Numerical Analysis, 2nd edn. Wiley, New York (1989)
7. Bhat, R.B., Dukkipati, R.V.: Advanced Dynamics. Alpha Science, Pangbourne, England (2001)
[zbMATH]
8. Baranowski, L., Gadowski, B., Szymonik, J., Majewski, P.: Comparison of explicit and implicit forms of the modified point mass trajectory model. J. Theor. Appl. Mech. **54**(4), 1183–1195 (2016)
9. Baranowski, L., Furmanek, W.: The problem of validation of the trajectory model of 35 mm calibre projectile TP-T in the normal conditions (in Polish). Problemy Techniki Uzbrojenia **125**, 35–44 (2013)
10. Baruh, H.: Analytical Dynamics. McGraw-Hill, New York (1999)
11. Bazaraa, M.S., Sherali, H.D., Shetty, C.M.: Nonlinear Programming: Theory and Algorithms, 2nd edn. Wiley, New York (1993)
- 12.

Beatty, M.F.: Principles of Engineering Mechanics, Volume 2: Dynamics–The Analysis of Motion. Springer, New York (2006)

13. Bellomo, N., Preziosi, L., Romano, A.: Mechanics and Dynamical Systems with Mathematica. Birkhäuser, Boston (2000)
[zbMATH]
14. Ben-Asher, J.Z.: Optimal Control Theory with Aerospace Applications. American Institute of Aeronautics and Astronautics, Reston, Virginia (2010)
15. Berkovitz, L.D.: Optimal Control Theory. Springer, New York (1974)
[zbMATH]
16. Bernardin, L., Chin, P., DeMarco, P., Geddes, K.O., et al.: Maple 16 Programming Guide. Maplesoft, Waterloo Maple Inc., Waterloo, Canada (2012)
17. Bertsekas, D.P.: Dynamic Programming: Deterministic and Stochastic Models. Prentice-Hall, Englewood Cliffs, New Jersey (1987)
18. Blundell, M., Harty, D.: The Multibody Systems Approach to Vehicle Dynamics. Elsevier Butterworth-Heinemann, Oxford (2004)
19. Breiman, L.: Probability. SIAM, Philadelphia (1992)
[zbMATH]
20. Bremaud, P.: Point Processes and Queues: Martingale Dynamics. Springer, New York (1981)
[zbMATH]
21. Bryson, A.E., Ho, Y.C.: Applied Optimal Control, revised printing. Hemisphere Publishing Corporation, New York (1975)
22. Burden, R.L., Faires, J.D.: Numerical Analysis, 4th edn. PWS-Kent, Boston (1989)
23. Champion, G., Bastin, G., D'Andrea-Novel, B.: Structural properties and classification of kinematic and dynamic models of wheeled mobile robots. IEEE Trans. Robot. Autom. **12**(1), 47–62 (1996)
24. Carlucci, D.E., Jacobson, S.S.: Ballistics: Theory and Design of Guns and Ammunition. CRC, Boca Raton, Florida (2008)
25. Caracciolo, L., De Luca, A., Iannitti, S.: Trajectory control of a four-wheel differentially driven mobile robot. In: Proceedings of the 1999 IEEE International Conference on Robotics & Automation, Detroit, Michigan, May 1999, pp. 2632–2638. IEEE, New Jersey (1999)
26. Chen, C.K., Shih, C.H.: Spatial dynamics of tank motion for real-time simulation. Veh. Syst. Dyn. **42**(4), 259–288 (2004)
27. Cheney, W., Kincaid, D.: Numerical Mathematics and Computing, 5th edn. Thomson Learning, Belmont, California (2004)
- 28.

Chernousko, F.L., Ananievski, I.M., Reshmin, S.A.: Control of Nonlinear Systems: Methods and Applications. Springer, Berlin (2008)
[\[zbMATH\]](#)

29. Cho, B.K., Oh, J.H., Kim, J.H.: Online balance controllers for a hopping and running humanoid robot. *Adv. Robot.* **25**(9–10), 1209–1225 (2011)
30. Chong, E.K.P., Zak, S.H.: An Introduction to Optimization, 3rd edn. Wiley, New Jersey (2008)
31. Conte, G., Moog, C.H., Perdon, A.M.: Algebraic Methods for Nonlinear Control Systems, 2nd edn. Springer, London (2007)
32. Conte, S.D., de Boor, C.: Elementary Numerical Analysis, 2nd edn. McGraw-Hill, Tokyo (1972)
33. Corless, R.M., Jeffrey, D.J.: The Turing factorization of a rectangular matrix. *SIGSAM Bull.* **31**(3), 20–28 (1997)
34. Cortes, J.C., Jodar, L., Villafuerte, L.: Mean square numerical solution of random differential equations: facts and possibilities. *Comput. Math. Appl.* **53**, 1098–1106 (2007)
35. Craig, J.J.: Introduction to Robotics: Mechanics and Control, 3rd edn. Pearson Prentice Hall, Upper Saddle River, New Jersey (2005)
36. Crandall, S.H., Karnopp, D.C., Kurtz, E.F., Pridmore-Brown, D.C.: Dynamics of Mechanical and Electromechanical Systems. Krieger, Malabar, Florida (1982)
37. Craven, B.D.: Control Optimization. Chapman & Hall, London (1995)
[\[zbMATH\]](#)
38. Crespo da Silva, M.R.M.: Intermediate Dynamics. McGraw-Hill, New York (2004)
39. Dankowicz, H.: Multibody Mechanics and Visualization. Springer, London (2005)
[\[zbMATH\]](#)
40. Deitz, P.H., Reed, H.L., Klopčic, J.T., Walbert, J.N.: Fundamentals of Ground Combat System Ballistic Vulnerability/Lethality. American Institute of Aeronautics and Astronautics, Reston, Virginia (2009)
41. De Sapia, V., Khatib, O., Delp, S.: Task-level approaches for the control of constrained multibody systems. *Multibody Syst. Dyn.* **16**(1), 73–102 (2006)
[\[MathSciNet\]](#)[\[zbMATH\]](#)
42. de Silva, C.W.: Mechatronics: An Integrated Approach. CRC Press, Boca Raton, Florida (2005)
43. Eaton, J.W.: GNU Octave Manual, 2nd printing. Network Theory, Bristol (2005)
44. Edsberg, L.: Introduction to Computation and Modelling for Differential Equations. Wiley, Hoboken, New Jersey (2008)
[\[zbMATH\]](#)

45. Escalona, J.L., Recuero, A.M.: A bicycle model for education in multibody dynamics and real-time interactive simulation. *Multibody Syst. Dyn.* **27**, 383–402 (2012)
[[MathSciNet](#)][[zbMATH](#)]
46. Etkin, B.: *Dynamics of Atmospheric Flight*. Dover Publications, Mineola, New York (2005)
47. Ehlers, G.W., Yavin, Y., Frangos, C.: On the motion of a disk rolling on a horizontal plane: path controllability and feedback control. *Comput. Methods Appl. Mech. Eng.* **137**, 345–356 (1996)
[[zbMATH](#)]
48. Einstein, A: “Life is like riding a bicycle. To keep your balance you must keep moving”. Observation attributed to Albert Einstein. Information obtained partly from the following website: <https://smallbusiness.com/monday-morning-motivation/einstein-quotations-bicycle/>
49. Fantoni, I., Lozano, R.: *Non-linear Control for Underactuated Mechanical Systems*. Springer, London (2002)
50. Featherstone, R.: *Rigid Body Dynamics Algorithms*. Springer Science, New York (2008)
[[zbMATH](#)]
51. Flannery, M.R.: D'Alembert-Lagrange Dynamics for Nonholonomic Systems. *Journal of Mathematical Physics* **52**, 032705-1 - 032705-29 (2011)
52. Fleming, W.H., Soner, H.M.: *Controlled Markov Processes and Viscosity Solutions*. Springer, New York (1993)
[[zbMATH](#)]
53. Fliess, M., Hazewinkel, M. (eds.): *Algebraic and Geometric Methods in Nonlinear Control Theory*. D. Reidel Publishing Company, Dordrecht, The Netherlands (1986)
[[zbMATH](#)]
54. Fradkov, A.L., Miroshnik, I.V., Nikiforov, V.O.: *Nonlinear and Adaptive Control of Complex Systems*. Kluwer Academic Publishers, Dordrecht, The Netherlands (1999)
[[zbMATH](#)]
55. Frangos, C., Yavin, Y.: Feasible output feedback controller design for linear systems. *Opt. Control Appl. Methods* **18**, 109–122 (1997)
[[MathSciNet](#)][[zbMATH](#)]
56. Frangos, C., Yavin, Y.: Feasible controller design for stochastic systems. *AIAA J. Guidance Control Dyn.* **20**(3), 535–541 (1997)
[[zbMATH](#)]
57. Frangos, C., Yavin, Y., Sniedovich, M.: Control strategies for a stochastic flexible manufacturing and assembly system model. *Comput. Math. Appl.* **38**, 243–249 (1999)
[[MathSciNet](#)][[zbMATH](#)]
58. Frangos, C., Yavin, Y.: Tracking control of a rolling disk. *IEEE Trans. Syst. Man Cybern. Part B: Cybern.* **30**(2), 364–372 (2000)
- 59.

- Frangos, C., Zenios, S., Yavin, Y.: Computation of feasible portfolio control strategies for an insurance company using a discrete-time asset/liability model. *Math. Computer Model.* **40**, 423–446 (2004)
[\[MathSciNet\]](#)[\[zbMATH\]](#)
60. Frangos, C.: Dynamic modelling and maneuvering control of a front-wheel-drive autonomous vehicle. *Dyn. Contin. Discrete Impulsive Syst. Ser. B: Appl. Algorith.* **16**(5), 675–697 (2009)
[\[MathSciNet\]](#)[\[zbMATH\]](#)
61. Frangos, C.: Mathematical modelling and control of an autonomous vehicle with rear-wheel-drive. *Dyn. Contin. Discrete Impulsive Syst. Ser. B: Appl. Algorith.* **19**(6), 667–696 (2012)
[\[MathSciNet\]](#)[\[zbMATH\]](#)
62. Frangos, C.: Dynamic modelling and nonlinear control of a front-wheel-drive vehicle subject to holonomic and nonholonomic constraints. *Dyn. Contin. Discrete Impulsive Syst. Ser. B: Appl. Algorith.* **21**(6), 307–365 (2014)
[\[MathSciNet\]](#)
63. Frangos, C.: Mathematical modelling and nonlinear control of a rear-wheel-drive vehicle by using the Newton-Euler equations - Part 1. *Dyn. Contin. Discrete Impulsive Syst. Ser. B: Appl. Algorith.* **26**(6), 381–446 (2019)
64. Frangos, C.: Mathematical modelling and nonlinear control of a rear-wheel-drive vehicle by using the Newton-Euler equations - Part 2. *Dyn. Contin. Discrete Impulsive Syst. Ser. B: Appl. Algorith.*, accepted for publication (2018)
65. Friedberg, S.H., Insel, A.J., Spence, L.E.: *Linear Algebra*, 4th edn. Prentice Hall, Upper Saddle River, New Jersey (2003)
66. Gantmacher, F.: *Lectures in Analytical Mechanics*. MIR Publishers, Moscow (1970)
67. Gard, T.C.: *Introduction to Stochastic Differential Equations*. Marcel Dekker, New York (1988)
[\[zbMATH\]](#)
68. Gerald, C.F., Wheatly, P.O.: *Applied Numerical Analysis*, 5th edn. Addison-Wesley Publishing Company, Reading, Massachusetts (1994)
69. Germershausen, R. (ed.): *Handbook on Weaponry*. Rheinmetall, Düsseldorf, Germany (1982)
70. Ginsberg, J.H.: *Advanced Engineering Dynamics*, 2nd edn. Cambridge University Press, Cambridge, England (1998)
71. Golub, G.H., van Loan, C.F.: *Matrix Computations*, 2nd edn. Johns Hopkins University Press, Baltimore, Maryland (1989)
72. Gonnet, P.: A review of error estimation in adaptive quadrature. *ACM Comput. Surv.* **44**(4), 1–36 (2012)
[\[zbMATH\]](#)

73. Greenwood, D.T.: Advanced Dynamics. Cambridge University Press, Cambridge (2003)
74. Gutzwiller, M.C.: Moon-earth-sun: the oldest three body problem. *Rev. Modern Phys.* **70**(2), 589–639 (1998)
75. Hahn, H.: Rigid Body Dynamics of Mechanisms, Part 1: Theoretical Basis. Springer, Berlin (2002)
[zbMATH]
76. Hahn, H.: Rigid Body Dynamics of Mechanisms, Part 2: Applications. Springer, Berlin (2003)
[zbMATH]
77. Hairer, E., Nørsett, S.P., Wanner, G.: Solving Ordinary Differential Equations I: Nonstiff Problems, 2nd revised edn. Springer, Berlin (1993)
78. Hammond, W.E.: Design Methodologies for Space Transportation Systems. American Institute of Aeronautics and Astronautics, Reston, Virginia (2001)
79. Hart, D., Croft, T.: Modelling with Projectiles. Ellis Horwood, Chichester, England (1988)
[zbMATH]
80. Harville, D.A.: Matrix Algebra from a Statistician's Perspective. Springer, New York (1997)
[zbMATH]
81. Haug, E.J.: Intermediate Dynamics. Prentice Hall, Englewood Cliffs, New Jersey (1992)
[zbMATH]
82. Hemami, H., Weimer, F.C.: Modeling of nonholonomic systems with applications. *ASME J. Appl. Mech.* **48**, 177–182 (1981)
[zbMATH]
83. Hsu, H.P.: Probability, Random Variables, & Random Processes. Schaum's Outline Series, McGraw-Hill, New York (1997)
84. Huston, R.L.: Multibody Dynamics. Butterworth-Heinemann, New York (1990)
[zbMATH]
85. Huston, R.L.: Constraint forces and undetermined multipliers in constrained multibody systems. *Multibody Syst. Dyn.* **3**, 381–389 (1999)
[MathSciNet][zbMATH]
86. Hyun, D.: Predictive Modelling and Active Control of Rollover in Heavy Vehicles. PhD Dissertation, Department of Mechanical Engineering, Texas A&M University, College Station, Texas, USA (2001)
87. Hyun, D., Langari, R.: Development of a parsimonious dynamic model of tractor-semitrailers. *J. Heavy Veh. Syst.* **9**(2), 298–318 (2002)
88. Isidori, A.: Nonlinear Control Systems, 3rd edn. Springer, London (1995)
89. Jacobson, D.H., Martin, D.H., Pachter, M., Geveci, T.: Extensions of Linear-Quadratic Control

Theory. Springer, Berlin (1980)
[zbMATH]

90. Jazwinski, A.H.: Stochastic Processes and Filtering Theory. Dover Publications, Mineola, New York (2007)
[zbMATH]
91. Jeffrey, D.J., Corless, R.M.: Linear algebra in Maple. In: Hogben, L. (ed.) Handbook of Linear Algebra, pp. 72-1 - 72-21. Chapman and Hall/CRC, Boca Raton, Florida (2006)
92. Johnson, R.W.: AMGKQ: An efficient implementation of adaptive multivariate Gauss-Kronrod quadrature for simultaneous integrands in Octave/MATLAB, ArXiv e-prints, [arXiv.org/abs/1410.1064](https://arxiv.org/abs/1410.1064), submitted (2014)
93. Katz, A.: Computational Rigid Vehicle Dynamics. Krieger Publishing Company, Malabar, Florida (1997)
[zbMATH]
94. Kim, P.: Rigid Body Dynamics for Beginners: Euler Angles and Quaternions. CreateSpace Independent Publishing Platform, ISBN-13: 978-1493598205 (2013)
95. Kimbrell, J.T.: Kinematics Analysis and Synthesis. McGraw-Hill, New York (1991)
96. Kirk, D.E.: Optimal Control Theory. Dover Publications, Mineola, New York (2004)
97. Kushner, H.J.: Introduction to Stochastic Control. Holt, Rinehart and Winston, New York (1971)
[zbMATH]
98. Kushner, H.J., Dupuis, P.G.: Numerical Methods for Stochastic Control Problems in Continuous Time. Springer, New York (1992)
[zbMATH]
99. Kwatny, H.G., Blankenship, G.L.: Nonlinear Control and Analytical Mechanics: A Computational Approach. Birkhäuser, Boston (2000)
[zbMATH]
100. Larson, R.E., Casti, J.L.: Principles of Dynamic Programming: Part 2. Marcel Dekker, New York (1982)
[zbMATH]
101. Laumond, J.P. (ed.): Robot Motion Planning and Control. Springer, Berlin (1998)
102. Leitmann, G.: Calculus of Variations and Optimal Control - An Introduction. Plenum Press, New York (1981)
[zbMATH]
103. Levine, J.: Analysis and Control of Nonlinear Systems. Springer, Berlin (2009)
[zbMATH]
104. Lipschutz, M.: Differential Geometry. Schaum's Outline Series, McGraw-Hill, New York (1969)

[zbMATH]

105. Lipschutz, S.: General Topology. Schaum's Outline Series, McGraw-Hill, New York (1965)
[zbMATH]
106. Low, K.H., Leow, Y.P.: Kinematic modelling, mobility analysis and design of wheeled mobile robots. *Adv. Robot.* **19**(1), 73–99 (2005)
107. Lurie, A.I.: Analytical Mechanics. Springer, Berlin (2002)
108. MacFadzean, R.: Surface-Based Air Defence System Analysis. Artech House, London (1992)
109. Marquez, H.J.: Nonlinear Control Systems: Analysis and Design. Wiley, New Jersey (2003)
[zbMATH]
110. MATLAB 2007b User's Guide. The MathWorks Inc., Natick, Massachusetts (2007)
111. MATLAB 2007b Optimization Toolbox User's Guide. The MathWorks Inc., Natick, Massachusetts (2007)
112. MATLAB 2007b Symbolic Toolbox User's Guide. The MathWorks Inc., Natick, Massachusetts (2007)
113. MATLAB program stdatmo.m implementing the ISA 1976 atmospheric model obtained from the following website: <http://www.mathworks.com/matlabcentral/fileexchange/authors/101715>
114. Maxima Computer Algebra System obtained from the following website: <http://maxima.sourceforge.net/download.html>
115. McCoy, R.L.: The Effect of Wind on Flat-Fire Trajectories. Ballistic Research Laboratories Report No. ADB012872, Aberdeen Proving Ground, Maryland, USA (1976)
116. McCoy, R.L.: Modern Exterior Ballistics: The Launch and Flight Dynamics of Symmetric Projectiles, revised, 2nd edn. Schiffer, Atglen (2012)
117. McPhee, J.: Dynamics of Multibody Systems: Conventional and Graph-Theoretic Methods. SD 652 Course Notes, Department of Systems Design Engineering, University of Waterloo, Ontario, Canada N2L 3G1 (2004)
118. Merritt, R.W.: Methodology for Probability of Kill Against a Moving Target in Air-To-Ground Gunnery. MS Thesis, Department of Industrial and Systems Engineering, Georgia Institute of Technology, Atlanta, Georgia, USA (1978)
119. Miller, R.K., Michel, A.N.: Ordinary Differential Equations. Academic Press, New York (1982)
[zbMATH]
120. Moler, C.: Are we there yet? Zero crossing and event handling for differential equations. MATLAB News and Notes, Simulink 2 Special Edition, 1617 (1997)
- 121.

- Mood, A.M., Graybill, F.A., Boes, D.C.: Introduction to the Theory of Statistics, 3rd edn. McGraw-Hill, New York (1974)
122. Moulton, F.R.: Methods in Exterior Ballistics. Dover Publications, Mineola, New York (1962)
[zbMATH]
 123. Munro, N. (ed.): Symbolic Methods in Control System Analysis and Design. IEE Control Engineering Series 56, IEE, London (1999)
 124. Murray, R.M., Li, Z.X., Sastry, S.S.: A Mathematical Introduction to Robotic Manipulation. CRC Press, Boca Raton, Florida (1994)
[zbMATH]
 125. Nakamura, Y.: Advanced Robotics: Redundancy and Optimization. Addison-Wesley, Reading, Massachusetts (1991)
 126. Nakos, G., Joyner, D.: Linear Algebra with Applications. Brooks-Cole, Pacific Grove, California (1998)
 127. Navarro, A.: Computational Methods for Random Differential Equations: Theory and Applications. PhD Dissertation, Department of Applied Mathematics, Polytechnic University of Valencia, Spain (2017)
 128. Neckel, T., Rupp, F.: Random Differential Equations in Scientific Computing. De Gruyter Publishers, Berlin (2013)
[zbMATH]
 129. Neimark, J.I., Fufaev, N.A.: Dynamics of Nonholonomic Systems. American Mathematical Society, Providence, Rhode Island (1972)
[zbMATH]
 130. Nijmeijer, H., van der Schaft, A.J.: Nonlinear Dynamical Control Systems. Springer, New York (1990)
[zbMATH]
 131. Nikravesh, P.E.: Computer-Aided Analysis of Mechanical Systems. Prentice Hall, Englewood Cliffs, New Jersey (1988)
 132. Oberkampf, W.L., Roy, C.J.: Verification and Validation in Scientific Computing. Cambridge University Press, Cambridge (2010)
[zbMATH]
 133. Octave Symbolic Package using SymPy obtained from the following website: <https://octave.sourceforge.io/symbolic/>
 134. Ortega, R., Loria, A., Nicklasson, P.J., Sira-Ramirez, H.: Passivity-based Control of Euler-Lagrange Systems. Springer, London (1998)
 135. Pages, G.: Numerical Probability: An Introduction with Applications to Finance. Springer, Cham, Switzerland (2018)
[zbMATH]

136. Papoulis, A., Pillai, S.U.: Probability, Random Variables and Stochastic Processes, 4th edn. McGraw-Hill, New York (2002)
137. Pars, L.A.: A Treatise on Analytical Dynamics. Ox Bow Press, Woodbridge, Connecticut (1979)
[\[zbMATH\]](#)
138. Pavelle, R., Rothstein, M., Fitch, J.: Computer Algebra. *Scient. Am.*, 136–152 (1981)
139. Peebles, P.Z.: Probability Random Variables and Random Signal Principles. McGraw-Hill, New York (2001)
140. Peressini, A.L., Sullivan, F.E., Uhl, J.J.: The Mathematics of Nonlinear Programming. Springer, New York (1988)
[\[zbMATH\]](#)
141. Pfeiffer, F.: Mechanical System Dynamics. Springer, Berlin (2005)
[\[zbMATH\]](#)
142. Przemieniecki, J.S.: Mathematical Methods in Defence Analyses, 3rd edn. American Institute of Aeronautics and Astronautics, Reston, Virginia (2000)
143. Pontryagin, L.S., Boltyanskii, V.G., Gamkrelidze, R.V., Mishchenko, E.F.: The Mathematical Theory of Optimal Processes. Wiley, New York (1962)
[\[zbMATH\]](#)
144. Popp, K., Schiehlen, W.: Ground Vehicle Dynamics. Springer, Berlin (2010)
145. Rabier, P.J., Rheinboldt, W.C.: Nonholonomic Motion of Rigid Mechanical Systems from a DAE Viewpoint. SIAM, Philadelphia (2000)
[\[zbMATH\]](#)
146. Rajagopalan, R.: A generic kinematic formulation for wheeled mobile robots. *J. Robot Syst.* **14**(2), 77–91 (1997)
147. Rosenberg, R.M.: Analytical Dynamics of Discrete Systems. Plenum Press, New York (1991)
148. Ross, S.M.: Introduction to Probability Models, 7th edn. Academic Press, San Diego, California (2000)
149. Saaty, T.L., Bram, J.: Nonlinear Mathematics. Dover Publications, Mineola, New York (1981)
[\[zbMATH\]](#)
150. Samin, J.C., Fisette, P.: Symbolic Modelling of Multibody Systems. Kluwer Academic Publishers, Dordrecht, The Netherlands (2003)
[\[zbMATH\]](#)
151. Scherrer, M., McPhee, J.: Dynamic modelling of electromechanical multibody systems. *Multibody Syst. Dyn.* **9**, 87–115 (2003)
[\[zbMATH\]](#)

152. Schilling, R.J., Harris, S.L.: Applied Numerical Methods for Engineers Using Matlab and C. Brooks/Cole, Pacific Grove, California (2000)
153. Sciavicco, L., Siciliano, B.: Modelling and Control of Robot Manipulators. Springer, London (2000)
[zbMATH]
154. Seifried, R.: Dynamics of Underactuated Multibody Systems. Springer, Cham, Switzerland (2014)
[zbMATH]
155. Shabana, A.A.: Computational Dynamics, 2nd edn. Wiley, New York (2001)
156. Shampine, L.F., Allen, R.C., Pruess, S.: Fundamentals of Numerical Computing. Wiley, New York (1997)
[zbMATH]
157. Shanmugan, K.S., Breipohl, A.M.: Random Signals: Detection, Estimation and Data Analysis. Wiley, New York (1988)
158. Sherman, M.A., Seth, A., Delp, S.L.: Simbody: multibody dynamics for biomedical research. 2011 Symposium on Human Body Dynamics, Procedia IUTAM 2, pp. 241–261 (2011)
159. Sherman, M.A.: Simbody Theory Manual. Simbios Center at Stanford University (2011)
160. Shi, P., McPhee, J.: Symbolic programming of a graph-theoretic approach to flexible multibody dynamics. Mech. Struct. Mach. **30**, 123–154 (2002)
161. Shiryaev, A.N.: Probability, 2nd edn. Springer, Berlin (1996)
162. Siciliano, B., Khatib, O. (eds.): Handbook of Robotics, 2nd edn. Springer, Berlin (2016)
163. Sniedovich, M.: Dynamic Programming. Marcel Dekker, New York (1992)
[zbMATH]
164. Snyman, J.A., Wilke, D.N.: Practical Mathematical Optimization, 2nd edn. Springer Nature, Cham, Switzerland (2018)
165. Soong, T.T.: Random Differential Equations in Science and Engineering. Academic Press, New York (1973)
[zbMATH]
166. Speyer, J.L., Jacobson, D.H.: Primer on Optimal Control Theory. Society for Industrial and Applied Mathematics (SIAM), Philadelphia (2010)
[zbMATH]
167. Spong, M.W., Vidyasagar, M.: Robot Dynamics and Control. Wiley, New York (1989)
168. Spivak, M.: Physics for Mathematicians: Mechanics I. Publish or Perish, <http://www.mathpop.com> (2010)
169. Stevens, B.L., Lewis, F.L.: Aircraft Control and Simulation, 2nd edn. Wiley, Hoboken, New

Jersey (2003)

170. Tertychny-Dauri, V.Y.: Adaptive Mechanics. Kluwer Academic Publishers, Dordrecht, The Netherlands (2002)
[\[zbMATH\]](#)
171. Thomasian, A.J.: The Structure of Probability Theory with Applications. McGraw-Hill, New York (1969)
[\[zbMATH\]](#)
172. Torby, B.J.: Advanced Dynamics for Engineers. Holt, Rinehart and Winston, New York (1984)
173. Tucker, H.G.: A Graduate Course in Probability. Academic Press, New York (1967)
[\[zbMATH\]](#)
174. Uchida, T., Callejo, A., Garcia de Jalon, J., McPhee, J.: On the Gröbner basis triangularization of constraint equations in natural coordinates. *Multibody Syst. Dyn.* **31**, 371–392 (2014)
175. van Loan, C.F.: Introduction to Scientific Computing, 2nd edn. Prentice-Hall, Upper Saddle River, New Jersey (2000)
176. Vlasenko, D., Kasper, R.: Algorithm for component based simulation of multibody dynamics. *Technische Mechanik* **16**(1), 77–88 (2006)
177. Vlasenko, D., Kasper, R.: Implementation of the symbolic simplification for the calculation of accelerations of multibodies. *Proceedings of Industrial Simulation Conference*, 9–11 June, 2008, Lyon, France (2008)
178. Vujanovic, B.D., Atanackovic, T.M.: An Introduction to Modern Variational Techniques in Mechanics and Engineering. Birkhäuser, Boston (2004)
[\[zbMATH\]](#)
179. Wells, D.A.: Schaum's Outline of Theory and Problems of Lagrangian Dynamics. McGraw-Hill, New York (1967)
180. White, F.M.: Fluid Mechanics, 6th edn. McGraw-Hill, New York (2008)
181. Wittenburg, J.: Dynamics of Multibody Systems, 2nd edn. Springer, Berlin (2008)
182. Woernle, C.: Control of robotic systems by exact linearization. In: Angeles, J., Zakhariiev, E. (eds.): *Computational Methods in Mechanical Systems*, NATO ASI Series, Series F: Computer and Systems Sciences, Vol. 161, pp. 296–325. Springer, Berlin (1998)
183. Wolfram, S.: The Mathematica Book, 4th edn. Cambridge University Press, Cambridge (1999)
184. Wong, E., Hajek, B.: Stochastic Processes in Engineering Systems. Springer, New York (1985)
[\[zbMATH\]](#)
185. Wong, J.Y.: Theory of Ground Vehicles, 3rd edn. Wiley, New York (2001)

186. Wright, F.: Computing with Maple. Chapman & Hall, London (2002)
[\[zbMATH\]](#)
187. Yavin, Y., Friedman, M., Solomon, E.: Optimal control of a non-linear noisy sine wave oscillator. *Int. J. Non-Linear Mech.* **14**, 205–219 (1979)
[\[zbMATH\]](#)
188. Yavin, Y., Friedman, M.: Estimation and control for a class of non-linear stochastic systems. *Int. J. Syst. Sci.* **12**, 587–600 (1981)
[\[zbMATH\]](#)
189. Yavin, Y.: Bang-bang strategies using interrupted observations for steering a random motion of a point. *Comput. Methods Appl. Mech. Eng.* **29**, 351–364 (1981)
[\[MathSciNet\]](#)[\[zbMATH\]](#)
190. Yavin, Y.: A discrete Kalman filter for a class of non-linear stochastic systems. *Int. J. Syst. Sci.* **13**, 1233–1246 (1982)
[\[zbMATH\]](#)
191. Yavin, Y.: Strategies using an observer for steering a random motion of a point in a multitarget environment. *Comput. Methods Appl. Mech. Eng.* **39**, 297–310 (1983)
[\[MathSciNet\]](#)[\[zbMATH\]](#)
192. Yavin, Y.: Feedback Strategies for Partially Observable Stochastic Systems. Springer, Berlin (1983)
[\[zbMATH\]](#)
193. Yavin, Y.: Numerical Studies in Non-Linear Filtering. Springer, Berlin (1985)
[\[zbMATH\]](#)
194. Yavin, Y.: Stochastic pursuit-evasion differential games in the plane. *J. Optim. Theory Appl.* **50**, 495–523 (1986)
[\[MathSciNet\]](#)[\[zbMATH\]](#)
195. Yavin, Y.: A pursuit-evasion differential game with noisy measurements of the evader's bearing from the pursuer. *J. Optim. Theory Appl.* **51**, 161–177 (1986)
[\[MathSciNet\]](#)[\[zbMATH\]](#)
196. Yavin, Y., Miloh, T.: Stochastic two-target pursuit-evasion differential games in 3-D. *Optim. Control Appl. Methods* **8**, 311–325 (1987)
[\[MathSciNet\]](#)
197. Yavin, Y., de Villiers, R.: The game of two cars: The case of variable speed. *J. Optim. Theory Appl.* **60**, 327–339 (1989)
[\[MathSciNet\]](#)[\[zbMATH\]](#)
198. Yavin, Y., de Villiers, R.: Proportional navigation and the game of two cars in 3D: a time-dependent stochastic differential game. *Adv. Control Dyn. Syst.* **32**(2), 39–52 (1990)
[\[zbMATH\]](#)
199. Yavin, Y., de Villiers, R.: Applications of stochastic differential games to medium-range air-to-air missiles. *J. Optim. Theory Appl.* **67**, 355–367 (1990)

[\[MathSciNet\]](#)[\[zbMATH\]](#)

200. Yavin, Y., Frangos, C.: Application of stochastic optimal control to the design of an electromagnetic actuator. *Mathem. Comput. Model.* **13**(10), 51–57 (1990)
[\[MathSciNet\]](#)[\[zbMATH\]](#)
201. Yavin, Y., Frangos, C., Fourie, J.P.: On the performance of a projectile which uses a bang-bang type guidance law: Part 1. *Comput. Mathem. Appl.* **23**, 111–118 (1992)
[\[zbMATH\]](#)
202. Yavin, Y., Frangos, C., Fourie, J.P.: On the performance of a projectile which uses a bang-bang type guidance law: Part 2 - A semi rigid body model. *Comput. Mathem. Appl.* **24**(4), 85–92 (1992)
203. Yavin, Y., Frangos, C.: Optimal control of some queueing networks. *Mathem. Comput. Model.* **16**(5), 3–12 (1992)
204. Yavin, Y., Frangos, C.: An optimal selection policy for a flexible manufacturing cell feeding several production lines. *Comput. Mathem. Appl.* **23**(10), 57–63 (1992)
205. Yavin, Y., Frangos, C.: Optimal control of a manufacturing system which consists of three assembly machines. *Int. J. Syst. Sci.* **23**(12), 2407–2412 (1992)
[\[MathSciNet\]](#)[\[zbMATH\]](#)
206. Yavin, Y., Frangos, C., Fourie, J.P.: The performance of a projectile which uses a bang-bang type guidance law: Part 3—The point-mass model revisited. *Comput. Mathem. Appl.* **25**(4), 27–37 (1993)
[\[zbMATH\]](#)
207. Yavin, Y.: Application of stochastic optimal control to the suboptimal design of thrust-mass profiles. *J. Optim. Theory Appl.* **78**(1), 77–91 (1993)
[\[MathSciNet\]](#)[\[zbMATH\]](#)
208. Yavin, Y., Miloh, T.: On the control and guidance of the motion of an immersed body: some problems in stochastic control. *J. Optim. Theory Appl.* **77**(3), 613–641 (1993)
[\[MathSciNet\]](#)[\[zbMATH\]](#)
209. Yavin, Y., Frangos, C.: Optimal two layer selection policy for a flexible manufacturing system. *J. Optim. Theory Appl.* **77**(2), 359–371 (1993)
[\[MathSciNet\]](#)[\[zbMATH\]](#)
210. Yavin, Y., Frangos, C.: Feasible strategies for the control of a disk rolling on a moving horizontal plane. *Mathem. Comput. Model.* **20**(12), 81–95 (1994)
211. Yavin, Y., Frangos, C.: Open-loop strategies for the control of a disk rolling on a horizontal plane. *Comput. Methods Appl. Mech. Eng.* **127**(1–4), 227–240 (1995)
[\[zbMATH\]](#)
212. Yavin, Y., Frangos, C., Zilman, G., Miloh, T.: Computation of feasible command strategies for the navigation of a ship in a narrow zigzag channel. *Comput. Mathem. Appl.* **30**(10), 79–101 (1995)
- 213.

Yavin, Y.: Stabilization and control of the motion of an autonomous bicycle by using a rotor for the tilting moment. *Comput. Methods Appl. Mech. Eng.* **178**, 233–243 (1999)
[\[MathSciNet\]](#)[\[zbMATH\]](#)

214. Ying, S.J.: *Advanced Dynamics*. American Institute of Aeronautics and Astronautics, Reston, Virginia (1997)
[\[zbMATH\]](#)

215. Yoshikawa, T.: *Foundations of Robotics: Analysis and Control*. MIT Press, Cambridge, Massachusetts (1990)

Index

A

AA gun

AA gun aiming angles

AA Gun Tracking Mode GM1

AA Gun Tracking Mode GM1A

AA Gun Tracking Mode GM1B

AA Gun Tracking Mode GM2

AA projectile trajectories

acceleration constraints

acceleration kinematic model

Accumulative probability of destroying the AAT

accumulative probability of destroying the AAT

Ackermann steering system

admissible region or set

aerodynamic drag force

aiming vector of the AA gun

air-density

altitude

angular acceleration

angular momentum

angular velocity

applied forces

applied torques

arc length

asymptotic tracking results

augmented matrix

azimuth and elevation angles of the AA gun
Azimuth error angle

B

basic dynamic model
basis
Bellman dynamic programming equation
binomial
body co-ordinate system
body of the AAT
body reference frame
bounding set
Burst of AA projectiles

C

center of mass
Chetaev principle
closed-form expression
closed-form expressions
closed-form solution
closest point of approach (CPA)
column space
Computational method NM1
Computational method NM2
consistent simultaneous linear equations (SLEs)
constrained motion of the controlled dynamic model
constrained rigid multibody system
constraint forces
constraint torques
control objective
cross wind
Crypto-deterministic system
cylinder

D

d'Alembert-Lagrange principle
decoupled kinematic models
defended location

dependent variables
deployment of the mobile ADS
Deterministic initial conditions
deviation of the inertial angles of the FC vector from the inertial angles
of the LOS vector
differential gearbox
dimensions of the AAT
domains of integration
double integral
drag coefficient
drive system
dynamics

E

elementary row operations
Elevation error angle
equality
Euclidean norm
Euler angles
Euler parameters

F

Feasible control
feasible control
feedback variables
finite time horizon
fire control problem FCA
Firing Rate of the AA Gun
firing time
firing time of the AA projectile
Firing Times of the AA Projectiles
form of the kinematic model
free-body diagram
full column rank

G

Gaussian
general solution

generalized applied forces
generalized constraint forces
generalized gravitational forces
generic firing speed
generic firing velocity of the AA projectile
geometric constraint
Geometric constraints
geometric constraints
Geometry of the AAT
gravitational acceleration
gravitational force
ground impact inertial position
ground impact inertial velocity
ground impact range
ground impact time

H

half-sphere
Hamilton-Jacobi-Bellman (HJB) partial differential equation (PDE)
hinge point H of the AA gun
holonomic constraint
holonomic velocity constraint
holonomic velocity constraints
homogeneous equation
homogeneous solution
homogeneous system
Hurwitz

I

ideal AA projectile
independent generalized co-ordinates
independent generalized velocities
independent variables
independent velocity constraints
independent virtual displacement
inequalities
inertia matrix
inertial acceleration

inertial angles of the FC vector
inertial angles of the LOS vector
inertial azimuth and elevation angles
inertial azimuth and elevation angles of the fire control vector
inertial azimuth angle of the FC vector
inertial azimuth angle of the LOS vector
inertial co-ordinate system
inertial elevation angle of the velocity vector of the AA projectile
Inertial position
inertial position
inertial position of the AA gun muzzle
inertial position of the center of mass of the AAT
Inertial reference frame
inertial reference frame
Inertial trajectory of the AAT
inertial velocity
inertial velocity of the AA gun muzzle
inertial velocity of the AA projectile at the firing time
inertial velocity of the AA projectile relative to the wind
inertial velocity of the center of mass of the AAT
Initial value problem
initial value problem
Initial velocity of the AA projectile
intercept times
inverse dynamics transformation
inverse transformation
ISA model

J

joint probability density function (PDF)

K

kill probability
kinematic constraints
kinematic model
kinematic model of the *turret and AA gun system*
kinematic model of the *vehicle system*
kinematics

kinetic energy
Kushner, Harold J.

L

Lagrange equations
Lagrange multipliers
Langrange multipliers
lead angles of the FC vector
lead azimuth angle
lead elevation angle
line-of-intercept (LOI) vector
line-of-sight (LOS) vector
linear algebra
linear transformation
locally flat surface of the earth

M

Maple
mass
mass matrix
Mathematica
mathematical modelling
MATLAB
MATLAB function odezero
MATLAB Optimization Toolbox
MATLAB Symbolic Toolbox
matrix inverse
Maxima
mils
miss distance
Moore-Penrose conditions
Moore-Penrose generalized inverse
Moore-Penrose generalizedinverse
motion trajectory
multibody system
Muzzle of the AA gun

N

neutrally stable
Newton's second law
Newton's third law
Newton-Euler equations
nonholonomic constraint
nonholonomic velocity constraint
Nonholonomic velocity constraints
nonholonomic velocity constraints
nonlinear control
nonlinear feedback control law
Not independent velocity constraints
not unique
null space
null space matrix
numerical approximation method
numerical integration algorithm
numerical solution

O

Octave
Octave Symbolic Package
Operational Mode OM1
Operational Mode OM1A
Operational Mode OM1B
Operational Mode OM2
Operational Mode OM3
operational modes of the mobile ADS
optimal control
orthogonal
orthogonal complement
orthogonal matrices

P

parameters
parametric form
particular solution
penalty function
performance evaluation

Point mass flight dynamics model of the AA projectile
point mass flight dynamics model of the AA projectile
point of contact of wheel i

positive definite

potential energy

principle of constraint release

probability mass function (PMF)

probability of destroying the AAT

Probability that a burst of AA projectiles will destroy the AAT

Probability that the AA projectile will impact the body of the AAT

R

Random differential equation

random disturbances

Random initial conditions

random initial conditions

Random vector

Realization

reduced dynamic model

reduced row echelon form

redundant velocity constraints

reference trajectories

regula falsi

regular curve in three dimensional space

relative intercept speed

relative speed of the AA projectile

resultant aerodynamic force

resultant applied force

resultant applied torque

resultant constraint force

resultant constraint torque

x Cartesian co-ordinate systems

rigid body

rotation axis sequences

Rotation matrix

rotation matrix

rotational kinetic energy

rotational motion
rotor of the AA gun electric motor
rotor of the turret electric motor
row space
Runge-Kutta algorithm

S

sequence of intercept times
singular value decomposition
singular values
six degrees of freedom
skew-symmetric matrices
solution set
span
spanning set
special engagement scenario
speed of sound
spin-stabilized
standard deviation
state space form
state vector
stationary sphere
steering system
Stochastic model of the dispersion of the AA projectiles
stochastic optimal control
stochastically independent and identically distributed (IID)
symbolic expressions
symmetric

T

target bounding sphere (TBS)
time of flight of the AA projectile to the CM of the AAT
time of flight to ground impact
time-step
translational kinetic energy
translational motion
turret

U

unique
Unique mean square solution
Unique solution
unique solution
unit vectors

V

vector equality constraint
vector of applied torques
vector of control inputs
vector of generalized co-ordinates
vector of generalized velocities
vehicle body
Vehicle Body Tracking Mode VM1
Vehicle Body Tracking Mode VM1A
Vehicle Body Tracking Mode VM2
velocity constraints
velocity constraints matrix
Verification method VMB
virtual displacement
virtual wheel
virtual work
Vulnerability model of the AAT

W

wheels 1, 2, 3 and 4
white measurement noise
white state noise
wind velocity

Y

Yavin, Yaakov (1935-2006)

Z

zero dynamics

Footnotes

¹ In the main part of the research monograph m represents the number of velocity constraints, n represents the number of generalized velocities, and δ_3 represents the number of independent generalized velocities.